Small Inorganic Ring Systems: Understanding Cyclization and Bond Activation Processes

Dissertation

zur Erlangung des

DOKTORGRADES DER NATURWISSENSCHAFTEN

(DR. RER. NAT)

an der Fakultät für Chemie und Pharmazie

der Universität Regensburg

vorgelegt von

Alexander Falk

aus Burglengenfeld

im Jahr 2024

Eidesstattliche Erklärung

Ich erkläre hiermit an Eides statt, dass ich die vorliegende Arbeit selbstständig verfasst und keine anderen als die angegebenen Quellen und Hilfsmittel benutzt habe. Die aus fremden Quellen direkt oder indirekt übernommenen Gedanken sind als solche gekennzeichnet. Die Arbeit wurde bisher in gleicher oder ähnlicher Form keiner anderen Prüfungsbehörde vorgelegt und auch nicht veröffentlicht.

Ort, Datum	Unterschrift

Die vorliegende Arbeit entstand in der Zeit von April 2021 bis März 2024 am Institut für Anorganische Chemie der naturwissenschaftlichen Fakultät IV für Chemie und Pharmazie der Universität Regensburg unter Anleitung von Herrn PD. Dr. Jonathan O. Bauer.

Promotionsgesuch	September 2024
Promotion	November 2024
Prüfungsausschuss:	
Vorsitz:	Prof. Dr. Hubert Motschmann
Erster Gutachter:	PD Dr. Jonathan O. Bauer
Zweiter Gutachter:	Prof. Dr. Manfred Scheer
Dritter Prüfer:	Prof. Dr. Frank-Michael Matysik

Publikationsliste:

Interplay of Hydrogen and Halogen Bonding in the Crystal Structures of 2,6-Dihalogenated Phenols

J. O. Bauer, S. Koschabek, A. Falk

ChemistrySelect **2021**, *6*, 8736–8740.

Molecular Scissors for Tailor-Made Modification of Siloxane Scaffolds

T. Götz, A. Falk, J. O. Bauer

Chem. Eur. J. **2022**, *28*, e202103531.

Structural and Electronic Effects on Phosphine Chalcogenide-Stabilized Silicon Centers in Four-Membered Heterocyclic Cations

A. Falk, J. O. Bauer

Inorg. Chem. **2022**, *61*, 15576–15588.

Stereochemically Pure *Si*-Chiral Aminochlorosilanes

M. Kümper, T. Götz, N. A. Espinosa-Jalapa, A. Falk, R. Rothfelder, J. O. Bauer

Z. Anorg. Allg. Chem. **2023**, *649*, e202300067.

Regio-, diastereo- and enantioselectivity in the photocatalytic generation of carbanions via hydrogen atom transfer and reductive radical-polar crossover

S. Grotjahn, L. Müller, A. Pattanaik, A. Falk, G. Barison, J. O. Bauer, J. Rehbein, R. M. Gschwind, B. König

Org. Chem. Front. **2024**, 10.1039/D4QO01219D

Preface

The herein presented results have already been published in part during the preparation of this thesis (see above). The corresponding citations are given at the beginning of the respective chapters.

Each chapter includes a list of authors and the individual contribution of each author is described.

Furthermore, all chapters have their own numeration of compounds. The molecular structures in the schemes and figures may differ slightly in style. In the beginning of this thesis, a general introduction and objectives of the work are presented together with a comprehensive conclusion at the end of this thesis.

Abbreviations

Ar	Aryl
DFT	Density functional theory
d.r.	Diastereomeric ratio
e.r.	Enantiomeric ratio
EI	Electron impact ionization
Et	Ethyl
FD	Field desorption ionization
h	Hour(s)
HR	High resolution
HAT	Hydrogen-atom transfer
*i*Pr	*Iso*-propyl
Me	Methyl
Mes	Mesityl = 2,3,5-trimethylbenzene
min	Minute(s)
mol	Moles
MS	Mass spectrometry
NMR	Nuclear magnetic resonance
Ph	Phenyl
RT	Room temperature
RPC	Reversal-polarity catalysis
RRPCO	Reductive radical-polar crossover
TMP	Trimethoxyphenyl = 2,3,5-trimethoxybenzene
*t*Bu	*Tert*-Butyl
Tf	Triflate = Trifluoromethanesulfonate
THF	Tetrahydrofurane

Table of contents

1 Introduction

1.1 Lewis acids and bases

The concept of Lewis acids and bases proposed by Gilbert N. Lewis in 1923, represents a fundamental principle of chemistry. It elucidates the behavior of substances in various chemical reactions. In accordance with this theory, a Lewis acid is defined as an electron pair acceptor, while a Lewis base is characterized as an electron pair donor. Lewis acids encompass a wide range of chemical species, including metal ions, metal complexes, and main group compounds with vacant orbitals capable of accepting an electron pair.[1] Common examples include metal cations such as Ti^{4+}, Ce^{3+} and Fe^{3+}, or main group compounds such as BCl_3, $AlCl_3$ and $SiCl_4$. Conversely, Lewis bases encompass molecules with lone electron pairs available for donation. Notable Lewis bases include ammonia (NH_3), water (H_2O), and various organic compounds containing nitrogen, oxygen, or sulfur atoms. The interaction between Lewis acids and bases typically involves the formation of coordinate covalent bonds. In this process, the Lewis acid accepts a lone pair from the Lewis base, leading to the formation of a coordinate covalent bond or a Lewis adduct (Scheme 1).

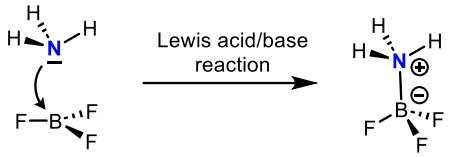

Scheme 1: A typical example for a Lewis acid / base reaction.

The strength of the interaction is hereby not only influenced by the Lewis acidity/basicity of the individual parts, but also by the ability of the Lewis acid to change its coordination sphere.[2] This becomes evident when looking at the BF_3 Lewis acid in Scheme 1 which goes from a trigonal-planar coordination mode, with ideal bonding angles of 180° between the fluorine substituents, to a tetrahedral coordination mode, with ideal bonding angles of 109.5 ° between the fluorine substituents, once the NH_3 Lewis base is bonded to it. When more bulky substituents at boron are present the Lewis acidity significantly decreases, due to the increased energy demand from the transformation into a tetrahedral form with smaller bonding angles. This interaction plays a crucial role in numerous chemical processes, including coordination chemistry, catalysis and organic synthesis.[3] Understanding the principles governing Lewis acid-base interactions is essential for designing novel catalysts, elucidating reaction mechanisms, and predicting molecular behavior in complex systems. Boron, which is located in group 13, is renowned for its Lewis acidic properties, particularly in the form of boron trifluoride (BF_3), boron trichloride (BCl_3) and in the last decade especially tris(pentafluorophenyl)borane [$B(C_6F_5)_3$], and related boranes with fluorinated aryl groups.[4] These compounds readily accept electron pairs from Lewis bases, forming stable adducts and participating in diverse catalytic processes.

1.2 Silicon-based Lewis acids

When navigating across the periodic table, to group 14, the tendency to exhibit Lewis acidic behavior is slightly lower compared to group 13 elements. Nevertheless, especially certain silicon compounds, including silicon tetrahalides, can function as potent Lewis acids under appropriate conditions.[5] For instance, highly Lewis acidic Si(IV)- and Si(II) cations were found to efficiently catalyze Diels-Alder additions, Friedel-Crafts reactions, C–F hydrodefluorinations, and even olefin- and carbonyl hydrosilylations (Scheme 2).[6]

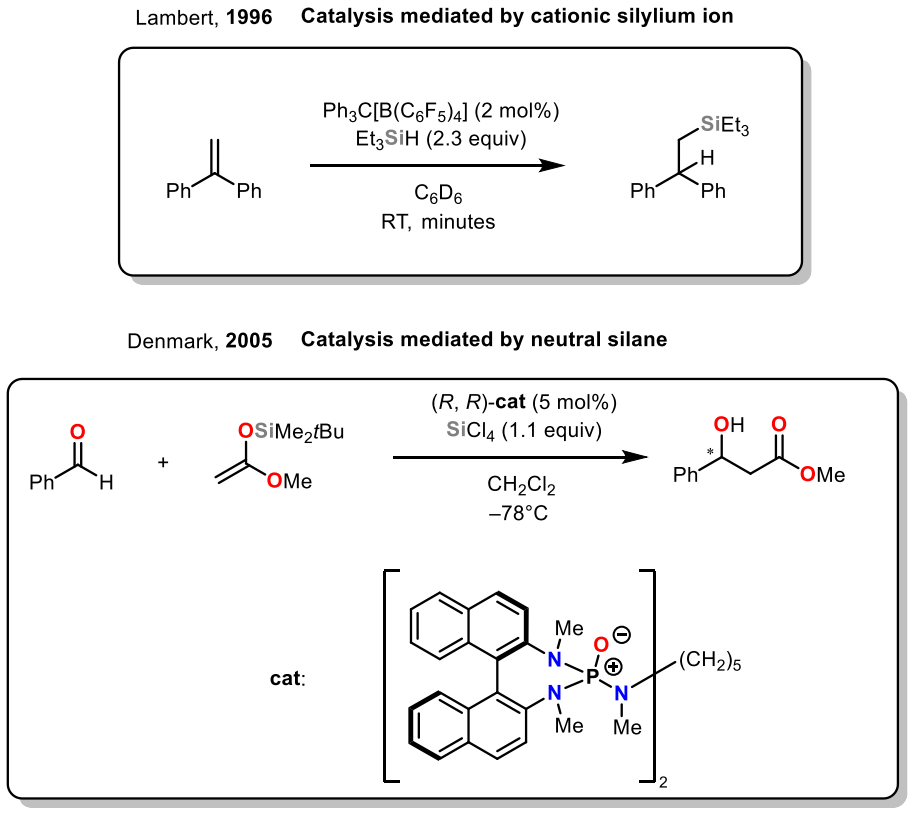

Scheme 2: Cationic silicon Lewis acid catalyzed hydrosilylation and enantioselective neutral silicon co-catalyzed aldol reaction.[7]

The utilization of silicon for potential catalytic applications is highly favorable due to its abundance and easy accessibility.[8] Lewis acidic silicon compounds can be roughly divided into two categories. The first category comprises cationic silylium-based compounds, which exhibit high Lewis acidity due to the presence of a vacant p-orbital and their general cationic nature. The second category encompasses neutral silanes, which display Lewis acidity due to their ability to form higher coordination compounds with sufficiently Lewis basic moieties. Neutral Lewis acidic silanes display remarkable versatility in catalytic applications, participating in a variety of transformations spanning organic synthesis, polymerization, and material science.[9] However, traditional neutral silicon acids, such as $SiCl_4$, are constrained in their applications due to the highly reactive Si–Cl bonds. In recent years, this issue has been circumvented by the introduction of geometrically constraining and/or perfluorinated alkyl- or aryl groups.[10] Greb et al. demonstrated the utility of silicon-based catalysts in promoting various organic reactions, including Diels-Alder

cycloadditions, ring-opening polymerizations, and C–H bond activations.[11] One of the first examples was published by Tilley and coworkers (Scheme 3).[12]

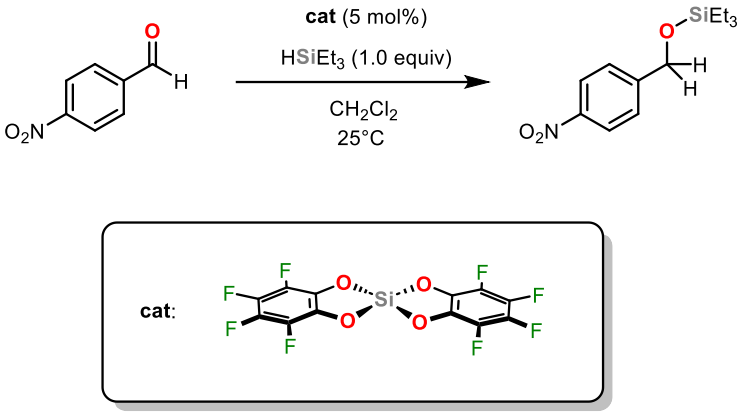

Scheme 3: Hydrosilylation by a neutral bis(catecholato)-substituted silicon Lewis acid.

The employed bis(perfluorocatecholato)silane [Si(cat^F)$_2$] demonstrated remarkable Lewis acidity, even surpassing B(C_6F_5)$_3$, when tested by the Gutmann-Beckett method. Futhermore, the hydrosilylation mechanism with Si(cat^F)$_2$ was found to proceed in an entirely different manner than the hydrosilylation process with B(C_6F_5)$_3$ (Figure 1). It was demonstrated that the Si(cat^F)$_2$-catalyzed hydrosilylation of aldehydes with enantiopure silanes is highly dependent on the polarity of the solvent. In the case of unpolar solvents, such as cyclohexane, a retention of the stereochemical configuration was observed to be predominant (70% ee). As the polarity of the solvent increased, a greater degree of racemization was observed. The authors detected, that the ^{1}H-NMR chemical shift of Et_3SiH does not change upon mixing with Si(cat^F)$_2$, therefore they were able to propose an alternative mechanism (Figure 1). First, the initial stage of the catalytic cycle was found to differ from the one observed in B(C_6F_5)$_3$-catalyzed hydrosilylations.[13] Instead of the anticipated interaction between the Lewis acid and the silicon hydride, the coordination of the Lewis basic aldehyde to Si(cat^F)$_2$ was identified as the initial step. This is followed up by a hydride transfer from the silane to the now highly electron deficient aldehyde. This results in the formation of a highly reactive silylium alkoxysilicate intermediate, which undergoes rapid silicon–oxygen bond formation, releasing the Si(cat^F)$_2$ catalyst and forming the hydrosilylated product (Figure 1). This step is likely to be the one most heavily influenced by solvent effects, leading to the observed loss of stereo information with more polar solvents. In contrast, B(C_6F_5)$_3$-catalyzed hydrosilylations initiate their catalytic cycle with the complexation of the Si–H moiety by the Lewis acid, resulting in a positive polarization of the silicon atom (Figure 1). This is followed by a nucleophilic attack of a Lewis basic moiety, such as an aldehyde or ketone, onto the activated silicon moiety, forming an Si–O bond. Subsequent to this, a hydride transfer from the B–H moiety occurs onto the electrophilic carbonyl carbon atom, releasing the product and B(C_6F_5)$_3$.

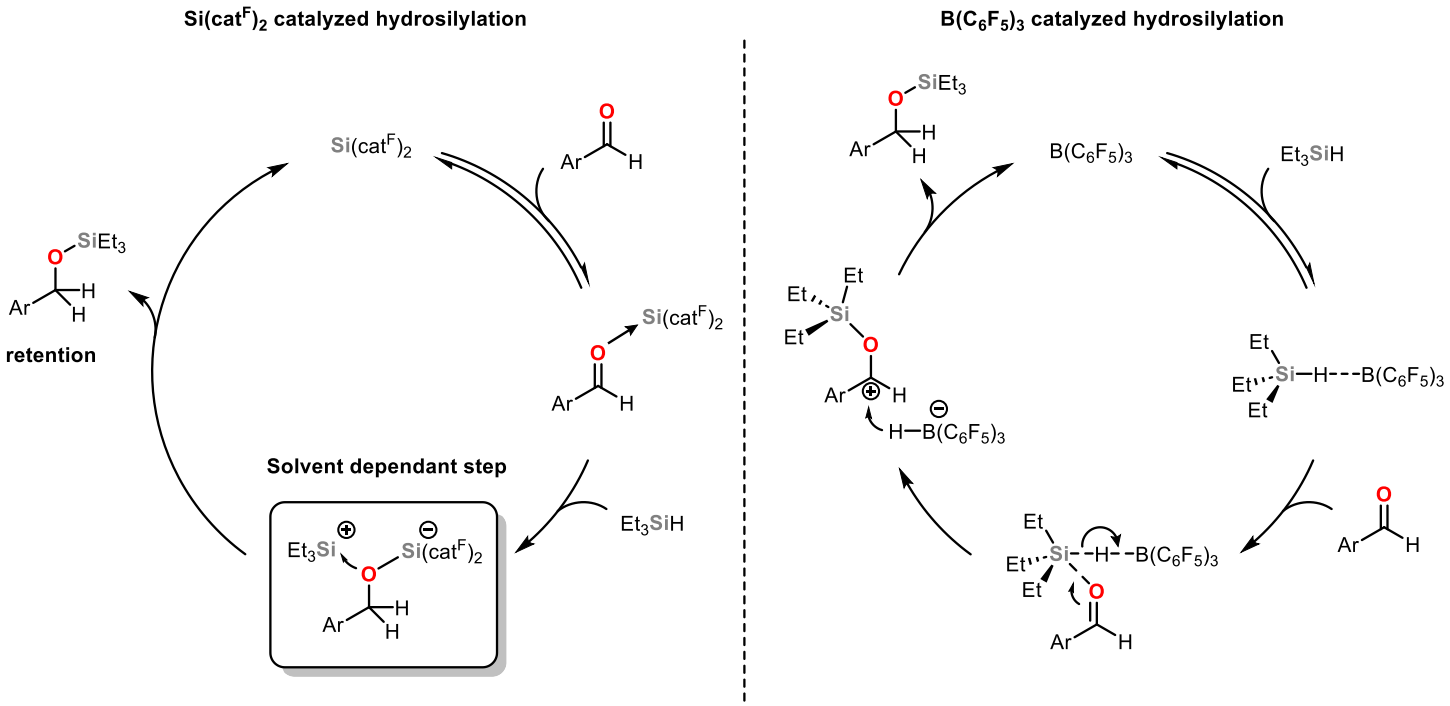

Figure 1: Mechanism of the hydrosilylation of aldehydes with bis(perfluorocatecholato)silane and $B(C_6F_5)_3$.[12,13]

This illustrates the potential of silicon-based Lewis acids in elucidating novel pathways in catalysis that remain unexplored.

1.2.1 Silylium ions

The class of silicon-based Lewis acids with the highest Lewis acidity are the cationic silylium ions. In contrast to their smaller group 14 homologues, carbenium ions, silylium ions emerged much later, sparking controversial debates regarding their existence in condensed phases.[14] Despite their delated introduction to the chemical field, the synthetic utilization of silylium ions as reactive intermediates and catalysts has recently gained momentum, marking a notable shift from their initial obscurity nearly four decades ago.[6c,15] The difficulties encountered in the isolation and characterization of silylium ions in their “free” form (Figure 2), coupled with the intricacies of their coordination chemistry, contributed to their slow start.

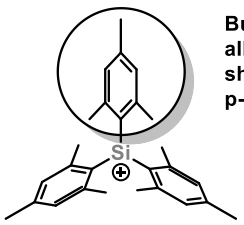

Bulky mesityl groups allow for a complete shielding of the vacant p-orbital at silicon

$^-[B(C_6F_5)_4]$

$\delta(^{29}Si)$ = 225.5 ppm

Figure 2: The first truly free silylium ion reported by Lambert and coworkers in 1997.[16]

The first report on a solvent and counter-anion free silylium ion was reported by Lambert and coworkers in 1997. They used the extremely bulky mesityl groups for the steric shielding of the vacant p-orbital at silicon (Figure 2).[16] Due to the high Lewis acidity resulting from their three-coordinate cationic nature, as well as the highly electrophilic character of the silylium ion, the selection of a suitable solvent and counter-anion is a challenging task. This is because virtually any Lewis base can form a Lewis pair with the silylium ion. Consequently, unless adequately shielded, silylium ions are typically stabilized by Lewis-basic moieties, resulting in the formation of Lewis-base-stabilized silylium cations.

1.2.2 Synthesis of silylium ions

The choice of solvent and counterion represents the most critical aspects in the successful synthesis of silylium ions. The advancement of silylium ion chemistry has been paralleled by the evolution of weakly coordinating anions (WCAs).[6b] Only a select few weakly coordinating counterions are oxidatively robust, do not serve as a fluorine ions source, and are not nucleophilic enough to react irreversibly with silylium ions. Two anions in particular have emerged as promising candidates for the synthesis of silylium ions. The perfluorinated aryl borate $[B(C_6F_5)_4]^-$ and the perhalogenated *closo*-dodecaborate $[B_{12}Cl_{12}]^{2-}$ (Figure 3).[17]

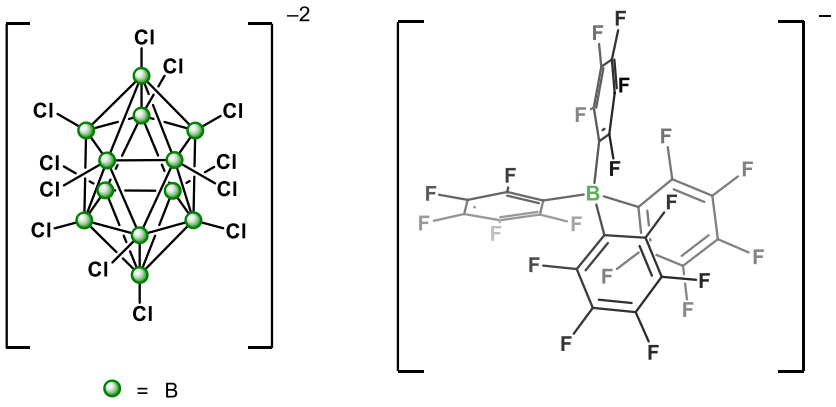

Figure 3: The perhalogenated *closo*-dodecaborate $[B_{12}Cl_{12}]^{2-}$ and the perfluorinated aryl borate $[B(C_6F_5)_4]^-$.

It is important to note that even when using fluorinated WCAs caution must be exercised. Compounds with $C(sp^3)$–F bonds, such as the fluorinated aryl borate $[B(Ar^F)_4]^-$ (Ar^F = (3,5-CF_3)C_6H_3), are unstable and decompose through fluoride abstraction by the highly Lewis acidic silylium ions, when the latter are not stabilized by Lewis bases.[18] In general, the perchlorinated *closo*-borates exhibit greater nucleophilicity towards silylium ions than the perfluorinated aryl borate $[B(C_6F_5)_4]^-$, binding through one of the chlorine atoms to the silicon cation.[19] However, the superior crystallization properties exhibited by *closo*-borates and *closo*-carborates, which are imparted to their salts, compensate for the negative aspect of slightly higher nucleophilicity. The superior crystallization properties of *closo*-

carboranes were effectively demonstrated through the solid-state characterization of the elusive SiH_3^+ cation by Oestreich and colleagues.[20] It is equally, if not more, crucial to select an appropriate solvent for the synthesis of silylium ions. Due to the extreme electrophilicity of silylium ions, all solvents except simple alkanes act as Lewis bases.[6b] However, the method of synthesis of silylium ions renders alkanes as unsuitable solvents, since they are unable to solubilize the reagents. A compromise between the Lewis basicity of the solvent and the solubility of the reagents was found in aromatic hydrocarbons, halogenated arenes, or even silanes.[6b,15b] The employed arenes either serve as π- or σ-donors, depending on the substituents, resulting in the formation of silylarenium ions,[21] silylated arylhalonium ions[22] or bissilylhydronium ions[22b,23] (Figure 4).

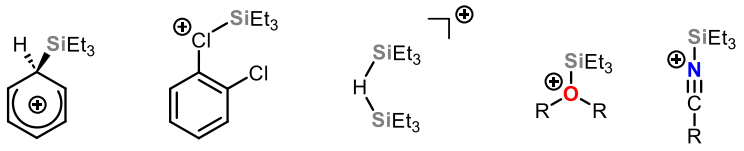

Figure 3: Different solvent adducts with the triethylsilylium ion.

In general, the fluorinated arenes are more reactive than the chlorinated arenes, due to the high fluorophilicity of the silylium cation.[24] It is unfortunate that aromatic hydrocarbons, halogenated arenes, or silanes are poor solvents for the salt-like nature of silylium ions. This often results in long reaction times and the formation of two phases, with the denser lower phase containing the silylium ion species. Such oily layers are often challenging to purify by recrystallization. The use of solvents with higher basicity, such as ethers and nitriles, results in the formation of silyloxonium ions[18] and silylnitrilium ions[25] (Figure 3), rendering them unsuitable for the handling of “free” silylium ion species. Halogenated alkanes, such as CH_2Cl_2, represent an ideal solvent for the chemistry of organic salts. Nevertheless, for the synthesis of non-stabilized silylium ions, CH_2Cl_2 can only be employed up to temperatures of –40°C. Extended exposure to temperatures above –40°C results in the formation of chlorosilanes and the decomposition of the solvent.[18,26] The early synthesis of silylium cations were conducted in accordance with established procedures, derived from the synthesis of carbocations. These procedures included the heterolytic cleavage of Si–X (X = Hal, OAlkyl) bonds. Nevertheless, while these techniques proved effective for the synthesis of carbocations, they were unsuccessful for the synthesis of silylium cations. One of the difficulties encountered was demonstrated by the attempt at synthesizing silylium cations by Olah and colleagues (Scheme 4).[27]

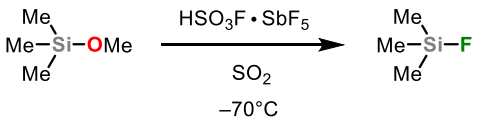

Scheme 4: Attempted synthesis of silylium cations by Olah and coworkers in 1969.[27]

The reaction of trimethyl(methoxy)silane with magic acid ($HSO_3F{\cdot}SbF_5$) in liquid sulfur dioxide demonstrated that the highly Lewis acidic environment indeed protonated the trimethyl(methoxy)silane, resulting in the formation of trimethyl(fluoro)silane. The trimethyl(fluoro)silane interacts with SbF_5, yet no silylium cation intermediate could be

observed (Scheme 4).[27] Despite the absence of evidence for the presence of silylium cations in this example, subsequent attempts for the synthesis of silylium cations via the cleavage of Si–X (X=Hal, OAlkyl) bonds have identified a bissilylated halonium intermediate (**1**) (Scheme 5).[28]

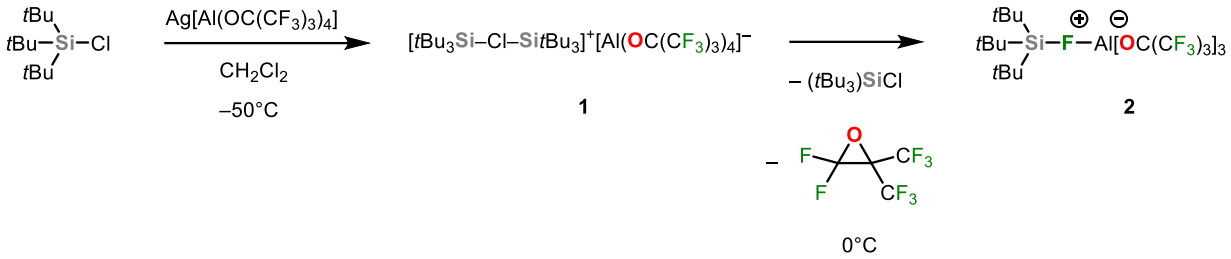

Scheme 5: Reactivity of the bissilylated halonium ion **1**.

The obtained bissilylated halonium ion **1** slowly decomposes above –50°C forming tri-*tert*-butylchlorosilane and the highly reactive tri-*tert*-butyl silylium cation, which immediately abstracts a fluorine atom from the aluminate counter-anion forming the zwitterionic silylium fluoroaluminate species **2** (Scheme 5). This demonstrates that halogen moieties, particularly fluorine atoms, should be avoided during the synthesis and handling of silylium ions. Nowadays the most successful method for synthesizing silylium ions is a specific version of the Bartlett-Condon-Schneider hydride transfer[29], referred to as the Corey reaction.[30] The reaction is initiated by the heterolytic cleavage of an Si–H bond by a strong electrophile, which is paired with a robust weakly coordinating anion. In the overwhelming majority of cases, the electrophile of choice is the triphenylmethylium cation [trityl, Ph_3C^+]. Upon reaction with silanes, the inert side product Ph_3CH is formed. This is possible due to the thermodynamic driving force involved in the Corey reaction. Due to the more electropositive nature of silicon (Pauling electronegativities: (Si) 1.9, (C) 2.6) compared to carbon, silyl cations are thermodynamically more stable than carbocations. Ab initio calculations indicate that $[H_3Si]^+$ is more stable than $[H_3C]^+$ by 225 kJ mol^{-1}. Both silylium ions and carbocations are stabilized by the same type of substituents, but silicon to a much lesser extent. For instance, $[Ph_3Si]^+$ is stabilized by 244 kJ mol^{-1} in comparison to $[H_3Si]^+$, whereas $[Ph_3C]^+$ is more stable than $[H_3C]^+$ by 454 kJ mol^{-1}.[31] This discrepancy can be attributed to the dissimilarities in the dimensions of the 2p orbitals of carbon and the 3p orbitals of silicon. In the case of silylium cations, this results in a less efficient overlap of orbitals, which in turn leads to less efficient hyperconjugative interactions and resonance effects between the central silylium cation and its carbon substituents. The trityl cation can be prepared with a variety of different weakly coordinating anions (WCAs). Examples include perfluorinated tetraarylborates,[32] perhalogenated *closo*-carborates,[33] perhalogenated *closo*-borates[34] and perfluorinated aluminates.[35] The selection of counter-anion has a crucial influence on the course of the Corey reaction when conducted in unpolar solvents (Scheme 6).

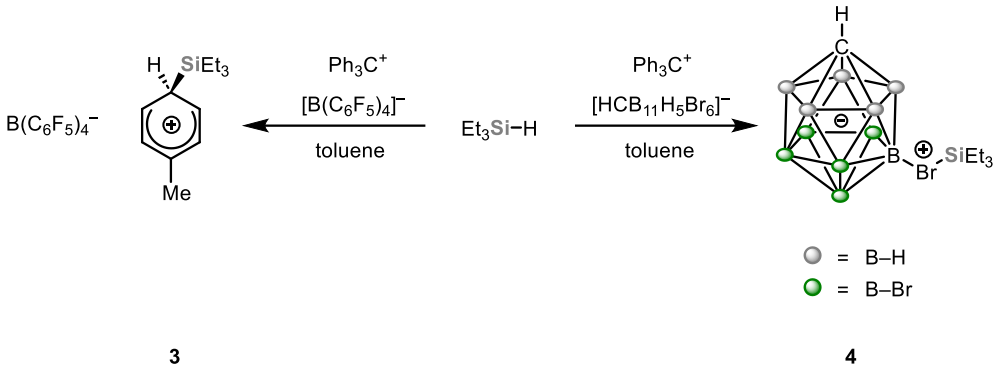

Scheme 6: Different outcomes of the Corey reaction with the triphenylmethylium cation, depending on the WCA used.

In unpolar solvents such as toluene, hydride abstraction from triethylsilane with tritylium tetrakis(pentafluorophenyl)borate leads to the formation of the solvent-stabilized silylated arenium ion **3**. The same reaction, when performed with the *closo*-carborate, yielded the anion-stabilized silylium ion **4**, owing to the fact that these anions are stronger donors than the solvent itself. When both reactions are performed in solvents with a higher polarity, such as halogenated arenes, ethers, or nitriles, the outcome of both reaction pathways is the same due to both reactions forming the corresponding silylonium ions.[6b] The reaction times are also highly dependent on the choice of counterions. While reactions of tritylium salts with perfluorinated arylborate counterions usually proceed within minutes at room temperature, reactions with tritylium salts of *closo*-carborates or *closo*-borates usually extend to a few hours or days of reaction time. In polar solvents, the reaction times of both *closo*-carborates and *closo*-borates are significantly shortened due to their higher solubility, while the reaction times of perfluorinated arylborates are not significantly affected.[22b,23] Another well-established synthesis pathway for silylium ions is the dehydrogenative protolysis by strong Brønsted acids.[20,36] The protonation of di-*tert*-butylsilane with Reeds benzenium ion $[H(C_6H_6)]$ $[HCB_{11}H_5Br_6]$ results in the evolution of dihydrogen and the formation of the corresponding silylium ion (Scheme 7).[20]

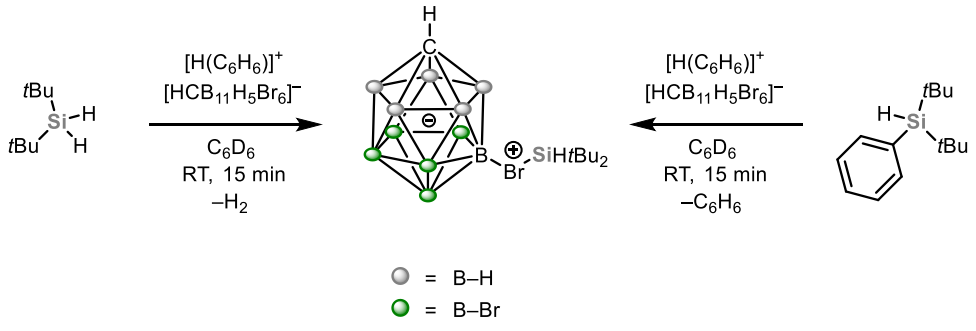

Scheme 7: Reaction of Reeds benzenium ion with different silanes.[20]

The chemoselectivity of this protonation remains incompletely understood, as evidenced by the observation that in the case of di-*tert*-butylphenylsilane, no dihydrogen is evolved, but rather protodesilylation of the phenyl group is observed (Scheme 7). This observation is analogous to previously investigated protodesilylations of silanes with trifluoroacetic

acid.[37] However, when Brookharts acid $(H(OEt_2)_2)[BAr^F{}_4]$ (Ar^F = 3,5-$(CF_3)_2C_6H_3$) is employed in the same reaction, which is typically not a suitable counterion for silylium cations due to C(sp^3)–F bond activation, the Si–H group of di-*tert*-butylphenylsilane is selectively cleaved over the phenyl moiety. A crucial aspect to be considered is the solvent present. Current research indicates that more polar solvents, such as Et_2O, tend to favor the dehydrogenative pathway, whereas unpolar solvents tend to lead to protodesilylation of the phenyl group. This protocol is not limited to Si–H or silylated arenes; it can also be extended to other Si–C(sp^2) bonds.[38]

1.2.3 Stabilized silylium ions

Silylium ions, which possess high electrophilicity, are almost always stabilized in some manner, even when seemingly non-Lewis basic moieties such as arenes or silanes are used as solvents. Consequently, the formation of truly free silylium ions is only possible when the highly electrophilic cationic silicon center is shielded from any interactions by bulky ligands (see Figure 2). However, the use of bulky ligands results in the inhibition or limitation of the catalytic activity of silylium cations.[16] Therefore, a finely tuned stabilization of silylium ions is necessary in order to allow their practical application in catalysis.[15b] The stabilization of silylium ions can be achieved in two ways: by adding a Lewis base to the already solvent-stabilized silylium ions or by preparation of the silylium ion in the presence of a stabilizing base either inter- or intramolecularly. Alternatively, the silylium ion can be stabilized by an anion. The stabilizing approach presents both advantages and disadvantages. One advantage is that less electrophilic reagents are required for the preparation of silylium ions. This is exemplified by the case of the preparation of stabilized silylium ions through heterolytic cleavage of Si–Cl bonds with the silver or sodium salts of weakly coordinating anions. This approach is only viable when strongly donating Lewis bases are present. Furthermore, solvents such as CH_2Cl_2 can be employed, which are typically incompatible with less stabilized silylium ions.[18,39] One disadvantage of this methodology is that it may result in a reduction of reaction speed, as the electrophiles employed, such as the tritylium cation, do compete with the hydride abstraction process, leading to the formation of a Lewis adduct (Scheme 8).

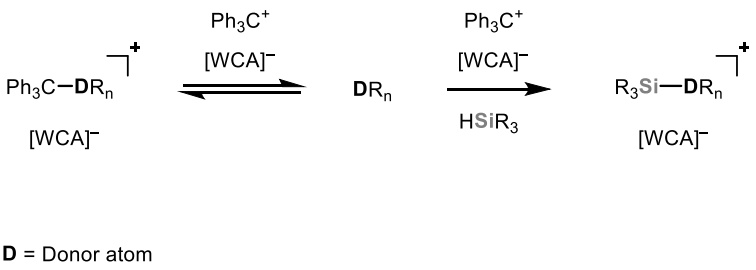

Scheme 8: Competing reactions in the formation of donor stabilized silylium ions.

Due to the large σ-donor influence by pnictogen- and chalcogen atoms one may ask the question whether these atoms should be classified as silylium ions or rather silylated onium ions. Although the σ-electron donation significantly lowers the Lewis acidity of the silylium cation, the positive charge remains largely on silicon due to its relatively low electronegativity.[40] The extent to which the silicon center loses its Lewis acidity is contingent upon the type of heteroatom selected and the steric environment surrounding

the Lewis acidic silylium cation and the donor Lewis base.[40] Consequently, a judicious choice of donor-types and steric hinderance enables the tailored tuning of the Lewis acidity of silylium ions for Lewis acid catalysis.[41] Silylonium ions have been identified as key intermediates in transformations mediated by silicon based Lewis acids, whereby the energy of the lowest unoccupied orbital of the Lewis basic substrate is lowered by Lewis adduct formation.[15b] A prominent class of reactions following this principle are silylium ion-promoted deoxygenation reactions (Scheme 9). In these reactions, carbonyl moieties are reduced to the corresponding alkyl groups using silanes. It is noteworthy that the reactivity of silylonium ion-based Lewis acids differs markedly from that of boron-based Lewis acids, which only reduce carbonyl moieties to the corresponding alcohols via a hydrosilylation mechanism. In an demonstrative example by Piers and colleagues, acetophenone was reduced to ethylbenzene in the presence of catalytic amounts of $[Ph_3C][B(C_6F_5)_4]$ (Scheme 9).[42] In conjunction with previous studies conducted by the group of Kira, which reported the deoxygenation of benzophenone in the presence of *in situ* prepared $[Ph_3C][B(3,5\text{-}(CF_3)C_6H_3)_4]$, a mechanism could be formulated (Scheme 9).[43]

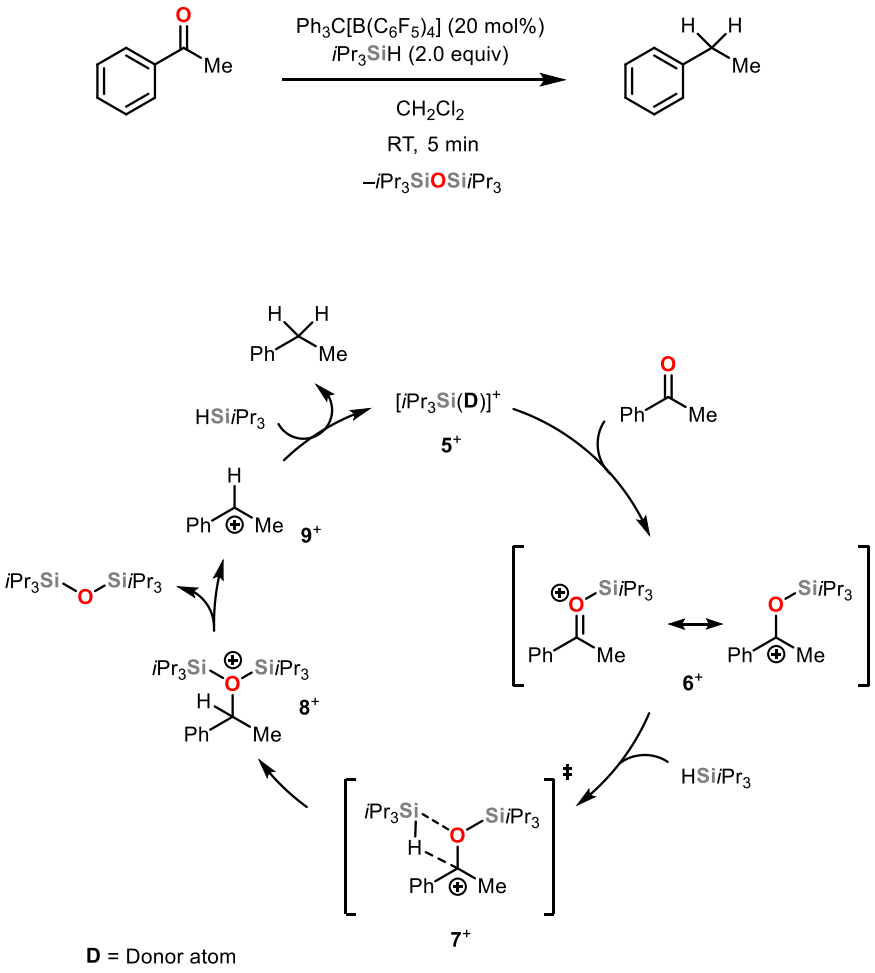

Scheme 9: Deoxygenation of acetophenone and the proposed catalytic cycle of deoxygenations mediated by silylonium ions.[42,43]

First, the silylium cation **5**$^+$, stabilized by a donor moiety, either solvent, hexa-*iso*-propyldisiloxane or tri-*iso*-propylsilane coordinates to the Lewis basic carbonyl function of acetophenone. This forms the Lewis adduct **6**$^+$, to which a tri-*iso*-propylsilane molecule

can transfer its hydride, possibly assisted by the oxygen atom (transition state **7**$^+$). The newly formed hexa-*iso*-propyldisiloxane in is a superb leaving group, therefore leaving the oxonium ion **8**$^+$ and forming the carbocation **9**$^+$. The newly formed carbenium ion **9**$^+$ is Lewis acidic enough to abstract a hydride from tri-*iso*-propylsilane, thereby regenerating the donor stabilized silylium ion **5**$^+$ and forming ethylbenzene in the process.[42] The groups of Müther and Oestreich demonstrated that this catalytic cycle can be modified to yield the intermediate alcohol by using silanes with an enhanced hydricity. This enables hydride transfer directly to the Lewis adduct **6**$^+$ without needing to proceed to the oxonium assisted transition state **7**$^+$.[44] The electrophilic activation of carbonyl groups induced by silylium ions can also be transferred to carbon monoxide moieties. In a notable example from 2018, it was demonstrated that the electrophilic formylation of arenes was feasible with silylium ions and carbon monoxide (Scheme 10). However, the quantum chemical calculations indicated that carbon monoxide is not the activated species in this case, but rather the silyl-arene cation. This is based on the observation that both the $[Et_3Si(CO)]^+$ and $[Et_3Si(OC)]^+$ cations are more stable than the arene-stabilized cation $[Et_3Si(C_6H_6)]^+$.[45]

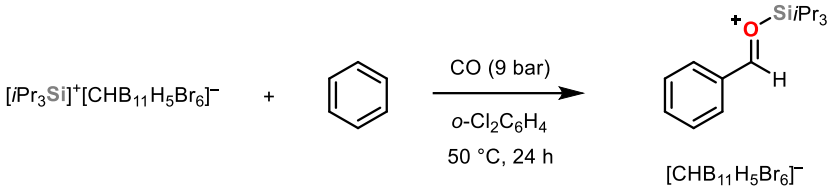

Scheme 10: Formylation of benzene mediated by the tri-*iso*-propylsilylium cation.[45]

This formylation reaction reflects nicely, that the reactivity of stabilized silylium ions is analogous to that of frustrated Lewis pairs (FLPs). In a certain sense, stabilized silylium ions can also be regarded as frustrated Lewis pairs, when both Lewis centers are shielded properly from each other.

1.3 Frustrated Lewis Pairs (FLPs)

Over the past few decades, organometallic chemistry has yielded a plethora of groundbreaking reactions, made possible by the meticulous selection of ligand systems and transition metals. Examples of such applications include hydrogenation catalysis,[46] chiral catalysts for asymmetric synthesis,[47] cross-coupling reactions for the formation of new C–C bonds[48] and metathesis catalysis.[49] All of these reactions make use of the bifunctional role of transition metals, which possess the capacity to accept electron density from a substrate molecule and donate electron density to the anti-bonding orbitals via back-bonding. This facilitates the lowering of the activation barrier of substrates, thereby rendering them more susceptible to chemical transformations. In main group chemistry, the ability to accept electron density, particularly among group 13 elements, has long been recognized and has been extensively employed in Lewis acid catalysis (for examples see section 1.2). Similarly, the ability to donate electron density into anti-orbitals has also been well-documented and utilized in the form of Lewis base catalysis.[50] However, combining both concepts into a bifunctional role usually results in the formation of a Lewis acid-base adduct, which negates the desired effects of both Lewis acid and base. In the mid-2000s,

a selection of seminal publications from the group of Douglas W. Stephan emerged, successfully combining both concepts, and paving the way for a chemistry which is known today as Frustrated Lewis Pairs (FLPs).[51] The fundamental concept is relatively straightforward: Lewis acids and bases are prevented from combining by geometrical and/or steric hindrance (Figure 4).

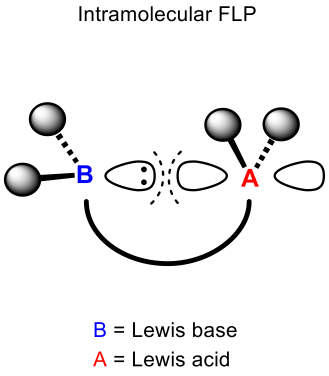

Figure 4: Representation of the concept of an intramolecular frustrated Lewis pair.

Nevertheless, it is important to recognize that the synthesis of FLPs is not straightforward. It should be noted that not all possible combinations are viable. It is necessary that either the Lewis acid or base be sufficiently Lewis acidic or basic, to generate an electric field between both moieties strong enough, to enable substrate activation.[52] The electric field generated by the Lewis acid and base is also highly dependent on the distance between both Lewis centers.[53] In the event that both Lewis centers are situated at an excessive distance from one another, no reaction will occur due to the electric field being insufficient or the orbital distance being excessively disparate. Conversely, if both Lewis centers are positioned in close proximity, Lewis acid/base adduct formation will occur, once more impeding reactivity.[51d] In the event that all of the aforementioned parameters are met, there remains the possibility that the substrates may be unable to reach the reaction center due to steric shielding preventing their approach.[54] Nevertheless countless successful examples were reported in the literature within the last two decades.[55] The most successful class of FLPs are undoubtedly boron/phosphorus Lewis pairs with numerous examples able to catalyze hydrogenation reactions (Figure 5).[51b,51d]

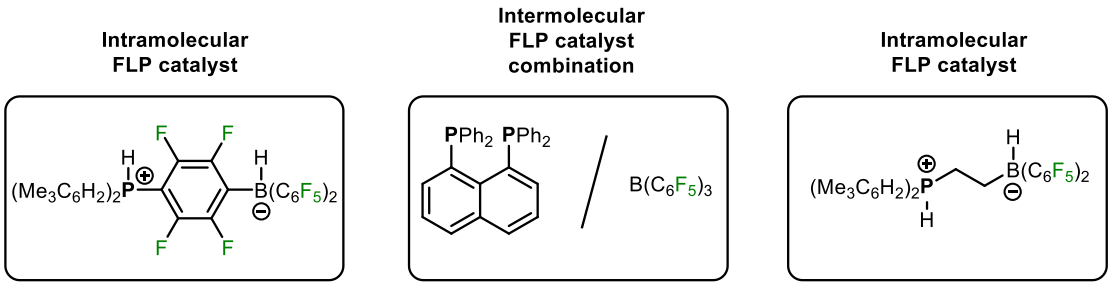

Figure 5: Examples of intra- and intermolecular P/B FLPs hydrogenation catalysts.

Although intermolecular FLPs are more readily synthesized than intramolecular FLPs, typically involving the simple mixing of a Lewis acid like $B(C_6F_5)_3$ with commercially

available bases, the effort expended in synthesis is worthwhile due to the markedly enhanced ability of intramolecular FLPs to activate and transfer dihydrogen.[54] The combination of group 13 and group 15 elements has attracted considerable attention in the field of FLP chemistry. This is in stark contrast to combinations with group 14 elements such as silicon. As previously mentioned in chapter 1.2.1, silylium cations are strong Lewis acids, isolobal to boranes, but with a higher electrophilicity due to the longer silicon-alkyl/aryl bonds shielding the silylium cation less efficiently. Consequently, they should be ideal candidates for the synthesis of new FLPs based on silicon, albeit more difficult to shield from Lewis bases. The higher Lewis acidity of the positively charged silylium ion compared to boranes should also enhance the reactivity spectrum of the FLPs, making the use of lower Lewis basic moieties possible.[56] Indeed, the Müller group demonstrated that the combination of the sterically encumbered silylium ion $[Si(C_6Me_5)_3]^+$ $[B(C_6F_5)_4]^-$ with the shielded phosphorus Lewis base $P(Mes)_3$ will irreversibly activate H_2 at room temperature (Scheme 12). However, the selection of the Lewis base was of paramount importance, as other employed Lewis bases, such as $P(C_6F_5)_3$, yielded an unidentifiable mixture of products.[57] The steric hindrance of silylium-based FLPs is also of particular significance, as it can not only result in the quenching of FLP reactivity but also in the occurrence of a protonation side reaction (Scheme 12). It is known that trialkyl silylium ions can form silylated arenium complexes, which act as Brønsted acids (Scheme 12).[58]

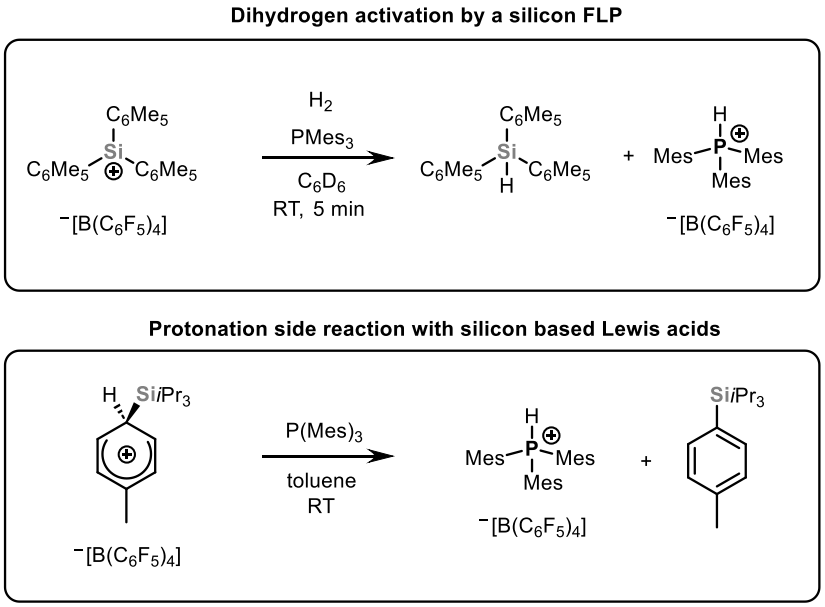

Scheme 12: Activation of H_2 by silicon Lewis acid based FLP and silylated arenium salts behaving as Brønsted acids. [58]

The Müller group circumvented this problem by employing highly sterically demanding aryl groups, which do not form solvent complexes due to their steric shielding (Scheme 12).[59] The limited current empirical evidence on the mechanism by which FLPs can heterolytically cleave dihydrogen provides only an incomplete picture.[60] However, two main mechanisms have been discussed in the literature based on theoretical and computational methods (Figure 6).[61] Pápai and colleagues initially proposed a model wherein the electron density is transferred from the lone electron pair of the Lewis base into the antibonding σ*-orbital of dihydrogen and simultaneously from the bonding σ-orbital of dihydrogen into the empty p-orbital of the Lewis acid. These synergistic electron transfers result in a weakening of the bond to the point of heterolytic cleavage (Figure

6a).[62] Subsequent research conducted by Grimme and colleagues demonstrated the presence of a substantial electrical field within the encounter complex of frustrated Lewis pairs. The computational methods employed demonstrated that a sufficiently strong electrical field can split dihydrogen heterolytically, which led to the formulation of the electric field theory (Figure 6b).[63] This mechanism can allow for a heterolytic pathway, as well as a homolytic cleavage pathway, which has also been observed empirically in frustrated Lewis pairs.[64] Further research utilizing the Localized Molecular Orbital Energy Decomposition Analysis (LMOEDA) with the classical FLP model NH_3–BCl_3 has demonstrated that electrical fields do play a significant role in the initial polarization of the H_2 molecule. However, their overall contribution in comparison to orbital interactions is relatively minor, suggesting that the electrical fields generated by FLPs are not sufficiently strong enough to split dihydrogen on their own.[60c,65] In conclusion, the current state of knowledge is a combination of both the electric field model and the electron transfer model, with the electric field model being dominant in the initial polarization of the H_2 molecule allowing for the subsequent splitting of the H–H bond via the mechanism of the electron transfer model.[65]

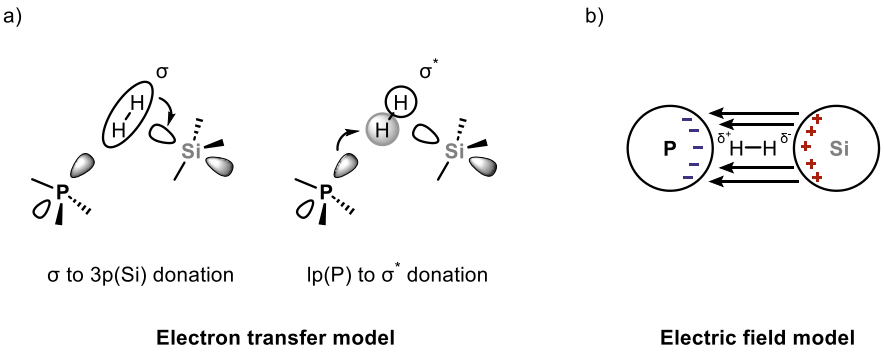

Figure 6: The two discussed models by which FLPs can activate and split dihydrogen.

The activation of the dihydrogen molecule is a challenging process due to the low polarizability of the H–H bond. In contrast, small unpolar molecules like CO_2 are more readily fixated, particularly when considering the high oxophilicity of silicon. Nevertheless, even in this case, certain challenges do arise, as Müller and colleagues have demonstrated (Scheme 13).[59]

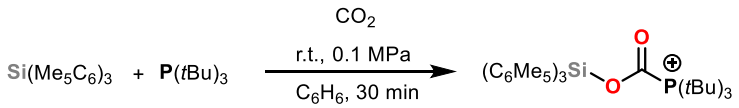

Scheme 13: Fixation of CO_2 by a Si/P FLP (Counterion $B(C_6F_5)_4^-$ omitted for clarity).

The same silylium ion $[Si(C_6Me_5)_3]^+$ $[B(C_6F_5)_4]^-$ which was employed for dihydrogen activation in Scheme 12 with the same solvent and reaction conditions, was employed for CO_2 fixation aswell. However, in this case triarylphosphanes showed no reaction towards CO_2. The use of trialkylphosphanes resulted in the fixation of CO_2. These findings demonstrate that subtle alterations in steric and electronic properties can profoundly

influence the reactivity of FLPs. Consequently, further investigation into this topic is essential.

1.3.1 Intramolecular FLPs

As previously mentioned, Frustrated Lewis pairs consist of a Lewis base and acid, which are sterically or geometrically restrained from combining into a Lewis acid/base adduct. If both Lewis centers are contained within one molecule these species are called intramolecular frustrated Lewis pairs. Compared to intermolecular FLPs these species are generally more reactive, since intramolecular reactions are always faster than intermolecular reactions.[54] This makes the intramolecular FLPs the species of choice for catalytic applications such as hydrogenations (see Figure 5).[51b,51d] Steric factors play an important role in the design and the reactivity of FLPs (see section 1.3), however when intramolecular FLPs are considered another steric factor needs to be taken into consideration, which is the ring strain. Consequently, the strength of interaction of a Lewis acid with its Lewis basic counterpart within an intramolecular FLP is also dependent upon the ring size. In 2015 Müller *et al.* has published a study of the interaction of silylium cations with pnictogen Lewis bases (Scheme 14).[66] In this study of Müller the cyclization reactions towards differently sized silylated phosphonium ions were studied. It was found, that the cyclization reaction only yielded the desired phosphonium ion ring systems when five-or higher membered rings were obtained (Scheme 14). For lower-membered ring systems a Lewis acid/base reaction between the Lewis basic phosphine moiety and the Lewis acidic tritylium cation $[Ph_3C]^+$ was observed (Scheme 14).[66]

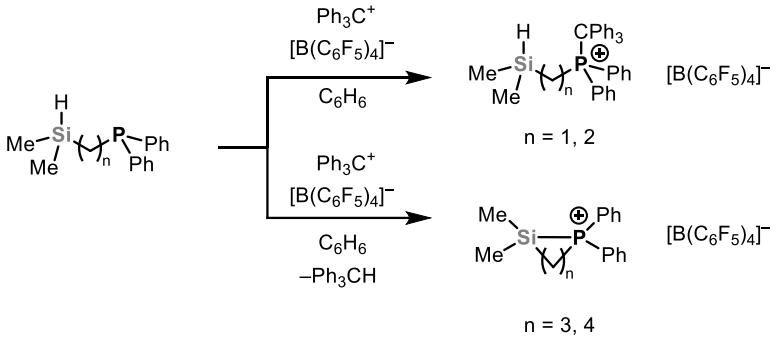

Scheme 14: Cyclization reaction of silylated phosphonium ions of different ring sizes.

The root cause of this discrepancy in reactivity was found to be the thermodynamic preference of the Lewis acid/base reaction, over the hydride abstraction, when three-or four-membered cyclic phosphonium ions would be the products.[66] While smaller, four-membered ring systems, are known for donors like nitrogen,[67] no four-membered ring systems, utilizing phosphine chalcogenides as donors for stabilizing silylium ions, are known. The smallest ring size synthesized, with $Ph_3C[B(C_6F_5)]_4$ as an hydride abstracting reagent, were just five-membered cycles.[68] In 2021 our group circumvented this problem by employing $B(C_6F_5)_3$ as an hydride abstracting reagent, finally making access to the four-membered phosphonium ions possible (Scheme 15).[69]

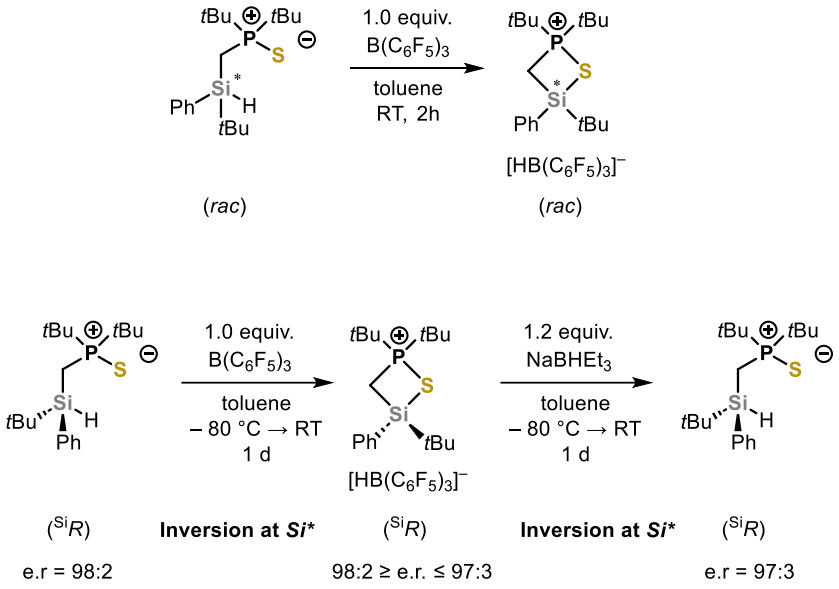

Scheme 15: Synthesis of four-membered heterocyclic silyl phosphonium sulfide cations.

Furthermore, light could be shed onto the mechanism by which tris(pentafluorophenyl)borane abstracts the hydride from silicon to form the four-membered ring systems. This was achieved by employing an enantiopure silicon center as a stereochemical probe.[69] It was found that the hydride abstracting proceeds via an backside attack from the P^+–S^- donor moiety onto the silicon center. While the mechanism was elucidated, little is known about the steric effects making this cyclization to four-membered phosphonium ions even possible. In the aforementioned example by Müller it is obvious that ring strain plays a significant role in the cyclization of these systems,[66] however the steric and electronic effects governing these reactions are still unknown.

1.4 References

(1) Lewis, G. N., *Valence and the Structure of Atoms and Molecules*, Dover Publications Inc., New York, **1923**.

(2) (a) Laurence, C.; Graton, J.; Gal, J.-F. An Overview of Lewis Basicity and Affinity Scales. *J. Chem. Educ.* **2011**, *88*, 1651–1657. (b) John Wiley: Chichester (Ed.) Lewis basicity and Affinity Scales: Data and Measurement, West Sussex, **2010**. (c) Liantonio, R.; Luzzati, S.; Metrangolo, P.; Pilati, T.; Resnati, G. Perfluorocarbon–hydrocarbon self-assembly. Part 16: Anilines as new electron donor modules for halogen bonded infinite chain formation. *Tetrahedron* **2002**, *58*, 4023–4029. (d) R. W., A. Strain effects on amine basicities. *Chem. Rev.* **1989**, *89*, 1215–1223.

(3) Pearson, R. G. Hard and Soft Acids and Bases. *J. Am. Chem. Soc.* **1963**, *85*, 3533–3539.

(4) (a) Chatterjee, I.; Oestreich, M. $B(C_6F_5)_3$-catalyzed transfer hydrogenation of imines and related heteroarenes using cyclohexa-1,4-dienes as a dihydrogen source. *Angew. Chem. Int. Ed.* **2015**, *54*, 1965–1968. (b) Erker, G. Tris(pentafluorophenyl)borane: a special boron Lewis acid for special reactions. *Dalton Trans.* **2005**, 1883–1890. (c) Hackel, T.; McGrath, N. A. Tris(pentafluorophenyl)borane-Catalyzed Reactions Using Silanes. *Molecules* **2019**, *24*. (d) Kumar, G.; Roy, S.; Chatterjee, I. Tris(pentafluorophenyl)borane catalyzed C-C and C-heteroatom bond formation. *Org. Biomol. Chem.* **2021**, *19*, 1230–1267. (e) Parks, D. J.; H. Spence, R. E. von; Piers, W. E. Bis(pentafluorophenyl)borane: Synthesis, properties, and hydroboration chemistry of a highly electrophilic borane reagent. *Angew. Chem. Int. Ed.* **1995**, *34*, 809–811. (f) Patrick, E. A.; Piers, W. E. Twenty-five years of bis-pentafluorophenyl borane: A versatile reagent for catalyst and materials synthesis. *Chem. Commun.* **2020**, *56*, 841–853. (g) Yin, Q.; Soltani, Y.; Melen, R. L.; Oestreich, M. $BAr^F{}_3$ -Catalyzed Imine Hydroboration with pinacolborane not requiring the assistance of an additional lewis base. *Organometallics* **2017**, *36*, 2381–2384.

(5) P. L. Holland, G. Parkin, K. Meyer, D. O'Hare, E. Boros, L. J. Daumann (Eds.) Comprehensive organometallic chemistry IV, Elsevier, Amsterdam, **2023**.

(6) (a) Fritz-Langhals, E. Silicon(II) Cation Cp^*Si^+ X^- : A New Class of Efficient Catalysts in Organosilicon Chemistry. *Org. Process Res. Dev.* **2019**, *23*, 2369–2377. (b) Klare, H. F. T.; Albers, L.; Süsse, L.; Keess, S.; Müller, T.; Oestreich, M. Silylium Ions: From Elusive Reactive Intermediates to Potent Catalysts. *Chem. Rev.* **2021**, *121*, 5889–5985. (c) Walker, J. C. L.; Klare, H. F. T.; Oestreich, M. Cationic silicon lewis acids in catalysis. *Nat. Rev. Chem.* **2020**, *4*, 54–62.

(7) (a) Lambert, J. B.; Zhao, Y. A Stable β-Silyl Carbocation. *J. Am. Chem. Soc.* **1996**, *118*, 7867–7868. (b) Denmark, S. E.; Beutner, G. L.; Wynn, T.; Eastgate, M. D. Lewis base activation of Lewis acids: catalytic, enantioselective addition of silyl ketene acetals to aldehydes. *J. Am. Chem. Soc.* **2005**, *127*, 3774–3789.

(8) Holleman, A. F.; Wiberg, N., *Anorganische Chemie*, De Gruyter, Berlin, Boston, **2017**.

(9) Sergio, R.; M., B.; A., G. Organic reactions mediated by tetrachlorosilane. *Tetrahedron* **2014**, *70*, 2065–2080.

(10) (a) Hartmann, D.; Schädler, M.; Greb, L. Bis(catecholato)silanes: assessing, rationalizing and increasing silicon's Lewis superacidity. *Chem. Sci.* **2019**, *10*, 7379–7388. (b) Maskey, R.; Schädler, M.; Legler, C.; Greb, L. Bis(perchlorocatecholato)silane-A Neutral Silicon Lewis Super Acid. *Angew. Chem. Int. Ed.* **2018**, *57*, 1717–1720. (c) Tschernuth, F. S.; Thorwart, T.;

Greb, L.; Hanusch, F.; Inoue, S. Bis(perfluoropinacolato)silane: A Neutral Silane Lewis Superacid Activates Si-F Bonds. *Angew. Chem. Int. Ed.* **2021**, *60*, 25799–25803. (d) Hermannsdorfer, A.; Driess, M. Silicon Tetrakis(trifluoromethanesulfonate): A Simple Neutral Silane Acting as a Soft and Hard Lewis Superacid. *Angew. Chem. Int. Ed.* **2021**, *60*, 13656–13660.

(11) (a) Thorwart, T.; Hartmann, D.; Greb, L. Dihydrogen Activation with a Neutral, Intermolecular Silicon(IV)-amine Frustrated Lewis Pair. *Chem. Eur. J.* **2022**, *28*, e202202273. (b) Thorwart, T.; Greb, L. Reversible C–H bond silylation with a neutral silicon Lewis acid. *Chem. Sci.* **2023**, *14*, 11237–11242. (c) Ansmann, N.; Thorwart, T.; Greb, L. Silicon Catalyzed C-O Bond Ring Closing Metathesis of Polyethers. *Angew. Chem. Int. Ed.* **2022**, *61*, e202210132.

(12) Liberman-Martin, A. L.; Bergman, R. G.; Tilley, T. D. Lewis Acidity of Bis(perfluorocatecholato)silane: Aldehyde Hydrosilylation Catalyzed by a Neutral Silicon Compound. *J. Am. Chem. Soc.* **2015**, *137*, 5328–5331.

(13) (a) Rubin, M.; Schwier, T.; Gevorgyan, V. Highly efficient $B(C_6F_5)_3$-catalyzed hydrosilylation of olefins. *J. Org. Chem.* **2002**, *67*, 1936–1940. (b) Blackwell, J. M.; Piers, W. E.; McDonald, R. Mechanistic studies on the $B(C_6F_5)_3$ catalyzed allylstannation of aromatic aldehydes with ortho donor substituents. *J. Am. Chem. Soc.* **2002**, *124*, 1295–1306.

(14) (a) Eaborn, C. A contribution to the silicenium ion debate. *J. Organomet. Chem.* **1991**, *405*, 173–177. (b) Lickiss, P. D. Do R_3Si^+ ions exist in solution? *Dalton Trans.* **1992**, 1333. (c) Ragué Schleyer, P. von; Buzek, P.; Müller, T.; Apeloig, Y.; Siehl, H.-U. The Search for an Isolable Silyl Cation Must Continue. *Angew. Chem. Int. Ed.* **1993**, *32*, 1471–1473. (d) Corriu, R.J.P.; Henner, M. The siliconium ion question. *J. Organomet. Chem.* **1974**, *74*, 1–28.

(15) (a) Klare, H. F. T. Catalytic C–H Arylation of Unactivated C–H Bonds by Silylium Ion-Promoted $C(sp^2)$–F Bond Activation. *ACS Catal.* **2017**, *7*, 6999–7002. (b) Klare, H. F. T.; Oestreich, M. Silylium ions in catalysis. *Dalton Trans.* **2010**, *39*, 9176–9184. (c) Schulz, A.; Villinger, A. “Tamed” silylium ions: Versatile in catalysis. *Angew. Chem. Int. Ed.* **2012**, *51*, 4526–4528.

(16) Lambert, J. B.; Zhao, Y. The Trimesitylsilylium Cation. *Angew. Chem. Int. Ed.* **1997**, *36*, 400–401.

(17) (a) Engesser, T. A.; Lichtenthaler, M. R.; Schleep, M.; Krossing, I. Reactive p-block cations stabilized by weakly coordinating anions. *Chem. Soc. Rev.* **2016**, *45*, 789–899. (b) Krossing, I.; Raabe, I. Noncoordinating anions—fact or fiction? A survey of likely candidates. *Angew. Chem. Int. Ed.* **2004**, *43*, 2066–2090. (c) Riddlestone, I. M.; Kraft, A.; Schaefer, J.; Krossing, I. Taming the Cationic Beast: Novel Developments in the Synthesis and Application of Weakly Coordinating Anions. *Angew. Chem. Int. Ed.* **2018**, *57*, 13982–14024.

(18) Kira, M.; Hino, T.; Sakurai, H. Chemistry of organosilicon compounds. 292. An NMR study of the formation of silyloxonium ions by using tetrakis[3,5-*bis*(trifluoromethyl)phenyl]borate as counteranion. *J. Am. Chem. Soc.* **1992**, *114*, 6697–6700.

(19) (a) Kessler, M.; Knapp, C.; Sagawe, V.; Scherer, H.; Uzun, R. Synthesis, characterization, and crystal structures of silylium compounds of the weakly coordinating dianion $B_{12}Cl_{12}^{2-}$. *Inorg. Chem.* **2010**, *49*, 5223–5230. (b) Reed, C. A.; Xie, Z.; Bau, R.; Benesi, A. Closely Approaching the Silylium Ion (R_3Si^+). *Science* **1993**, *262*, 402–404. (c) Xie, Z.; Liston, D. J.; Jelínek, T.; Mitro, V.; Bau, R.; Reed, C. A. A new weakly coordinating anion: Approaching the silylium (silicenium) ion. *Chem. Commun.* **1993**, 384–386.

(20) Wu, Q.; Irran, E.; Müller, R.; Kaupp, M.; Klare, H. F. T.; Oestreich, M. Characterization of hydrogen-substituted silylium ions in the condensed phase. *Science* **2019**, *365*, 168–172.

(21) (a) Lambert, J. B.; Zhang, S.; Stern, C. L.; Huffman, J. C. Crystal structure of a silyl cation with no coordination to anion and distant coordination to solvent. *Science* **1993**, *260*, 1917–1918. (b) Lambert, J. B.; Zhang, S. Tetrakis(pentafluorophenyl)borate: a new anion for silylium cations in the condensed phase. *Chem. Commun.* **1993**, 383. (c) Lambert, J. B.; Zhang, S.; Ciro, S. M. Silyl Cations in the Solid and in Solution. *Organometallics* **1994**, *13*, 2430–2443. (d) Ibad, M. F.; Langer, P.; Schulz, A.; Villinger, A. Silylium-arene adducts: an experimental and theoretical study. *J. Am. Chem. Soc.* **2011**, *133*, 21016–21027.

(22) (a) Schäfer, A.; Saak, W.; Haase, D.; Müller, T. Silyl cation mediated conversion of CO_2 into benzoic acid, formic acid, and methanol. *Angew. Chem. Int. Ed.* **2012**, *51*, 2981–2984. (b) Hoffmann, S. P.; Kato, T.; Tham, F. S.; Reed, C. A. Novel weak coordination to silylium ions: formation of nearly linear Si–H–Si bonds. *Chem. Commun.* **2006**, 767–769.

(23) (a) Nava, M.; Reed, C. A. Triethylsilyl Perfluoro-Tetraphenylborate, $Et_3Si\ F_{20}$-BPh_4, a widely used Non-Existent Compound. *Organometallics* **2011**, *30*, 4798–4800. (b) Connelly, S. J.; Kaminsky, W.; Heinekey, D. M. Structure and Solution Reactivity of (Triethylsilylium)triethylsilane Cations. *Organometallics* **2013**, *32*, 7478–7481.

(24) Duttwyler, S.; Douvris, C.; Fackler, N. L. P.; Tham, F. S.; Reed, C. A.; Baldridge, K. K.; Siegel, J. S. C-F activation of fluorobenzene by silylium carboranes: evidence for incipient phenyl cation reactivity. *Angew. Chem. Int. Ed.* **2010**, *49*, 7519–7522.

(25) Bahr, S. R.; Boudjouk, P. Stable silylnitrilium ions. *J. Am. Chem. Soc.* **1993**, *115*, 4514–4519.

(26) (a) Klare, H. F. T.; Bergander, K.; Oestreich, M. Taming the silylium ion for low-temperature Diels-Alder reactions. *Angew. Chem. Int. Ed.* **2009**, *48*, 9077–9079. (b) Nishinaga, T.; Izukawa, Y.; Komatsu, K. The first cyclic π-conjugated silylium ion: The silatropylium ion annelated with rigid σ-frameworks. *J. Am. Chem. Soc.* **2000**, *122*, 9312–9313. (c) Nishinaga, T.; Izukawa, Y.; Komatsu, K. The first silatropylium ion stabilized by rigid σ-frameworks: Preparation, properties, and some reactions. *Tetrahedron* **2001**, *57*, 3645–3656.

(27) Olah, G. A.; O'Brien, D. H.; Lui, C. Y. Stable carbonium ions. LXXIV. Protonated alkoxysilanes and disiloxanes and their cleavage in fluorosulfuric acid-antimony pentafluoide solution. *J. Am. Chem. Soc.* **1969**, *91*, 701–706.

(28) Budanow, A.; Bolte, M.; Wagner, M.; Lerner, H.-W. The ion-like supersilylium compound $t$$Bu_3Si$–F–$Al[OC(CF_3)_3]_3$. *Eur. J. Inorg. Chem.* **2015**, *2015*, 2524–2527.

(29) Bartlett, P. D.; Condon, F. E.; Schneider, A. Exchanges of Halogen and Hydrogen between Organic Halides and Isoparaffins in the Presence of Aluminum Halides. *J. Am. Chem. Soc.* **1944**, *66*, 1531–1539.

(30) (a) Y. Corey, J.; Gust, D.; Mislow, K. Generation of a ferrocenylsilicenium ion. *J. Organomet. Chem.* **1975**, *101*, C7-C8. (b) Corey, J. Y. Generation of a silicenium ion in solution. *J. Am. Chem. Soc.* **1975**, *97*, 3237–3238. (c) Corey, J. Y.; West, R. Hydrogen-Halogen Exchange between Silanes and Triphenylmethyl Halides. *J. Am. Chem. Soc.* **1963**, *85*, 2430–2433. (d) Bickart, P.; Llort, F. M.; Mislow, K. On the evidence for the generation of a ferrocenylsilicenium ion. *J. Organomet. Chem.* **1976**, *116*, C1-C2.

(31) (a) *Advances in Organometallic Chemistry*, *Vol. 53*, Academic Press, Amsterdam, **2005**. (b) Müller, T. in *Advances in Organometallic Chemistry*, *Vol. 53*, Academic Press, Amsterdam, **2005**, pp. 155–215.

(32) (a) Jia, L.; Yang, X.; Stern, C. L.; Marks, T. J. Cationic Metallocene Polymerization Catalysts Based on Tetrakis(pentafluorophenyl)borate and Its Derivatives. Probing the Limits of Anion "Noncoordination" via a Synthetic, Solution Dynamic, Structural, and Catalytic Olefin Polymerization Study. *Organometallics* **1997**, *16*, 842–857. (b) Chien, J. C. W.; Tsai, W. M.; Rausch, M. D. Isospecific polymerization of propylene catalyzed by *rac*-ethylenebis(indenyl)methylzirconium cation. *J. Am. Chem. Soc.* **1991**, *113*, 8570–8571.

(33) (a) Reed, C. A. H^+, CH_3^+, and R_3Si^+ carborane reagents: When triflates fail. *Acc. Chem. Res.* **2010**, *43*, 121–128. (b) Xie, Z.; Jelinek, T.; Bau, R.; Reed, C. A. New Weakly Coordinating Anions. III. Useful Silver and Trityl Salt Reagents of Carborane Anions. *J. Am. Chem. Soc.* **1994**, *116*, 1907–1913. (c) Hepp, A.; Labbow, R.; Reiß, F.; Schulz, A.; Villinger, A. Carba-*closo*-dodecaborates – Synthesis, Structure, and Energetics. *Eur. J. Inorg. Chem.* **2018**, *2018*, 2905–2914.

(34) (a) Avelar, A.; Tham, F. S.; Reed, C. A. Superacidity of boron acids $H_2(B_{12}X_{12})$ (X = Cl, Br). *Angew. Chem. Int. Ed.* **2009**, *48*, 3491–3493. (b) Geis, V.; Guttsche, K.; Knapp, C.; Scherer, H.; Uzun, R. Synthesis and characterization of synthetically useful salts of the weakly-coordinating dianion $B_{12}Cl_{12}^{2-}$. *Dalton Trans.* **2009**, 2687–2694. (c) Ivanov, S. V.; Miller, S. M.; Anderson, O. P.; Solntsev, K. A.; Strauss, S. H. Synthesis and stability of reactive salts of dodecafluoro-*closo*-dodecaborate(2-). *J. Am. Chem. Soc.* **2003**, *125*, 4694–4695.

(35) Krossing, I.; Brands, H.; Feuerhake, R.; Koenig, S. New reagents to introduce weakly coordinating anions of type $Al(OR^F)_4^-$: Synthesis, structure and characterization of Cs and trityl salts. *J. Fluor. Chem.* **2001**, *112*, 83–90.

(36) Chen, Q.-A.; Klare, H. F. T.; Oestreich, M. Brønsted Acid-Promoted Formation of Stabilized Silylium Ions for Catalytic Friedel-Crafts C–H Silylation. *J. Am. Chem. Soc.* **2016**, *138*, 7868–7871.

(37) Uhlig, W. Silyl Triflates – Valuable Synthetic Materials in Organosilicon Chemistry. *Chem. Ber.* **1996**, *129*, 733–739.

(38) Wu, Q.; Qu, Z.-W.; Omann, L.; Irran, E.; Klare, H. F. T.; Oestreich, M. Cleavage of Unactivated Si–C(sp^3) bonds with Reed's Carborane Acids: Formation of Known and Unknown Silylium Ions. *Angew. Chem. Int. Ed.* **2018**, *57*, 9176–9179.

(39) Yanagisawa, M.; Shimamura, T.; Iida, D.; Matsuo, J. I.; Mukaiyama, T. Aldol reaction of enol esters catalyzed by cationic species paired with tetrakis(pentafluorophenyl)borate. *Chem. Pharm. Bull.* **2000**, *48*, 1838–1840.

(40) Künzler, S.; Rathjen, S.; Merk, A.; Schmidtmann, M.; Müller, T. An Experimental Acidity Scale for Intramolecularly Stabilized Silyl Lewis Acids. *Chem. Eur. J.* **2019**, *25*, 15123–15130.

(41) Rohde, V. H. G.; Pommerening, P.; Klare, H. F. T.; Oestreich, M. Intramolecularly Sulfur-Stabilized Silicon Cations as Lewis Acid Catalysts. *Organometallics* **2014**, *33*, 3618–3628.

(42) Parks, D. J.; Blackwell, J. M.; Piers, W. E. Studies on the mechanism of $B(C_6F_5)_3$-catalyzed hydrosilation of carbonyl functions. *J. Org. Chem.* **2000**, *65*, 3090–3098.

(43) Kira, M.; Hino, T.; Sakurai, H. Siloxycarbenium Tetrakis[3,5-bis(trifluoromethyl)phenyl]borates and their role in reactions of Ketones with Nucleophiles. *Chemistry Letters* **1992**, *21*, 555–558.

(44) Müther, K.; Oestreich, M. Self-regeneration of a silylium ion catalyst in carbonyl reduction. *Chem. Commun.* **2011**, *47*, 334–336.

(45) Omann, L.; Qu, Z.-W.; Irran, E.; Klare, H. F. T.; Grimme, S.; Oestreich, M. Electrophilic Formylation of Arenes by Silylium Ion Mediated Activation of Carbon Monoxide. *Angew. Chem. Int. Ed.* **2018**, *57*, 8301–8305.

(46) (a) Evans, D.; Osborn, J. A.; Jardine, F. H.; Wilkinson, G. Homogeneous Hydrogenation and Hydroformylation using Ruthenium Complexes. *Nature* **1965**, *208*, 1203–1204. (b) Young, J. F.; Osborn, J. A.; Jardine, F. H.; Wilkinson, G. Hydride intermediates in homogeneous hydrogenation reactions of olefins and acetylenes using rhodium catalysts. *Chem. Commun.* **1965**, 131.

(47) (a) Noyori, R. Asymmetric Catalysis: Science and Opportunities. *Angew. Chem. Int. Ed.* **2002**, *41*, 2008. (b) Knowles, W. S. Asymmetric Hydrogenations (Nobel Lecture). *Angew. Chem. Int. Ed.* **2002**, *41*, 1998.

(48) T. Colacot (Ed.) *RSC catalysis series*, *Vol. 21*, Royal Society of Chemistry, Cambridge, **2015**.

(49) (a) Schrock, R. R. Multiple metal-carbon bonds for catalytic metathesis reactions. *Angew. Chem. Int. Ed.* **2006**, *45*, 3748–3759. (b) Grubbs, R. H. Olefin-metathesis catalysts for the preparation of molecules and materials. *Angew. Chem. Int. Ed.* **2006**, *45*, 3760–3765.

(50) Denmark, S. E.; Beutner, G. L. Lewis base catalysis in organic synthesis. *Angew. Chem. Int. Ed.* **2008**, *47*, 1560–1638.

(51) (a) Welch, G. C.; Stephan, D. W. Facile heterolytic cleavage of dihydrogen by phosphines and boranes. *J. Am. Chem. Soc.* **2007**, *129*, 1880–1881. (b) Spies, P.; Erker, G.; Kehr, G.; Bergander, K.; Fröhlich, R.; Grimme, S.; Stephan, D. W. Rapid intramolecular heterolytic dihydrogen activation by a four-membered heterocyclic phosphane-borane adduct. *Chem. Commun.* **2007**, 5072–5074. (c) McCahill, J. S. J.; Welch, G. C.; Stephan, D. W. Reactivity of “frustrated Lewis pairs”: three-component reactions of phosphines, a borane, and olefins. *Angew. Chem. Int. Ed.* **2007**, *46*, 4968–4971. (d) Welch, G. C.; San Juan, R. R.; Masuda, J. D.; Stephan, D. W. Reversible, metal-free hydrogen activation. *Science* **2006**, *314*, 1124–1126.

(52) Stephan, D. W. “Frustrated Lewis pairs”: A concept for new reactivity and catalysis. *Org. Biomol. Chem.* **2008**, *6*, 1535–1539.

(53) Stephan, D. W. The broadening reach of frustrated Lewis pair chemistry. *Science* **2016**, *354*.

(54) Stephan, D. W.; Erker, G. Frustrated Lewis pair chemistry: Development and perspectives. *Angew. Chem. Int. Ed.* **2015**, *54*, 6400–6441.

(55) Stephan, D. W. Frustrated Lewis Pairs. *J. Am. Chem. Soc.* **2015**, *137*, 10018–10032.

(56) Rokob, T. A.; Hamza, A.; Pápai, I. Rationalizing the reactivity of frustrated Lewis pairs: Thermodynamics of H_2 activation and the role of acid-base properties. *J. Am. Chem. Soc.* **2009**, *131*, 10701–10710.

(57) Schäfer, A.; Reissmann, M.; Schäfer, A.; Saak, W.; Haase, D.; Müller, T. A new synthesis of triarylsilylium ions and their application in dihydrogen activation. *Angew. Chem. Int. Ed.* **2011**, *50*, 12636–12638.

(58) Driess, M.; Monsé, C.; Merz, K.; van Wüllen, C. Perstannylated Ammonium and Phosphonium Ions: Organometallic Onium Ions That Are also Base-Stabilized Stannylium Ions. *Angew. Chem. Int. Ed.* **2000**, *39*, 3684–3686.

(59) Reißmann, M.; Schäfer, A.; Jung, S.; Müller, T. Silylium Ion/Phosphane Lewis Pairs. *Organometallics* **2013**, *32*, 6736–6744.

(60) (a) Sumerin, V.; Schulz, F.; Nieger, M.; Atsumi, M.; Wang, C.; Leskelä, M.; Pyykkö, P.; Repo, T.; Rieger, B. Experimental and theoretical treatment of hydrogen splitting and storage in boron–nitrogen systems. *J. Organomet. Chem.* **2009**, *694*, 2654–2660. (b) Sumerin, V.; Schulz, F.; Nieger, M.; Leskelä, M.; Repo, T.; Rieger, B. Facile heterolytic H_2 activation by amines and $B(C_6F_5)_3$. *Angew. Chem. Int. Ed.* **2008**, *47*, 6001–6003. (c) Kronig, S.; Theuergarten, E.; Holschumacher, D.; Bannenberg, T.; Daniliuc, C. G.; Jones, P. G.; Tamm, M. Dihydrogen activation by frustrated carbene-borane Lewis pairs: An experimental and theoretical study of carbene variation. *Inorg. Chem.* **2011**, *50*, 7344–7359.

(61) Marwitz, A. J. V.; Dutton, J. L.; Mercier, L. G.; Piers, W. E. Dihydrogen activation with *t*$Bu_3P/B(C_6F_5)_3$: A chemically competent indirect mechanism via in situ-generated *p*-*t*Bu_2P-C_6F_4-$B(C_6F_5)_2$. *J. Am. Chem. Soc.* **2011**, *133*, 10026–10029.

(62) (a) Bakó, I.; Stirling, A.; Bálint, S.; Pápai, I. Association of frustrated phosphine-borane pairs in toluene: molecular dynamics simulations. *Dalton Trans.* **2012**, *41*, 9023–9025. (b) Hamza, A.; Stirling, A.; András Rokob, T.; Pápai, I. Mechanism of hydrogen activation by frustrated Lewis pairs: A molecular orbital approach. *Int. J. of Quantum Chem.* **2009**, *109*, 2416–2425. (c) Rokob, T. A.; Bakó, I.; Stirling, A.; Hamza, A.; Pápai, I. Reactivity models of hydrogen activation by frustrated Lewis pairs: Synergistic electron transfers or polarization by electric field? *J. Am. Chem. Soc.* **2013**, *135*, 4425–4437. (d) Rokob, T. A.; Hamza, A.; Stirling, A.; Soós, T.; Pápai, I. Turning frustration into bond activation: A theoretical mechanistic study on heterolytic hydrogen splitting by frustrated Lewis pairs. *Angew. Chem. Int. Ed.* **2008**, *47*, 2435–2438.

(63) (a) Grimme, S.; Kruse, H.; Goerigk, L.; Erker, G. The mechanism of dihydrogen activation by frustrated Lewis pairs revisited. *Angew. Chem. Int. Ed.* **2010**, *49*, 1402–1405. (b) Schirmer, B.; Grimme, S. Electric field induced activation of H_2--Can DFT do the job? *Chem. Commun.* **2010**, *46*, 7942–7944.

(64) Dasgupta, A.; Richards, E.; Melen, R. L. Frustrated Radical Pairs: Insights from EPR Spectroscopy. *Angew. Chem. Int. Ed.* **2021**, *60*, 53–65.

(65) Skara, G.; Vleeschouwer, F. de; Geerlings, P.; Proft, F. de; Pinter, B. Heterolytic Splitting of Molecular Hydrogen by Frustrated and Classical Lewis Pairs: A Unified Reactivity Concept. *Sci. Rep.* **2017**, *7*, 16024.

(66) Reissmann, M.; Schäfer, A.; Panisch, R.; Schmidtmann, M.; Bolte, M.; Müller, T. Cyclic silylated onium ions of group 15 elements. *Inorg. Chem.* **2015**, *54*, 2393–2402.

(67) Fernandes, A.; Laye, C.; Pramanik, S.; Palmeira, D.; Pekel, Ö. Ö.; Massip, S.; Schmidtmann, M.; Müller, T.; Robert, F.; Landais, Y. Chiral Memory in Silyl-Pyridinium and Quinolinium Cations. *J. Am. Chem. Soc.* **2020**, *142*, 564–572.

(68) Denhof, A.; Olaru, M.; Lork, E.; Mebs, S.; Chęcińska, L.; Beckmann, J. Silyl Cations Stabilized by Pincer Type Ligands with Adjustable Donor Atoms. *Eur. J. Inorg. Chem.* **2020**, *2020*, 4093–4110.

(69) Fontana, N.; Espinosa-Jalapa, N. A.; Seidl, M.; Bauer, J. O. Easy Access to Enantiomerically Pure Heterocyclic Silicon-Chiral Phosphonium Cations and the Matched/Mismatched Case of Dihydrogen Release. *Chem. Eur. J.* **2021**, *27*, 2649–2653.

2 Research Objectives

As previously stated in the introduction, silicon can function as a robust Lewis acid in both its tetravalent coordination state and its cationic tricoordinate state. In the cationic silylium ion state, partial stabilization by a Lewis base is required to use these highly reactive species in catalytic applications. The introduction of a steric separation which allows for the stabilization of the silylium ion, but does not fully quench its Lewis acidity, has the potential to act as a frustrated Lewis pair, further enhancing the possibility of catalytic applications. The objective of the third chapter was to stabilize the highly electrophilic and Lewis acidic silylium cation by employing different phosphine chalcogenide Lewis bases. The ability to synthesize the four-membered heterocycles is influenced by the presence of different types of chalcogens and steric factors. Our objective was to quantify the amount of stabilization obtained by different substitution patterns. Furthermore, the question of whether ring strain in these four-membered heterocycles contributes to the reduction in Lewis base stabilization was examined. In chapter four, this study was extended to phosphinimide-stabilized cationic silylium ions. The possibility to introduce another substituent when using nitrogen-based donor moieties, different to chalcogen-based donor moieties, allowed us to deepen our understanding of steric and electronic factors influencing the Lewis acidity at silicon. This also allowed us to introduce a second boron-based Lewis acid, which competed with the silicon center for the Lewis basic phosphinimine electron density. As a result, the electronic destabilization, induced by boron Lewis acid competition, of the phosphinimine-silicon interaction could be studied. For the first time, this motif of destabilization allowed us to successfully employ these species as a catalyst for hydrosilylations. In chapter five neutral silicon-based Lewis acids instead of cationic silylium ions were anchored to phosphine sulfides and their interaction was studied in terms of Lewis acidity and strength of donor-acceptor interaction. Different substituents on silicon were tested for their ability to increase the Lewis acidity at silicon. Due to the less electrophilic and Lewis acidic nature of neutral silicon Lewis acids compared to cationic silylium-based Lewis acids, the thermodynamic and kinetic barriers for a reversible donor coordination to the Lewis acid were lowered. Therefore, a reversible Lewis acid/base interaction could be observed, which revealed a dynamic equilibrium between the tetra- and pentacoordinate states of the Lewis acidic silicon center. Finally, it was shown, that this equilibrium is not indefinitely stable and the pentacoordinate silicon state undergoes a clean and uncatalyzed dehydrogenative Si–H/N–H coupling forming again a tetravalent silane in the process.

Silanethiols have emerged as potent hydrogen-atom transfer catalysts in radical-chemistry over the past two decades. They are particularly useful in polarity-reversal catalysis (PRC), replacing one single polarity-mismatching reaction step with two polarity-matching reaction steps, thereby significantly enhancing the overall reaction rate. However, their employment has been limited to only a few examples. This is in part due to the lack of synthetic procedures for this class of built for purpose only compounds, especially considering enantiopure silanethiols. The sixth chapter is devoted to the synthesis and characterization of novel enantiopure silanethiols and their subsequent application as asymmetric hydrogen-atom-transfer catalysts in a deracemization sequence consisting of a hydrogen-atom transfer, photocatalytic radical-polar crossover, and subsequent protonation for benzylic substrates.

The objectives of this work can be summarized as follows:

- Development of an innovative, efficient synthetic pathway towards novel phosphine chalcogenide or phosphine imine modified silanes.
- Synthesis and characterization of novel neutral silicon Lewis acids and investigation of their dynamic Lewis base stabilization behavior.
- Synthesis and characterization of novel enantiopure silanethiols, and determination of their efficacy as enantioselective catalysts in a deracemization sequence for benzylic substrates consisting of an enantioselective hydrogen atom transfer followed by a photocatalytic radical-polar crossover and finally protonation.
- Evaluation of the influence of donor-atom type and steric factors on Lewis base stabilization of silylium cations in four-membered heterocyclic rings.
- Obtaining detailed information about the bonding situation within four-membered phosphine chalcogenide-stabilized silicon centers, and evaluation of crucial steric and electronic parameters influencing the stabilization of the Lewis acidic silicon center using computational methods.

3 Structural and Electronic Effects on Phosphine Chalcogenide-Stabilized Silylium Centers in Four-Membered Heterocyclic Cations

Preface

A synthetic version of the following chapter has already been published.

Reprinted (adapted) with permission from A. Falk, J. O. Bauer *Inorg. Chem.* **2022**, *61*, 15576–15588.

Author contribution

All reported syntheses and characterizations were performed by A. Falk. Quantum chemical calculations were performed by Dr. J. O. Bauer. The original script and supporting information were prepared by A. Falk and revised by Dr. J. O. Bauer.

Acknowledgements

This work was supported by the Deutsche Forschungsgemeinschaft (DFG, German Research Foundation) through the Research Training Group “Ion Pair Effects in Molecular Reactivity” (RTG 2620, project 426795949). The authors also thank Prof. Dr. Manfred Scheer for generous support, Dr. Michael Seidl for helpful discussions regarding X-ray crystallography, and Prof. Dr. Hendrik Zipse for inspiring discussions on the calculations.

3.1 Abstract

Understanding the interplay of structural and electronic parameters in the stabilization of Lewis acidic silicon centers is crucial for stereochemical questions and applications in bond activation and catalytic transformations. Phosphine chalcogenide-functionalized (Ch = O, S, Se) hydrosilanes having *tert*-butyl or 2,4,6-trimethoxyphenyl (TMP) substituents on the silicon atom were synthesized and the ring-closing reactions to afford the heterocyclic four-membered CPChSi cations investigated. Synthetic access was only achieved for the sulfur- and selenium-based cations. A thorough study by means of single-crystal X-ray structure determination, NMR spectroscopic data, and density functional theory (DFT) calculations provided insight into important electronic and structural parameters affecting the stability of the intramolecularly stabilized cations. The angular strain within the four-membered rings appears to be quite balanced in all four-membered CPChSi rings investigated. Thermochemical investigations showed that the substituents on the silicon and phosphorus atoms play an important role for the strength of the intramolecular Ch–Si coordination. In the absence of large steric repulsions through bulky substituents (methyl groups on silicon, *tert*-butyl groups on phosphorus), a stability sequence depending on the chalcogen atom in the direction Se ≤ S < O can be observed. However, the order is reversed (O < S < Se) in case of strong repulsions between sterically demanding substituents (*tert*-butyl groups on both silicon and phosphorus atoms). Natural bond orbital (NBO) analysis supported the explanations for the observed deshielding trends in ^{31}P NMR spectroscopy, and revealed that the O–Si bond is more ionic in nature compared to the S–Si and Se–Si bonds, the latter exhibiting higher covalent character due to a more efficient charge transfer through an $n_{Ch} \rightarrow p_{Si}$ interaction.

3.2 Introduction

Small inorganic ring systems are an interesting class of compounds and often show intriguing electronic properties.[1] The chemistry of heterocyclic main-group element compounds in which a donor function intramolecularly stabilizes a Lewis acidic center has received considerable attention for many years. Initially, the focus of interest was on intramolecularly stabilized group 13 elements,[2] which gained renewed attention particularly in the context of the developments in the field of frustrated Lewis pairs (FLPs).[3] In the last decades, as a result of the exploration of new reactions catalyzed by Lewis acidic compounds,[4] the potential of the tremendous Lewis acidity of silylium ions has increasingly been recognized.[5] This significantly affected the development of entirely new synthesis methods and stimulated progress in the design of novel silicon-based Lewis acid catalysts.[6] Now, the scope of catalytic applications using silylium ions covers a wide range of transformations.[7] Silylium ions stabilized intramolecularly by a Lewis base became attractive targets, as this allows their strong Lewis acidity to be tamed and adjusted, and stereochemical information to be transferred to the silicon center. Oestreich and co-workers reported the intramolecular stabilization of a silylium center by sulfur and nitrogen donor atoms introduced through dithioacetal and oxazoline functions, respectively, and studied the effect of the donor atom on the reactivity.[8] Müller et al. studied cyclic silylated group 15 element onium ions and the dependence of the intramolecular stabilization on the ring size and the nature of the pnictogen atom.[9] Five- and six-membered cycles were synthesized, but no smaller ring sizes could be achieved.[9] The study of the intramolecular chalcogen–silicon bond in catalytically active cyclic chalconium ions by the same group surprisingly revealed that the Si–O bond was the weakest of the Si–Ch interactions (Ch = chalcogen).[10] Consequently, the oxonium ion was also assigned the highest Lewis acidity of all cyclic chalconium ions.[11] This concept of intramolecular stabilization of silyl cationic centers has also been extended to halogen substituents, which show that the silicon Lewis

acidity decreases as the halogen atom gets heavier.[12] Other intriguing examples of nitrogen-, phosphorus-, oxygen-, and sulfur-stabilized silylium ions have stimulated promising applications in bond activation and catalysis.[13] In recent years, the intramolecular stabilization of silylium ions has been further explored, particularly with regard to the generation of stereogenic Lewis acidic silicon centers with defined configurations.[14,15] Phosphine chalcogenide functions are known for their interesting coordinating abilities.[16] We recently reported a new type of four-membered heterocyclic cations in which the elusive silyl cationic center is intramolecularly stabilized, thus generating a configurationally stable stereogenic silicon center.[15] The starting compounds chosen for these studies were equipped with a P^+–S^- moiety that intramolecularly promoted the hydride abstraction by $B(C_6F_5)_3$ (Scheme 1, top). Consistent with a strong silicon–sulfur interaction and a strongly tamed Lewis acidity, we classified these cyclic cations as phosphonium rather than silylium ions. Starting from a protonated hydrosilane, we were also able to generate different substituent patterns on the silicon atom via an elimination reaction, which enables an easy switch in chemoselectivity depending on the solvent mixture (Scheme 1, bottom).[15]

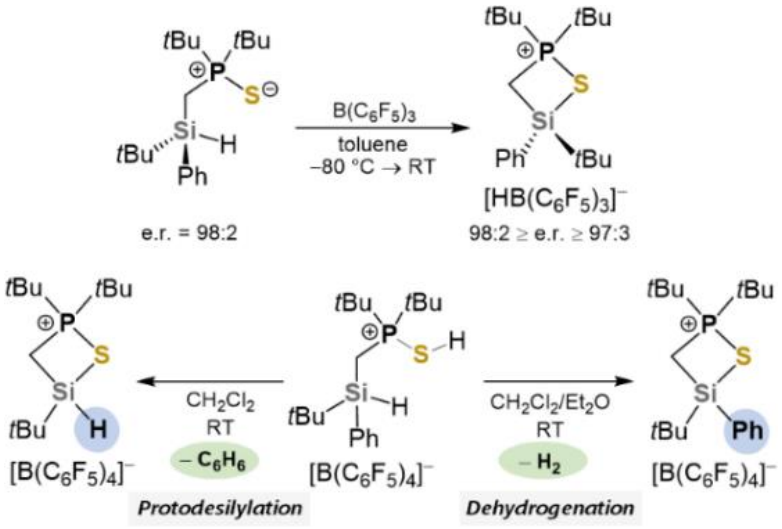

Scheme 1: Previously reported access toward four-membered heterocycles by our group.[15] Top: Stereospecific ring formation. Bottom: Solvent-dependent chemoselectivity switching starting from a protonated hydrosilane

Continuing our research on main group element-based heterocyclic systems,[17] we herein set out to systematically investigate the structural properties (angular strain, substituent effects) and the electronic nature of four-membered heterocyclic CPChSi cations. Phosphine chalcogenide-functionalized hydrosilanes were synthesized and their ring-closing reactions studied. The effect of the chalcogenide of the P^+–Ch^- (Ch = O, S, Se) unit and the influence of the substituents bound to the silicon atom (*tert*-butyl, methyl, and 2,4,6-trimethoxyphenyl) on the strength of the intramolecular stabilization of a silylium center in four-membered cycles were elucidated. Structural, NMR spectroscopic, and quantum chemical data were evaluated in detail to provide a comprehensive picture of the key parameters affecting the stability of the P–Ch–Si linkage.

3.3 Results and Discussion

Synthetic Approach, Molecular Structures, and NMR Spectroscopy. We started our investigations with the synthesis of the silylated phosphorus(V) chalcogenides **3–6** (Scheme 2). The phosphine sulfides **3** and **4** were synthesized according to our previously reported procedure[15] by direct reaction of the corresponding chlorosilane **1** or **2** with $LiCH_2P(S)(tBu)_2$ in good yields of 85% and 77%, respectively. For both the phosphine oxide **5** and the selenide **6** an alternative synthetic route was employed. First, di-*tert*-butylchlorosilane (**1**) was reacted with freshly prepared $LiCH_2P(tBu)_2$[17,18] followed by oxidation of the phosphorus(III) intermediate either with oxygen, resulting in compound **5**, or using grey selenium to afford compound **6**. The two products were obtained in moderate (**5**: 26%) and good (**6**: 71%) yields over two steps.

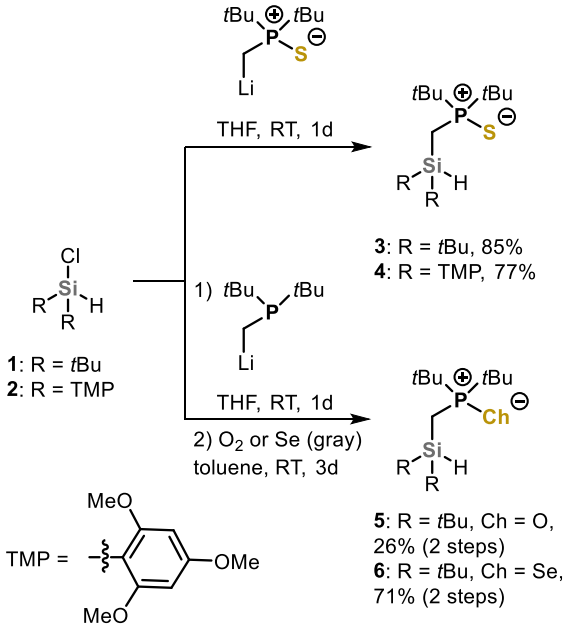

Scheme 2: Synthesis of silyl phosphine chalcogenides **3**–**6**

The phosphine chalcogenides **3–6** crystallized in the monoclinic crystal system, space groups $P2_1/c$ (**3–5**) and $P2_1/n$ (**6**) (Figures 1 and 2). All compounds show an enlarged P–C–Si angle caused by the high steric demand of the substituents bound to the silicon and the phosphorus atom. The (di-*tert*-butyl)silyl-substituted species **5** (Ch = O), **3** (Ch = S), and **6** (Ch = Se) follow a trend of slightly increasing P–C–Si angles [121.02(6)° < 123.19(7)° < 124.3(1)°] in the same direction as the atomic radii of the chalcogenides and the P–Ch bond lengths increase [P–O: 1.4958(8) Å < P–S: 1.9650(5) Å < P–Se 2.1164(7) Å]. The bis(2,4,6-trimethoxyphenyl)silane **4** shows the smallest P–C–Si angle with 118.90(9)° due to the lower steric demand of the substituents around the silicon atom.

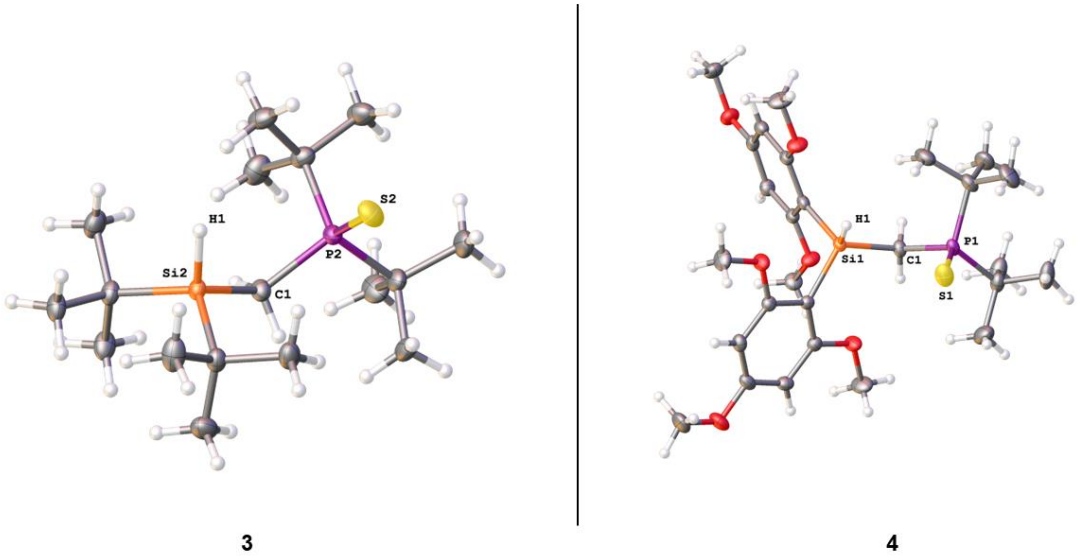

Figure 1: Molecular structures of phosphine chalcogenides **3** and **4** in the crystal (displacement ellipsoids set at the 50 % probability level). Selected bond lengths (Å) and angles (°) of **3** (123.0(1) K): P(2)–S(2) 1.9650(5), P(2)–C(26) 1.824(1), Si(2)–C(26) 1.906(1), P(2)–C(26)–Si(2) 123.19(7), C(26)–P(2)–S(2) 114.34(5). **4** (122.9(1) K): S(1)–P(1) 1.9699(6), P(1)–C(1) 1.8179(6), Si(1)–C(1) 1.8991(6), P(1)–C(1)–Si(1) 118.90(9), C(1)–P(1)–S(1) 113.51(6).

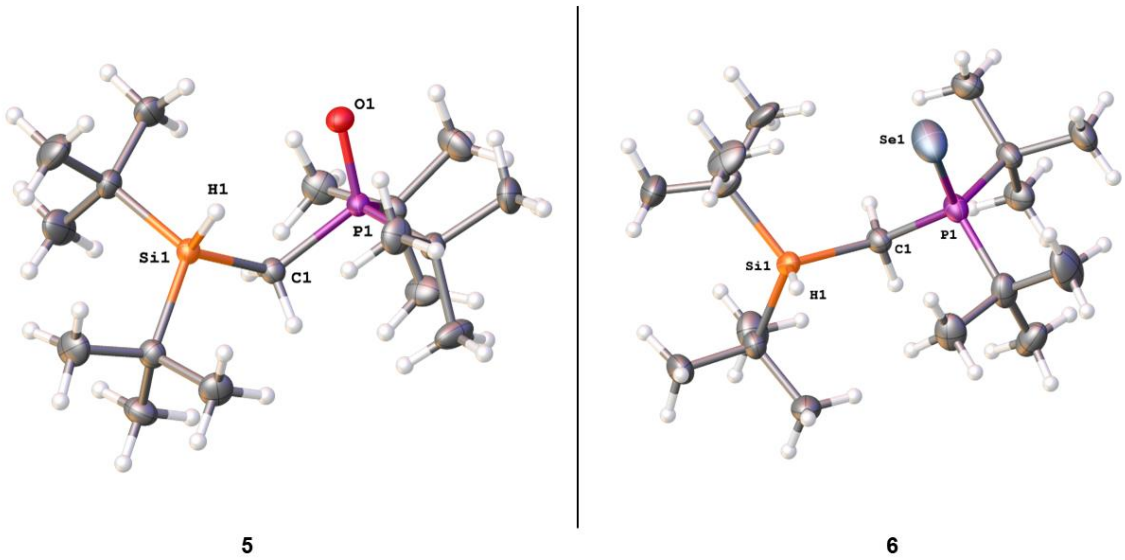

Figure 2: Molecular structures of phosphine chalcogenides **5** and **6** in the crystal (displacement ellipsoids set at the 50 % probability level). Selected bond lengths (Å) and angles (°) of **5** (123.0(1) K): P(1)–O(1) 1.4958(8), P(1)–C(1) 1.814(1), Si(1)–C(1) 1.893(1), O(1)–P(1)–C(1) 114.09(5), P(1)–C(1)–Si(1) 121.02(6). **6** (123.0(1) K): P(1)–Se(1) 2.1164(7), P(1)–C(1) 1.822(2), Si(1)–C(1) 1.905(2), P(1)–C(1)–Si(1) 124.3(1), C(1)–P(1)–Se(1) 114.45(8).

Phosphine sulfide **3** and selenide **6** were easily converted into the corresponding heterocyclic phosphonium–hydroborate ion pairs **7**[HB(C_6F_5)$_3$] and **8**[HB(C_6F_5)$_3$] by hydride abstraction with tris(pentafluorophenyl)borane (Scheme 3). After 7 days exposure to B(C_6F_5)$_3$ in pentane, products **7**[HB(C_6F_5)$_3$] and **8**[HB(C_6F_5)$_3$] were directly obtained in crystalline form in good yields of 77% and 93%, respectively. It is noteworthy that the formation of the cyclic phosphonium ions **7** and **8** from the reactions of compounds **3** and **6**, respectively, using [Ph_3C][B(C_6F_5)$_4$] as hydride abstracting reagent was unsuccessful. In contrast, the reaction of the bis(2,4,6-trimethoxyphenyl)-substituted compound **4** with [Ph_3C][B(C_6F_5)$_4$] resulted in clean hydride abstraction and gave rise to the ion pair **9**[B(C_6F_5)$_4$] (Scheme 3). Although in this case the formation of the cyclic cation **9** is also possible when using B(C_6F_5)$_3$, the isolation of the pure product **9**[HB(C_6F_5)$_3$] turned out to be much more difficult.

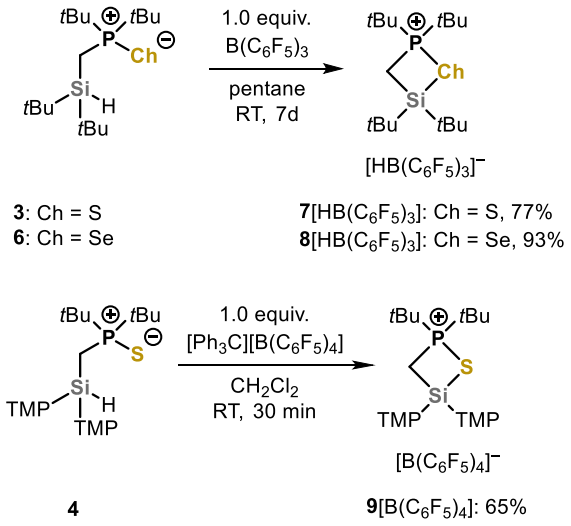

Scheme 3: Synthesis of heterocyclic phosphonium chalcogenide cations **7**–**9**. TMP = 2,4,6-trimethoxyphenyl

Compared to the corresponding hydrosilanes **3** [δ(^{29}Si) = 7.7 ppm] and **4** [δ(^{29}Si) = –40.1 ppm], the ^{29}Si NMR signals of the sulfur-stabilized silicon atoms are noticeably shifted downfield to δ = 31.4 ppm for **7**[HB(C_6F_5)$_3$] and to δ = –12.5 ppm for **9**[B(C_6F_5)$_4$], with a chemical shift difference [$\Delta\delta$(^{29}Si)] of 23.7 ppm and 27.6 ppm, respectively (Table 1). However, the clearly highfield shifted absolute values of the ^{29}Si NMR signals of compounds **4** and **9**[B(C_6F_5)$_4$] nicely reflect the influence of the electron rich TMP groups in contrast to the *tert*-butyl groups. The ^{29}Si NMR chemical shift is often taken as a measure of the silylium character of a silicon center.[6c] However, the chemical shift is a function of different contributions, with the ring size also influencing the shielding of the ^{29}Si nucleus.[19] At least for related systems like those studied herein, the downfield shift [$\Delta\delta$(^{29}Si)] of the ^{29}Si NMR signal upon hydride abstraction and ring formation may be regarded as an estimate for the electronic stabilization of the Lewis acidic silicon center by the Lewis basic chalcogenide functionality. Accordingly, for the formation of the four-membered cyclic cations, the phosphine selenide function appears to induce a stronger electron occupation of silicon-located orbitals via a covalent σ-type Se–Si bond than the phosphine sulfide function, as suggested by the smaller downfield shift of $\Delta\delta$(^{29}Si) = 17.3 ppm between compounds **6** [δ(^{29}Si) = 8.1 ppm] and **8**[HB(C_6F_5)$_3$] [δ(^{29}Si) = 25.4 ppm] compared to the sulfur-based compounds. This correlates with the stronger polarizability and the lower electronegativity of the selenium atom. Consequently, we expected the P–O function to be

the least effective Lewis base of the phosphine chalcogenide series to stabilize the silicon center via covalent contributions of the σ-type O–Si bond (see also discussion of the NBO calculations below).

Table 1: Chemical shifts (δ in ppm) of ^{29}Si and ^{31}P NMR signals

Compound	$\delta(^{29}Si)$	$\delta(^{31}P)$
3	7.7	77.4
7[HB(C_6F_5)$_3$]	31.4	88.7
6	8.1	73.8
8[HB(C_6F_5)$_3$]	25.4	75.8
4	–40.1	78.1
9[B(C_6F_5)$_4$]	–12.5	88.6
5	9.1	58.9
10	32.0	96.6

Surprisingly, neither the reaction of the phosphine oxide **5** with B(C_6F_5)$_3$ nor with [Ph_3C][B(C_6F_5)$_4$] resulted in hydride abstraction and cation formation, even when heated to 50 °C. As another strategy to provide the oxygen-containing heterocycle, we considered a method, which was recently reported by Beckmann et al. for the generation of pincer-type phosphine oxide-stabilized silylium centers, and which is based on a reaction of a hydrosilane with two equivalents of bromine.[20] However, also this approach was unsuccessful for our system. Instead, we obtained the hydrogen bromide adduct of the brominated intermediate (**10**) (Scheme 4).

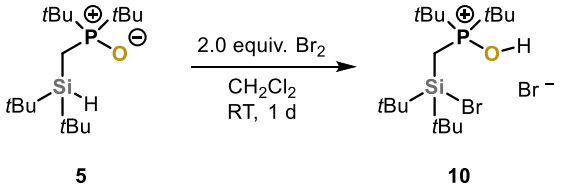

5 **10**

Scheme 4: Ring closure attempt using bromine

Ion pairs **7**[HB(C_6F_5)$_3$], **8**[HB(C_6F_5)$_3$], and **9**[B(C_6F_5)$_4$] crystallized in the monoclinic crystal system, the former two in the space group $P2_1/c$ and the latter in the space group $P2_1/n$ (Figure 3). X-Ray diffraction analysis gave insight into some important structural parameters. The molecular structures of the heterocyclic cations in the crystalline state show a decrease in the P–C–Si bond angle in the direction Se > S [100.0(1)° (**8**) > 94.5(3)° (**7**) ≈ 95.3(4)° (**9**)] and hence an increasing deviation from the ideal tetrahedral angle around the carbon atom. The P–Ch bond lengths in the cyclic cations **7** [P–S: 2.012(7) Å], **8** [P–Se: 2.2277(6) Å], and **9** [P–S: 2.052(1) Å] differ only slightly from the respective bond lengths in the starting compounds **3** [P–S: 1.9650(5) Å], **6** [P–Se: 2.1164(7) Å], and **4** [P–S: 1.9699(6) Å] (Figures 1, 2, and 3).

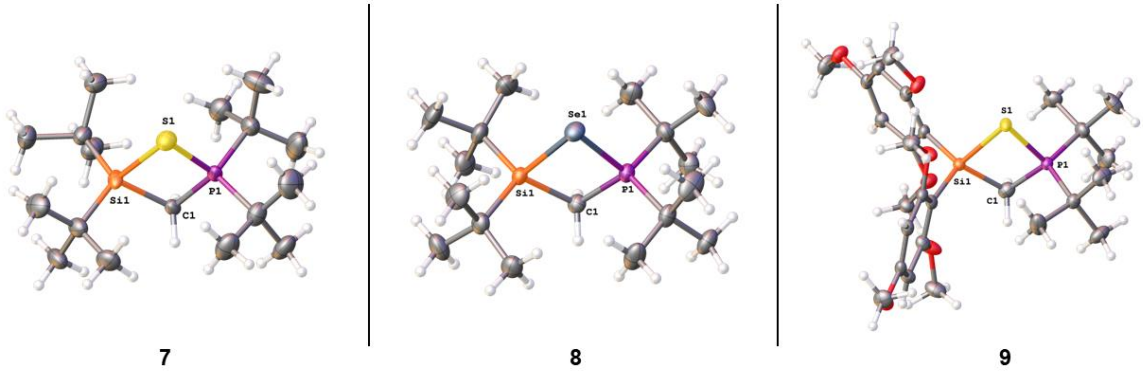

7 8 9

Figure 3: Molecular structures of cations **7**, **8**, and **9** in the crystal (displacement ellipsoids set at the 50 % probability level). Counteranions are omitted for clarity. Selected bond lengths (Å) and angles (°) of **7** (122.9(1) K): Si(1)–S(1) 2.285(7), P(1)–S(1) 2.012(7), P(1)–C(1) 1.840(8), Si(1)–C(1) 1.954(8), P(1)–S(1)–Si(1) 80.6(4), P(1)–C(1)–Si(1) 94.5(3). **8** (123.0(1) K): Si(1)–Se(1) 2.3567(6), P(1)–Se(1) 2.2277(6), P(1)–C(1) 1.834(2), Si(1)–C(1) 1.915(2), P(1)–Se(1)–Si(1) 77.55(2), P(1)–C(1)–Si(1) 100.0(1). **9** (123.15 K): Si(1)–S(1) 2.205(1), P(1)–S(1) 2.052(1), P(1)–S(1)–Si(1) 80.00(4), P(1)–C(1)–Si(1) 95.3(4).

In a fundamental theoretical ^{31}P NMR investigation by Letcher and van Watzer, the ^{31}P-NMR chemical shift was found to be predominantly influenced by asymmetric electronic occupation of orbitals located at the phosphorus atom, which should be less pronounced for tetravalent phosphorus compounds than for trivalent posphines.[21] The phosphine chalcogenide moiety corresponds to the picture of a polarized P–Ch σ-bond, which is superimposed by an $n_{Ch} \rightarrow \sigma^*_{P-C}$ hyperconjugative interaction. This bonding situation is a result of theoretical bond analyses[22] and expressed in the zwitterionic P^+–Ch^- notation. Following from this, the silicon–chalcogen interaction in our cyclic cations has only a marginal influence on the electronic occupation of phosphorus-centered orbitals in the case of the P–S bond and even a negligible influence in case of the P–Se bond; this can be seen from the small ^{31}P NMR chemical shifts toward lower field upon ring formation, changing from 77.4 ppm to 88.7 ppm [$\Delta\delta(^{31}P)$ = 11.3 ppm, **3** → **7**] and from 73.8 ppm to 75.8 ppm [$\Delta\delta(^{31}P)$ = 2.0 ppm, **6** → **8**] (Table 1). Also the TMP substituents at the silicon atoms have no dramatic influence on the ^{31}P NMR chemical shifts [$\Delta\delta(^{31}P)$ = 10.5 ppm, **4** → **9**]. In contrast, the protonation of the P–O function (see Scheme 4) leads to a much stronger deshielding of the phosphorus atom, which is evident from the significant ^{31}P NMR downfield shift of $\Delta\delta(^{31}P)$ = 37.7 ppm between compounds **5** [$\delta(^{31}P)$ = 58.9 ppm] and **10** [$\delta(^{31}P)$ = 96.6 ppm]. Previous results in our group[15] showed that the ^{31}P NMR spectroscopic data of a protonated P–S function can be used as a good estimate for a silylated P–S function incorporated in a four-membered ring. The observed chemical shift differences [$\Delta\delta(^{31}P)$] in the direction O >> S > Se correlate very well with the supposed change in hyperconjugative $n_{Ch} \rightarrow \sigma^*_{P-C}$ contributions (see also discussion of the NBO calculations below). Based on the ^{31}P NMR spectroscopic findings, we therefore assume that the P–Ch σ-bond in all phosphine-chalcogenide functions remains largely unaffected upon coordination to the silicon center and that changes in hyperconjugative $n_{Ch} \rightarrow \sigma^*_{P-C}$ contributions are likely responsible for an asymmetric electronic occupation at the ^{31}P nucleus in our tetravalent phosphorus compounds.[21] This effect should indeed be grater for the P–O[22b] than for the P–S and P–Se bonds[22c]. In general, the $^2J_{Si-P}$ coupling constants increase when the phosphine chalcogenide functionality binds to a Lewis acidic center either intra- or intermolecularly (Table 1). Upon tetracyclic ring formation, this change $\Delta(^2J_{Si-P})$ is somewhat more pronounced with sulfur [$\Delta(^2J_{Si-P})$ = 1.7 Hz, **3** → **7**] than with selenium [$\Delta(^2J_{Si-P})$ = 1.0 Hz, **6** → **8**] and appears to be greater as more aryl groups are bound to the silicon atom; some $\Delta(^2J_{Si-P})$ values of similar systems, all of which have

(tBu)$_2$P–S functions, reflect this latter trend: Si(tBu)$_2$ (1.7 Hz) < Si(tBu)Ph[15] (7.3 Hz) < Si(TMP)$_2$ (14.6 Hz). For the absolute value of the $^2J_{Si–P}$ coupling constants in the ring systems, it should be taken into account that the Si–P coupling can also occur via the P–Ch–Si linkage.[17] The ^{77}Se NMR spectroscopic parameters are most affected through the ring formation. The ^{77}Se NMR spectrum of the selenium-based starting compound **6** shows a doublet at –381.6 ppm and a $^1J_{P–Se}$ coupling constant of 717.6 Hz (Table 1). The ^{77}Se NMR signal, although more highfield-shifted due to the aliphatic phosphorus-bound substituents, and the $^1J_{P–Se}$ coupling constant are in the expected region, typical for phosphine selenides.[20] Upon ring formation, the $^1J_{P–Se}$ coupling constant drops down by more than half to a value of 323.6 Hz in **8**[HB(C$_6$F$_5$)$_3$], accompanied by a significantly large downfield shift $\Delta\delta(^{77}Se)$ of –381.6 ppm to $\delta(^{77}Se)$ = –72.9 ppm. These changes are much more pronounced in the systems studied herein than in the case of the formation of five-membered rings with a pincer-type coordination of the P–Se moiety to a silylium center reported by Beckmann et al.[20] The decrease in the $^1J_{P–Se}$ coupling constant may also be attributed to an elongation of the P–Se bond upon ring formation. In general, the ^{77}Se nucleus as an NMR probe for the direct Ch–Si interaction indicates a particularly strong intramolecular coordination of the phosphine chalcogenide function to the silicon center.

Thermochemistry and Structural Properties. Quantum chemical calculations on the M062X/6-311+G(d,p) level of theory[23] allowed also structural insight into the hitherto experimentally inaccessible oxygen analogue (**11**) in comparison with the heavier sulfur (**7**) and selenium (**8**) species of the chalcogenide series. First, we calculated the Gibbs energy (ΔG) required to break the intramolecular Ch–Si coordination within the cyclic cations **11** (Ch = O), **7** (Ch = S), and **8** (Ch = Se) to form the open, trigonal planar silylium ions **11-o**, **7-o**, and **8-o** (Figure 4). This can be regarded as a good measure of the strength of the intramolecular coordination in the corresponding cyclic cations considering the sum of both structural and electronic contributions. Our computational investigations showed a clear increase in the stabilization energy (ring-opening energy) of the Ch–Si linkage of the all-*tert*-butyl-substituted cyclic cations in the order O–Si (+29.6 kcal mol^{-1}) < S–Si (+34.2 kcal mol^{-1}) ≤ Se–Si (+34.9 kcal mol^{-1}). This order of stability is consistent with the trend also found for Ch–Si bonds in chalconium ions.[10,11] For the TMP-substituted cyclic cation **9**, an energy of only +26.5 kcal mol^{-1} for the opening of the S–Si linkage was calculated, since one *ortho*-methoxy group of a TMP ring weakly stabilizes the silyl cationic center, resulting in an oxonium species (**9-o**) with a distorted trigonal pyramidal coordination around the silicon atom (Figure 4).

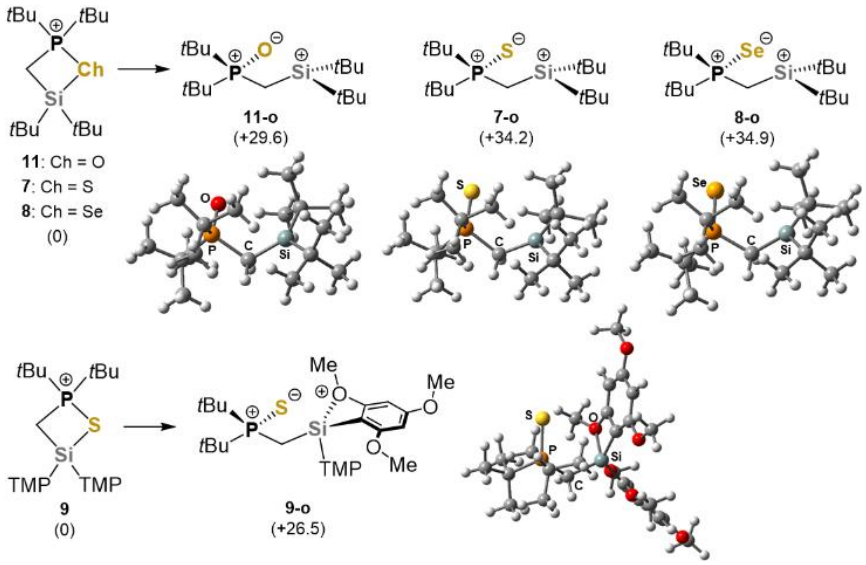

Figure 4: Gibbs energies (ΔG) [kcal mol–1] for the ring-opening as a measure of the stabilization provided by the intramolecular coordination of the phosphine chalcogenide function to the silylium center, calculated on the M062X/6-311+G(d,p) level of theory.[23] TMP = 2,4,6-trimethoxyphenyl.

All cyclic cores of the three cations (**11**, **7**, and **8**) form a nearly perfect plane, which forces the two pairs of bulky *tert*-butyl groups on the phosphorus and silicon atoms into an unfavorable ecliptic arrangement (Figure 5). With respect to the corresponding hydrosilanes, the P–Ch bond lengths decrease only slightly by about the same amount in all three cyclic cations (**5** → **11**: 0.114 Å; **3** → **7**: 0.106 Å; **6** → **8**: 0.101 Å). The angle around the heterocyclic carbon atom is strongly dependent on the chalcogenide of the P–Ch function (Table 2). The calculated oxygen analogue (**11**) exhibits the smalles P–C–Si bond angle of 86.4°, caused by the short P–O (1.618 Å) and O–Si (1.773 Å) bond lengths, which is far beyond the P–C–Si angles of the cyclic sulfur- and selenium-based cations **7** (96.6°) and **8** (100.1°), and even below an orthogonal geometry (Table 2). For comparison, the calculated O–Si bond length in cation **11** of 1.773 Å is approximately 0.1 Å shorter than the O–Si distance found in the molecular structure of a zwitterionic four-membered CPOSi heterocycle with a penta-coordinate silicon atom reported by Mitzel et al.[24] These structural properties cause a substantial steric repulsion between the bulky *tert*-butyl groups on the phosphorus and silicon atoms in cation **11**, thereby weakening the intramolecular donor–acceptor interaction. This may be an important reason for the easier opening of the O–Si bond compared to the S–Si and Se–Si bonds within the four-membered CPChSi heterocycles (see Figure 4). Unlike the P–C–Si angle, the P–Ch–Si angle increases in the opposite direction (Se < S < O) with angles far below 90° within the selenium- (77.2°) and sulfur-based cations (80.4°) and an angle of 99.5° within the oxygen analogue (Table 2).

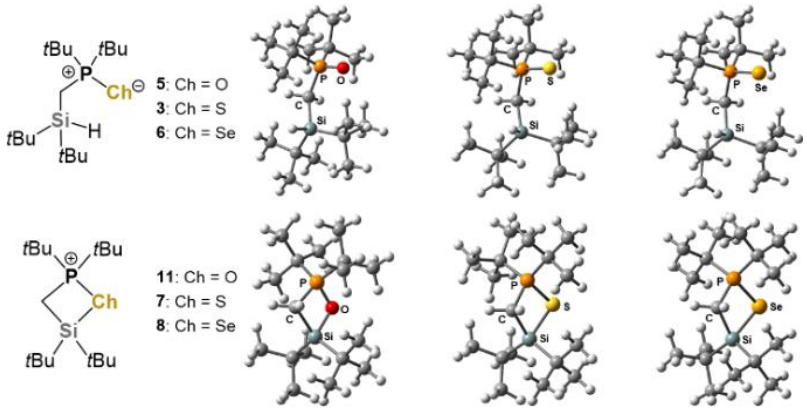

Figure 5: Optimized structures of the phosphine chalcogenide-functionalized hydrosilanes and the cyclic all-*tert*-butyl cations. M062X/6-311+G(d,p).[23]

Table 2: Structural properties of the phosphine chalcogenide-functionalized hydrosilanes and cyclic cations[a]

Compound	P–Ch bond length [Å]	Ch–Si bond length [Å]	P–C–Si angle [°]	P–Ch–Si angle [°]
5 (Ch = O)	1.504		125.1	
11 (Ch = O)	1.618	1.773	86.4	99.5
13 (Ch = O)	1.616	1.751	85.1	97.5
3 (Ch = S)	1.981		123.0	
7 (Ch = S)	2.087	2.262	96.6	80.4
14 (Ch = S)	2.089	2.227	94.8	79.1
6 (Ch = Se)	2.138		123.9	
8 (Ch = Se)	2.239	2.396	100.1	77.2
15 (Ch = Se)	2.237	2.363	97.6	75.4

[a][M062X/6-311+G(d,p)].[23]

This can in fact result in a quite balanced ring strain in all three cations, given that the second-row elements (carbon and oxygen) tend to have angles as close as possible to the tetrahedral angle, while the heavier elements (sulfur and selenium) prefer angles closer to 90°. This means that, for example, in cation **11** the ring strain caused by an unfavorably small P–C–Si angle is partially counterbalanced by a larger P–O–Si angle. We therefore hypothesized that the steric repulsion between the space-filling *tert*-butyl groups might be the main reason for the found stability order (O < S < Se) of the all-*tert*-butyl-substituted four-membered cyclic CPChSi cations. To further support this hypothesis, we exchanged the *tert*-butyl groups on the silicon atom for methyl groups and calculated the ring-opening energy (Figure 6). The successive exchange of the two *tert*-butyl groups by two methyl groups in the oxygen-based cation led to a remarkable increase in stability (ring-opening energy) of the four-membered cyclic cations from +29.6 kcal mol^{-1} for **11** to +41.8 kcal mol^{-1} for **12** to +47.6 kcal mol^{-1} for **13**, which now even surpasses that of the dimethyl-substituted sulfur- and selenium-based cations (**14** → **14-o**: +44.9 kcal mol^{-1}; **15** → **15-o**: +43.5 kcal mol^{-1}). This leads to an inverted chalcogenide-dependent stability order (Se ≤ S < O) and indeed confirms an intrinsically stronger intramolecular interaction between silicon and oxygen. Incidentally, the structural parameters of the cyclic four-membered core do not differ significantly from the all-*tert*-butyl derivatives (Table 2). Hence, disproportionately large steric repulsions between bulky groups on the phosphorus and silicon atoms of the CPOSi heterocycle, caused by the short P–O and O–Si bond lengths, can significantly counteract the greater inherent stability of the O–Si interaction compared to the S–Si and Se–Si interactions. This stability trend follows the one reported for phosphine chalcogenide-stabilized silylium centers in pincer-type bonding modes.[20]

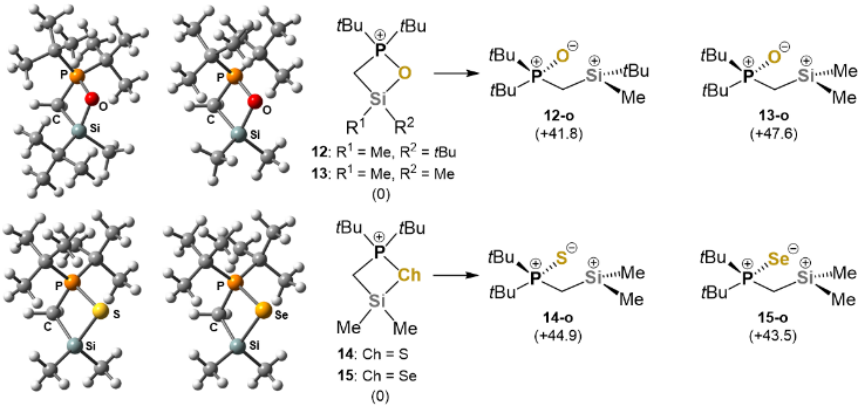

Figure 6: Gibbs energies (Δ*G*) [kcal mol^{-1}] for the ring-opening to estimate the effect of steric repulsion on the strength of the intramolecular coordination within the four-membered cyclic CPChSi cations. M062X/6-311+G(d,p).[23]

NBO Calculations. Table 3 summarizes the results of the natural bond orbital (NBO) analysis[25] performed on the M062X/6-311+G(d,p) level of theory[23] allowing for an investigation of inductive and hyperconjugative electronic bonding components[26] within the heterocyclic cations. As a comparison of the three pairs of compounds **5**/**11** (Ch = O), **3**/**7** (Ch = S), and **6**/**8** (Ch = Se) shows, the natural atomic charges on the phosphorus atom (Q_P) do not change significantly upon intramolecular coordination (row 3 in Table 3). The same applies to the bond ionicity values (i_{PCh}) (row 1 in Table 3), with the P–O bond being in general much more ionic (5/11: i_{PO} = 0.493/0.564) than the P–S (3/7: i_{PS} = 0.028/0.118) and P–Se bonds (6/8: i_{PSe} = 0.064/0.037). This corresponds to the electrovalent bonding situation as expressed in the zwitterionic notation P$^+$–Ch$^-$ (Ch = O,

S, Se), in qualitative agreement with atoms-in-molecules (AIM) studies on P–Ch bonds,[22b,c] and shows that the inductive charge distribution along the P–Ch σ-bond is only marginally affected through the Ch–Si interaction.[27] In general, the Ch–Si bonds of the cyclic cations are for all chalcogen atoms more polar than the P–Ch bonds, as is evident from the bond ionicities (rows 1 and 2 in Table 3), and which is the reason for the preferential opening of the Ch–Si bond in reactions with nucleophilic reagents. However, the negative charge of the chalcogen atom (Q_{Ch}) decreases noticeably for sulfur and selenium upon ring formation, but remains almost constant for oxygen (row 4 in Table 3). This means that significant charge transfer from a chalcogen lone electron pair to the silicon-located empty p-orbital through an $n_{Ch} \rightarrow p_{Si}$ interaction only occurs with the phosphine sulfide and selenide functions and increases the covalent character of the Ch–Si σ-bond in cations **7** (Ch = S) and **8** (Ch = Se), in accordance with the higher polarizability of the heavier sulfur and selenium atoms. This can also be seen at the significantly higher s-character of the natural hybrid (h_O) on the oxygen atom contributing to the O–Si bond (40.3%) compared to the s-character of h_S and h_{Se} participating in the S–Si (22.5%) and Se–Si bonds (19.8%) (row 6 in Table 3). The higher ionic nature of the O–Si interaction[24] is also reflected in the far greater ionicity value of the O–Si bond (i_{OSi} = 0.781) and the higher positive charge of the silicon atom (Q_{Si} = 2.193) in cation **11** compared to **7** (Q_{Si} = 1.899) and **8** (Q_{Si} = 1.843) (rows 2 and 5 in Table 3). These findings are in line with the results of experimental and theoretical studies on the nature of O–Si bonds incorporated in ring systems.[20,28]

Table 3: Results of the natural bond orbital (NBO) calculations regarding bond polarity parameters, hybridization, and hyperconjugative properties of the phosphine chalcogenide-functionalized hydrosilanes and cyclic cations[a]

Property	**5** (Ch = O)	**11** (Ch = O)	**3** (Ch = S)	**7** (Ch = S)	**6** (Ch = Se)	**8** (Ch = Se)
i_{PCh}[b]	0.493	0.564	0.028	0.118	0.064	0.037
i_{ChSi}[b]		0.781		0.518		0.458
Q_P[c]	2.063	1.988	1.477	1.530	1.405	1.473
Q_{Ch}[c]	–1.148	–1.169	–0.633	–0.401	–0.564	–0.263
Q_{Si}[c]	1.602	2.193	1.611	1.899	1.610	1.843
h_{Ch} (% s)[d]		$sp^{1.48}$ (40.3)		$sp^{3.44}$ (22.5)		$sp^{4.00}$ (19.8)
h_{Si} (% s)[d]		$sp^{4.47}$ (17.8)		$sp^{5.04}$ (16.4)		$sp^{5.17}$ (16.1)
$E^{(2)}$ ($n_{Ch} \rightarrow \sigma^*_{P-C}$)[e]	–74.0	–20.27	–64.34	–19.42	–56.67	–16.44

[a][M062X/6-311+G(d,p)].[23] [b]Bond ionicities (i_{PCh}, i_{ChSi}) of the P–Ch and Ch–Si bonds ($i_{AB} = |c_A^2 - c_B^2|$ with c_A and c_B being NBO polarization coefficients). [c]Natural atomic charges (Q_P, Q_{Ch}, Q_{Si}) at atoms P, Ch, and Si . [d]Natural hybrid types (h_{Ch}, h_{Si}) and their % s-character at atoms Ch and Si in the Ch–Si bond. [e]Hyperconjugative stabilization energy estimates ($E^{(2)}$ in kcal mol^{-1}) from the second order perturbation theory analysis for the $n_{Ch} \rightarrow \sigma^*_{P-C}$ interactions.

In addition, second-order perturbation theory analysis gave an estimate for the loss of $n_{Ch} \rightarrow \sigma^*_{P-C}$ hyperconjugative stabilization energy ($E^{(2)}$) upon intramolecular Ch–Si coordination (row 8 in Table 3). This loss ($\Delta E^{(2)}$) is greatest in the case of the O–Si coordination with 53.73 kcal mol^{-1}, from –74.0 kcal mol^{-1} in hydrosilane **5** to –20.27 kcal mol^{-1} in cation **11**, and decreases in the series S ($\Delta E^{(2)}$ = 44.92 kcal mol^{-1}) > Se ($\Delta E^{(2)}$ = 40.23 kcal mol^{-1}). This rather than inductive effects from P–Ch σ-bond contributions might be an explanation for the observed deshielding trend in ^{31}P NMR spectroscopy[21] in the direction O >> S > Se (^{31}P NMR data for the oxygen analogue refer to the protonated P–O function of compound **10**) (see Table 1 and discussion of the ^{31}P NMR chemical shifts above).

Reactivity. Finally, we set out to investigated the Lewis acidity of the sulfur- and selenium-containing cations **7**, **8**, and **9** with reference to the Lewis acidity scale based on diagnostic NMR spectroscopic parameters of the interaction with *para*-fluorobenzonitrile (*p*-FBN).[11]

While no interaction between the cation and *p*-FBN was observed in the ^{19}F NMR spectrum when using **9**[$B(C_6F_5)_4$], treatment of the ion pairs **7**[$HB(C_6F_5)_3$] and **8**[$HB(C_6F_5)_3$] with one equivalent of *p*-FBN each resulted in a reaction (Scheme 5). According to NMR spectroscopic analysis, the reaction products were unambiguously identified as the hydrosilylated nitriles **16** and **17**, respectively, and the borane–nitrile adduct[11] **18** which were formed in an approximate 1:1 ratio with half an equivalent of unreacted starting material (either **7**[$HB(C_6F_5)_3$] or **8**[$HB(C_6F_5)_3$]) left. $B(C_6F_5)_3$-catalyzed reductive silylation of nitriles to afford imines and amines,[29] and denitrogenation of aromatic nitriles[30] have been reported previously. Notably, the six-membered cyclic siloxane-based cations in combination with hydroborate counterions, which were recently synthesized in our group,[17] did not show a hydrosilylation reaction with *p*-FBN, indicating a higher Lewis acidity of the four-membered cyclic cations and also supporting the previously observed robustness of the siloxane-based systems.[17]

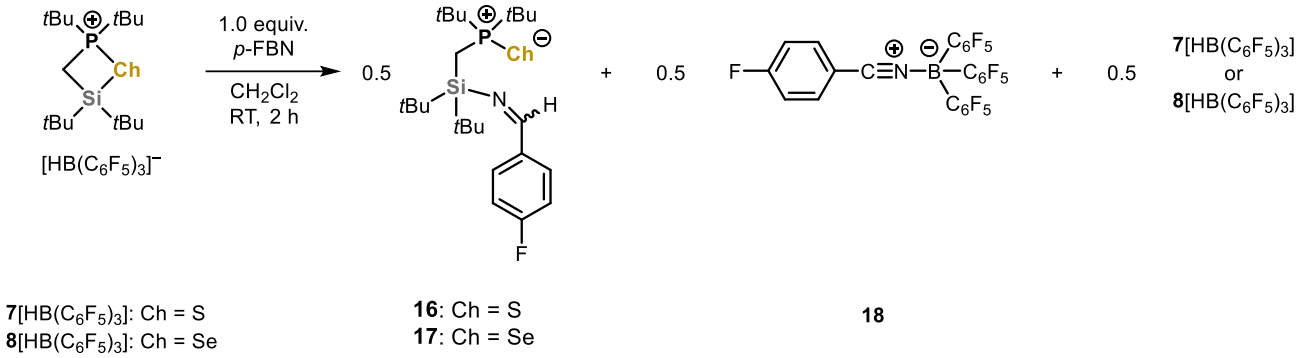

Scheme 5: Hydrosilylation of *para*-fluorobenzonitrile (*p*-FBN) by ion pairs **7**[$HB(C_6F_5)_3$] and **8**[$HB(C_6F_5)_3$]

3.4 Conclusions

Four phosphine chalcogenide-functionalized hydrosilanes (**3**–**6**) (Ch = O, S, Se) having *tert*-butyl or 2,4,6-trimethoxyphenyl (TMP) substituents bound to the silicon atom were synthesized and characterized by single-crystal X-ray structure determination. Only the sulfur and selenium based cyclic cations (**7**–**9**) could be obtained via ring-closing reaction with either $B(C_6F_5)_3$ (access to all three cations **7**–**9**) or $[Ph_3C][B(C_6F_5)_4]$ (access only to cation **9**) and their molecular structures investigated by X-ray crystallography. Thermochemical studies on the ring-opening energy of *tert*-butyl- and methyl-substituted heterocyclic CPChSi cations demonstrated that the steric repulsion between the bulky *tert*-butyl groups on the silicon and phosphorus atoms becomes crucial for the oxygen-based cation in such a way that the Si–O bond was found to be the easiest to open among the all-*tert*-butyl-patterned cations **11**, **7**, and **8**. However, in the absence of significant steric repulsion the stability of the intramolecular Ch–Si interaction indeed decreases as the chalcogenide atom becomes heavier (O > S ≥ Se). Although the small P–C–Si angle could be well balanced by a larger P–O–Si angle in the cyclic product, the unfavorable bending may potentially adversely affect the activation barrier of the P–O-assisted hydride abstraction, thereby complicating access to the oxygen-based cation **11**. ^{31}P NMR spectroscopy shows a small (Ch = S) or a negligible (Ch = Se) effect of the Ch–Si interaction on the ^{31}P NMR chemical shifts toward lower field. However, this effect seems to be greatest in the oxygen case, as assumed by ^{31}P NMR data of the isolated protonated species **10**. Bond polarity parameters from the NBO calculations correspond to a

zwitterionic bond description (P^+–Ch^-) of the phosphine chalcogenide group and show almost no changes in the inductive charge distribution along the P–Ch σ-bond upon ring formation thus assuming the loss of hyperconjugative $n_{Ch} \rightarrow \sigma^*_{P-C}$ stabilization as a measure for the deshielding trend in the ^{31}P NMR spectra (O >> S > Se). Instead, a clearly increasing σ-type $n_{Ch} \rightarrow p_{Si}$ charge transfer (i.e. an increasing covalent character of the Ch–Si bond) in the direction O < S < Se within the cyclic cations was found. As another important result, the found TMP-substituted oxonium species **9**-**o** has potential for further development and electronic optimization en route to a cooperatively working functional cation that might act as a frustrated Lewis pair.

3.5 References

(1) a) Veith, M. Unsaturated Molecules Containing Main Group Metals. *Angew. Chem., Int. Ed., Engl.* **1987**, *26*, 1-14; b) Bertrand, G. Ylidic Four π Electron Four-Membered λ^5-Phosphorus Heterocycles: Electronical Isomers of Heterocyclobutadienes. *Angew. Chem., Int. Ed.* **1998**, *37*, 270-281; c) Sen, S. S.; Khan, S.; Roesky, H. W.; Kratzert, D.; Meindl, K.; Henn, J.; Stalke, D.; Demers, J.-P.; Lange, A. Zwitterionic Si-C-Si-P and Si-P-Si-P Four-Membered Rings with Two-Coordinate Phosphorus Atoms. *Angew. Chem., Int. Ed.* **2011**, *50*, 2322-2325; d) Sen, S. S.; Hey, J.; Eckhardt, M.; Herbst-Irmer, R.; Maedl, E.; Mata, R. A.; Roesky, H. W.; Scheer, M.; Stalke, D. A Stable Cation of a CSi_3P Five-Membered Ring with a Weakly Coordinating Chloride Anion. *Angew. Chem., Int. Ed.* **2011**, *50*, 12510-12513; e) Lehmann, M.; Schulz, A.; Villinger, A. Cyclic Distiba- and Dibismadiazenium Cations. *Angew. Chem., Int. Ed.* **2012**, *51*, 8087-8091; f) Bisai, M. K.; Sharma, V.; Gonnade, R. G.; Sen, S. S. Reactivities of Silaimines with Boranes: From Cooperative B–H Bond Activation to Donor Stabilized Silyl Cation. *Organometallics* **2021**, *40*, 2133-2138.

(2) a) Schumann, H.; Hartmann, U.; Dietrich, A.; Pickardt, J. Intramolecularly Stabilized Organogallium Compounds. *Angew. Chem., Int. Ed., Engl.* **1988**, *27*, 1077-1078; b) Schumann, H.; Hartmann, U.; Wassermann, W.; Dietrich, A.; Görlitz, F. H.; Pohl, L.; Hostalek, M. Intramolecularly Stabilized Organoaluminium, -gallium and -indium Derivatives. Crystal Structures of {*o*-[(Dimethylamino)methyl]phenyl}dimethylgallium and {*o*-[(Diethylamino)methyl]phenyl}dimethylindium. *Chem. Ber.* **1990**, *123*, 2093-2099.

(3) a) Spies, P.; Erker, G.; Kehr, G.; Bergander, K.; Fröhlich, R.; Grimme, S.; Stephan, D. W. Rapid intramolecular heterolytic dihydrogen activation by a four-membered heterocyclic phosphane–borane adduct. *Chem. Commun.* **2007**, 5072-5074; b) Stephan, D. W.; Erker, G. Frustrated Lewis Pairs: Metal-free Hydrogen Activation and More. *Angew. Chem., Int. Ed.* **2010**, *49*, 46-76.

(4) Oestreich, M.; Hermeke, J.; Mohr, J. A unified survey of Si–H and H–H bond activation catalysed by electron-deficient boranes. *Chem. Soc. Rev.* **2015**, *44*, 2202-2220.

(5) For some seminal contributions in silylium chemistry, see: a) Lambert, J. B.; Zhang, S.; Stern, C. L.; Huffman, J. C. Crystal Structure of a Silyl Cation with No Coordination to Anion and Distant Coordination to Solvent. *Science* **1993**, *260*, 1917-1918; b) Reed, C. A.; Xie, Z.; Bau, R.; Benesi, A. Closely Approaching the Silylium Ion (R_3Si^+). *Science* **1993**, *262*, 402-404; c) Duttwyler, S.; Douvris, C.; Fackler, N. L. P.; Tham, F. S.; Reed, C. A.; Baldridge K. K.; Siegel, J. S. C–F Activation of Fluorobenzene by Silylium Carboranes: Evidence for Incipient Phenyl Cation Reactivity. *Angew. Chem., Int. Ed.* **2010**, *49*, 7519-7522; d) Müther, K.; Fröhlich, R.; Mück-Lichtenfeld, C.; Grimme, S.; Oestreich, M. A Unique Transition Metal-Stabilized Silicon Cation. *J. Am. Chem. Soc.* **2011**, *133*, 12442-12444; e) Schäfer, A.; Reißmann, M.; Schäfer, A.; Saak, W.; Haase, D.; Müller, T. A New Synthesis of Triarylsilylium Ions and Their Application in Dihydrogen Activation. *Angew. Chem., Int. Ed.* **2011**, *50*, 12636-12638; f) Merk, A.; Großekappenberg, H.; Schmidtmann, M.; Luecke, M.-P.; Lorent, C.; Driess, M.; Oestreich, M.; Klare, H. F. T.; Müller, T. Single-Electron Transfer Reactions in Frustrated and Conventional Silylium Ion/Phosphane Lewis Pairs. *Angew. Chem., Int. Ed.* **2018**, *57*, 15267-15271; g) Wu, Q.; Irran, E.; Müller, R.; Kaupp, M.; Klare, H. F. T.; Oestreich, M. Characterization of hydrogen-substituted silylium ions in the condensed phase. *Science* **2019**, *365*, 168-172; h) Fernandes, A.; Laye, C.; Pramanik, S.; Palmeira, D.; Pekel, Ö. Ö.; Massip, S.; Schmidtmann, M.; Müller, T.; Robert, F.; Landais, Y. Chiral Memory in Silyl-Pyridinium and Quinolinium Cations. *J. Am. Chem. Soc.* **2020**, *142*, 564-572; i) Wu, Q.; Roy, A.; Wang, G.; Irran, E.; Klare, H. F. T.; Oestreich, M. Synthesis of a Counteranion-Stabilized Bis(silylium) Ion. *Angew. Chem., Int. Ed.* **2020**, *59*, 10523-10526.

(6) a) Panisch, R.; Bolte, M.; Müller, T. Hydrogen- and Fluorine-Bridged Disilyl Cations and Their Use in Catalytic C–F Activation. *J. Am. Chem. Soc.* **2006**, *128*, 9676-9682; b) Douvris, C.; Ozerov, O. V. Hydrodefluorination of Perfluoroalkyl Groups Using Silylium-Carborane Catalysts. *Science* **2008**, *321*, 1188-1190; c) Klare, H. F. T.; Bergander, K.; Oestreich, M. Taming the Silylium Ion for Low-Temperature Diels–Alder Reactions. *Angew. Chem., Int. Ed.* **2009**, *48*, 9077-9079; d) Allemann, O.; Duttwyler, S.; Romanato, P.; Baldridge, K. K.; Siegel, J. S. Proton-Catalyzed, Silane-Fueled Friedel-Crafts Coupling of Fluoroarenes. *Science* **2011**, *332*, 574-577; e) Schulz, A.;

Villinger, A. “Tamed” Silylium Ions: Versatile in Catalysis. *Angew. Chem., Int. Ed.* **2012**, *51*, 4526-4528; f) Gatzenmeier, t.; van Gemmeren, M.; Xie, Y.; Höfler, D.; Leutzsch, M.; List, B. Asymmetric Lewis acid organocatalysis of the Diels–Alder reaction by a silylated C–H acid. *Science* **2016**, *351*, 949-952.

(7) a) Dilman, A. D.; Ioffe, S. L. Carbon–Carbon Bond Forming Reactions Mediated by Silicon Lewis Acids. *Chem. Rev.* **2003**, *103*, 733-772; b) Klare, H. F. T.; Oestreich, M. Silylium ions in catalysis. *Dalton Trans.* **2010**, *39*, 9176-9184; c) Shaykhutdinova, P.; Keess, S.; Oestreich, M. Organosilicon Chemistry: Novel Approaches and Reactions (Eds.: Hiyama, T.; Oestreich, M.), Wiley-VCH, Weinheim, Germany, 2020, pp. 131-170; d) Siegel, J. S. Silylium ions: from controversial beginnings to useful catalysts. *Nat. Rev. Chem.* **2020**, *4*, 4-5; e) Walker, J. C. L.; Klare, H. F. T.; Oestreich, M. Cationic silicon Lewis acids in catalysis. *Nat. Rev. Chem.* **2020**, *4*, 54-62; f) Klare, H. F. T.; Albers, L.; Süsse, L.; Keess, S.; Müller, T.; Oestreich, M. Silylium Ions: From Elusive Reactive Intermediates to Potent Catalysts. *Chem. Rev.* **2021**, *121*, 5889-5985.

(8) a) Rohde, V. H. G.; Pommerening, P.; Klare, H. F. T.; Oestreich, M. Intramolecularly Sulfur-Stabilized Silicon Cations as Lewis Acid Catalysts. *Organometallics* **2014**, *33*, 3618-3628; b) Rohde, V. H. G.; Müller, M. F.; Oestreich, M. Intramolecularly Sulfur-Stabilized Silicon Cations with Chiral Binaphthyl Backbones: Synthesis of Three Different Motifs and Their Application in Enantioselective Diels–Alder Reactions. *Organometallics* **2015**, *34*, 3358-3373; c) Shaykhutdinova, P.; Oestreich, M. Enantioselective Diels–Alder Reactions of Cyclohexa-1,3-diene and Chalcones Catalyzed by Intramolecular Silicon–Sulfur Lewis Pairs as Chiral Lewis Acids. *Organometallics* **2016**, *35*, 2768-2771.

(9) a) Reißmann, M.; Schäfer, A.; Panisch, R.; Schmidtmann, M.; Bolte, M.; Müller, T. Cyclic Silylated Onium Ions of Group 15 Elements. *Inorg. Chem.* **2015**, *54*, 2393-2402.

(10) Kordts, N.; Künzler, S.; Rathjen, S.; Sieling, T.; Großekappenberg, H.; Schmidtmann, M.; Müller, T. Silyl Chalconium Ions: Synthesis, Structure and Application in Hydrodefluorination Reactions *Chem.–Eur. J.* **2017**, *23*, 10068-10079.

(11) Künzler, S.; Rathjen, S.; Merk, A.; Schmidtmann, M.; Müller, T. An Experimental Acidity Scale for Intramolecularly Stabilized Silyl Lewis Acids. *Chem.–Eur. J.* **2019**, *25*, 15123-15130.

(12) Merk, A.; Bührmann, L.; Kordts, N.; Görtemaker, K.; Schmidtmann, M.; Müller, T. Intramolecular Halo Stabilization of Silyl Cations — Silylated Halonium- and Bis-Halo-Substituted Siliconium Borates. *Chem.–Eur. J.* **2021**, *27*, 3496-3503.

(13) a) Devillard, M.; de Bruin, B.; Siegler, M. A.; van der Vlugt, J. I. Transition-Metal-Free Cleavage of CO. *Chem.–Eur. J.* **2017**, *23*, 13628-13632; b) Dajnak, A.; Maerten, E.; Saffon-Merceron, N.; Baceiredo, A.; Kato, T. Synthesis of Norbornene-Based Phosphine-Stabilized Silylium Ions Behaving as Masked Frustrated Lewis Pairs. *Organometallics* **2020**, *39*, 3403-3412; c) Kumar, N.; Laye, C.; Robert, F.; Landais, Y. Quinoline-Based Silylium Ions: Synthesis, Structure and Lewis Acidity. *Eur. J. Org. Chem.* **2021**, 3613-3621; d) Fernandes, A. J.; Robert, F.; Landais, Y.; Künzler, S.; Müller, T. On the Origin of the Non-Planarity in Biarylsilyloxonium Ions. *Chem.–Eur. J.* **2021**, *27*, 15496-15500; e) Dajnak, A.; Özpinar, G. A.; Lenk, R.; Saffon-Merceron, N.; Baceiredo, A.; Kato, T.; Müller, T.; Maerten, E. Norbornene based-sulfide-stabilized silylium ions: synthesis, structure and application in catalysis. *Dalton Trans.* **2022**, *51*, 1407-1414.

(14) a) Ducos, P.; Liautard, V.; Robert, F.; Landais, Y. Chiral Memory in Silylium Ions. *Chem.–Eur. J.* **2015**, *21*, 11573-11578; b) Fernandes, A.; Laye, C.; Pramanik, S.; Palmeira, D.; Pekel, Ö. Ö.; Massip, S.; Schmidtmann, M.; Müller, T.; Robert, F.; Landais, Y. Chiral Memory in Silyl-Pyridinium and Quinolinium Cations. *J. Am. Chem. Soc.* **2020**, *142*, 564-572; c) Künzler, S.; Rathjen, S.: Rüger, K.; Würdemann, M. S.; Wernke, M.; Tholen, P.; Girschik, C.; Schmidtmann, M.; Landais, Y.; Müller, T. Chiral Chalcogenyl-Substituted Naphthyl- and Acenaphthyl-Silanes and Their Cations. *Chem.–Eur. J.* **2020**, *26*, 16441-16449.

(15) Fontana, N.; Espinosa-Jalapa, N. A.; Seidl, M.; Bauer, J. O. Easy Access to Enantiomerically Pure Heterocyclic Silicon-Chiral Phosphonium Cations and the Matched/Mismatched Case of Dihydrogen Release. *Chem.–Eur. J.* **2021**, *27*, 2649-2653.

(16) a) Müller, J. F. K.; Neuburger, M.; Spingler, B. Structural Investigation of a Dilithiated Phosphonate in the Solid State. *Angew. Chem., Int. Ed.* **1999**, *38*, 92-94; b) Molitor, S.; Gessner, V. H. Alkali Metal Carbenoids: A Case of Higher Stability of the Heavier Congeners. *Angew. Chem., Int. Ed.* **2016**, *55*, 7712-7716.

(17) Fontana, N.; Espinosa-Jalapa, N. A.; Seidl, M.; Bauer, J. O. Hidden silylium-type reactivity of a siloxane-based phosphonium**–**hydroborate ion pair. *Chem. Commun.* **2022**, *58*, 2144-2147.

(18) Fink, L.; Samigullin, K.; Bodach, A.; Alig, E.; Wagner, M.; Lerner, H.-W. Donor-unsupported Phosphanylmethanides Li[CH2P*R*$_2$] (*R* = *t*Bu, Ph) – Crystal Structure of Li[CH$_2$P*t*Bu$_2$] Solved by XRPD and DFT-D Calculations. *Z. Anorg. Allg. Chem.* **2016**, *642*, 282-287.

(19) Seyferth, D.; Friedrich, H.; Krska, S. W. Radical-Initiated Hydrosilylation-Cyclization Reactions of Bis(vinyldimethylsilyl) Compounds, CH$_2$=CH(CH$_3$)$_2$SiXSi(CH$_3$)$_2$CH=CH$_2$ (X = O, CH$_2$, NH, NCH$_3$, NSi(CH$_3$)$_3$. *Z. Naturforsch.* **1994**, *49b*, 1818-1826.

(20) Denhof, A.; Olaru, M.; Lork, E.; Mebs, S.; Chęcińska, L.; Beckmann, J. Silyl Cations Stabilized by Pincer Type Ligands with Adjustable Donor Atoms. *Eur. J. Inorg. Chem.* **2020**, 4093-4110.

(21) Letcher, J. H.; van Wazer, J. R. Theoretical Interpretation of ^{31}P NMR Chemical Shifts. I. *J. Chem. Phys.* **1966**, *44*, 815-829.

(22) a) Reed, A. E.; Schleyer, P. v. R. Chemical Bonding in Hypervalent Molecules. The Dominance of Ionic Bonding and Negative Hyperconjugation over d-Orbital Participation. *J. Am. Chem. Soc.* **1990**, *112*, 1434-1445; b) Chesnut, D. B. An Ab Initio Nuclear Magnetic Resonance and Atoms-in-Molecules Study of the PO Bond in Phosphine Oxides. *J. Am. Chem. Soc.* **1998**, *120*, 10504-10510; c) Kuivalainen, T., El-Bahraoui, J.; Uggla, R.; Kostiainen, R.; Sundberg, M. R. Correlation of the ^{31}P NMR Chemical Shift with the Position of Bond Critical Points in Some Phosphorothionates. *J. Am. Chem. Soc.* **2000**, *122*, 8073-8074.

(23) Frisch, M. J.; Trucks, G. W.; Schlegel, H. B.; Scuseria, G. E.; Robb, M. A.; Cheeseman, J. R.; Scalmani, G.; Barone, V.; Mennucci, B.; Petersson, G. A.; Nakatsuji, H.; Caricato, M.; Li, X.; Hratchian, H. P.; Izmaylov, A. F.; Bloino, J.; Zheng, G.; Sonnenberg, J. L.; Hada, M.; Ehara, M.; Toyota, K.; Fukuda, R.; Hasegawa, J.; Ishida, M.; Nakajima, T.; Honda, Y.; Kitao, O.; Nakai, H.; Vreven, T.; Montgomery, Jr., J. A.; Peralta, J. E.; Ogliaro, F.; Bearpark, M.; Heyd, J. J.; Brothers, E.; Kudin, K. N.; Staroverov, V. N.; Keith, T.; Kobayashi, R.; Normand, J.; Raghavachari, K.; Rendell, A.; Burant, J. C.; Iyengar, S. S.; Tomasi, J.; Cossi, M.; Rega, N.; Millam, J. M.; Klene, M.; Knox, J. E.; Cross, J. B.; Bakken, V.; Adamo, C.; Jaramillo, J.; Gomperts, R.; Stratmann, R. E.; Yazyev, O.; Austin, A. J.; Cammi, R.; Pomelli, C.; Ochterski, J. W.; Martin, R. L.; Morokuma, K.; Zakrzewski, V. G.; Voth, G. A.; Salvador, P.; Dannenberg, J. J.; Dapprich, S.; Daniels, A. D.; Farkas, O.; Foresman, J. B.; Ortiz, J. V.; Cioslowski, J.; Fox, D. J. *Gaussian 09*. Revision E.01; Gaussian, Inc.: Wallingford, CT, USA, 2013.

(24) Kinder, T. A.; Pior, R.; Blomeyer, S.; Neumann, B.; Stammler, H.-G.; Mitzel, N. W. A Neutral Germanium/Phosphorus Frustrated Lewis Pair and Its Contrasting Reactivity Compared to Its Silicon Analogue. *Chem.–Eur. J.* **2019**, *25*, 5899-5903.

(25) Weinhold, F.; Landis, C. R. *Valency and Bonding: A Natural Bond Orbital Donor-Acceptor Perspective*; Cambridge University Press: Cambridge, U.K., 2005.

(26) a) Weinhold, F.; West, R. The Nature of the Silicon–Oxygen Bond. *Organometallics* **2011**, *30*, 5815-5824; b) Weinhold, F.; West, R. Hyperconjugative Interactions in Permethylated Siloxanes and Ethers: The Nature of the SiO Bond. *J. Am. Chem. Soc.* **2013**, *135*, 5762-5767; c) Bauer, J. O. Influence of Amino Functions on the Coordination Ability of Silyl Ethers and Disiloxanes. *Organometallics* **2022**, *41*, 321-327.

(27) a) Kutzelnigg, W. Chemical Bonding in Higher Main Group Elements. *Angew. Chem., Int. Ed. Engl.* **1984**, *23*, 272-295; b) Leusser, D.; Henn, J.; Kocher, N.; Engels, B.; Stalke, D. S=N versus S^{+}**–**N^{-}: An Experimental and Theoretical Charge Density Study. *J. Am. Chem. Soc.* **2004**, *126*, 1781-1793; c) Schmøkel, M. S.; Cenedese, S.; Overgaard, J.; Jørgensen, M. R. V.; Chen, Y.-S.; Gatti, C.; Stalke, D.; Iversen, B. B. Testing the Concept of Hypervalency: Charge Density Analysis of K_2SO_4. *Inorg. Chem.* **2012**, *51*, 8607-8616.

(28) Kocher, N.; Henn, J.; Gostevskii, B.; Kost, D.; Kalikhman, I.; Engels, B.; Stalke, D. Si–E (E = N, O, F) Bonding in a Hexacoordinated Silicon Complex: New Facts from Experimental and Theoretical Charge Density Studies. *J. Am. Chem. Soc.* **2004**, *126*, 5563-5568.

(29) Gandhamsetty, N.; Jeong, J.; Park, J.; Park, S.; Chang, S. Boron-Catalyzed Silylative Reduction of Nitriles in Accessing Primary Amines and Imines. *J. Org. Chem.* **2015**, *80*, 7281-7287.

(30) Peng, Y.; Oestreich, M. $B(C_6F_5)_3$-Catalyzed Reductive Denitrogenation of Benzonitrile Derivatives. *Org. Lett.* **2022**, *24*, 2940-2943.

3.6 Synthesis and Characterizations

3.6.1 General remarks

All experiments were performed in an inert atmosphere of purified nitrogen by using standard Schlenk techniques or an MBraun Unilab 1200/780 glovebox. Glassware was heated at 600 °C prior to use. Dichloromethane (DCM), hexane, pentane, tetrahydrofuran (THF), and toluene were dried and degassed with an MBraun SP800 solvent purification system. *n*-Butyllithium (2.5 M or 1.6 M solution in hexane, Merck KGaA), *tert*-butyllithium (1.6 M solution in pentane, Merck KGaA), di-*tert*-butylchlorosilane (97%, Merck KGaA), di-*tert*-butylmethylphosphine (97%, Merck KGaA), trichlorosilane (99%, Merck KGaA), 1,3,5-trimethoxybenzene (≥99%, Merck KGaA), and sulfur (99%, Merck KGaA) were used as received without further purification. (Di-*tert*-butylphosphanyl)methyllithium,[1,2] di-*tert*-butylmethylphosphine sulfide,[3] tris(pentafluorophenyl)borane,[4] and tritylium tetrakis(pentafluorophenyl)borate[5] were synthesized according to reported literature procedures. C_6D_6, CD_2Cl_2, and 1,2-dichlorobenzene (1,2-$C_6H_4Cl_2$) used for NMR spectroscopy were dried over 3 Å molecular sieves and degassed by a standard freeze-pump-thaw procedure. NMR spectra were either recorded on a Bruker Avance 300 (300.13 MHz), a Bruker Avance 400 (400.13 MHz) or on a Bruker Avance III HD 400 (400.13 MHz) at 25 °C. Chemical shifts (δ) are reported in parts per million (ppm). ^{1}H and $^{13}C\{^{1}H\}$ NMR spectra are referenced to tetramethylsilane ($SiMe_4$, δ = 0.0 ppm) as external standard, with the deuterium signal of the solvent serving as internal lock and the residual solvent signal as an additional reference. $^{11}B\{^{1}H\}$, $^{19}F\{^{1}H\}$, $^{31}P\{^{1}H\}$, $^{77}Se\{^{1}H\}$, and $^{29}Si\{^{1}H\}$ NMR spectra are referenced to $BF_3{\cdot}OEt_2$, $CFCl_3$, 85% H_3PO_4, $SeMe_2$, and $SiMe_4$, respectively. For the assignment of the multiplicities, the following abbreviations are used: s = singlet, bs = broad singlet, d = doublet, t = triplet, bq = broad quartet, m = multiplet. For simplicity, multiplets of order higher than one are described by approximating them to the closest first-order type. High-resolution mass spectrometry was carried out on a Jeol AccuTOF GCX and an Agilent Q-TOF 6540 UHD spectrometer. Elemental analyses were performed on a Vario MICRO cube apparatus.

3.6.2 Synthesis of compound 2

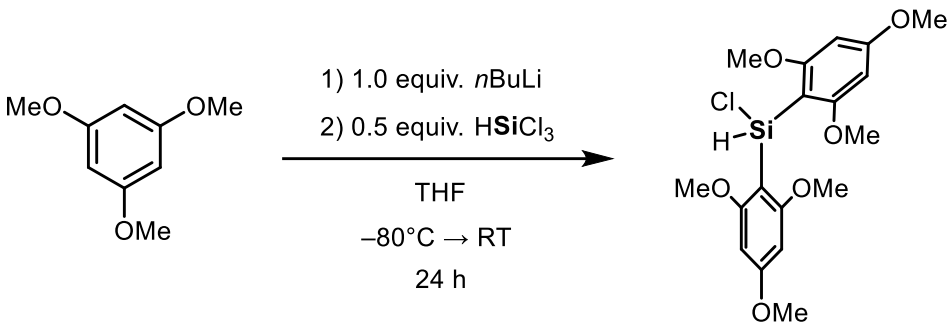

2

n-Butyllithium (4.0 mL of a 2.5 M solution in hexane, 10 mmol, 1.0 equiv.) was slowly added to a solution of 1,3,5-trimethoxybenzene (1.68 g, 10 mmol, 1.0 equiv.) in 100 mL THF at **–** 80 °C. The reaction mixture was stirred in the cooling bath for 2 h and further 30 min at room temperature. Then, all volatiles were removed *in vacuo*. The resulting yellowish powder was washed once with 50 mL of hexane and dried *in vacuo*. Then, the powder was dissolved in 100 mL THF and cooled to **–**80°C. Trichlorosilane (0.505 mL, 5.0 mmol, 0.5 equiv.) was added to this solution and the mixture stirred for 24 h at room temperature. Then, all volatiles were removed *in vacuo*. The resulting solid was suspended in DCM and filtered using a P3-Frit with added Celite®. All volatiles of the filtrate were removed *in vacuo* and the resulting crude oil purified *via* Kugelrohr distillation (200 – 215 °C oven temperature, $1.3 \cdot 10^{-3}$ mbar). Compound **2** was obtained as a colorless oil. Yield: 1.2 g (3.0 mmol, 60%).

^{1}H NMR (400.13 MHz, C_6D_6, 298 K): δ 6.67 (s, 1H, Si*H*), 6.02 (s, 4H, CH_{meta}), 3.33 [s, 6H, C(OCH_3)$_{para}$], 3.32 [s, 12H, C(OCH_3)$_{ortho}$].

^{13}C{^{1}H} NMR (100.61 MHz, C_6D_6, 298 K): δ 166.7 [s, *C*(OCH$_3$)$_{ortho}$], 164.4 [s, *C*(OCH$_3$)$_{para}$], 103.2 (s, *C*$_{ipso}$), 90.8 (s, *C*H$_{meta}$), 55.0 [s, C(O*C*H$_3$)$_{ortho}$], 54.4 [s, C(O*C*H$_3$)$_{para}$].

^{29}Si{^{1}H} NMR (79.49 MHz, C_6D_6, 298 K): δ –26.0 (s, *Si*H).

HR(EI)-MS: Calcd *m/z* for $C_{18}H_{23}ClO_6Si$ $[M]^+$: 398.0946. Found: 398.0934.

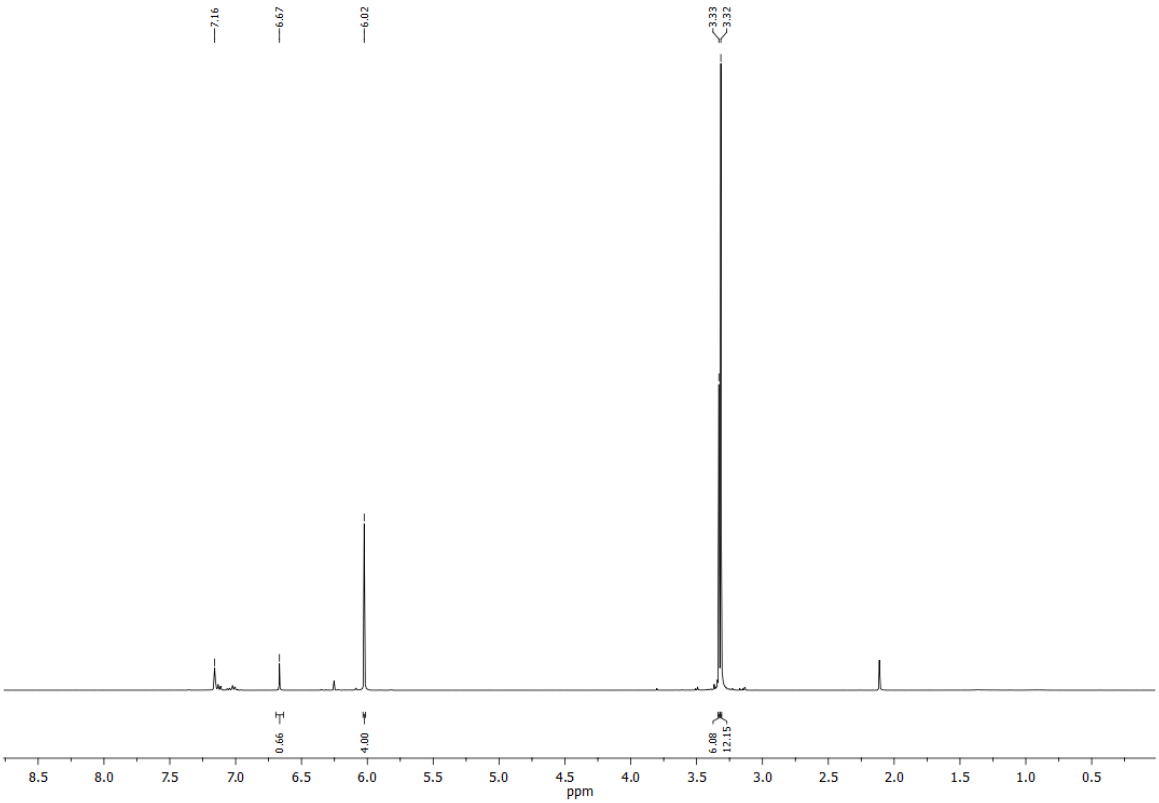

Figure S1: ^{1}H NMR (400.13 MHz, C_6D_6, 298 K) of compound **2**. TMP = 2,4,6-trimethoxyphenyl.

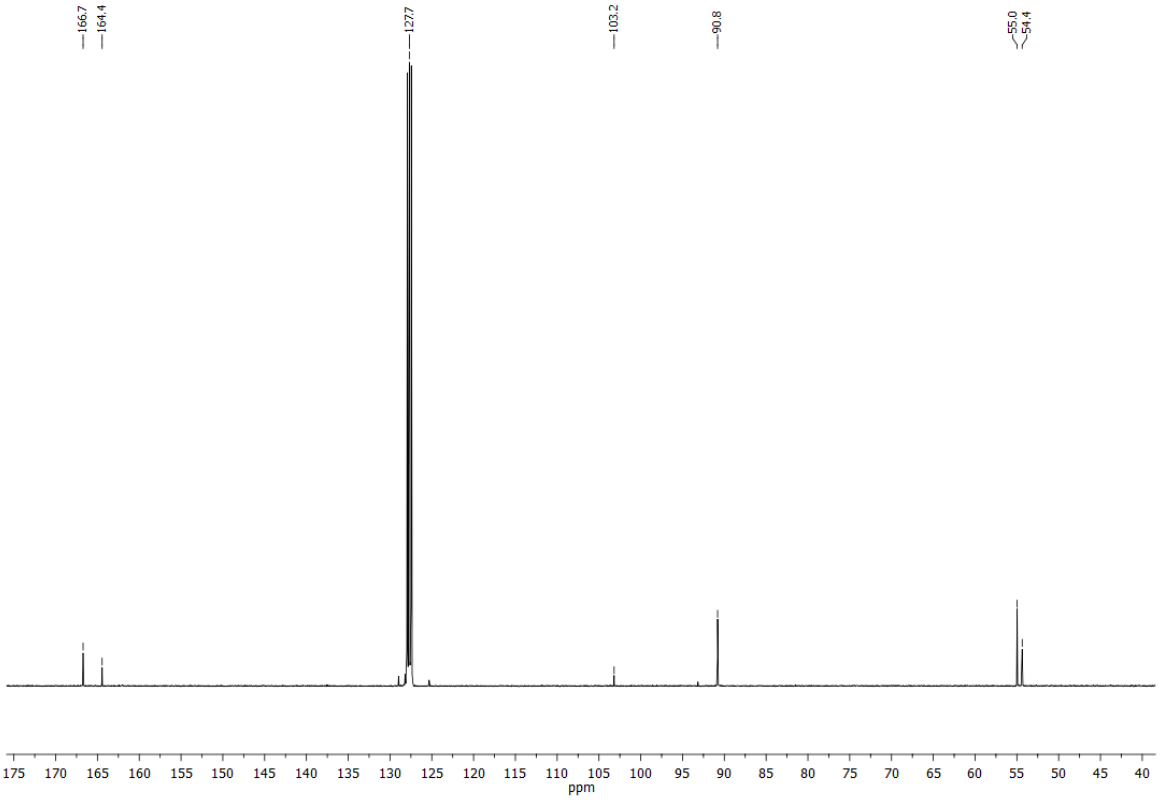

Figure S2: $^{13}C\{^{1}H\}$ NMR (100.61 MHz, C_6D_6, 298 K) of compound **2**.

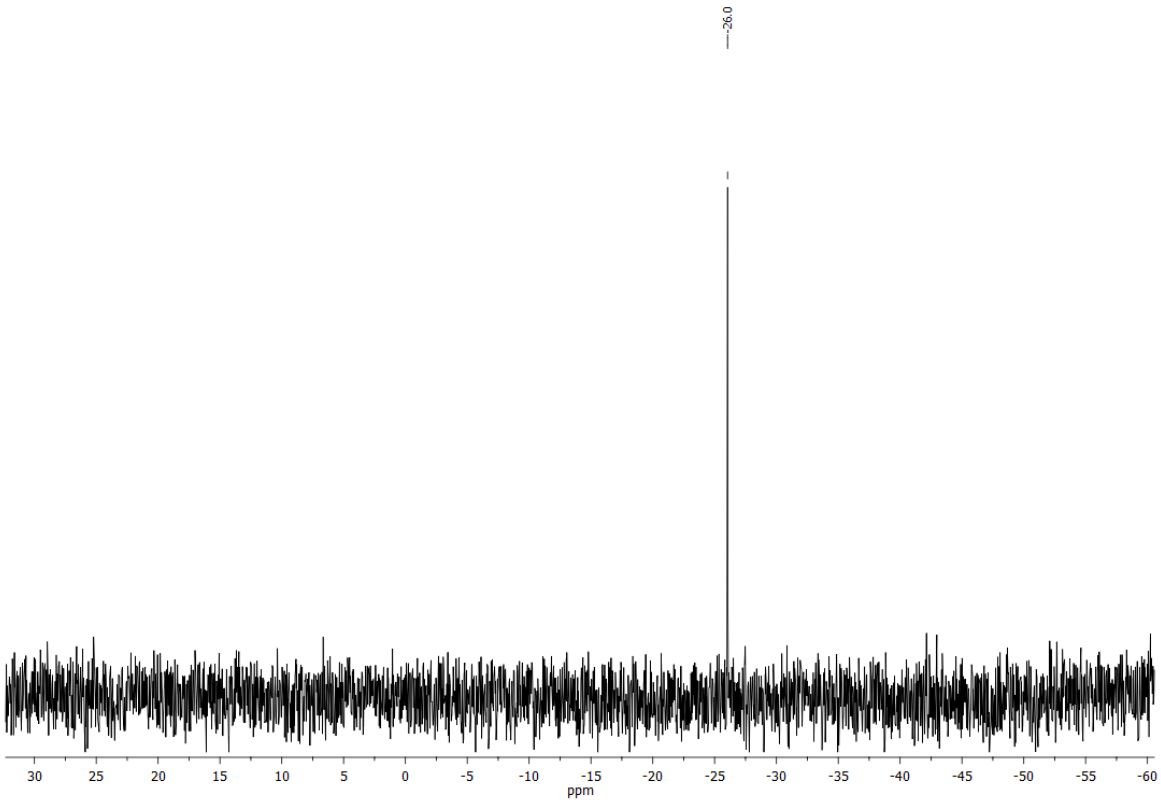

Figure S3: $^{29}Si\{^{1}H\}$ NMR (79.49 MHz, C_6D_6, 298 K) of compound **2**.

3.6.3 Synthesis of compound 3

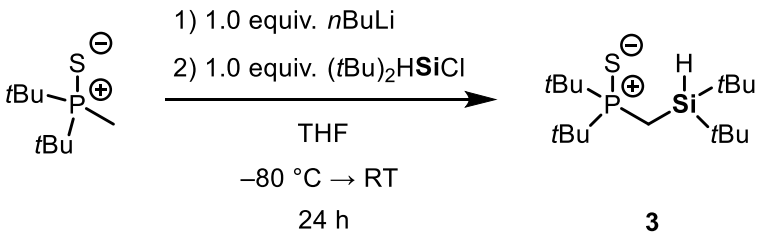

3

n-Butyllithium (5.15 mL of a 1.6 M solution in hexane, 8.24 mmol, 1.2 equiv.) was slowly added to a solution of di-*tert*-butylmethylphosphine sulfide (1.44 g, 7.49 mmol, 1.1 equiv.) in 15 mL pentane at 0 °C. The reaction mixture was allowed to stir for 24 h at room temperature. Then, the solvent was removed *via* filtration and the remaining white powder dried *in vacuo*. The powder was dissolved in 20 mL THF and cooled to **–**80 °C. Then, di-*tert*-butylchlorosilane (1.33 g, 7.42 mmol, 1.0 equiv.) was added, the solution allowed to warm to room temperature and stirred for 24 h. Then, all volatiles were removed *in vacuo*, the residue suspended in hot hexane and filtered. Crystals suitable for single-crystal X-ray diffraction analysis were obtained from the filtrate at **–**30 °C. The crystalline compound **3** was isolated *via* filtration, washed twice with 5 mL pentane and dried *in vacuo*. Yield: 2.1 g (6.3 mmol, 85%).

^{1}H NMR (400.13 MHz, C_6D_6, 298 K): δ 4.16 (m, 1H, Si*H*), 1.24 {d, $^{3}J_{P-H}$ = 14.6 Hz, 18H, PS[C(C*H*$_3$)$_3$]$_2$}, 1.23 (d, $^{2}J_{P-H}$ = 14.4 Hz, 2H, SiC*H*$_2$PS), 1.14 {s, 18H, Si[C(C*H*$_3$)$_3$]$_2$}.

^{13}C{^{1}H} NMR (100.61 MHz, C_6D_6, 298 K): δ 39.1 {d, $^{1}J_{C-P}$ = 43.1 Hz, PS[*C*(CH$_3$)$_3$]$_2$}, 30.0 {s, Si[C(*C*H$_3$)$_3$]$_2$}, 28.0 {d, $^{2}J_{C-P}$ = 1.6 Hz, PS[C(*C*H$_3$)$_3$]$_2$}, 19.5 {d, $^{3}J_{C-P}$ = 2.5 Hz, Si[*C*(CH$_3$)$_3$]$_2$}, 4.0 (d, $^{1}J_{C-P}$ = 32.5 Hz, Si*C*H$_2$PS).

^{29}Si{^{1}H} NMR (79.49 MHz, C_6D_6, 298 K): δ 7.74 (d, $^{2}J_{Si-P}$ = 8.4 Hz, *Si*CH$_2$PS).

^{31}P{^{1}H} NMR (162.04 MHz, C_6D_6, 298 K): δ 77.4 (s, SiCH$_2$*P*S).

EI-MS: Calcd *m/z* for $C_{17}H_{39}PSSi$ $[M]^{+\bullet}$: 334.23. Found: 277.1594 $[M - C_4H_9]^{+\bullet}$.

CHN Analysis: Calcd for $C_{17}H_{39}PSSi$: C, 61.01; H, 11.75. Found: C, 61.06; H, 11.52.

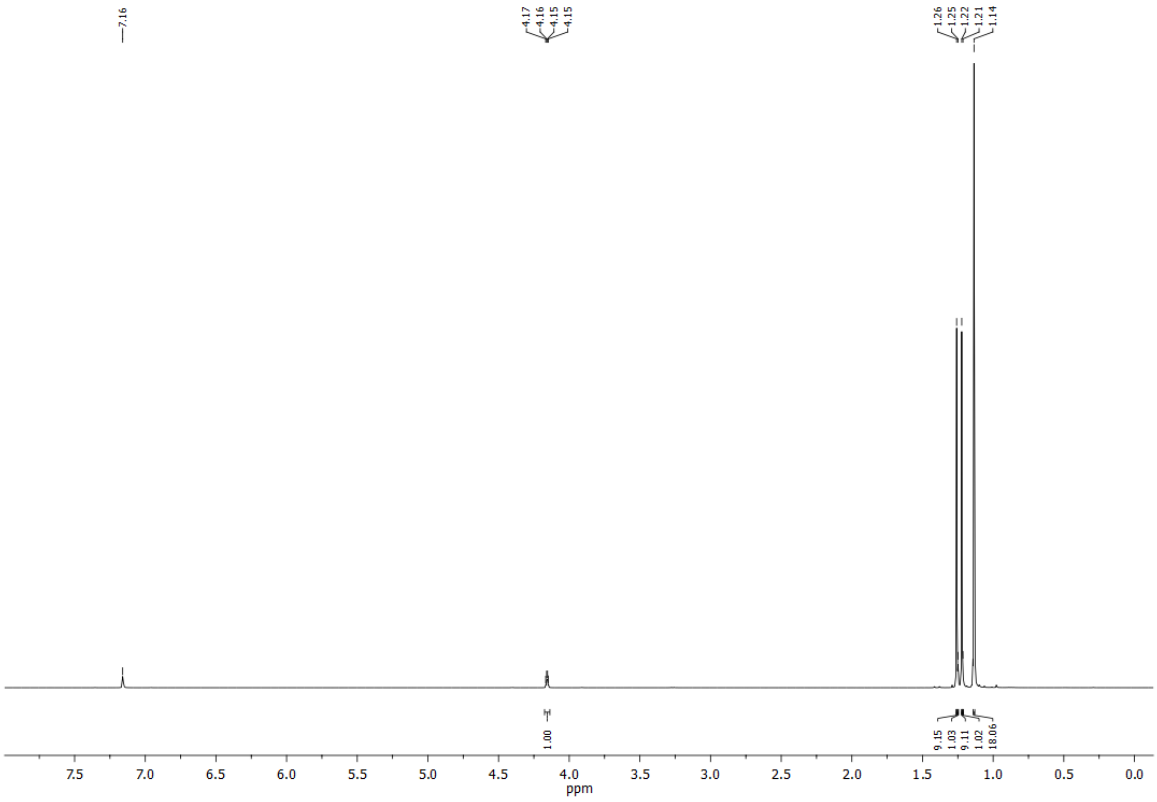

Figure S4: ^{1}H NMR (400.13 MHz, C_6D_6, 298 K) of compound **3**.

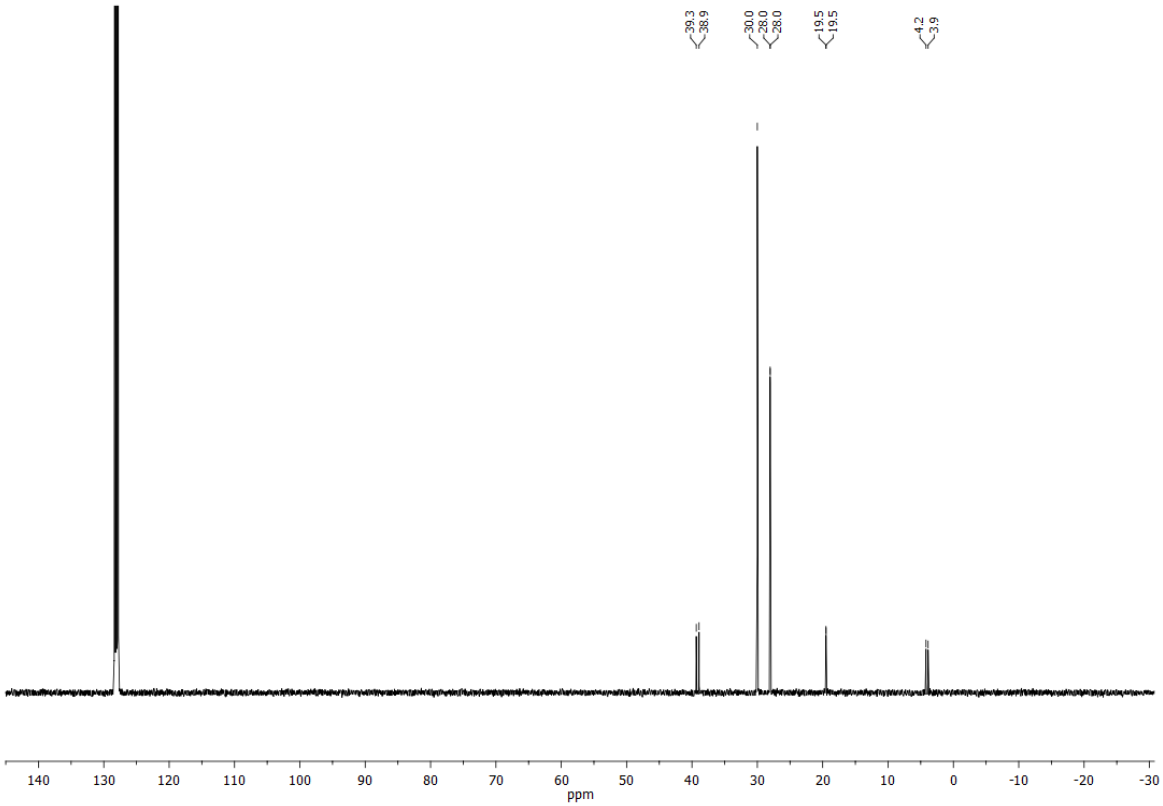

Figure S5: $^{13}C\{^{1}H\}$ NMR (100.61 MHz, C_6D_6, 298 K) of compound **3**.

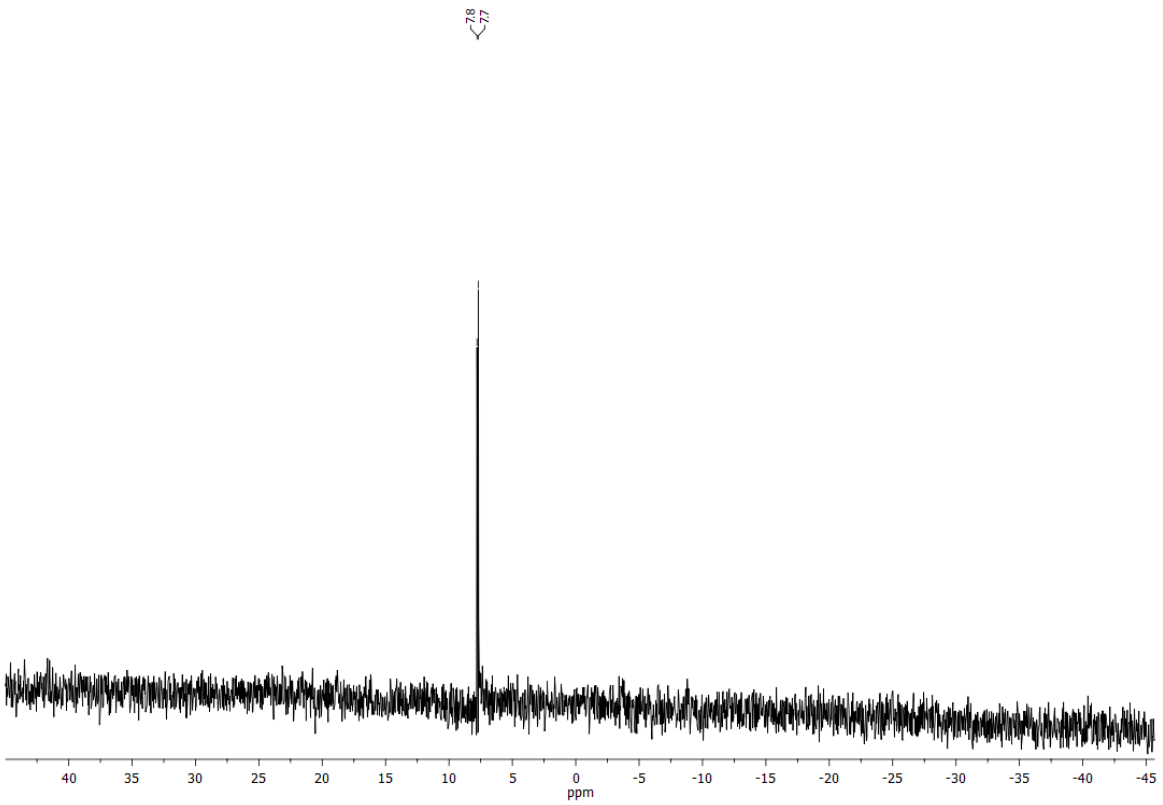

Figure S6: $^{29}Si\{^{1}H\}$ NMR (C_6D_6, 298 K) spectrum of compound **3.**

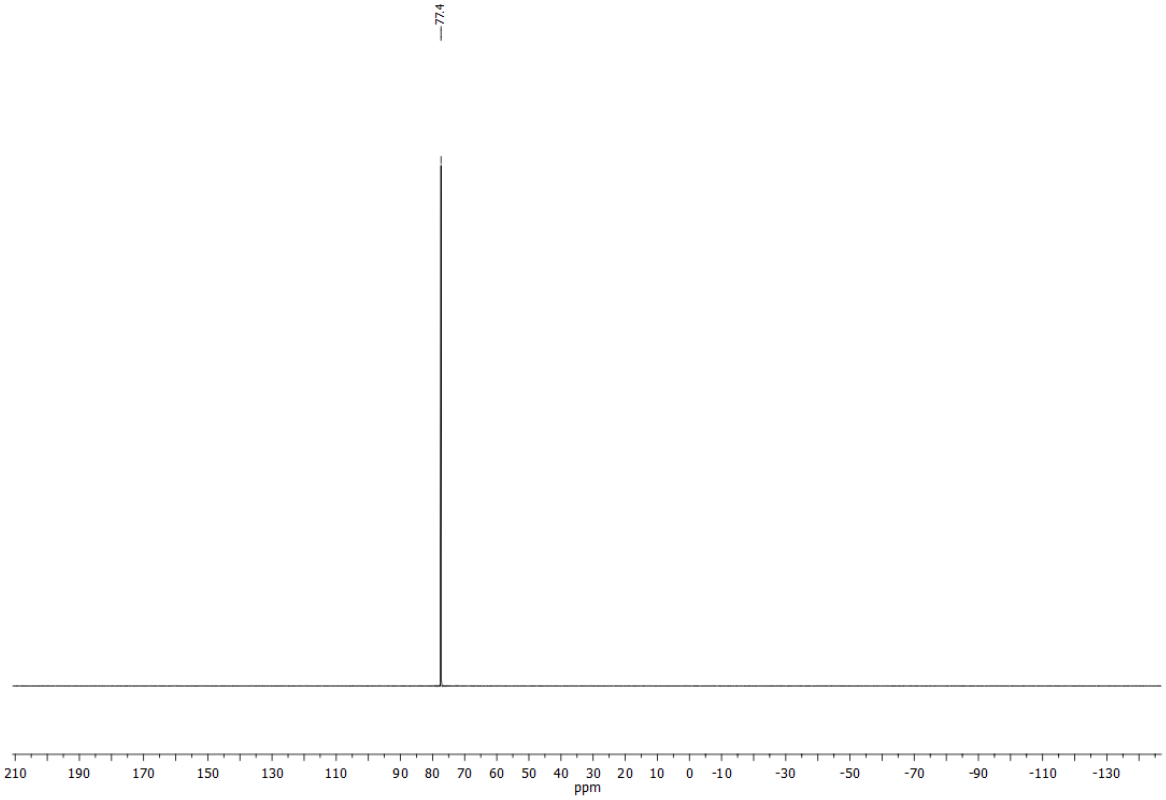

Figure S7: $^{31}P\{^{1}H\}$ NMR (162.04 MHz, C_6D_6, 298 K) of compound **3**.

3.6.4 Synthesis of compound 4

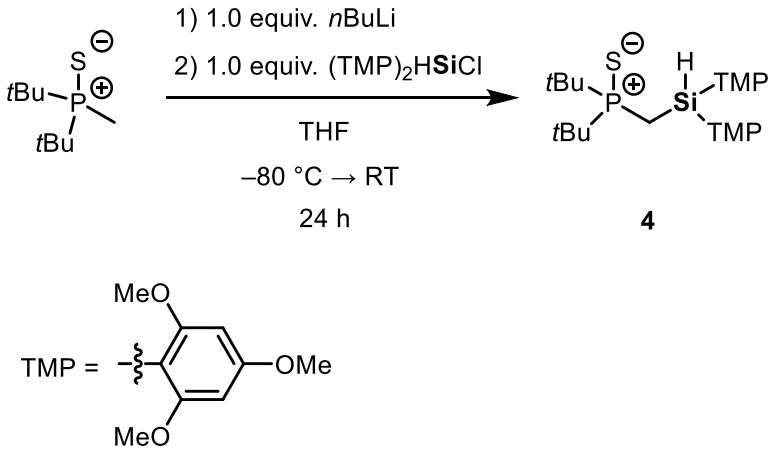

n-Butyllithium (0.33 mL of a 2.5 M solution in hexane, 0.752 mmol, 1.0 equiv.) was slowly added to a solution of di-*tert*-butylmethylphosphine sulfide (144 mg, 0.752 mmol, 1.0 equiv.) in 15 mL pentane at 0 °C. The reaction mixture was allowed to stir for 4 h at room temperature. Then, the solvent was removed *via* filtration and the remaining white powder dried *in vacuo*. The powder was dissolved in 10 mL THF and cooled to **–**80 °C. In a separate Schlenk flask, compound **2** (300 mg, 0.752 mmol, 1.0 equiv.) was dissolved in 5

mL THF and then slowly added to the previously prepared solution of the powder in THF. The reaction mixture was stirred for 24 h at room temperature. Then, all volatiles were removed *in vacuo*. The oily residue was washed twice with 10 mL of hexane. The resulting white powder was suspended in DCM and filtered over a P3-frit with added Celite®. The solvent of the filtrate was removed to obtain compound **4** as a white powder. Yield: 323 mg (0.58 mmol, 77%). Colorless crystals of compound **4** suitable for single-crystal X-ray diffraction analysis were obtained by recrystallization from hot toluene.

^{1}H NMR (400.13 MHz, C_6D_6, 298 K): δ 6.14 (dd, $^{3}J_{P-H}$ = 5.6 Hz, $^{3}J_{H-H}$ = 3.0 Hz, 1H, Si*H*), 6.07 (s, 4H, C*H*$_{meta}$), 3.40 [s, 12H, C(OC*H*$_3$)$_{ortho}$], 3.35 [s, 6H, C(OC*H*$_3$)$_{para}$], 2.35 (dd, $^{2}J_{P-H}$ = 12.8 Hz, $^{3}J_{H-H}$ = 3.0 Hz, 2H, SiC*H*$_2$PS), 1.35 {d, $^{3}J_{P-H}$ = 14.3 Hz, 18H, PS[C(C*H*$_3$)$_3$]$_2$}.

^{13}C{^{1}H} NMR (100.61 MHz, C_6D_6, 298 K): δ 166.7 [s, *C*(OCH$_3$)$_{ortho}$], 163.9 [s, *C*(OCH$_3$)$_{para}$], 105.2 (s, *C*$_{ipso}$), 91.3 (s, *C*H$_{meta}$), 55.3 [s, C(O*C*H$_3$)$_{ortho}$], 54.7 [s, C(O*C*H$_3$)$_{para}$], 38.3 {d, $^{1}J_{C-P}$ = 42.6 Hz, PS[*C*(CH$_3$)$_3$]$_2$}, 27.9 {d, $^{2}J_{C-P}$ = 1.7 Hz, PS[C(*C*H$_3$)$_3$]$_2$}, 8.7 (d, $^{1}J_{C-P}$ = 36.0 Hz, Si*C*H$_2$PS).

^{29}Si{^{1}H} NMR (79.49 MHz, C_6D_6, 298 K): δ –40.1 (d, $^{2}J_{Si-P}$ = 5.2 Hz, *Si*CH$_2$PS).

^{31}P{^{1}H} NMR (162.04 MHz, C_6D_6, 298 K): δ 78.1 (s, SiCH$_2$*P*S).

HR(ESI)-MS: Calcd *m/z* for $C_{27}H_{43}NaO_6PSSi$ [M + Na]$^+$: 577.2293. Found: 577.2185.

CHN Analysis: Calcd for $C_{27}H_{43}O_6PSSi$: C, 58.46; H, 7.81. Found: C, 57.77; H, 7.80.

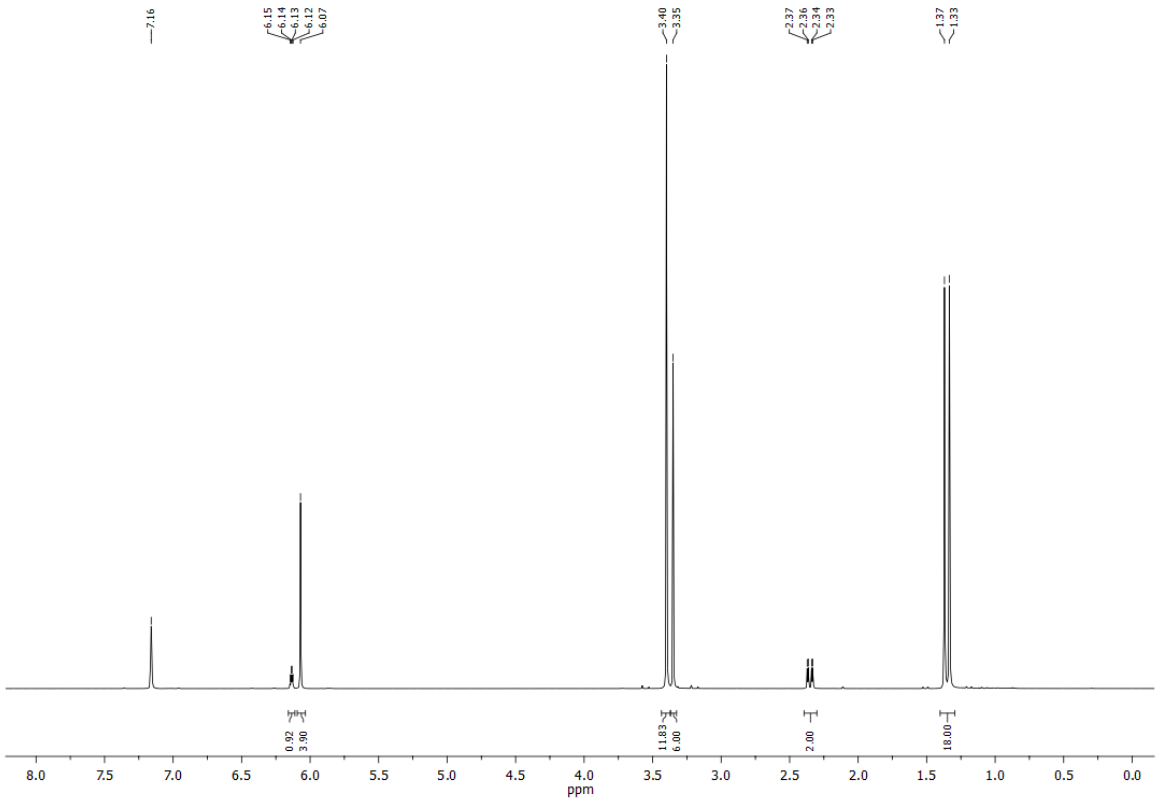

Figure S8: ^{1}H NMR (400.13 MHz, C_6D_6, 298 K) of compound **4**.

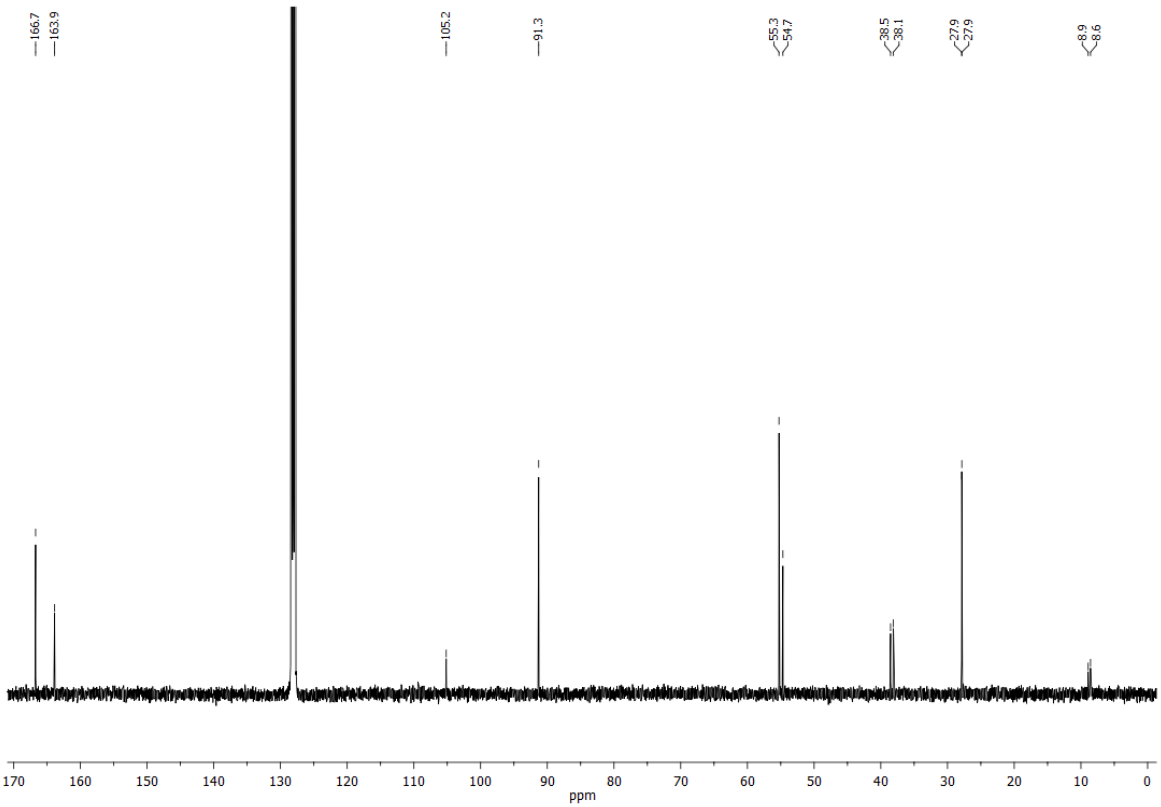

Figure S9: $^{13}C\{^{1}H\}$ NMR (100.61 MHz, C_6D_6, 298 K) of compound **4**.

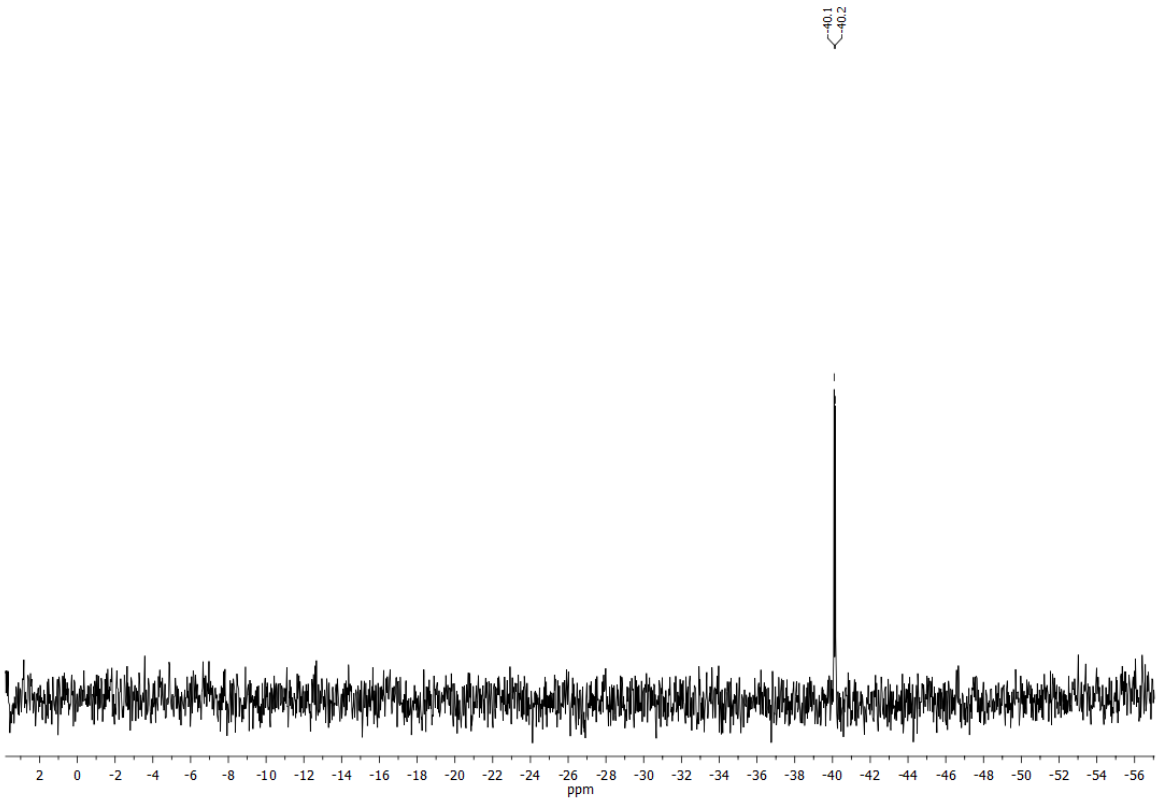

Figure S10: $^{29}Si\{^{1}H\}$ NMR (79.49 MHz, C_6D_6, 298 K) of compound **4**.

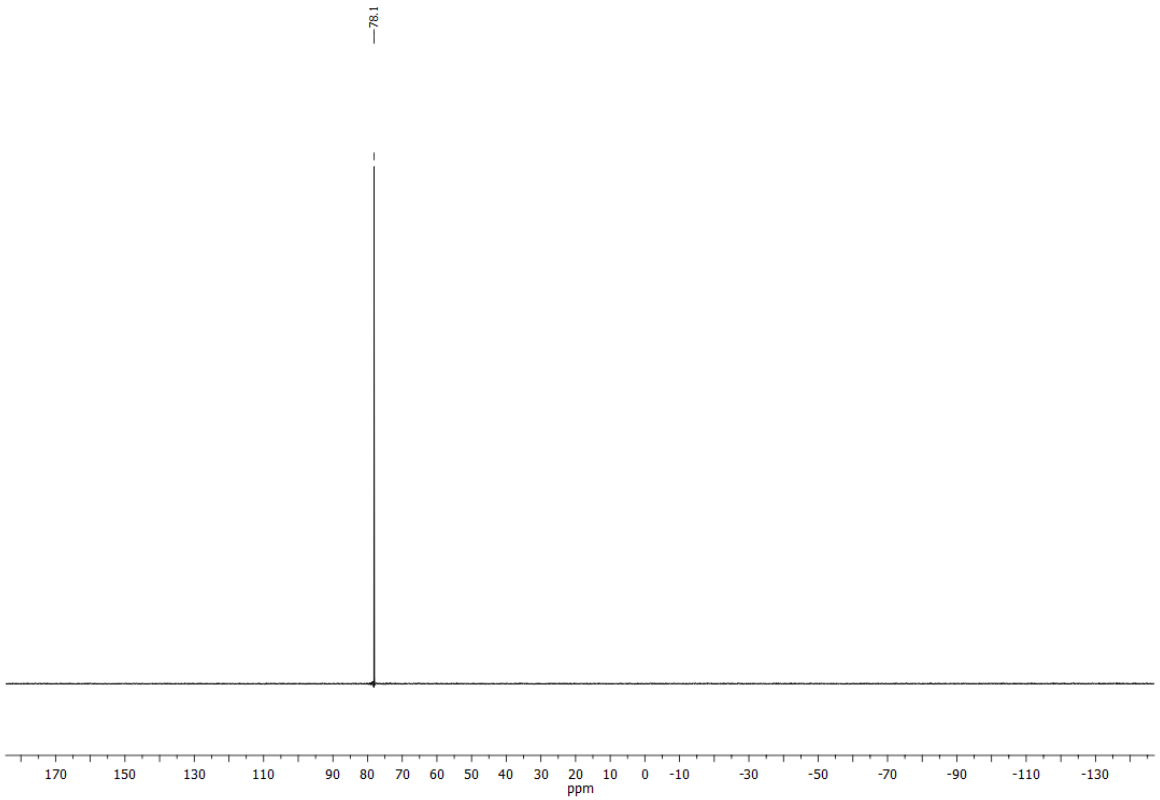

Figure S11: $^{31}P\{^{1}H\}$ NMR (162.04 MHz, C_6D_6, 298 K) of compound **4**.

3.6.5 Synthesis of Di-*tert*-butyl[(di-*tert*butylsilyl)methyl] phosphine

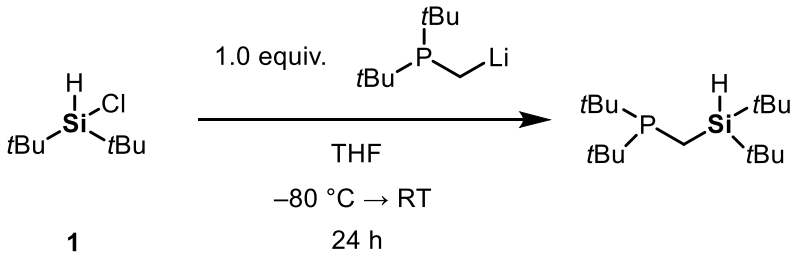

1

Di-*tert*-butylchlorosilane (0.811 mL, 4.01 mmol, 1.0 equiv.) was dissolved in 50 mL THF and cooled to **–**80 °C. Then, a freshly prepared solution of (di-*tert*-butylphosphanyl)methyllithium (666 mg, 4.01 mmol, 1.0 equiv.) in 20 mL THF was cooled to **–**80 °C and slowly added to the previously prepared solution of di-*tert*-butyl(chloro)silane in THF *via* teflon cannula. The reaction mixture was allowed to stir at room temperature for 24 h. Then, all volatiles were removed *in vacuo* and the residue dissolved in DCM. The resulting suspension was filtered through a P3-frit with added Celite®. All volatiles of the filtrate were removed *in vacuo* and the resulting oil purified *via* Kugelrohr distillation (80 – 90 °C oven temperature, $1.8 \cdot 10^{-3}$ mbar). Di-*tert*-butyl[(di-*tert*-butylsilyl)methyl]phosphine was obtained as a colorless oil. Yield: 994 mg (3.28 mmol, 82%).

^{1}H NMR (400.13 MHz, C_6D_6, 298 K): δ 3.86 (dd, $^{3}J_{P–H}$ = 5.3 Hz, $^{3}J_{H–H}$ = 3.5 Hz, 1H, Si*H*), 1.15 {d, 18H, $^{3}J_{P–H}$ = 10.5 Hz, P[C(C*H*$_3$)$_3$]$_2$}, 1.14 {s, 18H, Si[C(C*H*$_3$)$_3$]$_2$}, 0.68 (dd, $^{3}J_{H–H}$ = 3.5 Hz, $^{2}J_{P–H}$ = 1.4 Hz, 2H, SiC*H*$_2$P).

^{13}C{^{1}H} NMR (100.61 MHz, C_6D_6, 298 K): δ 32.4 {d, $^{1}J_{C–P}$ = 26.4 Hz, P[*C*(CH$_3$)$_3$]$_2$}, 30.0 {d, $^{2}J_{C–P}$ = 14.0 Hz, PS[C(*C*H$_3$)$_3$]$_2$}, 29.6 {d, $^{4}J_{C–P}$ = 2.8 Hz, Si[C(*C*H$_3$)$_3$]$_2$}, 20.0 {d, $^{3}J_{C–P}$ = 2.6 Hz, Si[*C*(CH$_3$)$_3$]$_2$}, –1.1 (d, $^{1}J_{C–P}$ = 46.6 Hz, Si*C*H$_2$P).

^{29}Si{^{1}H} NMR (79.49 MHz, C_6D_6, 298 K): δ 7.7 (d, $^{2}J_{Si–P}$ = 8.4 Hz, *Si*CH$_2$P).

^{31}P{^{1}H} NMR (162. 04 MHz, C_6D_6, 298 K): δ 22.4 (s, SiCH$_2$*P*).

HR(EI)-MS: Calcd *m/z* for $C_{17}H_{39}PSi$ $[M]^+$: 302.2553. Found: 302.2553.

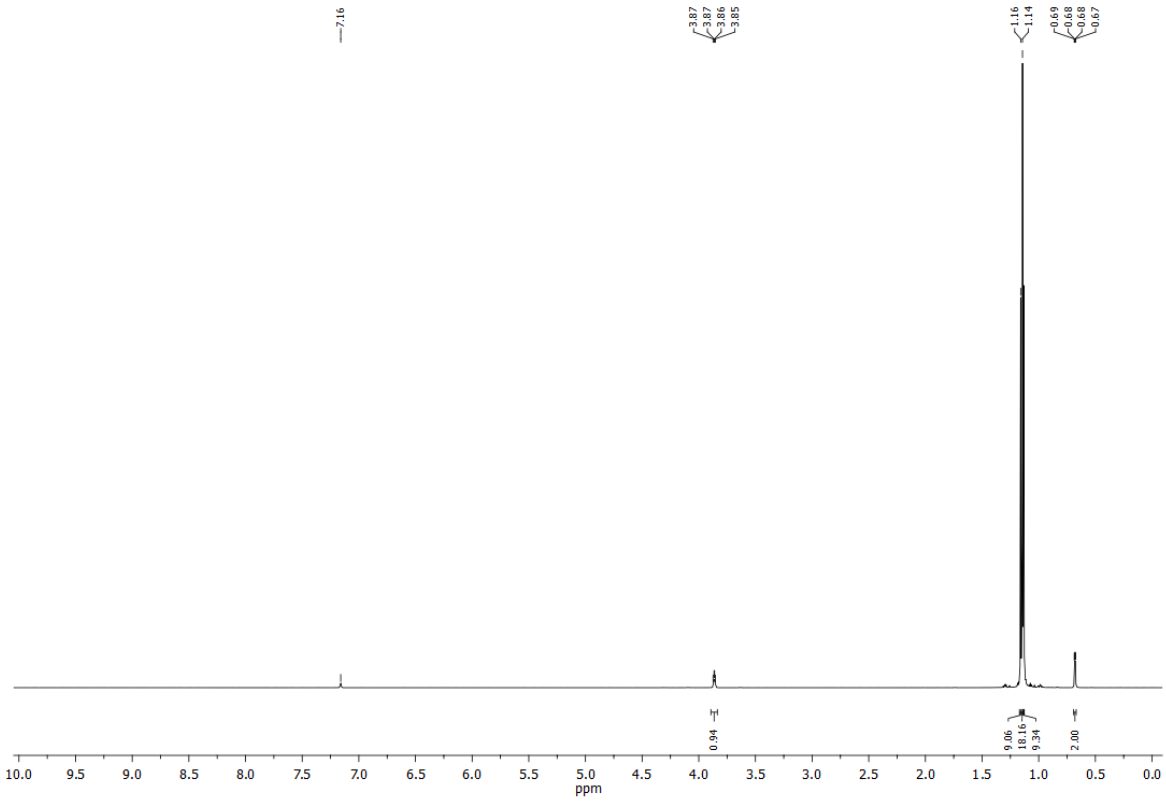

Figure S12: ^{1}H NMR spectrum (C_6D_6, 298 K) of di-*tert*-butyl[(di-*tert*-butylsilyl)methyl]phosphine.

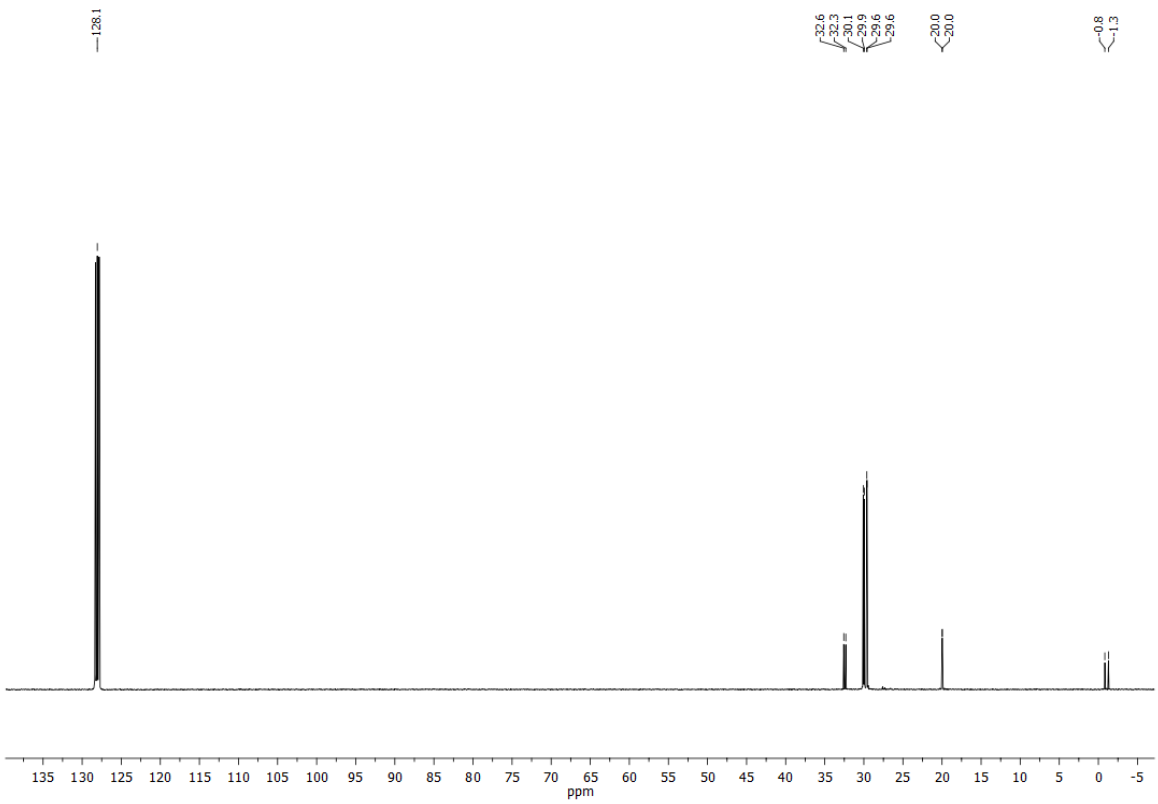

Figure S13: $^{13}C\{^{1}H\}$ NMR spectrum (C_6D_6, 298 K) of di-*tert*-butyl[(di-*tert*-butylsilyl)methyl]phosphine.

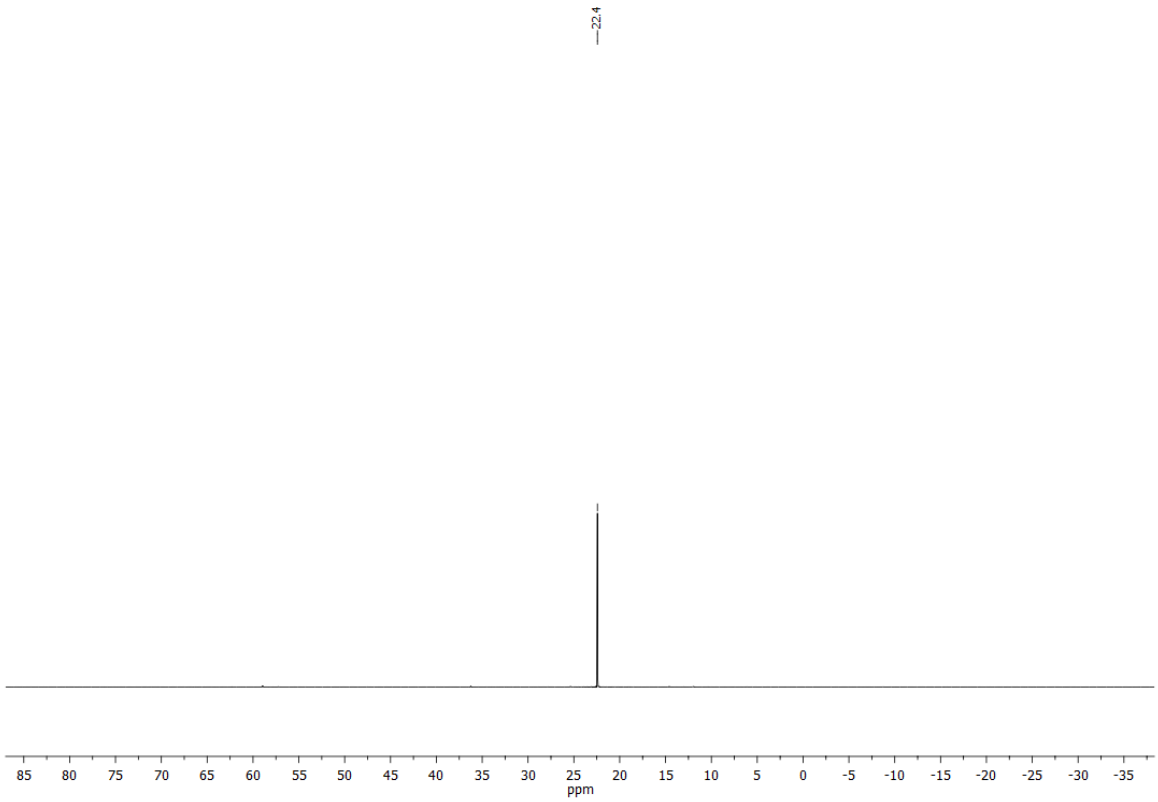

Figure S14: $^{31}P\{^{1}H\}$ NMR spectrum (C_6D_6, 298 K) of di-*tert*-butyl[(di-*tert*-butylsilyl)methyl]phosphine.

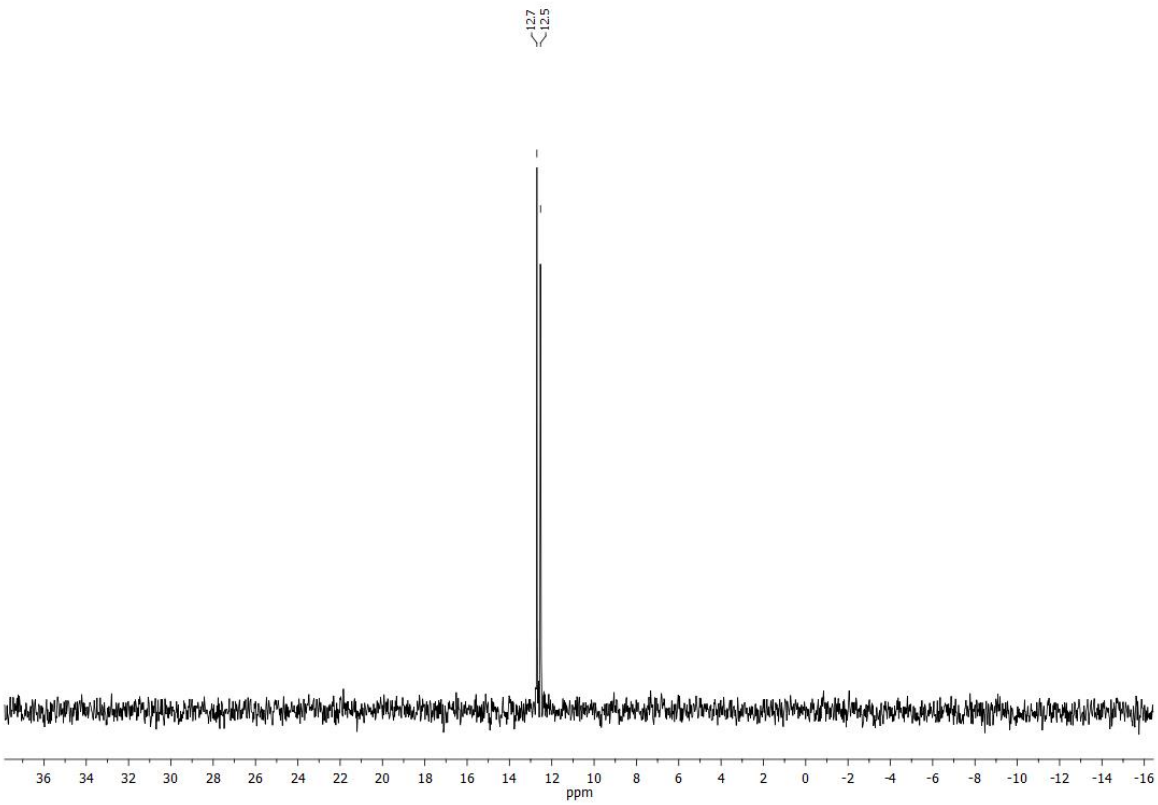

Figure S15: $^{29}Si\{^{1}H\}$ NMR (C_6D_6, 298 K) spectrum of di-*tert*-butyl[(di-*tert*-butylsilyl)methyl]phosphine.

3.6.6 Synthesis of compound 5

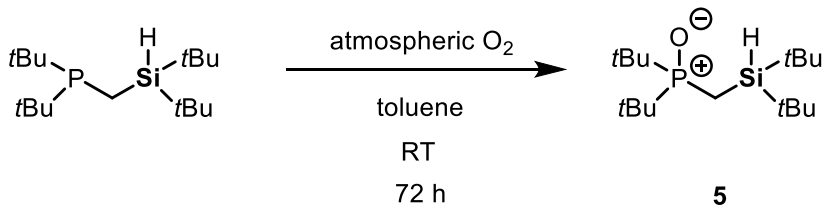

Di-*tert*-butyl[(di-*tert*-butylsilyl)methyl]phosphine (449 mg, 1.48 mmol, 1.0 equiv.) was dissolved in 10 mL toluene. Then, a drying tube filled with orange silica gel beads and dry sodium hydroxide was attached. The tube was opened to air and the solution vigorously stirred for 72 h. Then, all volatiles were removed *in vacuo*. The resulting colorless oil was dissolved in 3 mL pentane and cooled to **–**30 °C. The formed colorless crystals of compound **5** were suitable for single-crystal X-ray diffraction analysis. Yield: 150 mg (0.47 mmol, 32%).

^{1}H NMR (400.13 MHz, C_6D_6, 298 K): δ 4.08 (m, 1H, Si*H*), 1.18 {d, $^{3}J_{P-H}$ = 13.0 Hz, 18H, PO[C(CH_3)$_3$]$_2$}, 1.14 {s, 18H, Si[C(CH_3)$_3$]$_2$}, 1.01 (dd, $^{2}J_{P-H}$ = 12.6 Hz, $^{3}J_{H-H}$ = 3.0, SiCH_2PO).

$^{13}C\{^1H\}$ NMR (100.61 MHz, C_6D_6, 298 K): δ 36.9 {d, $^1J_{C-P}$ = 61.1 Hz, PO[*C*$(CH_3)_3]_2$}, 29.4 {s, PO[C(*C*$H_3)_3]_2$}, 27.6 {s, Si[C(*C*$H_3)_3]_2$}, 19.3 {d, $^3J_{C-P}$ = 2.3 Hz, Si[*C*$(CH_3)_3]_2$}, 2.6 (d, $^1J_{C-P}$ = 47.1 Hz, Si*C*H_2PO).

$^{29}Si\{^1H\}$ NMR (79.49 MHz, C_6D_6, 298 K): δ 9.1 (d, $^2J_{Si-P}$ = 8.3 Hz, *Si*CH_2PO).

$^{31}P\{^1H\}$ NMR (162.04 MHz, C_6D_6, 298 K): δ 58.9 (s, $SiCH_2$*P*O).

HR(ESI)-MS: Calcd *m/z* for $C_{18}H_{39}OPSi$ $[M + H]^+$: 319.26. Found: 319.2586.

CHN Analysis: Calcd for $C_{17}H_{39}OPSi$: C, 64.1; H, 12.3. Found: C, 63.65; H, 12.2.

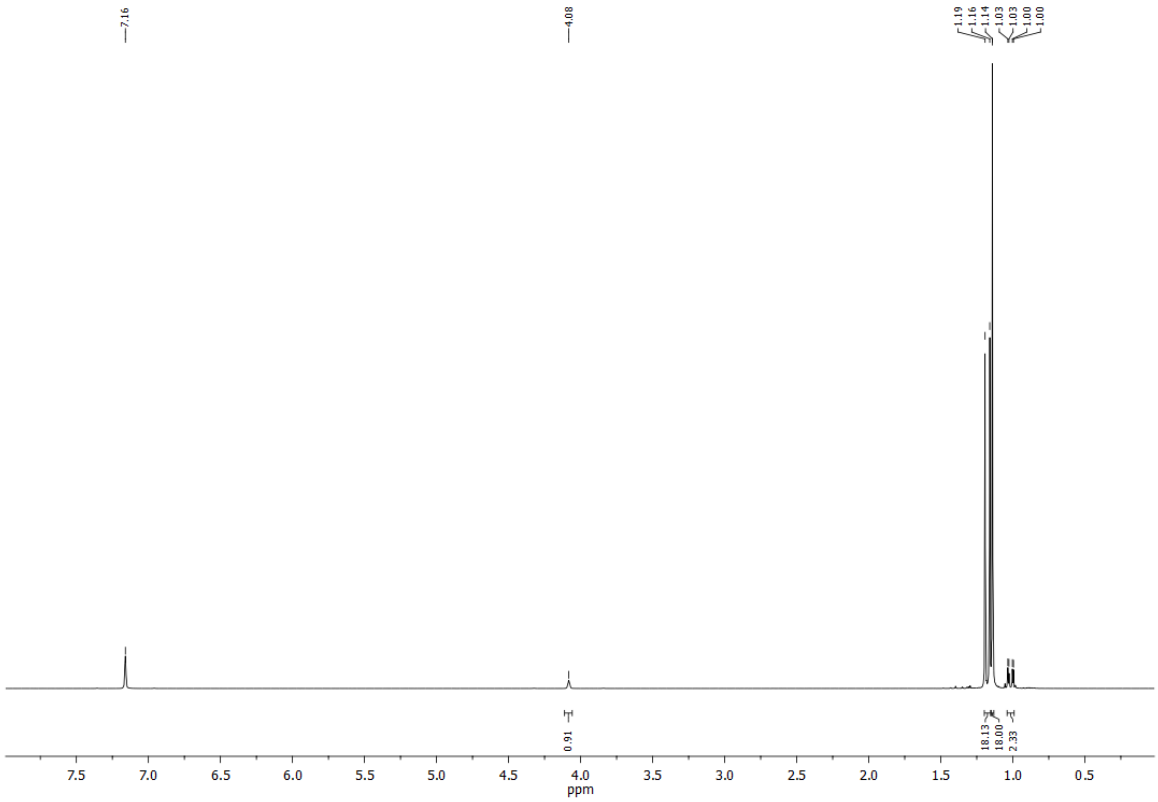

Figure S16: ^1H NMR spectrum (C_6D_6, 298 K) of compound **5.**

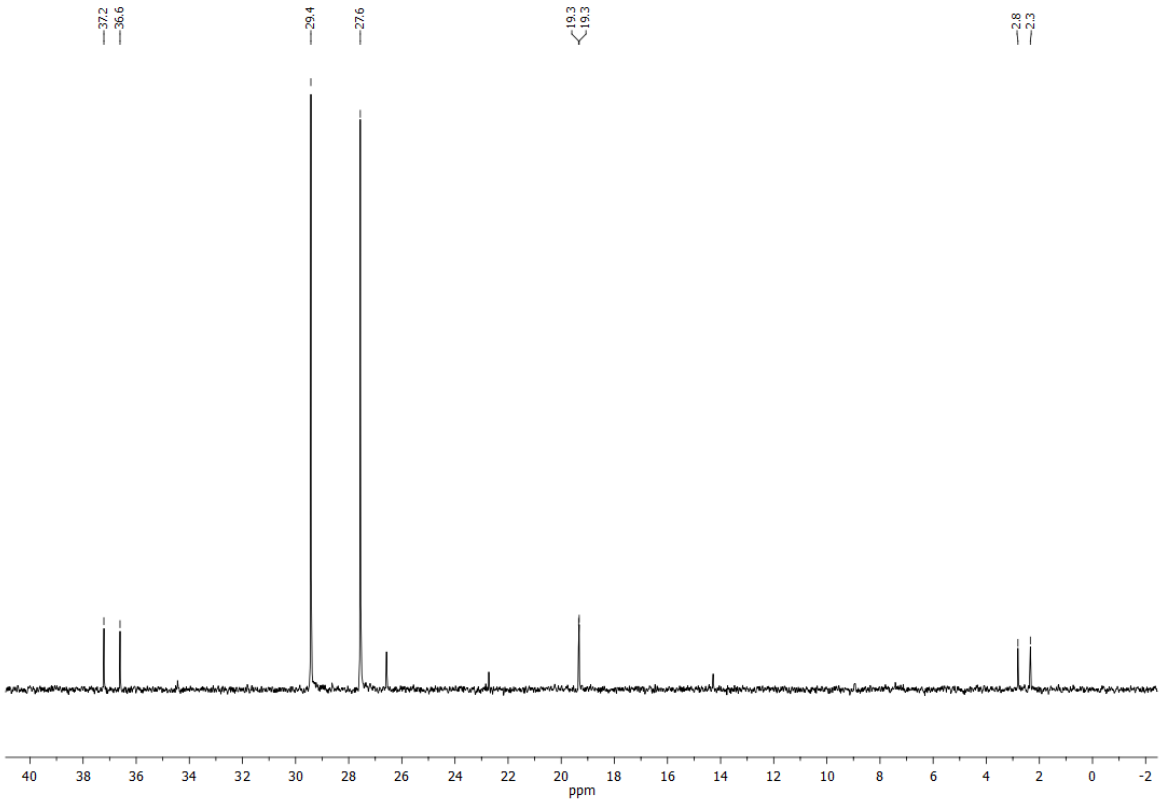

Figure S17: $^{13}C\{^{1}H\}$ NMR spectrum (C_6D_6, 298 K) of compound **5**.

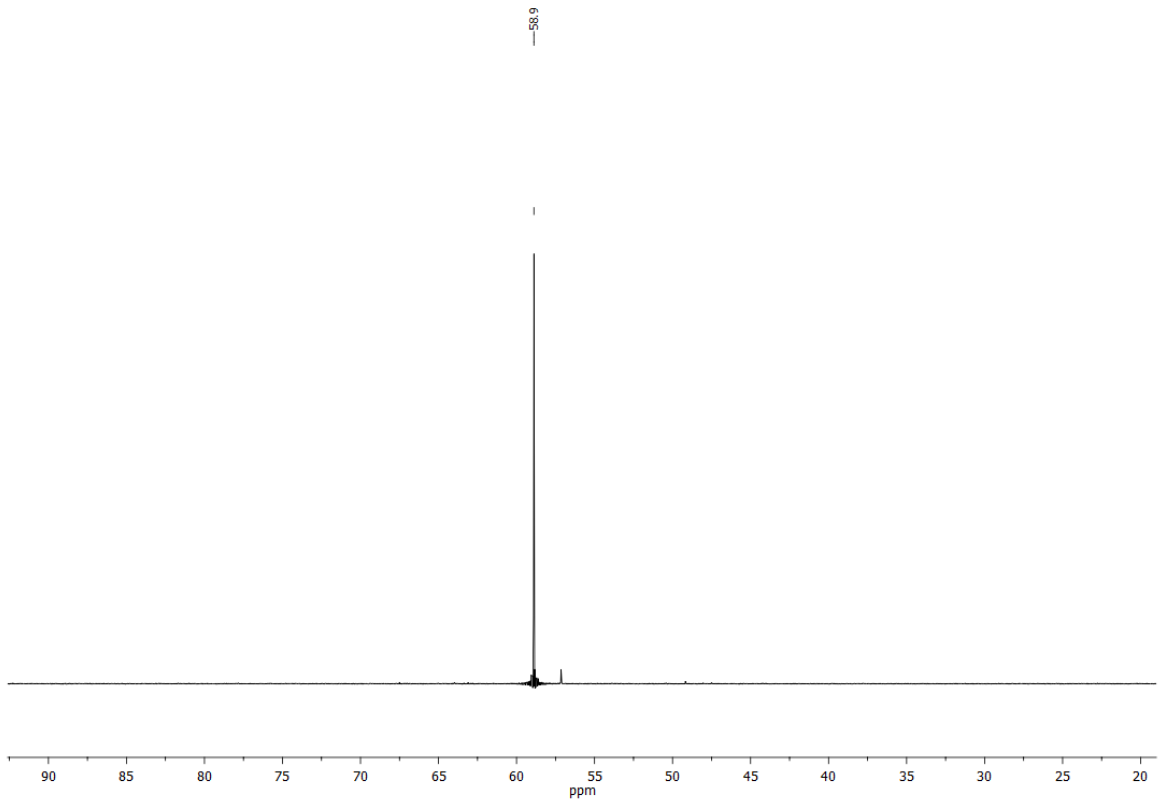

Figure S18: $^{31}P\{^{1}H\}$ NMR spectrum (C_6D_6, 298 K) of compound **5**.

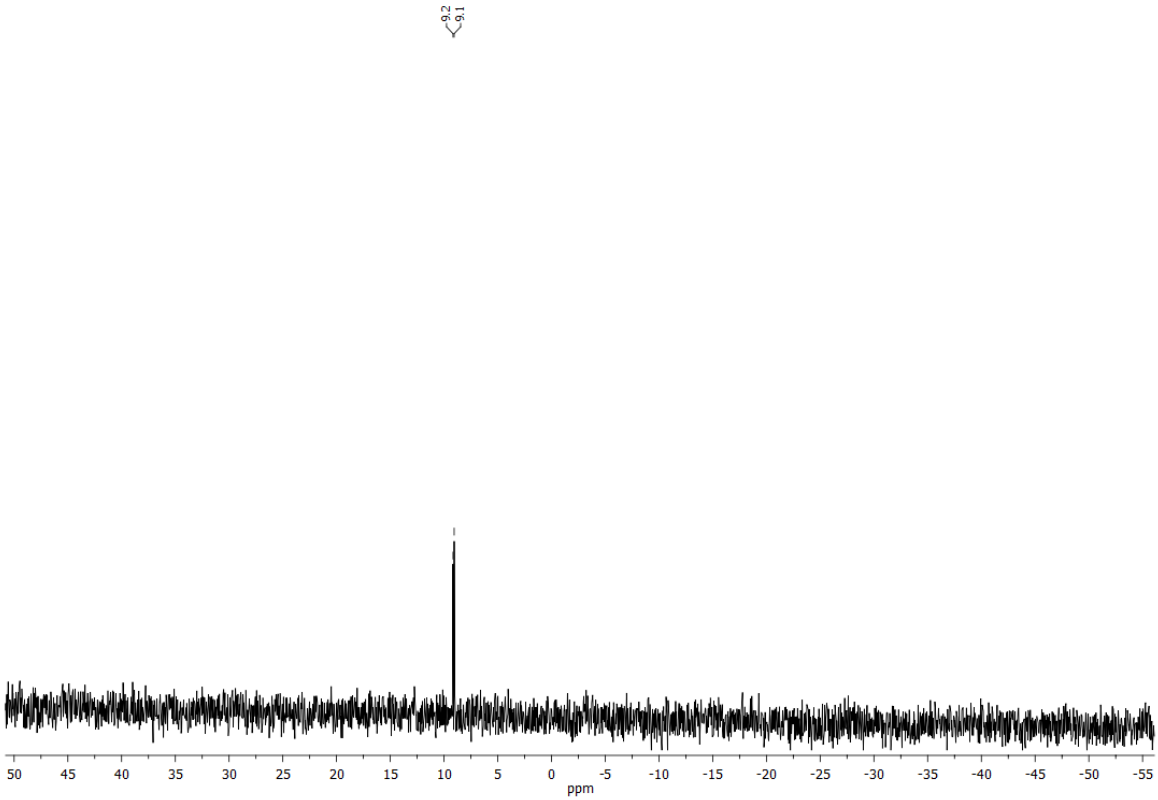

Figure S19: $^{29}Si\{^{1}H\}$ NMR (C_6D_6, 298 K) spectrum of compound **5**.

3.6.7 Synthesis of compound 6

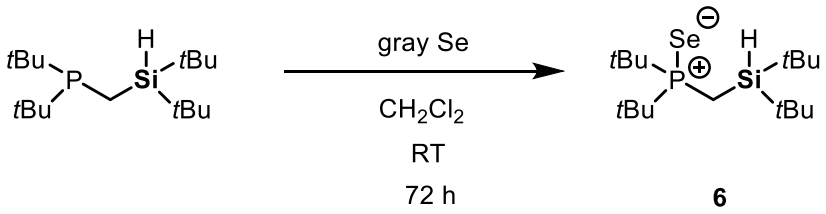

Di-*tert*-butyl[(di-*tert*-butylsilyl)methyl]phosphine (680 mg, 2.25 mmol, 1.0 equiv.) was dissolved in 5 mL DCM at room temperature. The solution was then cooled to **–**30 °C. Grey selenium (177.5 mg, 2.25 mmol, 1.0 equiv.) was added and the solution allowed to stir at room temperature for 72 h. Then, the solution was filtered and all volatiles of the filtrate removed *in vacuo*. Colorless crystals of compound **6** suitable for single-crystal X-ray diffraction analysis were obtained by recrystallization from 1 mL hexane at **–**30 °C. Yield: 737 mg (1.93 mmol, 86%).

^{1}H NMR (400.13 MHz, C_6D_6, 298 K): δ 4.16 (m, 1H, Si*H*), 1.37 (dd, $^{2}J_{P-H}$ = 14.9 Hz, $^{3}J_{H-H}$ = 2.4 Hz, 2H, SiCH_2PSe), 1.25 {d, $^{3}J_{P-H}$ = 14.9 Hz, 18H, PSe[C(CH_3)$_3$]$_2$}, 1.14 {s, 18H, Si[C(CH_3)$_3$]$_2$}.

$^{13}C\{^1H\}$ NMR (100.61 MHz, C_6D_6, 298 K): δ 38.2 {d, $^1J_{C-P}$ = 34.8 Hz, PSe[*C*$(CH_3)_3]_2$}, 29.8 {s, Si[C(*C*$H_3)_3]_2$}, 27.9 {d, $^2J_{C-P}$ = 1.9 Hz, PSe[C(*C*$H_3)_3]_2$}, 19.1 {d, $^3J_{C-P}$ = 2.6 Hz, Si[*C*$(CH_3)_3]_2$}, 3.4 (d, $^1J_{C-P}$ = 25 Hz, Si*C*H_2PSe).

$^{29}Si\{^1H\}$ NMR (79.49 MHz, C_6D_6, 298 K): δ 8.1 (d, $^2J_{Si-P}$ = 8.2 Hz, *Si*CH_2PSe).

$^{31}P\{^1H\}$ NMR (162.04 MHz, C_6D_6, 298 K): δ 73.8 (s, SiCH_2*P*Se).

$^{77}Se\{^1H\}$ NMR (76 MHz, C_6D_6, 298 K): δ –381.6 (d, $^1J_{P-Se}$ = 717.6 Hz, P*Se*).

HR(ESI)-MS: Calcd *m/z* for $C_{17}H_{40}PSeSi$ $[M + H]^+$: 383.1797. Found: 383.1797 $[M + H]^+$.

CHN Analysis: Calcd for $C_{17}H_{39}PSeSi$: C, 53.3; H, 10.3. Found: C, 53.29; H, 10.21.

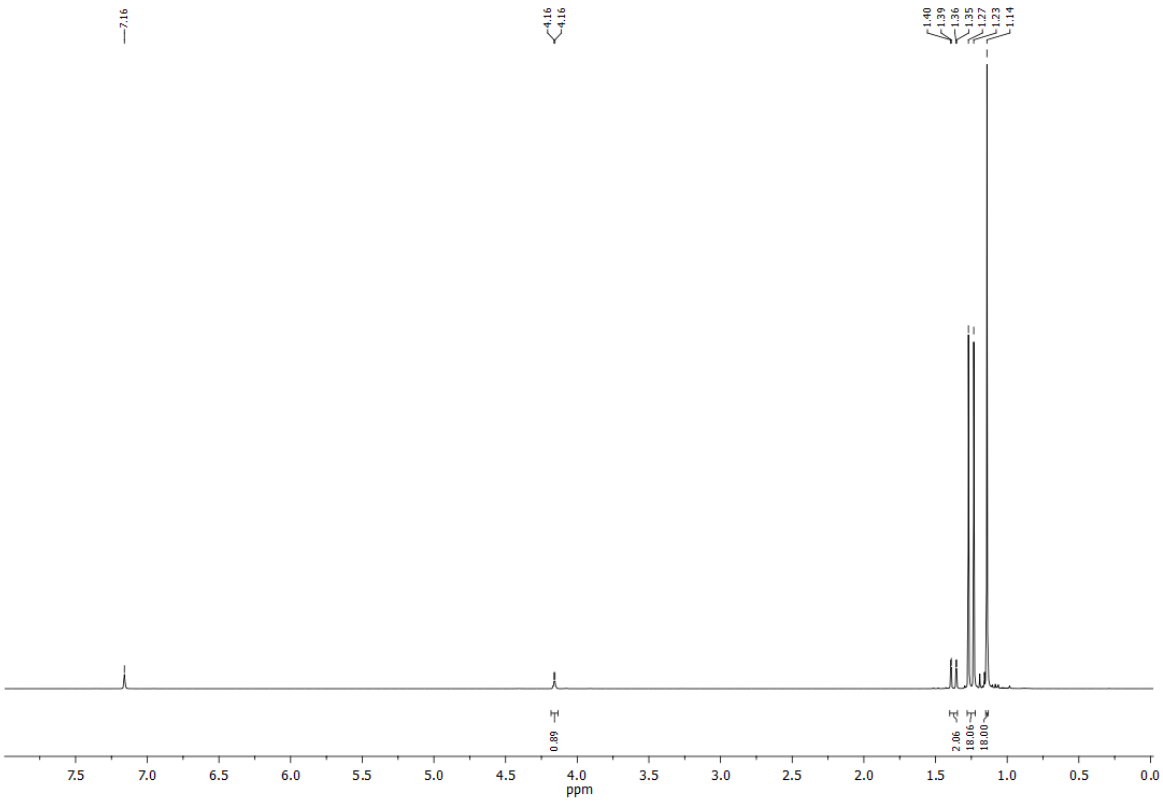

Figure S20: ^1H NMR spectrum (C_6D_6, 298 K) of compound **6**.

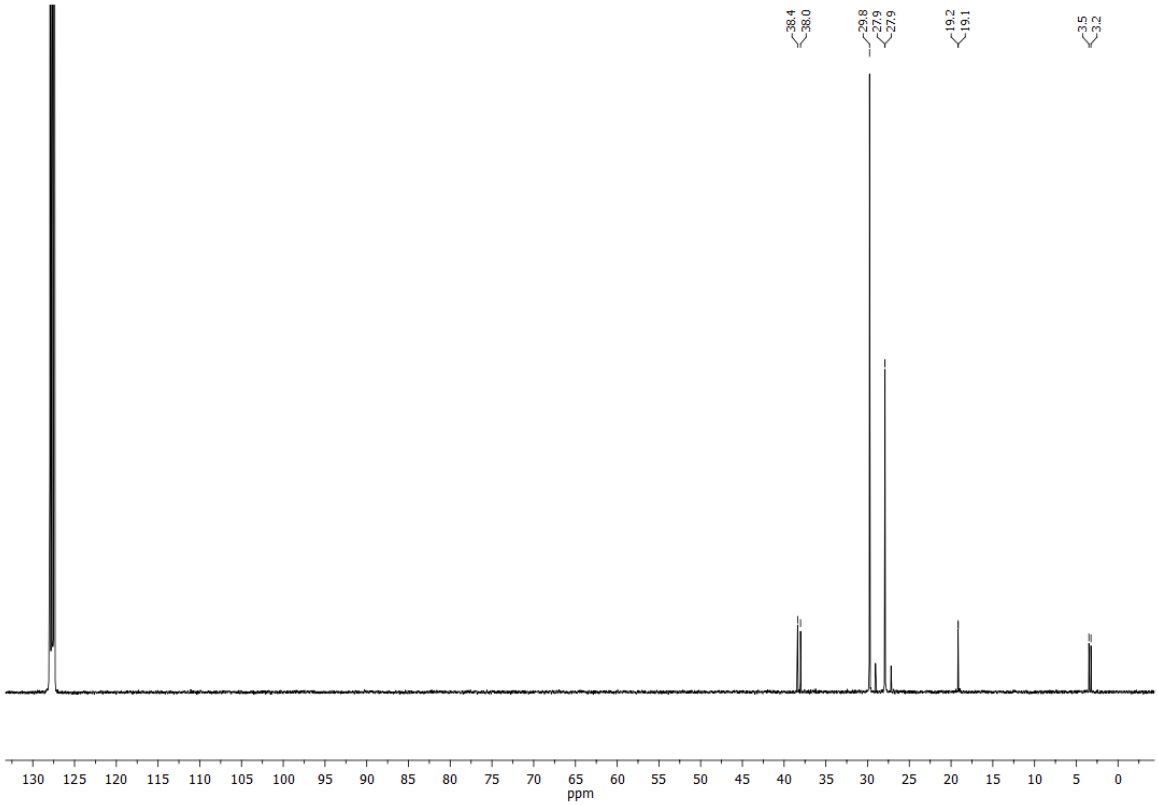

Figure S21: $^{13}C\{^{1}H\}$ NMR spectrum (C_6D_6, 298 K) of compound **6**.

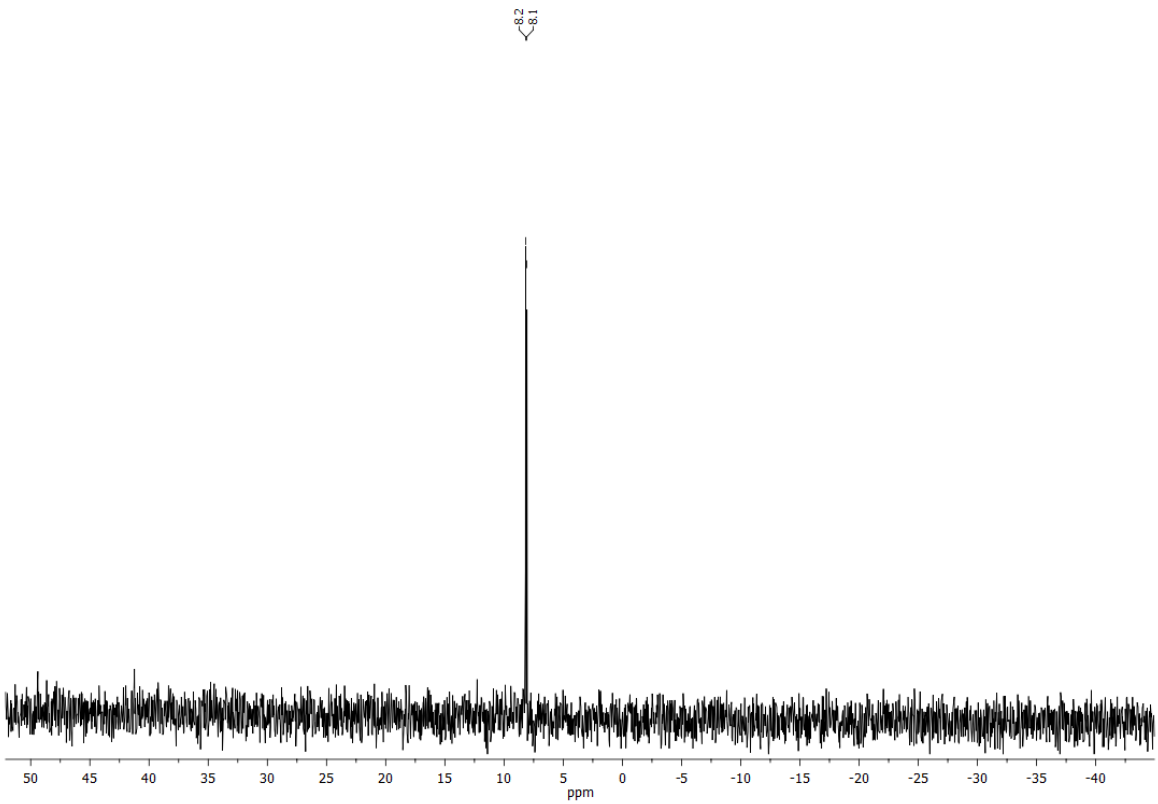

Figure S22: $^{29}Si\{^{1}H\}$ NMR (C_6D_6, 298 K) spectrum of compound **6**.

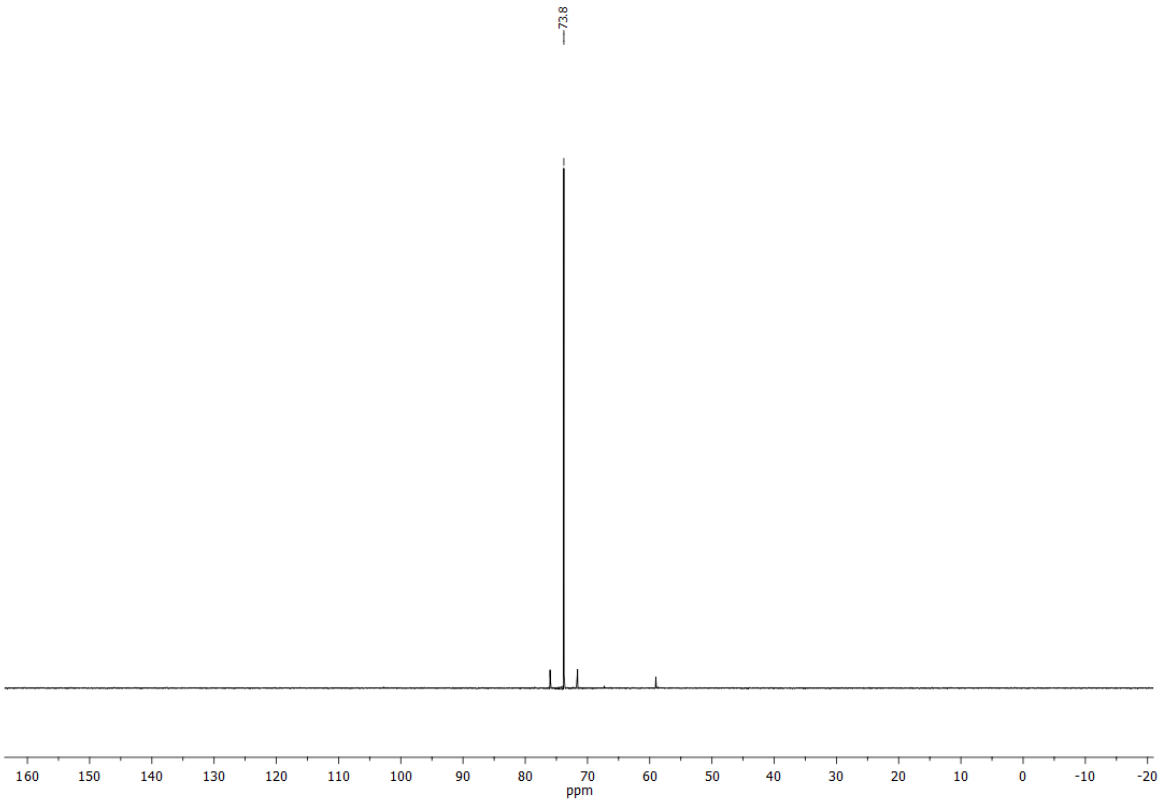

Figure S23: $^{31}P\{^{1}H\}$ NMR spectrum (C_6D_6, 298 K) of compound **6**.

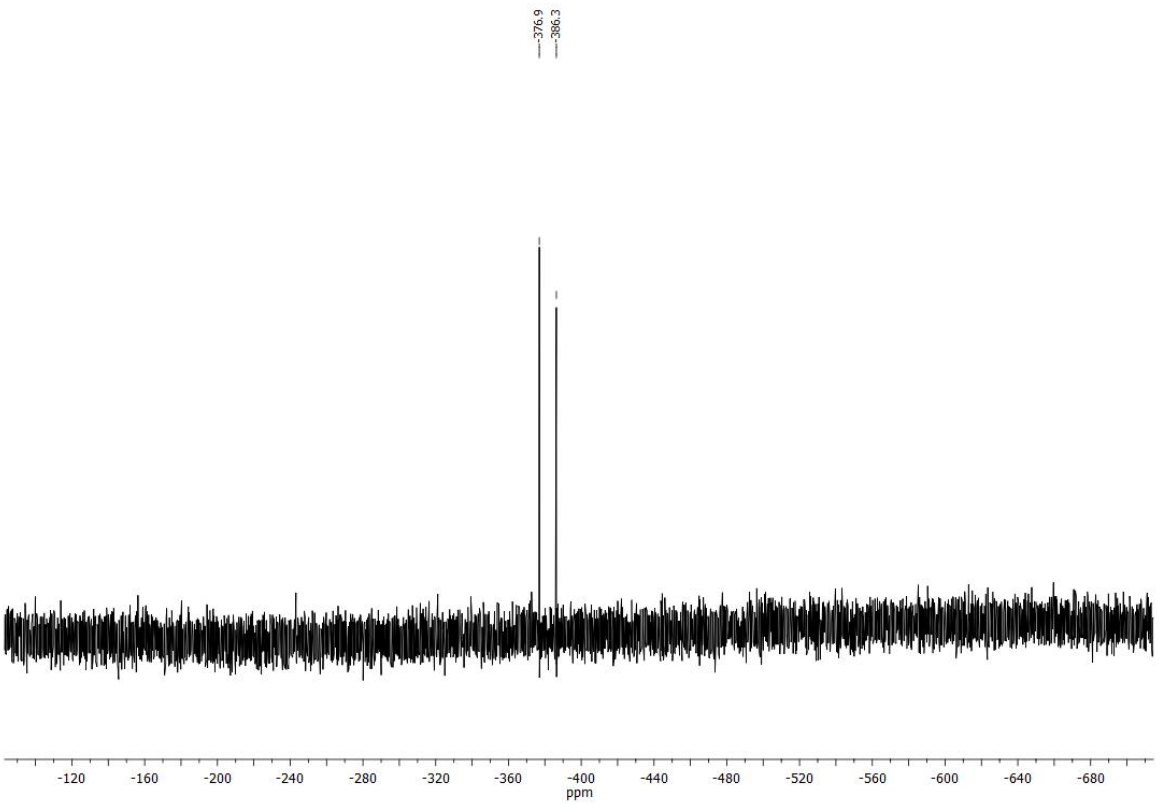

Figure S24: $^{77}Se\{^{1}H\}$ NMR spectrum (C_6D_6, 298 K) of compound **6**.

3.6.8 Synthesis of compound 7[H(B$_6$F$_5$)$_3$]

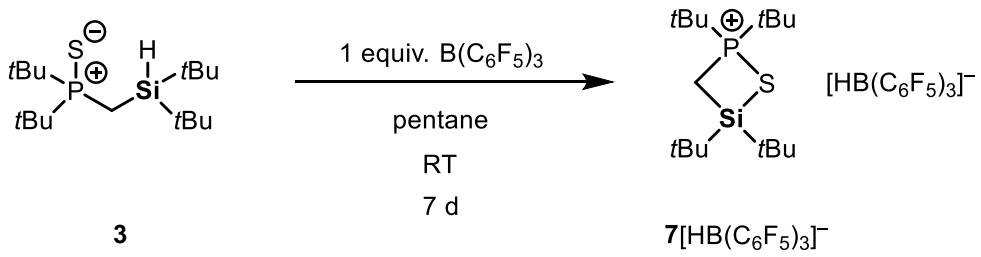

3 **7**[HB(C$_6$F$_5$)$_3$]$^-$

Compound **3** (150 mg, 0.448 mmol, 1,0 equiv.) and tris(pentafluorophenyl)borane (230 mg, 0.448 mmol, 1.0 equiv.) were dissolved in 3 mL pentane at room temperature. The solution was stirred until all solids were dissolved. Then, the stir bar was removed and the solution allowed to react undisturbed for 7 d. During this time, colorless crystals of compound **7**[HB(C$_6$F$_5$)$_3$] suitable for single-crystal X-ray diffraction analysis slowly formed. Yield: 115.3 mg (0.345 mmol, 77.1%).

^{1}H NMR (400.13 MHz, C$_6$D$_6$/1,2-C$_6$H$_4$Cl$_2$, 298 K): δ 1.98 (d, $^2J_{P-H}$ = 12.2 Hz, 2H, SiCH_2PS), 1.06 {d, $^3J_{P-H}$ = 18.4, 18H, PS[C(CH_3)$_3$]$_2$}, 0.9 {s, 18H, Si[C(CH_3)$_3$]$_2$}.

^{13}C{^{1}H} NMR (100.61 MHz, C$_6$D$_6$/1,2-C$_6$H$_4$Cl$_2$, 298 K): δ 40.6 {d, $^1J_{C-P}$ = 21.2 Hz, PS[*C*(CH$_3$)$_3$]$_2$}, 28.5 {s, Si[C(*C*H$_3$)$_3$]$_2$}, 27.2 {d, $^2J_{C-P}$ = 2.3 Hz, PS[C(*C*H$_3$)$_3$]$_2$}, 23.7 {s, Si[*C*(CH$_3$)$_3$]$_2$}, 8.9 (d, $^1J_{C-P}$ = 20.4 Hz, Si*C*H$_2$PS).

^{29}Si{^{1}H} NMR (79.49 MHz, C$_6$D$_6$/1,2-C$_6$H$_4$Cl$_2$, 298 K): δ 31.4 (d, $^2J_{Si-P}$ = 10.1 Hz, *Si*CH$_2$PS).

^{31}P{^{1}H} NMR (162.04 MHz, C$_6$D$_6$/1,2-C$_6$H$_4$Cl$_2$, 298 K): δ 88.7 (s, SiCH$_2$*P*S).

^{19}F{^{1}H} NMR (376.66 MHz, C$_6$D$_6$/1,2-C$_6$H$_4$Cl$_2$, 298 K): δ –132.1 (s, 6H, CF_{ortho}), –163.5 (bs, 3H, CF_{para}), –166.1 (s, 6H, CF_{meta}).

^{11}B{^{1}H} NMR (128.43 MHz, C$_6$D$_6$/1,2-C$_6$H$_4$Cl$_2$, 298 K): δ –25.7 (s, *B*H).

CHN Analysis: Calcd for C$_{35}$H$_{39}$BF$_{15}$PSSi: C, 49.66; H, 4.64. Found: C, 48.77; H, 4.07.

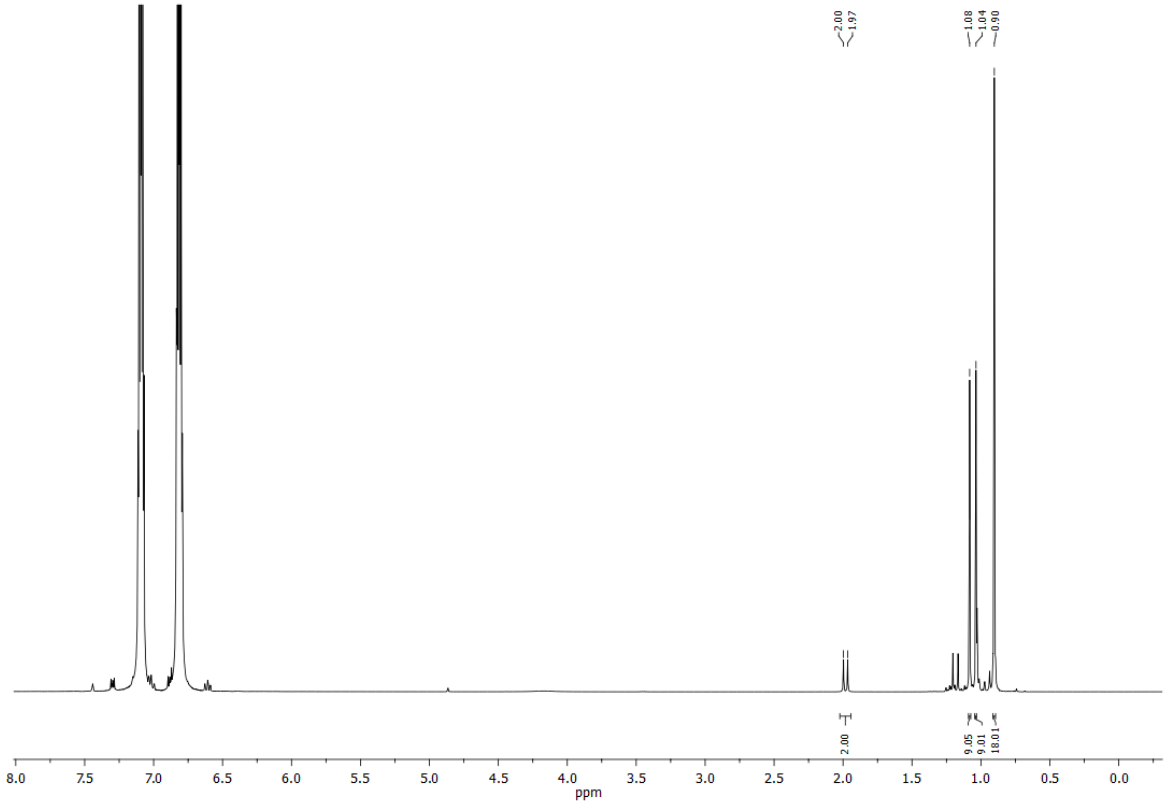

Figure S25: ^{1}H NMR spectrum (C_6D_6 + 1,2-dichlorobenzene, 298 K) of compound **7**[$HB(C_6F_5)_3$].

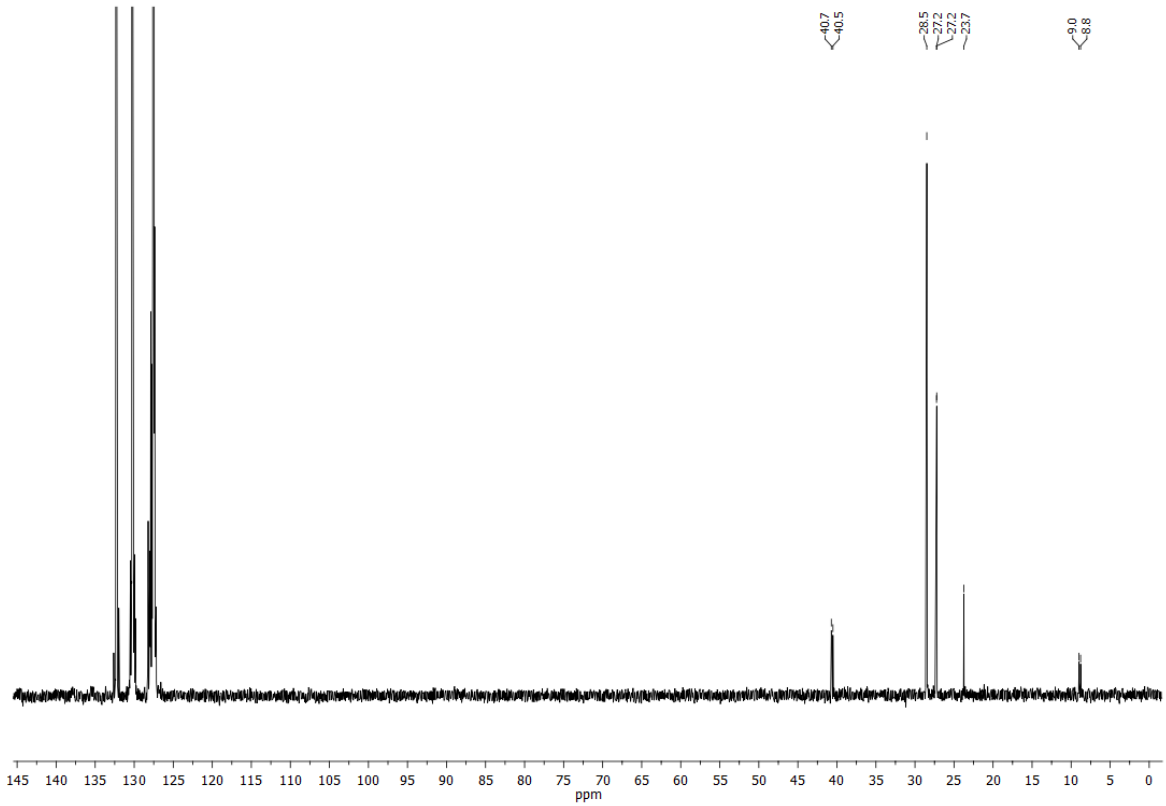

Figure S26: $^{13}C\{^{1}H\}$ NMR spectrum (C_6D_6 + 1,2-dichlorobenzene, 298 K) of compound **7**[$HB(C_6F_5)_3$].

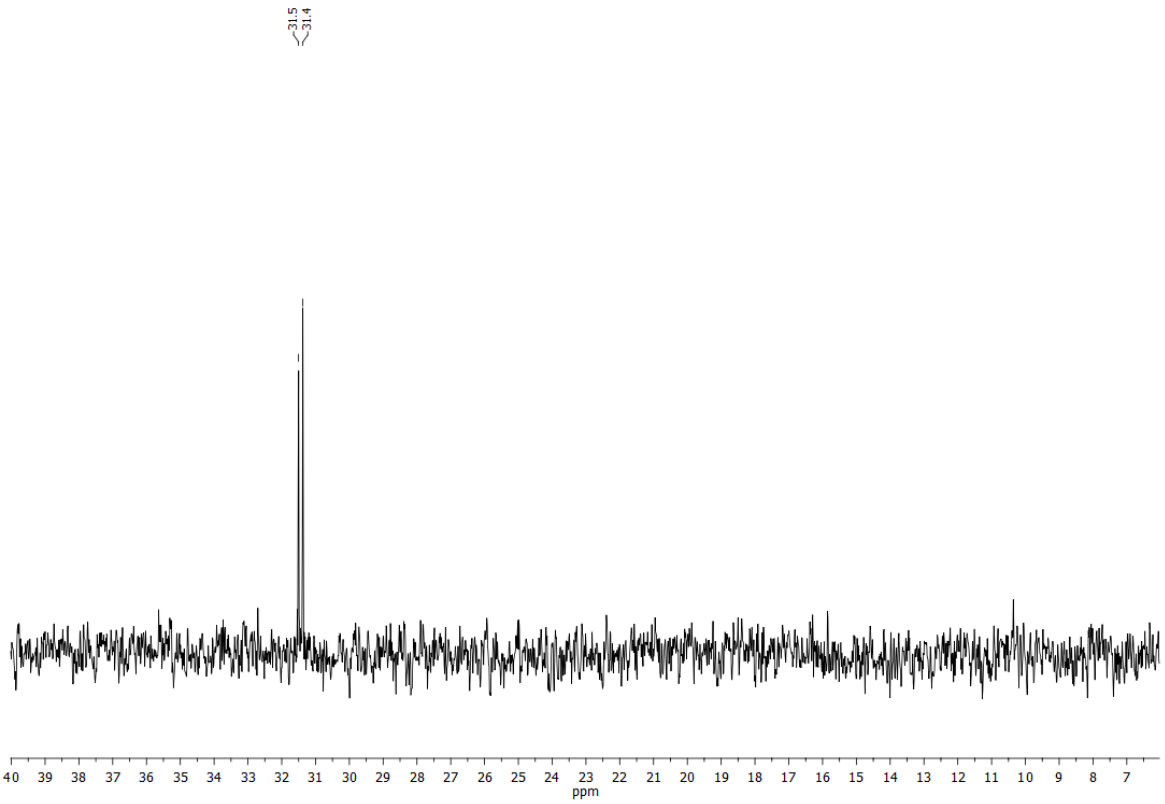

Figure S27: $^{29}Si\{^{1}H\}$ NMR spectrum (C_6D_6 + 1,2-dichlorobenzene, 298 K) of compound **7**[$HB(C_6F_5)_3$].

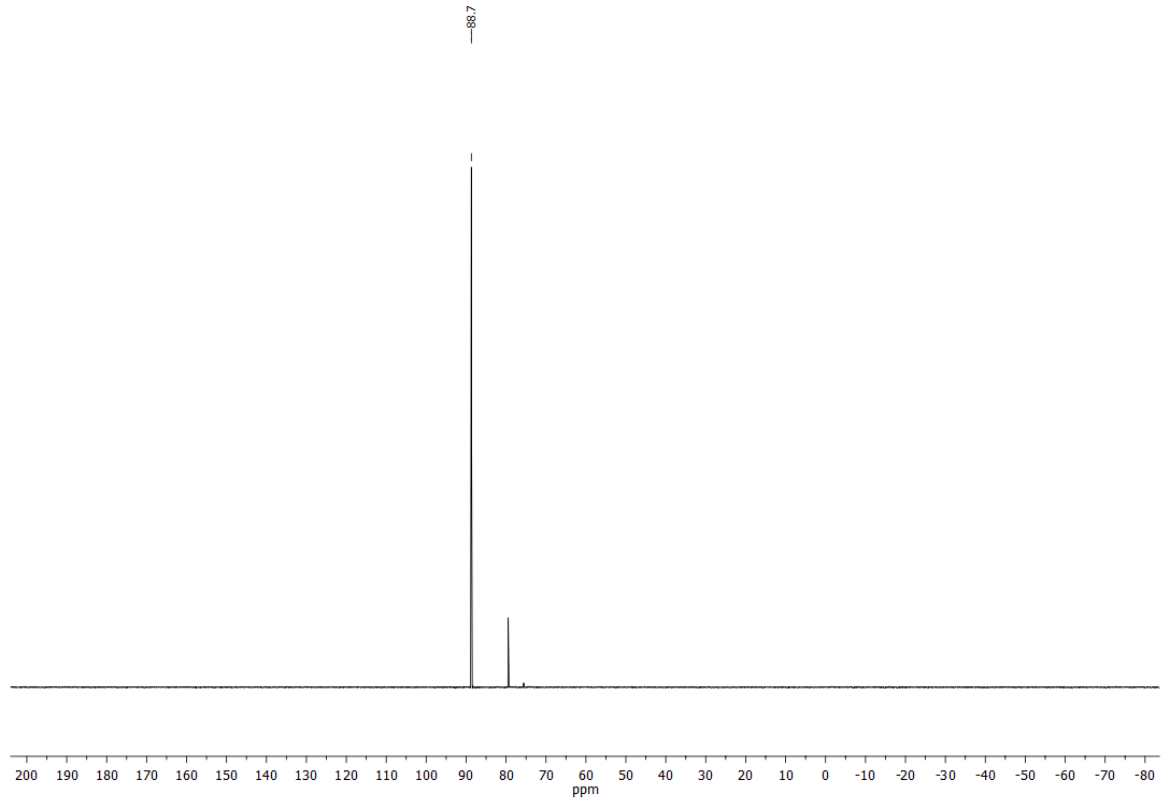

Figure S28: $^{31}P\{^{1}H\}$ NMR spectrum (C_6D_6 + 1,2-dichlorobenzene, 298 K) of compound **7**[$HB(C_6F_5)_3$].

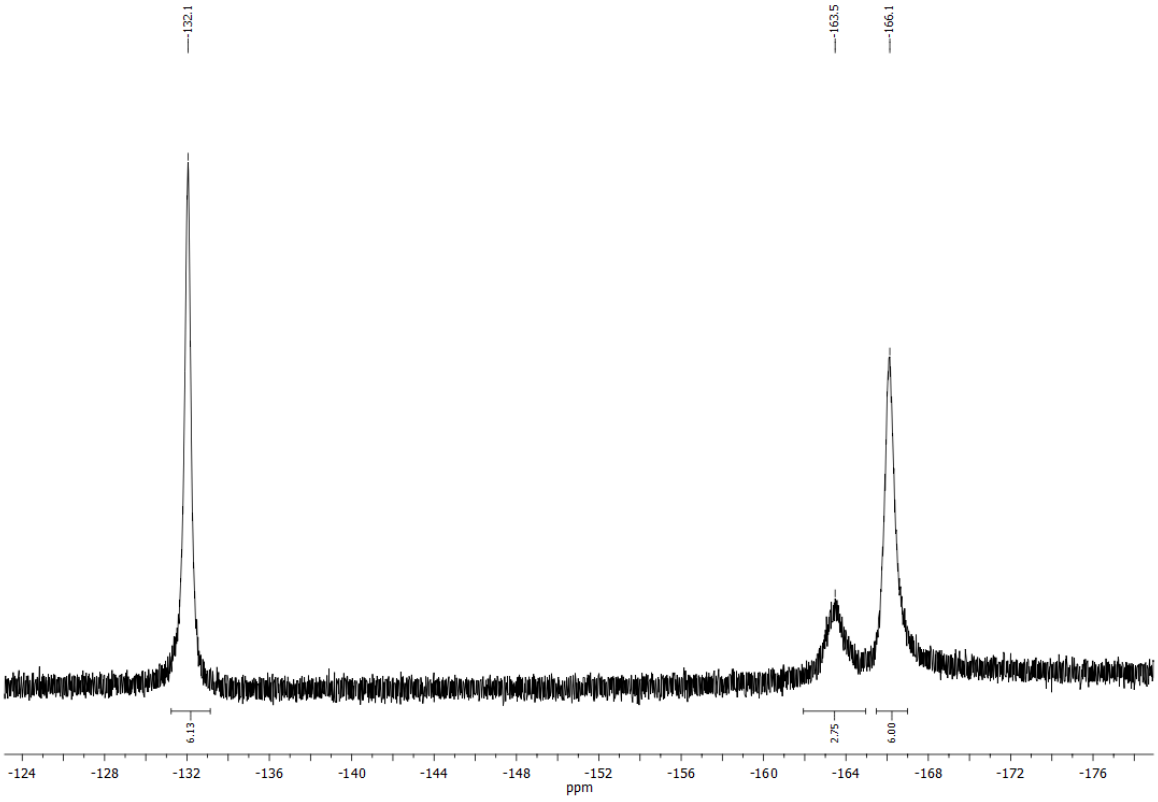

Figure S29: $^{19}F\{^{1}H\}$ NMR spectrum (C_6D_6 + 1,2-dichlorobenzene, 298 K) of compound **7**[$HB(C_6F_5)_3$].

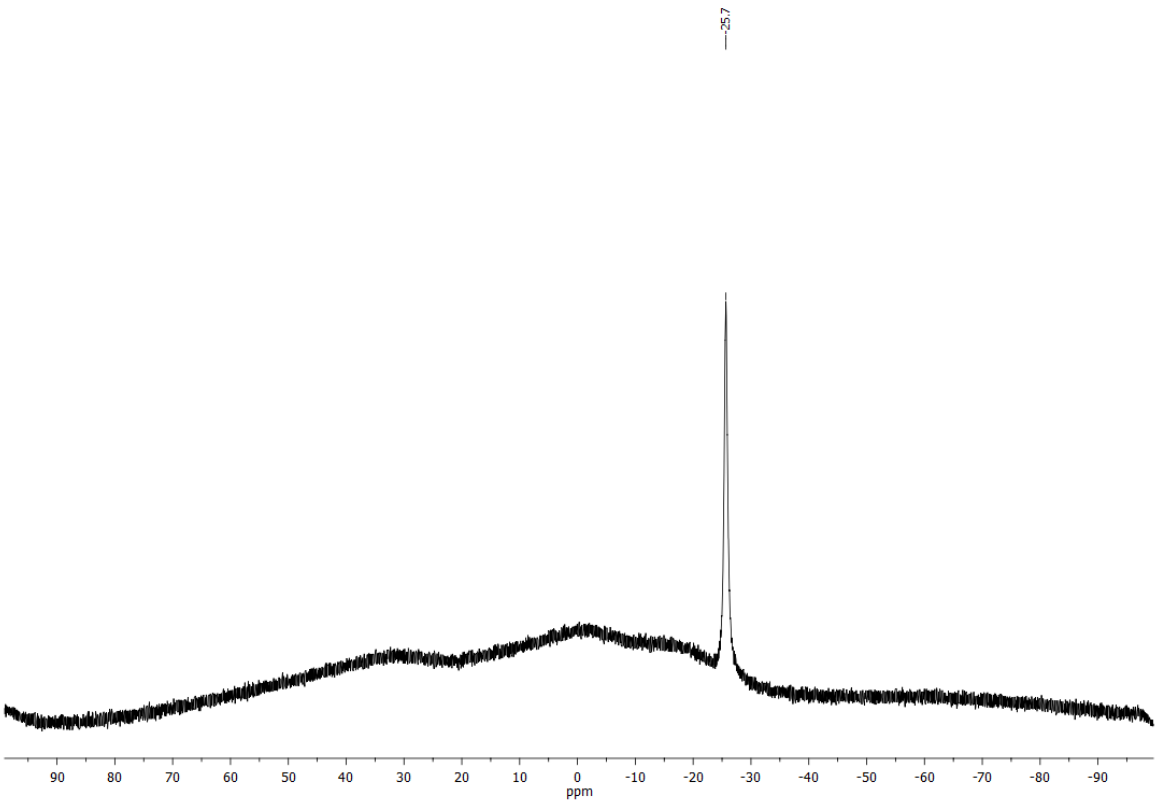

Figure S30: $^{11}B\{^{1}H\}$ NMR spectrum (C_6D_6 + 1,2-dichlorobenzene, 298 K) of compound **7**[$HB(C_6F_5)_3$].

3.6.9 Synthesis of compound 8[HB(C$_6$F$_5$)$_4$]

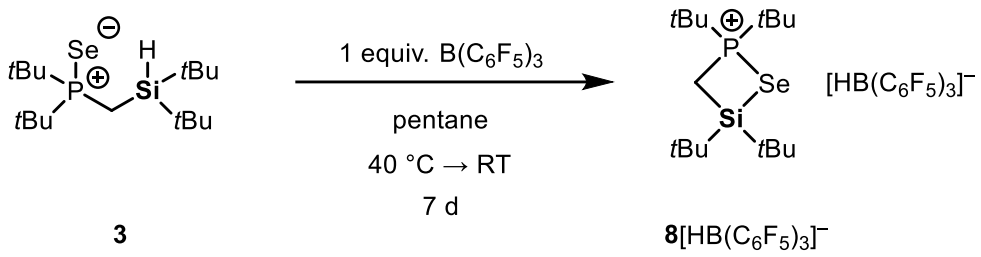

3 **8**[HB(C$_6$F$_5$)$_3$]$^-$

Compound **6** (160 mg, 0.419 mmol, 1.0 equiv.) and tris(pentafluorophenyl)borane (215 mg, 0.419 mmol, 1.0 equiv.) were dissolved in 3 mL pentane at room temperature. The solution was stirred and gently heated to 40 °C until all solids were dissolved. Then, the stir bar was removed and the solution allowed to react undisturbed for 7 d. During this time, colorless crystals of compound **8**[HB(C$_6$F$_5$)$_3$] suitable for single-crystal X-ray diffraction analysis slowly formed. Yield: 149 mg (0.391 mmol, 93.4%).

^{1}H NMR (400.13 MHz, CD_2Cl_2, 298 K): δ 3.59 (bq, 1H, $^1J_{B-H}$ = 87.1 Hz, B*H*), 2.69 (d, $^2J_{P-H}$ = 14.9 Hz, 2H, SiC*H*$_2$PSe), 1.57 {d, $^3J_{P-H}$ = 18.7 Hz, 18H, PSe[C(C*H*$_3$)$_3$]$_2$}, 1.30 {s, 18H, Si[C(C*H*$_3$)$_3$]$_2$}.

^{13}C{^{1}H} NMR (100.61 MHz, CD_2Cl_2, 298 K): δ 40.9 {d, $^1J_{C-P}$ = 16.7 Hz, PSe[*C*(CH$_3$)$_3$]$_2$}, 29.7 {s, Si[C(*C*H$_3$)$_3$]$_2$}, 28.1 {d, $^2J_{C-P}$ = 2.4 Hz, PSe[C(*C*H$_3$)$_3$]$_2$}, 24.5 {s, Si[*C*(CH$_3$)$_3$]$_2$}, 11.5 (d, $^1J_{C-P}$ = 18.5 Hz, Si*C*H$_2$PSe).

^{29}Si{^{1}H} NMR (79.49 MHz, CD_2Cl_2, 298 K): δ 25.4 (d, $^2J_{Si-P}$ = 9.2 Hz, *Si*CH$_2$PSe).

^{31}P{^{1}H} NMR (162.04 MHz, CD_2Cl_2, 298 K): δ 75.8 (s, SiCH$_2$*P*Se).

^{77}Se{^{1}H} NMR (76 MHz, CD_2Cl_2, 298 K): δ –72.9 (d, $^1J_{P-Se}$ = 323.6 Hz, P*Se*).

^{19}F{^{1}H} NMR (376.66 MHz, CD_2Cl_2, 298 K): δ –133.7 (s, 6H, C*F*$_{ortho}$), –164.6 (bs, 3H, C*F*$_{para}$), –167.4 (s, 6H, C*F*$_{meta}$).

^{11}B{^{1}H} NMR (128.43 MHz, CD_2Cl_2, 298 K): δ –25.65 (s, *B*H).

HR(ESI+)-MS: Calcd *m/z* for $C_{35}H_{38}PSeSi$ [Cation]: 381.1645. Found: 381.1725.

CHN Analysis: Calcd for $C_{35}H_{39}BF_{20}PSeSi$: C, 47.05; H, 4.40. Found: C, 46.93; H, 4.59.

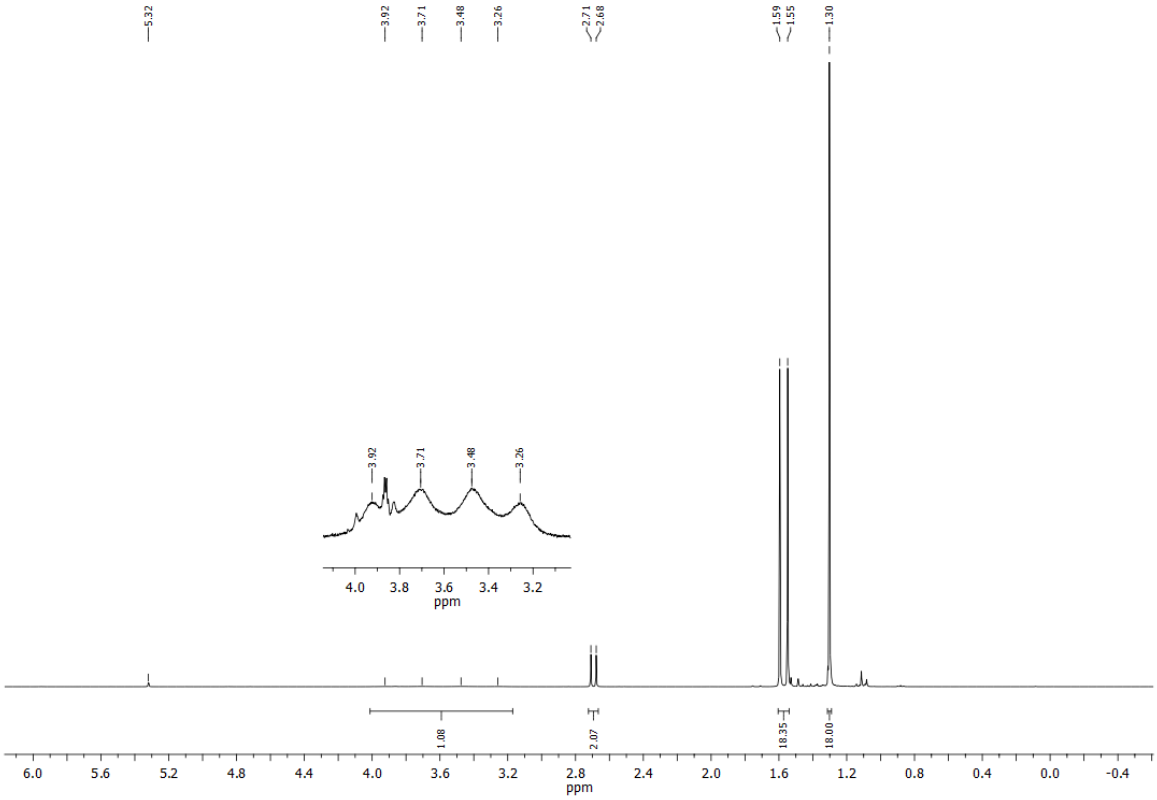

Figure S31: ^{1}H NMR spectrum (CD_2Cl_2, 298 K) of compound **8**[$HB(C_6F_5)_3$].

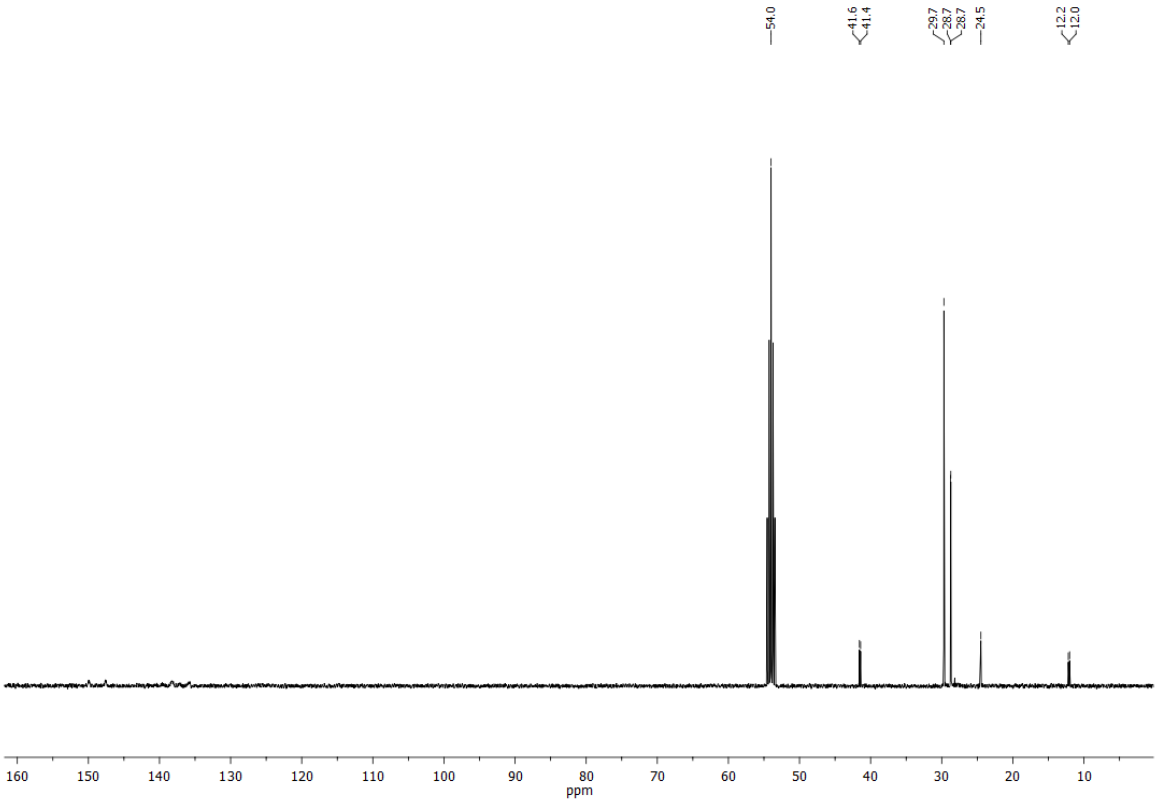

Figure S32: $^{13}C\{^{1}H\}$ NMR spectrum (CD_2Cl_2, 298 K) of compound **8**[$HB(C_6F_5)_3$].

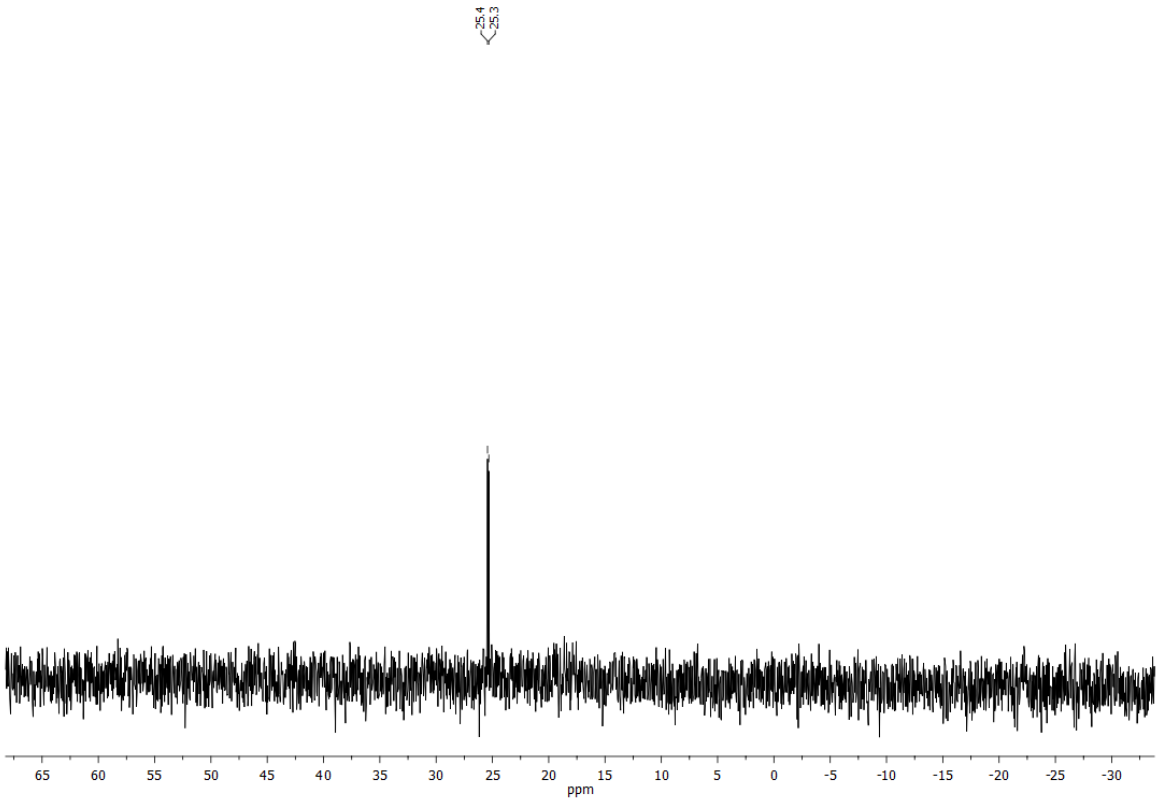

Figure S33: $^{29}Si\{^{1}H\}$ NMR spectrum (CD_2Cl_2, 298 K) of compound **8**[$HB(C_6F_5)_3$].

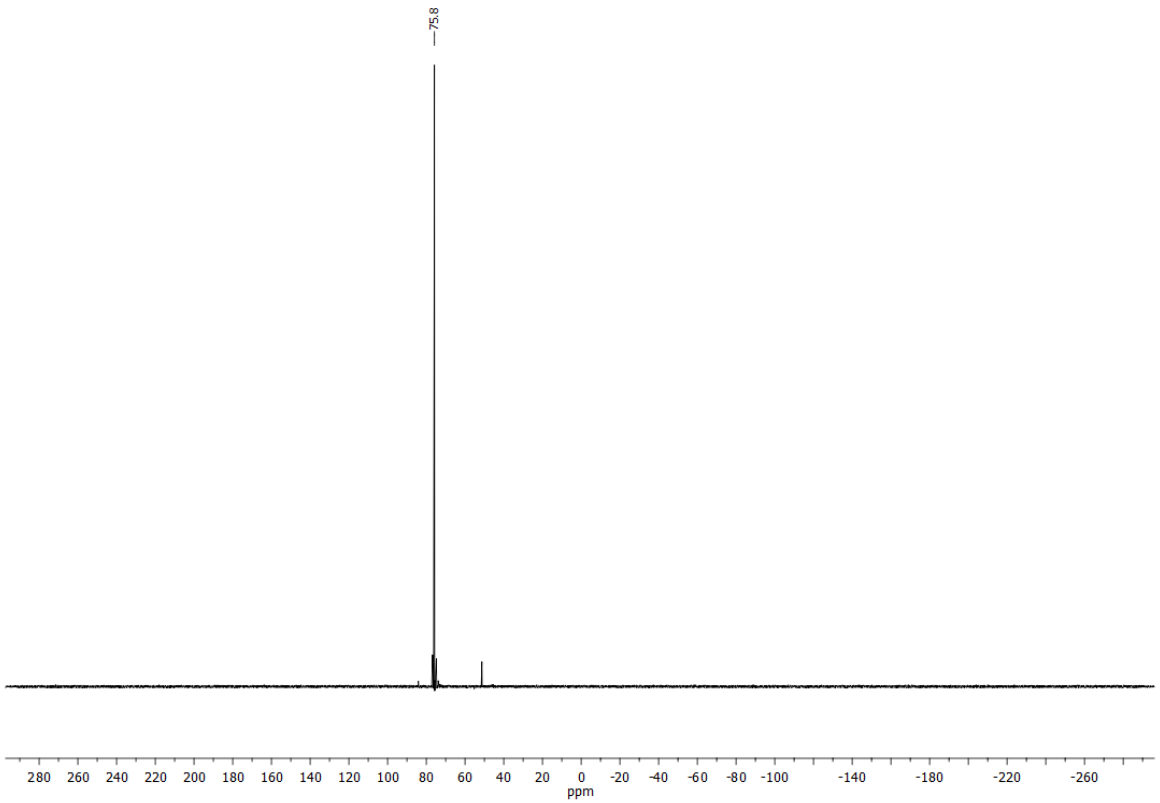

Figure S34: $^{31}P\{^{1}H\}$ NMR spectrum (CD_2Cl_2, 298 K) of compound **8**[$HB(C_6F_5)_3$].

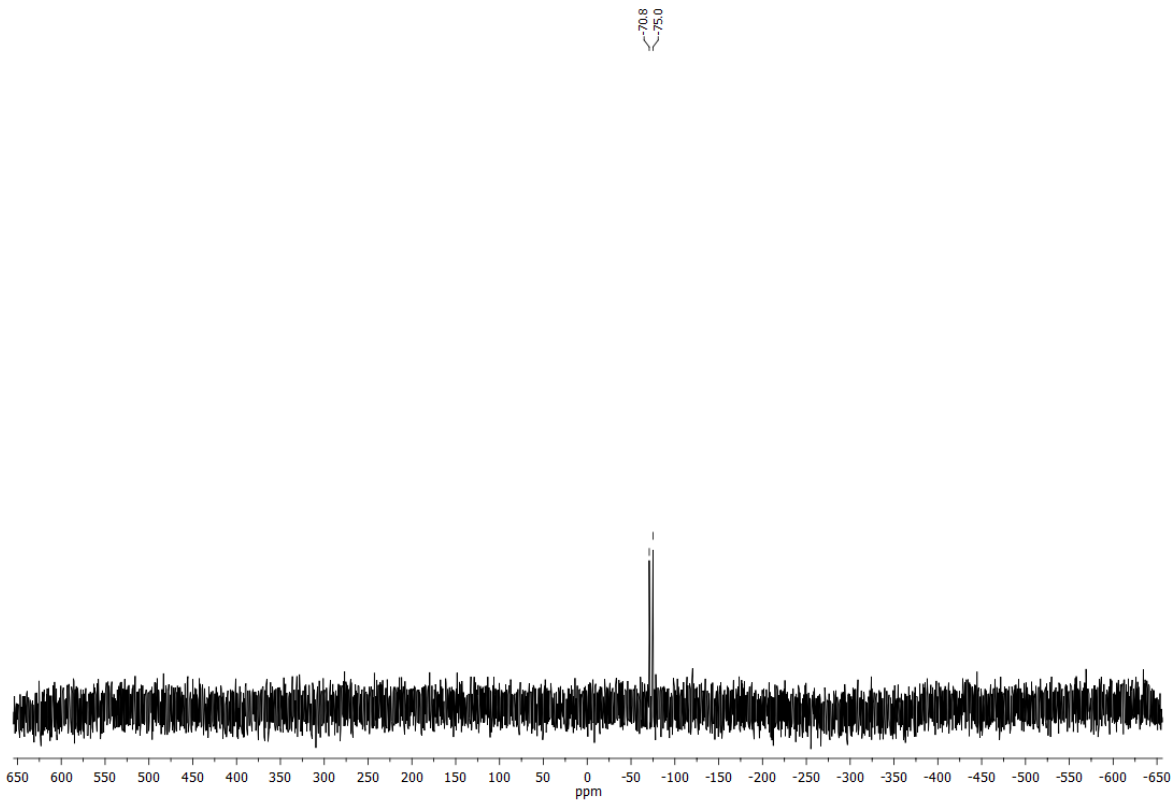

Figure S35: $^{77}Se\{^{1}H\}$ NMR spectrum (CD_2Cl_2, 298 K) of compound **8**[$HB(C_6F_5)_3$].

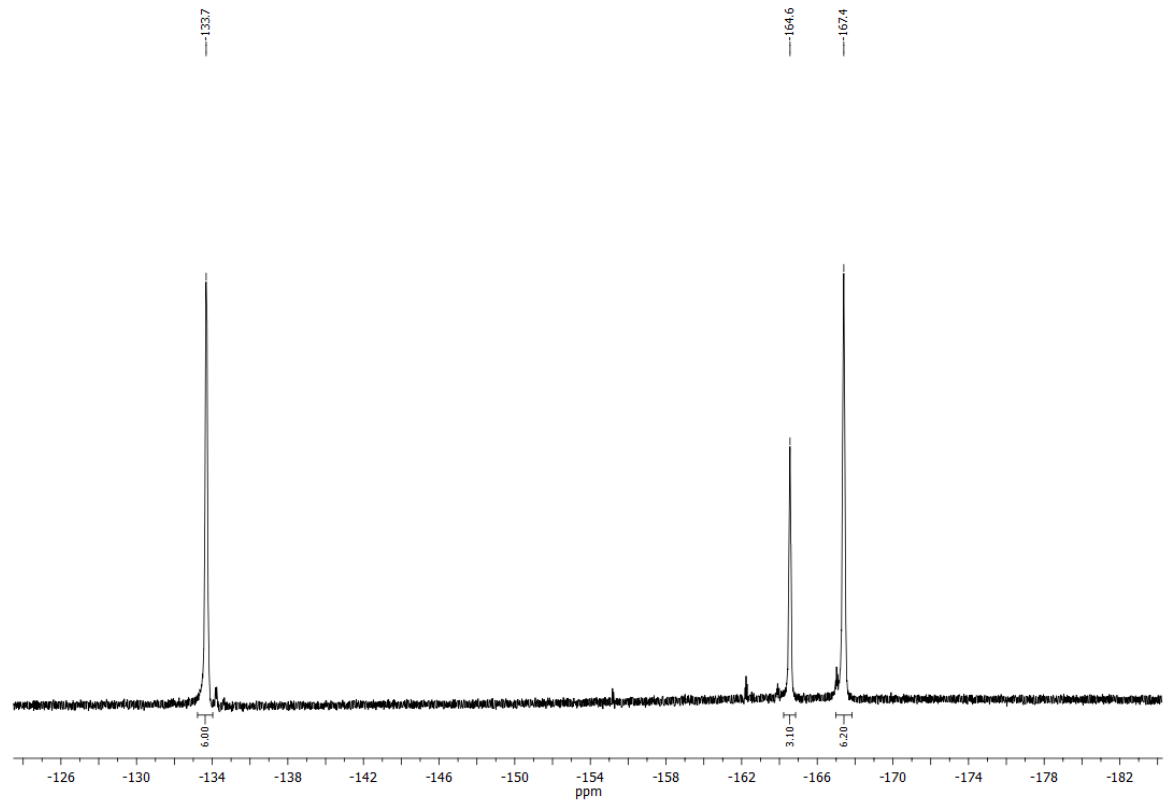

Figure S36: $^{19}F\{^{1}H\}$ NMR spectrum (CD_2Cl_2, 298 K) of compound **8**[$HB(C_6F_5)_3$].

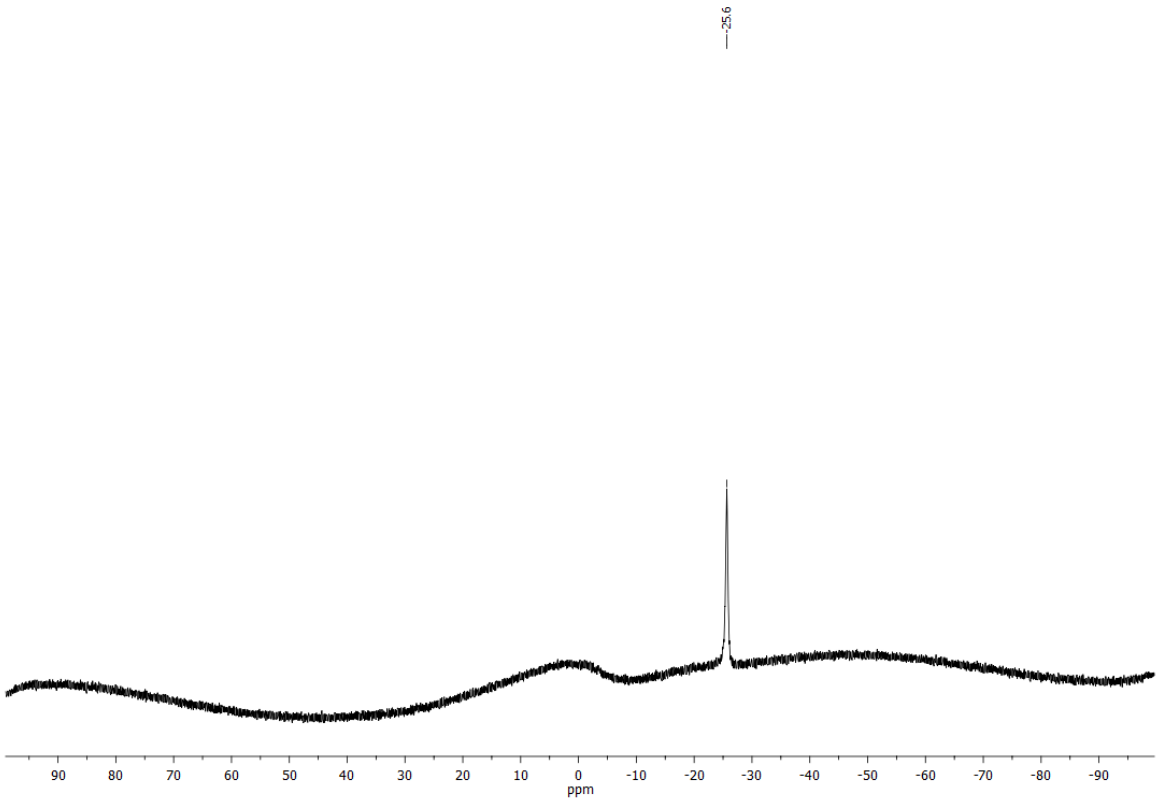

Figure S37: $^{11}B\{^{1}H\}$ NMR spectrum (CD_2Cl_2, 298 K) of compound **8**[$HB(C_6F_5)_3$].

3.6.10 Synthesis of compound 9[$B(C_6F_5)_4$]

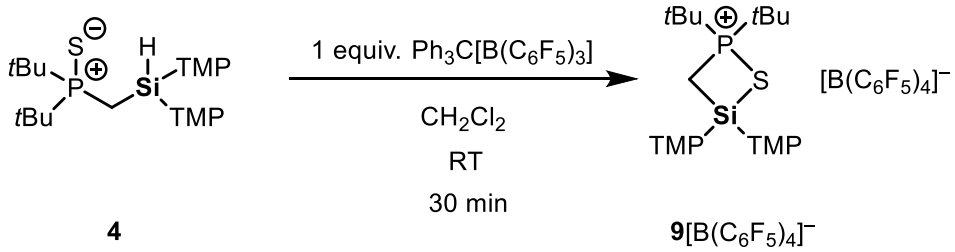

4 **9**[$B(C_6F_5)_4$]$^-$

Compound **4** (150 mg, 0.270 mmol, 1.0 equiv.) and tritylium tetrakis(pentafluorophenyl) borate (249 mg, 0.270 mmol, 1.0 equiv.) were dissolved in 5 mL DCM. The resulting solution was stirred for 30 min at room temperature. Then, all volatiles were removed *in vacuo* and the resulting oil was washed twice with 5 mL hexane. Colorless crystals of compound **9**[$B(C_6F_5)_4$] suitable for single-crystal X-ray diffraction analysis were obtained from a solution of the oil in 3 mL DCM layered with pentane at room temperature. Yield: 216 mg (0.175 mmol, 65%).

^{1}H NMR (400.13 MHz, CD_2Cl_2, 298 K): δ 6.10 (s, 4H, CH_{meta}), 3.81 [s, 6H, C(OCH_3)$_{para}$], 3.80 [s, 12H, C(OCH_3)$_{ortho}$], 2.78 (d, $^2J_{P-H}$ = 10.1 Hz, 2H, SiCH_2PS), 1.38 {d, $^3J_{P-H}$ = 17.7 Hz, 18H, PS[C(CH_3)$_3$]$_2$}.

$^{13}C\{^1H\}$ NMR (100.61 MHz, CD_2Cl_2, 298 K): δ 166.4 [s, $C(OCH_3)_{para}$], 166.0 [s, $C(OCH_3)_{ortho}$], 99.4 (s, C_{ipso}), 91.2 (s, CH_{meta}), 56.2 [s, $C(OCH_3)_{ortho}$], 56.0 [s, $C(OCH_3)_{para}$], 38.7 {d, $^1J_{C-P}$ = 24.8 Hz, PS[$C(CH_3)_3]_2$}, 26.1 {d, $^2J_{C-P}$ = 2.0 Hz, PS[$C(CH_3)_3]_2$}, 12.9 (d, $^1J_{C-P}$ = 24.6 Hz, $SiCH_2PS$).

$^{29}Si\{^1H\}$ NMR (79.49 MHz, CD_2Cl_2, 298 K): δ –12.5 (d, $^2J_{Si-P}$ = 19.8 Hz, $SiCH_2PS$).

$^{31}P\{^1H\}$ NMR (162.04 MHz, CD_2Cl_2, 298 K): δ 88.6 (s, $SiCH_2PS$).

$^{19}F\{^1H\}$ NMR (376.66 MHz, CD_2Cl_2, 298 K): δ –133.0 (s, 8F, CF_{ortho}), –163.6 (t, 4F, $^3J_{F-F}$ = 20.3 Hz, CF_{para}), –167.4 (t, 8F, $^3J_{F-F}$ = 17.2 Hz, CF_{meta}).

$^{11}B\{^1H\}$ NMR (128.43 MHz, CD_2Cl_2, 298 K): δ –16.9 (s, B).

HR(ESI–)-MS: Calcd *m/z* for $C_{24}BF_{20}$ $[M]^-$: 678.9773. Found: 678.9829.

CHN Analysis: Calcd for $C_{51}H_{42}BF_{20}O_6PSSi(0.45{\cdot}CH_2Cl_2)$: C, 48.6; H, 3.4. Found: C, 48.63; H, 3.45.

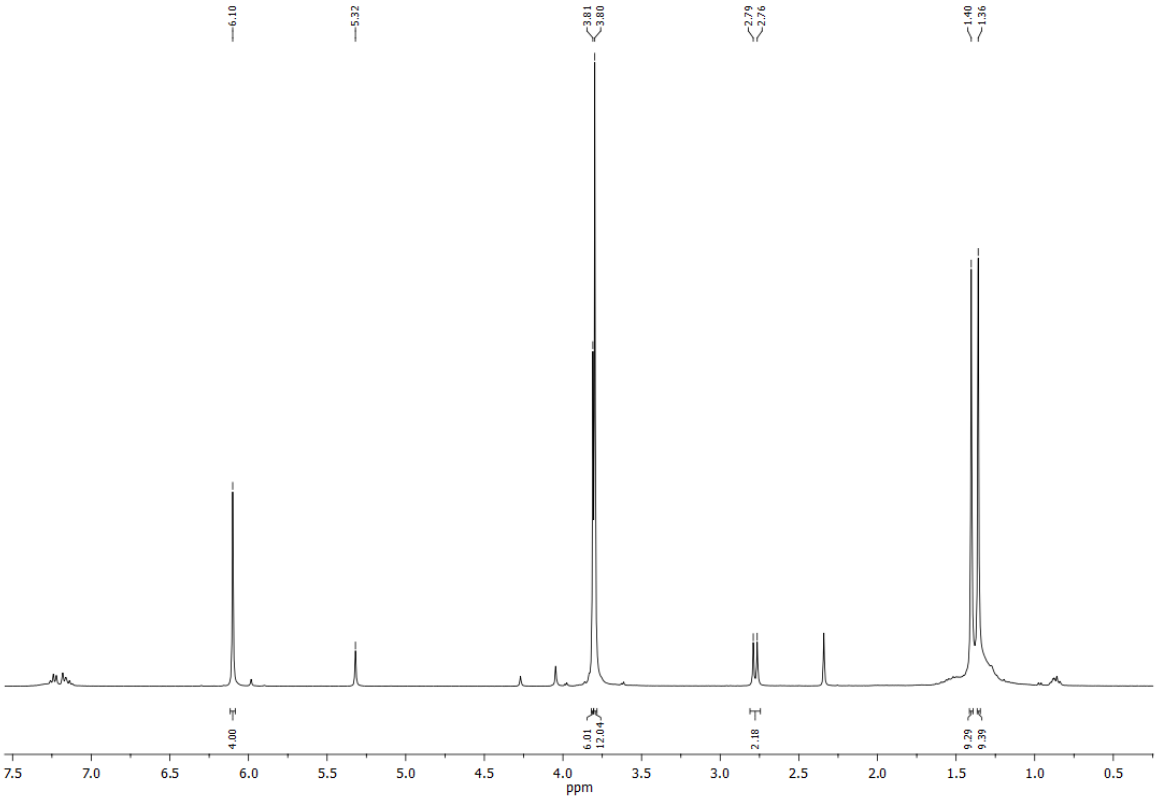

Figure S38: ^1H NMR spectrum (CD_2Cl_2, 298 K) of compound **9**[$B(C_6F_5)_4$]. TMP = 2,4,6-trimethoxyphenyl.

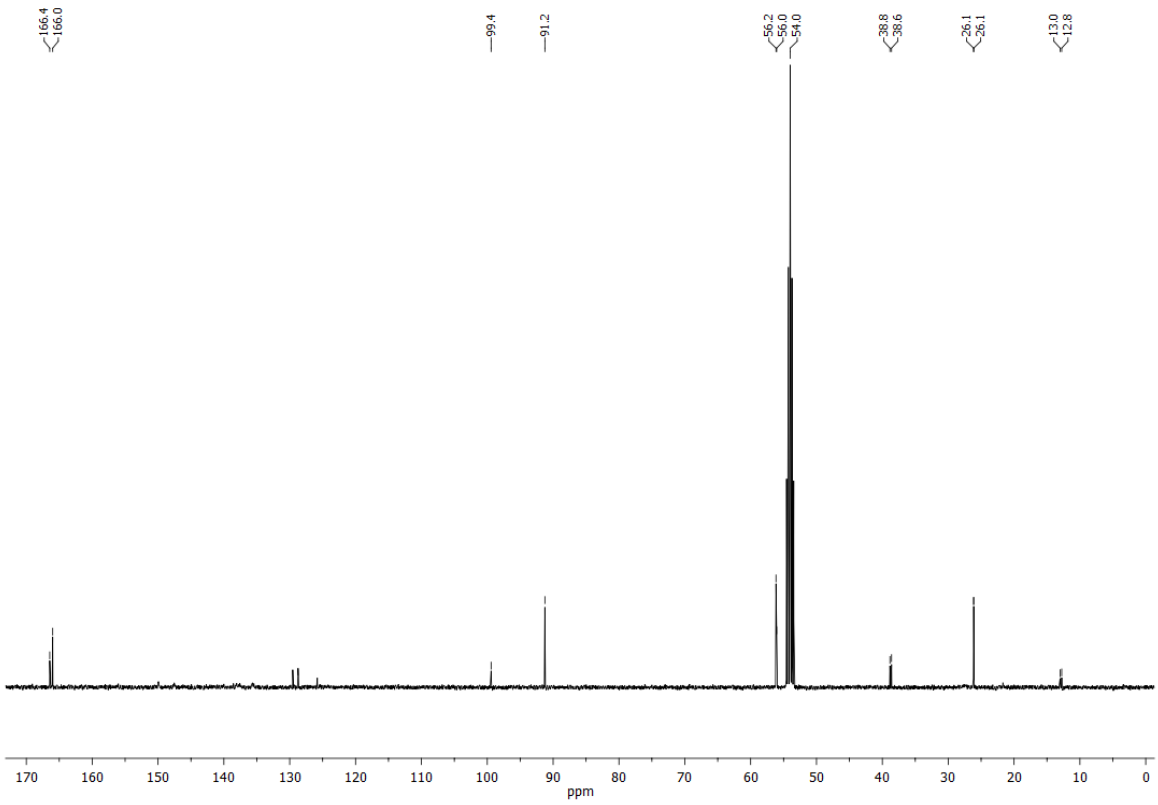

Figure S39: $^{13}C\{^{1}H\}$ NMR spectrum (CD_2Cl_2, 298 K) of compound **9**[$B(C_6F_5)_4$].

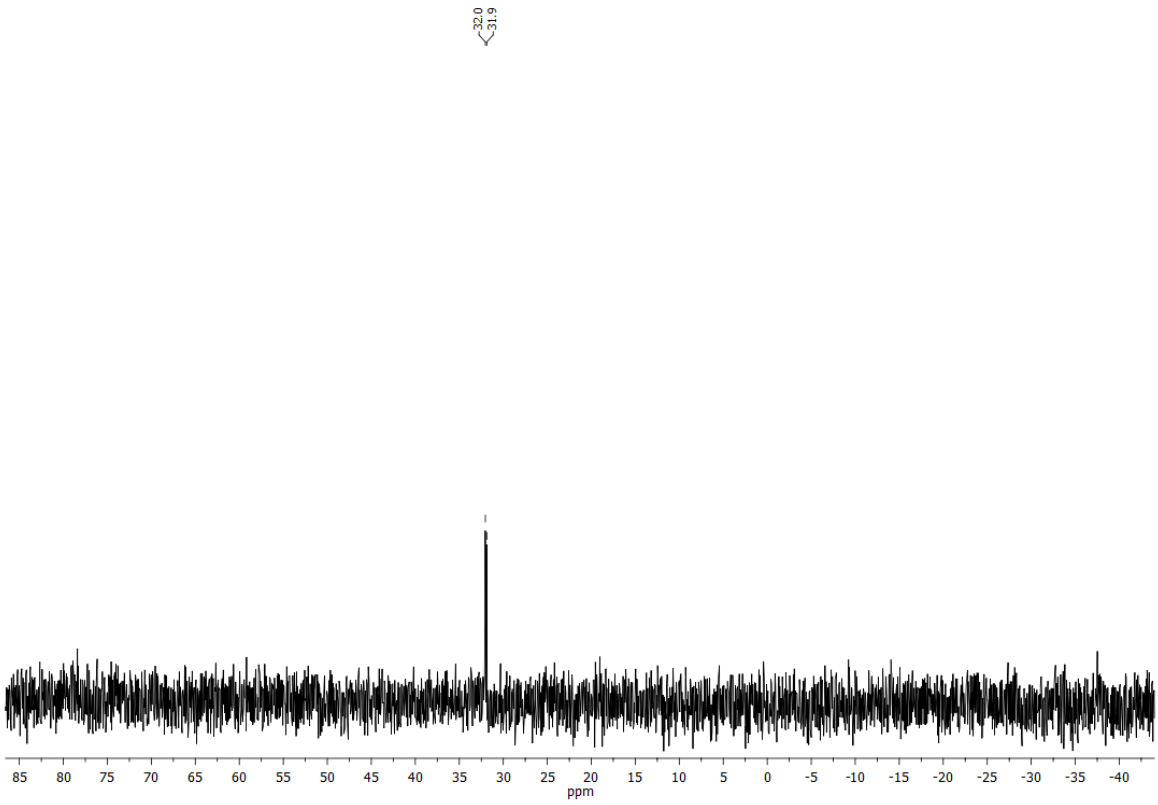

Figure S40: $^{29}Si\{^{1}H\}$ NMR spectrum (CD_2Cl_2, 298 K) of compound **9**[$B(C_6F_5)_4$].

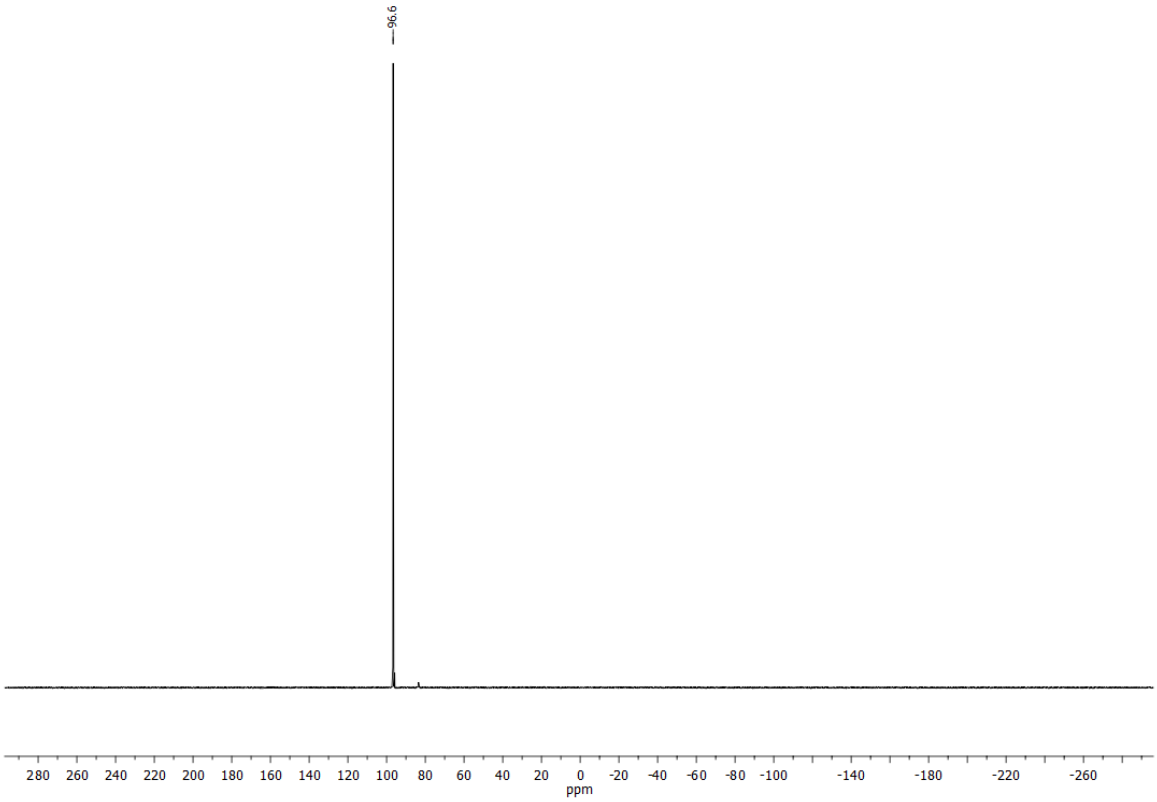

Figure S41: $^{31}P\{^{1}H\}$ NMR spectrum (CD_2Cl_2, 298 K) of compound **9**[$B(C_6F_5)_4$].

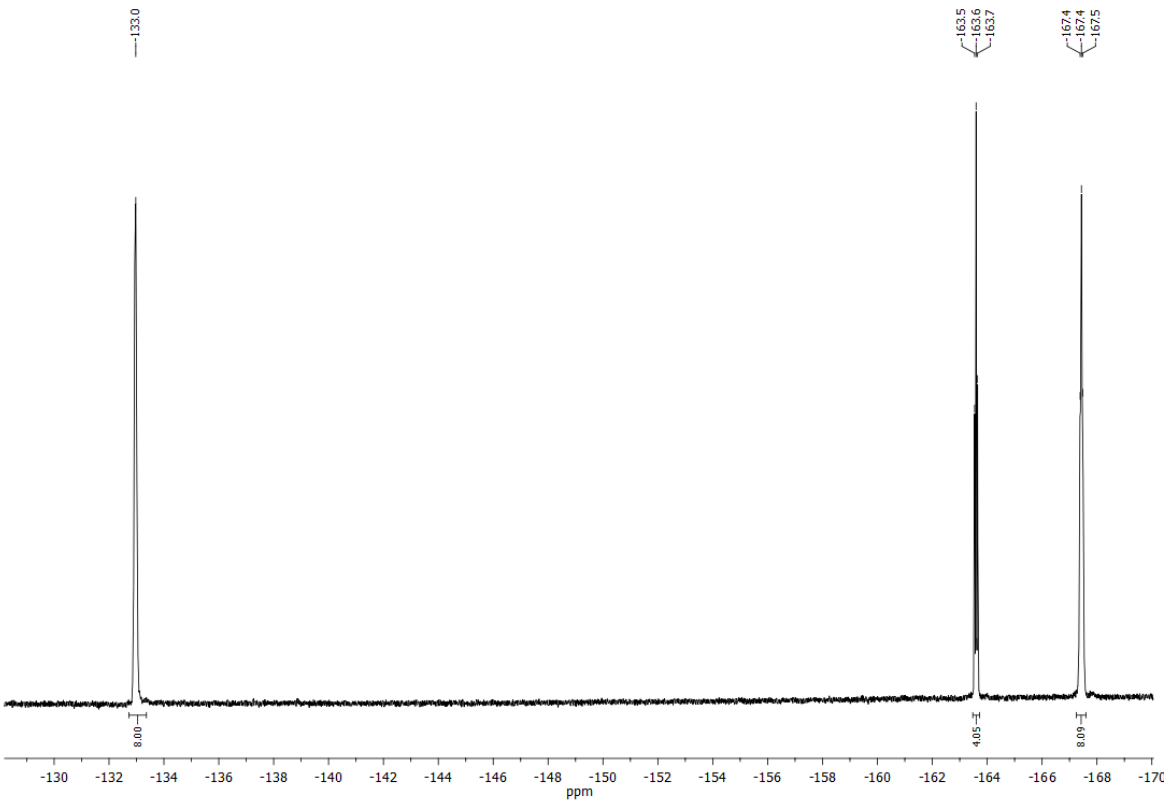

Figure S42: $^{19}F\{^{1}H\}$ NMR spectrum (CD_2Cl_2, 298 K) of compound **9**[$B(C_6F_5)_4$].

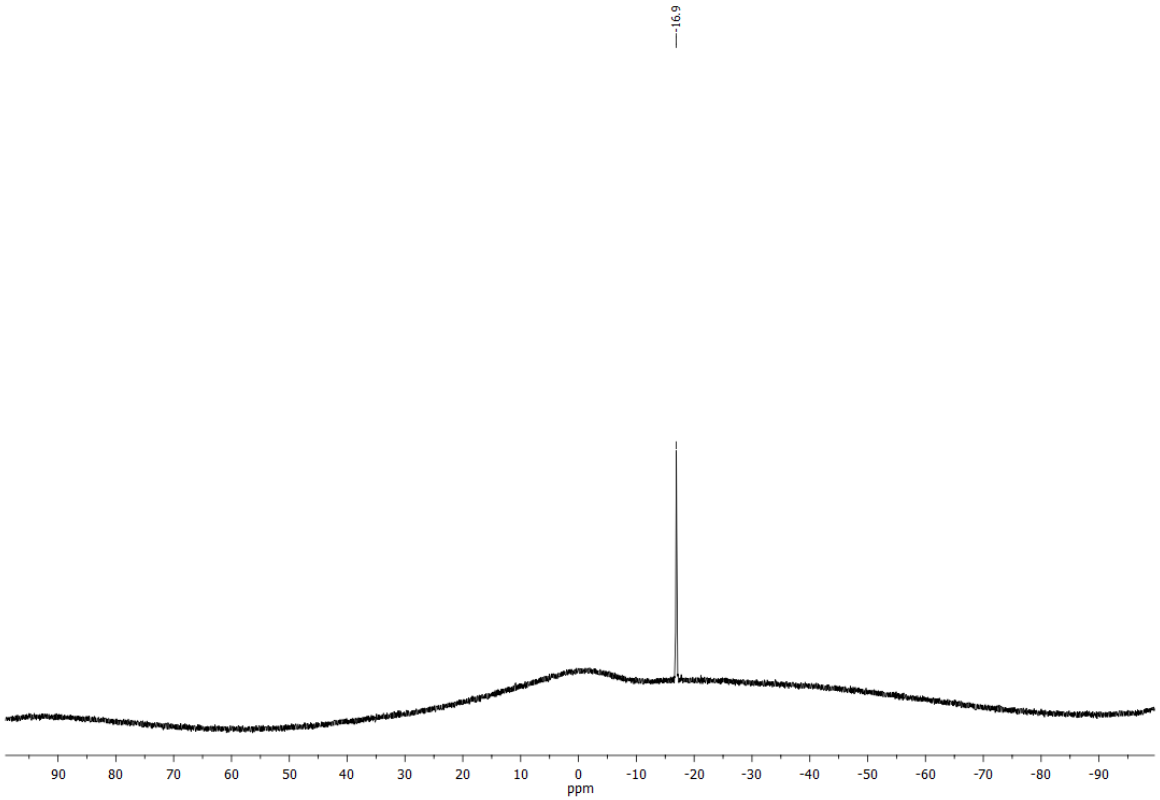

Figure S43: $^{11}B\{^{1}H\}$ NMR spectrum (CD_2Cl_2, 298 K) of compound **9**[$B(C_6F_5)_4$].

3.6.11 Synthesis of compound 10

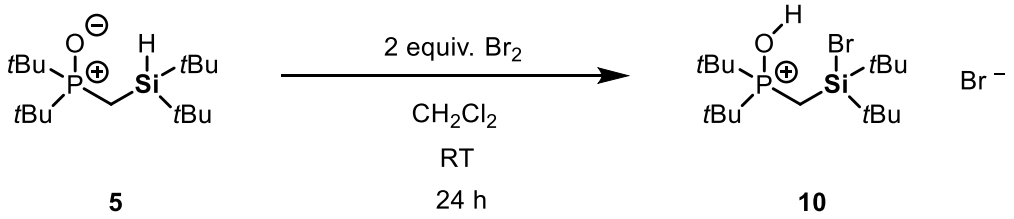

5 **10**

Bromine (0.1 mL, 1.95 mmol, 2.0 equiv.) was added to a solution of compound **5** (311 mg, 0.976 mmol, 1.0 equiv.) in 2 mL DCM. The mixture was stirred for 24 h at room temperature. Then, all volatiles were removed *in vacuo*. The remaining oil was washed three times with 3 mL of pentane to obtain compound **10** as a white powder. Yield 540 mg (0.96 mmol, 99%).

^{1}H NMR (400.13 MHz, CD_2Cl_2, 298 K): δ 12.19 (bs, 1H, O*H*), 1.64 [d, $^{2}J_{P-H}$ = 13.8 Hz, 2H, SiCH_2P(OH)], 1.53 {d, $^{3}J_{P-H}$ = 15.7 Hz, 18H, P(OH)[C(CH_3)$_3$]$_2$}, 1.19 {s, 18H, Si[C(CH_3)$_3$]$_2$}.

^{13}C{^{1}H} NMR (100.61 MHz, CD_2Cl_2, 298 K): δ 38.1 {d, $^{1}J_{C-P}$ = 50.5 Hz, P(OH)[*C*(CH$_3$)$_3$]$_2$}, 28.4 {s, Si[C(*C*H$_3$)$_3$]$_2$}, 27.7 {d, $^{2}J_{C-P}$ = 1.0 Hz, P(OH)[C(*C*H$_3$)$_3$]$_2$}, 24.0 {d, $^{3}J_{C-P}$ = 1.9 Hz, Si[*C*(CH$_3$)$_3$]$_2$}, 2.9 [d, $^{1}J_{C-P}$ = 58.9 Hz, Si*C*H$_2$P(OH)].

^{29}Si{^{1}H} NMR (79.49 MHz, CD_2Cl_2, 298 K): δ 32.0 [d, $^{2}J_{Si-P}$ = 12.9 Hz, *Si*CH_2P(OH)].

^{31}P{^{1}H} NMR (162.04 MHz, CD_2Cl_2, 298 K): δ 96.6 [s, $SiCH_2$*P*(OH)].

HR(ESI+)-MS: Calcd *m/z* for $C_{17}H_{39}BrOPSi$ $[M]^+$: 397.1669. Found: 397.1663.

CHN Analysis: Calcd for $C_{17}H_{39}Br_2OPSi$: C, 42.68; H, 8.22. Found: C, 42.41; H, 7.99.

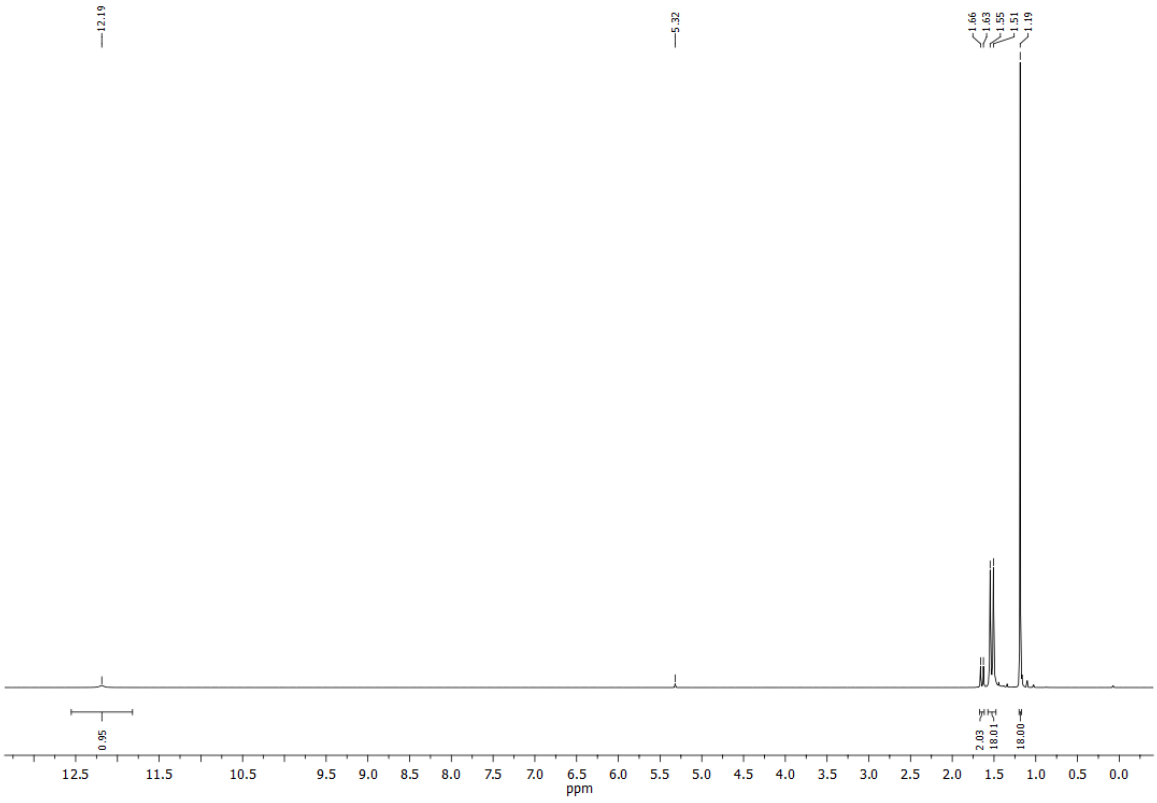

Figure S44: ^{1}H NMR spectrum (CD_2Cl_2, 298 K) of compound **10**.

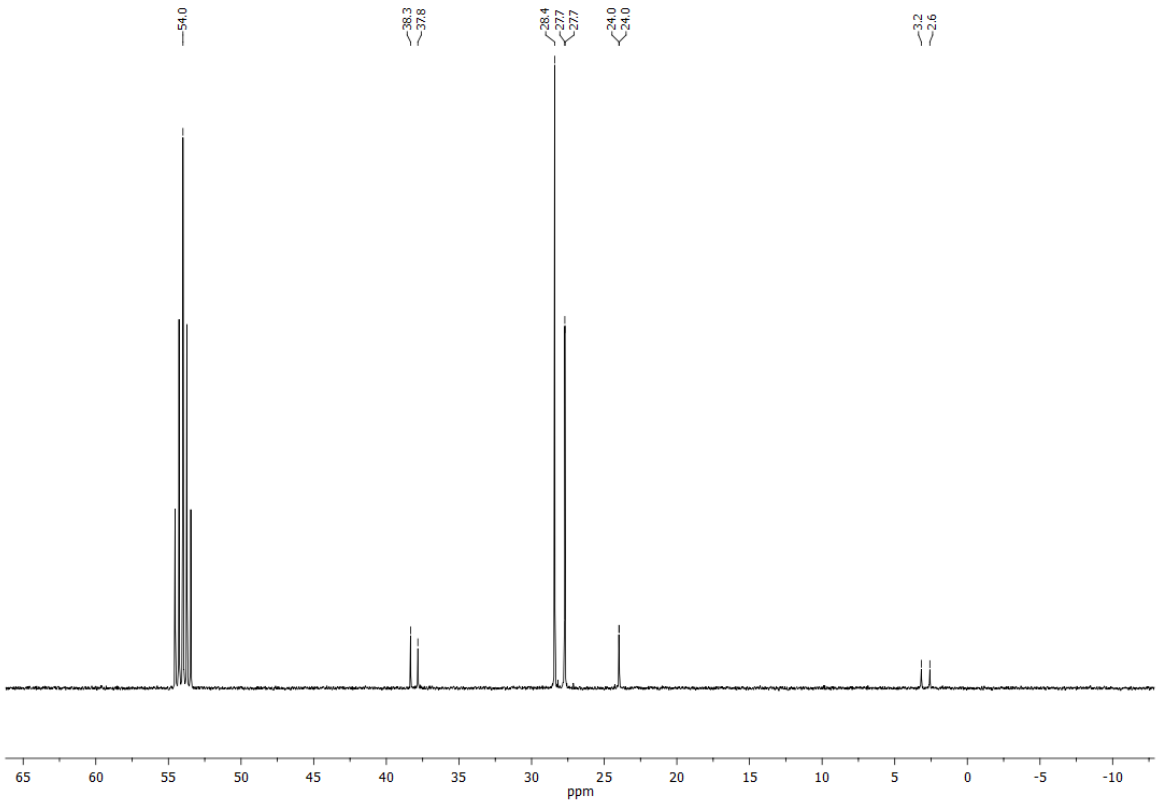

Figure S45: $^{13}C\{^{1}H\}$ NMR spectrum (CD_2Cl_2, 298 K) of compound **10**.

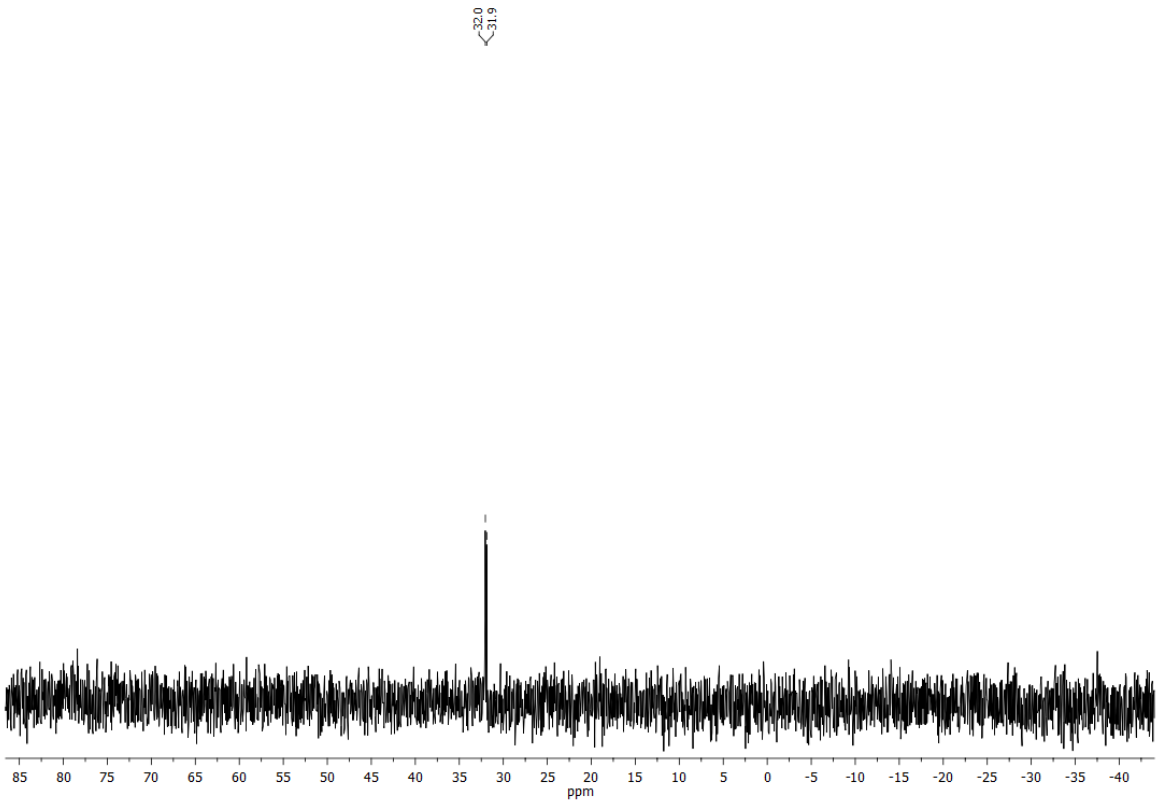

Figure S46: $^{29}Si\{^{1}H\}$ NMR spectrum (CD_2Cl_2, 298 K) of compound **10**.

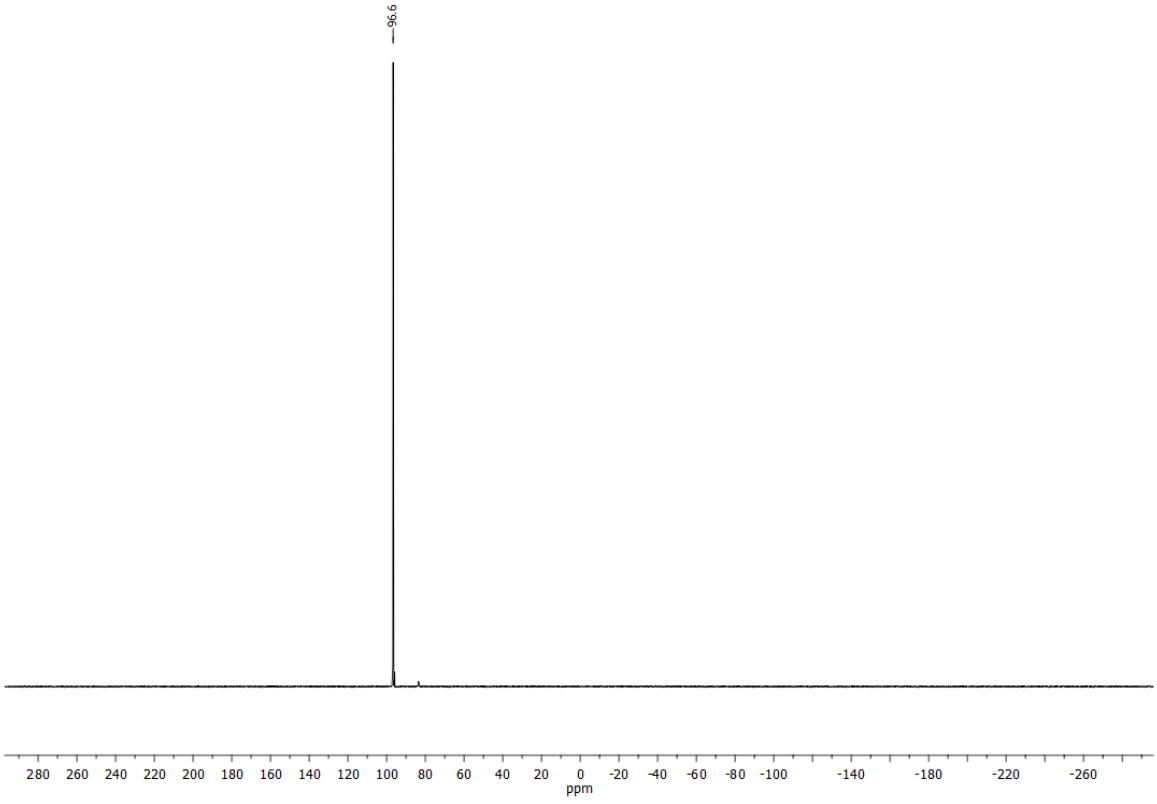

Figure S47: $^{31}P\{^{1}H\}$ NMR spectrum (CD_2Cl_2, 298 K) of compound **10**.

3.6.12 Reactions of Cyclic Silyl Phosphonium Ions with *para* Fluorobenzo-nitrile (*p*-FBN)

Compounds **7**[$HB(C_6F_5)_3$], **8**[$HB(C_6F_5)_3$], and **9**[$B(C_6F_5)_4$], respectively, (0.05 mmol, 1.0 equiv.) and *p*-FBN (0.05 mmol, 1.0 equiv.) were dissolved in 0.5 mL dichloromethane-d^2 and loaded into a Young-type NMR tube. The tube was left at room temperature for 2 h before subjecting the samples to NMR measurements.

7[$HB(C_6F_5)_3$]: Hydrosilylation of *p*-FBN was observed. Additional singals were identified as unreacted **7**[$HB(C_6F_5)_3$] (▲) and the tris(pentafluorophenyl)borane**–***p*-FBN adduct (★).

^{1}H NMR (400.13 MHz, CD_2Cl_2, 298 K): δ 9.65 (s, 1H, N=C*H*), 7.83 (m, 2H, CH_{Ar}), 7.13 (m, 2H, CH_{Ar}), 1.34 [s, 9H, P(S)C(CH_3)$_3$], 1.31 [s, 9H, P(S)C(CH_3)$_3$] (hidden under singlet of **7**), 1.16 {s, 18H, Si[C(CH_3)$_3$]$_2$}. **^{31}P{^{1}H} NMR** (162.04 MHz, CD_2Cl_2, 298 K): δ 78.5. **^{19}F{^{1}H} NMR** (376.66 MHz, CD_2Cl_2, 298 K): δ –109.6 (s, 1H).

8[$HB(C_6F_5)_3$]: Hydrosilylation of *p*-FBN was observed. Additional singals were identified as unreacted **8**[$HB(C_6F_5)_3$] (▲) and the tris(pentafluorophenyl)borane**–***p*-FBN adduct (★).

^{1}H NMR (400.13 MHz, CD_2Cl_2, 298 K): δ 9.69 (s, 1H, N=C*H*), 7.83 (m, 2H, CH_{Ar}), 7.13 (m, 2H, CH_{Ar}), 1.37 [s, 9H, P(Se)C(CH_3)$_3$], 1.33 [s, 9H, P(Se)C(CH_3)$_3$], 1.17 {s, 18H, Si[C(CH_3)$_3$]$_2$}. **^{31}P{^{1}H} NMR** (162.04 MHz, CD_2Cl_2, 298 K): δ 73.8. **^{19}F{^{1}H} NMR** (376.66 MHz, CD_2Cl_2, 298 K): δ –109.5 (s, 1H).

9[$B(C_6F_5)_4$]: The ^{19}F{^{1}H} NMR spectrum shows no interaction between cation **9** and *p*-FBN. The ^{19}F{^{1}H} NMR spectrum clearly shows free *p*-FBN at –103.2 ppm and unreacted **9**[$B(C_6F_5)_4$] (▲).

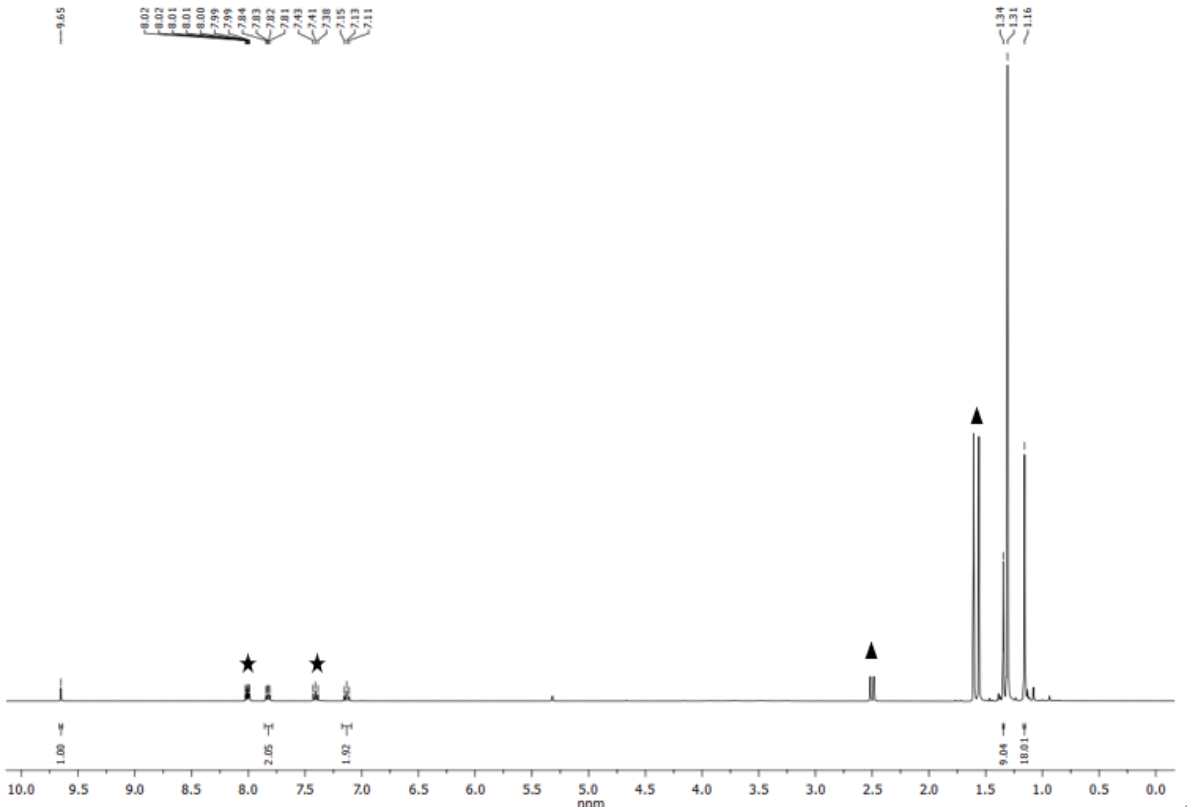

Figure S48: ^{1}H NMR spectrum (CD_2Cl_2, 298 K) of the reaction of compound **7**[$HB(C_6F_5)_3$] with *p*-FBN.

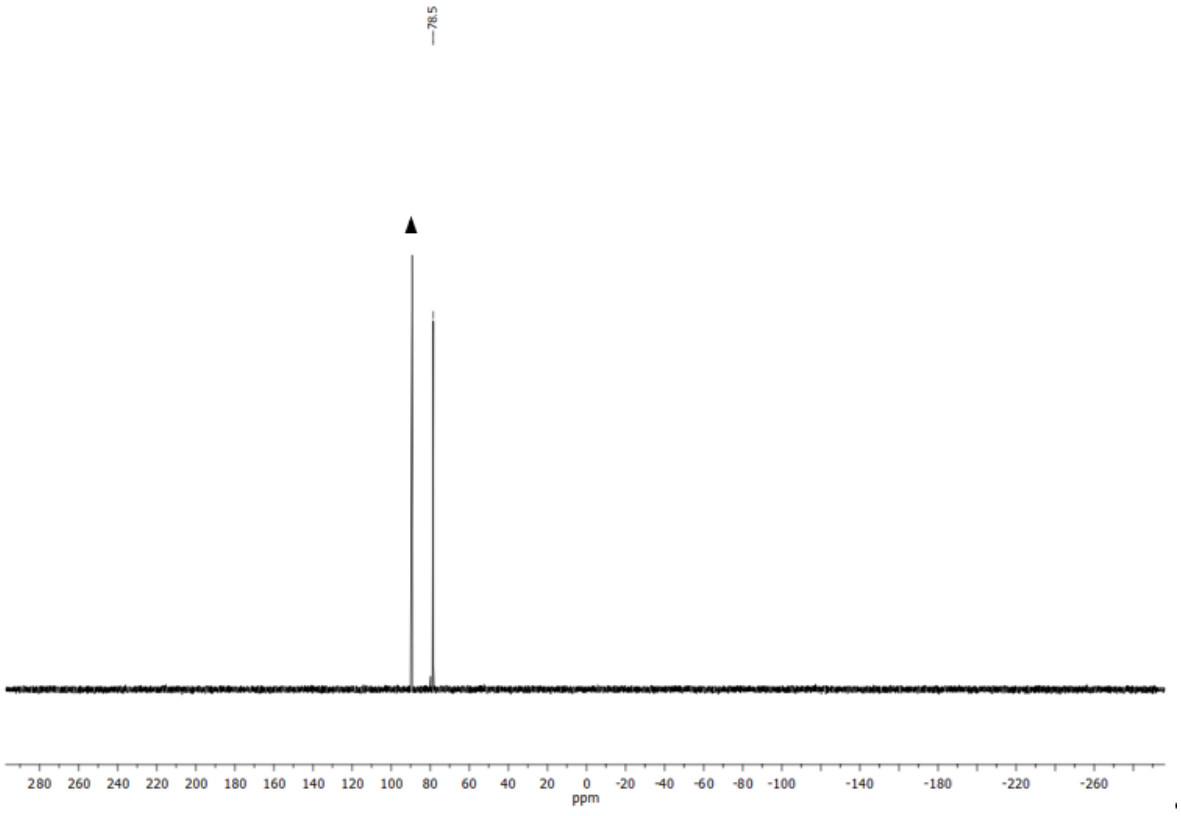

Figure S49: $^{31}P\{^{1}H\}$ NMR spectrum (CD_2Cl_2, 298 K) of the reaction of compound **7**[$HB(C_6F_5)_3$] with *p*-FBN.

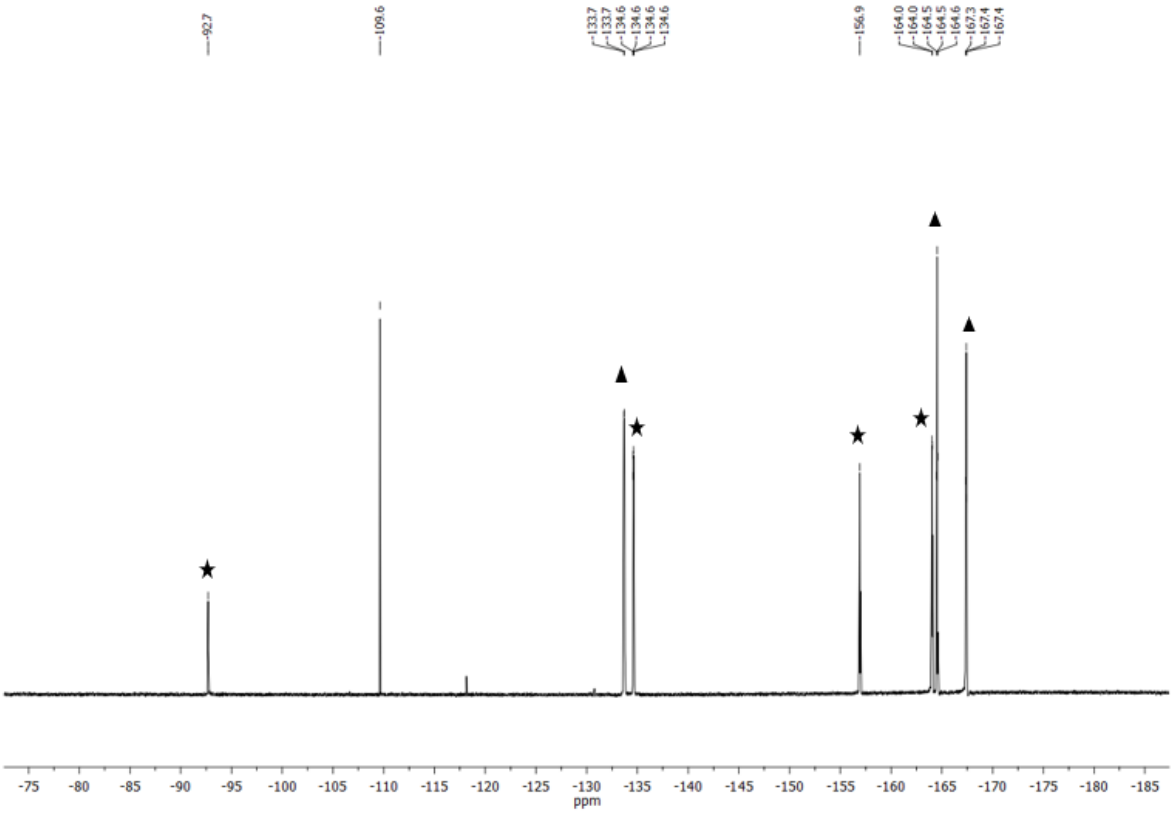

Figure S50: $^{19}F\{^{1}H\}$ NMR spectrum (CD_2Cl_2, 298 K) of the reaction of compound **7**[$HB(C_6F_5)_3$] with *p*-FBN.

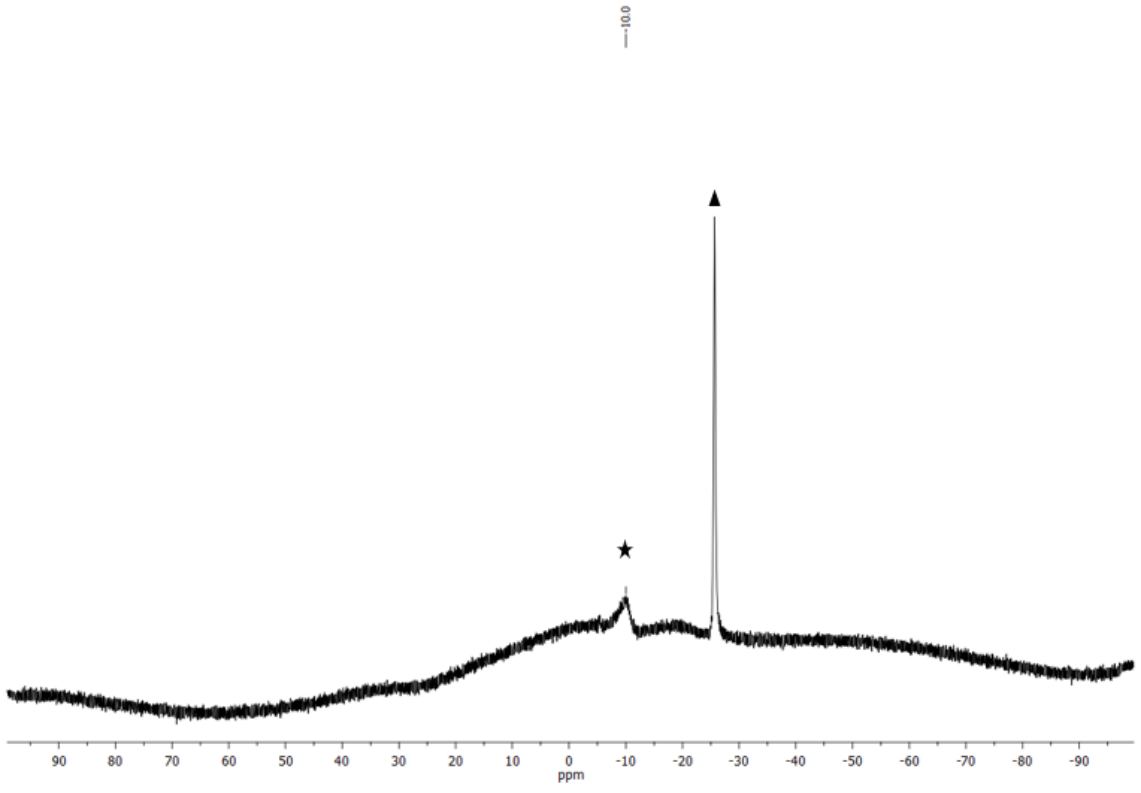

Figure S51: $^{11}B\{^{1}H\}$ NMR spectrum (CD_2Cl_2, 298 K) of the reaction of compound **7**[$HB(C_6F_5)_3$] with *p*-FBN.

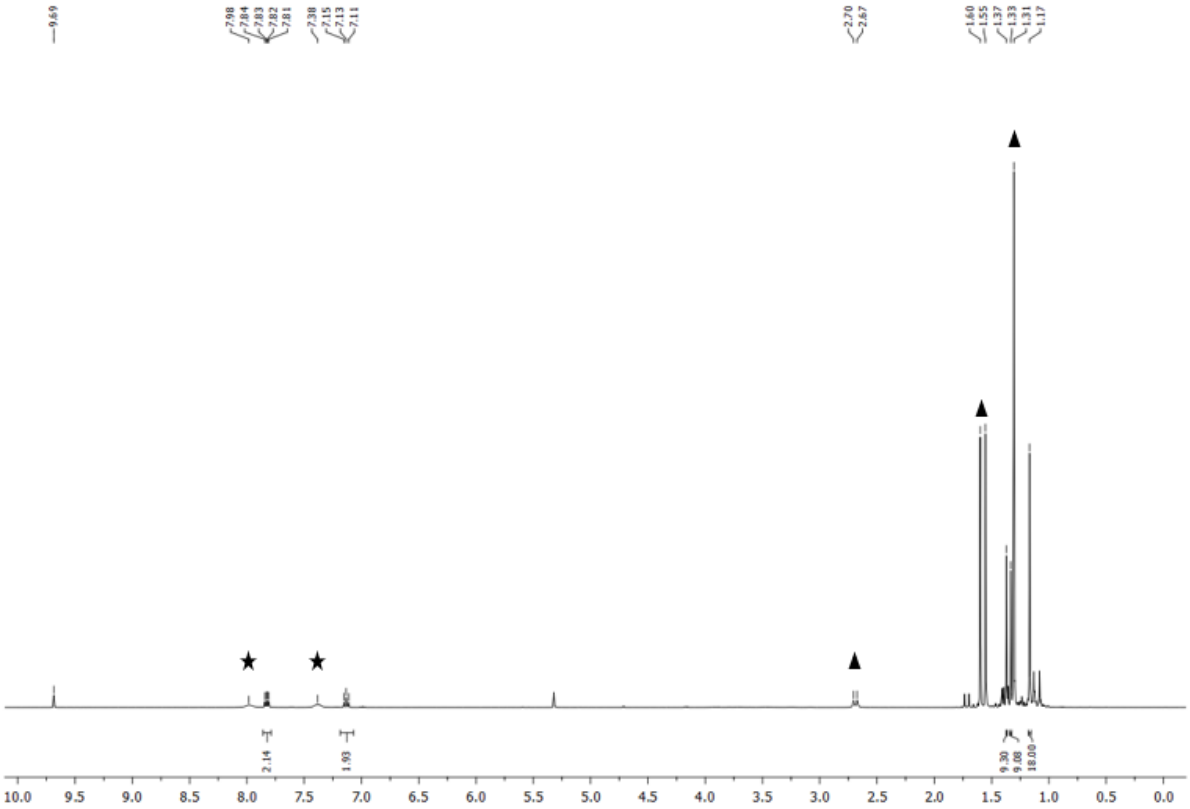

Figure S52: ^{1}H NMR spectrum (CD_2Cl_2, 298 K) of the reaction of compound **8**[$HB(C_6F_5)_3$] with *p*-FBN.

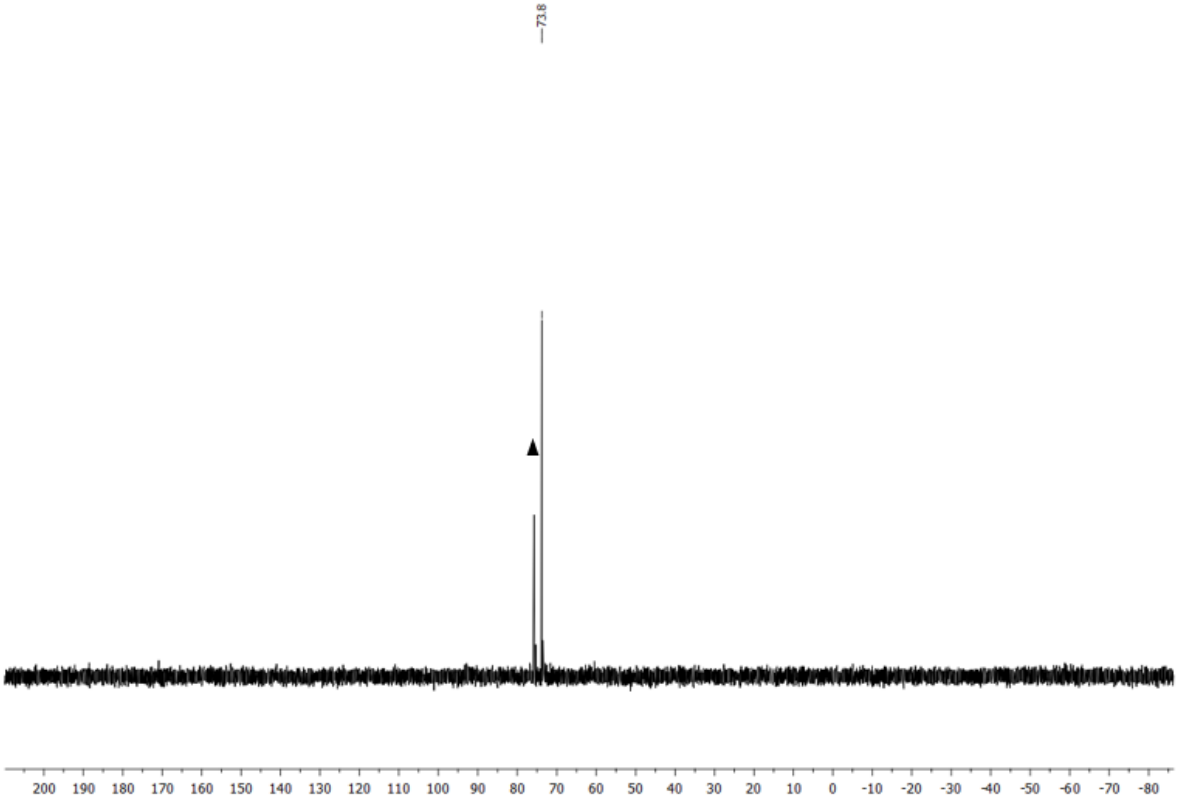

Figure S53: $^{31}P\{^{1}H\}$ NMR spectrum (CD_2Cl_2, 298 K) of the reaction of compound **8**[$HB(C_6F_5)_3$] with *p*-FBN.

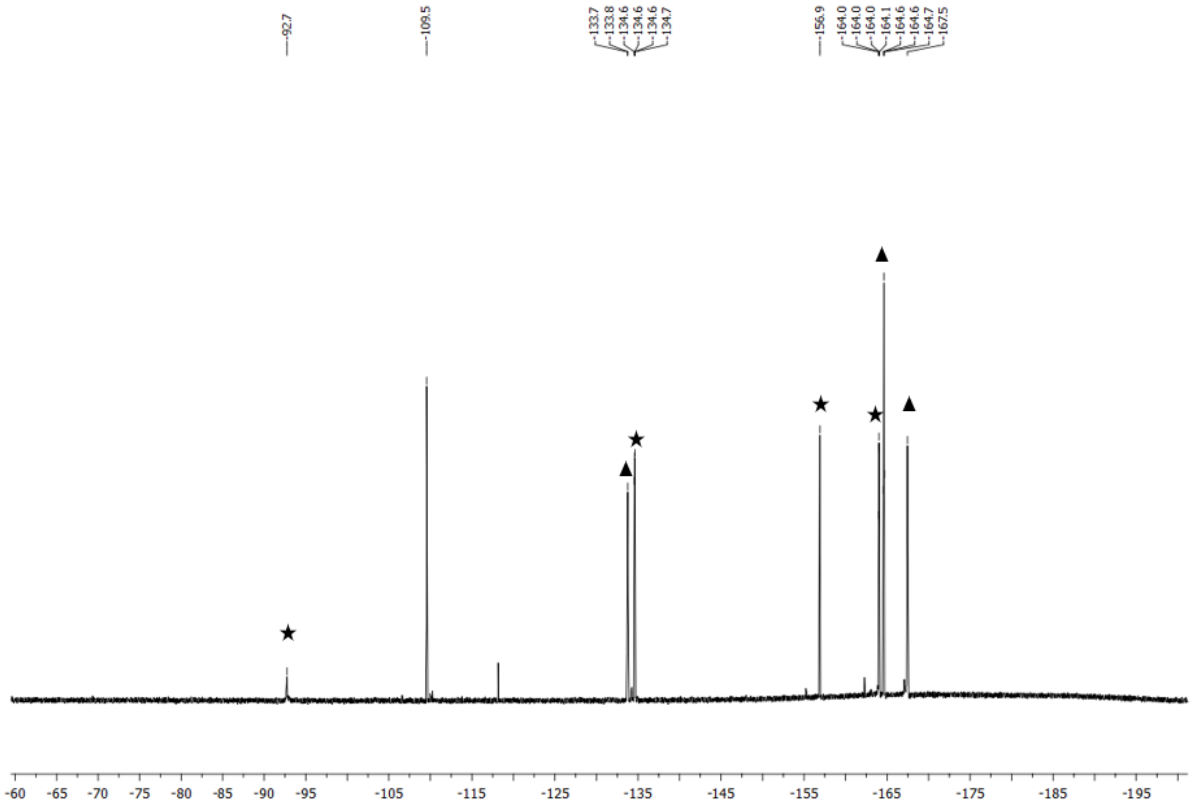

Figure S54: $^{19}F\{^{1}H\}$ NMR spectrum (CD_2Cl_2, 298 K) of the reaction of compound **8**[$HB(C_6F_5)_3$] with *p*-FBN.

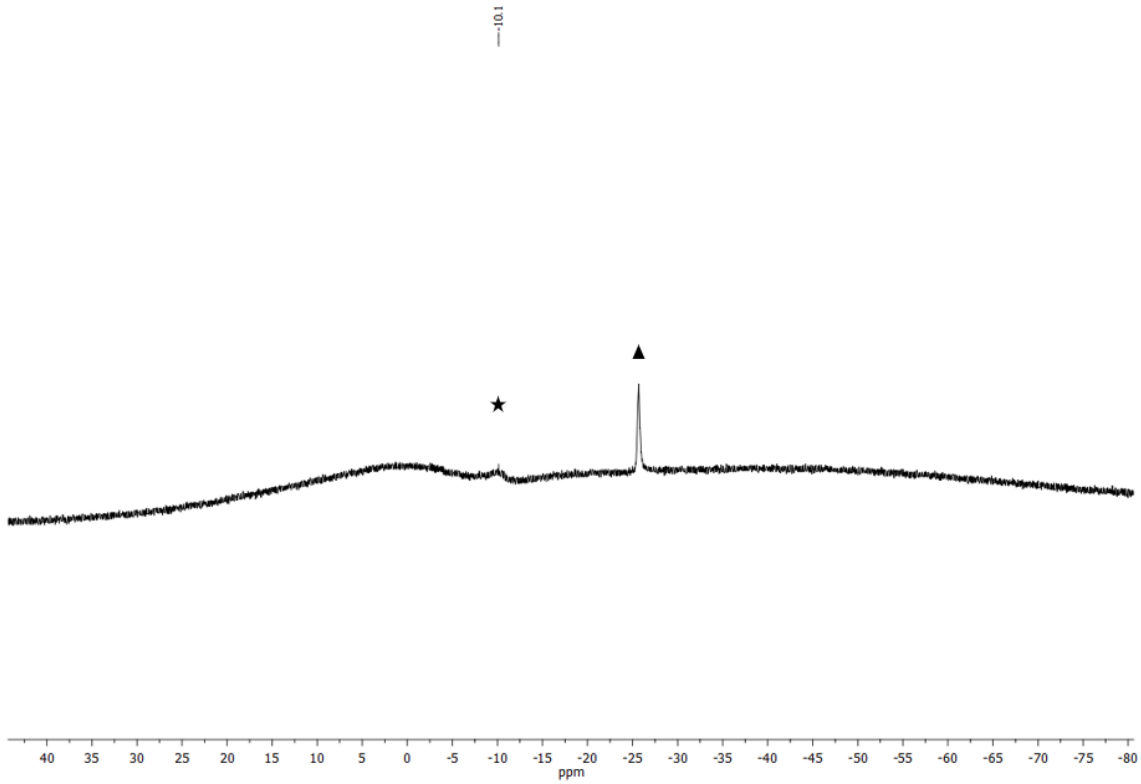

Figure S55: $^{11}B\{^{1}H\}$ NMR spectrum (CD_2Cl_2, 298 K) of the reaction of compound **8**[$HB(C_6F_5)_3$] with *p*-FBN.

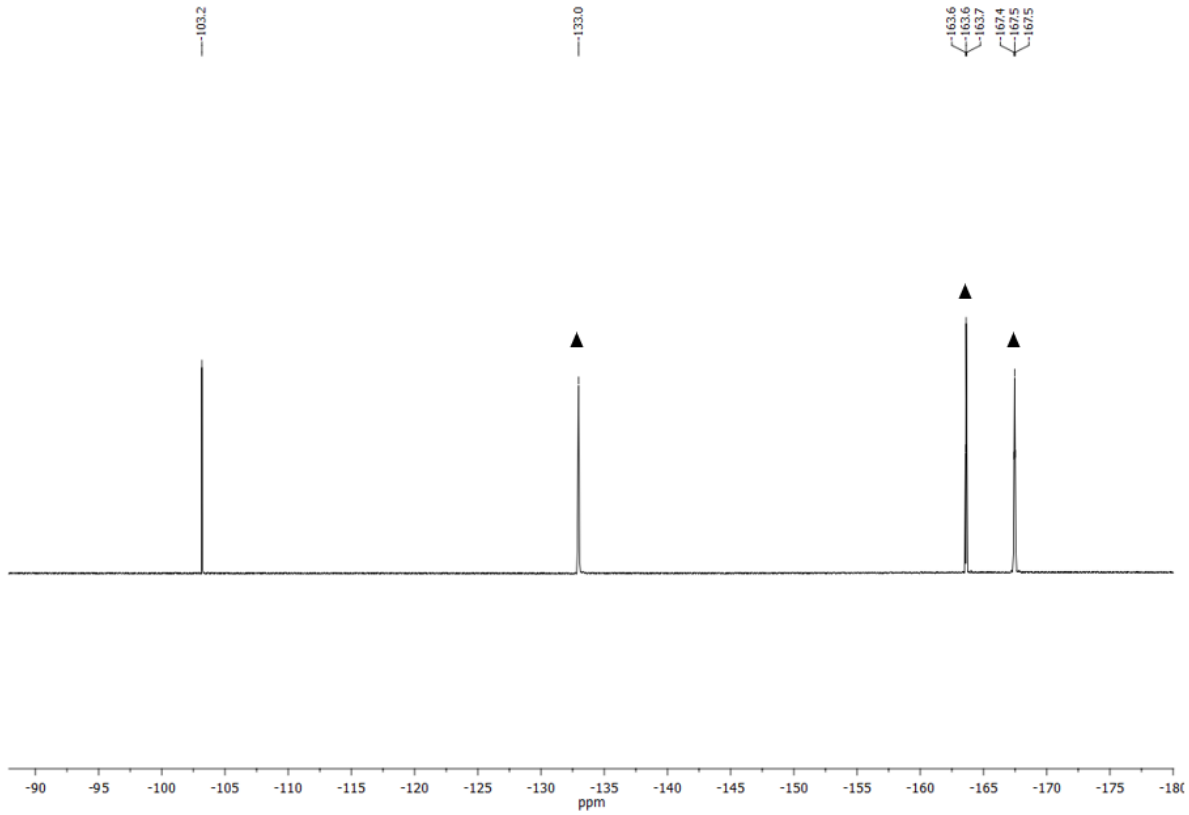

Figure S56: $^{19}F\{^{1}H\}$ NMR spectrum (CD_2Cl_2, 298 K) of compound **9**[$B(C_6F_5)_4$] and *p*-FBN.

3.6.13 Single-crystal X-ray diffraction

The crystals were selected and measured either on a SuperNova Dualflex diffractometer equipped with a TitanS2 detector {**4**, **7**[$HB(C_6F_5)_3$], and **9**[$B(C_6F_5)_4$]} or on a XtaLAB Synergy R, DW system, equipped with a HyPix-Arc 150 detector {**3**, **5**, **6**, and **8**[$HB(C_6F_5)_3$]}. Data collection and reduction were performed with CrysAlisPro {Version 1.171.41.90a for **7**[$HB(C_6F_5)_3$] and 1.171.41.93a for all other compounds}.[6] An analytical numeric absorption correction using a multifaceted crystal model, based on expressions derived by Clark and Reid,[7] and an empirical absorption correction using spherical harmonics, implemented in SCALE3 ABSPACK scaling algorithm, was applied for compound **7**[$HB(C_6F_5)_3$]. A numerical absorption correction based on Gaussian integration over a multifaceted crystal model, and an empirical absorption correction using spherical harmonics, implemented in SCALE3 ABSPACK scaling algorithm was applied for all other compounds. Using Olex2,[8] the structures were solved with ShelXT[9] and a least-square refinement on F^2 was carried out with ShelXL[10]. All non-hydrogen atoms were refined anisotropically. Hydrogen atoms at the carbon atoms were located in idealized positions and refined isotropically according to the riding model. Hydrogen atoms at the boron and silicon atoms were located from the difference Fourier map and refined without restraints. The figures in the paper were created with CrystalExplorer 17.5,[11] the figures in the Supporting Information were created with Olex2[8]. X-ray crystallographic data can be found in the Supporting Information.

Compound **3**: The asymmetric unit contains two molecules.

Compound **4**: The asymmetric unit contains one molecule.

Compound **5**: The asymmetric unit contains one molecule.

Compound **6**: The asymmetric unit contains one molecule. One *tert*-butyl fragment is disordered over two positions and split into two parts with occupancies of 60:40.

Compound **7**[$HB(C_6F_5)_3$]: The asymmetric unit contains two molecules. Two *tert*-butyl fragments are disordered over two positions and split into two parts with occupancies of 50:50. SADI, SIMU, and DFIX restraints were used to model the disorder of one of the two CPSSi rings (occupancies of 50:50).

Compound **8**[$HB(C_6F_5)_3$]: The asymmetric unit contains one molecule.

Compound **9**[$B(C_6F_5)_4$]: The asymmetric unit contains one molecule. The sulfur atom and the $–CH_2–$ moiety are each disordered over two positions and split into two parts with occupancies of 80:20.

Table S1: Crystallographic data for compounds **3**, **4**, and **5**.

Compound	**3**	**4**	**5**
Data Set (internal naming)	AF109	AF140	AF99
CCDC Number	2184165	2184166	2184167
Formula	$C_{17}H_{39}PSSi$	$C_{27}H_{43}O_6PSSi$	$C_{17}H_{39}OPSi$
$\rho_{calc.}$ / g·cm^{-3}	1.072	1.232	1.049
μ/mm^{-1}	2.580	2.153	1.726
Formula Weight	334.60	554.73	318.54
Color	clear colorless	clear colorless	clear colorless
Shape	plate	block	block
Size/mm^3	0.16 × 0.09 × 0.04	0.77 × 0.28 × 0.18	0.27 × 0.14 × 0.08
T/K	123.01(10)	122.97(10)	123.0(1)
Crystal System	monoclinic	monoclinic	monoclinic
Space Group	$P2_1/c$	$P2_1/c$	$P2_1/c$
a/Å	10.8678(2)	10.16340(10)	15.5121(3)
b/Å	25.1588(3)	14.39300(10)	10.9551(2)
c/Å	15.7629(2)	20.46580(10)	11.9723(2)
α/°	90	90	90
β/°	105.845(2)	92.3280(10)	97.383(2)
γ/°	90	90	90
V/Å^3	4146.14(11)	2991.30(4)	2017.66(6)
Z	8	4	4
Z'	2	1	1
Wavelength/Å	1.54184	1.54184	1.54184
Radiation Type	Cu K_α	Cu K_α	Cu K_α
$2\Theta_{min}$/°	6.806	7.512	5.744
$2\Theta_{max}$/°	146.686	159.578	149.88
Measured Refl.	63772	52297	24736
Independent Refl.	8172	5335	4112
R_{int}	0.0374	0.0598	0.0185
Parameters	393	341	197
Restraints	0	0	0
Largest Peak	0.38	0.50	0.31
Deepest Hole	−0.40	−0.33	−0.28
GooF	1.031	1.067	1.049
wR_2 (all data)	0.0855	0.1057	0.0801
wR_2	0.0842	0.0977	0.0794
R_1 (all data)	0.0340	0.0371	0.0305
R_1	0.0321	0.0371	0.0295

Table S2: Crystallographic data for compounds **6** and **7**[$HB(C_6F_5)_3$].

Compound	**6**	**7[$HB(C_6F_5)_3$]**
Data Set (internal naming)	AF178	AF_118c_mP_abs_ana
CCDC Number	2184168	2184169
Formula	$C_{17}H_{39}PSeSi$	$C_{35}H_{39}BF_{15}PSSi$
$\rho_{calc.}$ / g·cm^{-3}	1.199	1.483
μ/mm^{-1}	3.578	2.374
Formula Weight	381.50	846.59
Color	clear colorless	clear colorless
Shape	plate	block
Size/mm^3	0.18 × 0.15 × 0.03	0.374 × 0.12 × 0.032
T/K	123.00(11)	122.98(11)
Crystal System	monoclinic	monoclinic
Space Group	$P2_1/n$	$P2_1/c$
a/Å	8.76170(10)	21.5658(4)
b/Å	19.5303(2)	18.3748(3)
c/Å	12.42490(10)	21.8159(5)
α/°	90	90
β/°	96.3390(10)	118.683(3)
γ/°	90	90
V/Å^3	2113.13(4)	7584.1(3)
Z	4	8
Z'	1	2
Wavelength/Å	1.54184	1.54184
Radiation Type	Cu K_α	Cu K_α
$2\Theta_{min}$/°	8.472	6.706
$2\Theta_{max}$/°	148.784	133.77
Measured Refl.	39472	48673
Independent Refl.	4180	13307
R_{int}	0.0607	0.0523
Parameters	214	1100
Restraints	0	110
Largest Peak	0.87	0.41
Deepest Hole	−1.04	−0.37
GooF	1.076	1.052
wR_2 (all data)	0.1196	0.1338
wR_2	0.1147	0.1230
R_1 (all data)	0.0496	0.0669
R_1	0.0432	0.0492

Table S3: Crystallographic data for compounds **8**[$HB(C_6F_5)_3$] and **9**[$B(C_6F_5)_4$].

Compound	**8[$HB(C_6F_5)_3$]**	**9[$B(C_6F_5)_4$]**
Data Set (internal naming)	AF182	AF171new
CCDC Number	2184170	2184171
Formula	$C_{35}H_{39}BF_{15}PSeSi$	$C_{51}H_{42}BF_{20}O_6PSSi$
$\rho_{calc.}$ / g·cm^{-3}	1.560	1.598
μ/mm^{-1}	2.948	2.206
Formula Weight	893.62	1232.77
Color	clear colorless	clear colorless
Shape	hexagonal	block
Size/mm^3	0.23 × 0.07 × 0.06	0.23 × 0.15 × 0.07
T/K	123.01(10)	123.15
Crystal System	monoclinic	monoclinic
Space Group	$P2_1/c$	$P2_1/n$
a/Å	18.7778(2)	9.69440(10)
b/Å	12.15670(10)	36.1757(3)
c/Å	17.8431(2)	14.61320(10)
α/°	90	90
β/°	110.8870(10)	90.8070(10)
γ/°	90	90
V/Å^3	3805.49(7)	5124.37(8)
Z	4	4
Z'	1	1
Wavelength/Å	1.54184	1.54184
Radiation Type	Cu K_α	Cu K_α
$2\Theta_{min}$/°	5.038	7.778
$2\Theta_{max}$/°	150.038	133.364
Measured Refl.	38896	45394
Independent Refl.	7578	8906
R_{int}	0.0507	0.0485
Parameters	500	761
Restraints	0	12
Largest Peak	0.38	0.41
Deepest Hole	−0.78	−0.33
GooF	1.086	1.029
wR_2 (all data)	0.0985	0.0972
wR_2	0.0954	0.0938
R_1 (all data)	0.0422	0.0417
R_1	0.0360	0.0372

Compound **3**

Hydrogen atoms (except Si–H) omitted for clarity.

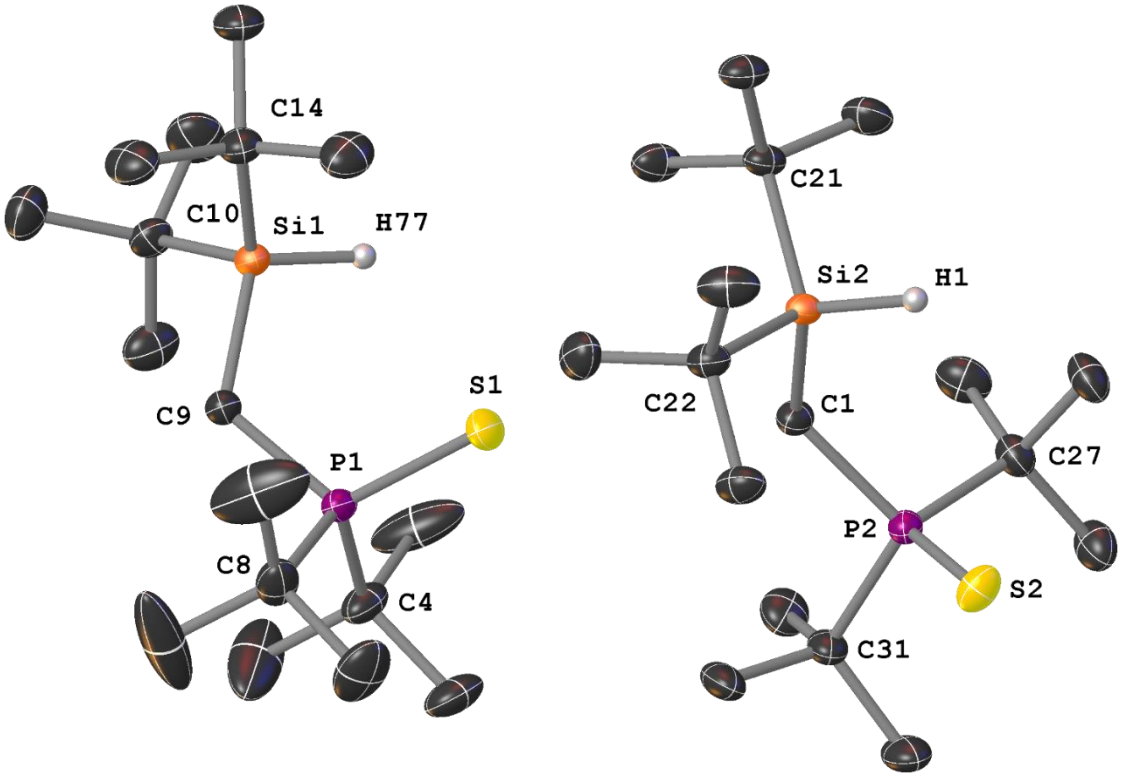

Selected Bond Lengths in Å		Selected Bond Angles in °	
P(2)–S(2)	1.9667(5)	**Si(2)–C(26)–P(2)**	122.63(7)
P(2)–C(26)	1.8249(5)	**S(2)–P(2)–C(27)**	109.40(5)
P(2)–C(27)	1.8756(15)	**S(2)–P(2)–C(26)**	115.11(5)

Compound **4**

Hydrogen atoms (except Si–H) omitted for clarity.

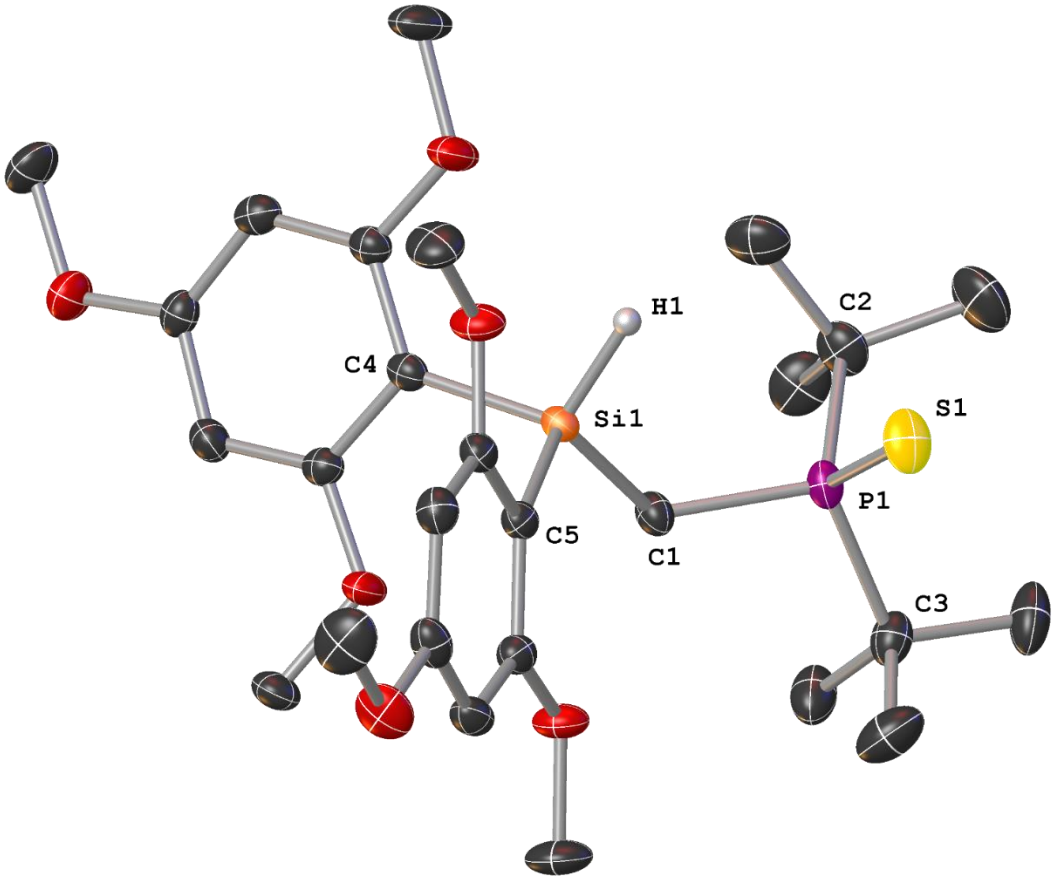

Selected Bond Lengths in Å		**Selected Bond Angles in °**	
S(1)–P(1)	1.9699(6)	**C(1)–P(1)–S(1)**	113.51(6)
P(1)–C(1)	1.8179(16)	**P(1)–C(1)–Si(1)**	118.90(9)
Si(1)–C(1)	1.8991(16)	**C(5)–Si(1)–C(1)**	114.64(7)
Si(1)–C(4)	1.8847(18)	**C(5)–Si(1)–C(4)**	109.21(7)
Si(1)–C(5)	1.8830(17)	**C(1)–P(1)–C(3)**	104.31(8)

Compound **5**

Hydrogen atoms (execpt Si–H) omitted for clarity.

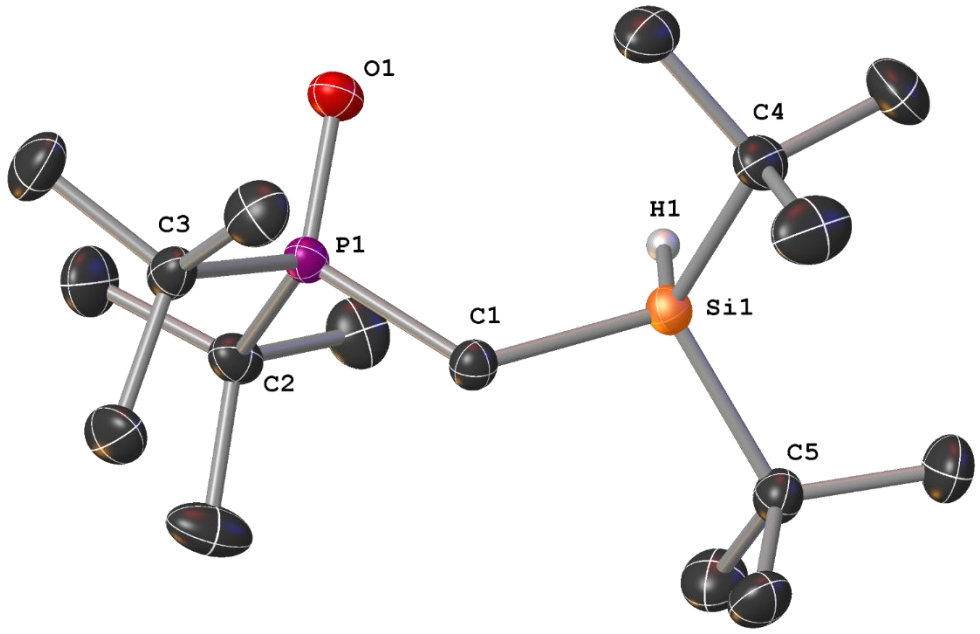

Selected Bond Lengths in Å		**Selected Bond Angles in °**	
P(1)–O(1)	1.4958(8)	**O(1)–P(1)–C(1)**	114.09(5)
P(1)–C(2)	1.8639(12)	**P(1)–C(1)–Si(1)**	121.01(6)
P(1)–C(1)	1.8147(11)	**C(1)–P(1)–C(2)**	105.59(5)
P(1)–C(3)	1.8631(12)	**C(1)–Si(1)–C(5)**	105.81
Si(1)–C(1)	1.8930(12)		
Si(1)–C(5)	1.9087(13)		
Si(1)–C(4)	1.9045(12)		

Compound **6**

Hydrogen atoms (except Si–H) omitted for clarity.

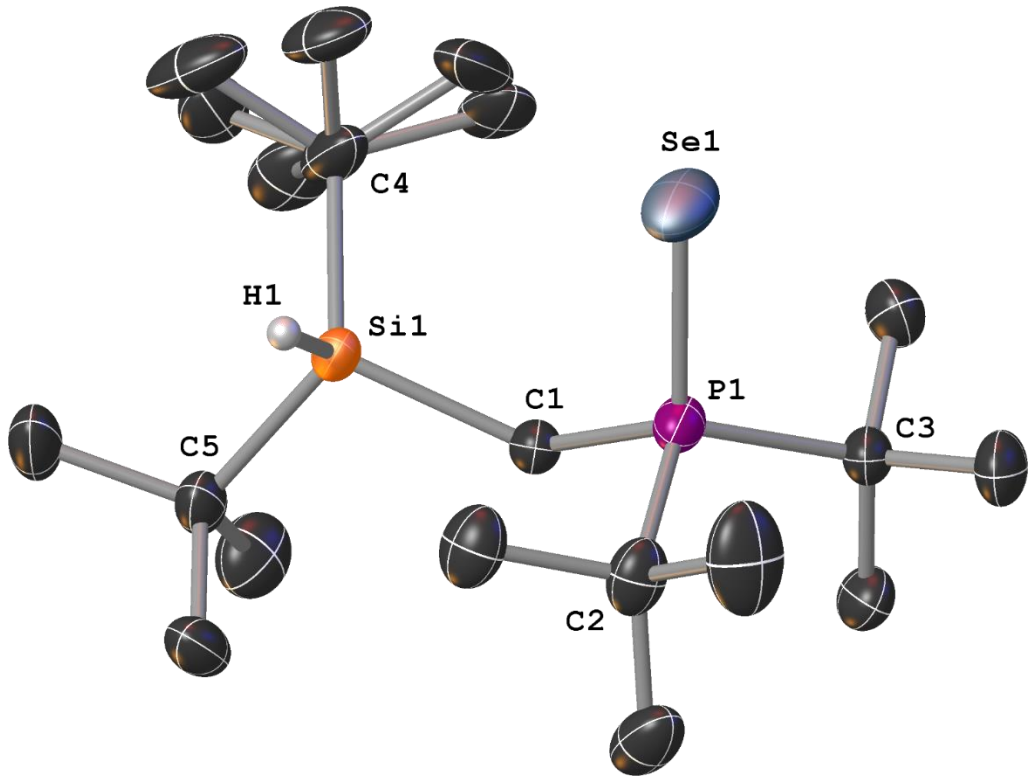

Selected Bond Lengths in Å		**Selected Bond Angles in °**	
Se(1)–P(1)	2.1163(7)	**C(1)–P(1)–Se(1)**	114.46(8)
Si(1)–C(1)	1.905(2)	**P(1)–C(1)–Si(1)**	124.31(14)
P(1)–C(1)	1.823(3)	**C(1)–Si(1)–C(5)**	105.44(12)

Compound **7**[$HB(C_6F_5)_3$]

Hydrogen atoms omitted for clarity.

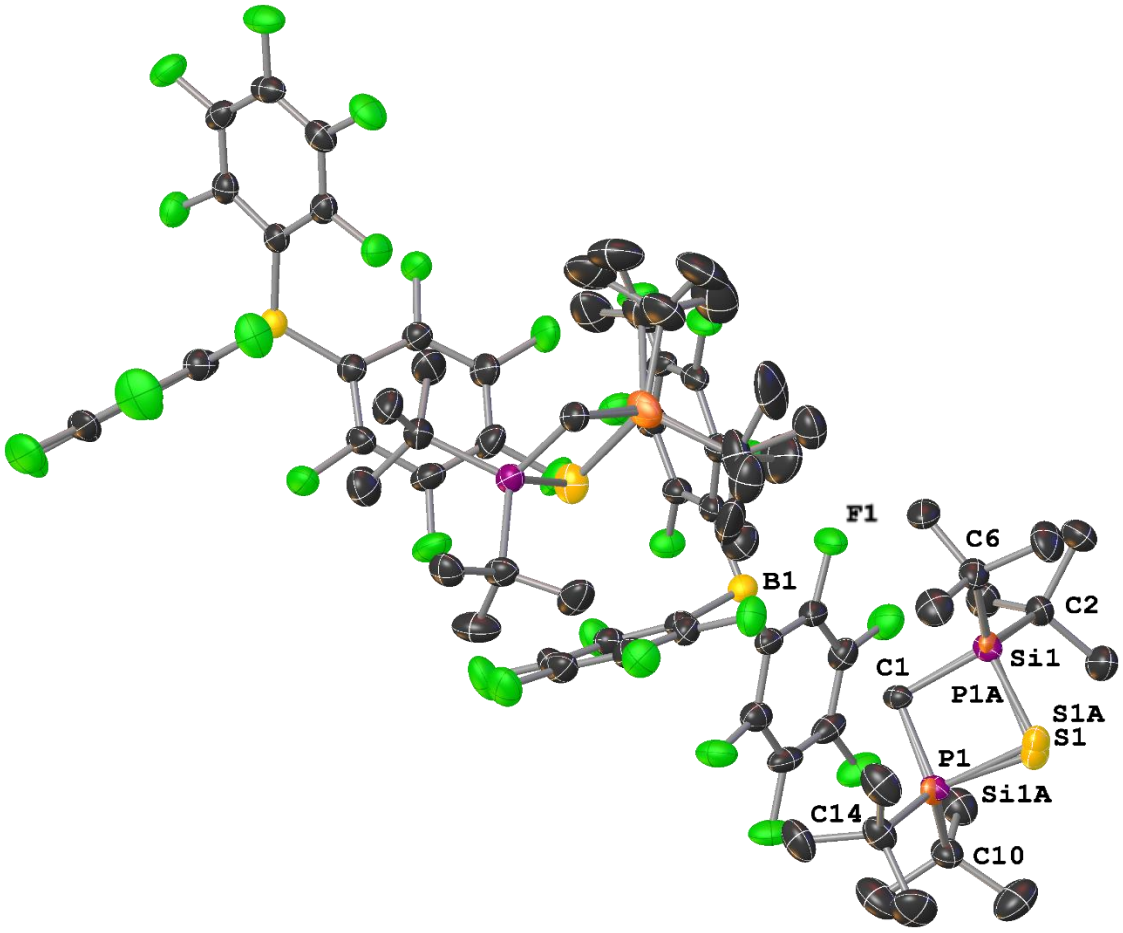

Selected Bond Lengths in Å		Selected Bond Angles in °	
Si(1)–S(1)	2.285(7)	**C(1)–Si(1)–S(1)**	86.5(4)
Si(1)–C(2)	1.887(8)	**C(1)–P(1)–S(1)**	98.2(4)
P(1)–S(1)	2.012(7)	**P(1)–S(1)–Si(1)**	80.6(4)
P(1)–C(1)	1.840(8)	**P(1)–C(1)–Si(1)**	94.5(3)

Compound **8**[$HB(C_6F_5)_3$]

Hydrogen atoms omitted for clarity.

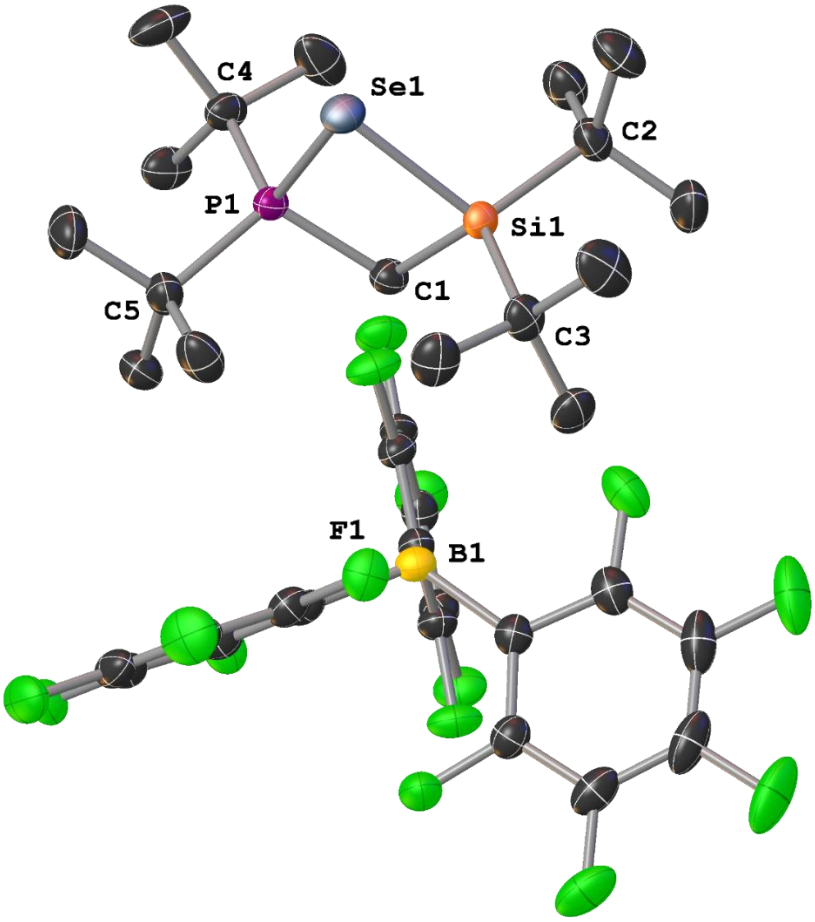

Selected Bond Lengths in Å		**Selected Bond Angles in °**	
Se(1)–P(1)	2.2277(6)	**P(1)–Se(1)–Si(1)**	77.55(2)
Se(1)–Si(1)	2.3567(6)	**C(1)–P(1)–Se(1)**	94.27(7)
P(1)–C(1)	1.834(2)	**C(1)–Si(1)–Se(1)**	88.17(7)
Si(1)–C(1)	1.915(2)	**P(1)–C(1)–Si(1)**	100.01(10)

Compound **9**[$B(C_6F_5)_4$]

Hydrogen atoms omitted for clarity.

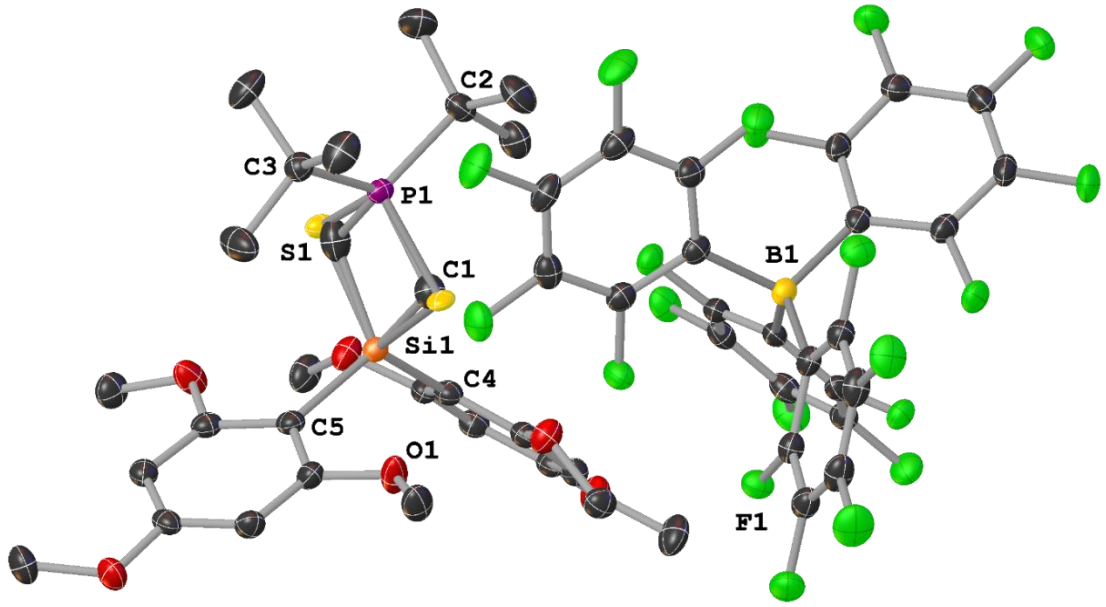

Selected Bond Lengths in Å		**Selected Bond Angles in °**	
P(1)–S(1)	2.0522(14)	**P(1)–S(1)–Si(1)**	80.00(4)
Si(1)–S(1)	2.2059(13)	**P(1)–C(1)–Si(1)**	95.3(4)
P(1)–C(1)	1.792(9)	**C(1)–Si(1)–S(1)**	88.0(3)
Si(1)–C(1)	1.912(9)	**C(1)–P(1)–S(1)**	96.3(3)

3.6.14 Details on quantum chemical calculations

Optimization in the gas phase and additional harmonic vibrational frequency analyses were performed with the software package Gaussian 09 (Revision E.01) on the M062X/6-311+G(d,p) level of theory without symmetry restrictions.[12] The GJF input files and the figures of the optimized structures were created with the program GaussView version 5.0.9.[13] For the ground state structures, the vibrational frequency analysis showed no imaginary frequency in the harmonical approximation. Natural bond orbital (NBO) analysis has been performed on the geometries optimized at the M062X/6-311+G(d,p) level of theory with the Gaussian NBO Version 3.1. Ring-opening energies (ΔG) are given based on the sum of electronic and thermal free energies (Gibbs energies) at 298.15 K in kcal mol^{-1}. The reaction enthalpies (ΔH) of the isodesmic reactions (see the Supporting Information) are given based on the sum of electronic and thermal enthalpies (enthalpies) at 298.15 K in kcal mol^{-1}. The total electronic energies (SCF), the sum of electronic and zero-point energies (ZPE), the sum of electronic and thermal enthalpies (enthalpies) at 298.15 K, the sum of electronic and thermal free energies (Gibbs energies) at 298.15 K, and the Cartesian coordinates of the calculated systems can be found in the Supporting Information. The Hartree units were converted as follows:[14] 1 Hartree = 2625.4995 kJ mol^{-1}, 1 cal = 4.184 J.

Table S4: Total electronic energies (SCF), sum of electronic and zero-point energies (ZPE), and sum of electronic and thermal free energies (Gibbs energies) at 298.15 K of the optimized structures.

Optimized structure	Method/Basis	SCF [Hartree]	ZPE [Hartree]	Enthalpies [Hartree]	Gibbs energies [Hartree]
3	M062X/6-311+G(d,p)	–1700.21613515	–1699.682649	–1699.653755	–1699.736307
5	M062X/6-311+G(d,p)	–1377.25146864	–1376.716884	–1376.688135	–1376.770587
6	M062X/6-311+G(d,p)	–3703.58621649	–3703.053442	–3703.024138	–3703.108197
7	M062X/6-311+G(d,p)	–1699.41413545	–1698.888000	–1698.859354	–1698.941193
7-o	M062X/6-311+G(d,p)	–1699.35656381	–1698.832531	–1698.803304	–1698.886695
8	M062X/6-311+G(d,p)	–3702.78598079	–3702.260322	–3702.231394	–3702.313736
8-o	M062X/6-311+G(d,p)	–3702.72538148	–3702.202670	–3702.172957	–3702.258148
9	M062X/6-311+G(d,p)	–2534.13475422	–2533.474363	–2533.431440	–2533.548238
9-o	M062X/6-311+G(d,p)	–2534.09212785	–2533.431936	–2533.388952	–2533.505941
11	M062X/6-311+G(d,p)	–1376.44969776	–1375.920598	–1375.892713	–1375.972372
11-o	M062X/6-311+G(d,p)	–1376.39549123	–1375.870860	–1375.841621	–1375.925326
12	M062X/6-311+G(d,p)	–1258.55928712	–1258.117595	–1258.093233	–1258.166426
12-o	M062X/6-311+G(d,p)	–1258.48907985	–1258.050018	–1258.025106	–1258.099582
13	M062X/6-311+G(d,p)	–1140.65370204	–1140.298325	–1140.277579	–1140.343543
13-o	M062X/6-311+G(d,p)	–1140.57521941	–1140.222249	–1140.201123	–1140.267706
14	M062X/6-311+G(d,p)	–1463.61045055	–1463.258223	–1463.236483	–1463.305686
14-o	M062X/6-311+G(d,p)	–1463.53990628	–1463.188183	–1463.166815	–1463.234073
15	M062X/6-311+G(d,p)	–3466.98034553	–3466.628006	–3466.606335	–3466.674690
15-o	M062X/6-311+G(d,p)	–3466.90960133	–3466.558560	–3466.536873	–3466.605525
16	M062X/6-311+G(d,p)	–904.818788550	–904.636248	–904.622565	–904.674788
17	M062X/6-311+G(d,p)	–1227.77348112	–1227.591306	–1227.577665	–1227.630418
18	M062X/6-311+G(d,p)	–3231.14440360	–3230.963615	–3231.003752	–3231.003752
19	M062X/6-311+G(d,p)	–76.4208162283	–76.399190	–76.395410	–76.416823
20	M062X/6-311+G(d,p)	–399.376110262	–399.360663	–399.356871	–399.380213
21	M062X/6-311+G(d,p)	–2402.73943169	–2402.725402	–2402.721599	–2402.746481
22	M062X/6-311+G(d,p)	–485.088298023	–484.964073	–484.953754	–484.997449
23	M062X/6-311+G(d,p)	–808.035108100	–807.914615	–807.904081	–807.948356
24	M062X/6-311+G(d,p)	–720.902557718	–720.606112	–720.588802	–720.646772
25	M062X/6-311+G(d,p)	–1043.85124249	–1043.558613	–1043.541021	–1043.600000
26	M062X/6-311+G(d,p)	–3047.21686451	–3046.925045	–3046.907355	–3046.966972
27	M062X/6-311+G(d,p)	–536.664556078	–536.536182	–536.526949	–536.567523
28	M062X/6-311+G(d,p)	–859.615152060	–859.490698	–859.481126	–859.522988
29	M062X/6-311+G(d,p)	–772.500427745	–772.200253	–772.183537	–772.240152
30	M062X/6-311+G(d,p)	–1095.45317975	–1095.156635	–1095.139874	–1095.196572
31	M062X/6-311+G(d,p)	–3098.82008767	–3098.525140	–3098.507977	–3098.566170
CH4	M062X/6-311+G(d,p)	–40.4967860493	–40.451680	–40.447869	–40.468994

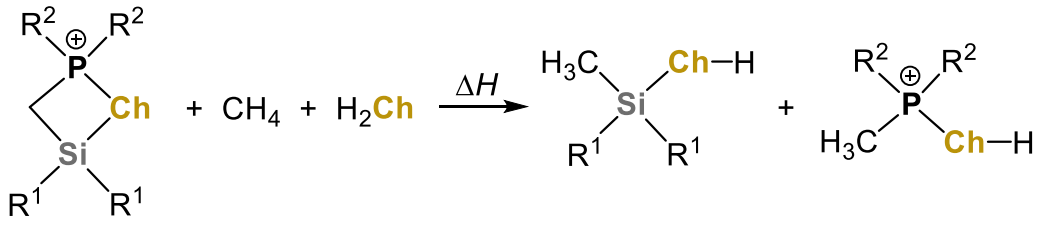

16: Ch = O, R^1 = Me, R^2 = Me
17: Ch = S, R^1 = Me, R^2 = Me
18: Ch = Se, R^1 = Me, R^2 = Me
11: Ch = O, R^1 = *t*Bu, R^2 = *t*Bu
7: Ch = S, R^1 = *t*Bu, R^2 = *t*Bu
8: Ch = Se, R^1 = *t*Bu, R^2 = *t*Bu

19: Ch = O
20: Ch = S
21: Ch = Se

22: Ch = O, R^1 = Me
23: Ch = S, R^1 = Me
24: Ch = O, R^1 = *t*Bu
25: Ch = S, R^1 = *t*Bu
26: Ch = Se, R^1 = *t*Bu

27: Ch = O, R^1 = Me
28: Ch = S, R^1 = Me
29: Ch = O, R^1 = *t*Bu
30: Ch = S, R^1 = *t*Bu
31: Ch = Se, R^1 = *t*Bu

Figure S57: Isodesmic reactions to estimate the angular strain in the four-membered heterocyclic cations and the interaction energy between the R^1 and R^2 groups, calculated on the M062X/6-311+G(d,p) level of theory.

Table S5: Reaction enthapies (ΔH) [kcal mol–1] of the isodesmic reactions of Figure S56, calculated on the M062X/6-311+G(d,p) level of theory.

Ch	R^1	R^2	Δ*H* [kcal mol^{-1}]
O	Me	Me	–9.3
S	Me	Me	–1.7
O	*t*Bu	*t*Bu	–22.7
S	*t*Bu	*t*Bu	–10.5
Se	*t*Bu	*t*Bu	–9.1

3.6.15 Supplementary References

(1) Fontana, N.; Espinosa-Jalapa, N. A.; Seidl, M.; Bauer, J. O. Hidden silylium-type reactivity of a siloxane-based phosphonium–hydroborate ion pair. *Chem. Commun.* **2022**, *58*, 2144-2147.

(2) Fink, L.; Samigullin, K.; Bodach, A.; Alig, E.; Wagner, M.; Lerner, H.-W. Donor-unsupported Phosphanylmethanides Li[CH2P*R*$_2$] (*R* = *t*Bu, Ph) – Crystal Structure of Li[CH_2P*t*Bu_2] Solved by XRPD and DFT-D Calculations. *Z. Anorg. Allg. Chem.* **2016**, *642*, 282-287.

(3) Hägele, G.; Tossing, G.; Kückelhaus, W.; Seega, J. Diastereomere Organophosphorverbindungen, I Darstellung und Eigenschaften von CH_3(*t*-C_4H_9)P(X)–Y–(Z)P(*t*-C_4H_9)CH_3. *Z. Naturforsch.* **1984**, *39b*, 1574-1580.

(4) Lehmann, M.; Schulz, A.; Villinger, A. Bissilylated Halonium Ions: [Me_3Si–X–$SiMe_3$][B(C_6F_5)$_4$] (X = F, Cl, Br, I). *Angew. Chem., Int. Ed.* **2009**, *48*, 7444-7447.

(5) Chien, J. C. W.; Tsai, W.-M.; Rausch, M. D. Isospecific Polymerization of Propylene Catalyzed by *rac*-Ethylenebis(indenyl)methylzirconium “Cation” *J. Am. Chem. Soc.* **1991**, *113*, 8570-8571.

(6) Rigaku Oxford Diffraction, CrysAlisPro Software System. 2020.

(7) Clark, R. C.; Reid, J. S. The analytical calculation of absorption in multifaceted crystals. *Acta Crystallogr.* **1995**, *A51*, 887-897.

(8) Dolomanov, O. V.; Bourhis, L. J.; Gildea, R. J.; Howard, J. A. K.; Puschmann, H. *OLEX2*: a complete structure solution, refinement and analysis program. *J. Appl. Crystallogr.* **2009**, *42*, 339-341.

(9) Sheldrick, G. M. *SHELXT* – Integrated space-group and crystal-structure determination. *Acta Crystallogr*. **2015**, *A71*, 3-8.

(10) Sheldrick, G. M. Crystal structure refinement with *SHELXL*. *Acta Crystallogr.* **2015**, *C71*, 3-8.

(11) Turner, M. J.; McKinnon, J. J.; Wolff, S. K.; Grimwood, D. J.; Spackman, P. R.; Jayatilaka, D.; Spackman, M. A. *CrystalExplorer17*; University of Western Australia, Perth, Australia, 2017.

(12) Frisch, M. J.; Trucks, G. W.; Schlegel, H. B.; Scuseria, G. E.; Robb, M. A.; Cheeseman, J. R.; Scalmani, G.; Barone, V.; Mennucci, B.; Petersson, G. A.; Nakatsuji, H.; Caricato, M.; Li, X.; Hratchian, H. P.; Izmaylov, A. F.; Bloino, J.; Zheng, G.; Sonnenberg, J. L.; Hada, M.; Ehara, M.; Toyota, K.; Fukuda, R.; Hasegawa, J.; Ishida, M.; Nakajima, T.; Honda, Y.; Kitao, O.; Nakai, H.; Vreven, T.; Montgomery, Jr., J. A.; Peralta, J. E.; Ogliaro, F.; Bearpark, M.; Heyd, J. J.; Brothers, E.; Kudin, K. N.; Staroverov, V. N.; Keith, T.; Kobayashi, R.; Normand, J.; Raghavachari, K.; Rendell, A.; Burant, J. C.; Iyengar, S. S.; Tomasi, J.; Cossi, M.; Rega, N.; Millam, J. M.; Klene, M.; Knox, J. E.; Cross, J. B.; Bakken, V.; Adamo, C.; Jaramillo, J.; Gomperts, R.; Stratmann, R. E.; Yazyev, O.; Austin, A. J.; Cammi, R.; Pomelli, C.; Ochterski, J. W.; Martin, R. L.; Morokuma, K.; Zakrzewski, V. G.; Voth, G. A.; Salvador, P.; Dannenberg, J. J.; Dapprich, S.; Daniels, A. D.; Farkas, O.; Foresman, J. B.; Ortiz, J. V.; Cioslowski, J.; Fox, D. J. Gaussian 09. Revision E.01; Gaussian, Inc.: Wallingford, CT, USA, 2013.

(13) Dennington, R. D., II; Keith, T. A.; Millam, J. M. *GaussView 5.0*; Gaussian, Inc.: Wallingford, CT, USA, 2008.

(14) Foresman, J. B.; Frisch, A. *Exploring Chemistry with Electronic Structure Methods*, 2nd Ed.; Gaussian, Inc.: Pittsburgh, PA, USA, 1996

4 Development of a weak Si–N linkage in four-membered cyclic CPNSi phosphonium ions.

Preface

The following chapter and supporting information are based on a manuscript in preparation about the synthesis of cyclic phosphinimine stabilized silylium cations and investigations in their structural and electronic properties.

Authors

A. Falk, J. O. Bauer

Author contribution

All the reported syntheses and characterizations were performed by A. Falk. The manuscript draft and supporting information was prepared by A. Falk and revised by J. O. Bauer.

Acknowledgements

This work was supported by the Deutsche Forschungsgemeinschaft (DFG, German Research Foundation) through the Research Training Group “Ion Pair Effects in Molecular Reactivity” (RTG 2620, project 426795949).

4.1 Abstract

The synthesis and reactivity of novel four-membered silyl cycles containing a phosphinimine moiety as a stabilizing donor group are presented. The compounds presented in this chapter are based on previously published silyl phosphonium chalcogenide heterocycles.[1] The similarities and differences of these new ring compounds in reactivity and steric strain are elaborated. In contrast to phosphine chalcogenides, phosphinimine donor moieties allow for further modification of donor strength by the influence of steric or electronic parameters. This was exploited for the synthesis of phosphinimine donor atoms with strongly electron-withdrawing boranes attached.

4.2 Introduction

Phosphinimines, also known as iminophosphoranes, and their respective deprotonated forms, called phosphinimides, have long been recognized as potent ligand systems in transition metal chemistry.[2] Over the course of decades, research has led to the development of tailored phosphinimine-based ligand systems, particularly for titanium complexes, which have been utilized as highly effective olefin polymerization catalysts.[3] Building on this success, subsequent research focused on the implementation of these powerful ligand systems into complexes of main group elements.[4] The Meyer group demonstrated that phosphinimines possess catalytic potential, exhibiting imine/imine and imine/carbodiimine cross-metathesis.[5] In main group phosphinimide complexes two terminal bonding modes either in the monomeric or dimeric form can occur (Scheme 1).[6]

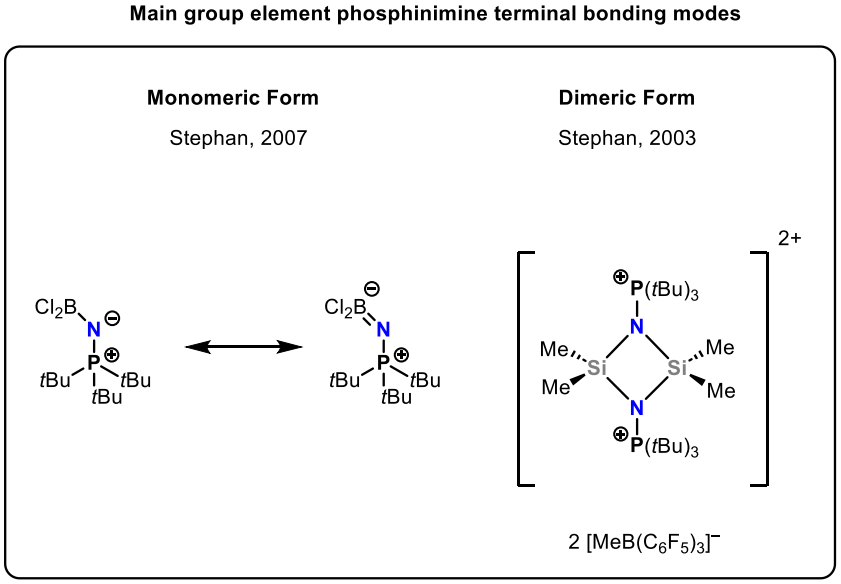

Scheme 1: Different types of bonding modes in main group element phosphinimines.[6,7]

Phosphinimines are valued in main group chemistry for their broad range of applications and bonding modes. In 2007, the Stephan group published a study that revealed a broad range of coordination modes in boron-substituted phosphinimines. It was discovered that sterically demanding substituents tend to favor the monomeric coordination form, which was of significant importance for the design of the systems presented in this chapter.[7]

A)

Stephan, 2007

Use as masked Frustrated Lewis Pair

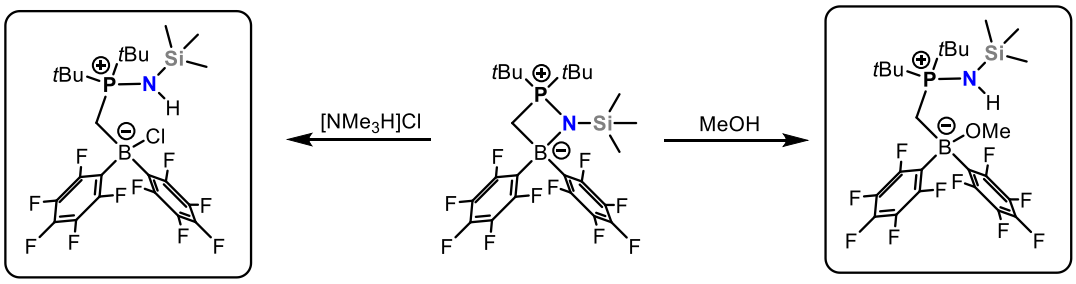

Four-membered ring system utilizing boron as Lewis acid and phosphinimide as Lewis base

B)

Kato, Müller, Maerten 2023

Use as hydrosilylation catalyst

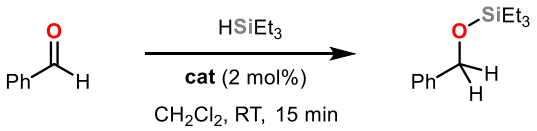

cat:

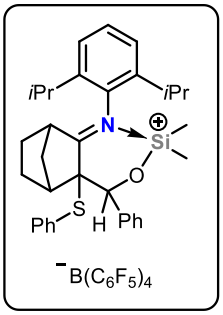

Six-membered ring system utilizing silicon as Lewis acid and imine as Lewis base

C)

This work

Four-membered ring system utilizing silicon as Lewis acid and phosphinimide as Lewis base

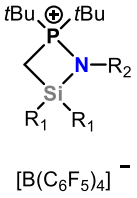

- **Use as hydrosilylation catalyst**
- **FLP activity ?**
- **Structural and electronic studies**

R_1 = Me, *i*Pr, *t*Bu
R_2 = $SiMe_3$, $B(3,5\text{-}CF_3(C_6H_3))_2$

Scheme 2: Rational behind the chosen design motifs and applications of similar systems.

Furthermore phosphinimines are known for their high Lewis basicity, which is beneficial for their use as one part of a frustrated Lewis pair (FLP).[8] This is due to the fact that the strength, meaning the ability to effectively polarize unpolar molecules, of a frustrated Lewis pair is in part described as the combination of the relative Lewis acid/base strengths of the individual parts.[9] In 2007, the Stephan group employed phosphinimines as Lewis bases in combination with the strongly Lewis acidic bis(pentafluorophenyl)borane as frustrated Lewis pairs. The substrates were found to be capable of splitting methanol and trimethylamine hydrochloride in an FLP-type manner, thereby demonstrating the viability of phosphinimines as donor moieties in FLPs (Scheme 2, A).[10] Very recently, Kato, Müller, and Maerten demonstrated that imine-stabilized silylium ions exhibit remarkable stability compared to other stabilized silylium ions. Additionally, the high Lewis acidity of the silicon center rendered them efficient hydrosilylation and allylsilylation catalysts (Scheme 2, B).[11] This illustrated the profound impact of carefully chosen stabilizing moieties in achieving a delicate balance between reactivity and stability, a quality essential for applications in catalysis. Building upon the knowledge of phosphinimide complexes containing silicon, our attention was drawn to the exploration of stabilized silylium ions containing a Lewis basic phosphinimide moiety as a Lewis basic center.[7] Combination of both concepts requires the elaboration of new synthetic pathways towards these novel type of ring systems. Our goal was the study of the structural properties and the reactivity profile of these novel ring systems (Scheme 2, C). These ring systems can be considered FLPs, as they contain a Lewis basic center, the phosphinimine, and a Lewis acidic center, the silylium ion. However, not all systems will exhibit this property and certain design choices have to be taken in order to fulfill the desired reactivity. First and foremost a steric hinderance has to be introduced between the intracyclic Lewis acidic silicon center and the Lewis basic phosphinimine moiety (Figure 1).

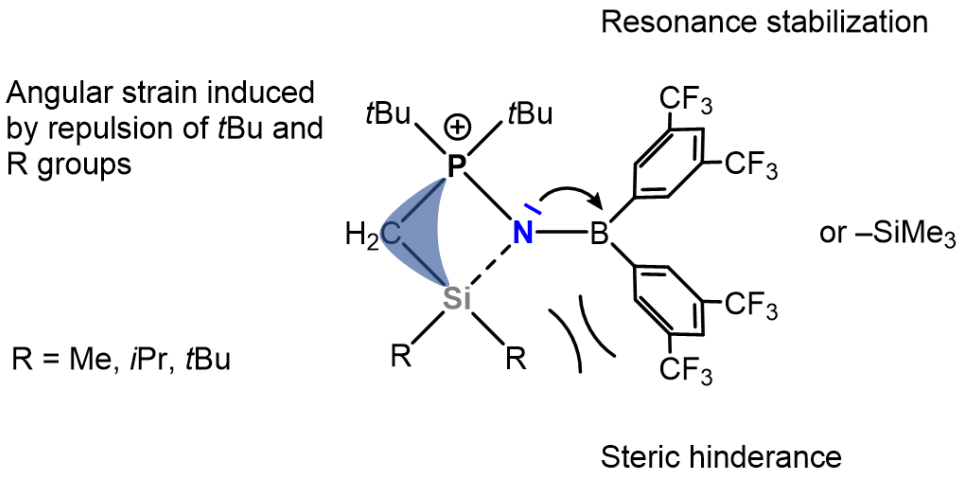

Figure 1: Design of the four-membered cations and their proposed implications on the system.

This serves to diminish the donor-acceptor interaction through steric repulsion. In our case this was achieved by the bulky, but easily introducible, $SiMe_3$ moiety on the Lewis basic side. The Lewis acidic silicon side was shielded by progressively more spatially demanding methyl, *iso*-propyl and *tert*-butyl groups in order to gauge the effect of direct steric repulsion on the system. Since our design allows for all atoms to be within a four-membered ring system, the interaction between the phosphinimine and the silicon atom can be further deteriorated by rising ring strain through a steric clash between the *tert*-butyl groups of the

phosphorus atom and the alkyl moieties bound to the intracyclic silicon atom. Further modifications, by replacement of the $SiMe_3$ moiety on the Lewis basic nitrogen atom, were meant to not only allow for steric repulsion, but also for introduction of electronic factors in order to further diminish the interaction between the phosphinimine moiety and the ring bound silicon atom. Herein, we report the rational synthesis towards these systems, the steric and electronic factors influencing these systems and the reactivity of these systems in regard to catalytic applications and FLP activity.

4.3 Results and Discussion

Our investigations started with the preparation of the phosphinimine donor moiety. In order to ensure comparability with previously published structures, the di-*tert*-butyl(methyl)phosphine scaffold was chosen.[1] The benefit of this scaffold is the high steric demand of the *tert*-butyl groups, which serve to inhibit the formation of dimeric structures when boron Lewis acids are attached. Compound **1** was obtained from di-*tert*-butyl(methyl)phosphine and trimethylsilyl azide in a Staudinger oxidation (Scheme 3).[12] Heating at 70 °C extruded dinitrogen and formed the final product **1**. Heating is required, since the Staudinger oxidation proceeds via a phosphazide intermediate, which forces the bulky substituents to come into close proximity during the decomposition process (Scheme 3).[13]

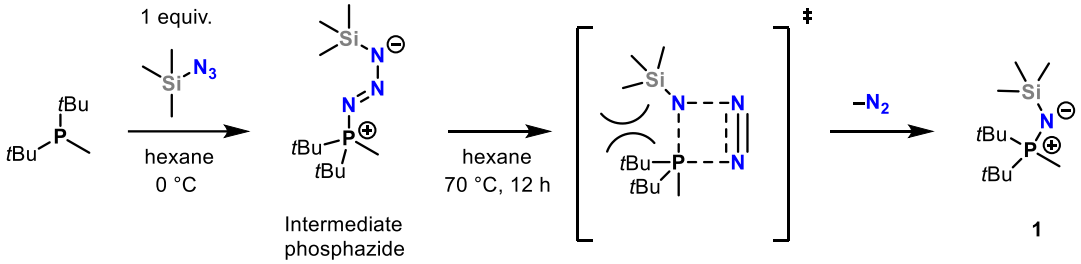

Scheme 3: Mechanistic pathway of the Staudinger oxidation with subsequent formation of **1**.

Subsequent attempts to replace the bulky trimethylsilyl moiety with the even more bulky adamantyl residue were unsuccessful, as the reaction terminated at the intermediate phosphazide (Figure 2). Although using a longer reaction time and higher temperatures, compared to the synthesis of compound **1**, only di-*tert*-butyl(methyl)phosphaadamantylazide (**12**) was obtained as crystals from the reaction mixture.

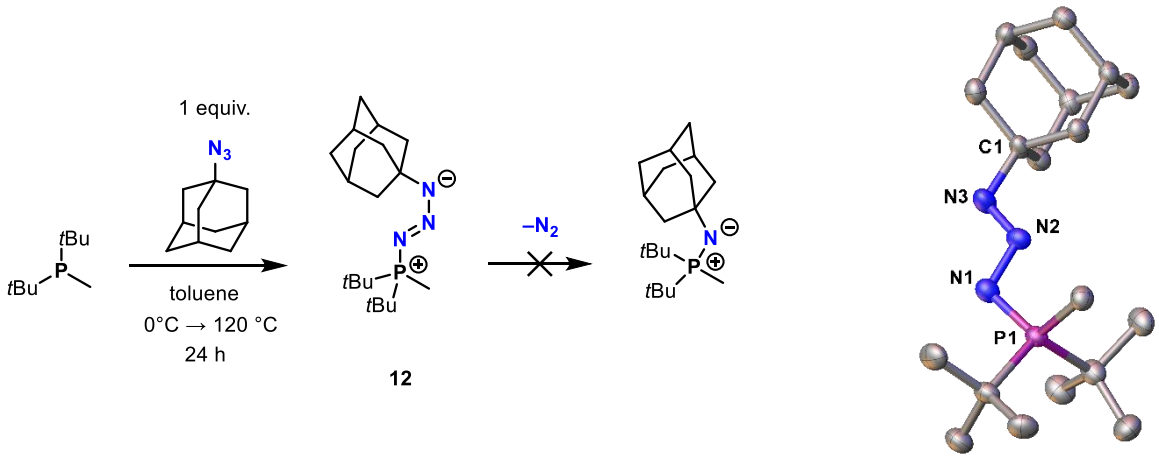

Figure 2: Reaction scheme from which the crystals were obtained and molecular structure of the di-*tert*-butyl(methyl)phosphadamantylazide (**12**) in the crystal (displacement ellipsoids set at the 50 % probability level). Selected bond lengths (Å) and angles (°): P(1)–N(1) 1.636(2), N(1)–N(2) 1.373(3), N(2)–N(3) 1.266(3), P(1)–N(1)–N(2) 108.53(2), N(1)–N(2)–N(3) 113.3(2), N(2)–N(3)–C(1) 112.4(2).

Single-crystals of the intermediate **12** were obtained and analyzed by single-crystal X-ray diffraction analysis (Figure 2). The N–N bonds [N(1)–N(2) 1.373(3) Å, N(2)–N(3) 1.266 (3) Å] are slightly shortened due to a partial double bond character. This obstacle in the synthesis of adamantyl substituted phosphinimides, as well as the inability to modify the phosphinimide substituent in later steps lead us to abandon this synthesis pathway and return our attention back to the trimethylsilyl-patterned structure **1**. We chose to retain the trimethylsilyl moiety, as no complications were observed during the synthesis and the trimethylsilyl moiety can be easily replaced by other functional groups, thereby extending the tunability of our final system.[4a,14] The synthesis of the silylated phosphinimines started with the literature known lithiation of **1** (Scheme 4).[15] These can then be easily coupled to various chlorosilanes to afford the products **2**, **3** and **4** in moderate to good yields (Scheme 4). The reason for choosing different chlorosilanes was their increasing steric crowding from methyl- to *iso*-propyl to *tert*-butyl groups. It is noteworthy that a downfield shift can be observed at the ^{29}Si nucleus in the NMR spectrum with increasing steric demand of the substituents.

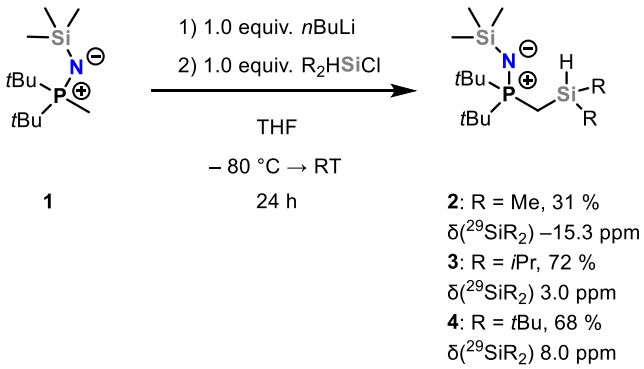

Scheme 4: Synthesis of silylated phosphinimines **2-4**.

While compounds **2** and **3** were obtained as colorless oils, compound **4** was obtained in a single-crystalline form and subjected to single-crystal X-ray structural analysis (Figure 3).

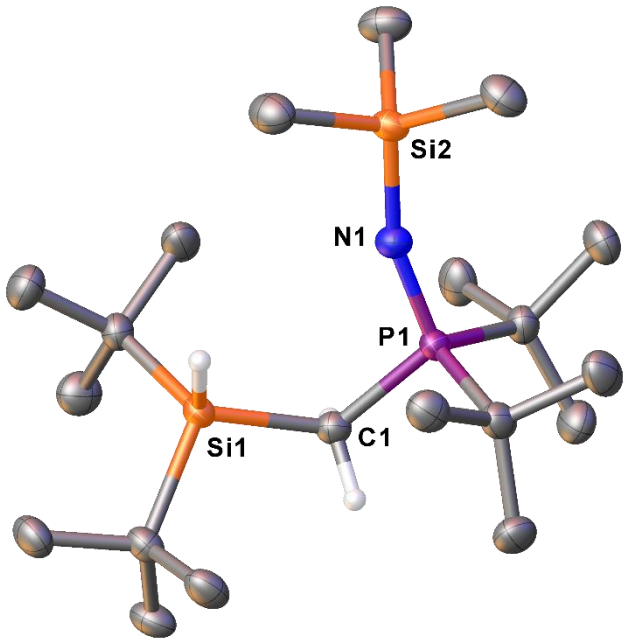

Figure 3: Molecular structure of compound **4** in the crystal (displacement ellipsoids set at the 50 % probability level). Selected bond lengths (Å) and angles (°): P(1)–N(1) 1.538(2), N(1)–Si(2) 1.665(2), Si(1)–C(1)–P(1) 118.85(13), P(1)–N(1)–Si(2) 160.92(15).

Compound **4** crystallized in the space group $P2_1/n$ and exhibits two molecules in the asymmetric unit. Due to the high steric demand of the *tert*-butyl groups the Si(1)–C(1)–P(1) angle is enlarged with a value of 118.858(13)°. However, the Si(1)–C(1)–P(1) angle is smaller than the same angle in related all *tert*-butyl-substituted systems with phosphine oxide-, sulfide-, and selenide donors.[1a] The P(1)–N(1) [1.538(2) Å] bond length is within the range observed in other *tert*-butyl substituted phosphinimines [tBu$_3$PNSiMe$_3$ · B(C$_6$F$_5$)$_3$, P–N 1.637(4) Å; (tBu$_3$PN)$_2$BH, P–N 1.535(7) Å] , and is slightly enlarged to the P–O bond length observed in a all-*tert*-butyl substituted silylphosphineoxide system [tBu$_2$P(O)CH$_2$Si(tBu$_2$)H, P–O 1.4958(8) Å].[1a,4a,6b,7] The P(1)–N(1)–Si(2) [160.92(15)] bond angle is notably expanded from the ideal 120 ° trigonal planar angle. This is due to steric repulsions between the trimethylsilyl group and the di-*tert*-butyl moiety of the phosphinimine. The phosphinimide fragment [R$_3$P$^+$–N$^-$]$^-$ is isoelectronic to the siloxide fragment R$_3$SiO$^-$, which makes the trimethylsilyl-phosphinimine ([R$_3$P$^+$–N$^-$]–SiMe$_3$) moiety isoelectronic to the disiloxane bond (R$_3$SiO–SiMe$_3$), which shows a significant decrease in the basicity of the oxygen atom.[16] It is also known that disiloxane bonds form almost linear bond angles. However, due to a less efficient n(N)→σ*(PR) orbital overlap of the phosphinimide fragment [R$_3$P$^+$–N$^-$]$^-$ the ([R$_3$P$^+$–N$^-$]–SiMe$_3$) fragments are of higher basicity compared to their isoelectronic relatives.[2,4b] This effect also leads to a more bent P(1)–N(1)–Si(2) angle. The synthesis of the four-membered CPNSi cycles required the use of a strong Lewis acid for hydride abstraction. The reactions of compounds **2** and **3** with tritylium tetrakis(pentafluorophenyl)borate resulted in the smooth hydride abstraction and the formation the of four-membered heterocyclic CPNSi cycles **5**[B(C$_6$F$_5$)$_4$] and **6**[B(C$_6$F$_5$)$_4$] (Scheme 5, top). However, in the case of the *tert*-butyl derivative **4**, no hydride abstraction occurred with tritylium tetrakis(pentafluorophenyl)borate nor with tris(pentafluorophenyl)borane, both of which have previously been successfully employed as hydride abstraction reagents to provide four-membered cyclic cations.[1] In light of these observations, we tried to make use of a reported dehydrogenative approach by protonation with a strong Brønsted acid, [H(OEt$_2$)$_2$][B(C$_6$F$_5$)$_4$], and subsequent H$_2$ release (Scheme 5, bottom).[1b,17,18]

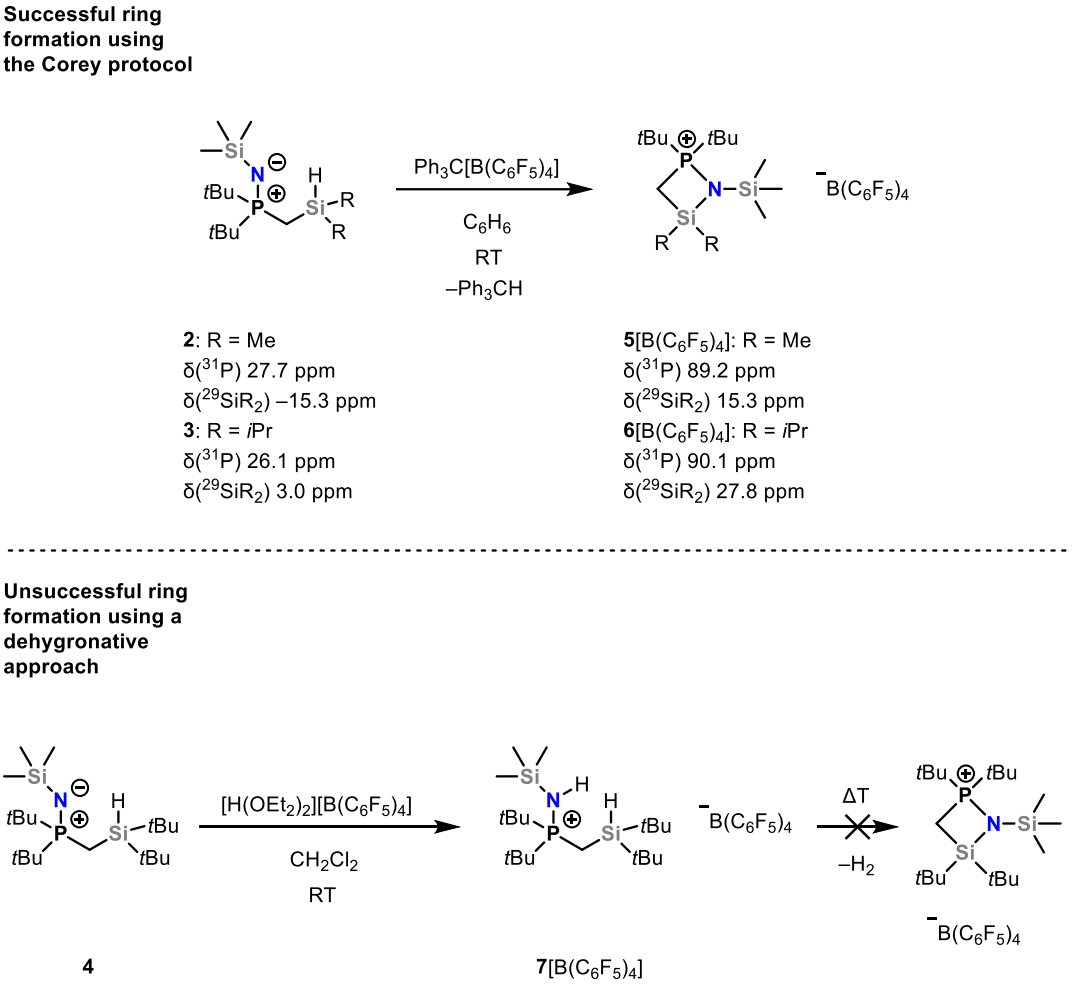

Scheme 5: Top: Synthesis and selected spectroscopic values of cationic cycles **5**[B(C$_6$F$_5$)$_4$] and **6**[B(C$_6$F$_5$)$_4$]. Bottom: Synthesis of **7**[B(C$_6$F$_5$)$_4$] by protonation and attempted dehydrogenative ring closure.

Unfortunately, this approach was also unsuccessful to achieve the corresponding *tert*-butyl-equipped ring, instead the protonated intermediate **7**[B(C$_6$F$_5$)$_4$] was the only product that could be isolated and analyzed by single-crystal X-ray diffraction analysis (Figure 4). Upon hydride abstraction, the ^{31}P NMR signals of **5**[B(C$_6$F$_5$)$_4$] [δ(^{31}P) = 89.2 ppm] and **6**[B(C$_6$F$_5$)$_4$] [δ(^{31}P) = 90.1 ppm] are noticeably shifted downfield compared to their precursors **2** [δ(^{31}P) = 27.7 ppm] and **3** [δ(^{31}P) = 26.1 ppm], which clearly shows the electron-withdrawing capability of the intracyclic silicon moiety attached to the nitrogen donor. In a previous publication we determined, that the change in ^{31}P NMR downfield shift [$\Delta\delta$(^{31}P)] observed upon formation of four-membered cations based on chalcogen-substituted phosphorus donors can be traced back to a change in hyperconjugative $n_{Ch} \rightarrow \sigma^*_{P-C}$ contributions and that this effect is greatest for phosphine oxides. The P–N bond in phosphinimines [R$_3$P$^+$–N$^-$]–R can, like phosphine chalcogenides, be best described as a polarized P–N σ-bond which is superimposed by an $n_N \rightarrow \sigma^*_{P-C}$ hyperconjugative interaction.[19] The large change in ^{31}P shift from **2** to **5**[B(C$_6$F$_5$)$_4$] [$\Delta\delta$(^{31}P) = 61.5 ppm] and **3** to **6**[B(C$_6$F$_5$)$_4$] [$\Delta\delta$(^{31}P) = 64 ppm] can therefore be expected since the [R$_3$P$^+$–N$^-$]$^-$ moiety is isoelectronic to the [R$_3$P$^+$–O$^-$] fragment, where also the biggest change in [$\Delta\delta$(^{31}P)] is expected.[1] A downfield shift trend can also be observed when the ^{29}Si NMR signals of the hydrosilanes **2** [δ(^{29}Si) = –15.3 ppm] and **3** [δ(^{29}Si) = 3.0 ppm] are

compared with their corresponding ionic forms **5**[B(C_6F_5)$_4$] [δ(^{29}Si) = 15.3 ppm] and **6**[B(C_6F_5)$_4$] δ(^{29}Si) = 27.8 ppm]. The relative changes in chemical ^{29}Si shift from **2** to **5**[B(C_6F_5)$_4$] [$\Delta\delta$(^{29}Si) = 30.6 ppm] and **3** to **6**[B(C_6F_5)$_4$] [$\Delta\delta$(^{29}Si) = 24.8 ppm] are in the same range to each other. Additionally, previously reported formations of four-membered phosphine sulfide containing systems show similar relative changes in chemical ^{29}Si shift.[1] The ^{29}Si NMR chemical shift is frequently utilized as an indicator of the silylium ion character associated with a silicon center. However, it should be noted that the chemical shift is influenced by a number of contributions, with the ring size also affecting the shielding of the ^{29}Si nucleus.[20] In systems such as those studied here, it is reasonable to regard the downfield shift [$\Delta\delta$(^{29}Si)] of the ^{29}Si NMR signal upon hydride abstraction and ring formation as an indication of the extent of electronic stabilization of the Lewis acidic silicon center by the Lewis basic phosphinimine functionality. Therefore it can be concluded that the effect of steric repulsion does increase the Lewis acidity of the ring bound silicon atom as seen in the absolute values of ^{29}Si signals in **5**[B(C_6F_5)$_4$] [δ(^{29}Si) = 15.3 ppm] and **6**[B(C_6F_5)$_4$] [δ(^{29}Si) = 27.8 ppm]. The bulkier *iso*-propyl substituents in **6**[B(C_6F_5)$_4$], compared to the methyl subsitutents in **5**[B(C_6F_5)$_4$], lead to less covalent contributions of the σ-type N–Si bond, therefore increasing the Lewis acidity of the intracyclic silicon center. However, the comparison of the absolute NMR signal values from the ring centered ^{31}P and ^{29}Si nuclei from cations **5** and **6** with literature examples suggests that the ^{29}Si chemical shift is not in the range of species classified as traditional silylium ions, however the ^{31}P chemical shift matches that of a phosphonium ion species. Ion pairs **6**[B(C_6F_5)$_4$] and **7**[B(C_6F_5)$_4$] crystallized both in the triclinic crystal system with the space group $P\bar{1}$ (Figure 4).

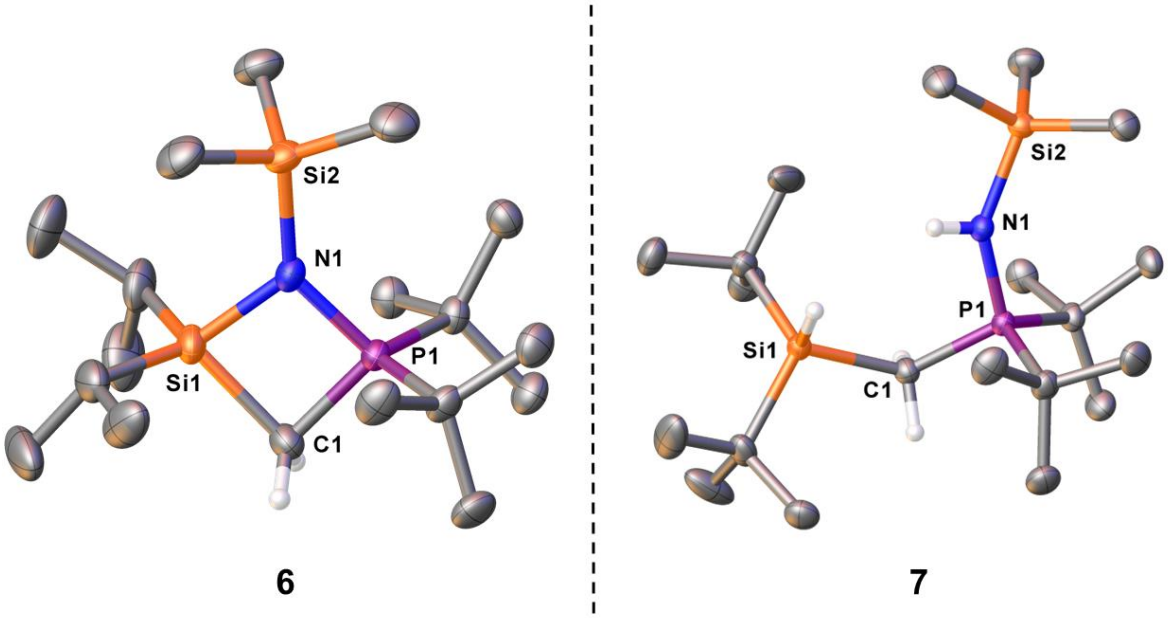

Figure 4: Molecular structures of cations **6** and **7** in the crystal (displacement ellipsoids set at the 50 % probability level). Selected bond lengths (Å) and angles (°) of **6**: Si(1)–N(1) 1.8087(19), N(1)–Si(2) 1.7722(19), P(1)–N(1) 1.6654(19), Si(1)–N(1)–Si(2) 126.70(11), Si(1)–C(1)–P(1) 87.60(10), Si(1)–N(1)–P(1) 95.14(9). **7**: Si(1)–C(1) 1.9224(14), C(1)–P(1) 1.8017(14), P(1)–N(1) 1.6433(12), N(1)–Si(2) 1.7902(12), C(4)–Si(1)–C(1) 109.57(6), Si(1)–C(1)–P(1) 124.02(8), C(1)–P(1)–N(1) 108.09(6), P(1)–N(1)–Si(2) 146.11(8).

A comparison of the Si(1)–N(1) [1.8087(19) Å] and Si(2)–N(1) [1.7722(19) Å] bond lengths within cation **6**, reveals that there is little to no silylium ion character, as the Si(1)–N(1)

bond is very similar in length to the Si(2)–N(1) bond, making both of them clearly covalent in nature. However the Si(1)–N(1) bond in cation **6** is considerably shortened in comparison to similar ([*t*Bu$_2$SiCH$_2$P(*t*Bu$_2$)S]$^+$, Si–S 2.285(7) Å; [*t*Bu$_2$SiCH$_2$P(*t*Bu$_2$)Se]$^+$, Si–Se 2.3567(6) Å) cationic chalcogen-stabilized four-membered heterocyclic rings. This is to be expected due to the increasing atomic radii of nitrogen, sulfur, and selenium (N<<S<Se) causing longer bond lenghts.[1a] Interestingly, the short Si(1)–N(1) bond in cation **6** may also provide insights into the reasons behind the unsuccessful hydride abstraction in compound **4**. In a previous publication we concluded, that the ring closure in all *tert*-butyl substituted systems is not possible for the oxygen modified compound *t*Bu$_2$SiHCH$_2$P(*t*Bu$_2$)O due to the resulting calculated short Si–O bond bringing the *tert*-butyl substituents closely together, therefore inducing a tremendous amount of steric repulsion.[1a] Therefore the ring closure of compound **4** may also be inhibited by the steric clash of *tert*-butyl groups due to a short Si–N bond in the resulting cycle, as implied by the Si–N bond length in *iso*-propyl and *tert*-butyl substituted cationic cycle **6**. The P(1)–N(1)–Si(2) [138.02(12) °] bond angle in the cyclic cation **6** is drastically decreased compared to the non-cyclic form of compound **4** with an P(1)–N(1)–Si(2) bond angle of 160.92(15) °. The Si(1)–C(1)–P(1) [87.60(10) °] bond angle of cation **6** is significantly distorted from the ideal tetrahedral angle of 109.5 °. With a C(1)–P(1)–N(1)–Si(2) [178.51(18) °] torsion angle, the nitrogen atom is almost perfectly planar, exhibiting minimal steric influence from the free lone electron pair at nitrogen. This is a result of the nitrogen atom in cation **6** being incorporated into a ring system, attached with substituents of high steric demand. Furthermore, the nitrogen lone pair can be effectively stabilized by the adjacent silicon and phosphorus atoms by hyperconjugative $n_N \rightarrow \sigma^*_{P-C}$ and $n_N \rightarrow \sigma^*_{Si-C}$ interactions.[21] Both compounds **5**[B(C$_6$F$_5$)$_4$] and **6**[B(C$_6$F$_5$)$_4$] were subjected to studies using CO_2 and H_2, yet no reaction was observed in any case (Scheme 6).

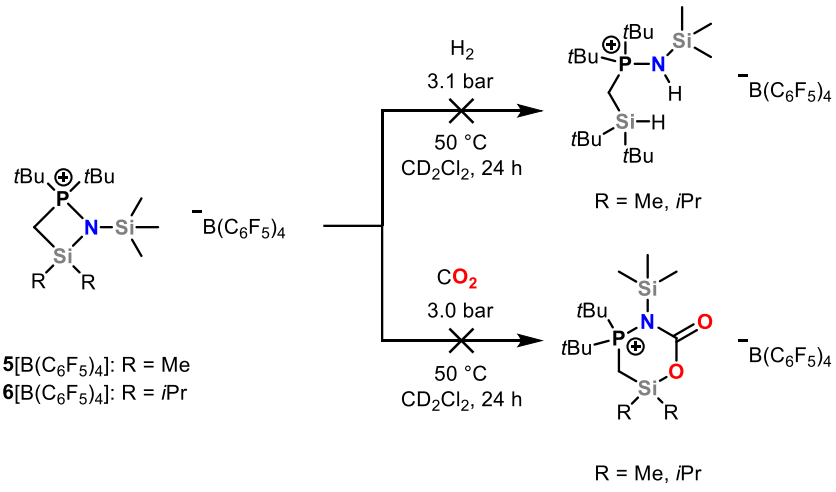

Scheme 6: Unsuccessful attempts at the activation of H_2 and CO_2 with the proposed reaction outcomes.

Since there is already a high steric demand in the case of compound **6**[B(C$_6$F$_5$)$_4$], and as shown for compound **4**, introduction of sterically more demanding groups like *tert*-butyl prevents the cyclization reaction, we set to tune the coordinating capability of the phosphinimine function by modifying the electronic structure of the substituent attached to the imine nitrogen atom. Our investigation of the X-ray crystallographic and NMR spectroscopic properties of compounds **5**[B(C$_6$F$_5$)$_4$] and **6**[B(C$_6$F$_5$)$_4$] showed, that the stabilization of the intracyclic silicon center provided by the phosphinimine moiety may be

too strong with the consequence of preventing the cations from acting as a frustrated Lewis pairs. In order to address this challenge, we next addressed the possibility to reduce the Lewis basicity of the phosphinimine fragment by incorporating a strongly electron withdrawing function at nitrogen, while maintaining a high steric repulsion between the nitrogen atom and the ring bound silicon atom. We considered these systems as optimal new candidates for introducing reactivity in the sense of masked Si/–N frustrated Lewis pairs. Our system of choice was a boron-substituted phosphinimine (Figure 1). The boron moiety can serve to reduce the Lewis basicity of phosphinimines through resonance stabilization, while the introduction of electron-withdrawing bulky substituents can also provide steric strain. An ideal motif for this purpose was the bis(3,5-trifluoromethylphenyl)borane moiety. The 3,5-trifluoromethylphenyl moiety provides two functions. First, the trifluoromethyl groups are an electron-withdrawing component, diminishing the Lewis basicity of the phosphinimine moiety by nitrogen-boron resonance stabilization and inductive effects. Second, they are sterically crowded, decreasing the interaction between the intracyclic silicon center and the Lewis basic phosphinimine. Taken together these effects are expected to facilitate ring opening and enable small molecule activation or even catalytic transformations. The synthetic procedure towards these species had to be slightly modified compared to compounds **2**-**4**.

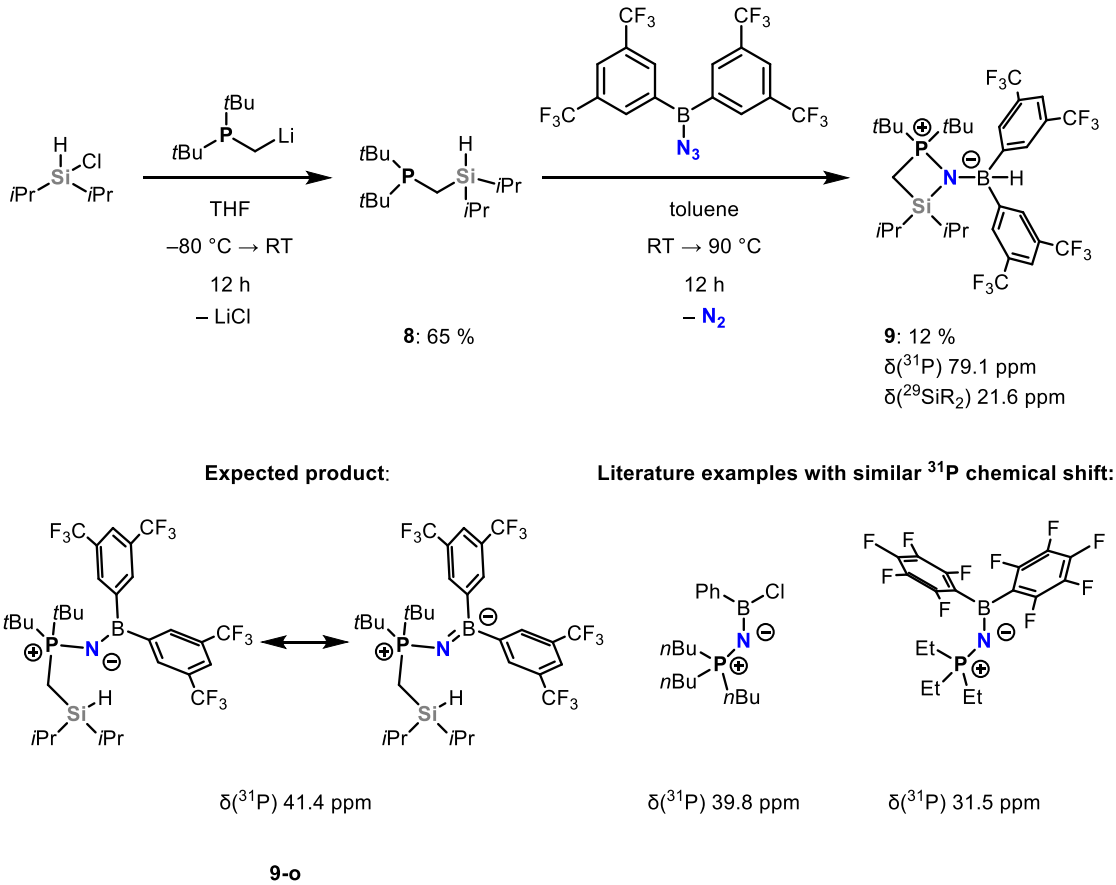

Scheme 7: Synthesis route towards the CPNSi cycle **9** and the expected product **9-o** with similar literature examples for comparison of their $^{31}P\{^{1}H\}$ spectroscopic values.[23]

Lithiation with *n*-butyllithium is not suitable when boranes are attached to the phosphinimine moiety, since nucleophilic attack at the boron atom would occur. This problem was circumvented by synthesis of the silicon substituted phosphorus(III) species

8 and subsequent Staudinger oxidation with boron azides (Scheme 7).[12] To our surprise this reaction did not give the expected "open" phosphinimine species **9-o**, similar to **2**–**4**, but rather the cyclic compound with a hydridoborate motif. The previously discussed ^{29}Si and ^{31}P NMR chemical shifts of the phosphinimine-based heterocycles **5**[B(C$_6$F$_5$)$_4$] and **6**[B(C$_6$F$_5$)$_4$] are comparable to the ^{29}Si and ^{31}P NMR chemical shifts of the silicon and phosphorus nuclei in the zwitterionic compound **9**. It is reasonable that compound **9** has a similar ^{29}Si NMR chemical shift for the intracyclic silicon nucleus similar to compounds **5**[B(C$_6$F$_5$)$_4$] and **6**[B(C$_6$F$_5$)$_4$]. Although the system is now formally neutral and not a cationic species anymore the ^{31}P NMR [79.1 ppm] and ^{11}B NMR [-6.7 ppm] chemical shifts clearly indicate a strong polarization within the molecule. In a way compound **9** can be seen as a zwitterionic combination between the anion and cation of compounds **5**[B(C$_6$F$_5$)$_4$] and **6**[B(C$_6$F$_5$)$_4$]. Because the tetracoordinate hydridoborate has no empty p-Orbital available for resonance stabilization of the free phosphinimine lone electron pair we expect no downfield shift in ^{31}P NMR compared to compounds **5**[B(C$_6$F$_5$)$_4$] and **6**[B(C$_6$F$_5$)$_4$]. We could show that, following a 12-hour period of stirring the crude reaction mixture for the synthesis of compound **9** at room temperature, the anticipated non-cyclic hydrosilane **9-o** is indeed initially formed (Figure 6). The ^{31}P NMR signal is in the expected range, as shown by comparison with **2-4** and the literature examples.[23] Furthermore, no characteristic B–H coupling can be observed in the crude ^{1}H NMR spectrum before heating occurs. These observations together with the accepted mechanistic picture of the Staudinger oxidation (see mechanistic pathway of the Staudinger oxidation, Scheme 3) strongly support our hypothesis of the initial formation of compound **9-o**. After heating intermediate **9-o** to 90°C for 12 hours, compound **9** is formed and can be isolated. It is obvious that the Lewis acidic (3,5-trifluoromethylphenyl)boryl moiety can function as a intermolecular hydride abstracting reagent, which has been demonstrated with other Lewis acidic boranes.[1]

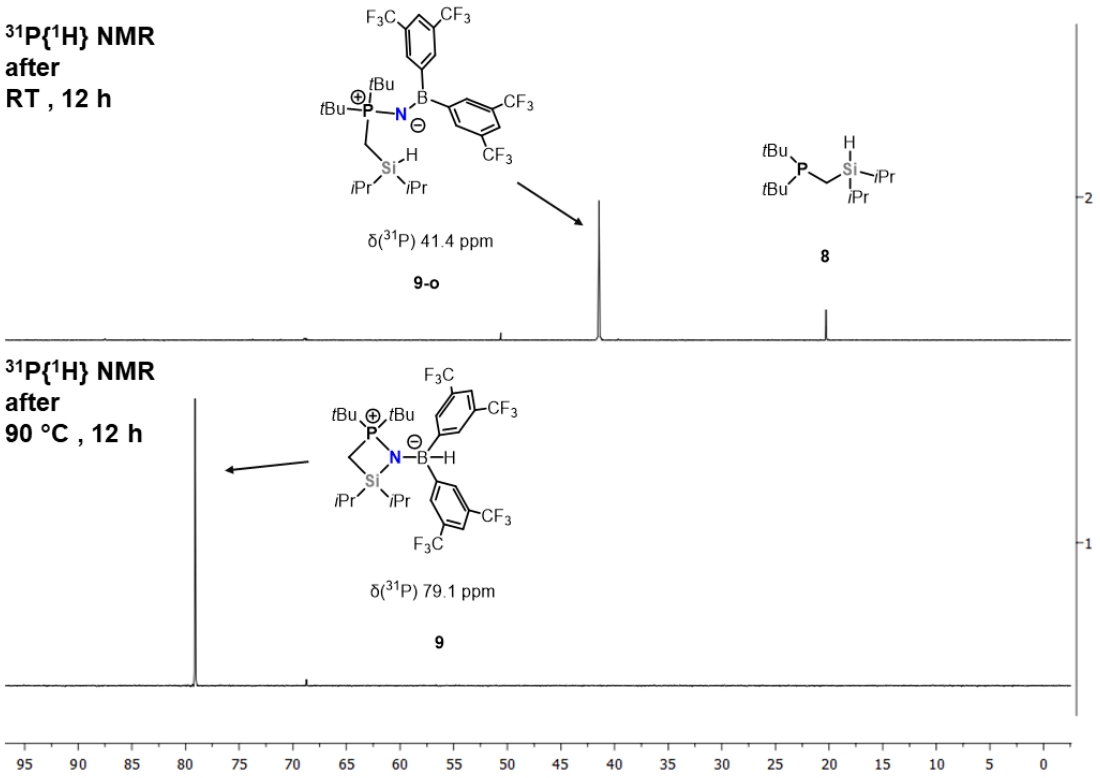

Figure 6: ^{31}P{^{1}H} NMR spectra of final isolated compound **9** after heating and the crude intermediate **9-o**.

What has not yet been clarified is the question of whether this process occurs inter- or intramolecularly. However, recent investigations of the stereochemical course of the ring formation by hydride abstraction with tris(pentafluorophenyl)borane, which is assisted by intramolecular neighboring group participation of a phosphine sulfide moiety, supports a mechanism via hydride abstraction from a backside attack (Scheme 8).[1b] Since the nitrogen donor atom and the Lewis acidic borane in **9-o** are geometrically restrained from adopting such a configuration a intermolecular mechanism is more likely.

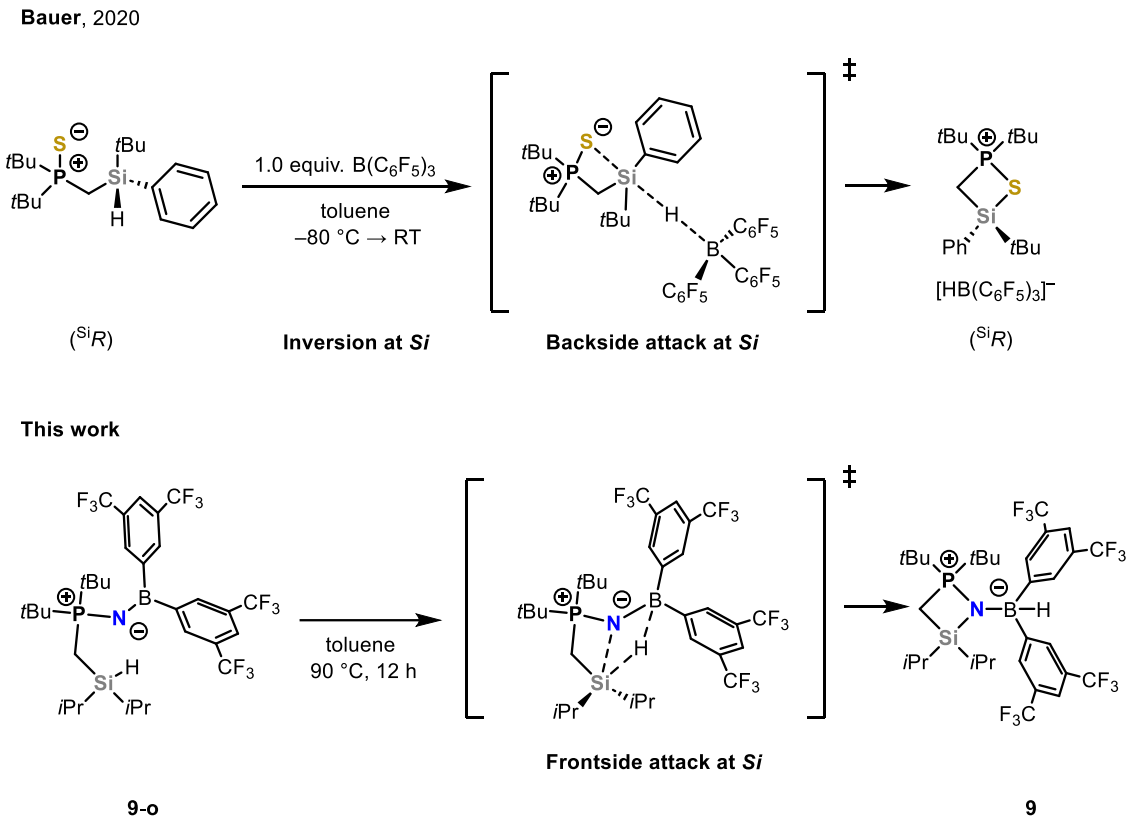

Scheme 8: The reported intramolecular backside attack on silicon and a possible intramolecular frontside attack on silicon in system **9-o**.[1b]

An intramolecular mechanism, although more unlikely, can also be formulated when using a concerted frontside attack on the silicon center (Scheme 8). Currently research is ongoing to shed light into the mechanism using a chiral silicon probe. Compound **9** crystallized in the monoclinic crystal system with the space group $P2_1/n$ (Figure 7).

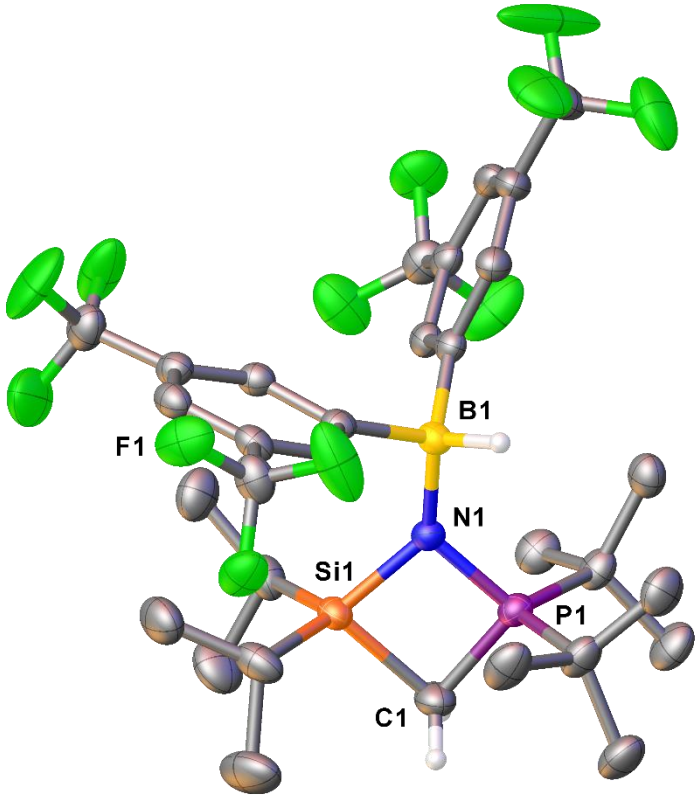

Figure 7: Molecular structure of compound **9** in the crystal (displacement ellipsoids set at the 50 % probability level). Selected bond lengths (Å) and angles (°): P(1)–N(1) 1.656(18), Si(1)–N(1) 1.7769(19), N(1)–B(1) 1.589(3), P(1)–C(1)–Si(1) 86.16(10), Si(1)–N(1)–P(1) 95.44(9), P(1)–N(1)–B(1) 127.99(5).

The Si(1)–N(1) [1.656(18) Å] bond length in **9** is slightly shorter than the same bond in cation **6** [1.8087(19) Å]. This can be explained by the higher steric demand from the trimethylsilyl group in cation **6** compared to the (3,5-trifluoromethylphenyl)borane group in the zwitterionic compound **9**. The P(1)–N(1) bond with 1.656(18) Å in compound **9** shows almost no change compared with cation **6** [1.6654(19) Å]. The Si(1)–C(1)–P(1) angle in compound **9** [86.16(10) °] is slightly decreased compared to cation **6** [87.60(10) °]. In contrast to the planar geometry around the nitrogen atom in cation **6** [C(1)–P(1)–N(1)–Si(2) 178.51(18) °], the nitrogen atom in zwitterion **9** is slightly pyramidalized, with a C(1)–P(1)–N(1)–B(1) torsion angle of 170.32(19)°. This is likely due to the lower steric hindrance of the (3,5-trifluoromethylphenyl)borane moiety with the *iso*-propyl and *tert*-butyl groups of the cyclic framework. Another reason may be the electronic stabilization of the nitrogen lone electron pair in cation **6** by $n_N \rightarrow \sigma^*_{Si-C}$ hyperconjugative interactions. It was found that the synthesis of **9** is highly dependent on the purity of the starting materials used. When bis(3,5-trifluoromethylphenyl)borane azide was used, which was not recrystallized three times prior to use, the reaction did not proceed straightforward to the desired product. Instead, additional signals were observed in the ^{31}P NMR spectrum, with the product **9-o** only being a minor product. One of those species could be characterized by single-crystal X-ray diffraction analysis (Figure 8).

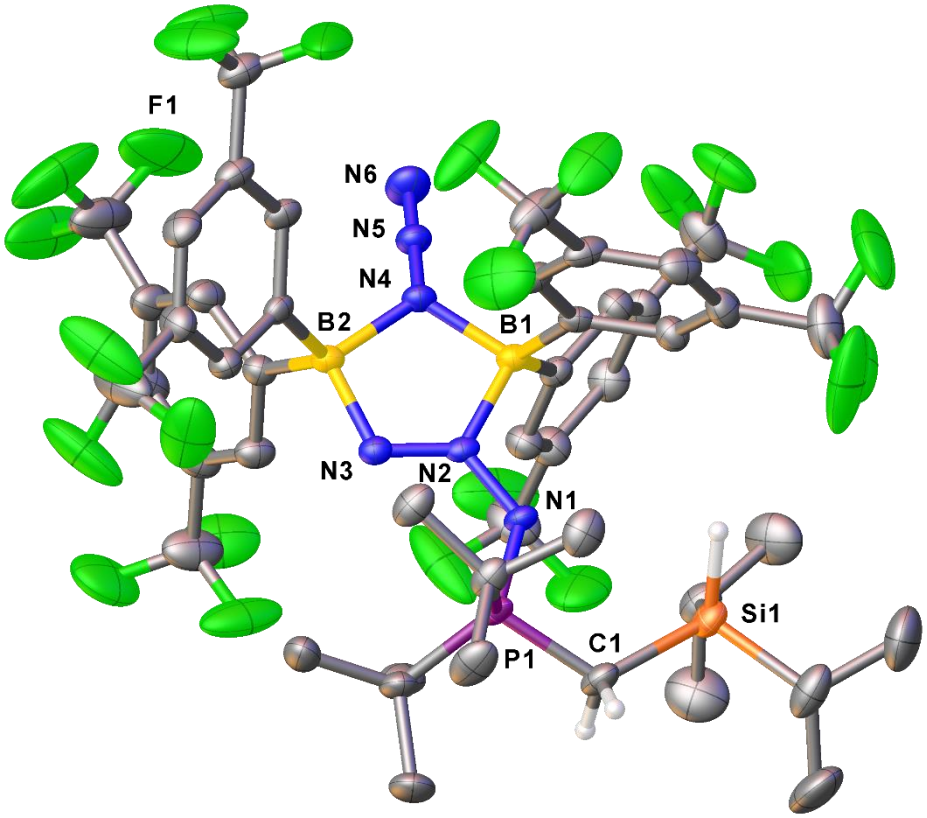

Figure 8: Molecular structure of compound **10** in the crystal (displacement ellipsoids set at the 50 % probability level). Selected bond lengths (Å) and angles (°): P(1)–N(1) 1.6535(19), N(1)–N(2) 1.335(3), N(2)–B(1) 1.598(3), P(1)–C(1) 1.804(2), P(1)–C(1)–Si(1) 118.70(14), P(1)–N(1)–N(2) 125.16(15), N(2)–B(1)–N(4) 94.72(17).

Compound **10** was found to crystallize in the monoclinic crystal system with the space group $P2_1/n$. The compound can be described as an oxidized boron-phosphazide species derived from **8** (Scheme 9, **9-o-Az**) with one fused bis(3,5-trifluoromethylphenyl)borane azide moiety attached. It is possible that compound **9-o-Az** and excess bis(3,5-trifluoromethylphenyl)borane azide may have undergone dimerization during crystallization of compound **9**, as has been observed for less bulky fluoroarylborane azides. However, this reaction only yields four-membered symmetric B_2N_2 cycles (Scheme 9).[24] A more probable mechanism is a click style reaction in solution of the intermediate phosphazide **9-o-Az** with another equivalent of bis(3,5-trifluoromethylphenyl)borane azide, analogous to the reported fluorophenylboron azide click reaction with alkynes. This reaction yields the observed five-membered B_2N_3 moieties (Scheme 9).[25] Therefore the crucial reason, of having clean bis(3,5-trifluoromethylphenyl)borane azide, is to avoid stoichiometric excess in relation of compound **8**.

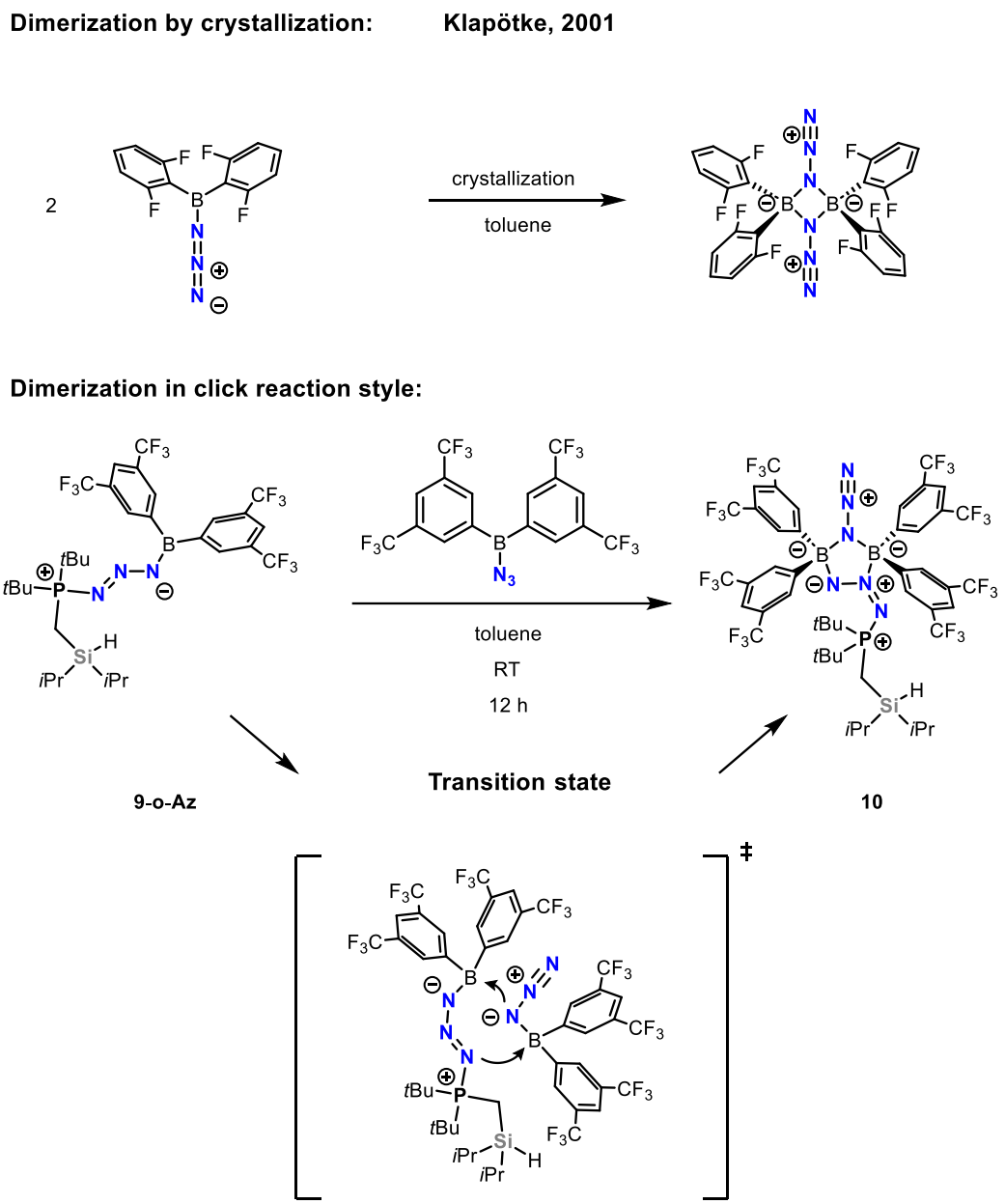

Scheme 9: Reported irreversible dimerization of boron azides and plausible reaction scheme leading to product **10**.[24]

Notably, compound **10** could not be transformed into compound **9** via extended heating in toluene. This suggests that the ring formation depicted in Scheme 8 is irreversible. Returning to compound **9**, our initial objective was to reduce the donating ability of the nitrogen atom in the phosphinimine moiety (Figure 1). In order to utilize the electron withdrawing properties caused by boron resonance stabilization, removal of the hydride from compound **9** is required. We achieved this by reaction of **9** with the strong Lewis acid tritylium tetrakis(pentafluorophenyl)borate to obtain the ionic compound **11**[$B(C_6F_5)_4$] (Scheme 10). The progress of the reaction can be monitored visually by observing a gradual decrease in the yellow color of tritylium tetrakis(pentafluorophenyl)borate and the formation of a biphasic system. Although obtaining single-crystals suitable for single-crystal X-ray crystallographic analysis was not yet possible, the desired product **11**[$B(C_6F_5)_4$] was unambiguously identified by multinuclear NMR analysis and

high-resolution mass spectrometry. Upon removal of the hydride from the borate, several key NMR spectroscopic properties undergo a significant change.

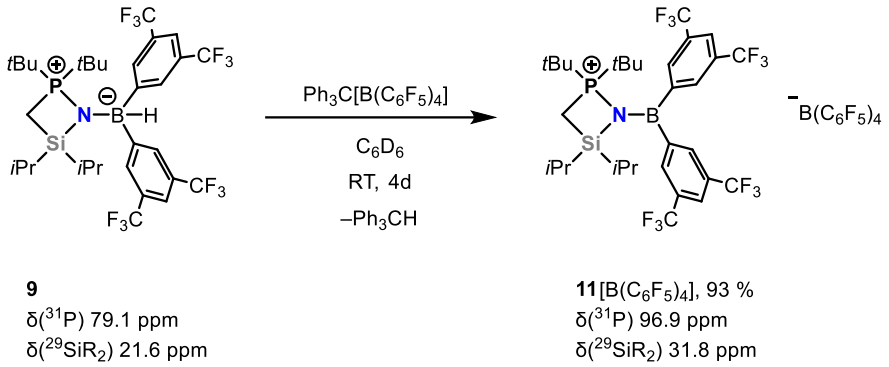

9
δ(^{31}P) 79.1 ppm
δ(^{29}SiR$_2$) 21.6 ppm

11[B(C$_6$F$_5$)$_4$], 93 %
δ(^{31}P) 96.9 ppm
δ(^{29}SiR$_2$) 31.8 ppm

Scheme 10: Synthesis of ion pair **11**[B(C$_6$F$_5$)$_4$] by hydride abstraction from the zwitterionic phosphonium borate **9**.

The ^{31}P{^{1}H} NMR signal is observed to be shifted downfield by 17.8 ppm, while the ^{29}Si{^{1}H} NMR signal is found to be shifted downfield by 10.2 ppm from 21.6 ppm to 31.8 ppm. The observation in the ^{29}Si{^{1}H} NMR spectrum that the silicon atom in **11**[B(C$_6$F$_5$)$_4$] is more deshielded than in compound **9** supports our hypothesis regarding the reduction of electronic stabilization of the silicon atom by the phosphinimine function. Upon subjecting compounds **9** and **11**[B(C$_6$F$_5$)$_4$] to H_2 and CO_2 pressure, no reaction was observed. However, preliminary results give rise to catalytic applications, since compound **9** shows catalytic activity in the hydrosilylation of nitriles (Scheme 11).

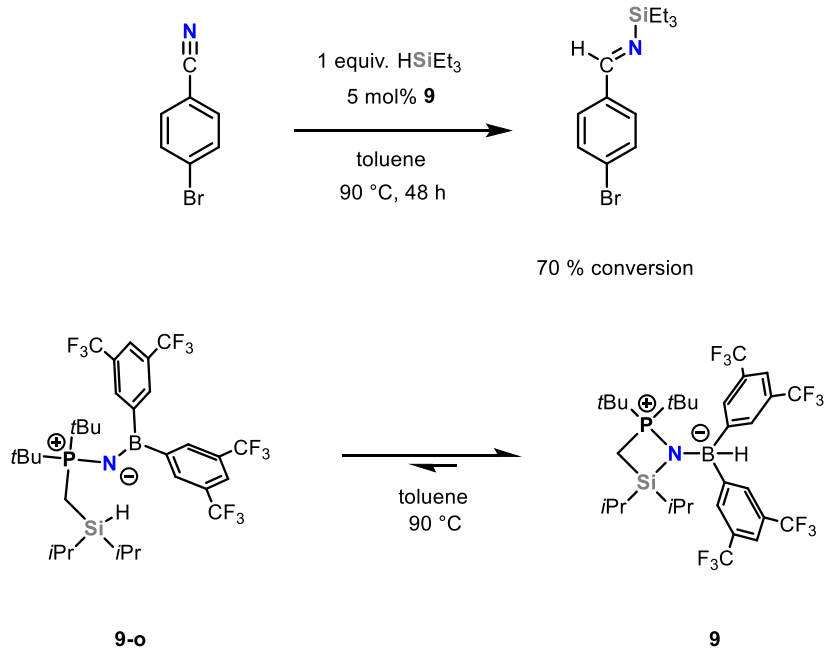

9-o **9**

Scheme 11: Hydrosilylation reaction catalyzed by compound **9**.

The conversion was determined by ^{1}H-NMR spectroscopy and unambiguously proves the formation of the hydrosilylated imine. Hydrosilylations catalyzed by main group

compounds are well known, particularly hydrosilylations catalyzed by boranes.[26] However, the fact that compound **9** acts as a hydrosilylation catalyst is unexpected, since no free Lewis acidic site is actually available in the closed form **9** to perform the catalytic cycle. This raises the question of whether an equilibrium between compound **9** and the open form **9**-**o** is established under the reaction conditions of the catalysis, with the latter compound reacting with $HSiEt_3$ via hydride abstraction, or whether the catalytic cycle even occurs in a cooperative catalytic fashion with the participation of the Lewis acidic silicon center in the hydride transfer reaction.

4.4 Conclusions

In conclusion, various four-membered CPNSi cycles were designed, synthesized and their structural and electronic properties were elucidated. It was determined that for compounds **5**[$B(C_6F_5)_4$] and **6**[$B(C_6F_5)_4$], steric shielding is insufficient to weaken the Si–N bond in order to permit reactivity as a frustrated Lewis pair. In fact, the Si–N bond is highly covalent in nature and relatively short. However, it was found that the successive introduction of sterically more demanding substituents led to a higher downfield-shifted silicon nucleus. In the case of *tert*-butyl groups (**4**), this ultimately resulted in a complete inhibition of hydride abstraction. Gaining valuable insights from these results we set out to design a system with a maximum of steric hinderance, while also preserving the necessary ability to remove the hydride from the Si–H moiety. Furthermore, an electrophilic borane moiety was introduced to probe the effect of electron withdrawing groups on the ability of these ring systems to reversibly open. This led to the development and synthesis of a boron substituted CPNSi cycle, which lead to the unexpected formation of the hydridoborate **9**. This observation prompted further investigation into the mechanism of intramolecular and intermolecular hydride abstraction, a topic that will be the subject of future research. While all compounds showed no reactivity towards CO_2 and H_2, success was obtained when compound **9** was observed to catalyze a hydrosilylation reaction. This reactivity may be a hint for a cooperative system at elevated temperatures, thereby validating our approach of combining steric and electronic factors to weaken the Si–N bond in compound **9**. This approach was further exploited by successfully removing the hydride from compound **9**, resulting in the formation of compound **11**[$B(C_6F_5)_4$]. As anticipated, this resulted in an enhancement of Lewis acidity, as evidenced by $^{29}Si\{^1H\}$ spectroscopy, which revealed a novel approach for weakening the donor interactions within this system by boron-nitrogen resonance stabilization. These results pave the way for future modifications of these systems in order to employ them as catalysts.

4.5 References

(1) (a) Falk, A.; Bauer, J. O. Structural and Electronic Effects on Phosphine Chalcogenide Stabilized Silicon Centers in Four-Membered Heterocyclic Cations. *Inorg. Chem.* **2022**, *61*, 15576–15588. (b) Fontana, N.; Espinosa-Jalapa, N. A.; Seidl, M.; Bauer, J. O. Easy Access to Enantiomerically Pure Heterocyclic Silicon-Chiral Phosphonium Cations and the Matched/Mismatched Case of Dihydrogen Release. *Chem. Eur. J.* **2021**, *27*, 2649–2653.

(2) Dehnicke, K.; Krieger, M.; Massa, W. Phosphoraneiminato complexes of transition metals. *Coord. Chem. Rev.* **1999**, *182*, 19–65.

(3) Stephan, D. W. The Road to Early-Transition-Metal Phosphinimide Olefin Polymerization Catalysts. *Organometallics* **2005**, *24*, 2548–2560.

(4) (a) Stephan, D. W. in *Advances in Organometallic Chemistry*, Elsevier, **2006**, pp. 267–291. (b) Dehnicke, K.; Weller, F. Phosphorane iminato complexes of main group elements. *Coord. Chem. Rev.* **1997**, *158*, 103–169.

(5) (a) Bell, S. A.; Meyer, T. Y.; Geib, S. J. Catalytic double-bond metathesis without the transition metal. *J. Am. Chem. Soc.* **2002**, *124*, 10698–10705. (b) Burland, M. C.; Meyer, T. Y. Iminophosphorane mediated imine metathesis. *Inorg. Chem.* **2003**, *42*, 3438–3444.

(6) (a) Dehnicke, K.; Strähle, J. *Polyhedron* **1989**, *8*, 707. (b) Courtenay, S.; Ong, C. M.; Stephan, D. W. Phosphinimido Complexes of Silicon, Tin, and Germanium. *Organometallics* **2003**, *22*, 818–825. (c) Möhlen, M.; Harms, K.; Magull, J.; Goesmann, H.; Fenske, D.; Dehnicke, K. Phosphanimin- und Phosphaniminato-Komplexe von Bor. Synthese und Kristallstrukturen von $[BF_3(Me_3SiNPEt_3)]$, $[BCl_2(NPPh_3)]_2$, $[BCl_2(NPEt_3)]_2$, $[B_2Cl_3(NPEt_3)_2]^+BCl_4^-$ und $[B_2Cl_2(NP\textit{i}Pr_3)^3]^+BCl_4^-$ *Z. Anorg. Allg. Chem.* **1996**, *10*, 1692–1700.

(7) Courtenay, S.; Walsh, D.; Hawkeswood, S.; Wei, P.; Das, A. K.; Stephan, D. W. Boron and aluminum complexes of sterically demanding phosphinimines and phosphinimides. *Inorg. Chem.* **2007**, *46*, 3623–3631.

(8) (a) T. Ishikawa (Ed.) Superbases for organic synthesis. *Guanidines, amidines and phosphazenes and related organocatalysts*, John Wiley & Sons, Chichester, UK, **2009**. (b) Weitkamp, R. F.; Neumann, B.; Stammler, H.-G.; Hoge, B. Phosphorus-Containing Superbases: Recent Progress in the Chemistry of Electron-Abundant Phosphines and Phosphazenes. *Chem. Eur. J.* **2021**, *27*, 10807–10825.

(9) Neu, R. C.; Ouyang, E. Y.; Geier, S. J.; Zhao, X.; Ramos, A.; Stephan, D. W. Probing substituent effects on the activation of H_2 by phosphorus and boron frustrated Lewis pairs. *Dalton Trans.* **2010**, *39*, 4285–4294.

(10) (a) Alhomaidan, O.; Hollink, E.; Stephan, D. W. Main Group Heterocycles from Lithiated Phosphinimines. *Organometallics* **2007**, *26*, 3041–3048. (b) Jiang, C.; Stephan, D. W. Phosphinimine-borane combinations in frustrated Lewis pair chemistry. *Dalton Trans.* **2013**, *42*, 630–637.

(11) Dajnak, A.; Shi, L.; Altınbaş Özpınar, G.; Lenk, R.; Saffon-Merceron, N.; Baceiredo, A.; Kato, T.; Müller, T.; Maerten, E. Imine-stabilized silylium ions: synthesis, structure and application in catalysis. *Dalton Trans.* **2023**, *52*, 3052–3058.

(12) Staudinger, H.; Meyer, J. Über neue organische Phosphorverbindungen III. Phosphinmethylenderivate und Phosphinimine. *Helvetica Chimica Acta* **1919**, *2*, 635–646.

(13) (a) Lin, F. L.; Hoyt, H. M.; van Halbeek, H.; Bergman, R. G.; Bertozzi, C. R. Mechanistic investigation of the staudinger ligation. *J. Am. Chem. Soc.* **2005**, *127*, 2686–2695. (b) Bebbington, M. W.P.; Bourissou, D. Stabilised phosphazides. *Coord. Chem. Rev.* **2009**, *253*, 1248–1261.

(14) (a) Wolfsberger, W. Monomere und dimere *N*-Trichlor(brom)germyltriorganophosphinimine. *Chem. Ztg.* **1979**, *103*, 338–340. (b) Wolfsberger, W. Tri(*tert*-butyl)phosphinimine. *Z. Naturforsch.* **1978**, *33b*, 1452–1456.

(15) Müller, A.; Neumüller, B.; Dehnicke, K. Lithiierte Phosphanimine. Synthese und Kristallstrukturen von $[LiCH_2PMe_2NSiMe_3]_4$ und $[LiCMe_2P(iPr)_2NSiMe_3]_2$. *Chem. Ber.* **1996**, *129*, 253–257.

(16) (a) Grabowsky, S.; Hesse, M. F.; Paulmann, C.; Luger, P.; Beckmann How to Make the Ionic Si−O Bond More Covalent and the Si−O−Si Linkage a Better Acceptor for Hydrogen Bonding. J. *Inorg. Chem.* **2009**, *48*, 4384–4393. (b) Weinhold, F.; West, R. The Nature of the Silicon–Oxygen bond. *Organometallics* **2011**, *30*, 5815–5824. (c) Weinhold, F.; West, R. Hyperconjugative Interactions in Permethylated Siloxanes and Ethers: The Nature of the Si–O Bond *J. Am. Chem. Soc.* **2013**, *135*, 5762–5767. (d) Bauer, J.O. Influence of Amino Functions on the Coordination Ability of Silyl Ethers and Disiloxanes. *Organometallics* **2022**, *41*, 321–327.

(17) Jutzi, P.; Müller, C.; Stammler, A.; Stammler, H.-G. Synthesis, Crystal Structure, and Application of the Oxonium Acid $[H(OEt_2)_2]^+$ $[B(C_6F_5)_4]^-$ *Organometallics*, **2000**, *19*, 1442.

(18) (a) Reissmann, M.; Schäfer, A.; Panisch, R.; Schmidtmann, M.; Bolte, M.; Müller, T. Cyclic silylated onium ions of group 15 elements. *Inorg. Chem.* **2015**, *54*, 2393–2402. (b) Wu, Q.; Irran, E.; Müller, R.; Kaupp, M.; Klare, H. F. T.; Oestreich, M. Characterization of hydrogen-substituted silylium ions in the condensed phase. *Science* **2019**, *365*, 168–172. (c) Chen, Q.-A.; Klare, H. F. T.; Oestreich, M. Brønsted Acid-Promoted Formation of Stabilized Silylium Ions for Catalytic Friedel-Crafts C-H Silylation. *J. Am. Chem. Soc.* **2016**, *138*, 7868–7871.

(19) Reed, A. E.; Schleyer, P. v.-R. Chemical bonding in hypervalent molecules. The dominance of ionic bonding and negative hyperconjugation over d-orbital participation. *J. Am. Chem. Soc.* **1990**, *112*, 4, 1434–1445.

(20) (a) Klare, H. F. T.; Bergander, K.; Oestreich, M. Taming the Silylium Ion for Low-Temperature Diels–Alder Reactions. *Angew. Chem., Int. Ed.* **2009**, *48*, 9077-9079. (b) Seyferth, D.; Friedrich, H.; Krska, S. W. Radical-Initiated Hydrosilylation-Cyclization Reactions of Bis(vinyldimethylsilyl) Compounds, $CH_2=CH(CH_3)_2SiXSi(CH_3)_2CH=CH_2$ (X = O, CH_2, NH, NCH_3, $NSi(CH_3)_3$. *Z. Naturforsch.* **1994**, *49b*, 1818-1826.

(21) Kocher, N.; Selinka, C.; Leusser, D.; Kost, D.; Kalikhman, I.; Stalke, D. Experimental Charge Density Studies of Cyclotetrasilazane and Metal Complexes Containing the Di- and Tetraanion *Z. Anorg. Allg. Chem.* **2004**, *630*, 1777–1793.

(22) Klare, H. F. T.; Albers, L.; Süsse, L.; Keess, S.; Müller, T.; Oestreich, M. Silylium Ions: From Elusive Reactive Intermediates to Potent Catalysts. *Chem. Rev.* **2021**, *121*, 5889–5985.

(23) Melen, R. L.; Lough, A. J.; Stephan, D. W. Boron azides in Staudinger oxidations and cycloadditions. *Dalton Trans.* **2013**, *42*, 8674–8683.

(24) Fraenk, W.; Klapötke, T. M.; Krumm, B.; Mayer, P.; Nöth, H.; Piotrowski, H.; Suter, M. Synthesis and structural studies on fluorophenylboron azides. *J. Fluor. Chem.* **2001**, *112*, 73–81.

(25) Melen, R. L.; Stephan, D. W. Cycloaddition reactions of $(C_6F_5)_2BN_3$ with dialkyl acetylenedicarboxylates. *Dalton Trans.* **2015**, *44*, 5045–5048.

(26) (a) Hermeke, J.; Mohr, J.; Oestreich, M. A unified survey of Si–H and H–H bond activation catalysed by electron-deficient boranes. *Chem. Soc. Rev.* **2015**, *44*, 2202–2220. (b) Gandhamsetty, N.; Jeong, J.; Park, J.; Park, S.; Chang, S. Boron-catalyzed silylative reduction of nitriles in accessing primary amines and imines. *J. Org. Chem.* **2015**, *80*, 7281–7287.

4.6 Synthesis and Characterizations

4.6.1 General remarks

All experiments were performed in an inert atmosphere of purified nitrogen by using standard Schlenk techniques or an MBraun Unilab 1200/780 glovebox. Glassware was heated at 600 °C prior to use. Dichloromethane (DCM), hexane, pentane, tetrahydrofuran (THF), and toluene were dried and de-gassed with an MBraun SP800 solvent purification system. *n*-Butyllithium (2.5 M or 1.6 M solution in hexane, Merck KGaA), di-*tert*-butylchlorosilane (97%, Merck KGaA), di-*iso*-propylchlorosilane (97%, Merck KGaA), dimethylchlorosilane (97%, Merck KGaA), trimethylsilyl azide (95 %, Merck KGaA) and di-*tert*-butylmethylphosphine (97%, Merck KGaA), 1-azidoadamantane (97 %, Merck KGaA) were used as received without further purification. (Di-*tert*-butylphosphaneyl)methyllithium[1], bis(3,5-trifluoromethylphenyl)chloroborane[2], tritylium tetrakis(pentafluorophenyl)borate[3] and $[H(OEt_2)_2][B(C_6F_5)_4]$[4] were synthesized according to reported literature procedures. C_6D_6 and CD_2Cl_2 used for NMR spectroscopy were dried over 3 Å molecular sieves and degassed by a standard freeze-pump-thaw procedure. NMR spectra were either recorded on a Bruker Avance 300 (300.13 MHz), a Bruker Avance 400 (400.13 MHz) or on a Bruker Avance III HD 400 (400.13 MHz) at 25 °C. Chemical shifts (*δ*) are reported in parts per million (ppm). ^{1}H and $^{13}C\{^{1}H\}$ NMR spectra are referenced to tetramethylsilane ($SiMe_4$, δ = 0.0 ppm) as external standard, with the deuterium signal of the solvent serving as internal lock and the residual solvent signal as an additional reference. $^{11}B\{^{1}H\}$, $^{19}F\{^{1}H\}$, $^{31}P\{^{1}H\}$, and $^{29}Si\{^{1}H\}$ NMR spectra are referenced to $BF_3{\cdot}OEt_2$, $CFCl_3$, 85% H_3PO_4 and $SiMe_4$, respectively. For the assignment of the multiplicities, the following abbreviations are used: s = singlet, bs = broad singlet, d = doublet, t = triplet, bq = broad quartet, m = multiplet. For simplicity, multiplets of order higher than one are described by approximating them to the closest first order type. High resolution mass spectrometry was carried out on a Jeol AccuTOF GCX and an Agilent Q-TOF 6540 UHD spectrometer. Elemental analyses were performed on a Vario MICRO cube apparatus.

4.6.2 Synthesis of starting materials

4.6.2.1 Synthesis of compound 1

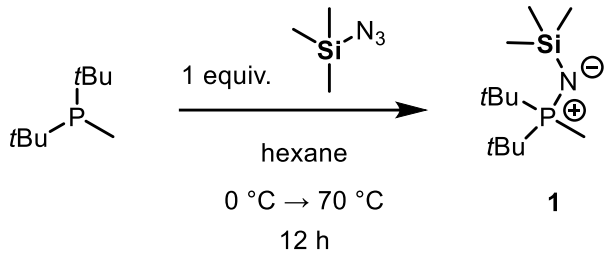

First di-*tert*-butylmethylphosphine (3.56 g, 22.25 mmol, 1 equiv) was diluted in 50 mL of hexane. This solution was cooled to 0°C and then azido(trimethyl)silane (2.56 g, 22.25 mmol, 1 equiv.) was added. The reaction mixture was left to warm up to room temperature, and then the mixture was stirred for 12h. Afterwards the reaction mixture was heated to 70°C with open overpressure for 1h. All volatiles were removed *in vacuo* and the remaining oil diluted in 20 mL of THF and filtered using a P3-Frit with added Celite. All volatiles of the filtrate were removed *in vacuo*. Compound **1** was obtained as a colorless oil. Yield: 3.8 g (15.36 mmol, 69%).

^{1}H NMR (400.13 MHz, C_6D_6, 298 K): δ 1.00 {d, $^{3}J_{P-H}$ = 13.6 Hz, 18H, NP[C(CH_3)$_3$]$_2$}, 0.88 [d, $^{2}J_{P-H}$ = 10.5 Hz, 3H, P(N)CH_3], 0.31 [s, 9H, PNSi(CH_3)$_3$].

^{31}P{^{1}H} NMR (162.04 MHz, C_6D_6, 298 K): δ 26.1 (s, SiN*P*).

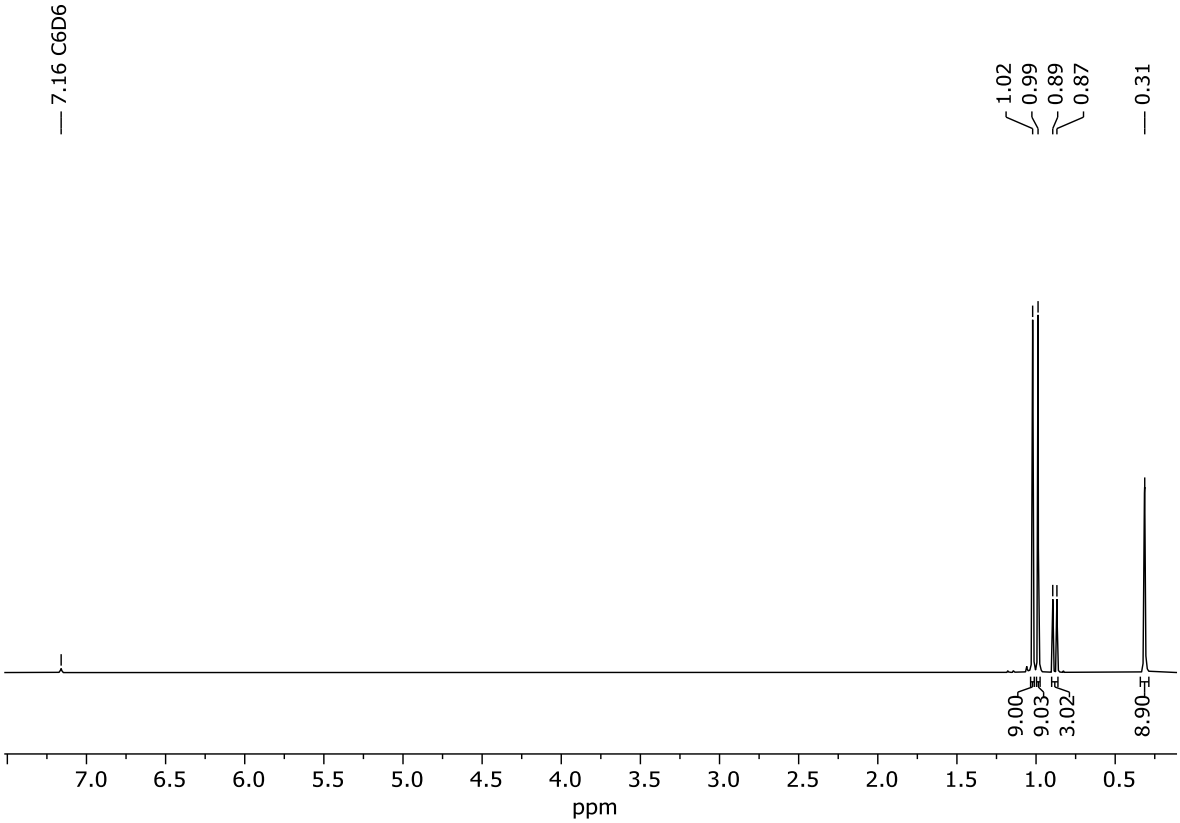

Figure S1: ^{1}H NMR (400.13 MHz, C_6D_6, 298 K) spectrum of **1**.

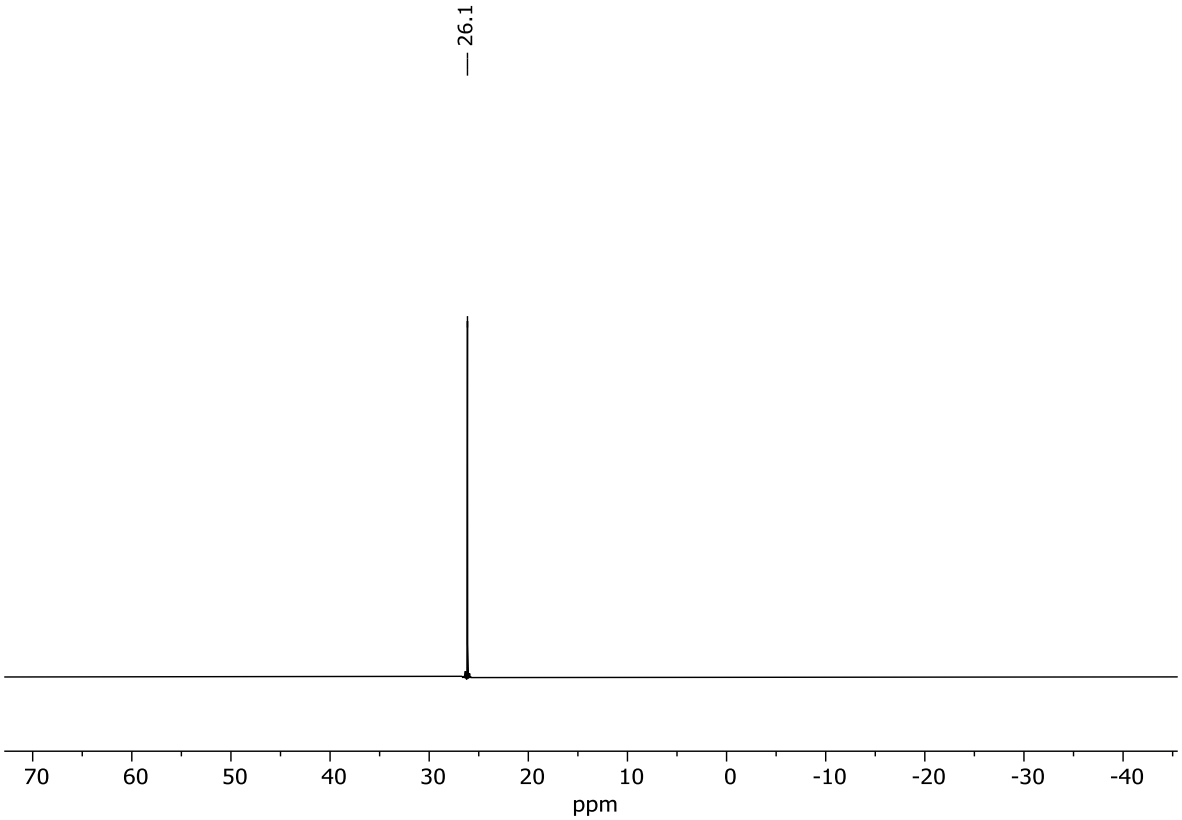

Figure S2: ^{31}P NMR (400.13 MHz, C6D6, 298 K) spectrum of 1.

4.6.2.2 Synthesis of compound 2.

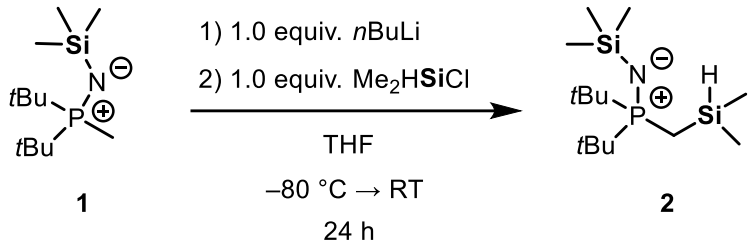

Compound **1** (3.6 g, 14.54 mmol, 1 equiv) was diluted in 50 mL of THF and cooled to –80°C. Then *n*-Butyllithium (6.40 mL of a 2.5 M solution in hexane, 16.0 mmol, 1.1 equiv) was added. The solution was removed from the cooling bath and left to stir for 3 min in a warm water bath at 40°C. Afterwards the solution was cooled down to –80°C. Then chlorodi(methyl)silane (1.38 g, 14.54 mmol, 1 equiv) was added. The reaction was left to warm up to room temperature and stirred for 12 h. Afterwards all volatiles were removed *in vacuo*. The resulting orange oily suspension was extracted with 20 mL of hexane and filtered. The filtrate was purified by fractional Kugelrohr distillation (75°C–80°C oven temperature, 1.0 x 10^{-3} mbar). Compound **2** was obtained as a slightly yellow oil. Yield: 1.4 g (4.58 mmol, 31%).

^{1}H NMR (400.13 MHz, C_6D_6, 298 K): δ 4.32 (m, 1H, Si*H*), 1.04 {d, $^3J_{P–H}$ = 13.6 Hz, 18H, NP[C(CH_3)$_3$]$_2$}, 0.82 (dd, $^2J_{P–H}$ = 10.6 Hz, $^3J_{H–H}$ = 3.1 Hz, 2H, NPCH_2SiH), 0.32 [s, 9H, PNSi(CH_3)$_3$], 0.20 [d, $^3J_{H–H}$ = 3.6 Hz, 6H, Si(CH_3)$_2$].

$^{13}C\{^1H\}$ NMR (100.61 MHz, C_6D_6, 298 K): δ 37.0 [d, $^1J_{P-C}$ = 60.2 Hz, P[*C*$(CH_3)]_2$}, 27.4 {d, $^2J_{P-C}$ = 1.6 Hz, P[C(*C*$H_3)]_2$}, 9.8 [d, $^1J_{P-C}$ = 59.7 Hz, P(N)*C*H_2Si], 5.1 [d, $^3J_{P-C}$ = 1.7 Hz, Si(*C*$H_3)_2$], –1.8 [d, $^3J_{P-C}$ = 2.7 Hz, PNSi(*C*$H_3)_3$].

$^{31}P\{^1H\}$ NMR (162.04 MHz, C_6D_6, 298 K): δ 27.7 (SiN*P*).

$^{29}Si\{^1H\}$ NMR (79.49 MHz, C_6D_6, 298 K): δ –15.3 (d, $^2J_{P-Si}$ = 8.7 Hz, PCH_2*Si*), –19.9 (d, $^2J_{P-Si}$ = 28.2 Hz, PN*Si*).

CHN Analysis: Calcd for $C_{14}H_{36}NPSi_2$: C, 55.0; H, 11.9; N, 4.6. Found: C, 54.60; H, 11.41; N, 4.15.

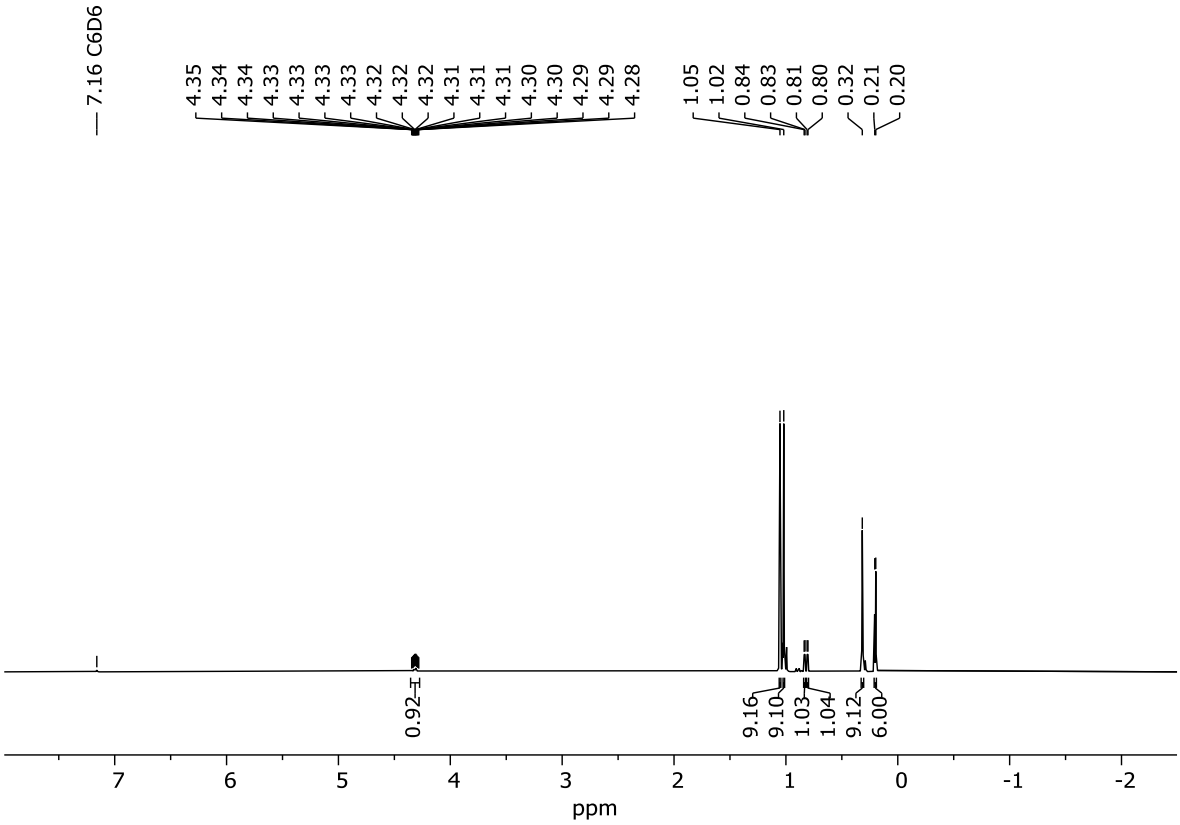

Figure S3: ^1H NMR (400.13 MHz, C_6D_6, 298 K) spectrum of **2**.

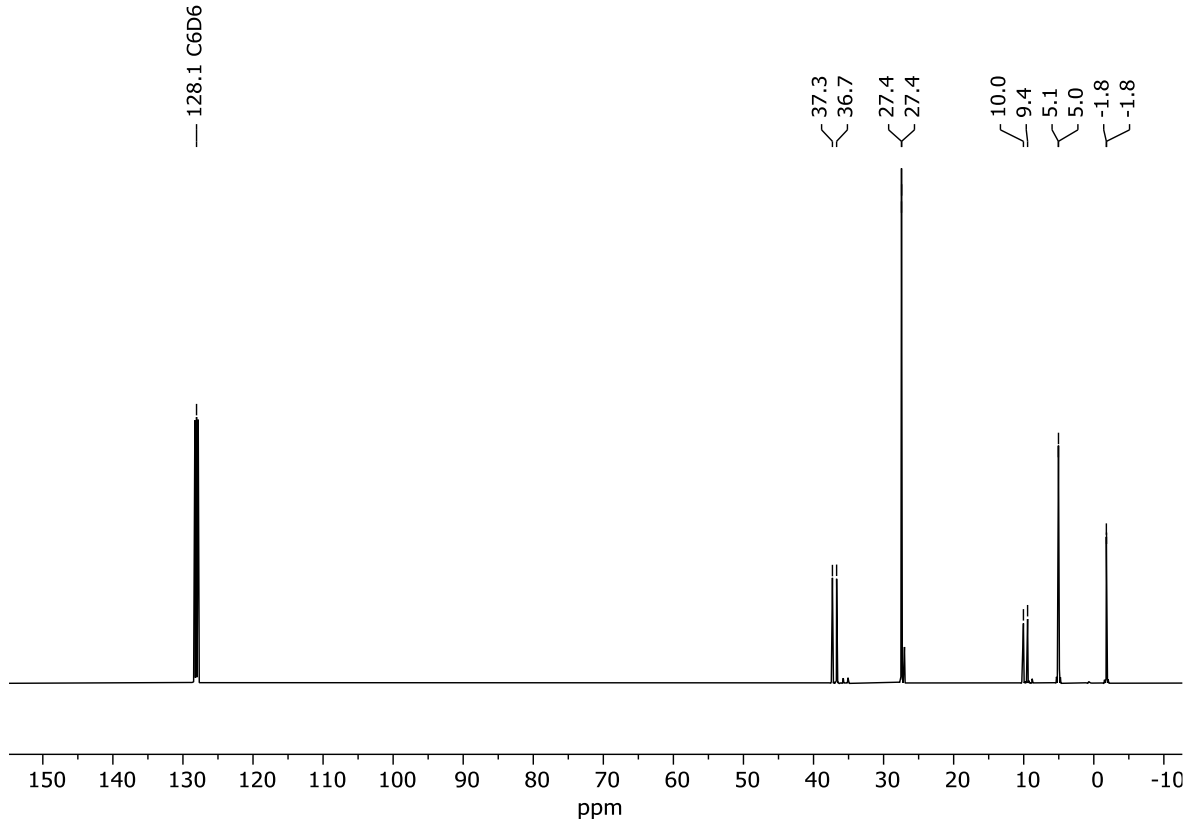

Figure S4: $^{13}C\{^{1}H\}$ NMR (100.61 MHz, C_6D_6, 298 K) of compound **2**.

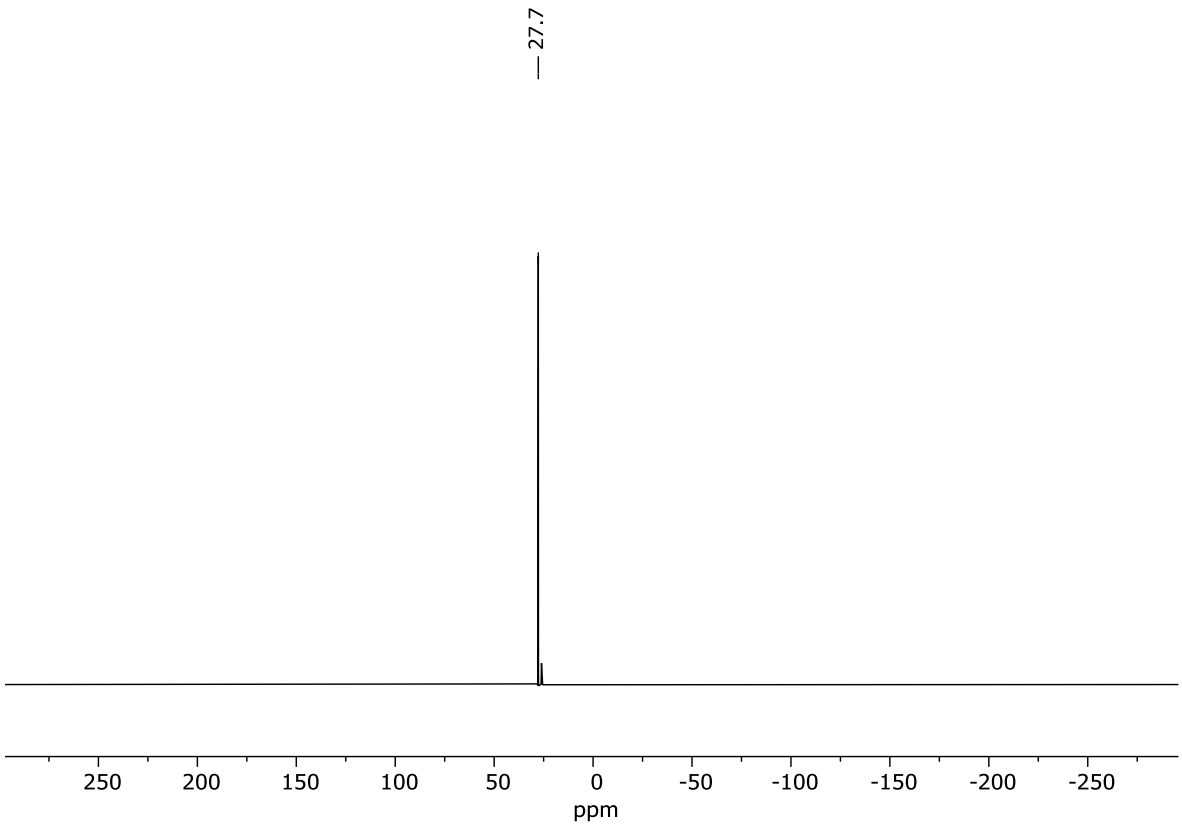

Figure S5: $^{31}P\{^{1}H\}$ NMR (162.04 MHz, C_6D_6, 298 K) of compound **2**.

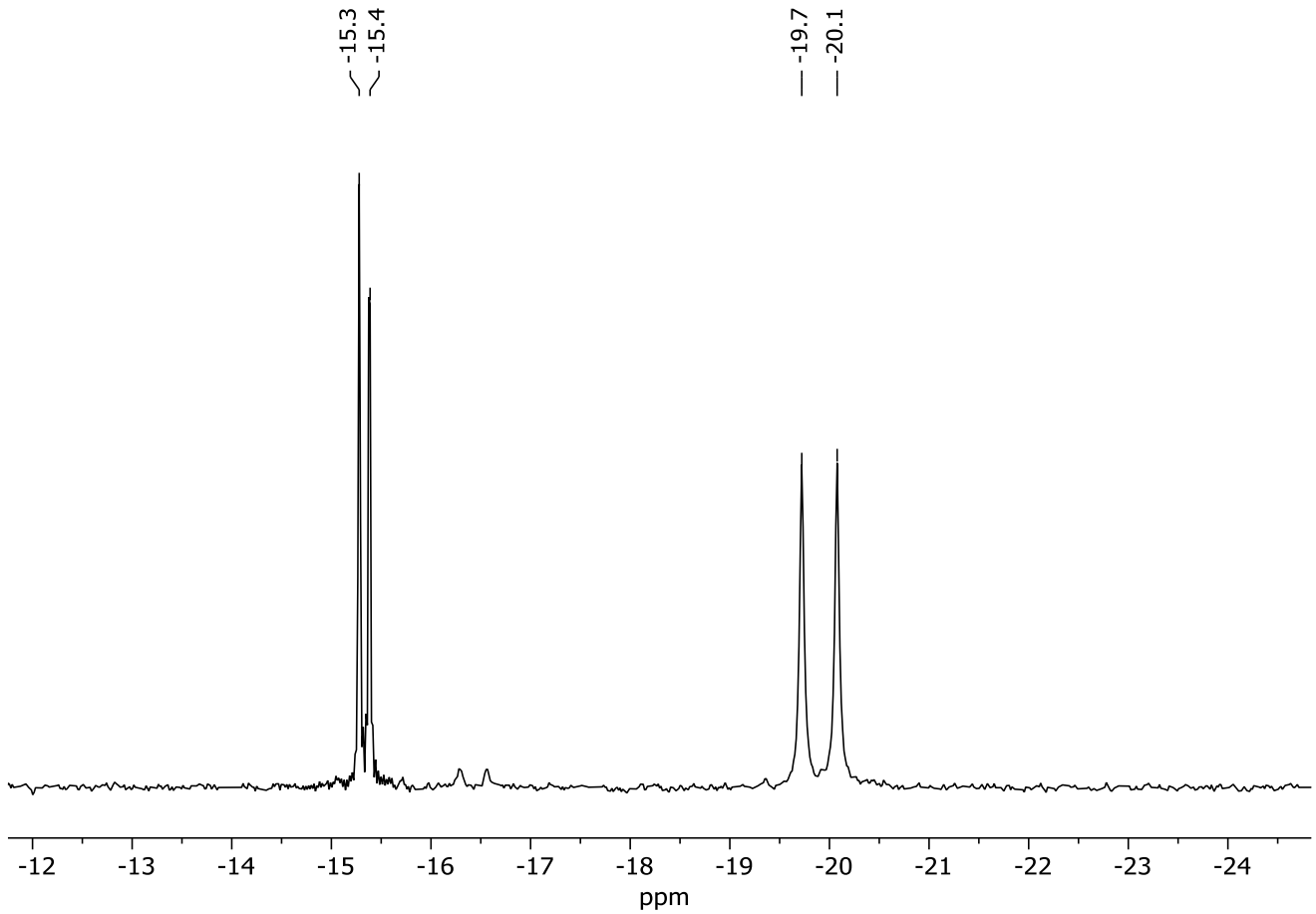

Figure S6: $^{29}Si\{^{1}H\}$ NMR (79.49 MHz, C_6D_6, 298 K) of compound **2**.

4.6.2.3 Synthesis of compound 3.

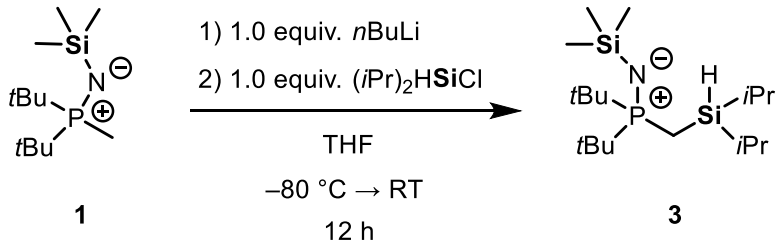

First compound **1** (1.28g, 5.17 mmol, 1 equiv) was dissolved in 30 mL of THF and cooled to 0°C. Next *n*-Butyllithium (2.07 mL of a 2.5 M solution in hexane, 5.17 mmol, 1 equiv) was slowly added. The mixture was stirred for 20 min at 0°C and then at room temperature for a further 20 min. Afterwards the solution was cooled to –80°C and di-*iso*-propyl(chloro)silane (0.779 g, 5.17 mmol, 1 equiv) was added. The resulting suspension was stirred for 12 h at room temperature. Next all volatiles were removed *in vacuo* and the resulting oily suspension diluted with 30 mL of hexane. The suspension was filtered using a P3-Frit with added celite, and the filtrate was purified using fractional Kugelrohr

distillation (130°C oven temperature, 1 x 10^{-3} mbar). Compound **3** was obtained as a colorless oil. Yield: 1.35 g (3.73 mmol, 72%).

^{1}H NMR (400.13 MHz, C_6D_6, 298 K): δ 4.08–4.07 (m, 1H, Si*H*), 1.27–1.21 [m, 2H, SiC*H*$(CH_3)_2$], 1.13 [s, 3H, SiCH(C*H*$_3)_2$], 1.12 [s, 3H, SiCH(C*H*$_3)_2$], 1.09 [s, 3H, SiCH(C*H*$_3)_2$], 1.09 [d, 18H, $^{3}J_{P-H}$ = 13.5 Hz, PC(C*H*$_3)_3$], 1.07 [s, 3H, SiCH(C*H*$_3)_2$], 0.88 (dd, $^{2}J_{P-H}$ = 11.3 Hz, $^{3}J_{H-H}$ = 3.1 Hz, 2H, PC*H*$_2$Si), 0.40 [s, 9H, Si(C*H*$_3)_3$].

^{13}C{^{1}H} NMR (100.61 MHz, C_6D_6, 298 K): δ 37.4 [d, $^{1}J_{P-C}$ = 59.9 Hz, P*C*$(CH_3)_3$], 27.6 [s, SiCH(*C*H$_3)_2$], 19.3 [d, $^{2}J_{P-C}$ = 76.6 Hz, PC(*C*H$_3)_3$], 11.7 [d, $^{3}J_{P-C}$ = 2.6 Hz, Si*C*H$(CH_3)_2$], 4.9 [d, $^{3}J_{P-C}$ = 1.8 Hz, PNSi(*C*H$_3)_3$], 3.4 (d, $^{1}J_{P-C}$ = 59.3 Hz, P*C*H$_2$Si).

^{31}P{^{1}H} NMR (162.04 MHz, C_6D_6, 298 K): δ 26.1 (SiN*P*).

^{29}Si{^{1}H} NMR (79.49 MHz, C_6D_6, 298 K): δ 3.0 (d, $^{2}J_{P-Si}$ = 7.9 Hz, PCH$_2$*Si*), –19.8 (d, $^{2}J_{P-Si}$ = 28.4 Hz, PN*Si*).

CHN Analysis: Calcd for $C_{18}H_{44}NPSi_2$: C, 59.77; H, 12.26; N, 3.87. Found: C, 59.42; H, 12.41; N, 3.70.

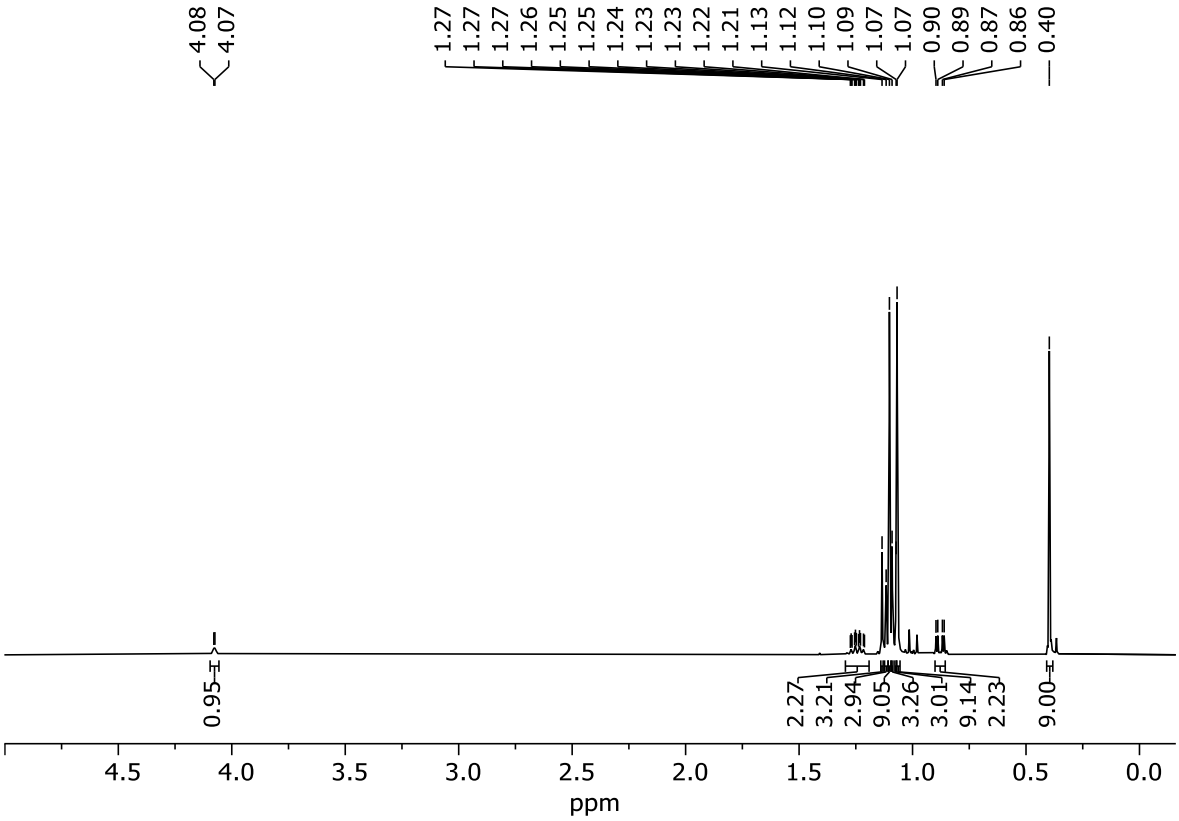

Figure S7: ^{1}H NMR (400.13 MHz, C_6D_6, 298 K) spectrum of **3**.

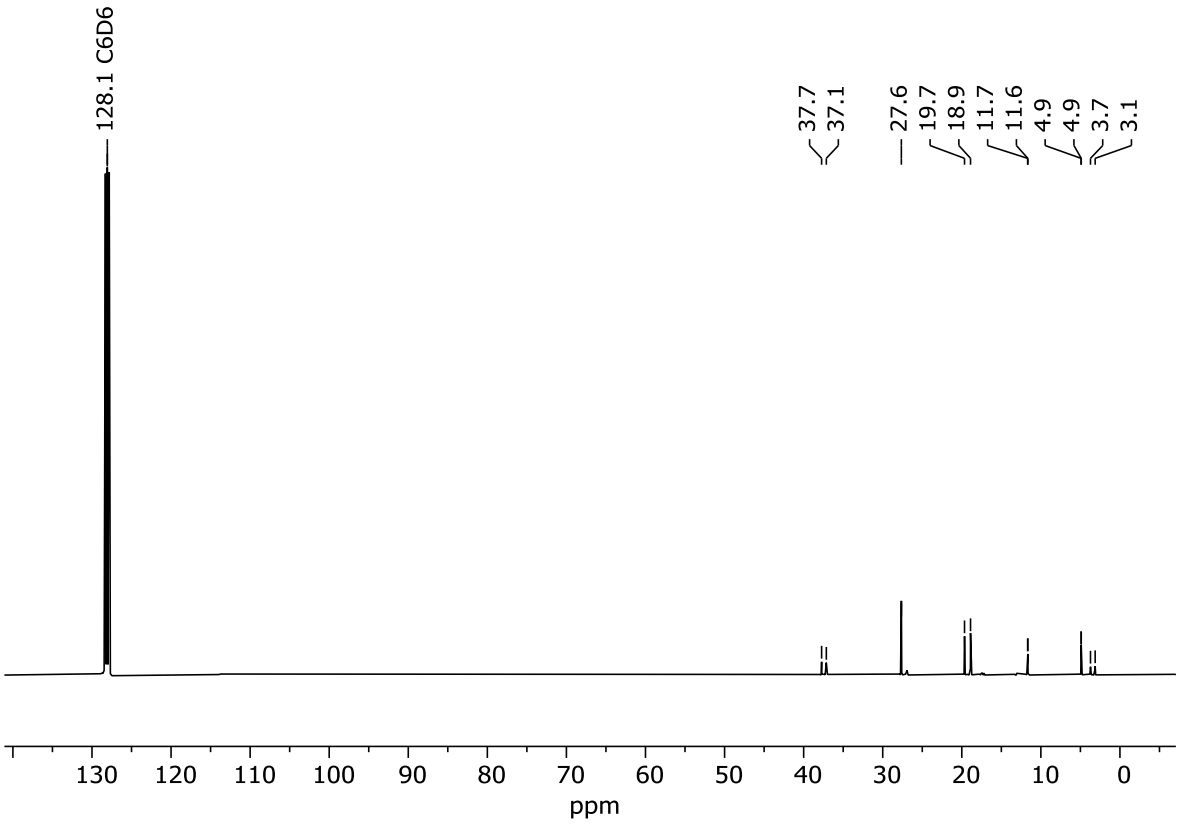

Figure S8: $^{13}C\{^{1}H\}$ NMR (100.61 MHz, C_6D_6, 298 K) of compound **3**.

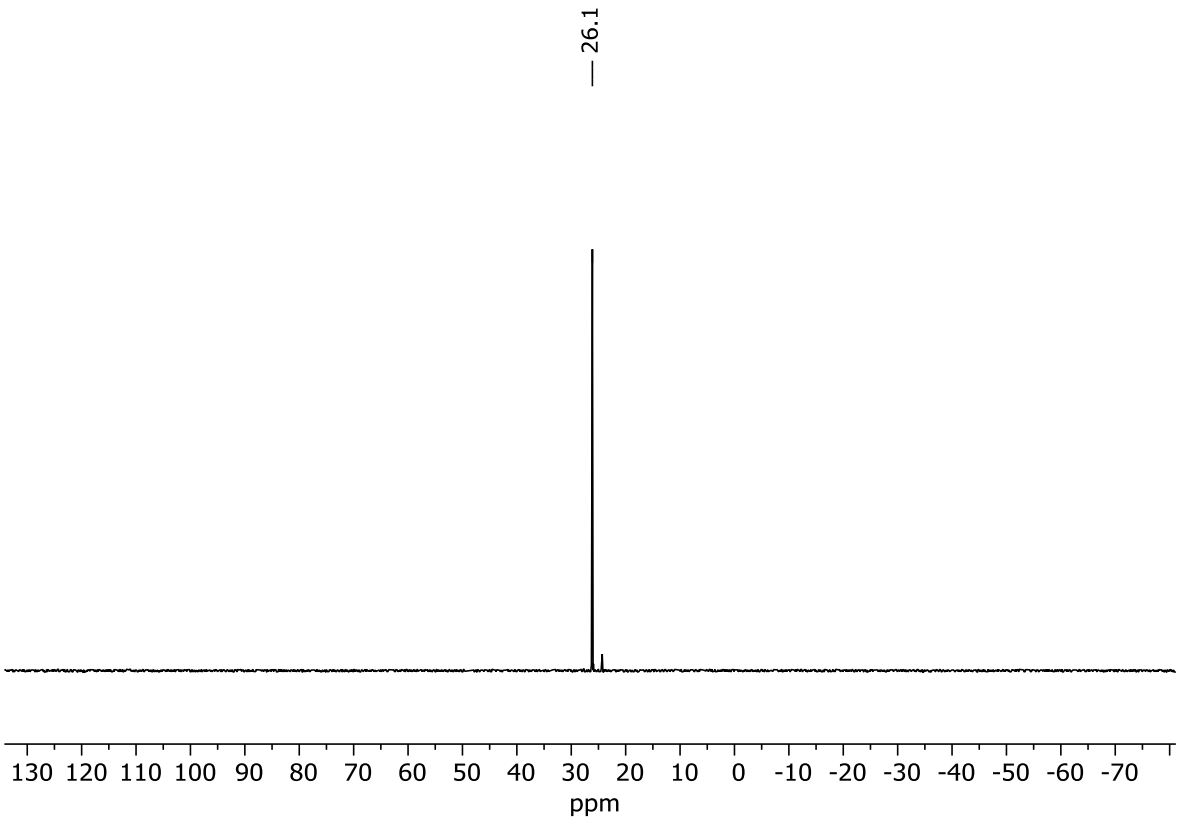

Figure S9: $^{31}P\{^{1}H\}$ NMR (162.04 MHz, C_6D_6, 298 K) of compound **3**.

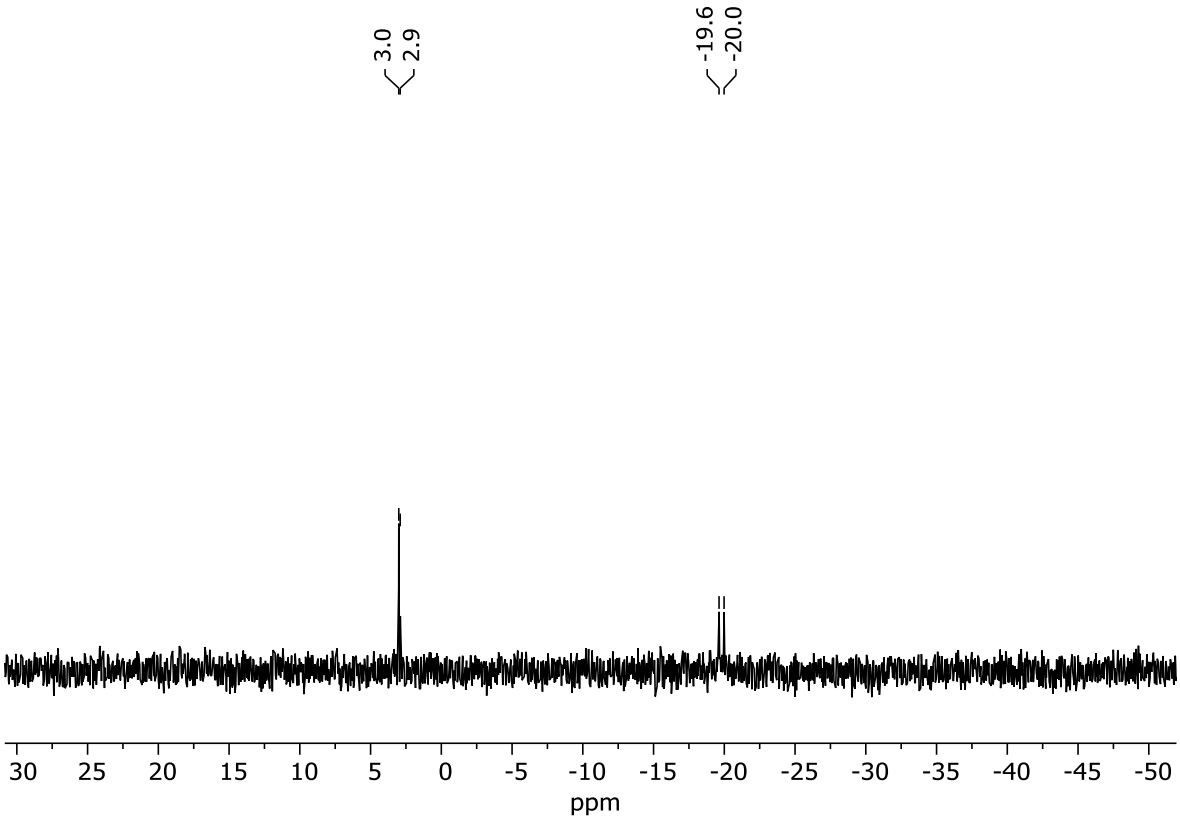

Figure S10: $^{29}Si\{^{1}H\}$ NMR (79.49 MHz, C_6D_6, 298 K) of compound **3**.

4.6.2.4 Synthesis of compound 4.

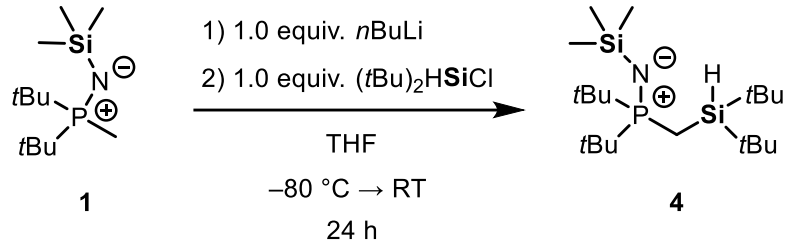

Compound **1** (3.8 g, 15.37 mmol, 1 equiv) was diluted in 50 mL of THF and cooled to –50°C. Then *n*-Butyllithium (6.76 mL of a 2.5 M solution in hexane, 16.9 mmol, 1.1 equiv) was added. The solution was removed from the cooling bath and left to stir for 20 min at room temperature. Afterwards the solution was cooled down to –80°C. Then di-*tert*-butylchlorosilane (2.75 g, 15.37 mmol, 1 equiv) was slowly added. The reaction was left to warm up to room temperature and stirred for 12 h. All volatiles were removed *in vacuo* and the resulting oil diluted in 5 mL of toluene. This solution was filtered using a P3-Frit with added Celite. Crystals suitable for single-crystal X-ray diffraction analysis were obtained from the filtrate at –30°C. The crystalline compound **4** was isolated via filtration and dried *in vacuo*. Yield: 4.12 g (10.57 mmol, 68%).

^{1}H NMR (400.13 MHz, C_6D_6, 298 K): δ 4.00 (m, 1H, Si*H*), 1.13 {d, $^{3}J_{P-H}$ = 13.5 Hz, 18H, NP[C(CH_3)$_3$]$_2$}, 1.10 {s, 18H, PSiH(CH_3)$_3$]$_2$}, 0.96 (dd, $^{2}J_{P-H}$ = 13.4 Hz, $^{3}J_{H-H}$ = 2.6 Hz, 2H, NPCH_2SiH), 0.40 [s, 9H, PNSi(CH_3)$_3$].

$^{13}C\{^1H\}$ NMR (100.61 MHz, C_6D_6, 298 K): δ 38.0 [d, $^1J_{P-C}$ = 60.3 Hz, P[*C*(CH_3)$_3$]$_2$}, 29.8 {s, Si[C(*C*H_3)$_3$]$_2$}, 28.2 {d, $^2J_{P-C}$ = 1.7 Hz, P[C(*C*H_3)$_3$]$_2$}, 19.4 {d, $^3J_{P-C}$ = 2.4 Hz, Si[*C*(CH_3)$_3$]$_2$}, 5.1 [d, $^3J_{P-C}$ = 1.7 Hz, PNSi(*C*H_3)$_3$], 3.5 (d, $^1J_{P-C}$ = 58.9 Hz, P(N)*C*H_2Si).

$^{31}P\{^1H\}$ NMR (162.04 MHz, C_6D_6, 298 K): δ 28.5 (s, SiN*P*).

$^{29}Si\{^1H\}$ NMR (79.49 MHz, C_6D_6, 298 K): δ 8.0 (d, $^2J_{P-Si}$ = 9.8 Hz, PCH_2*Si*), –19.7 (d, $^2J_{P-Si}$ = 27.5 Hz, PN*Si*).

FD-MS: Calcd *m/z* for $C_{20}H_{48}NPSi_2$ $[M]^{+\bullet}$: 389.3063. Found: 389.3049 $[M]^{+\bullet}$.

CHN Analysis: Calcd for $C_{20}H_{48}NPSi_2$: C, 61.6; H, 12.4; N, 3.6. Found: C, 61.39; H, 12.22; N, 3.41.

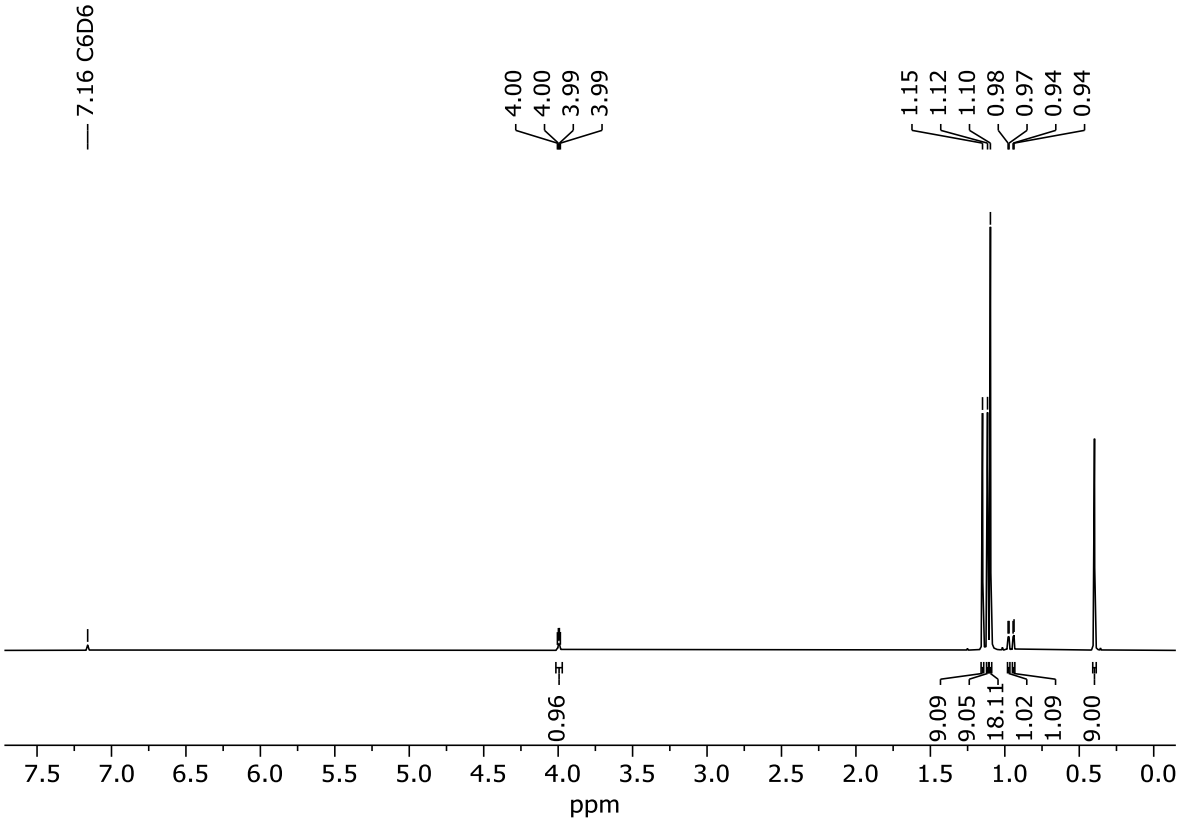

Figure S11: ^{1}H NMR (400.13 MHz, C_6D_6, 298 K) spectrum of **4.**

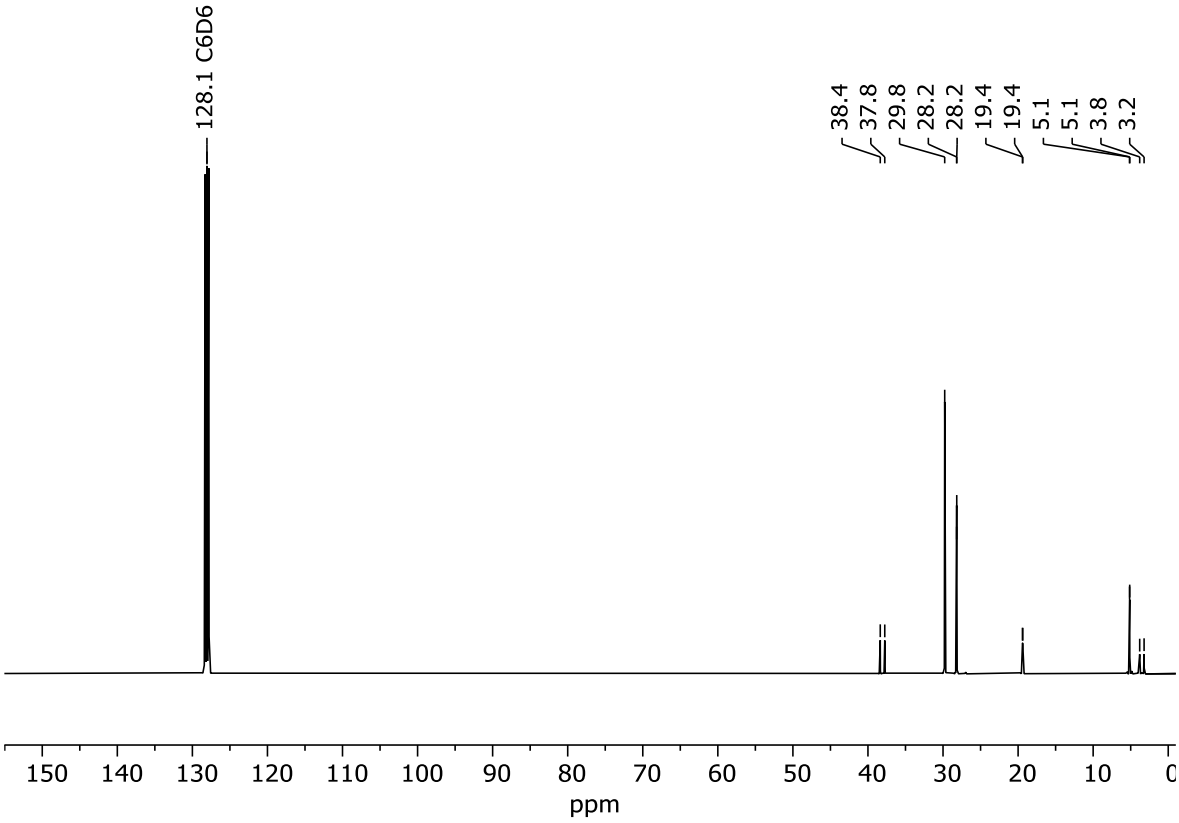

Figure S12: $^{13}C\{^{1}H\}$ NMR (100.61 MHz, C_6D_6, 298 K) of compound **4**.

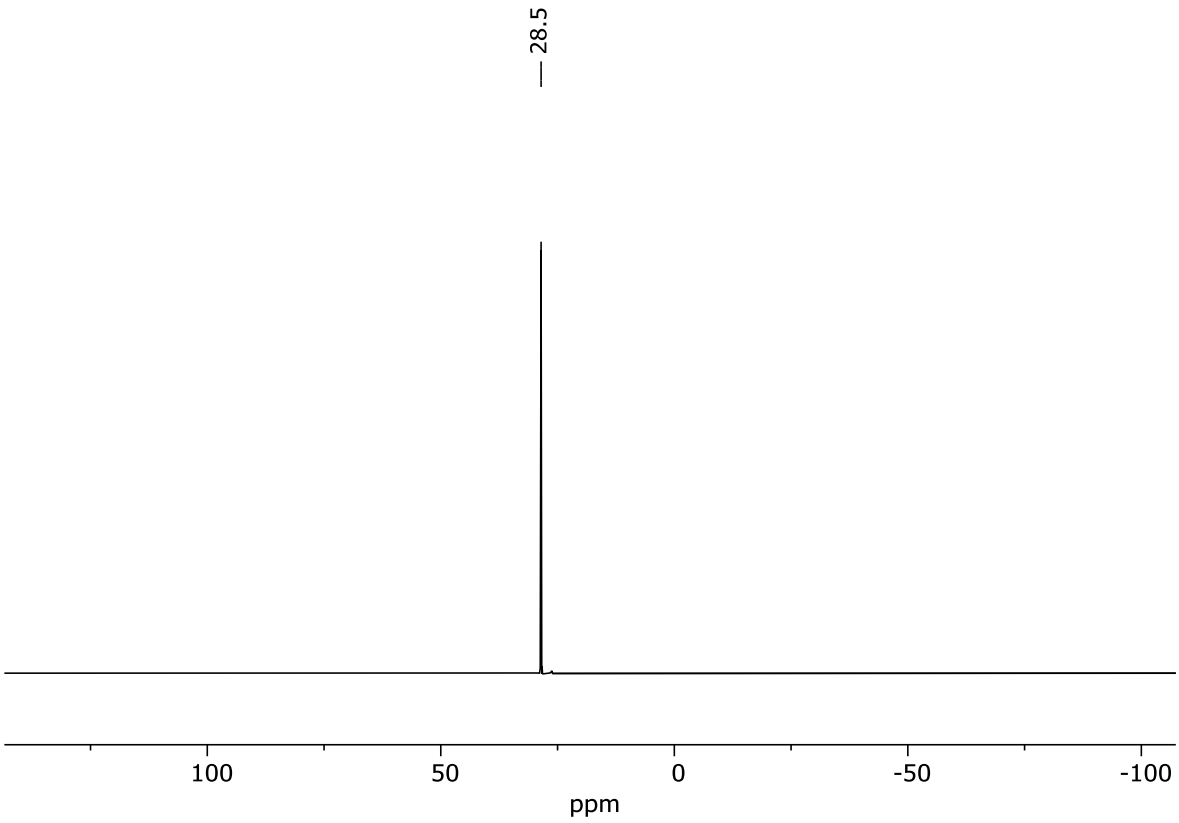

Figure S13: $^{31}P\{^{1}H\}$ NMR (162.04 MHz, C_6D_6, 298 K) of compound **4**.

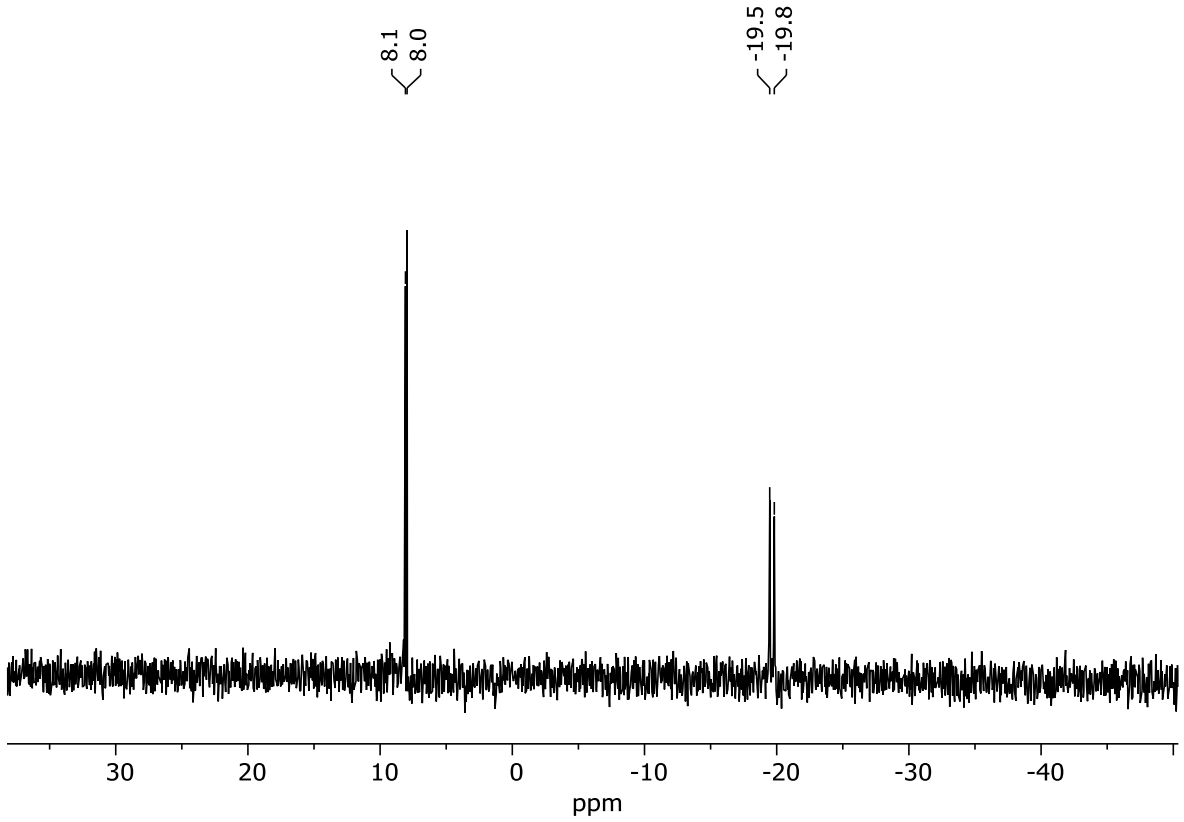

Figure S14: $^{29}Si\{^{1}H\}$ NMR (79.49 MHz, C_6D_6, 298 K) of compound **4**.

4.6.2.5 Synthesis of compound 8.

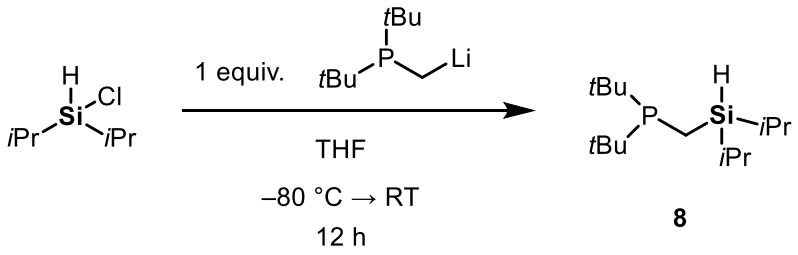

First di-*iso*-propyl(chloro)silane (3.30g, 21.89 mmol 1.1 equiv) was diluted in 10 mL of THF and cooled to –80°C. In a separate Schlenk flask ((di-*tert*-butylphosphaneyl)methyl)lithium[1] (3.31 g, 19.90 mmol, 1 equiv) was dissolved in 5 mL of THF and quickly added to the cooled solution. The mixture was allowed to slowly warm up to room temperature in the cooling bath and subsequently stirred for 24 h. Next all volatiles were removed *in vacuo* and the oily residue suspended in 10 mL of hexane. The suspension was filtered using a P3-Frit with added celite and the filtrate was subjected to fractional Kugelrohr distillation for purification (100°C oven temperature, 1 x 10^{-3} mbar). Compound **8** was obtained as a colorless oil. Yield: 3.6 g (13.11 mmol, 65%).

^{1}H NMR (400.13 MHz, C_6D_6, 298 K): δ 3.93 (m, 1H, Si*H*), 1.14 {m, 23H, Si[C*H*(CH_3)$_2$]$_2$+PC(CH_3)$_3$}, 1.11 [s, 9H, PC(CH_3)$_3$], 0.57 (dd, $^{2}J_{P-H}$ = 3.8 Hz, $^{3}J_{H-H}$ = 1.9 Hz, 2H, PCH_2Si).

$^{13}C\{^1H\}$ NMR (100.61 MHz, C_6D_6, 298 K): δ 32.0 [d, $^1J_{P-C}$ = 26.2 Hz, P*C*$(CH_3)_3$], 29.8 Hz [d, $^2J_{P-C}$ = 14.1 Hz, PC(CH$_3$)$_3$], 19.3 [s, SiCH(CH$_3$)$_2$], 11.9 [d, $^3J_{P-C}$ = 4.8 Hz, Si*C*H$(CH_3)_2$], –1.6 (d, $^1J_{P-C}$ = 44.6 Hz, P*C*H$_2$Si).

$^{31}P\{^1H\}$ NMR (162.04 MHz, C_6D_6, 298 K): δ 20.2 (*P*CH$_2$Si).

$^{29}Si\{^1H\}$ NMR (79.49 MHz, C_6D_6, 298 K): δ 7.7 (d, $^2J_{P-Si}$ = 18.7 Hz, PCH$_2$*Si*).

EI-MS: Calcd *m/z* for $C_{11}H_{27}PSi$ $[M]^{+\bullet}$: 274.2246. Found: 274.2233 $[M]^{+\bullet}$.

CHN Analysis: Calcd for $C_{11}H_{27}PSi$: C, 65.6; H, 12.85. Found: C, 62.19; H, 12.52.

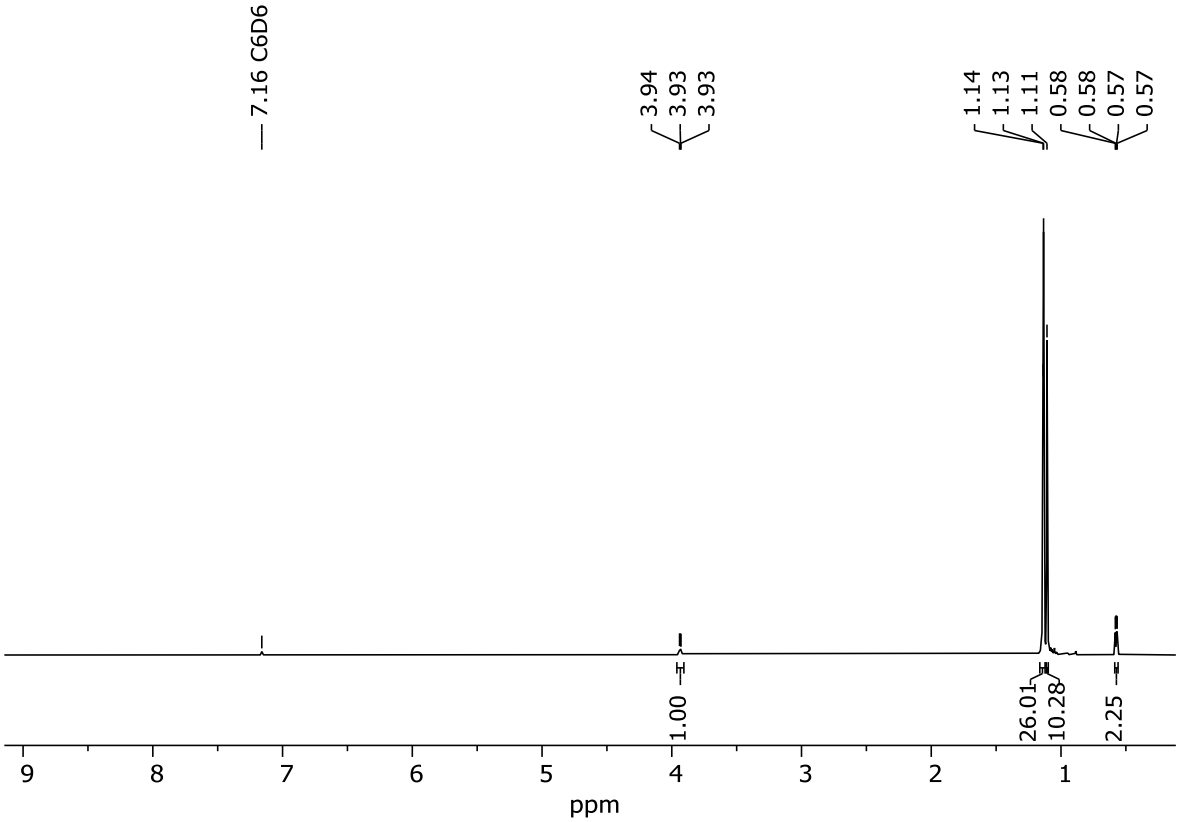

Figure S15: ^{1}H NMR (400.13 MHz, C_6D_6, 298 K) spectrum of **8**.

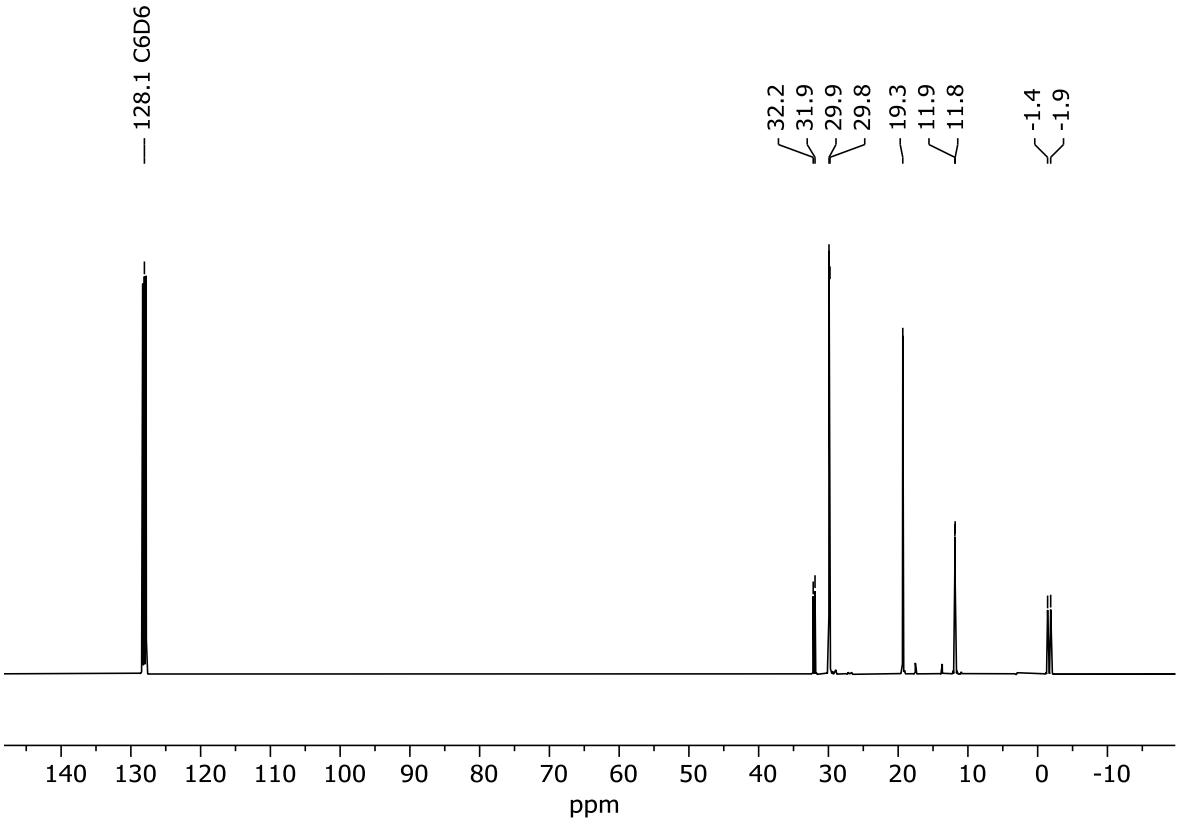

Figure S16: $^{13}C\{^{1}H\}$ NMR (100.61 MHz, C_6D_6, 298 K) of compound **8**.

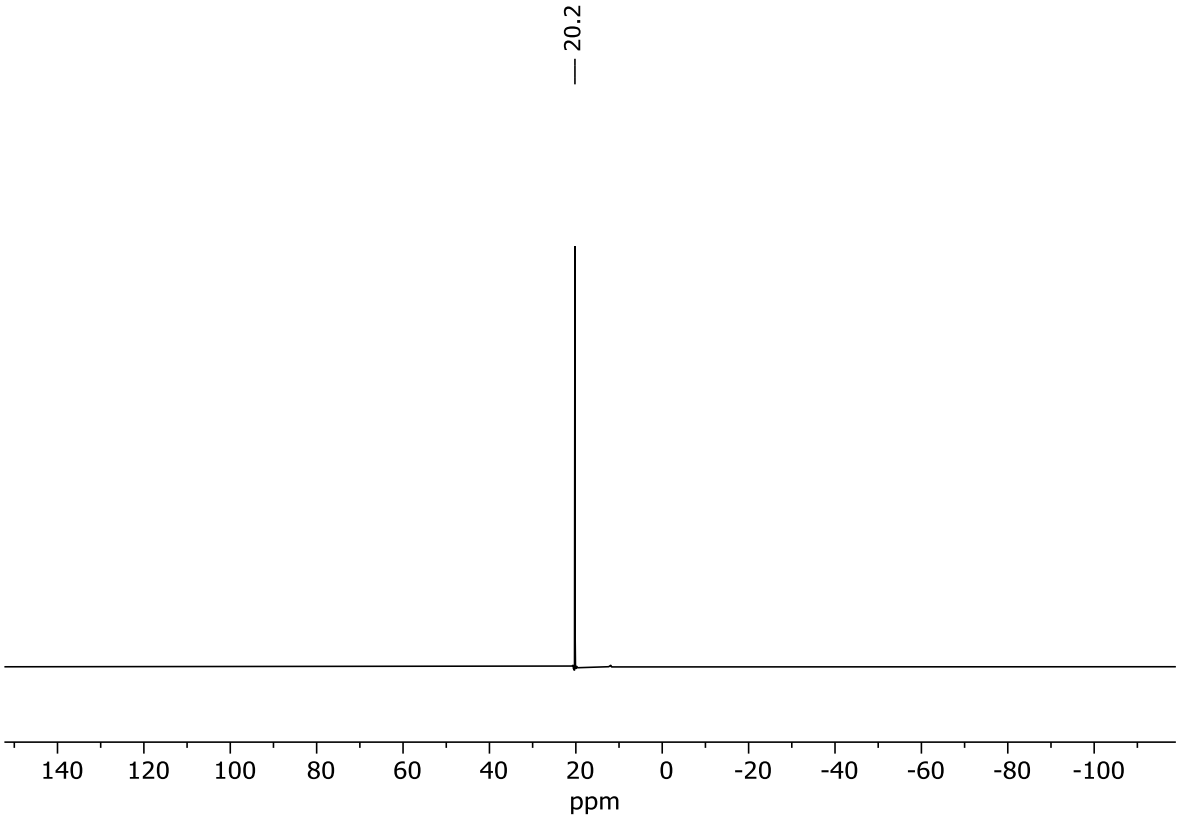

Figure S17: $^{31}P\{^{1}H\}$ NMR (162.04 MHz, C_6D_6, 298 K) of compound **8**.

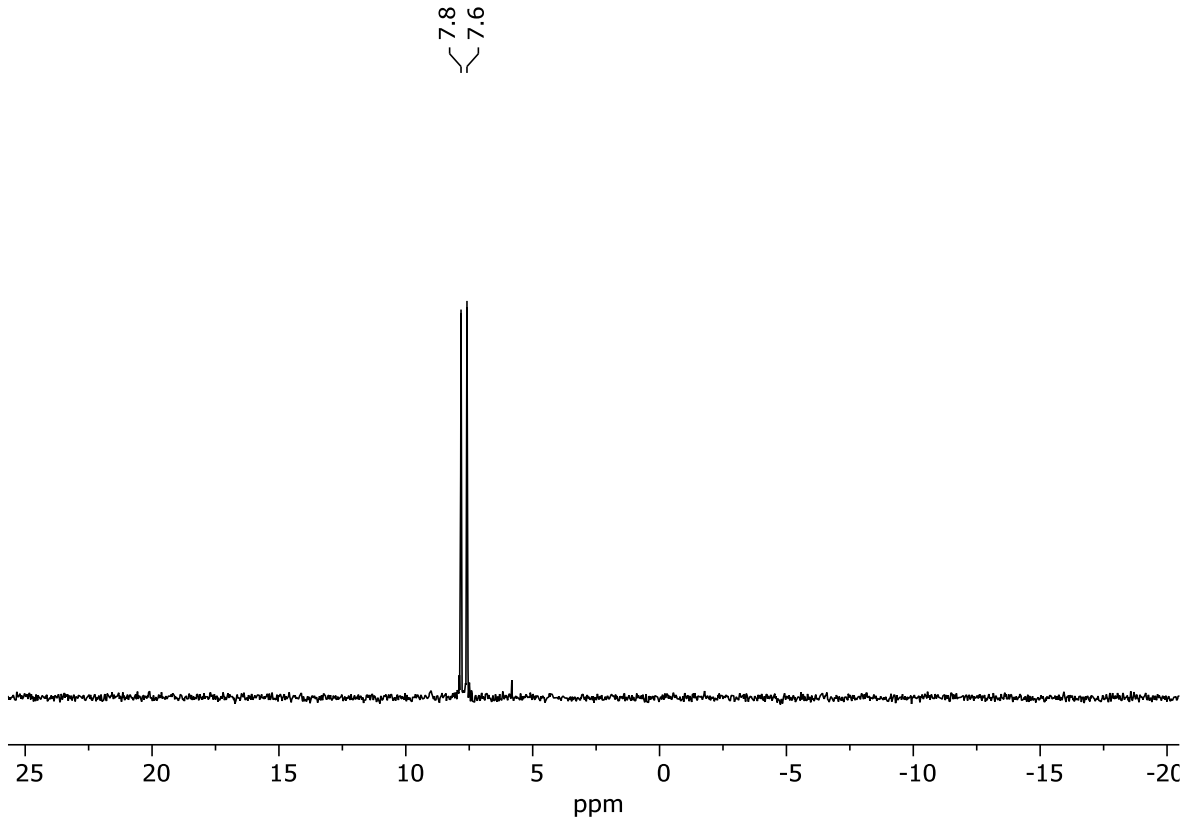

Figure S18: $^{29}Si\{^{1}H\}$ NMR (79.49 MHz, C_6D_6, 298 K) of compound **8**.

4.6.2.6 Synthesis of bis(3,5-trifluoromethylphenyl)borane azide.

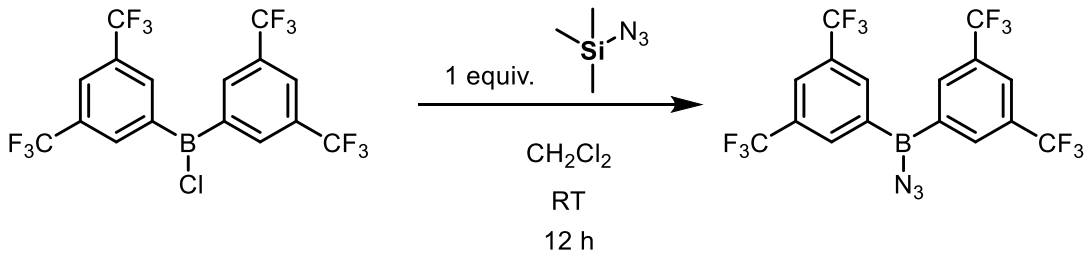

Prepared according to a modified literature procedure.[5]

First bis(3,5-bis(trifluoromethyl)phenyl)chloroborane[2] (1.02 g, 4.00 mmol, 1 equiv) was dissolved in 20 mL of DCM. Then strong stirring was activated. Next trimethylsilylazide (0.53 mmL, 4.00 mmol, 1 equiv) was added slowly over a period of 30 min. The reaction mixture was then stirred for 72 h at room temperature. Then the solvent was removed *in vacuo* and the oily yellow residue dissolved in 5 mL of toluene and crystallized at –30°C. The next day the crystals were isolated via filtration, washed once with 2 mL of pentane and dried *in vacuo*. The product was obtained as colorless crystals which were stored at –30°C in a Glovebox. Yield: 850 mg (1.77 mmol, 44%).

^{1}H NMR (400.13 MHz, C_6D_6, 298 K): δ 7.83 (s, 2H, C*H*$_{para}$), 7.73 (s, 4H, C*H*$_{ortho}$).

^{13}C{^{1}H} NMR (100.61 MHz, C_6D_6, 298 K): δ 134.6 (bm, *C*$_{ipso}$), 131.6 (q, $^{1}J_{C-F}$ = 33.4 Hz, *C*F_3), 125.8 (m, *C*$_{meta}$), 125.0 (s, *C*$_{para}$), 122.3 (s, *C*$_{ortho}$).

$^{19}F\{^{1}H\}$ NMR (376.66 MHz, C_6D_6, 298 K): δ –63.0 (s, C*F*$_3$).

$^{11}B\{^{1}H\}$ NMR (128.43 MHz, C_6D_6, 298 K): δ 48.0 (bs, *B*N_3).

CHN Analysis: Calcd for $C_{19}H_7BF_{12}O$: C, 42.33; H, 1.55; N, 0. Found: C, 42.62; H, 1.72; N, 0. (Compound hydrolyzed during the measurement).

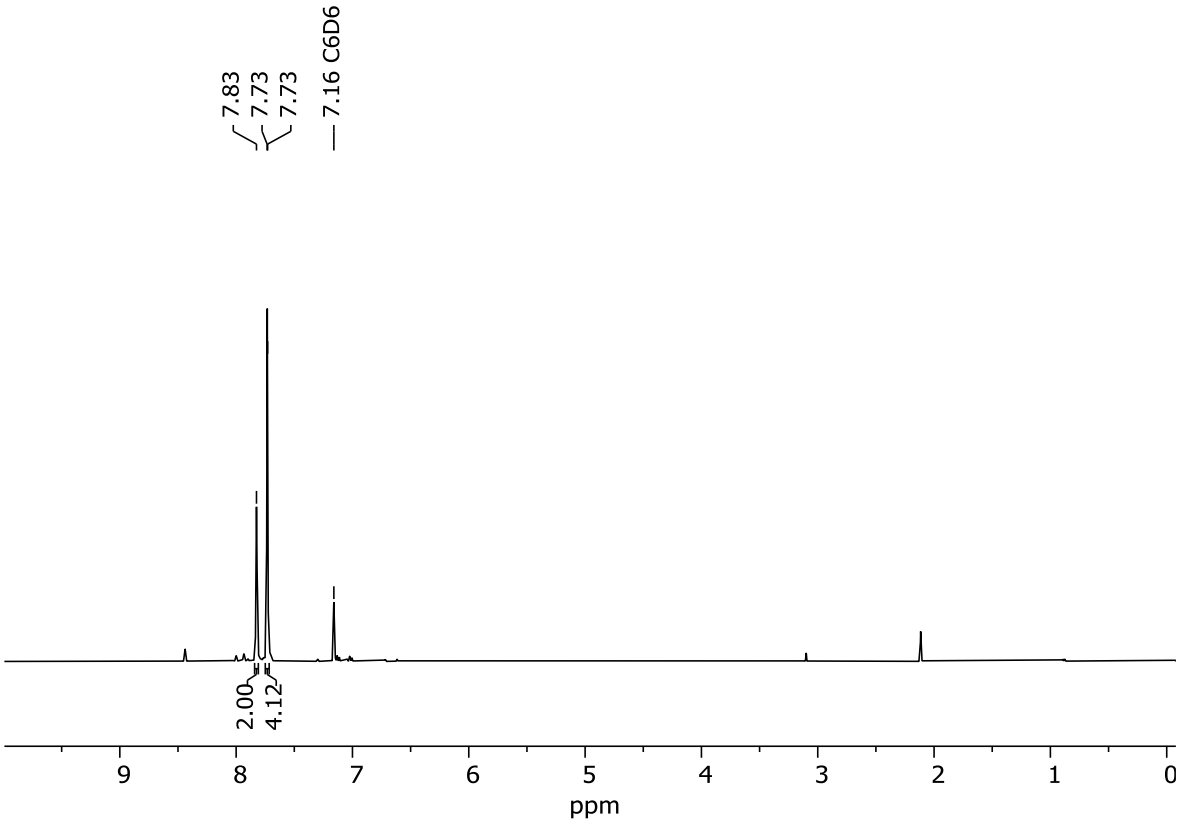

Figure S19: ^{1}H NMR (400.13 MHz, C_6D_6, 298 K) spectrum of bis(3,5-trifluoromethylphenyl)borane azide.

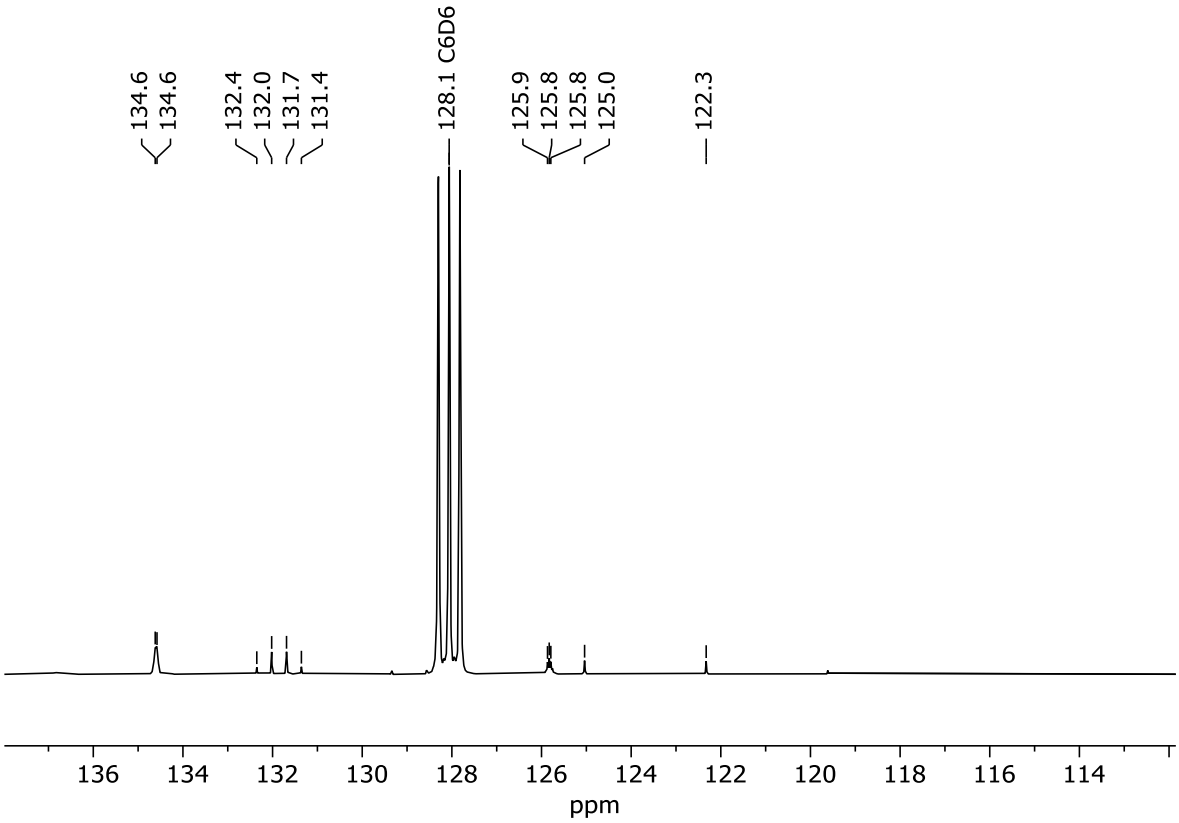

Figure S20: $^{13}C\{^{1}H\}$ NMR (100.61 MHz, C_6D_6, 298 K) of bis(3,5-trifluoromethylphenyl)borane azide.

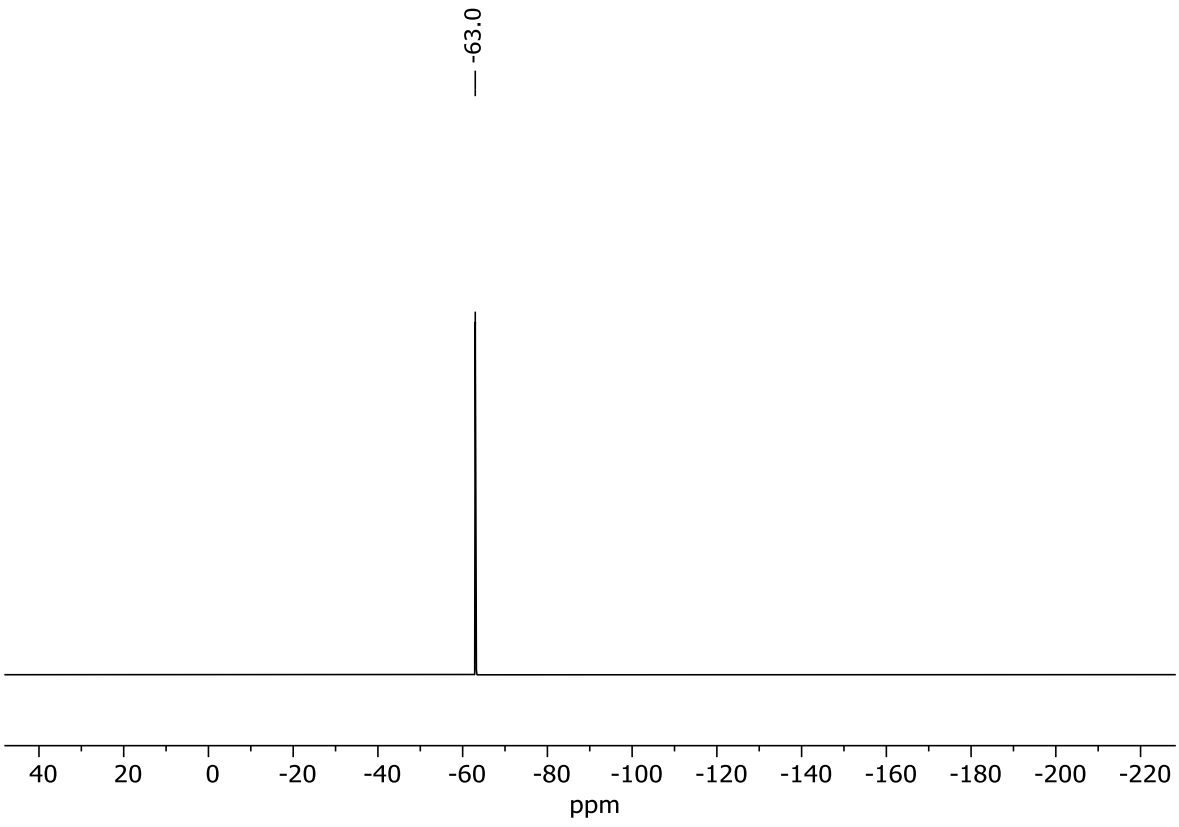

Figure S21: $^{19}F\{^{1}H\}$ NMR (376.66 MHz, C_6D_6, 298 K) of bis(3,5-trifluoromethylphenyl)borane azide.

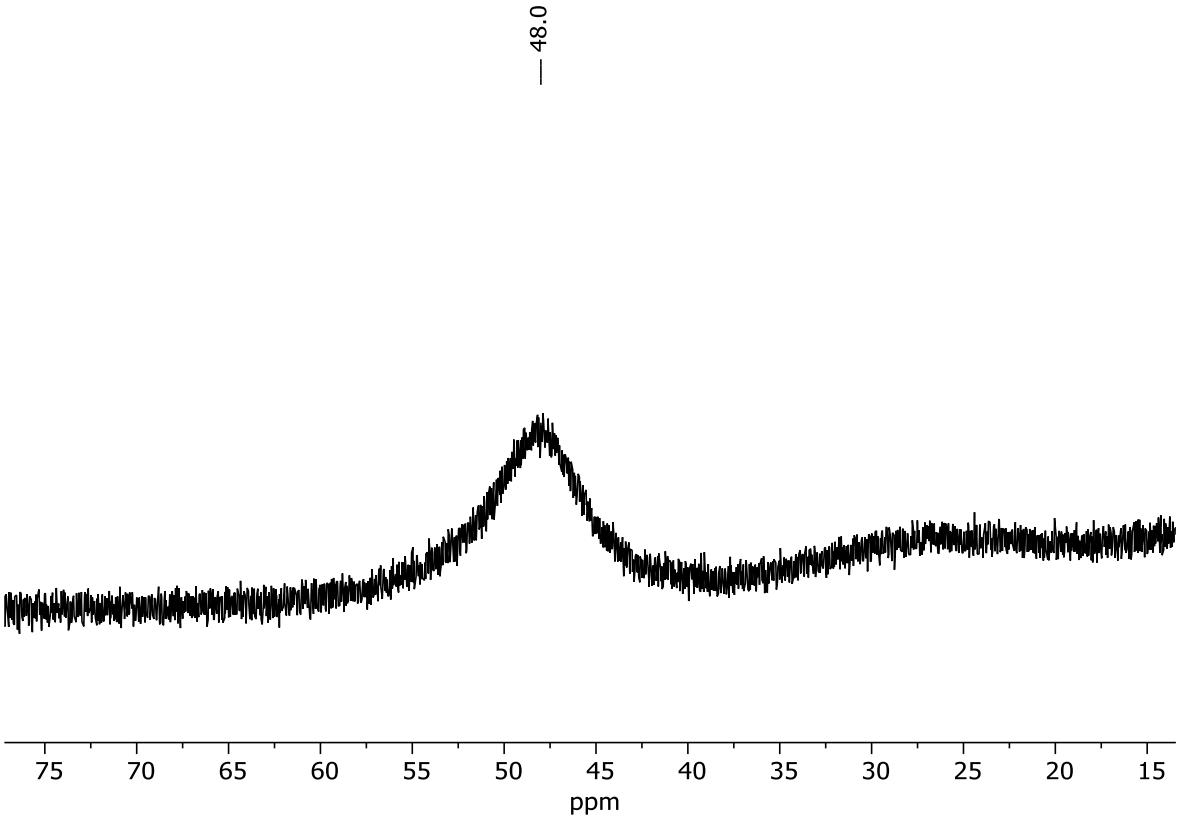

Figure S22: $^{11}B\{^{1}H\}$ NMR (128.43 MHz, C_6D_6, 298 K) of bis(3,5-trifluoromethyl)borane azide.

4.6.2.7 Synthesis of compound 12

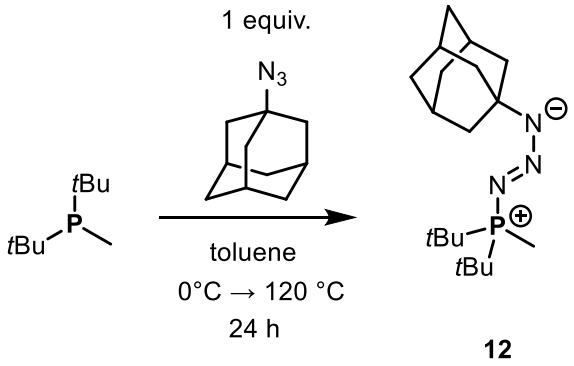

First di-*tert*-butylmethylphosphine (190 mg, 1.19 mmol, 1 equiv.) was diluted in 10 mL of toluene. This solution was cooled to 0°C and then a solution of 1-azidoadamantane (210 mg, 1.19 mmol, 1 equiv.) in 5 mL of toluene was added. The reaction mixture was left to warm up to room temperature, and then the mixture was heated for 24h at 120 °C. All volatiles were removed *in vacuo* and the remaining solid diluted in 3 mL of hexane and filtered using a P3-Frit with added Celite. The filtrate was placed at –30 °C and crystal suitable for single crystal X-ray diffraction analysis were obtained after one month. Since single-crystal analysis confirmed the crystals to be the undesired product **12** no further characterization was performed.

4.6.3 Synthesis of ion pairs.

4.6.3.1 Synthesis of compound 5[B(C$_6$F$_5$)$_4$]

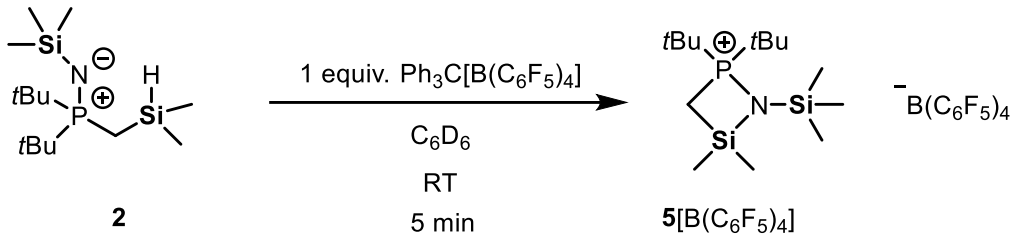

First tritylium tetrakis(pentafluorophenyl)borate (603 mg, 0.654 mmol, 1 equiv) was dissolved in 0.6 mL of C_6D_6 in a J-Young type NMR tube. To this compound **2** (200 mg, 0.654 mmol, 1 equiv) dissolved in 0.2 mL of C_6D_6 was added. The deep yellow color of the solution immediately faded and a slightly yellow solution with two layers was obtained. The upper C_6D_6 layer was carefully decanted, while the lower layer was washed twice with 0.1 mL of C_6D_6. The resulting slightly yellow oil was dried *in vacuo* and dissolved in 0.6 mL CD_2Cl_2 and subsequently subjected to NMR measurements. No yield could be determined.

^{1}H NMR (400.13 MHz, CD_2Cl_2, 298 K): δ 1.87 (d, $^2J_{P–H}$ = 10.3 Hz, 2H, PC*H*$_2$Si), 1.45 {d, $^3J_{P–C}$ = 16.7 Hz, 18H, NP[C(C*H*$_3$)$_3$]$_2$}, 0.70 [s, 6H, Si(C*H*$_3$)$_2$], 0.39 [s, 9H, Si(CH$_3$)$_3$].

^{31}P{^{1}H} NMR (162.04 MHz, CD_2Cl_2, 298 K): δ 89.2 (*P*NSi)

^{19}F{^{1}H} NMR (376.66 MHz, CD_2Cl_2, 298 K): δ –132.5 (m, 8F, C$_{Ar}$*F*), –163.3 (m, 4F, C$_{Ar}$*F*), –167.1 (m, 8F, C$_{Ar}$*F*).

^{11}B{^{1}H} NMR (128.43 MHz, CD_2Cl_2, 298 K): δ –16.7 (*B*$_{Ar}^F$)

^{29}Si{^{1}H} NMR (79.49 MHz, CD_2Cl_2, 298 K): δ 15.3 (s, PCH$_2$*Si*), 6.3 (s, PN*Si*).

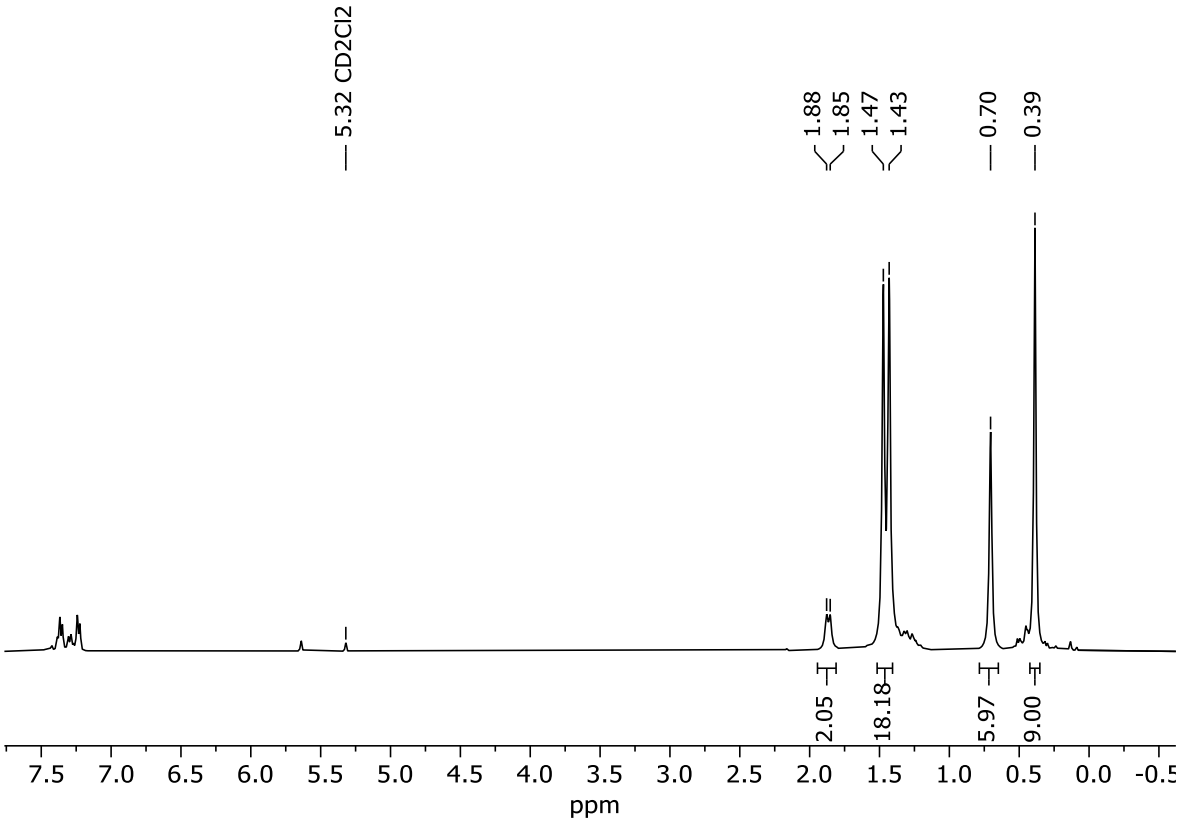

Figure S23: ^{1}H NMR (400.13 MHz, CD_2Cl_2, 298 K) spectrum of **5**[$B(C_6F_5)_4$].

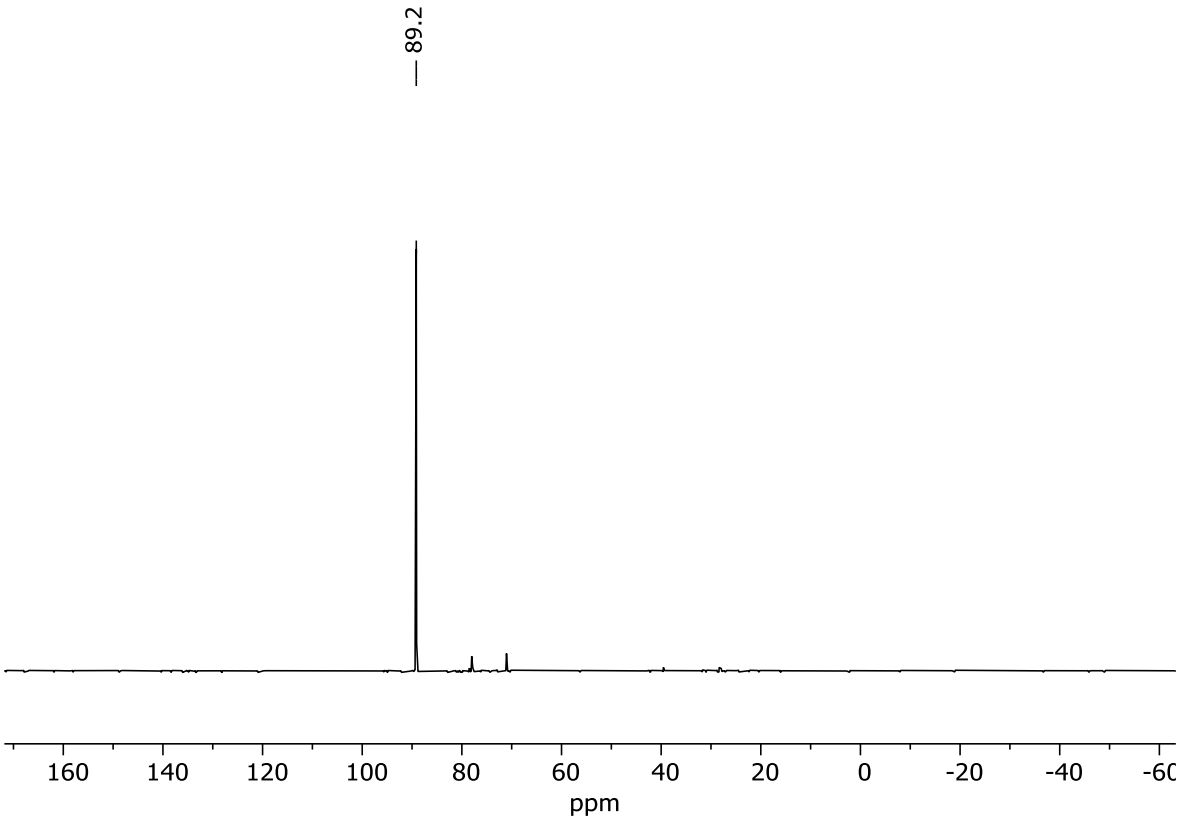

Figure S24: $^{31}P\{^{1}H\}$ NMR (162.04 MHz, CD_2Cl_2, 298 K) of compound **5**[$B(C_6F_5)_4$].

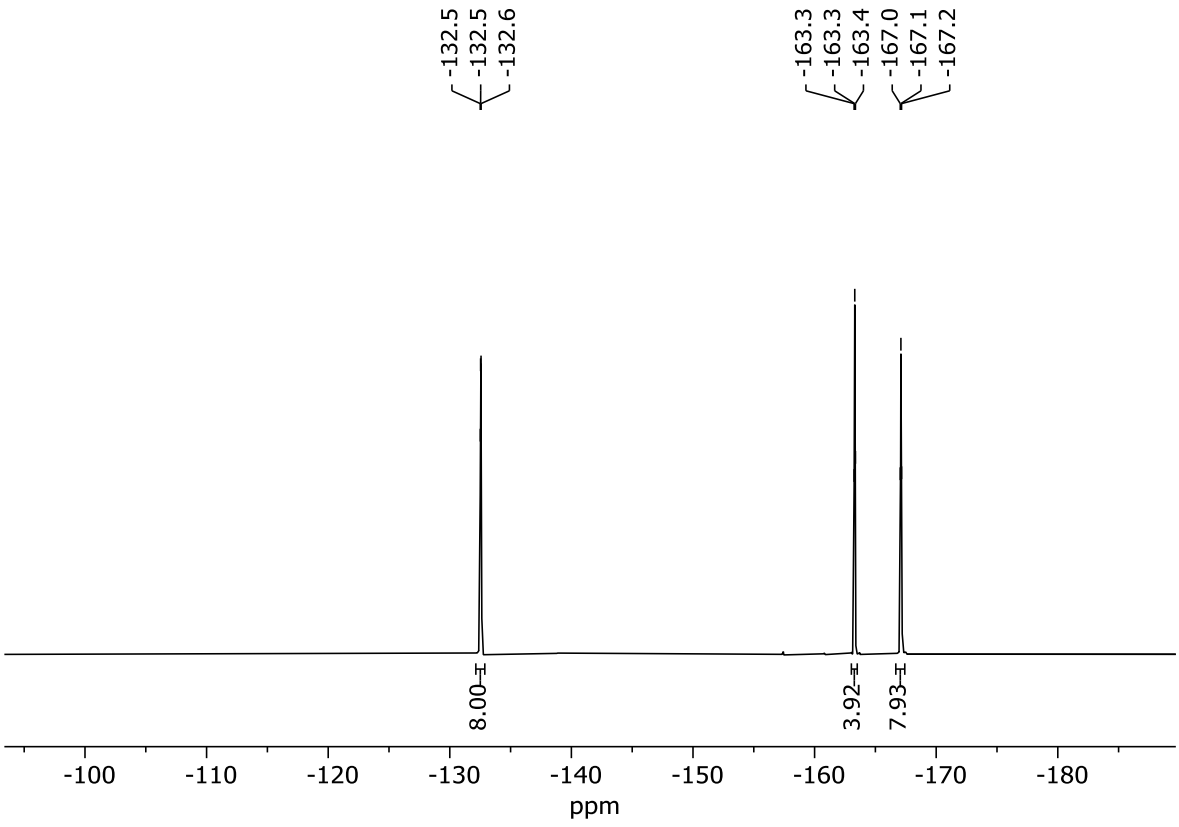

Figure S25: $^{19}F\{^{1}H\}$ NMR (376.66 MHz, CD_2Cl_2, 298 K) of compound **5**[$B(_6F_5)_4$].

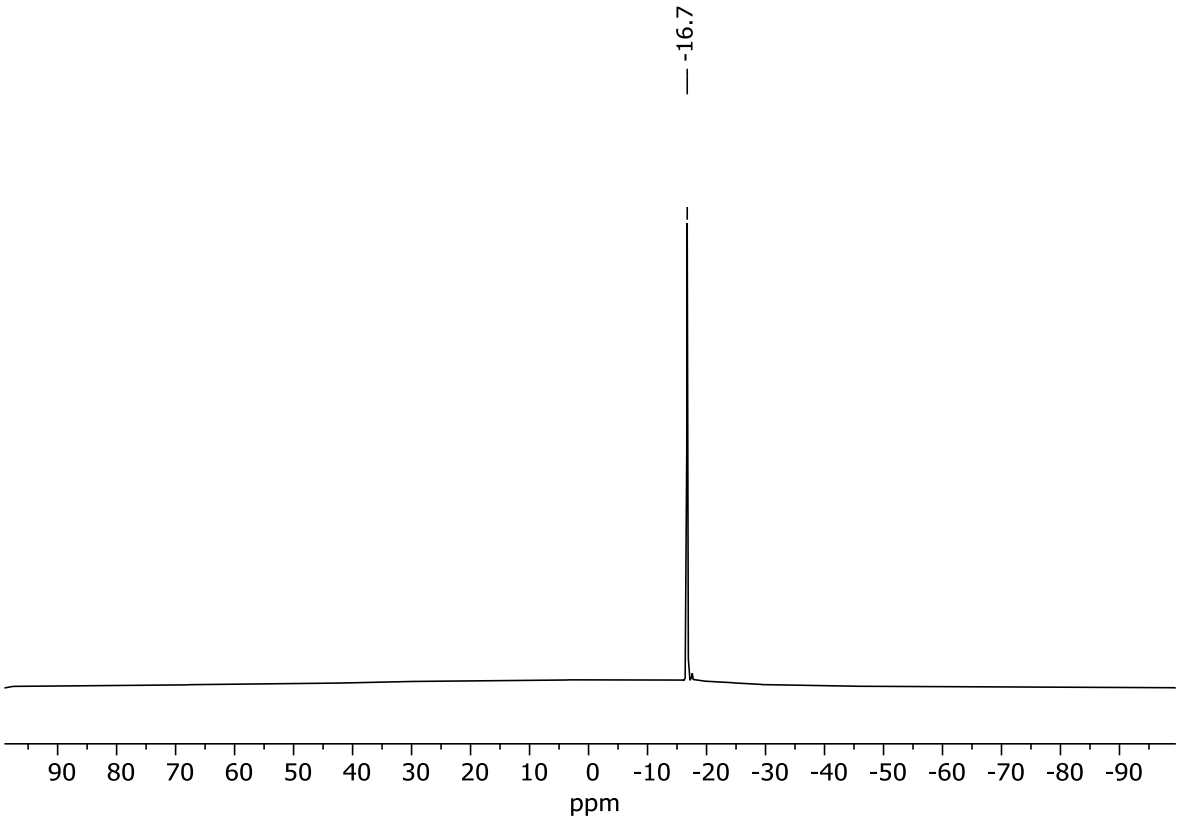

Figure S26: $^{11}B\{^{1}H\}$ NMR (128.43 MHz, CD_2Cl_2, 298 K) of compound **5**[$B(_6F_5)_4$].

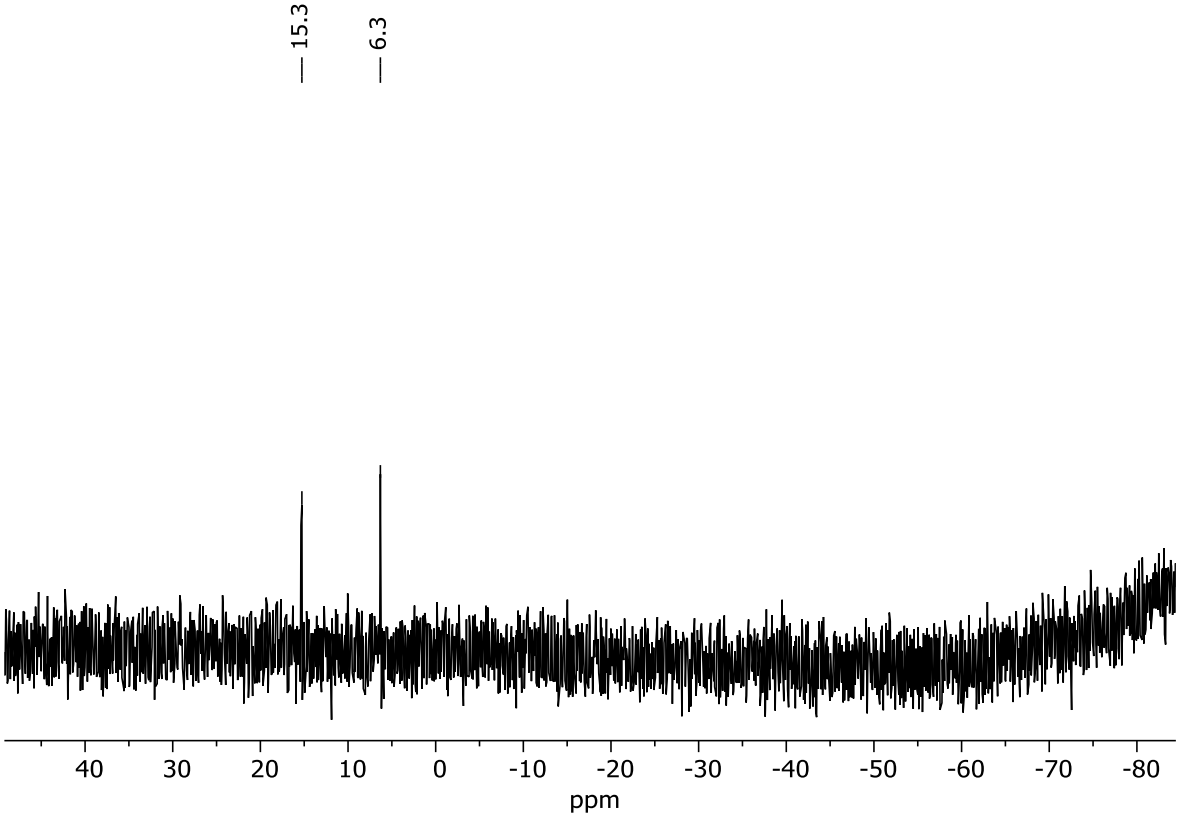

Figure S27: $^{29}Si\{^{1}H\}$ NMR (79.49 MHz, CD_2Cl_2, 298 K) of compound **5**[$B(_6F_5)_4$].

4.6.3.2 Synthesis of compound 6[B(C$_6$F$_5$)$_4$].

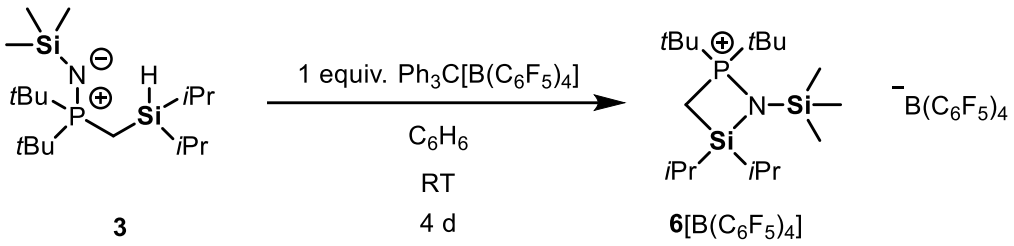

In a Glovebox a dry Schlenk flask was charged with compound **3** (388 mg, 1.07 mmol, 1 equiv) and tritylium tetrakis(pentafluorophenyl)borate (989 mg, 1.07 mmol, 1 equiv). Then 8 mL of benzene were added, and the mixture stirred for 4d at room temperature. Afterwards two layers formed. The upper layer was decanted, and the lower layer washed twice with 3 mL of benzene. The lower oily layer was dried *in vacuo* and the resulting foam dissolved in 6 mL of Et_2O. The resulting solution was crystallized at –30°C. The product was isolated via filtration, washed twice with 4 mL of Et_2O and dried *in vacuo*. Compound **6**[B(C$_6$F$_5$)$_4$] was obtained as colorless crystals suitable of single-crystal X-ray diffraction analysis. Yield: 162 mg (0.155 mmol, 14%).

^{1}H NMR (400.13 MHz, CD_2Cl_2, 298 K): δ 1.85 (d, $^2J_{P–H}$ = 10.8 Hz, 2H, SiC*H*$_2$P), 1.48 {d, $^3J_{P–H}$ = 16.7 Hz, 20H, P[C(C*H*$_3$)$_3$]$_2$ + Si[CH(C*H*$_3$)$_2$]$_2$}, 1.23 {d, $^3J_{H–H}$ = 15.4 Hz, 6H, Si[C*H*(CH$_3$)$_2$]$_2$}, 1.21 {d, $^3J_{H–H}$ = 15.7 Hz, 6H, Si[CH(C*H*$_3$)$_2$]$_2$}, 0.40 [s, 9H, Si(C*H*$_3$)$_3$].

^{13}C{^{1}H} NMR (100.61 MHz, CD_2Cl_2, 298 K): δ 39.2 {d, $^1J_{P–C}$ = 34.1 Hz, P[*C*(CH$_3$)$_3$]$_2$}, 27.6 {d, $^2J_{P–C}$ = 2.2 Hz, P[C(*C*H$_3$)$_3$]$_2$}, 18.4 [s, SiCH(*C*H$_3$)$_2$], 17.4 [s, SiCH(*C*H$_3$)$_2$], 16.6 [s, Si-*C*H(CH$_3$)$_2$], 4.8 (d, $^1J_{P–C}$ = 36.0, Si*C*H$_2$P), 3.1 [d, $^3J_{P–C}$ = 2.0 Hz, Si(*C*H$_3$)$_3$].

^{31}P{^{1}H} NMR (162.04 MHz, CD_2Cl_2, 298 K): δ 90.1 [s, P(N)Si(CH$_3$)$_3$].

^{19}F{^{1}H} NMR (376.66 MHz, CD_2Cl_2, 298 K): δ –133.0 (m, 8F, C*F*$_{Ar}$), –163.7 (m, 4F, C*F*$_{Ar}$), –167.5 (m, 8F, C*F*$_{Ar}$).

^{11}B{^{1}H} NMR (128.43 MHz, CD_2Cl_2, 298 K): δ –16.9 (s, *B*$_{Ar}^F$).

^{29}Si{^{1}H} NMR (79.49 MHz, CD_2Cl_2, 298 K): δ 27.8 (d, $^2J_{P–Si}$ = 20.4 Hz, PCH$_2$*Si*), 8.0 [s, *Si*(CH$_3$)$_3$].

CHN Analysis: Calcd for $C_{42}H_{43}BF_{20}NPSi_2$: C, 48.52; H, 4.17; N, 1.35. Found: C, 48.60; H, 4.22; N, 1.22.

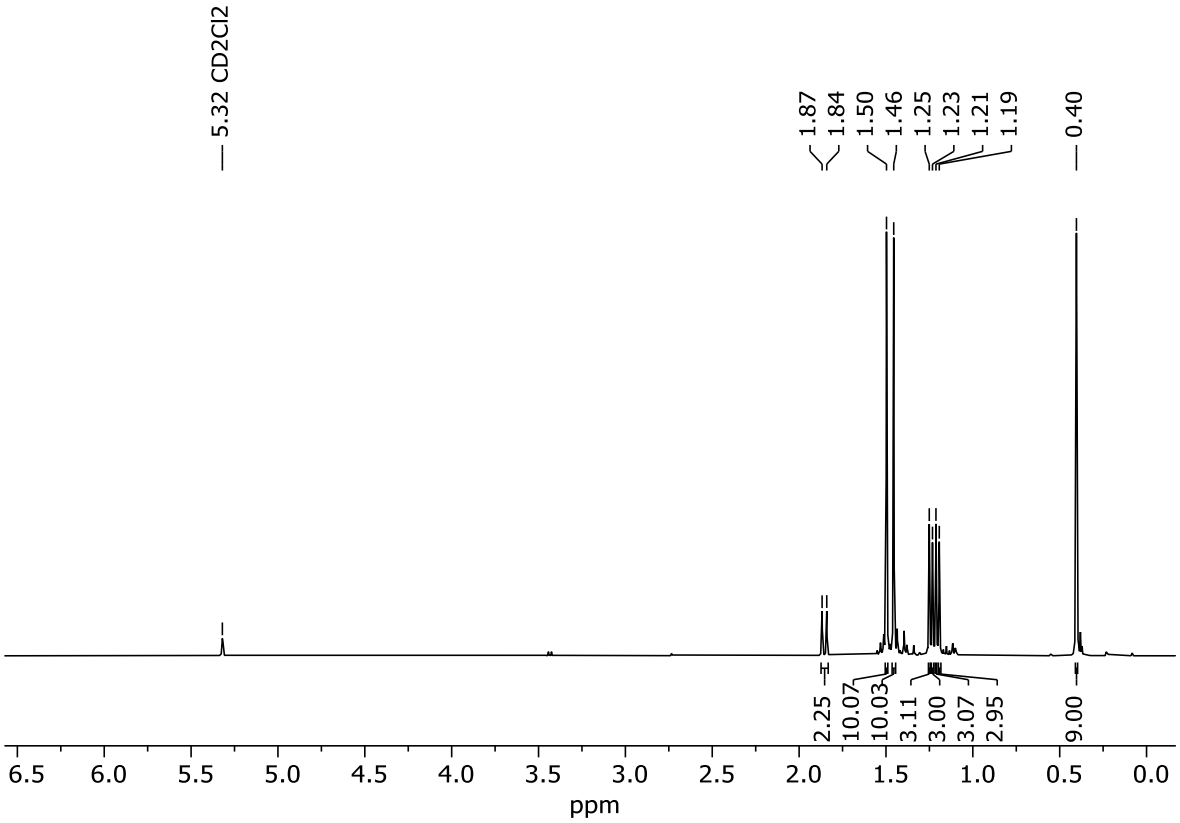

Figure S28: ^{1}H NMR (400.13 MHz, CD_2Cl_2, 298 K) spectrum of compound **6**[$B(C_6F_5)_4$].

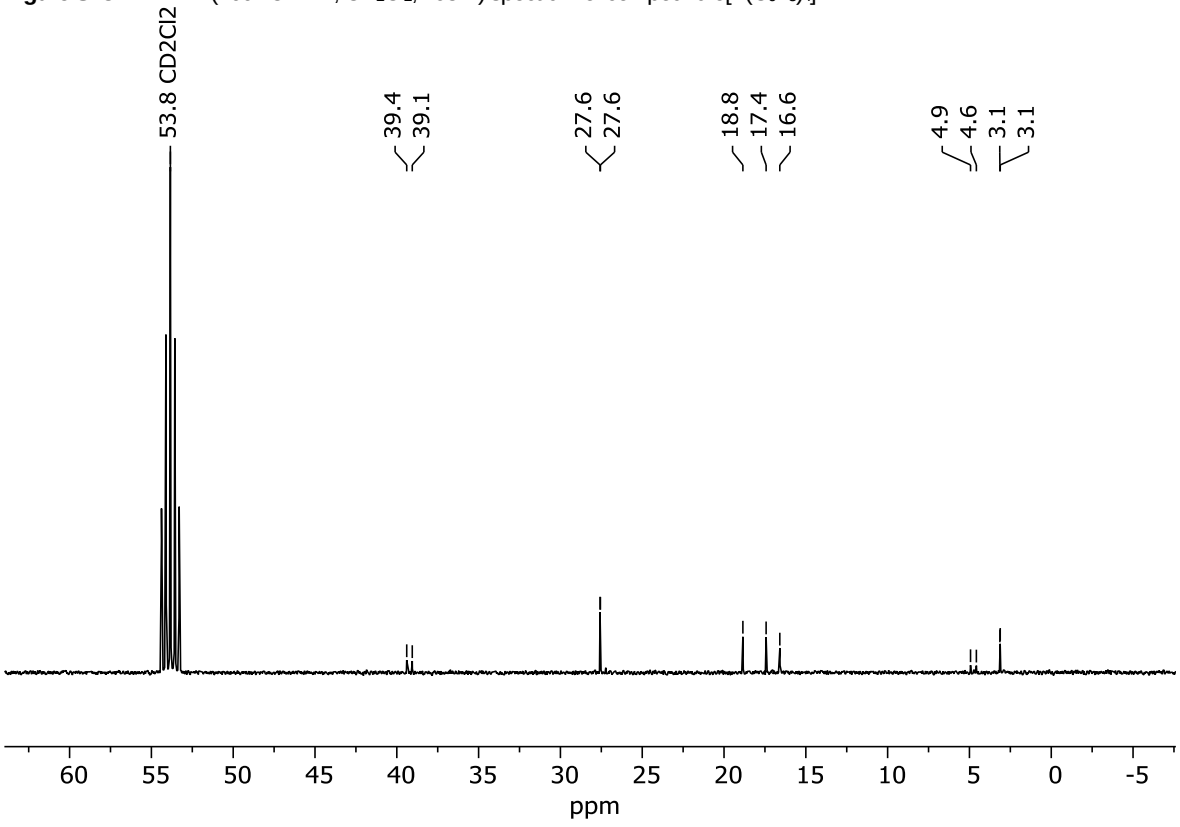

Figure S29: $^{13}C\{^{1}H\}$ NMR (100.61 MHz, CD_2Cl_2, 298 K) of compound **6**[$B(C_6F_5)_4$].

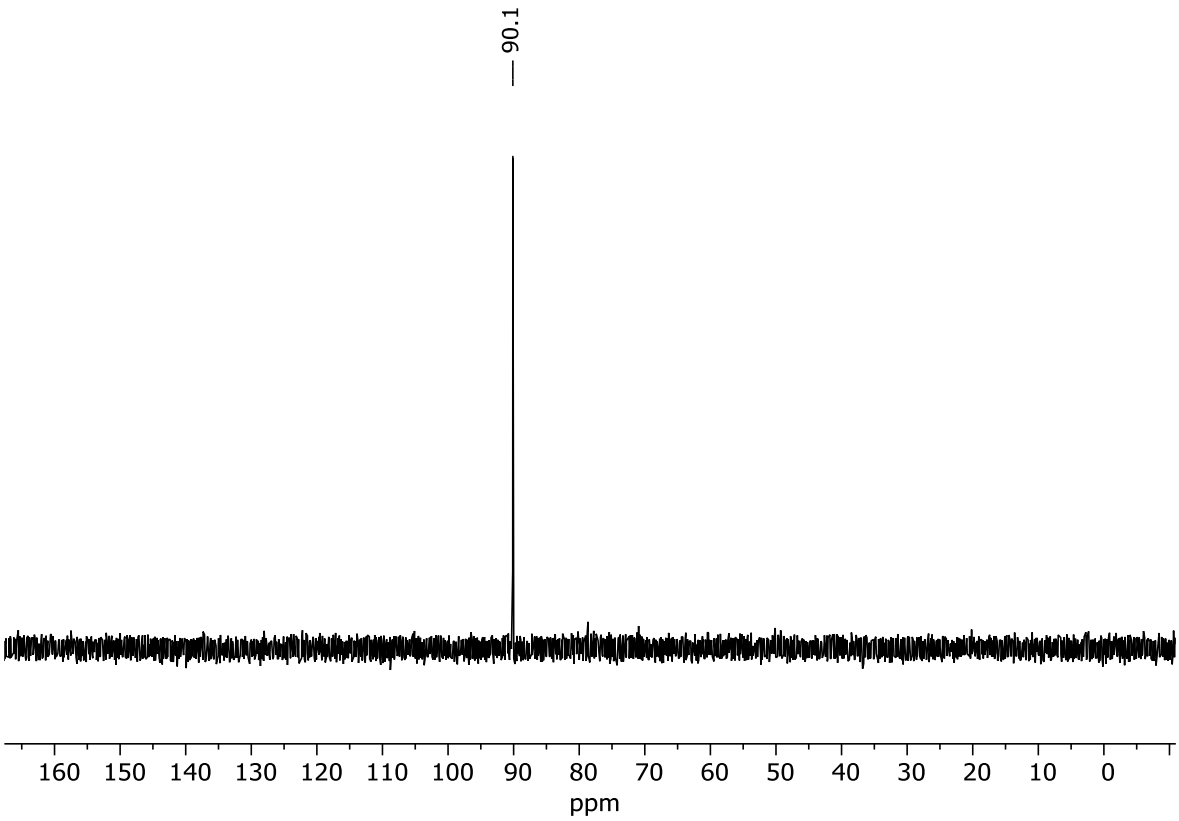

Figure S30: $^{31}P\{^{1}H\}$ NMR (162.04 MHz, CD_2Cl_2, 298 K) of compound **6**[$B(C_6F_5)_4$].

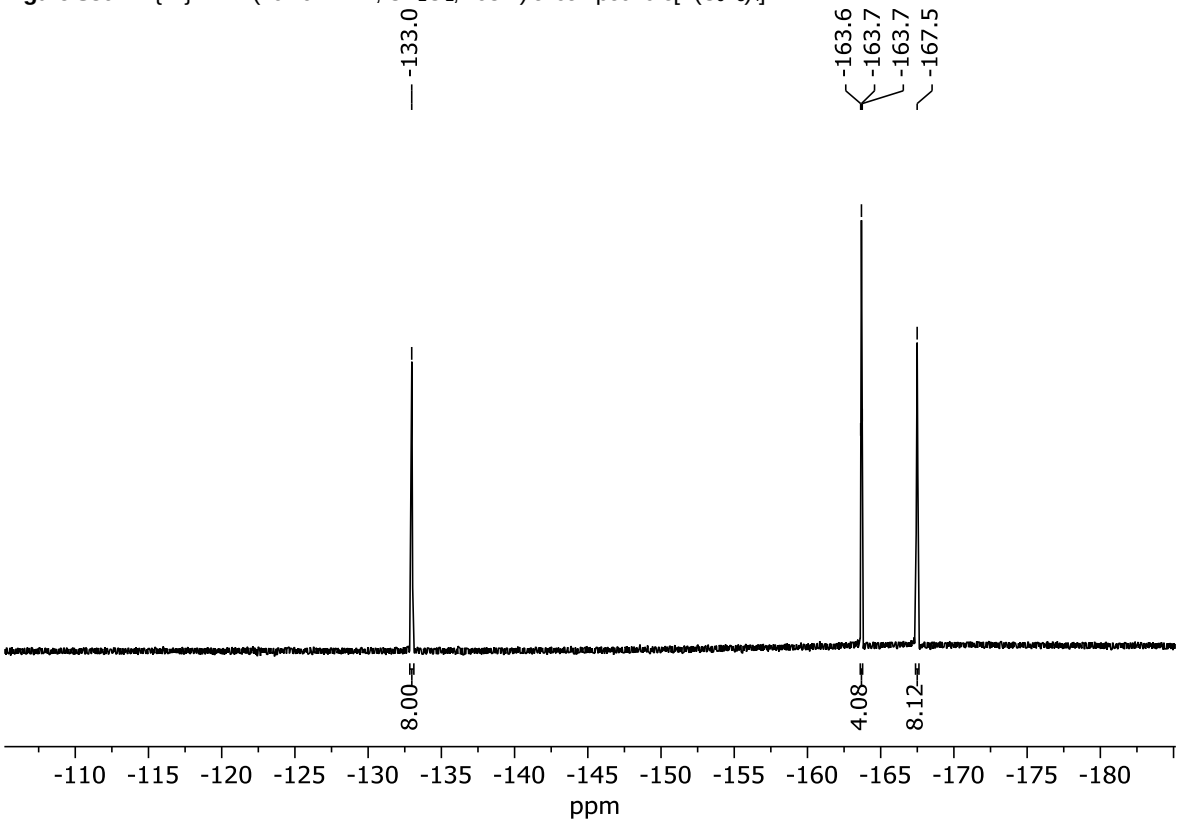

Figure S31: $^{19}F\{^{1}H\}$ NMR (376.66 MHz, CD_2Cl_2, 298 K) of compound **6**[$B(_6F_5)_4$].

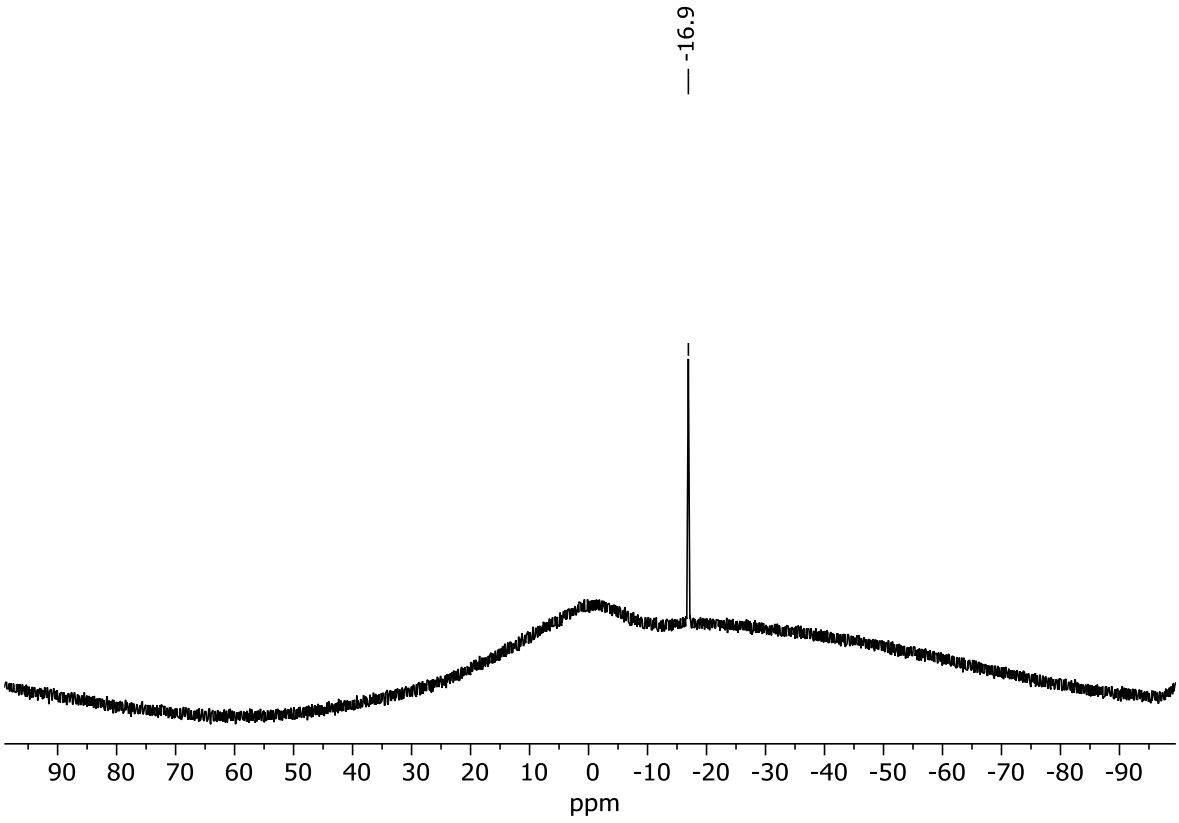

Figure S32: $^{11}B\{^{1}H\}$ NMR (128.43 MHz, CD_2Cl_2, 298 K) of compound **6**[$B(_6F_5)_4$].

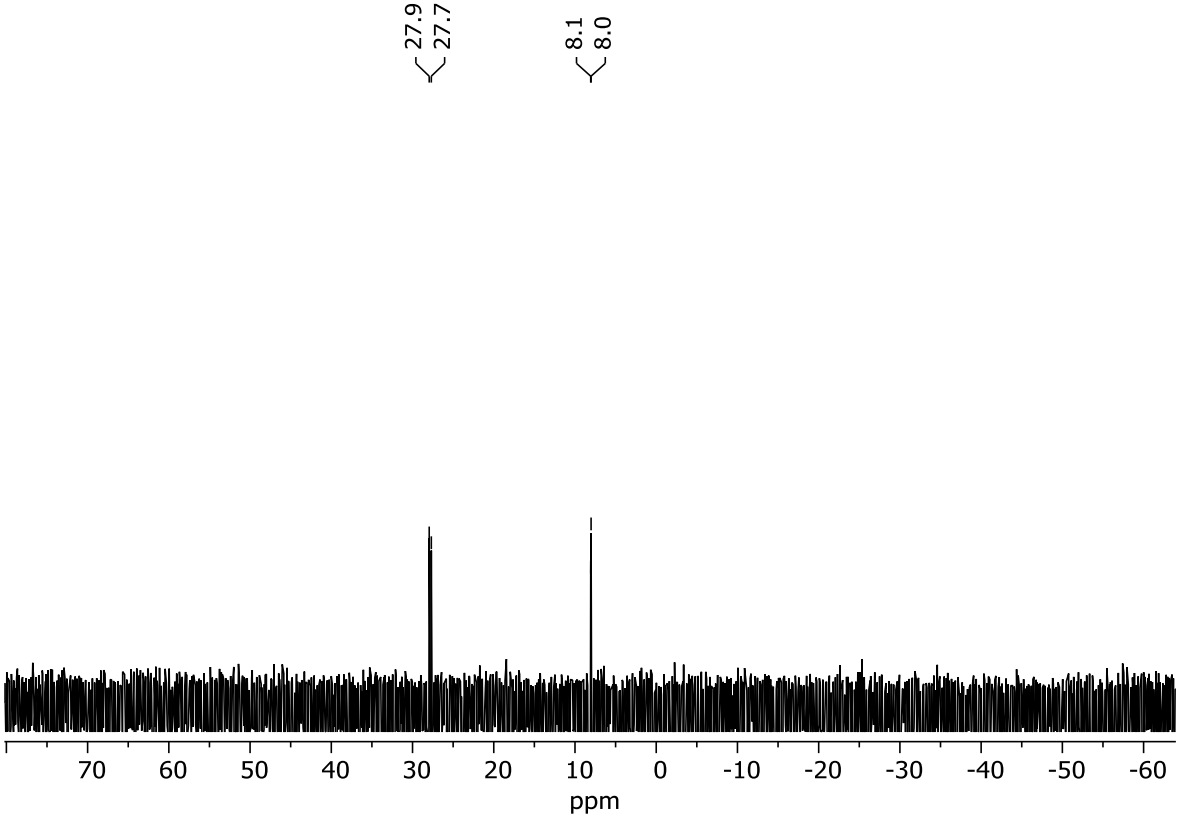

Figure S33: $^{29}Si\{^{1}H\}$ NMR (79.49 MHz, CD_2Cl_2, 298 K) of compound **6**[$B(_6F_5)_4$].

4.6.3.3 Synthesis of compound 7[B(C$_6$F$_5$)$_4$]

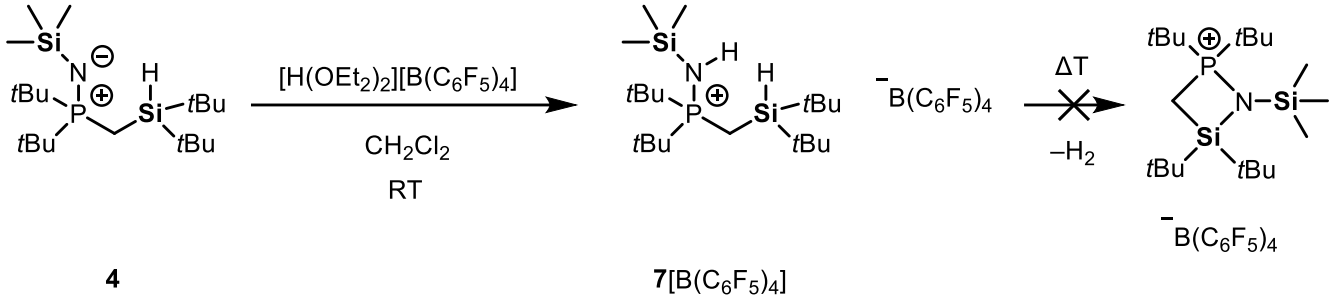

4 **7**[B(C$_6$F$_5$)$_4$]

A Schlenk flask was charged with compound **4** (235 mg, 0.603 mmol, 1 equiv) and [H(OEt$_2$)$_2$][B(C$_6$F$_5$)$_4$][4] (500 mg, 0.603 mmol, 1 equiv). Both solids were dissolved in 5 mL of CH_2Cl_2 and stirred for 24 h at room temperature. Afterwards the reaction mixture was filtered using a Teflon cannula and the solvent of the filtrate removed *in vacuo*. The resulting slightly yellow oil was washed twice with 5 mL of hexane which resulted in the formation of a white powder. The powder was dried *in vacuo* and while still being *in vacuo* heated slowly until the solid started to melt. The mixture was left molten for approximately one hour. Afterwards the melt was allowed to cool which resulted in the formation of a black oil. A ^{1}H-NMR of this black oil was made, which showed decomposition had occurred. This black oil was dissolved in 5 mL of hexane and left to crystallize at –30 °C. After several months compound **7**[B(C$_6$F$_5$)$_4$] was obtained as small crystals which were suitable for single-crystal X-ray diffraction analysis. Due to the small amount obtained no full characterization was possible.

4.6.3.4 Synthesis of compound 9.

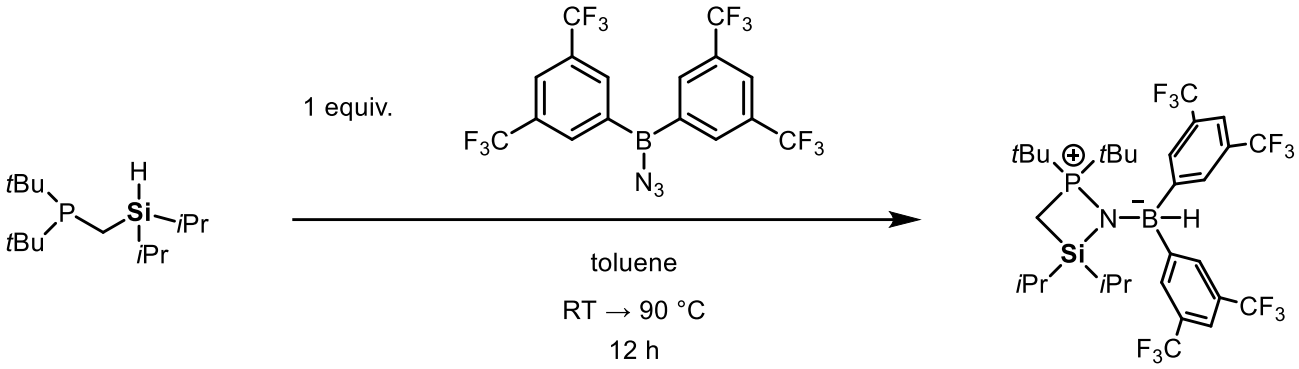

8 **9**

First bis(3,5-trifluoromethylphenyl)borane azide (500 mg, 1.04 mmol, 1 equiv) was dissolved in 30 mL of toluene. Then strong stirring was activated. Next compound **8** (286 mg, 1.04 mmol, 1 equiv) was steadily added. Strong gas evolution was observed during addition. The reaction mixture was left to stir for 12 h with open overpressure at room temperature. Afterwards the reaction mixture was heated to 90°C for 12 h. All volatiles were removed *in vacuo* and the yellow residue was dissolved in 5 mL of Et_2O. The solution was crystallized at –30°C. The crystals were isolated via filtration and dried *in vacuo*. Compound **9** was obtained as colorless crystals suitable for single-crystal X-ray diffraction analysis. Yield: 94.5 mg (0.13 mmol, 12%). **Note**: It was found that the outcome of this reaction is highly dependent on the purity of the starting materials.

^{1}H NMR (400.13 MHz, C_6D_6, 298 K): δ 8.20 (s, 4H, CH_{ortho}), 7.75 (s, 2H, CH_{para}), 3.80 (bd, $^{1}J_{B–H}$ = 117.6 Hz, 1H, B*H*), 1.20 {hept, $^{3}J_{H–H}$ = 7.6 Hz, 2H, Si[C*H*$(CH_3)_2]_2$}, 0.87 {d, $^{3}J_{P–H}$ = 15.2 Hz, 18H, NP[C(C$H_3)_3]_2$}, 0.86 [d, $^{3}J_{H–H}$ = 7.4 Hz, 6H, SiCH(C$H_3)_2$], 0.75 (d, $^{2}J_{P–H}$ = 10.6 Hz, 2H, PCH_2SiH), 0.70 [d, $^{3}J_{H–H}$ = 7.7 Hz, 6H, SiCH(C$H_3)_2$].

^{13}C{^{1}H} NMR (100.61 MHz, C_6D_6, 298 K): δ 134.8 (bm, C_{ipso}), 130.2 (q, $^{1}J_{C–F}$ = 31.6 Hz, CF_3), 128.2 (s, C_{para}), 128.0 (s, C_{ortho}), 119.1 (m, C_{meta}), 38.5 [d, $^{1}J_{P–C}$ = 37.2 Hz, P[$C(CH_3)]_2$}, 27.4 {d, $^{2}J_{P–C}$ = 1.3 Hz, P[C($CH_3)]_2$}, 18.8 [s, SiCH($CH_3)_2$], 17.6 [d, $^{3}J_{P–C}$ = 1.7 Hz, Si$CH(CH_3)_2$], 17.3 [s, SiCH($CH_3)_2$], 4.2 [d, $^{1}J_{P–C}$ = 33.7 Hz, P(N)CH_2Si].

^{31}P{^{1}H} NMR (162.04 MHz, C_6D_6, 298 K): δ 79.1 (SiN*P*).

^{19}F{^{1}H} NMR (376.66 MHz, C_6D_6, 298 K): δ –62.4 (s, CF_3).

^{11}B{^{1}H} NMR (128.43 MHz, C_6D_6, 298 K): δ –6.7 (bs, *B*H).

^{29}Si{^{1}H} NMR (79.49 MHz, C_6D_6, 298 K): δ 21.6 (d, $^{2}J_{P–Si}$ = 20.3 Hz, PCH_2*Si*).

CHN Analysis: Calcd for $C_{31}H_{41}BF_{12}NPSi$: C, 51.32; H, 5.70; N, 1.93. Found: C, 51.38; H, 5.75; N, 1.93.

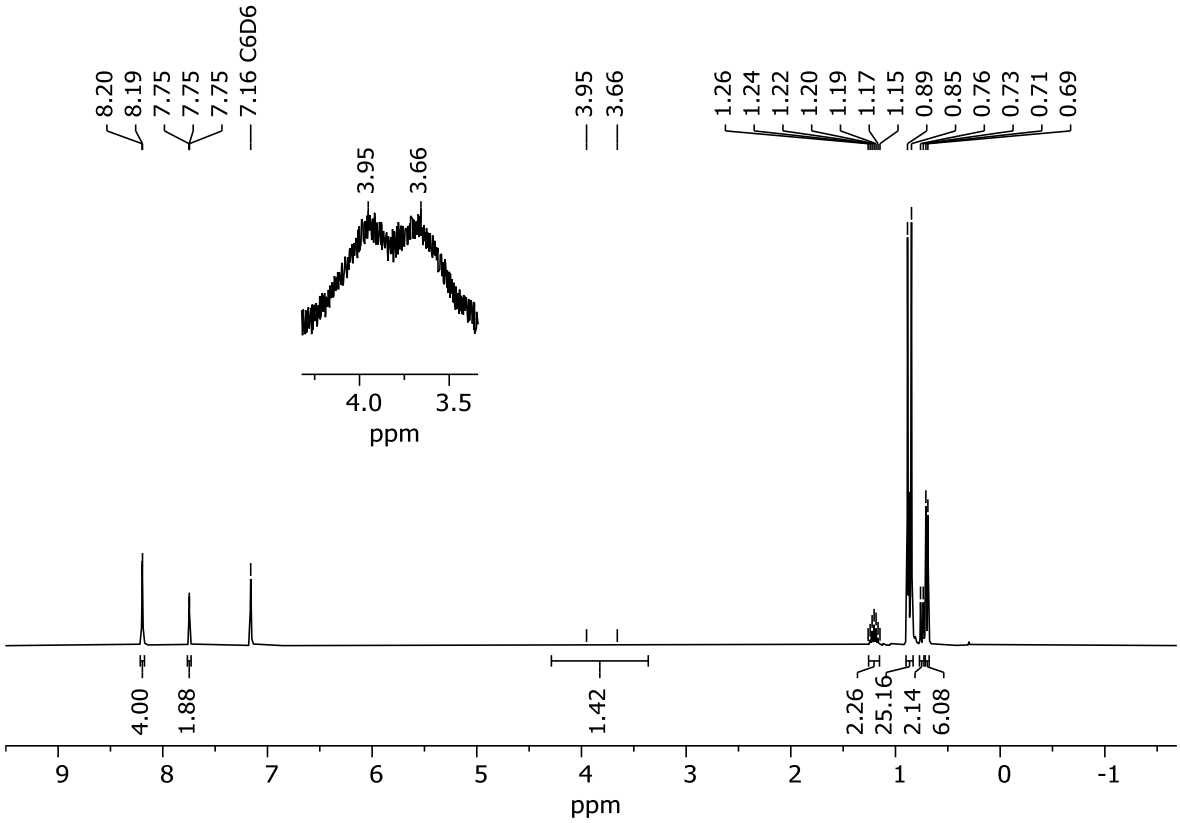

Figure S34: ^{1}H NMR (400.13 MHz, CD_2Cl_2, 298 K) spectrum of compound **9**.

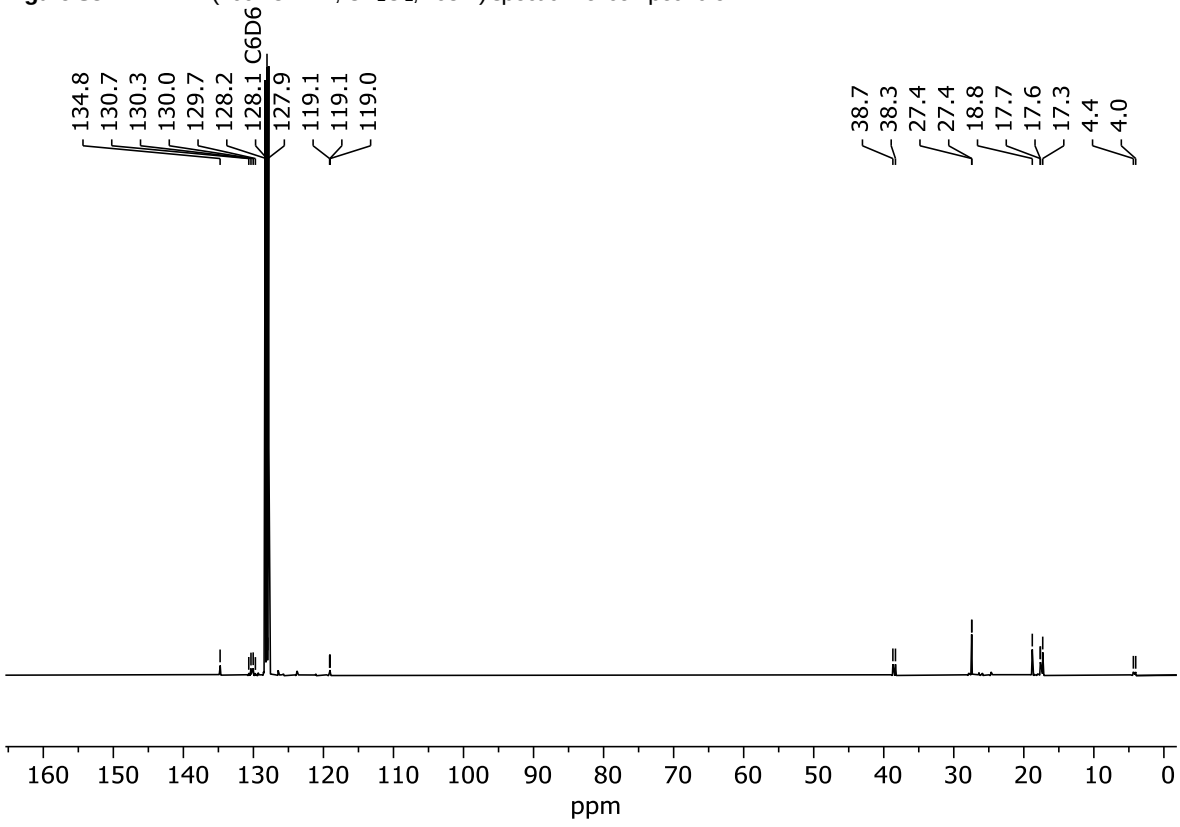

Figure S35: $^{13}C\{^{1}H\}$ NMR (100.61 MHz, CD_2Cl_2, 298 K) of compound **9**.

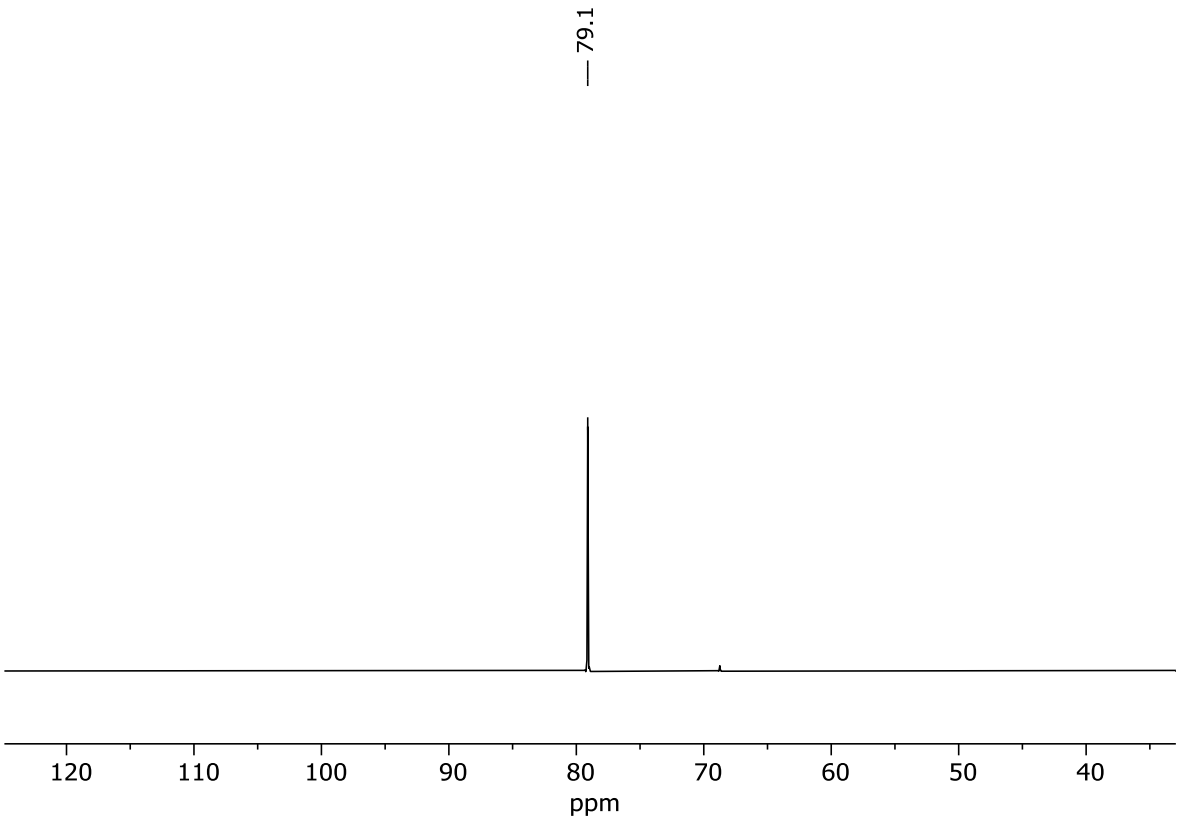

Figure S36: $^{31}P\{^{1}H\}$ NMR (162.04 MHz, CD_2Cl_2, 298 K) of compound **9**.

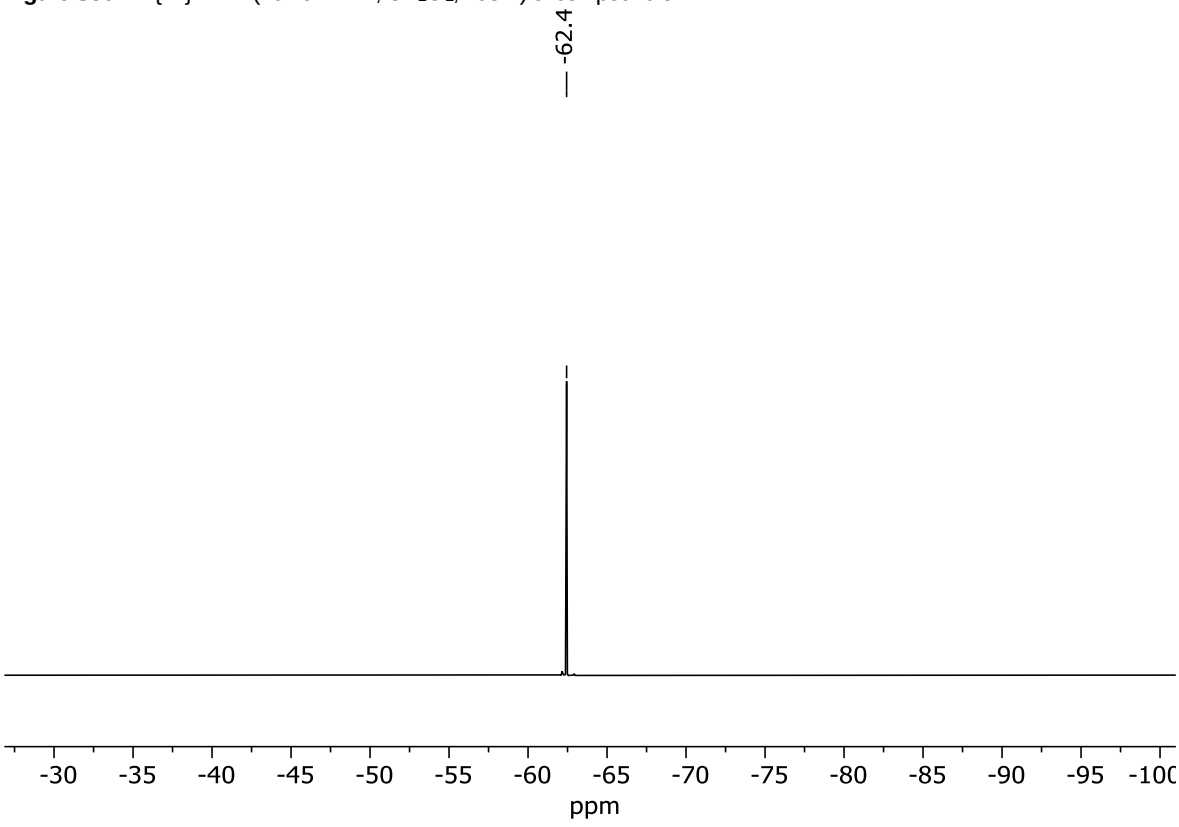

Figure S37: $^{19}F\{^{1}H\}$ NMR (376.66 MHz, CD_2Cl_2, 298 K) of compound **9**.

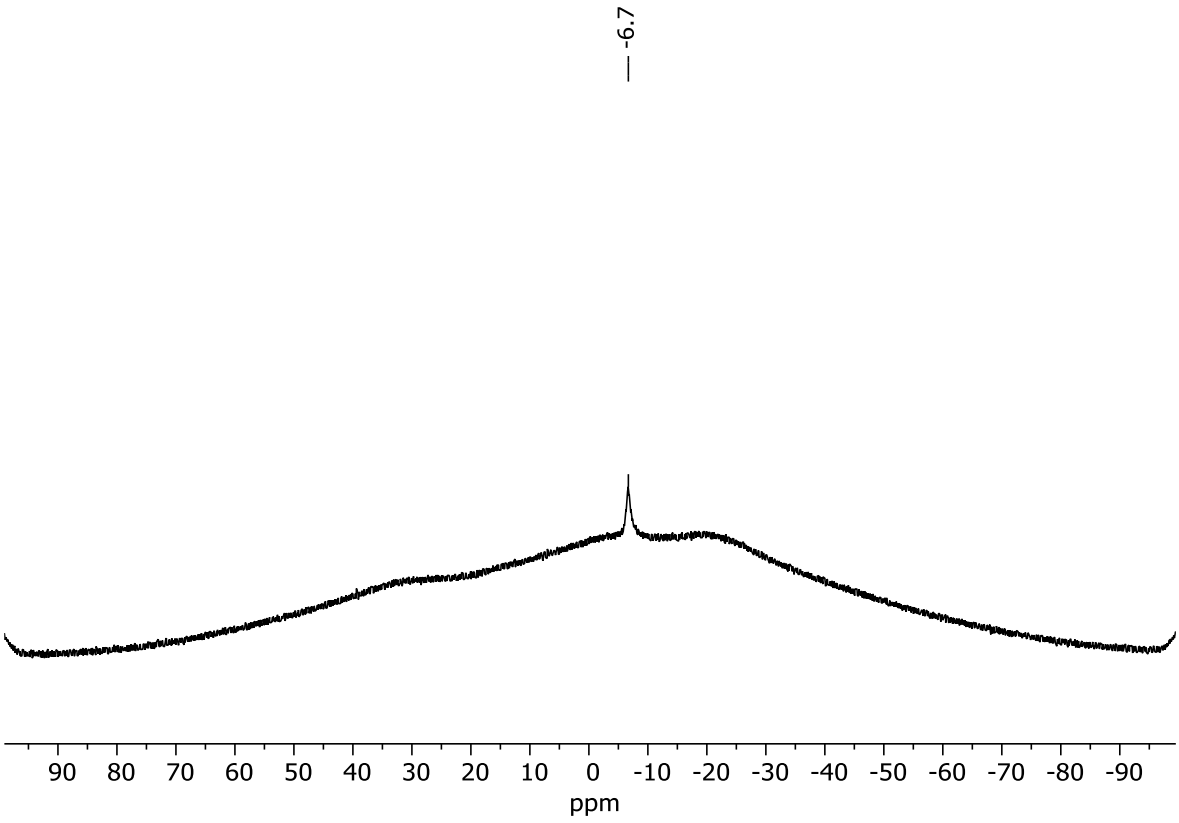

Figure S38: $^{11}B\{^{1}H\}$ NMR (128.43 MHz, CD_2Cl_2, 298 K) of compound **9**.

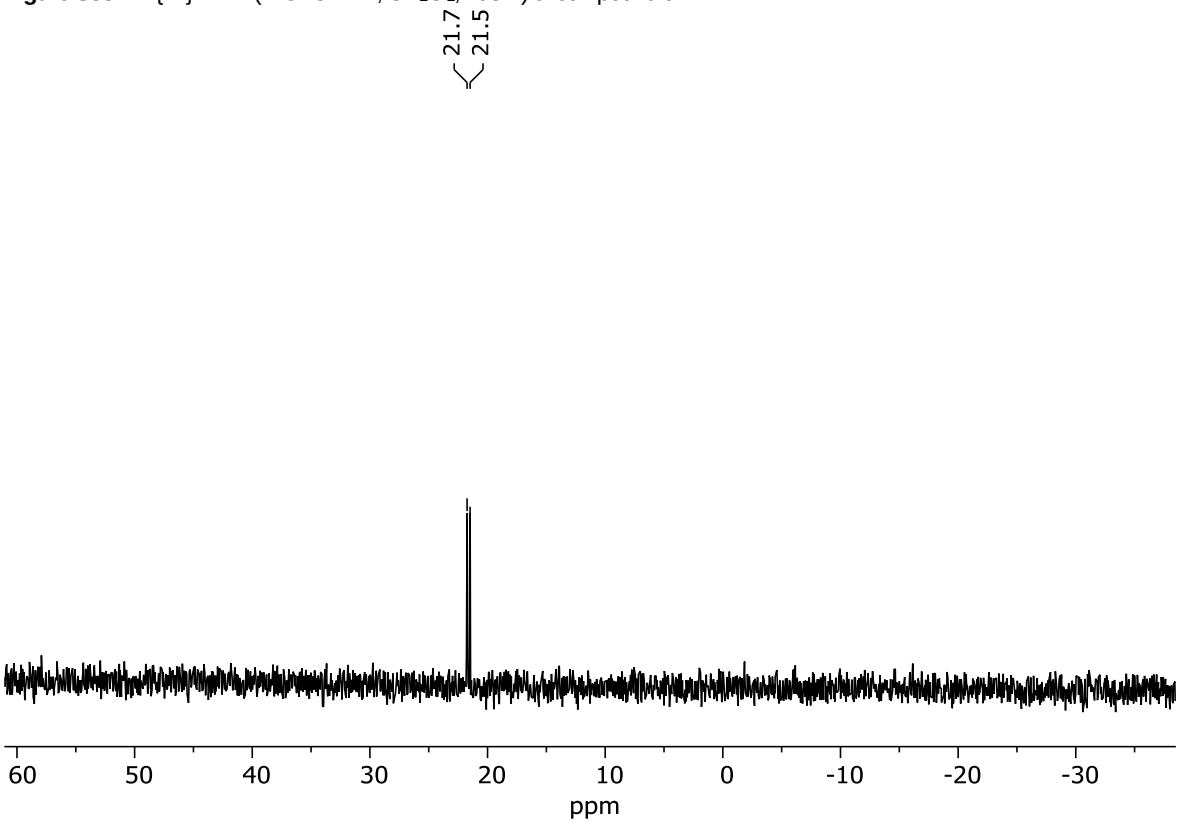

Figure S39: $^{29}Si\{^{1}H\}$ NMR (79.49 MHz, CD_2Cl_2, 298 K) of compound **9**.

4.6.3.5 Synthesis of compound 11[B(C$_6$F$_5$)$_4$].

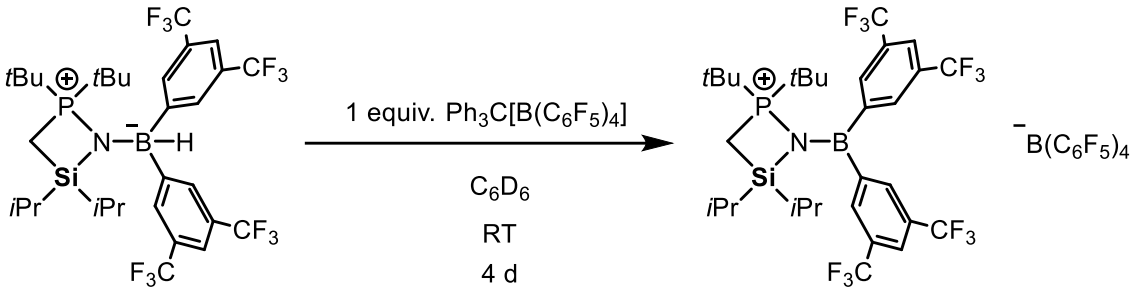

9 **11**[B(C$_6$F$_5$)$_4$]

In a Glovebox compound **9** (25.5 mg, 0.035 mmol, 1 equiv) was dissolved in 0.4 mL of C_6D_6 and transferred to a J-Young type NMR tube. Next tritylium tetrakis(pentafluorophenyl)borate (32.4 mg, 0.035 mmol, 1 equiv) was dissolved in 0.3 mL of C_6D_6 and added to the J-Young tube aswell. The NMR tube was tightly closed and stirred for 4 d at room temperature. Afterwards the mixture was completely discolored, and two layers had formed. The upper layer was decanted off using a teflon cannula and the lower layer was washed once with 0.3 mL of C_6D_6. Next all volatiles were removed *in vacuo* and the resulting oil dissolved in 0.6 mL of CD_2Cl_2 and the sample subjected for multinuclear NMR measurements. Compound **11**[B(C$_6$F$_5$)$_4$] was obtained as a slightly yellow oil. Yield: 46.2 mg (0.033 mmol, 93%).

^{1}H NMR (400.13 MHz, CD_2Cl_2, 298 K): δ 8.10 (s, 2H, C*H*$_{para}$), 7.84 (s, 4H, C*H*$_{ortho}$), 2.05 (d, $^2J_{P-H}$ = 10.8 Hz, 2H, PC*H*$_2$SiH), 1.53–1.46 {m, 2H, Si[C*H*(CH$_3$)$_2$]$_2$}, 1.39 {d, $^3J_{P-H}$ = 17.4 Hz, 18H, NP[C(C*H*$_3$)$_3$]$_2$}, 1.23 [d, $^3J_{H-H}$ = 7.7 Hz, 6H, SiCH(C*H*$_3$)$_2$], , 0.74 [d, $^3J_{H-H}$ = 7.4 Hz, 6H, SiCH(C*H*$_3$)$_2$].

^{13}C{^{1}H} NMR (100.61 MHz, CD_2Cl_2, 298 K): δ 148.6 (d, $^1J_{C-F}$ = 240.5 Hz, *C*$_{Ar}^F$), 141.9 (s, *C*$_{ipso}$), 138.6 (d, $^1J_{C-F}$ = 245.4 Hz, *C*$_{Ar}^F$), 136.7 (d, $^1J_{C-F}$ = 244.9 Hz, *C*$_{Ar}^F$), 132.5 (q, $^2J_{C-F}$ = 33.8 Hz, *C*$_{meta}$), 131.6 (s, *C*$_{ortho}$), 125.8 (s, *C*$_{para}$),123.2 (q, $^2J_{C-F}$ = 273.3 Hz, *C*F$_3$), 39.6 [d, $^1J_{P-C}$ = 28.0 Hz, P[*C*(CH$_3$)]$_2$}, 27.0 {s, P[C(*C*H$_3$)]$_2$}, 17.8 [s, SiCH(*C*H$_3$)$_2$], 17.6 [s, Si*C*H(CH$_3$)$_2$], 16.9 [s, SiCH(*C*H$_3$)$_2$], 4.2 [d, $^1J_{P-C}$ = 36.5 Hz, P(N)*C*H$_2$Si].

^{31}P{^{1}H} NMR (162.04 MHz, CD_2Cl_2, 298 K): δ 96.9 (SiN*P*).

^{19}F{^{1}H} NMR (376.66 MHz, CD_2Cl_2, 298 K): δ –63.5 (s, 6F, C*F*$_3$), –133.0 (m, 8F, C$_{Ar}$*F*), –163.5 (m, 4F, C$_{Ar}$*F*), –167.4 (m, 8F, C$_{Ar}$*F*).

^{11}B{^{1}H} NMR (128.43 MHz, CD_2Cl_2, 298 K): δ –16.9 (s, *B*$_{Ar}^F$).

^{29}Si{^{1}H} NMR (79.49 MHz, CD_2Cl_2, 298 K): δ 31.8 (d, $^2J_{P-Si}$ = 15.7 Hz, PCH$_2$*Si*).

+ESI-MS: Calcd *m/z* for $C_{31}H_{40}BF_{12}NPSi$ $[M]^+$: 724.2564. Found: 288.2269 $[MH–C_{16}H_6BF_{12}]^+$.

-ESI-MS: Calcd *m/z* for $C_{24}BF_{20}[M]^-$: 678.9779. Found: 678.9830 $[M]^-$.

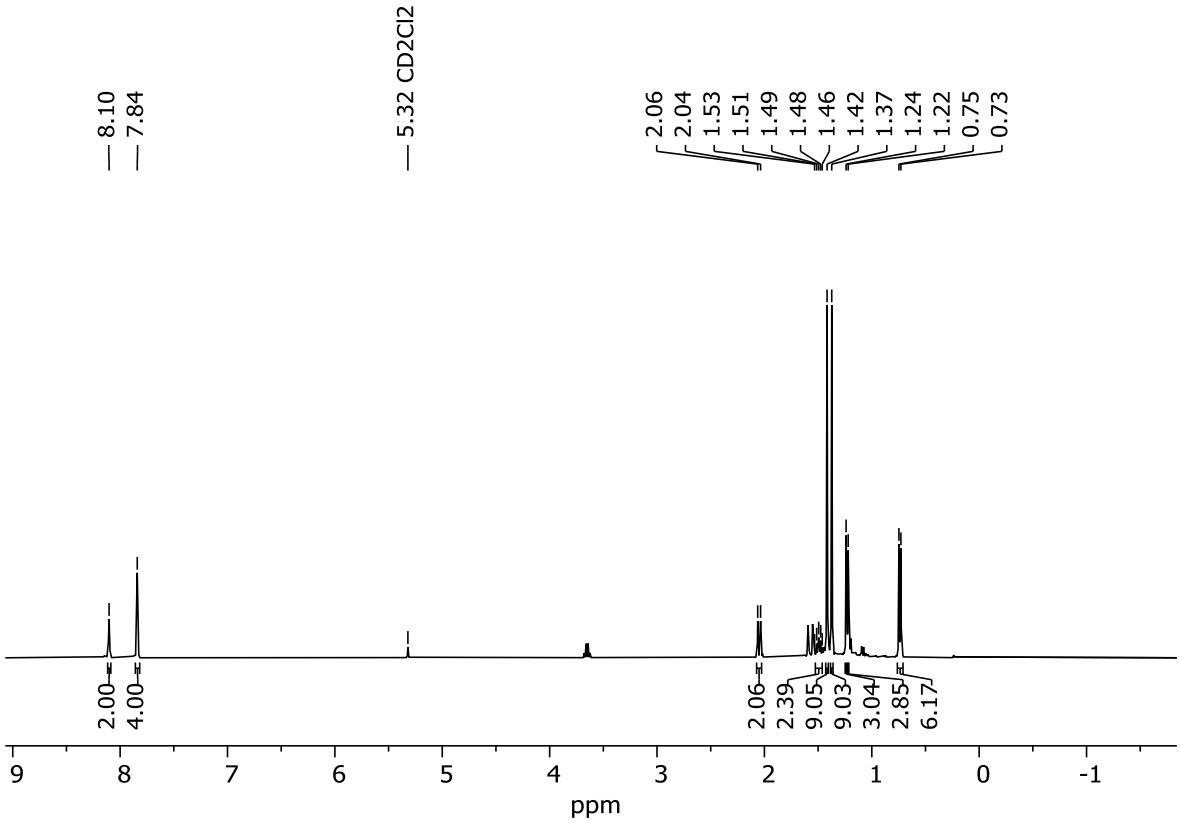

Figure S40: ^{1}H NMR (400.13 MHz, CD_2Cl_2, 298 K) spectrum of compound **11**[$B(C_6F_5)_4$].

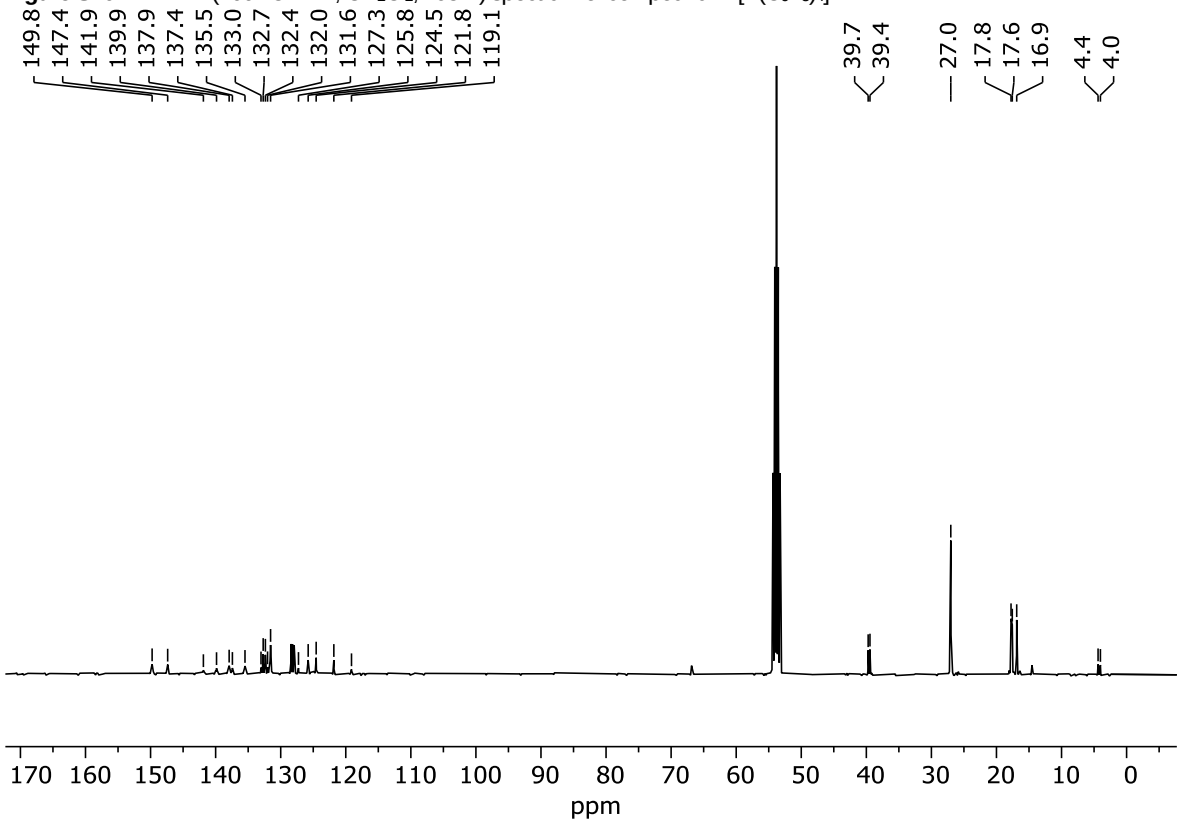

Figure S41: $^{13}C\{^{1}H\}$ NMR (100.61 MHz, CD_2Cl_2, 298 K) of compound **11**[$B(C_6F_5)_4$].

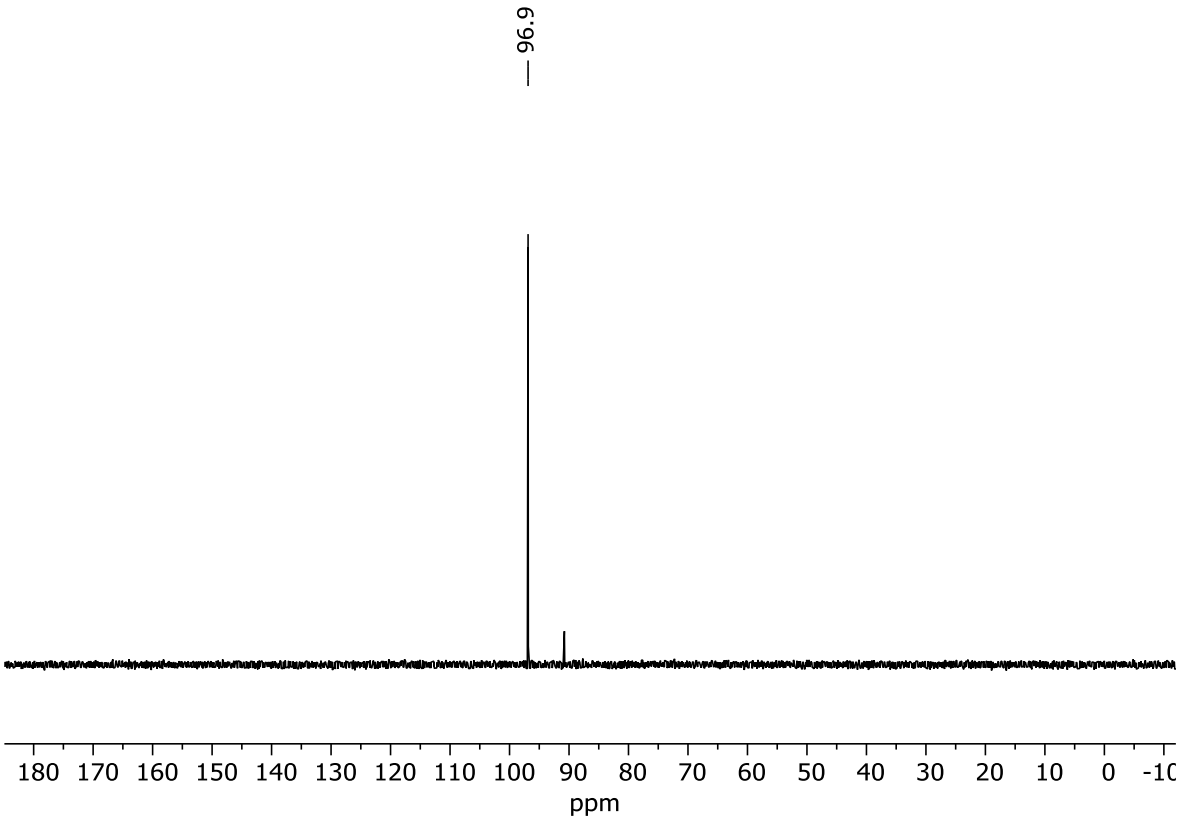

Figure S42: $^{31}P\{^{1}H\}$ NMR (162.04 MHz, CD_2Cl_2, 298 K) of compound **11**[$B(C_6F_5)_4$].

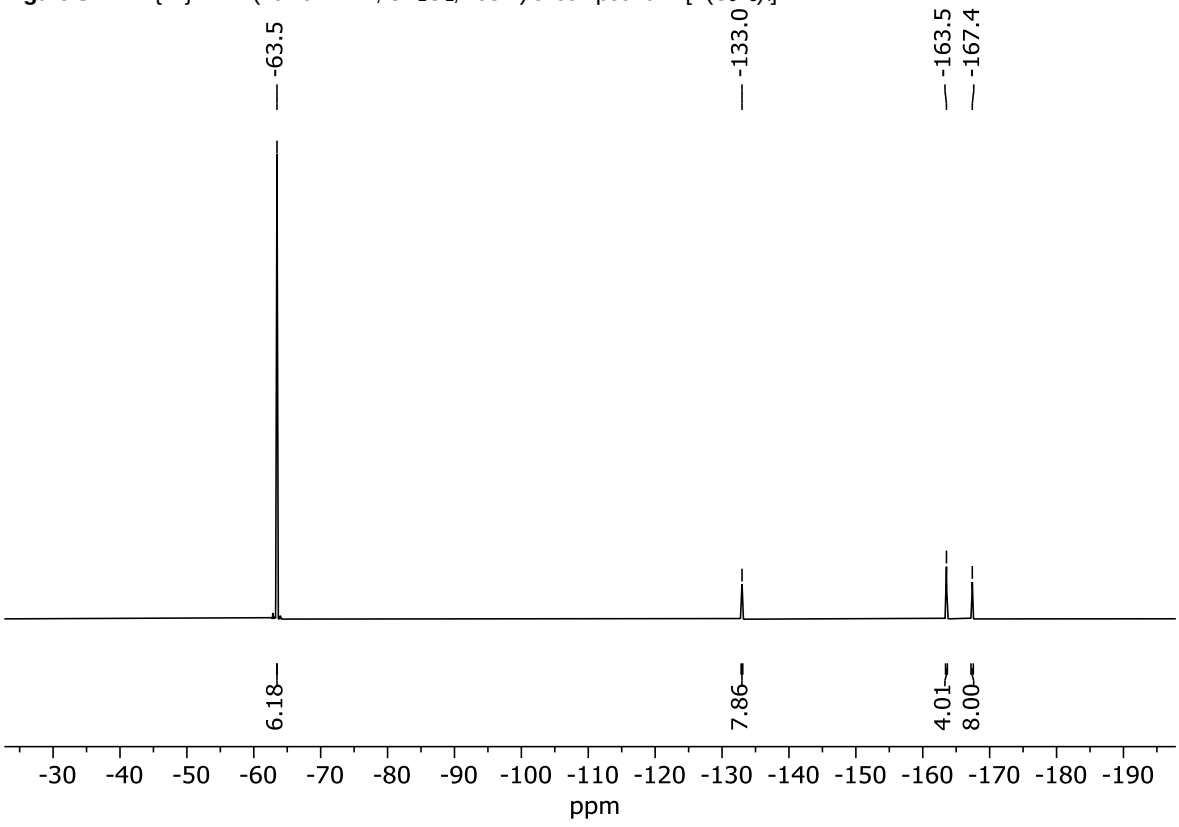

Figure S43: $^{19}F\{^{1}H\}$ NMR (376.66 MHz, CD_2Cl_2, 298 K) of compound **11**[$B(_6F_5)_4$].

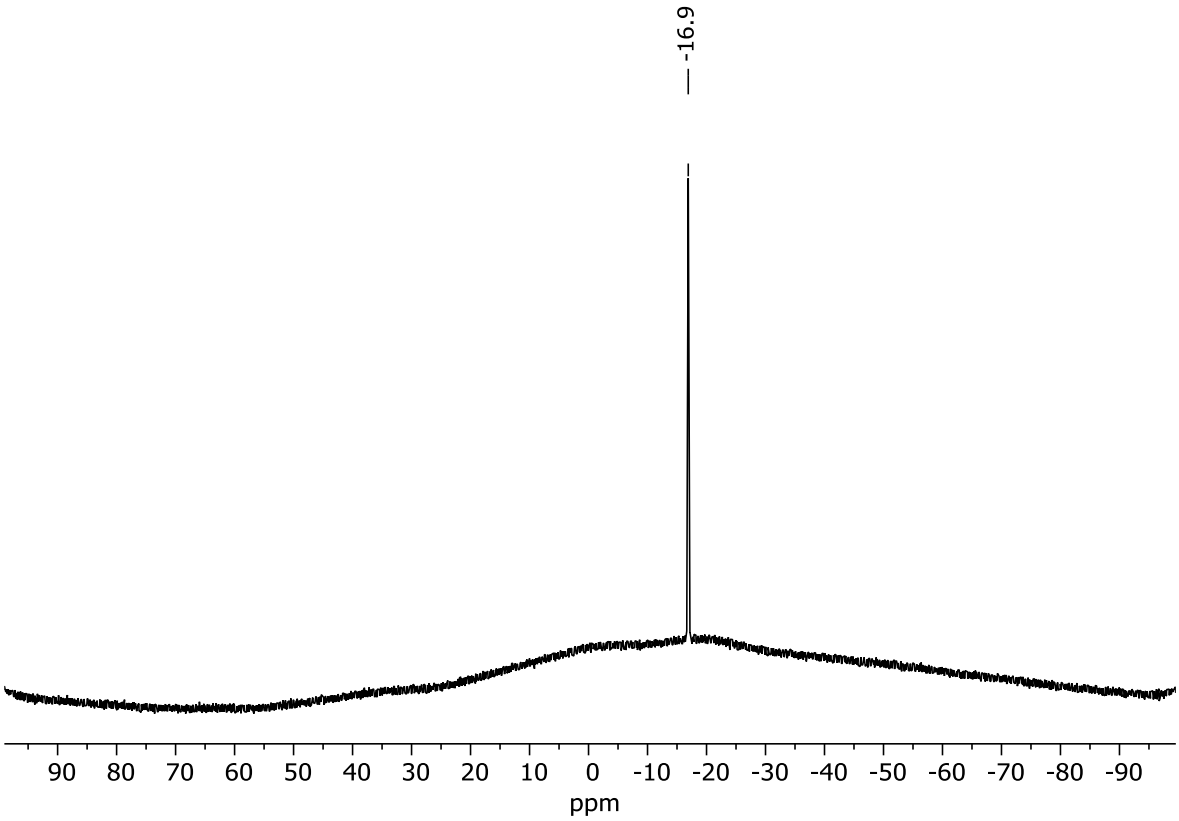

Figure S44: $^{11}B\{^{1}H\}$ NMR (128.43 MHz, CD_2Cl_2, 298 K) of compound **11**$[B(_6F_5)_4]$.

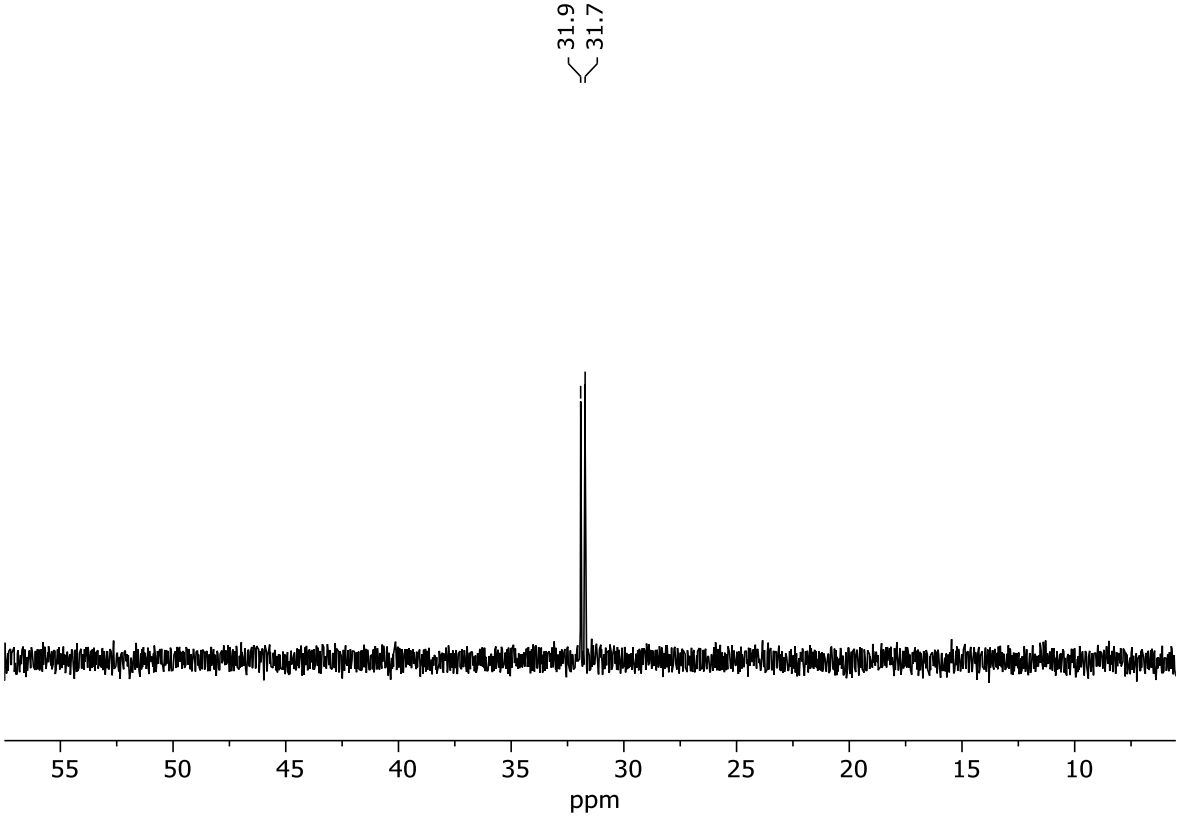

Figure S45: $^{29}Si\{^{1}H\}$ NMR (79.49 MHz, CD_2Cl_2, 298 K) of compound **11**$[B(C_6F_5)_4]$.

4.6.3.6 Hydrosilylation experiments

In a Glovebox compound **9** (10 mg, 0.0138 mmol, 1 equiv.) was combined with triethylsilane (32 mg, 0.275 mmol, 20 equiv.), 4-bromobenzonitrile (50 mg, 0.275 mmol, 20 equiv.) and dissolved in 0.7 mL of toluene-d8. When all solids were dissolved the mixture was transferred in a J-Young type NMR tube and submitted for ^{1}H-NMR analysis (Figure S45). Afterwards the closed NMR tube was heated at 90°C for 48 h. After cooling to room temperature, the NMR tube was again subjected to ^{1}H-NMR spectroscopy (Figure S46). The conversion was determined by integration of the C–H signals of the aryl groups (Figure S47).

Compound **9** + $HSiEt_3$ + 4-bromobenzonitrile at RT

^{1}H NMR (400.13 MHz, C_7D_8, 298 K): δ 6.82–6.80 (m, 2H, $C_{Ar}H$), 6.60–6.57 (m, 2H, $C_{Ar}H$), 3.82 (m, 1H, Si*H*), 0.98–0.94 (m, 9H, $SiCH_2CH_3$), 0.54–0.52 (m, 6H, $SiCH_2CH_3$).

Compound **9** + $HSiEt_3$ + 4-bromobenzonitrile after 48 h at 90 °C

Only the signals of the hydrosilyated product are given:

^{1}H NMR (400.13 MHz, C_7D_8, 298 K): δ 8.81 (s, 1H, $C_{sp2}H$), 7.40–7.38 (m, 2H, $C_{Ar}H$), 7.23–7.21 (m, 2H, $C_{Ar}H$), 1.04–1.00 (m, 9H, $SiCH_2CH_3$), 0.75–0.69 (m, 6H, $SiCH_2CH_3$).

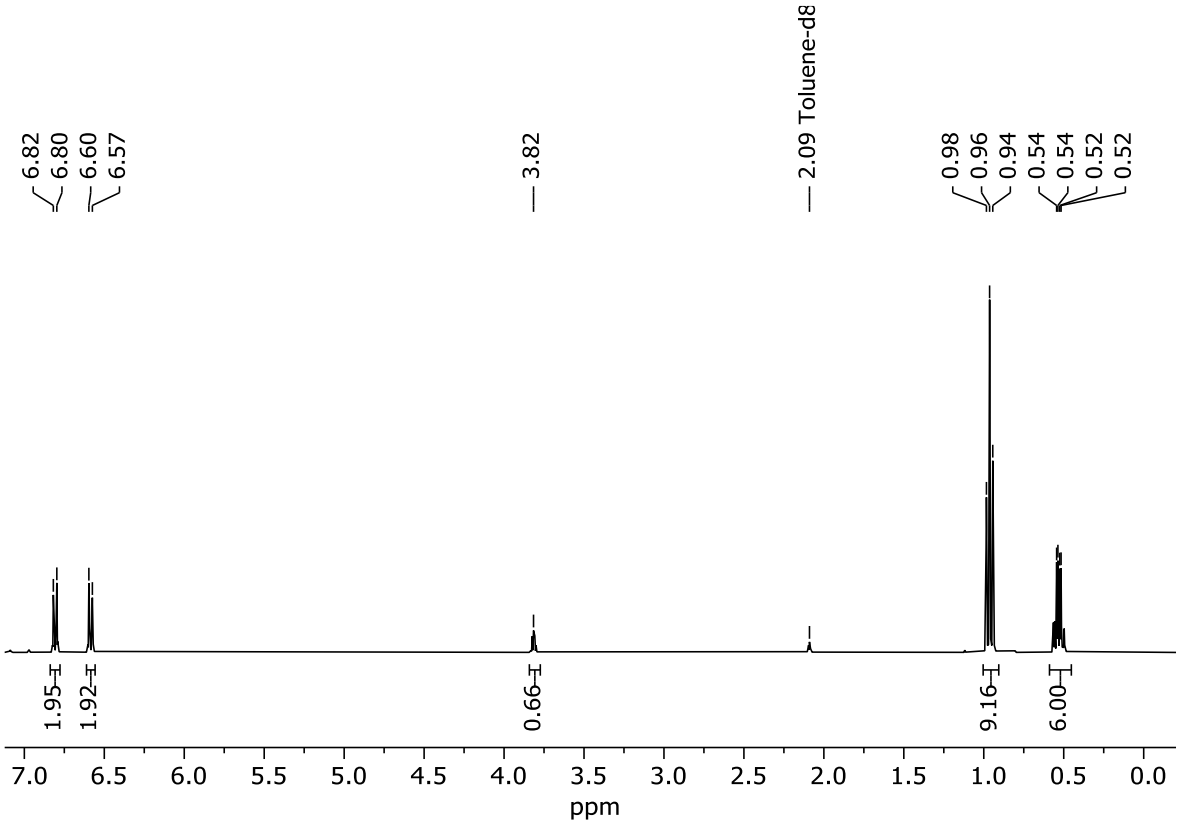

Figure S46: ^{1}H NMR (400.13 MHz, C_7D_8, 298 K) of the mixture of compound **9** (not visible), $HSiEt_3$ and 4-bromobenzonitrile.

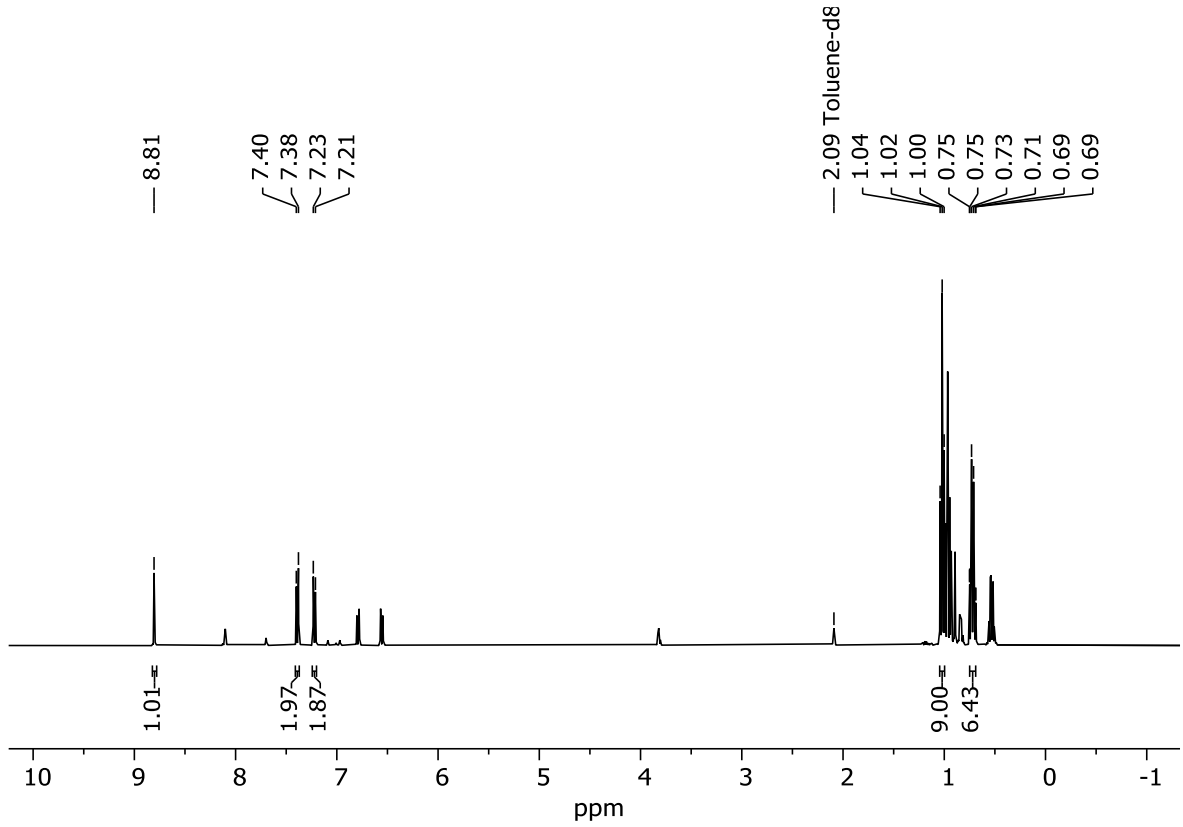

Figure S47: ^{1}H NMR (400.13 MHz, C_7D_8, 298 K) of the mixture of compound **9** (not visible), $HSiEt_3$, 4-bromobenzonitrile after 48 h at 90 °C.

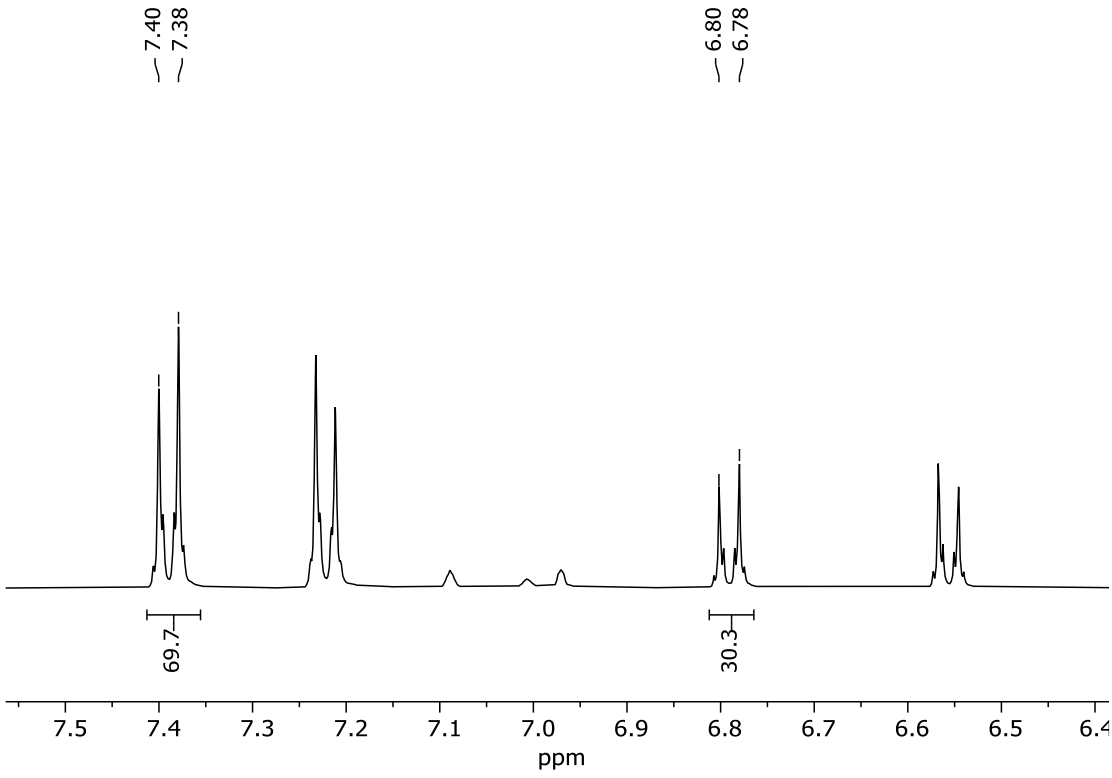

Figure S48: ^{1}H NMR (400.13 MHz, C_7D_8, 298 K) of the determination of conversion of 4-bromobenzonitrile.

4.6.4 X-ray crystallographic details

The crystals were selected and measured either on a SuperNova Dualflex diffractometer equipped with a TitanS2 detector {**4**, **6**[$B(C_6F_5)_4$]}, a XtaLAB Synergy R, DW system, equipped with a HyPix-Arc 150 detector {**12**, **7**[$B(C_6F_5)_4$]} or a Xcalibur Gemini Ultra diffractometer equipped with a TitanS2 detector (**9**, **10**). Data collection and reduction were performed with CrysAlisPro {Version 1.171.43.36a for all compounds}.[6] A numerical absorption correction based on Gaussian integration over a multifaceted crystal model, and an empirical absorption correction using spherical harmonics, implemented in SCALE3 ABSPACK scaling algorithm was applied for all compounds. Using Olex2,[7] the structures were solved with ShelXT[8] and a least-square refinement on F^2 was carried out with ShelXL[9]. All non-hydrogen atoms were refined anisotropically. Hydrogen atoms at the carbon atoms were located in idealized positions and refined isotropically according to the riding model. Hydrogen atoms at the boron, silicon and nitrogen atoms were located from the difference Fourier map and refined without restraints. The figures in the manuscript and Supporting Information were created with Olex2[7]. X-ray crystallographic data can be found in the Supporting Information.

Compound **12**: The asymmetric unit contains one molecule.

Compound **4**: The asymmetric unit contains two molecules.

Compound **6**[$B(C_6F_5)_4$]: The asymmetric unit contains one molecule.

Compound **7**[$B(C_6F_5)_4$]: The asymmetric unit contains one molecule.

Compound **9**: The asymmetric unit contains one molecule. Two of the four trifluoromethyl groups are disordered into two fragments with occupancies of (60:40) and (65:35).

Compound **10**: The asymmetric unit contains one molecule. Three of the eight trifluoromethyl groups are disordered into two fragments with occupancies of (70:30) and (55:45).

Table S1: Crystallographic information for compounds di-*tert*-butyl(methyl)phosphadamantylazide, **4** and **6**[$B(C_6F_5)_4$].

Compound	**12**	**4**	**6**[$B(C_6F_5)_4$]
Data Set (internal naming)	AF139	AF 143_full	AF 292
CCDC Number	-	-	-
Formula	$C_{19}H_{36}N_3P$	$C_{20}H_{48}NPSi_2$	$C_{42}H_{43}BF_{20}NPSi_2$
$\rho_{calc.}$ / g·cm^{-3}	1.139	1.014	1.541
μ/mm^{-1}	1.246	1.853	2.124
Formula Weight	337.48	389.74	1039.73
Color	clear colorless	clear colorless	clear colorless
Shape	needle	irregular	needle
Size/mm^3	0.13 x 0.04 x 0.03	0.18 x 0.14 x 0.08	0.85 x 0.15 x 0.14
T/K	100.00(10)	122.96(18)	123.00(10)
Crystal System	triclinic	monoclinic	triclinic
Space Group	$P\bar{1}$	$P2_1/n$	$P\bar{1}$
a/Å	6.4171(2)	16.5278(3)	10.9425(4)
b/Å	12.6631(6)	14.9902(3)	12.5905(5)
c/Å	13.1370(5)	21.2516(5)	17.2137(8)
α/°	108.110(4)	90	78.926/4)
β/°	100.565(3)	104.185(2)	78.459(3)
γ/°	95.597(3)	90	77.450(3)
V/Å^3	983.70(7)	5104.65(19)	2240.54(17)
Z	2	8	2
Z'	1	2	1
Wavelength/Å	1.54184	1.54184	1.54184
Radiation Type	Cu K_α	Cu K_α	Cu K_α
$2\Theta_{min}$/°	7.268	7.292	7.282
$2\Theta_{max}$/°	149.416	134.024	133.87
Measured Refl.	14542	46436	38583
Independent Refl.	3854	9010	7896
R_{int}	0.0684	0.0666	0.0662
Parameters	215	471	617
Restraints	0	0	0
Largest Peak	0.41	0.49	0.48
Deepest Hole	-0.53	-0.53	-0.46
GooF	1.076	1.024	1.024
wR_2 (all data)	0.1779	0.1689	0.1232
wR_2	0.1669	0.1535	0.1174
R_1 (all data)	0.0847	0.0690	0.0498
R_1	0.0638	0.0576	0.0446

Table S2: Crystallographic information for compounds di-*tert*-butyl(methyl)phosphadamantylazide, **4** and **6**[$B(C_6F_5)_4$].

Compound	**7**[$B(C_6F_5)_4$]	**9**	**10**
Data Set (internal naming)	AF 155	AF 162b	AF 162
CCDC Number	-	-	-
Formula	$C_{44}H_{49}BF_{20}NPSi_2$	$C_{31}H_{41}BF_{12}NPSi$	$C_{47}H_{47}B_2N_6F_{24}SiP$
$\rho_{calc.}$ / g·cm^{-3}	1.492	1.399	1.450
μ/mm^{-1}	2.014	1.840	1.713
Formula Weight	1070.01	725.52	1232.58
Color	clear colorless	clear colorless	colorless
Shape	irregular	block	irregular
Size/mm^3	0.14 x 0.12 x 0.11	0.23 x 0.2 x 0.12	0.27 x 0.22 x 0.16
T/K	123.00(10)	123.00(10)	123.00(10)
Crystal System	triclinic	monoclinic	monoclinic
Space Group	$P\bar{1}$	$P2_1/n$	$P2_1/n$
a/Å	12.79710(10)	13.8628(5)	11.9436(4)
b/Å	13.5020(2)	15.1601(6)	20.4773(10)
c/Å	15-7671(2)	16.4103(9)	23.1474(9)
α/°	106.4120(10)	90	90
β/°	112.5990(10)	92.439(4)	94.358(4)
γ/°	91.8230(10)	90	90
V/Å^3	2382.17(5)	3445.7(3)	5644.9(4)
Z	2	4	4
Z'	1	1	1
Wavelength/Å	1.54184	1.54184	1.54184
Radiation Type	Cu K_α	Cu K_α	Cu K_α
$2\Theta_{min}$/°	6.408	7.942	7.66
$2\Theta_{max}$/°	148.854	134.11	134.604
Measured Refl.	53169	24352	39587
Independent Refl.	9524	6073	9923
R_{int}	0.0268	0.0454	0.0535
Parameters	645	494	832
Restraints	0	0	0
Largest Peak	0.33	0.55	0.55
Deepest Hole	-0.35	-0.4	-0.48
GooF	1.054	1.045	1.022
wR_2 (all data)	0.0773	0.1380	0.1644
wR_2	0.0754	0.1311	0.1545
R_1 (all data)	0.0337	0.0603	0.0690
R_1	0.0299	0.0515	0.0585

Compound **12**

Hydrogen atoms are omitted for clarity.

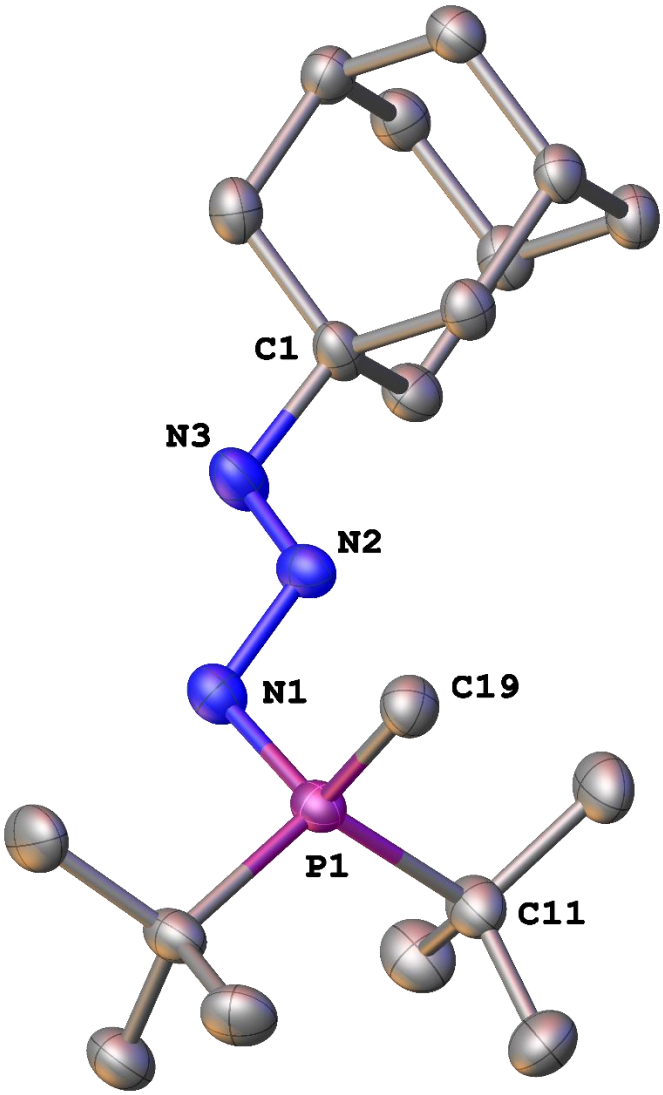

Selected Bond Lengths in Å		**Selected Bond Angles in °**	
P(1)–N(1)	1.636(2)	**P(1)–N(1)–N(2)**	108.53(17)
N(1)–N(2)	1.373(3)	**N(1)–N(2)–N(3)**	113.3(2)
N(2)–N(3)	1.266(3)	**N(2)–N(3)–C(1)**	112.4(2)

Compound **4**

Hydrogen atoms except Si–H omitted for clarity.

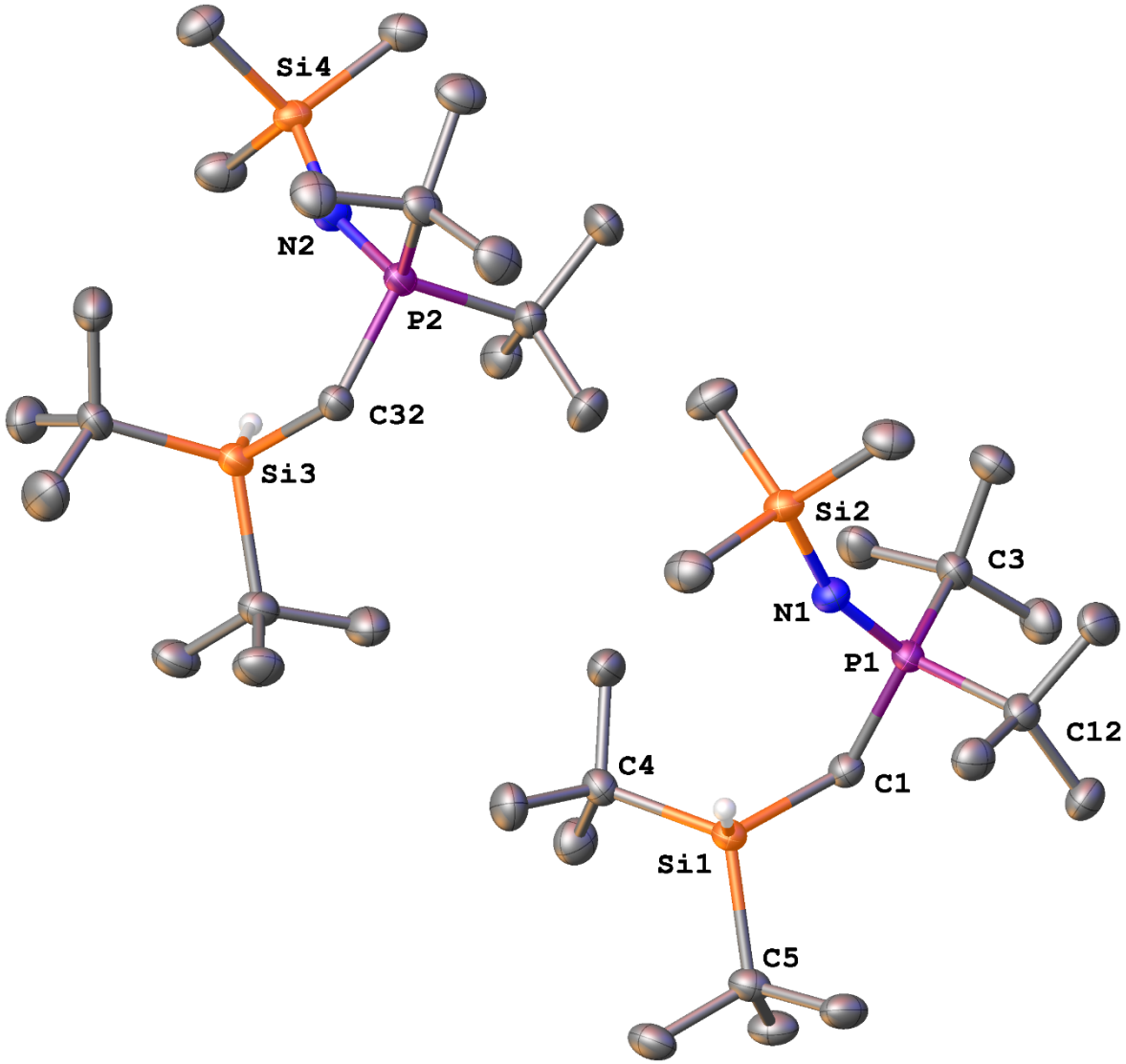

Selected Bond Lengths in Å		Selected Bond Angles in °	
Si(1)–C(1)	1.904(2)	**C(5)–Si(1)–C(1)**	114.96(11)
C(1)–P(1)	1.823(2)	**Si(1)–C(1)–P(1)**	118.85(13)
P(1)–N(1)	1.538(2)	**C(1)–P(1)–N(1)**	112.28(11)
N(1)–Si(2)	1.665(2)	**P(1)–N(1)–Si(2)**	160.92(15)

Compound **6**[$B(C_6F_5)_4$]

Hydrogen atoms are omitted for clarity.

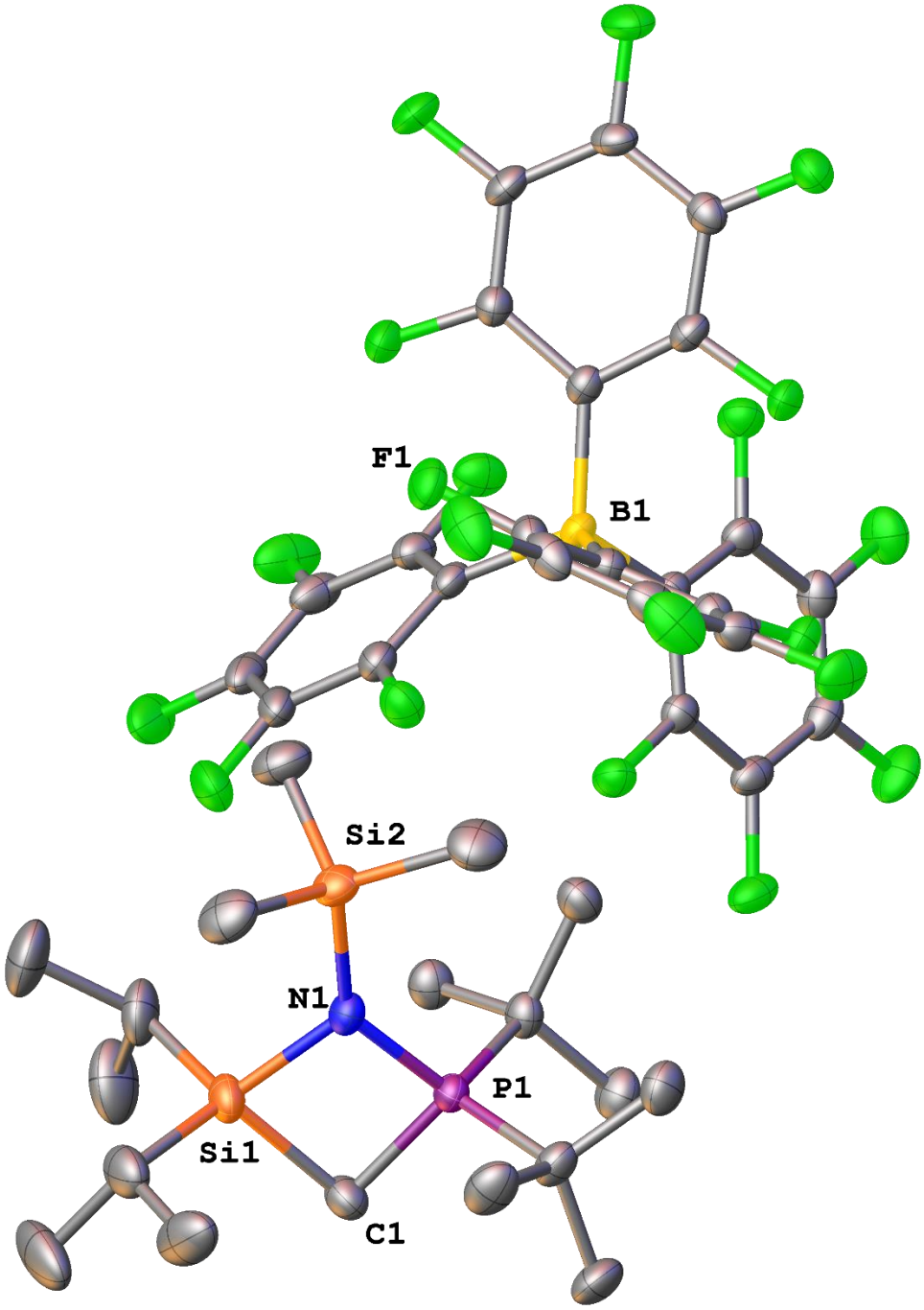

Selected Bond Lengths in Å		**Selected Bond Angles in °**	
Si(1)–N(1)	1.8087(19)	**Si(1)–N(1)–Si(2)**	126.70(11)
N(1)–Si(2)	1.7722(19)	**Si(1)–C(1)–P(1)**	87.60(10)
P(1)–N(1)	1.6654(19)	**Si(1)–N(1)–P(1)**	95.14(9)

Compound **7**[$B(C_6F_5)_4$]

Hydrogen atoms except Si–H and N–H are omitted for clarity.

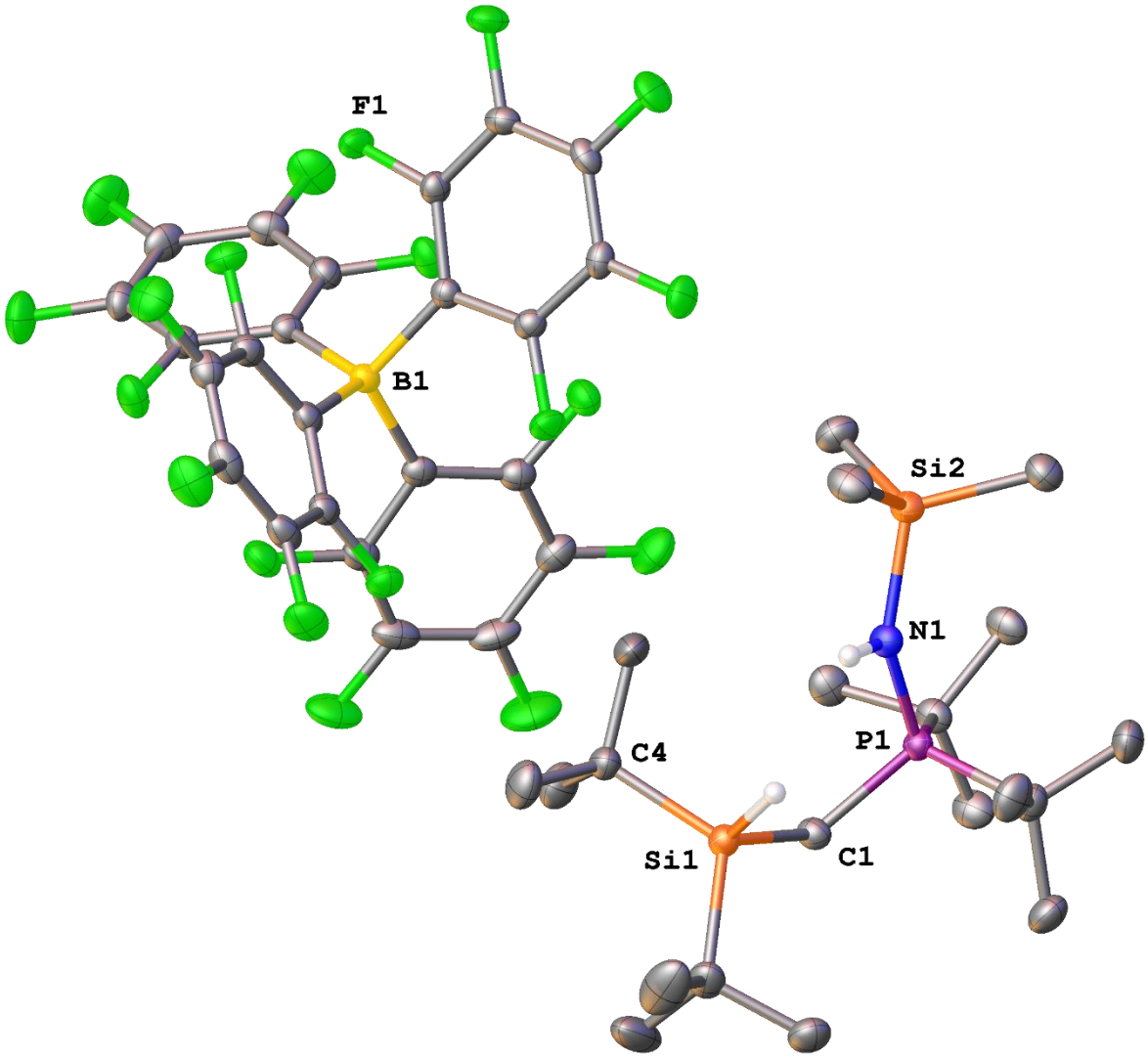

Selected Bond Lengths in Å		**Selected Bond Angles in °**	
Si(1)–C(1)	1.9224(14)	**C(4)–Si(1)–C(1)**	109.57(6)
C(1)–P(1)	1.8017(14)	**Si(1)–C(1)–P(1)**	124.02(8)
P(1)–N(1)	1.6433(12)	**C(1)–P(1)–N(1)**	108.09(6)
N(1)–Si(2)	1.7902(12)	**P(1)–N(1)–Si(2)**	146.11(8)

Compound **9**

Hydrogen atoms except B–H are omitted for clarity.

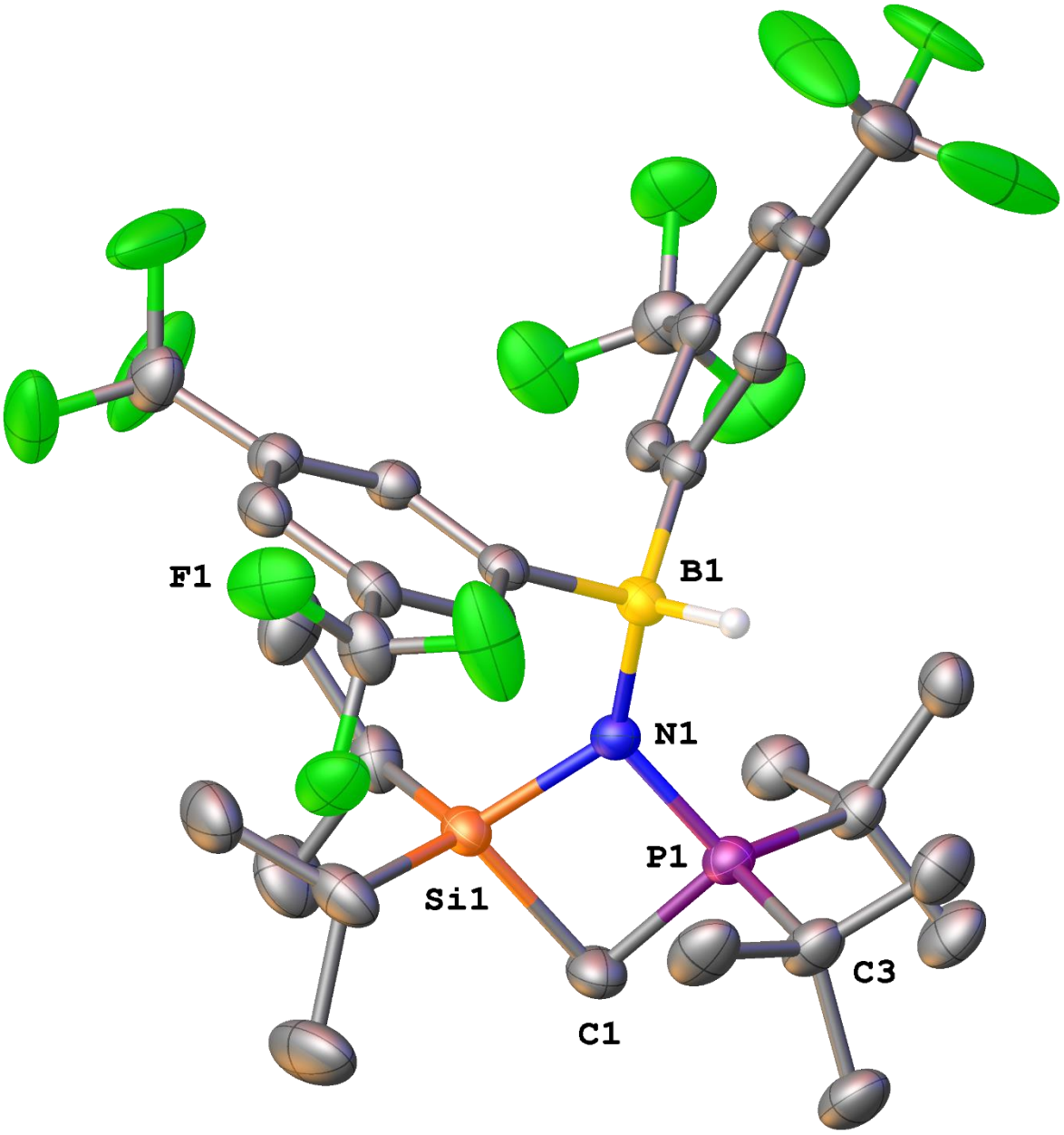

Selected Bond Lengths in Å		**Selected Bond Angles in °**	
P(1)–N(1)	1.656(18)	**P(1)–C(1)–Si(1)**	86.16(10)
Si(1)–N(1)	1.7769(19)	**Si(1)–N(1)–P(1)**	95.44(9)
N(1)–B(1)	1.589(3)	**P(1)–N(1)–B(1)**	127.99(15)
P(1)–C(1)	1.796(2)	**Si(1)–N(1)–B(1)**	135.20(14)

Compound **10**

Hydrogen atoms except Si–H are omitted for clarity.

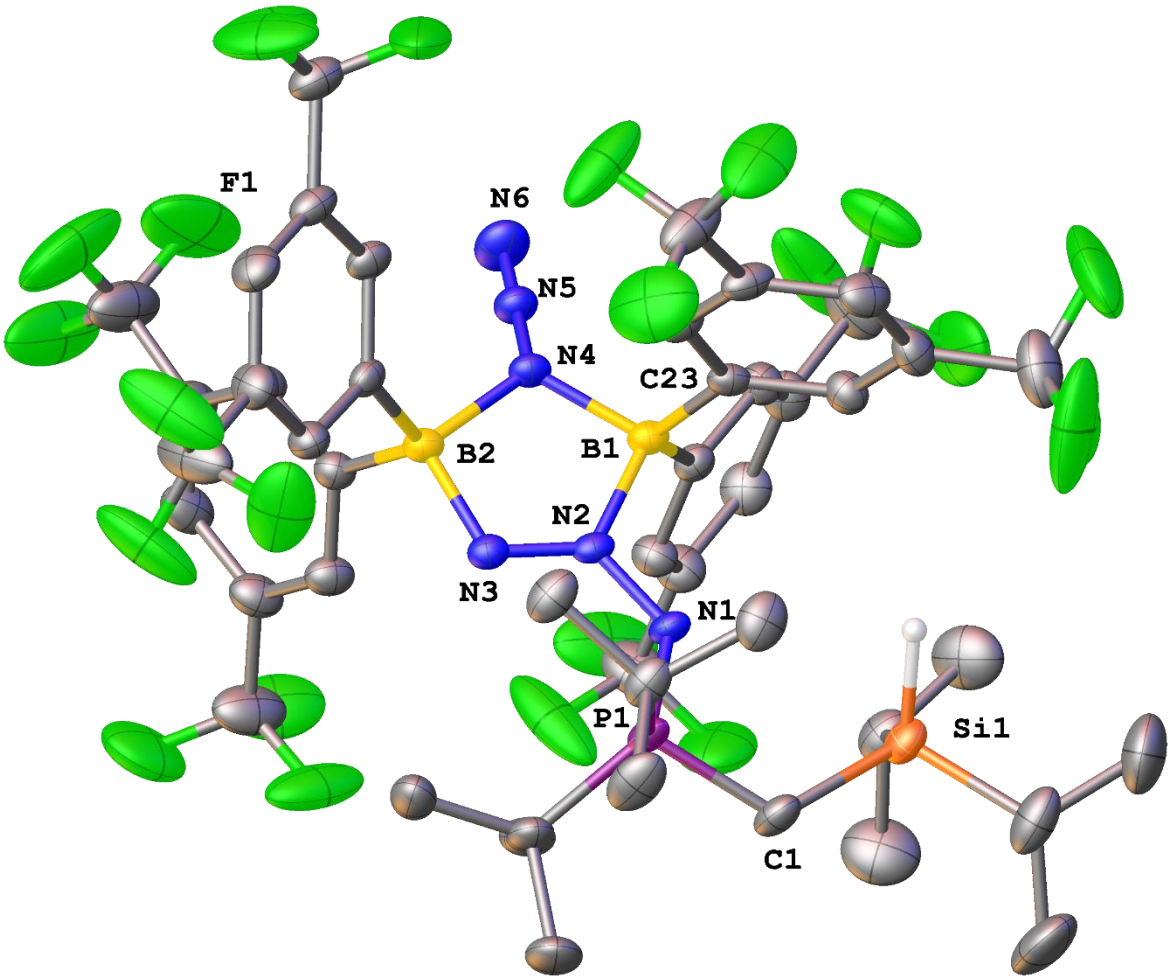

Selected Bond Lengths in Å		Selected Bond Angles in °	
P(1)–N(1)	1.6535(19)	**P(1)–C(1)–Si(1)**	118.70(14)
N(1)–N(2)	1.335(3)	**P(1)–N(1)–N(2)**	125.16(15)
N(2)–B(1)	1.598(3)	**N(2)–B(1)–N(4)**	94.72(17)
P(1)–C(1)	1.804(2)	**N(2)–B(1)–C(23)**	107.40(18)

4.6.5 Supplementary references

(1) (a) Fontana, N.; Espinosa-Jalapa, N. A.; Seidl, M.; Bauer, J. O. Hidden silylium-type reactivity of a siloxane-based phosphonium–hydroborate ion pair. *Chem. Commun.* **2022**, *58*, 2144-2147. (b) Fink, L.; Samigullin, K.; Bodach, A.; Alig, E.; Wagner, M.; Lerner, H.-W. Donor-unsupported Phosphanylmethanides Li[CH2P*R*$_2$] (*R* = *t*Bu, Ph) – Crystal Structure of Li[CH_2P*t*Bu_2] Solved by XRPD and DFT-D Calculations. *Z. Anorg. Allg. Chem.* **2016**, *642*, 282-287.

(2) Samigullin, K.; Bolte, M.; Lerner, H.W.; Wagner, M. Facile Synthesis of (3,5-$(CF_3)_2C_6H_3)_2$BX (X = H, OMe, F, Cl, Br): Reagents for the Introduction of a Strong Boryl Acceptor Unit. *Organometallics*. **2014**, *13*, 3564-3569.

(3) Chien, J. C. W.; Tsai, W.-M.; Rausch, M. D. Isospecific Polymerization of Propylene Catalyzed by *rac*-Ethylenebis(indenyl)methylzirconium “Cation” *J. Am. Chem. Soc.* **1991**, *113*, 8570-8571.

(4) (a) Rach, S. F.; Herdtweck E.; Kühn, F. E. *J. Organomet. Chem.* **2011**, *696*, 1817. (b) Jutzi, P.; Müller, C.; Stammler, A.; Stammler, H.-G. Synthesis, Crystal Structure, and Application of the Oxonium Acid [$H(OEt_2)_2$][$B(C_6F_5)_4$] -. *Organometallics* **2000**, *19*, 1442–1444.

(5) Fraenk, W.; Klapötke, T. M.; Krumm, B.; Mayer, P.; Nöth, H.; Piotrowski, H.; Suter, M. Synthesis and structural studies on fluorophenylboron azides. *Journal of Fluorine Chemistry* **2001**, *112*, 73–81.

(6) Rigaku Oxford Diffraction, CrysAlisPro Software System. 2020.

(7) Dolomanov, O. V.; Bourhis, L. J.; Gildea, R. J.; Howard, J. A. K.; Puschmann, H. *OLEX2*: a complete structure solution, refinement and analysis program. *J. Appl. Crystallogr.* **2009**, *42*, 339-341.

(8) Sheldrick, G. M. *SHELXT* – Integrated space-group and crystal-structure determination. *Acta Crystallogr*. **2015**, *A71*, 3-8.

(9) Sheldrick, G. M. Crystal structure refinement with *SHELXL*. *Acta Crystallogr.* **2015**, *C71*, 3-8.

5 Neutral silanes as Lewis acids in silyl phosphonium chalcogenides

Preface

The following chapter and supporting information are based on a manuscript in preparation about the synthesis and development of neutral silicon-based Lewis acids with attached phosphine sulfide Lewis bases.

Authors

A. Falk, J. O. Bauer

Author contribution

All the reported syntheses and characterizations were performed by A. Falk. The manuscript draft and supporting information was prepared by A. Falk and revised by J. O. Bauer.

Acknowledgements

This work was supported by the Deutsche Forschungsgemeinschaft (DFG, German Research Foundation) through the Research Training Group “Ion Pair Effects in Molecular Reactivity” (RTG 2620, project 426795949).

5.1 Abstract

Following our exploration of four-membered heterocyclic silyl phosphonium chalcogenides (chapter 3)[1] we changed the donor moiety to phosphinimines, in order to investigate four-membered heterocyclic silyl phosphinimine ions (chapter 4). While the use of phosphinimines as donors resulted in changed properties of these ions, the basic principle of using silylium ions as Lewis acids remained unchanged compared to the silyl phosphonium chalcogenides of chapter 3. In this chapter we aimed to change the nature of the employed Lewis acid from a silylium ion to a neutral silane. This enables us to form the cyclic four-membered phosphonium chalcogenide ions without hydride removal, therefore yielding zwitterionic species. These species contain a pentacoordinate silicon atom within the four-membered cycles, which is in stark contrast to the neutral tetravalent silanes in the phosphonium chalcogenide and phosphinimine cycles of chapters 3 and 4. Several novel neutral Lewis acidic silanes were prepared and incorporated within the previously described CPSSi cycles (chapter 3). By varying the electron-withdrawing groups from pentafluorophenyl [-C_6F_5] over pentafluorophenoxy [-OC_6F_5] to tetrafluorocatecholato [-$O_2C_6F_4$] moieties, a discernible difference in Lewis acidity at the silicon center was observed.

5.2 Introduction

Over the past decade, the field of Frustrated Lewis Pairs (FLPs) has attracted considerable scientific interest, resulting in the discovery of an ever-increasing number of suitable Lewis acid/base combinations. In this context, FLPs based on main group elements have emerged as a particularly interesting substrate class, because they exhibit properties that were previously observed only in transition metal chemistry.[2] The most prevalent and enduring class of FLPs is based on group 13 Lewis acids, particularly boranes, in combination with a multitude of Lewis bases, particularly phosphines.[3] Due to their empty 2p-orbitals, boranes are naturally suited for use as Lewis acids. Upon moving to Group 14 in the periodic table, it is expected that the same reactivity will be observed with the isolobal tricoordinate cations belonging to this group. In the case of silicon, specifically the silylium ions, this will be the case. And indeed, highly reactive FLPs were made from the combination of silylium ions with phosphines.[4] However, the high Lewis acidity of silylium ions has a decisive drawback. The heterolytic splitting of molecules lead to the formation of products in a thermodynamic sink, rendering these combinations unsuitable for catalytic applications.[4] This is where neutral Lewis acidic silanes make their debut. In contrast to their smaller carbon atom analogues, neutral silanes can act as strong Lewis acids and have been used extensively as such in the past.[5] A classic example for their discerning properties is the difference of $SiCl_4$ and CCl_4, with the latter being an inert solvent with no Lewis acidic properties and $SiCl_4$ being highly Lewis acidic. The first intramolecular FLP system based on a neutral silicon-based Lewis acid was published in 2015 by the Mitzel group (Scheme 1).[6] This novel system has demonstrated the fixation of carbon dioxide and the activation of dihydrogen, as evidenced by a H/D scrambling experiment. An essential aspect of the design of neutral highly acidic silanes is the energetic promotion of the pentacoordinate state.[7] The stability of the pentacoordinate state, and therefore the Lewis acidity of the tetravalent state of silicon, is not only contingent upon the electronic nature of its substituents, but also upon the steric demand of the substituents. Substituents that facilitate a less energetically demanding transition from a tetrahedral to a trigonal bipyramidal conformation result in higher neutral Lewis acidic silanes.[7,8]

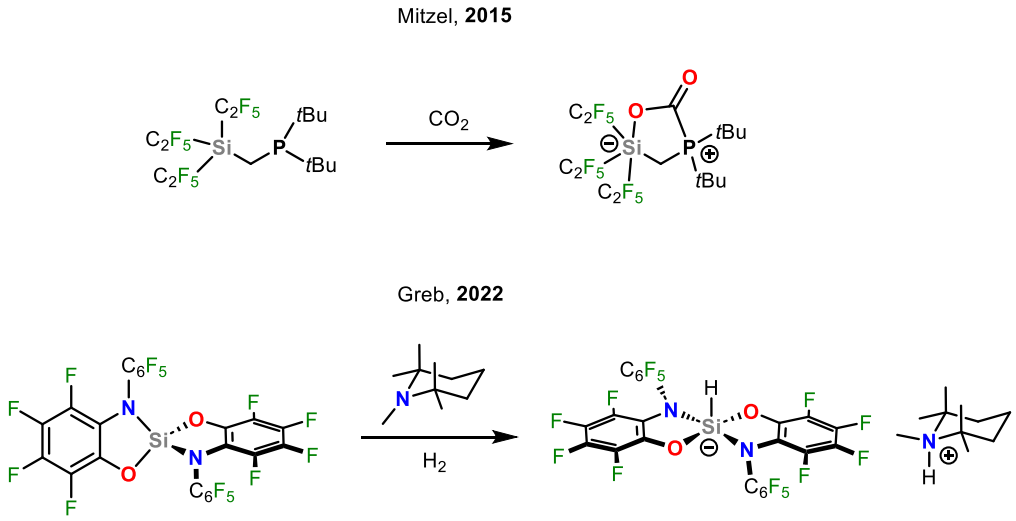

Scheme 1: Frustrated Lewis Pairs based on neutral Lewis acidic silanes.

The steric effect may be exploited through the synthesis of pentacoordinate silanes by strain release of the respective tetravalent species.[8] One particularly noteworthy instance of steric effects in pentacoordinate silanes is the class of bis(catecholo)silanes, which are represented by the general formula [Si(cat)$_2^X$] (X = EWG), were X represents an electron withdrawing group (Example given in Scheme 1). In this case, the pentacoordinate silicon state does not adopt the lower energy trigonal-bipyramidal form; rather, a distortion towards a square pyramidal configuration is observed (Scheme 1).[9] The stabilization of the square pyramidal configuration can be explained by the diminished electron density at the mutually repulsive oxygen lone pairs in the catechol plane.[10] This result is consistent with subsequent findings indicating an augmented π-backdonation of the free oxygen lone pairs into the halogenated aryl rings.[9b] A novel *ortho*-aminophenol, which exhibits analogous properties to the aforementioned bis(catecholo)silanes, was employed by the Greb group in 2022 to generate an intermolecular FLP utilizing a neutral silane as an Lewis acid (Scheme 1). This FLP was found to be capable of activating dihydrogen, and subsequent research demonstrated that this neutral silicon Lewis acid was also able to perform silylations at C–H bonds, thereby illustrating the remarkable power and versatile nature of neutral silicon-based Lewis acids.[5d,11] Our previously published four-membered heterocyclic silyl phosphonium chalcogenides were ideal platforms for the introduction of highly Lewis acidic neutral silanes, since their synthesis can be easily modified towards the introduction of these silanes. Additionally, being four-membered ring systems, steric strain can assist in the weakening of the Si–S bond allowing for heterolytic activation of small molecules (Scheme 2). The reactivity of these systems is enhanced by the fact that the P$^+$–S$^-$ moiety is just a moderately strong donor moiety and is furthermore shielded from the Lewis acidic silicon center with the bulky di-*tert*-butyl phosphine moiety. By using the pentacoordinate state it is possible to increase the positive polarization at silicon therefore increasing the reactivity of the Si–H bond, allowing it to be transferred to electrophilic substrates. The variation of electron withdrawing groups allows us to gradually increase the thermodynamic stability of the pentacoordinate silicon state, and therefore the corresponding Lewis acidity of the tetravalent state.

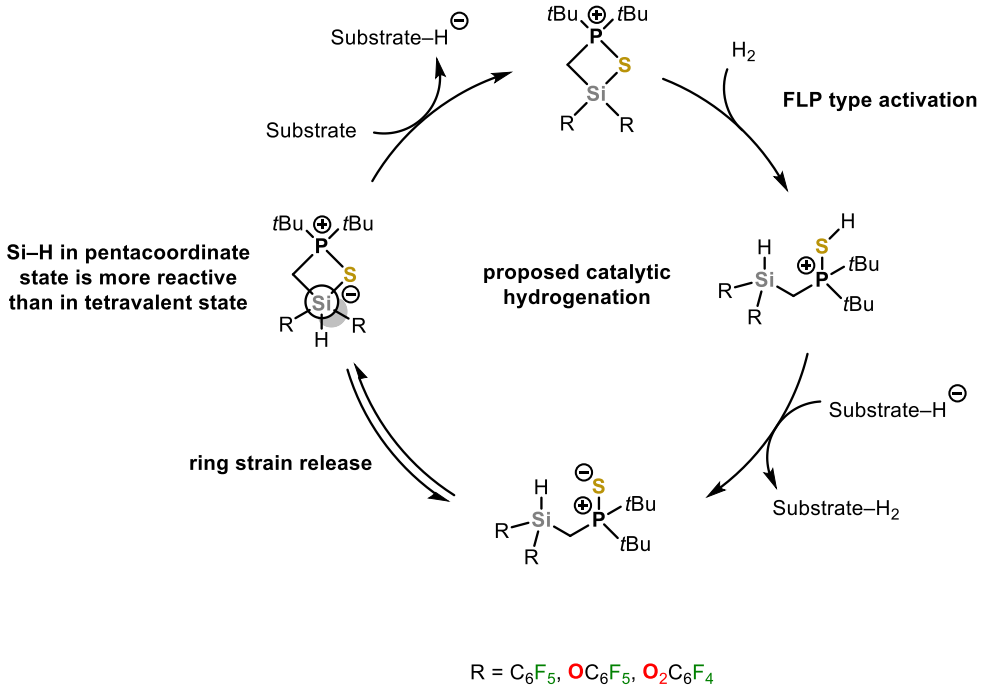

Scheme 2: Our goal of utilizing pentacoordinate silanes in a catalytic hydrogenation.

Finetuning the stability of the pentacoordinate state is crucial, as we want it to be energetically favorable enough to from the tetravalent state, but unstable enough to easily transfer the Si–H moiety. All of the above-mentioned design factors allow for the sensible formulation of a full catalytic cycle (Scheme 2). Our goal was the exploration of neutral silanes attached with either pentafluorophenyl [-C_6F_5], pentafluorophenoxy [-OC_6F_5] and tetrafluorocatecholato [-$O_2C_6F_4$] moieties in order to gauge their influence on Lewis acidity of the silicon atom and incorporate them within the previously studied four-membered heterocyclic silyl-phosphonium ring systems in order to obtain catalytically active species.

5.3 Results and Discussion

The initial objective was to modify our previously published scaffolds with pentafluorophenyl groups [-C_6F_5], based on previous findings that demonstrated a promising increase in Lewis acidity at silicon when these groups were introduced.[1,12] Pentafluorophenyl [-C_6F_5] substituted chlorosilanes cannot be obtained selectively from pentafluorophenyl lithium and the corresponding tri- or dichlorosilanes due to the high reactivity of the nucleophile. Therefore, we developed an alternative procedure using the previously published di-pentafluorophenyl(phenyl)silane as our starting material (Scheme 3).[13]

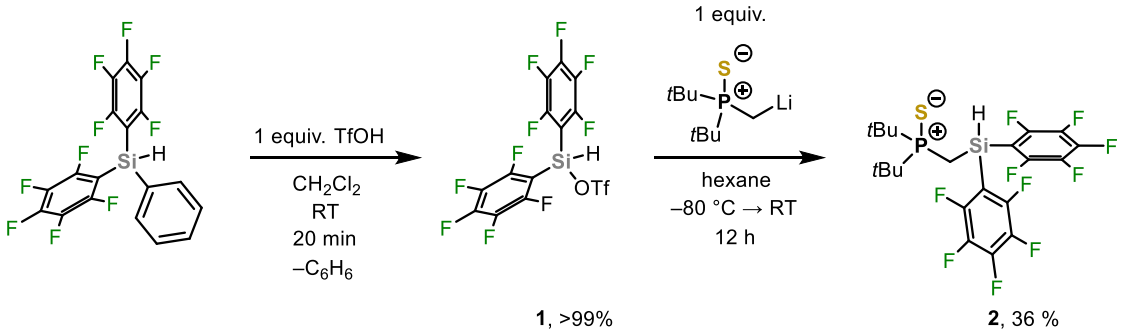

Scheme 3: Synthesis of compound **2** *via* protodesilylation with triflic acid and subsequent nucleophilic substitution with ((di-*tert*-butylphosphorothioyl)methyl)lithium.

Di-pentafluorophenyl(phenyl)silane can be readily obtained from commercially available dichloro(phenyl)silane and *in situ* prepared pentafluorophenyl lithium. The reaction of di-pentafluorophenyl(phenyl)silane with an exact equivalent of triflic acid results in the selective protodesilylation of the phenyl moiety, yielding silyl triflate **1** and benzene in a satisfactory yield. The selectivity and reactivity of triflic acid with other silanes have been previously published.[14] Nucleophilic substitution of the reactive triflate group in **1** with ((di-*tert*-butylphosphorothioyl)methyl)lithium gave the desired hydridosilane **2** in a moderate yield. In order to have a reference molecule to measure the effect of the electron withdrawing pentafluorophenyl [-C_6F_5] groups, we also synthesized the non-fluorinated equivalent of **2**, the diphenyl substituted silyl phosphine sulfide **3** (Scheme 4).

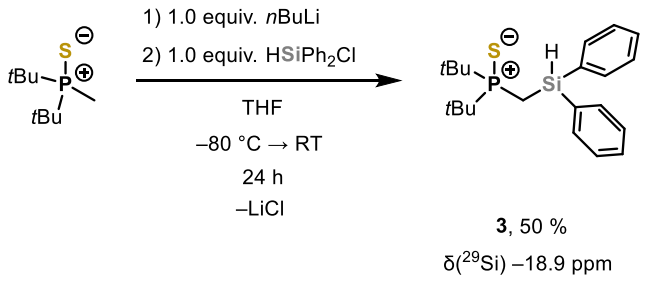

Scheme 4: Synthesis of compound **3** *via* lithiation of di-*tert*-butylphosphinesulfide and reaction with diphenyl(chloro)silane.

The synthesis was achieved through a reaction between diphenyl(chloro)silane and ((di-*tert*-butylphosphorothioyl)methyl)lithium. NMR spectroscopy of compound **2** revealed a significant upfield shift to –43.4 ppm in the $^{29}Si\{^1H\}$ spectrum. This value is in strong

contrast to compound **3** [δ(^{29}Si) = –18.9 ppm] and a *tert*-butyl substituted similar compound [*t*Bu$_2$P(S)CH$_2$Si(*t*Bu$_2$)H, δ(^{29}Si) = 7.7 ppm].[1] This shows the siginificant electronic influence of the [-C$_6$F$_5$] substitutents on the silicon nucelus. However, although the influence of the pentafluorophenyö [-C$_6$F$_5$] substitutents are significant, the absolute value of the ^{29}Si-NMR signal is not in the range of other previously reported pentacoordinated silanes.[7,9,10] Furthermore the ^{31}P{^{1}H}-NMR signal at 74.6 ppm is within the area of the *tert*-butyl-substituted silylphosphine sulfide [*t*Bu$_2$P(S)CH$_2$Si(*t*Bu$_2$)H, ^{31}P{^{1}H} = 77.4 ppm] and compound **3** [^{31}P{^{1}H} = 76.0 ppm] indicating no interaction of the P$^+$–S$^-$ moiety with the silicon center in compound **2**.[1] This observation is further supported by single-crystal X-ray diffraction data of compound **2** where no Si–S donor interaction with can be observed in the solid state (Figure 1).

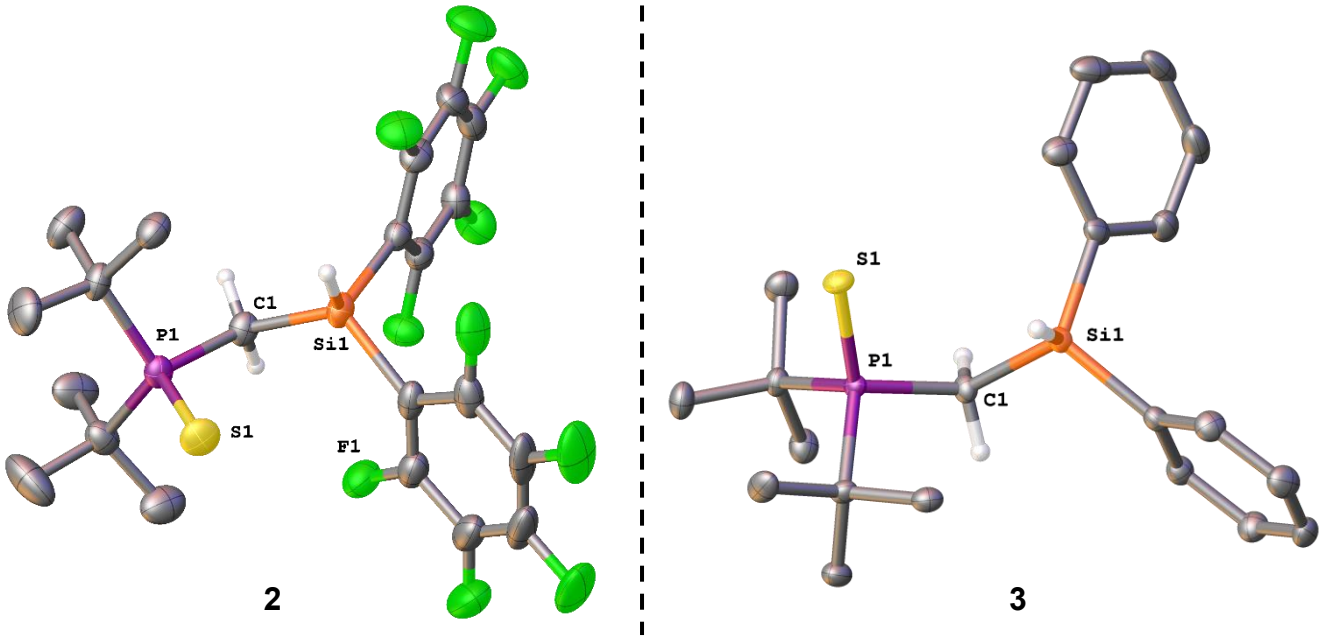

Figure 1: Molecular structures of compounds **2** and **3** in the crystal (displacement ellipsoids set at the 50 % probability level). Selected bond lengths (Å) and angles (°) of **2**: P(1)–S(1) 1.9697(13), P(1)–C(1) 1.817(4), Si(1)–C(4) 1.887(5), Si(1)-C(1)–P(1) 116.8(2), S(1)–P(1)–C(1) 110.04(13), C(1)–Si(1)–C(4) 116.79(19). **3**: P(1)–S(1) 1.9737(8), P(1)–C(1) 1.817(2), Si(1)–C(1) 1.902(2), Si(1)–C(1)–P(1) 117.64(11), S(1)–P(1)–C(1) 111.85(8), C(1)–Si(1)–C(3) 109.55(10).

Compound **2** crystallized in the monoclinic crystal system with the space group *Cc* and compound **3** crystallized in the triclinic crystal system with the space group $P2_12_12_1$. Both P$^+$–S$^-$ donor moieties have similar bond lengths [**2**: 1.9697(13) Å, **3**: 1.9737(8) Å], again indicating no interaction between the P$^+$–S$^-$ donor moiety and the silicon atom in compound **2**. The electron withdrawing effect of the pentafluorophenyl [-C$_6$F$_5$] groups in compound **2** results in a slightly shorter Si(1)–C(1) bond length [1.869(4) Å] compared to compound **3** [1.902(2) Å]. The same electron withdrawing effect is also responsible for a marginally tighter Si(1)–C(1)–P(1) bond angle in compound **2** [116.8(2) °] compared to compound **3** [117.64(11) °]. This is rather interesting since the pentafluorophenyl [-C$_6$F$_5$] groups in compound **2** possess a larger steric hinderance compared to the phenyl groups [-C$_6$H$_6$] in compound **3**, which should result in an enlargement of the Si(1)–C(1)–P(1) bond angle in compound **2**. Since no P$^+$–S$^-$ donor interaction with the silicon atom could be observed, compound **2** did not exhibit the desired Lewis acidic properties we were aiming for (see Scheme 2). In order to enhance the Lewis acidity of compound **2** we attempted hydride

atom abstraction with tris(pentafluorophenyl)borane and tritylium tetrakis(pentafluorophenyl)borate, with the objective of forming the corresponding four-membered cationic CPSSi cycle compound **2-c** (Scheme 5). This would allow us to form a cationic species with additional ring strain, a strategy which has been successfully employed by other groups to increase the Lewis acidity at silicon.[8] While crude NMR analysis of the reaction with one equivalent of tris(pentafluorophenyl)borane in dichloromethane shows successful conversion to the desired product **2-c**, isolation and full characterization has yet to be achieved.

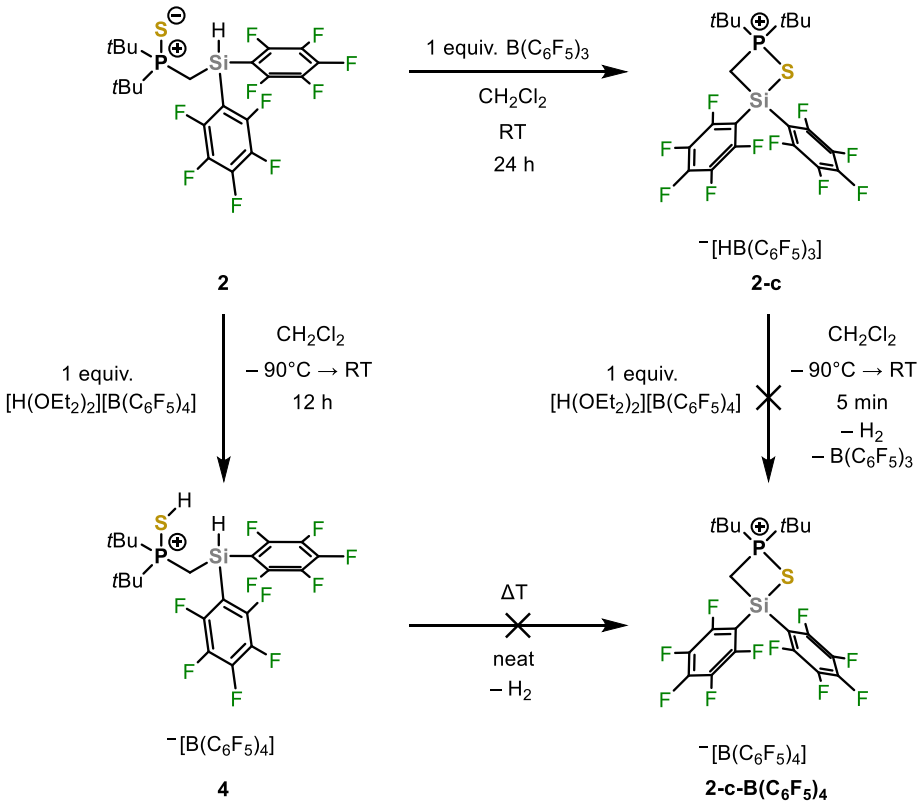

Scheme 5: Synthesis of compounds **2-c** and **4** as well as attempted pathways towards compound **2-c-B(C_6F_5)$_4$**.

Due to the problems faced with the isolation of compound **2-c**, we attempted to improve its crystallization properties by a dehydrogenative anion exchange with $[H(OEt_2)_2][B(C_6F_5)_4]$,[15] a strategy which as has been previously successfully employed in our group.[16] However, this reaction was unselective and produced a unidentifiable mixture of products and not the desired compound **2-c-B(C_6F_5)$_4$**. Still attempting to characterize compound **2-c** we turned to an alternative procedure, which was also previously employed within our group.[16a] Therefore we protonated compound **2** with the strong Brønsted acid $[H(OEt_2)_2][B(C_6F_5)_4]$[15] to obtain the protonated intermediate **4**. Upon heating of the isolated compound **4**, melting but no hydrogen evolution could be observed. NMR-spectroscopy of the melt confirmed decomposition of compound **4** had taken place (Scheme 5). Since we were currently not able to move forward with the approach of increasing the Lewis acidity at silicon in this way, we turned to the introduction of other electron-withdrawing groups. Inoue and colleagues have recently published a new method for increasing Lewis acidity at silicon.[17] This involves introducing an oxygen bridge between the perfluorinated aryl groups e.g. pentafluorophenyl [-C_6F_5] and the silicon center, which is understood to

increase the Lewis acidity at silicon. The objective was to achieve a sufficient increase in Lewis acidity by replacing the pentafluorophenyl groups [-C_6F_5] in compound **2** with pentafluorophenoxy groups [-OC_6F_5]. Initially, an attempt was made to synthesize the compound via the same route used for the synthesis of compound **2** (Scheme 3). However, it became evident that the protodesilylation of compound **5** was not selective, necessitating the adoption of an alternative synthesis route (Scheme 6).

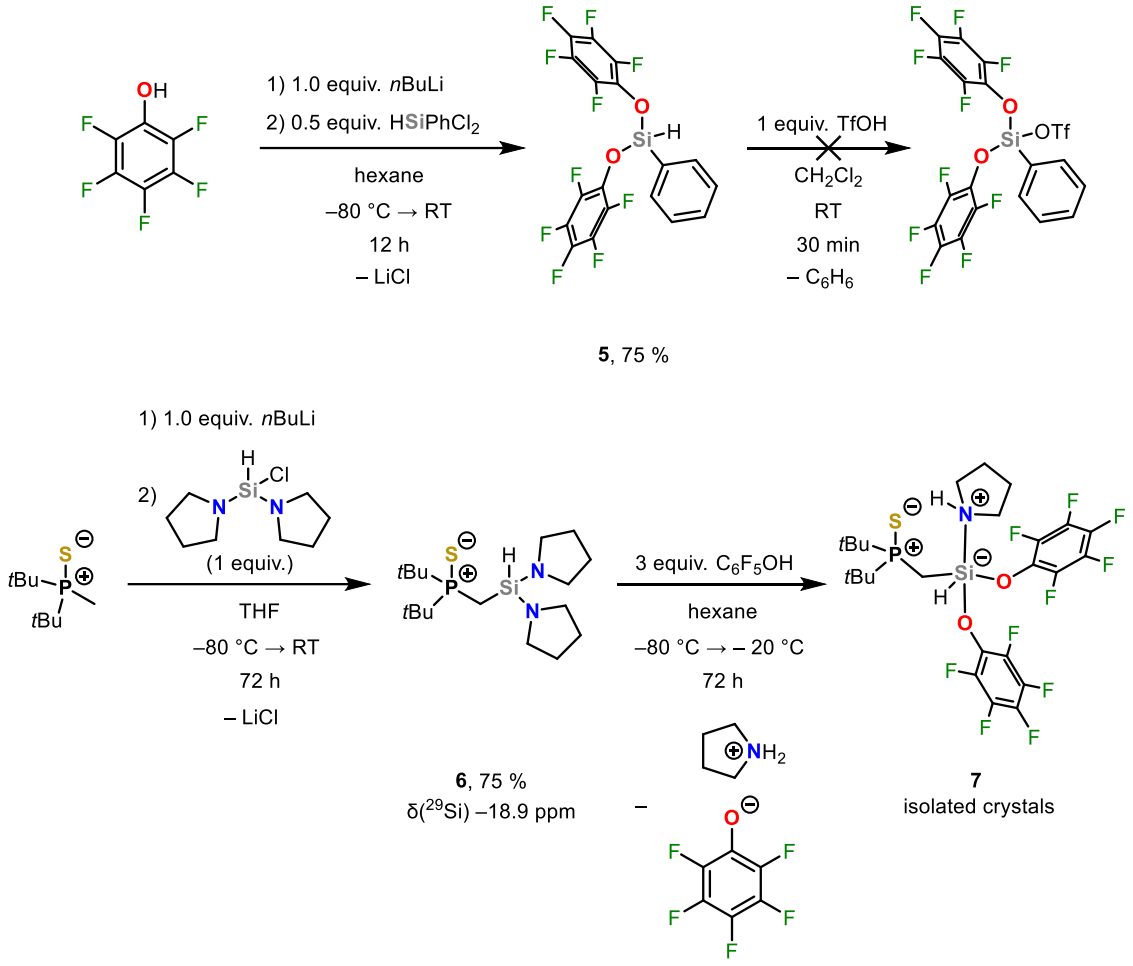

Scheme 6: Unsuccessful protodesilylation of compound **5** and synthesis of compound **7**.

In the first step compound **6** was prepared in satisfactory yield from the reaction of ((di-*tert*-butylphosphorothioyl)methyl)lithium and dipyrrolidine(chloro)silane. The reaction of compound **6** with two equivalents of the moderately Brønsted acidic pentafluorophenol resulted in the formation of compound **7**. Compound **7** was obtained as crystalline material which was suitable for single-crystal X-ray diffraction analysis, confirming the structure of compound **7** (Scheme 6) (Figure 2). Both compounds **6** and **7** crystallized in the monoclinic crystal system with the space group *C*2/*c* for **6** and $P2_1/n$. Compound **7** was crystallized at –80°C from *n*hexane and features a trigonal-bipyramidal pentacoordinated silicon atom with two pentafluorophenoxy [-OC_6F_5] groups in the axial and equatorial position. The hydridic Si–H function is located in the equatorial position. The protic N–H function is stabilized *via* an intramolecular hydrogen bond by the Lewis basic P^+–S^- moiety. This substitution pattern is highly unusual as anionic pentacoordinate silicon hydrides are generally highly reducing in nature and only a handful of literature examples are known.[18]

The main reason for their high tendency for reduction reactions is the low hydride affinity of the corresponding neutral silanes, which are among the lowest known for neutral molecules akin to benzene.[19] This results in anionic pentacoordinate silicon hydrides being able to transform C_{sp2}–F bonds to C_{sp2}–H bonds.[20] Therefore it is even more surprising to observe the presence of a Si–H bond in an anionic pentacoordinate silane in the direct vicinity of a protic N–H bond in compound **7**.

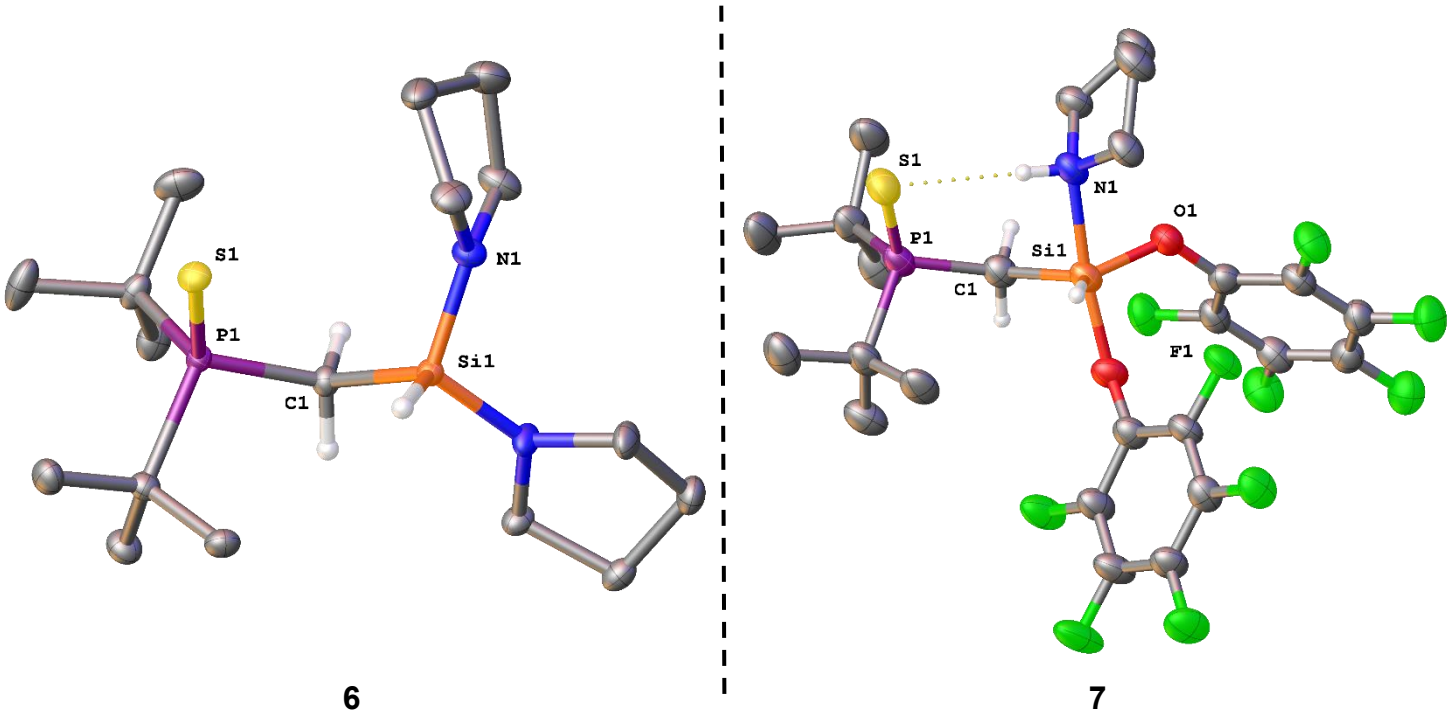

Figure 2: Molecular structures of compounds **6** and **7** in the crystal (displacement ellipsoids set at the 50 % probability level). Selected bond lengths (Å) and angles (°) of **6**: P(1)–S(1) 1.9700(5), P(1)–C(1) 1.8144(16), Si(1)–N(1) 1.7033(13), Si(1)–C(1)–P(1) 117.15(9), S(1)–P(1)–C(1) 113.06(5), C(1)–Si(1)–N(1) 113.65(7). **7**: P(1)–S(1) 1.9766(13), Si(1)–O(1) 1.702(2), Si(1)–N(1) 1.986(3), Si(1)–C(1)–P(1) 125.25(18), N(1)–Si(1)–O(1) 83.31(12), N(1)–Si(1)–O(2) 173.18(11).

To the best of our knowledge this is the only example of an intramolecular anionic pentacoordinate silicon hydride featuring a cationic protic N–H moiety. The only similar compound with a anionic pentacoordinate silicon hydride bond in the vicinity of a cationic N–H bond is a intermolecular example published by Greb *et al*. and is shown in Scheme 1.[11] The Si–N bond in compound **7** is elongated [1.9766(13) Å] compared to the starting material **6** [1.7033(13)]. The increased steric bulk in **7** results in a wider Si(1)–C(1)–P(1) angle [125.25(18) °] compared to **6** [117.15(9) °]. The N(1)–Si(1)–O(2) angle in **7** [173.18(11)] deviates slightly from its ideal 180 ° angle, presumably due to steric clash with the sterically demanding di-*tert*-butylphosphinesulfide moiety. The Si(1)–O(1) bond length [1.702(2) Å] is shortened compared to the Si(1)–O(2) bond length [1.774(2) Å] due to it being in the equatorial position and therefore having a higher s-character. Upon dissolution of crystals of compound **7** in C_6D_6 and subsequent NMR spectroscopy in a sealed J-Young-type NMR tube, three distinct sets of signals were observed (Figure 3). Its important to note that this experiment was conducted with crystals from different batches and at different stages of recrystallisation. The resulting recorded ^{1}H NMR spectra were consistently identical. Therefore, impurities are unlikely to be the source of the other signal sets observed in Figure 3. The most likely explanation for the observed results is a dynamic

behavior of the Si–N bond of compound **7** in solution. Further suggesting the dynamic behavior is the elongated Si(1)–N(1) bond length [1.9766(13) Å] in compound **7**, which indicates a weak bond and is known for dative Si←N bonds.[21] Transient coordination of Lewis bases onto silanes are known and have been used in the past to enhance the reactivity by increasing the positive polarization of the silicon atom.[22] The equilibrium between the pentacoordinated compound **7** and its tetracoordinated parent compound **7b** proposed in Figure 3 can be used to clearly assign all three signal sets within the ^{1}H NMR spectrum of compound **7** (Full assignment in experimental part). Further supporting the correct assignment of the signals in regard to the proposed equilibrium is the observation, that the –CH_2 and *tert*-butyl signals of compound **7** are diastereotopic (red triangle) which we expect from the pentacoordinated state, whereas the –CH_2 and *tert*-butyl signals of compound **7b** are not (black circle).

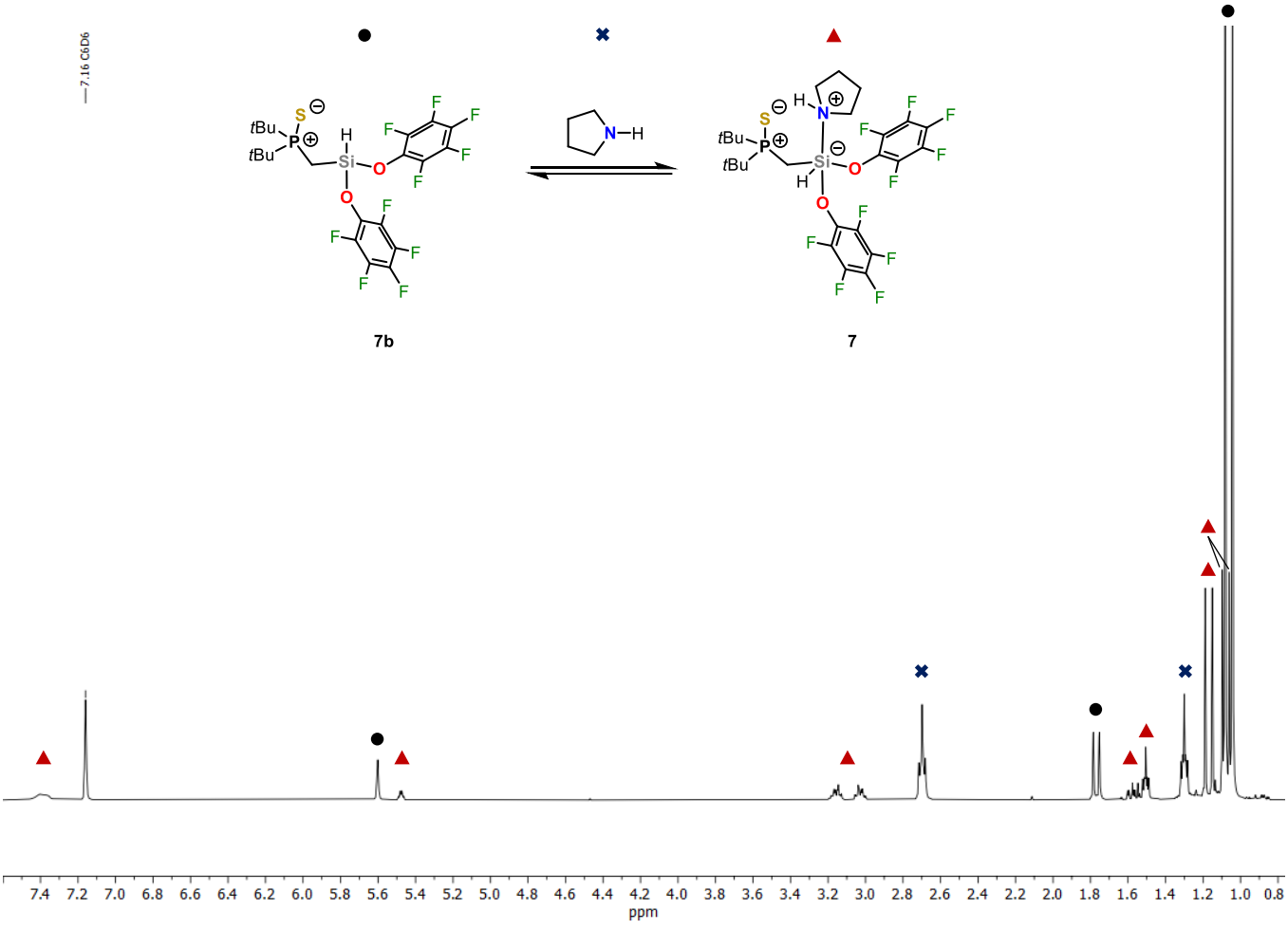

Figure 3: ^{1}H-NMR spectrum of the dissolved crystals of **7** with the proposed equilibrium and the assignment of signals.

Our initial objective of replacing the pentafluorophenyl [–C_6F_5] groups with more electron withdrawing pentafluorophenoxy [–OC_6F_5] groups was therefore very successful in increasing the Lewis acidity of the silicon center. The Lewis acidity of the silicon center is well balanced and might prove beneficial for the purpose of using compound **7** as a catalytic species as it allows Lewis basic moieties, like pyrrolidine, to reversibly coordinate (see Scheme 2 for catalytic cycle). However, the equilibrium between compounds **7** and

7b was found to be not indefinitely stable (Figure 4). Upon dissolution of crystals of compound **7** in C_6D_6 and subsequent storage in a closed J-Young type NMR tube for a period of two weeks at room temperature in the dark, new signals were observed within the ^{1}H-NMR spectrum (Figure 4). A new set of non-diastereotopic [–CH_2] pyrrolidine signals appear at 1.45 ppm and 3.2 ppm, as well as a new [–CH_2] duplet at 1.85 ppm and a new *tert*-butyl duplet at 1.1 ppm. These signals collectively indicate the formation of a tetravalent silane with an intact (C_4H_8N)Si–CH_2–P(*t*Bu)$_2$ framework (**8**). However, the most significant insight is derived from the observation that the newly formed compound is missing a Si–H and N–H signal, while another new singlet at 4.47 ppm could be identified as H_2.[23] The results strongly suggest that a dehydrogenative reaction pathway is operative in the formation of the new product (**8**). In light of the previously mentioned highly reductive properties of anionic pentacoordinate silicon hydrides, it seems plausible to suggest that a dehydrogenative pathway towards compound **8** can be formulated by loss of H_2 from compound **7** (Figure 4). Furthermore, the total integration of the Si–H signals in Figure 3 yields a ratio of 72:28 (**7b**:**7**). This ratio remains nearly unchanged after two weeks at room temperature when the formation of compound **8** occurs [71:29 (**7b**:**7**)] (Figure 4). This shows that, although compound **7** is continuously consumed in the formation of compound **8**, the ratio of **7b** to **7** remains constant. This further supports the existence of an equilibrium between compounds **7** and **7b** in solution.

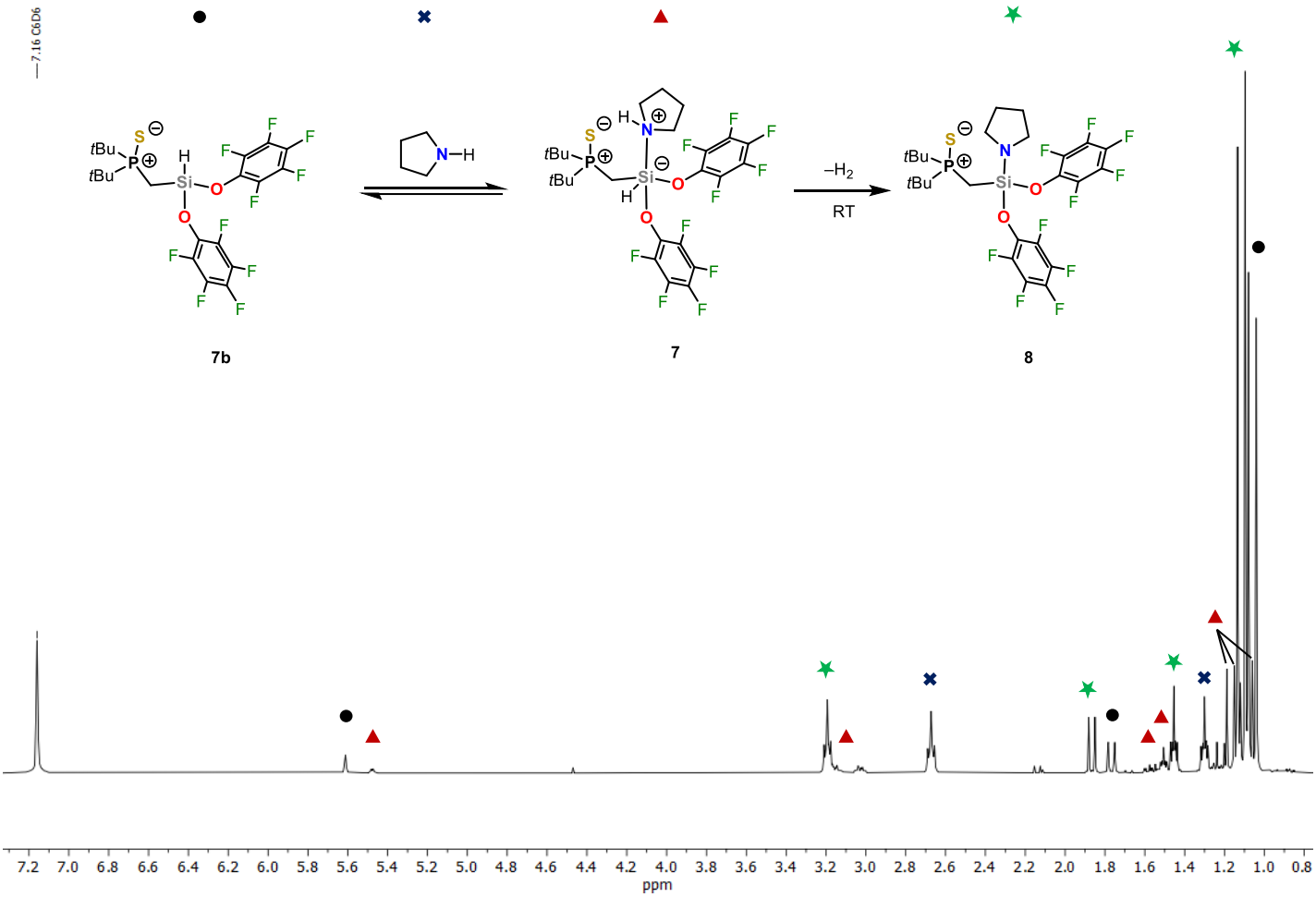

Figure 4: ^{1}H-NMR spectrum of the dissolved crystals of **7** after 2 weeks at room temperature with the proposed reaction product **8** and assignment of signals.

Given the overwhelming evidence for an equilibrium between compounds **7** and **7b**, we were curious to determine whether an equilibrium between compounds **8** and **7** would also be present. Since the only other compound where a protic N–H bond was stable in the presence of an anionic pentacoordinate hydrosilicate, was the product of a heterolytic cleavage of dihydrogen, this hypothesis appeared reasonable (Scheme 1).[11] However, pressurization of the J-Young NMR tube with dihydrogen did not result in a shift of the equilibrium (Figure 5, spectrum 4). Subsequent heating merely facilitated the formation of more compound **8** (Figure 5, spectrum 5). Indeed, upon prolonged observation, the reaction proceeded to yield a complete and almost uncontaminated formation of only compound **8** (Figure 5, spectra 1–5). Once more, the integration of the Si–H signals from compounds **7** and **7b** remained constant throughout the ^{1}H-NMR spectra (Figure 5, spectra 1–5).

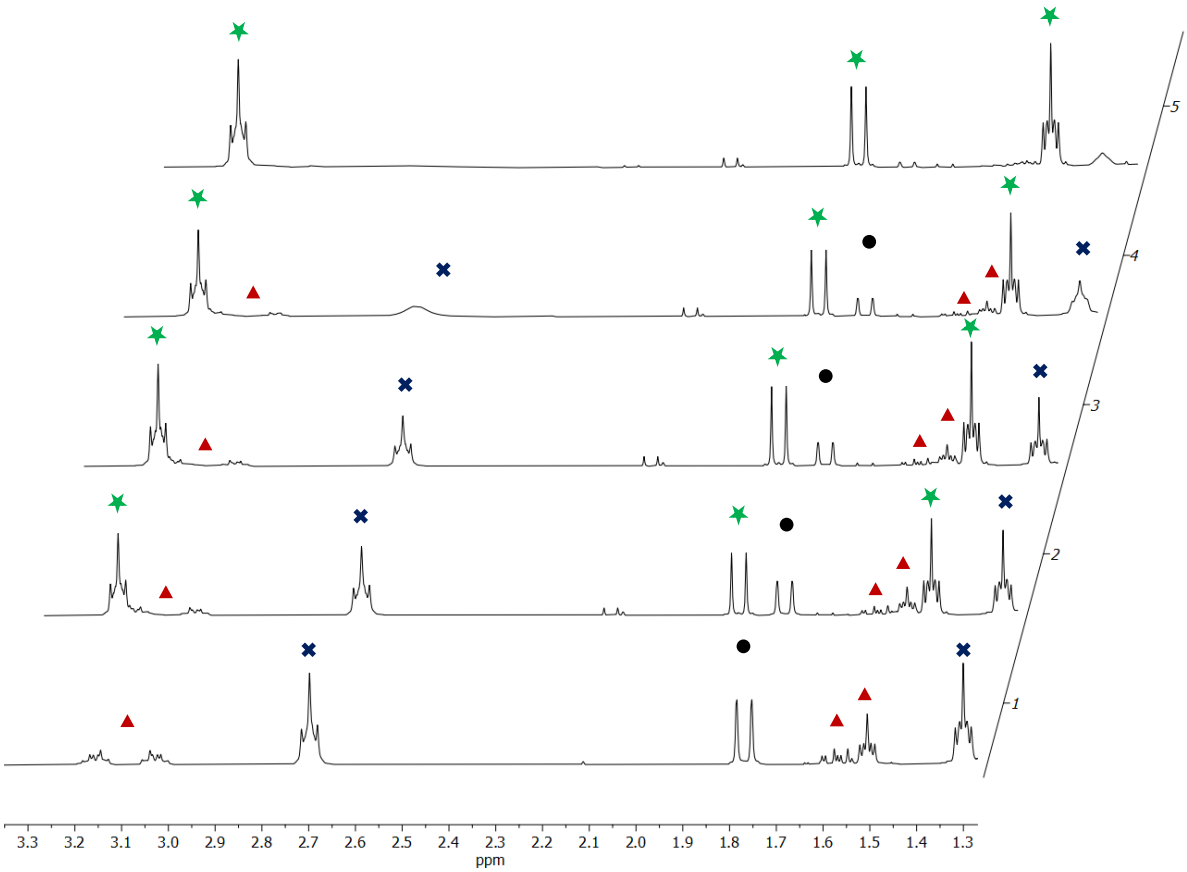

Figure 5: Cut out of the timeline of ^{1}H-NMRs of compound **7** from 1.2 ppm – 3.3 ppm. 1: ^{1}H-NMR of freshly dissolved crystals of **7**. 2: ^{1}H-NMR after 2 weeks at room temperature. 3: ^{1}H-NMR after 7h at 60°C. 4: ^{1}H-NMR after addition of 50 psi of H_2 pressure and 24 h at room temperature. 5: ^{1}H-NMR after heating to 80°C for 12 h with 50 psi of H_2 pressure.

Having demonstrated, that the Lewis acidity at silicon indeed increased from pentafluorophenyl [–C_6F_5] substituted compound **2** to pentafluorophenoxy [–OC_6F_5] substituted compound **7** we were curious to what extent the modification with tetrafluorocatcheol [–$O_2C_6F_4$] groups would impact the Lewis acidity at silicon. To introduce the desired tetrafluorocatechol [–$O_2C_6F_4$] groups, we could conveniently begin with the previously utilized compound **6** and react it with one equivalent of the commercially available tetrafluoro(phenyl)diol (Scheme 7). However, to our surprise, we did not obtain the desired monosubstituted product **9-H**, but rather the disubstituted product **9**, with

immediate loss of dihydrogen. Despite repeated attempts using various solvents and temperatures, the only products observed were compound **9** and the evolution of dihydrogen. In a related experiment, we attempted to react compound **3** with one equivalent of tetrafluoro(phenyl)diol to obtain the monosubstituted product **9-H**, however no reaction was observed in this instance (Scheme 7).

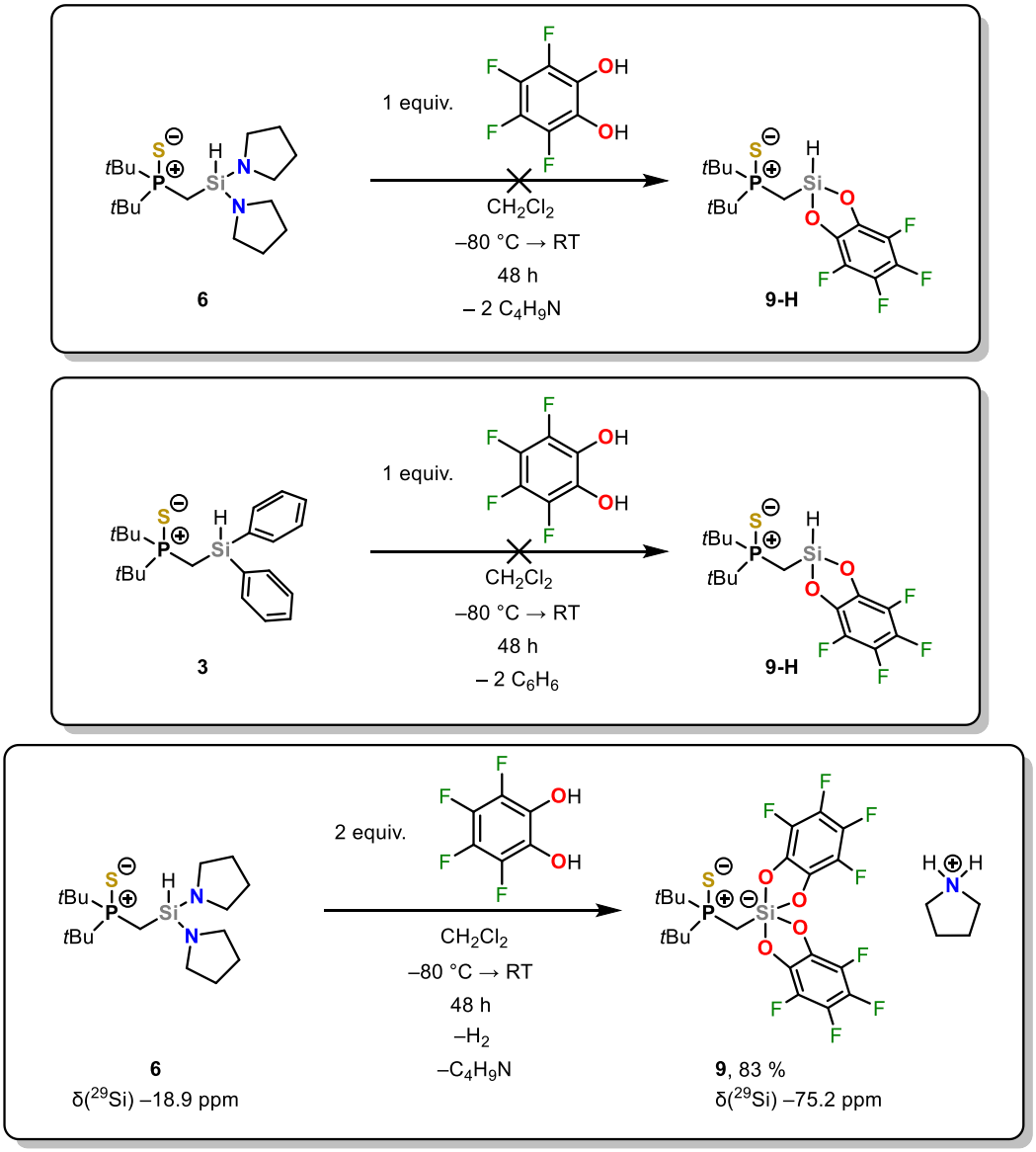

Scheme 7: Optimized synthesis of compound **9** and various approaches to the desired compound **9-H**.

After optimization of the synthesis of compound **9**, a yield of 83% was achieved by using two equivalents of tetrafluorocatechol in place of one (Scheme 7). The upfield shift of the ^{29}Si-NMR signal is indicative of the transition from a tetravalent silicon state in compound **6** [δ(^{29}Si) = –18.9 ppm] to a pentacoordinate state in compound **9** [δ(^{29}Si) = –75.2 ppm]. At present, it is not possible to obtain the desired monosubstituted hydridosilane **9-H**. Therefore, the reactivity of compound **9** towards dihydrogen and CO_2 was tested. Fortunately, the ability of compound **9** to act as a frustrated Lewis pair is not negated by the formation of a pentacoordinate silicon state. The silicon center is actually more

positively polarized in the pentacoordinate state and can therefore still act as a potent Lewis acid.[24] Therefore the silicon atom can accommodate another ligand to form the hexacoordinate state (Scheme 8).[24] However, in the case of compound **9**, no reactivity with dihydrogen was observed, and in the case of CO_2 the multiple reaction products were not defined and could not be characterized (Scheme 8).

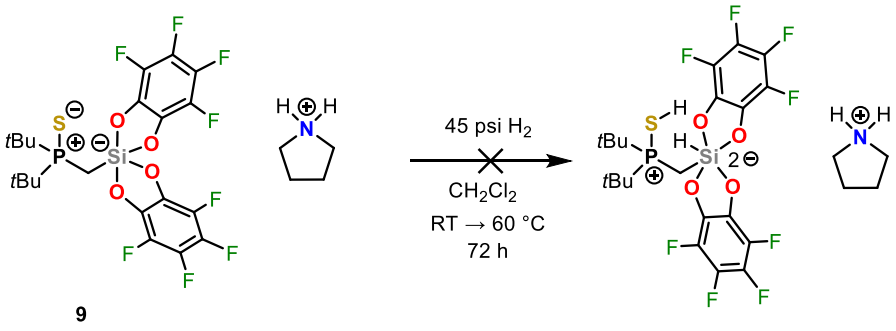

Scheme 8: Unsuccessful dihydrogen activation with compound **9**.

Compound **9** crystallized in the triclinic crystal system with the space group $P\bar{1}$ (Figure 6).

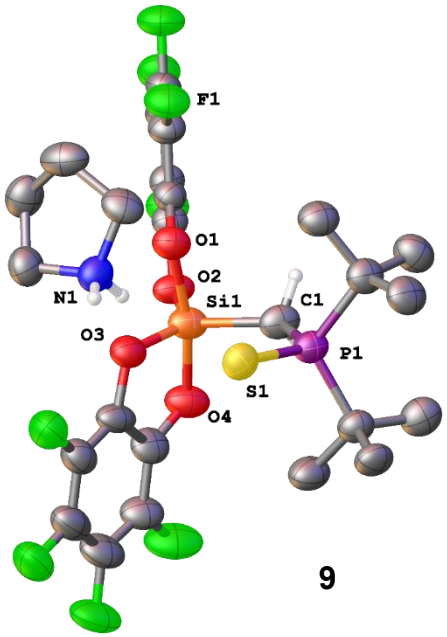

Figure 6: Molecular structures of compound **9** in the crystal (displacement ellipsoids set at the 50 % probability level). Selected bond lengths (Å) and angles (°) of **9**: P(1)–S(1) 1.988(2), Si(1)–O(1) 1.805(4), Si(1)–C(1) 1.891(7), Si(1)–C(1)–P(1) 121.4(4), O(1)–Si(1)–O(3) 84.7(2), C(1)–P(1)–S(1) 114.4(2).

Compound **9** exhibits a slightly distorted trigonal-bipyramidal coordination mode. This is rather interesting, since catechol-substituents at pentacoordinate silicon especially those with strongly electron withdrawing properties usually adopt a square-pyramid as the preferred structure.[9b,10,11] The apical Si(1)–O(1) bond length [1.805(4) Å] in compound **9** is slightly elongated compared to the apical Si(1)–O(1) bond length [1.774(2) Å] in compound **7**. The P(1)–S(1) bond length [1.988(2) Å] is nearly identical to that of the

starting material **6** [1.9700(5) Å], indicating that the donating P^+–S^- moiety does not interact with the silicon center to form a hexacoordinate silicon atom. Furthermore, the P^+–S^- donor moiety is twisted to lie in the equatorial plane, likely due to steric repulsion between the tetrafluoro(phenyl)diol [$–O_2C_6F_4$] moieties and the di-*tert*-butyl groups. Also interesting is, that the pyrrolidinium cation in compound **9** shows no hydrogen bonding with the Lewis basic P^+–S^- moiety contrary to compound **7** where this interaction was observed.

5.4 Conclusion

In conclusion, several novel silanes attached with substituents of different electron-withdrawing abilities, all of which possess a P^+–S^- donor moiety, have been synthesized and characterized. While the pentafluorophenyl [-C_6F_5]-substituted silane **2** did not show the desired Lewis acidic properties, we were successful in enhancing the Lewis acidity at silicon by the introduction of an oxygen bridge, resulting in the pentafluorophenoxy [-OC_6F_5]-substituted silane **7**. Compound **7** represents an unusual pentacoordinate silicon compound bearing a highly hydridic Si–H moiety in close proximity to a protic N–H moiety. Thorough NMR spectroscopic investigations showed that compound **7** is in equilibrium with the tetravalent silane **7b** in solution. Moreover, it was confirmed that compound **7** is not stable for a prolonged amount of time and undergoes a slow reaction with release of dihydrogen to form compound **8**. Our attempts in increasing the Lewis acidity at silicon further through the introduction of tetrafluorocatechol [-$O_2C_6F_4$] groups did not result in the formation of the desired monosubstituted compound **9-H**. Instead, an immediate release of dihydrogen occurred, giving rise to the disubstituted compound **9**. It is likely, that the tetrafluorocatechol [-$O_2C_6F_4$] groups favor the formation of the pentacoordinate state of silicon so much that the tetravalent precursor **9-H** is unstable. In conclusion, these results demonstrate the pivotal impact of diverse electron-withdrawing substituents on the Lewis acidity and stability of Si–H moieties at silicon. Further experiments concerning the reversibility of the dehydrogenative reaction of compound **7** to **8** are currently underway with the objective of elucidating new insights into this unusual compound.

5.5 References

(1) Falk, A.; Bauer, J. O. Structural and Electronic Effects on Phosphine Chalcogenide Stabilized Silicon Centers in Four-Membered Heterocyclic Cations. *Inorg. Chem.* **2022**, *61*, 15576–15588.

(2) (a) Chase, P. A.; Stephan, D. W. Hydrogen and amine activation by a frustrated Lewis pair of a bulky N-heterocyclic carbene and $B(C_6F_5)_3$. *Angew. Chem. Int. Ed.* **2008**, *47*, 7433–7437. (b) Geier, S. J.; Chase, P. A.; Stephan, D. W. Metal-free reductions of N-heterocycles via Lewis acid catalyzed hydrogenation. *Chem. Commun.* **2010**, *46*, 4884–4886. (c) Ramos, A.; Lough, A. J.; Stephan, D. W. Activation of H_2 by frustrated Lewis pairs derived from mono- and bis-phosphinoferrocenes and $B(C_6F_5)_3$. *Chem. Commun.* **2009**, 1118–1120. (d) Spies, P.; Erker, G.; Kehr, G.; Bergander, K.; Fröhlich, R.; Grimme, S.; Stephan, D. W. Rapid intramolecular heterolytic dihydrogen activation by a four-membered heterocyclic phosphane-borane adduct. *Chem. Commun.* **2007**, 5072–5074. (e) Stephan, D. W. Frustrated Lewis pairs: A new strategy to small molecule activation and hydrogenation catalysis. *Dalton Trans.* **2009**, 3129–3136.

(3) Stephan, D. W. Frustrated Lewis pairs: From concept to catalysis. *Acc. Chem. Res.* **2015**, *48*, 306–316.

(4) (a) Reißmann, M.; Schäfer, A.; Jung, S.; Müller, T. Silylium Ion/Phosphane Lewis Pairs. *Organometallics* **2013**, *32*, 6736–6744. (b) Schäfer, A.; Reissmann, M.; Schäfer, A.; Saak, W.; Haase, D.; Müller, T. A new synthesis of triarylsilylium ions and their application in dihydrogen activation. *Angew. Chem. Int. Ed.* **2011**, *50*, 12636–12638.

(5) (a) Liberman-Martin, A. L.; Bergman, R. G.; Tilley, T. D. Lewis Acidity of Bis(perfluorocatecholato)silane: Aldehyde Hydrosilylation Catalyzed by a Neutral Silicon Compound. *J. Am. Chem. Soc.* **2015**, *137*, 5328–5331. (b) Bader, J.; Maier, A. F. G.; Paradies, J.; Hoge, B. Perfluoroalkylated Main-Group Element Lewis Acids as Catalysts in Transfer Hydrogenation. *Eur. J. Inorg. Chem.* **2017**, *2017*, 3053–3056. (c) Maskey, R.; Schädler, M.; Legler, C.; Greb, L. Bis(perchlorocatecholato)silane-A Neutral Silicon Lewis Super Acid. *Angew. Chem. Int. Ed.* **2018**, *57*, 1717–1720. (d) Thorwart, T.; Greb, L. Reversible C–H bond silylation with a neutral silicon Lewis acid. *Chem. Sci.* **2023**, *14*, 11237–11242.

(6) Waerder, B.; Pieper, M.; Körte, L. A.; Kinder, T. A.; Mix, A.; Neumann, B.; Stammler, H.-G.; Mitzel, N. W. A Neutral Silicon/Phosphorus Frustrated Lewis Pair. *Angew. Chem. Int. Ed.* **2015**, *54*, 13416–13419.

(7) (a) Erdmann, P.; Greb, L. What Distinguishes the Strength and the Effect of a Lewis Acid: Analysis of the Gutmann-Beckett Method. *Angew. Chem. Int. Ed.* **2022**, *61*, e202114550. (b) Greb, L. Lewis Superacids: Classifications, Candidates, and Applications. *Chem. Eur. J.* **2018**, *24*, 17881–17896.

(8) (a) Myers, A. G.; Kephart, S. E.; Chen, H. Silicon-directed aldol reactions. Rate acceleration by small rings. *J. Am. Chem. Soc.* **1992**, *114*, 7922–7923. (b) Matsumoto, K.; Oshima, K.; Utimoto, K. Noncatalyzed Stereoselective Allylation of Carbonyl Compounds with Allylsilacyclobutanes. *J. Org. Chem.* **1994**, *59*, 7152–7155. (c) Kinnaird, J. W. A.; Ng, P. Y.; Kubota, K.; Wang, X.; Leighton, J. L. Strained silacycles in organic synthesis: A new reagent for the enantioselective allylation of aldehydes. *J. Am. Chem. Soc.* **2002**, *124*, 7920–7921. (d) Zhang, X.; Houk, K. N.; Leighton, J. L. Origins of stereoselectivity in strain-release allylations. *Angew. Chem. Int. Ed.* **2005**, *44*, 938–941. (e) Hrdina, R.; Müller, C. E.; Wende, R. C.; Lippert, K. M.; Benassi, M.; Spengler, B.; Schreiner, P. R. Silicon-(thio)urea Lewis acid catalysis. *J. Am. Chem. Soc.* **2011**, *133*, 7624–7627. (f) Chalifoux, W. A.; Reznik, S. K.; Leighton, J. L. Direct and highly regioselective and enantioselective allylation of β-diketones. *Nature* **2012**, *487*, 86–89.

(9) (a) Tacke, R.; Heermann, J.; Pülm, M.; Gottfried, E. A Zwitterionic λ^5Si-Silicate with an Almost Ideal Square-Pyramidal Si Coordination Polyhedron: Synthesis and Crystal Structure Analysis.

Monatshefte für Chemie **1999**, *130*, 99–107. (b) Hartmann, D.; Schädler, M.; Greb, L. Bis(catecholato)silanes: assessing, rationalizing and increasing silicon's Lewis superacidity. *Chem. Sci.* **2019**, *10*, 7379–7388.

(10) Dettlaff-Weglikowska, U.; Hey-Hawkins, E.; Schnering, H. G. von Einfluß des Kations auf die Struktur des $[Si(O_2C_6H_4)_2F]^-$-Anions: Struktur von $[K(18\text{-Krone-6})][Si(O_2C_6H_4)_2F]$. *Zeitschrift für Naturforschung B* **1991**, *46*, 609–614.

(11) Thorwart, T.; Hartmann, D.; Greb, L. Dihydrogen Activation with a Neutral, Intermolecular Silicon(IV)-Amine Frustrated Lewis Pair. *Chem. Eur. J.* **2022**, *28*, e202202273.

(12) (a) Frohn, H. J.; Giesen, M.; Klose, A.; Lewin, A.; Bardin, V. V. A convenient preparation of pentafluorophenyl(fluoro)silanes: reactivity of pentafluorophenyltrifluorosilane. *J. Organomet. Chem.* **1996**, *506*, 155–164. (b) Dilman, A. D.; Levin, V. V.; Korlyukov, A. A.; Belyakov, P. A.; Struchkova, M. I.; Antipin, M. Y.; Tartakovsky, V. A. Complexation of tris(pentafluorophenyl)silanes with neutral Lewis bases. *J. Organomet. Chem.* **2008**, *693*, 1005–1019. (c) Dilman, A. D.; Levin, V. V.; Karni, M.; Apeloig, Y. Activation of pentafluorophenylsilanes by weak Lewis bases in reaction with iminium cations. *J. Org. Chem.* **2006**, *71*, 7214–7223.

(13) Fearon, F.W.G.; Gilman, H. Polyhalo-organometallic and -organometalloidal compounds. *J. Organomet. Chem.* **1967**, *10*, 409–419.

(14) (a) Uhlig, W. Silyl Triflates – Valuable Synthetic Materials in Organosilicon Chemistry. *Chem. Ber.* **1996**, *129*, 733–739. (b) Emde, H.; Domsch, D.; Feger, H.; Frick, U.; Götz, A.; Hergott, H. H.; Hofmann, K.; Kober, W.; Krägeloh, K.; Oesterle, T. et al. Trialkylsilyl Perfluoroalkanesulfonates: Highly Reactive Silylating Agents and Lewis Acids in Organic Synthesis. *Synthesis* **1982**, *1982*, 1–26. (c) Levin, V. V.; Dilman, A. D.; Belyakov, P. A.; Korlyukov, A. A.; Struchkova, M. I.; Tartakovsky, V. A. Tris(pentafluorophenyl)silyl Triflate: Synthesis and Silylation of Carbonyl Compounds. *Eur. J. Org. Chem.* **2004**, *2004*, 5141–5148.

(15) Jutzi, P.; Müller, C.; Stammler, A.; Stammler, H.-G. Synthesis, Crystal Structure, and Application of the Oxonium Acid $[H(OEt_2)_2][B(C_6F_5)_4]$ -. *Organometallics* **2000**, *19*, 1442–1444.

(16) (a) Fontana, N.; Espinosa-Jalapa, N. A.; Seidl, M.; Bauer, J. O. Easy Access to Enantiomerically Pure Heterocyclic Silicon-Chiral Phosphonium Cations and the Matched/Mismatched Case of Dihydrogen Release. *Chem. Eur. J.* **2021**, *27*, 2649–2653. (b) Fontana, N.; Espinosa-Jalapa, N. A.; Seidl, M.; Bauer, J. O. Hidden silylium-type reactivity of a siloxane-based phosphonium-hydroborate ion pair. *Chem. Commun.* **2022**, *58*, 2144–2147.

(17) Tschernuth, F. S.; Bichlmaier, L.; Stigler, S.; Inoue, S. Tuning the Lewis Acidity of Neutral Silanes Using Perfluorinated Aryl- and Alkoxy Substituents. *Eur. J. Inorg. Chem.* **2023**, *26*, e202300388.

(18) (a) Bearpark, M. J.; McGrady, G. S.; Prince, P. D.; Steed, J. W. The first structurally characterized hypervalent silicon hydride: Unexpected molecular geometry and Si–H···K interactions. *J. Am. Chem. Soc.* **2001**, *123*, 7736–7737. (b) Prince, P. D.; Bearpark, M. J.; McGrady, G. S.; Steed, J. W. Hypervalent hydridosilicates: Synthesis, structure and hydride bridging. *Dalton Trans.* **2008**, 271–282. (c) Schuhknecht, D.; Leich, V.; Spaniol, T. P.; Okuda, J. Hypervalent Hydrosilicates Connected to Light Alkali Metal Amides: Synthesis, Structure, and Hydrosilylation Catalysis. *Chem. Eur. J.* **2018**, *24*, 13424–13427. (d) Ebner, F.; Greb, L. Calix[4]pyrrole Hydridosilicate: The Elusive Planar Tetracoordinate Silicon Imparts Striking Stability to Its Anionic Silicon Hydride. *J. Am. Chem. Soc.* **2018**, *140*, 17409–17412.

(19) (a) Windus, T. L.; Gordon, M. S.; Davis, L. P.; Burggraf, L. W. Theoretical Study of Pseudorotation of Pentacoordinated Silicon Anions: $SiH_{5-n}X_n^-$ (X = F, Cl). *J. Am. Chem. Soc.* **1994**, *116*, 3568–3579. (b) Hajdasz, D. J.; Squires, R. R. Hypervalent silicon hydrides: $(SiH_5)^-$. *J. Am.*

Chem. Soc. **1986**, *108*, 3139–3140. (c) Hajdasz, D. J.; Ho, Y.; Squires, R. R. Gas-Phase Chemistry of Pentacoordinate Silicon Hydride Ions. *J. Am. Chem. Soc.* **1994**, *116*, 10751–10760. (d) Damrauer, R.; Hankin, J. A. Chemistry and Thermochemistry of Silicon-Containing Anions in the Gas Phase. *Chem. Rev.* **1995**, *95*, 1137–1160.

(20) Kikushima, K.; Grellier, M.; Ohashi, M.; Ogoshi, S. Transition-Metal-Free Catalytic Hydrodefluorination of Polyfluoroarenes by Concerted Nucleophilic Aromatic Substitution with a Hydrosilicate. *Angew. Chem. Int. Ed.* **2017**, *56*, 16191–16196.

(21) (a) Carre, F. H.; Corriu, R. J. P.; Lanneau, G. F.; Yu, Z. Intramolecular coordination at silicon. The small effect of equatorial ligands on the stability of pentacoordinated organosilanes. *Organometallics* **1991**, *10*, 1236–1243. (b) Crystal Structure and Unambiguous Assignment of Two Ligand Exchange Barriers in Neutral Pentacoordinate Silicon Complexes: Correlation of ^{29}Si and ^{15}N Chemical Shifts and Si–N Cleavage Barriers. *Organometallics* **1996**, *15*, 5073–5076.

(22) (a) Yoshida, T.; Ilies, L.; Nakamura, E. Silylation of Aryl Halides with Monoorganosilanes Activated by Lithium Alkoxide. *Org. Lett.* **2018**, *20*, 2844–2847. (b) Kira, M.; Sato, K.; Sakurai, H. Reduction of carbonyl compounds with pentacoordinate hydridosilicates. *J. Org. Chem.* **1987**, *52*, 948–949. (c) Hosomi, A.; Hayashida, H.; Kohra, S.; Tominaga, Y. Pentacoordinate silicon compounds in synthesis: Chemo- and stereo-selective reduction of carbonyl compounds using trialkoxy-substituted silanes and alkali metal alkoxides. *J. Chem. Soc., Chem. Commun.* **1986**, 1411. (d) Schiffers, R.; Kagan, H. B. Asymmetric Catalytic Reduction of Ketones with Hypervalent Trialkoxysilanes. *Synlett* **1997**, *10*, 1175–1178. (e) Kobayashi, S.; Yasuda, M.; Hachiya, I. Trichlorosilane-Dimethylformamide (Cl_3SiH-DMF) as an Efficient Reducing Agent. Reduction of Aldehydes and Imines and Reductive Amination of Aldehydes under Mild Conditions Using Hypervalent Hydridosilicates. *Chem. Lett.* **1996**, *25*, 407–408.

(23) (a) Gottlieb, H. E.; Kotlyar, V.; Nudelman, A. NMR Chemical Shifts of Common Laboratory Solvents as Trace Impurities. *J. Org. Chem.* **1997**, *62*, 7512–7515. (b) Fulmer, G. R.; Miller, A. J. M.; Sherden, N. H.; Gottlieb, H. E.; Nudelman, A.; Stoltz, B. M.; Bercaw, J. E.; Goldberg, K. I. NMR Chemical Shifts of Trace Impurities: Common Laboratory Solvents, Organics, and Gases in Deuterated Solvents Relevant to the Organometallic Chemist. *Organometallics* **2010**, *29*, 2176–2179.

(24) (a) Z. Rappoport, Y. Apeloig (Eds.) *The chemistry of organic silicon compounds: The chemistry of functional groups*, *Vol. 2*, Wiley, Chichester, **1998**. (b) Denmark, S. E.; Beutner, G. L.; Wynn, T.; Eastgate, M. D. Lewis base activation of Lewis acids: Catalytic, enantioselective addition of silyl ketene acetals to aldehydes. *J. Am. Chem. Soc.* **2005**, *127*, 3774–3789. (c) Hartmann, D.; Braner, S.; Greb, L. Bis(perchlorocatecholato)silane and heteroleptic bidonors: Hidden frustrated Lewis pairs resulting from ring strain. *Chem. Commun.* **2021**, *57*, 8572–8575.

5.6 Synthesis and Characterizations

5.6.1 General remarks

All experiments were performed in an inert atmosphere of purified nitrogen by using standard Schlenk techniques or an MBraun Unilab 1200/780 glovebox. Glassware was heated at 600 °C prior to use. Dichloromethane (DCM), hexane, pentane, tetrahydrofuran (THF), and toluene were dried and de-gassed with an MBraun SP800 solvent purification system. *n*-Butyllithium (2.5 M or 1.6 M solution in hexane, Merck KGaA), di-*tert*-butylmethylphosphine (97%, Merck KGaA), sulfur (99%, Merck KGaA), diphenyl(chloro)silane (90%, Merck KGaA), dichloro(phenyl)silane (≥98%, Merck KGaA), trichlorosilane (99%, Merck KGaA), trifluoromethanesulfonic acid (≥99%, Merck KGaA), bromopentafluorobenzene (99%, Merck KGaA), pentafluorophenol (≥99%, Merck KGaA) and 3,4,5,6-tetrafluorobenzene-1,2-diol (97%, Merck KGaA) were used as received without further purification. Pyrrolidine (99%, Merck KGaA) was freshly distilled over sodium metal before use. Di-*tert*-butylmethylphosphine sulfide[1], di-pentafluorophenyl(phenyl)silane[2] and $[H(OEt_2)_2][B(C_6F_5)_4]$[3] were synthesized according to reported literature procedures. C_6D_6 and CD_2Cl_2 used for NMR spectroscopy were dried over 3 Å molecular sieves and degassed by a standard freeze-pump-thaw procedure. NMR spectra were either recorded on a Bruker Avance 300 (300.13 MHz), a Bruker Avance 400 (400.13 MHz) or on a Bruker Avance III HD 400 (400.13 MHz) at 25 °C. Chemical shifts (*δ*) are reported in parts per million (ppm). ^{1}H and $^{13}C\{^{1}H\}$ NMR spectra are referenced to tetramethylsilane ($SiMe_4$, δ = 0.0 ppm) as external standard, with the deuterium signal of the solvent serving as internal lock and the residual solvent signal as an additional reference.$^{19}F\{^{1}H\}$, $^{31}P\{^{1}H\}$, and $^{29}Si\{^{1}H\}$ NMR spectra are referenced to $CFCl_3$, 85% H_3PO_4 and $SiMe_4$, respectively. For the assignment of the multiplicities, the following abbreviations are used: s = singlet, bs = broad singlet, d = doublet, t = triplet, bq = broad quartet, m = multiplet. For simplicity, multiplets of order higher than one are described by approximating them to the closest first order type. High resolution mass spectrometry was carried out on a Jeol AccuTOF GCX and an Agilent Q-TOF 6540 UHD spectrometer. Elemental analyses were performed on a Vario MICRO cube apparatus.

5.6.2 Synthesis of compound 1

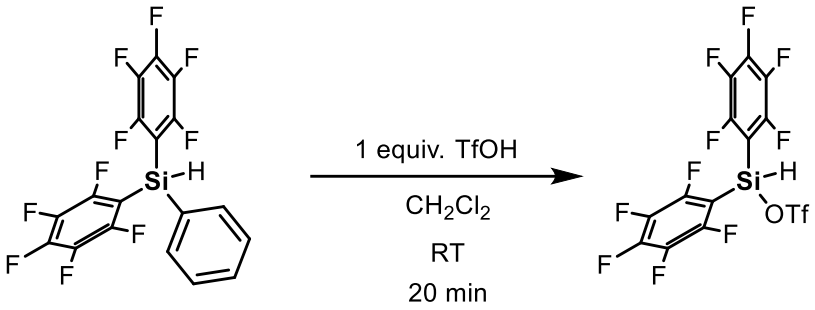

1

Prepared according to a modified literature procedure.[4]

First bis(pentafluorophenyl)phenylsilane[2] (1.18 g, 2.68 mmol, 1 equiv) was dissolved in 5 mL of DCM. Next triflic acid (0.442 mg, 2.95 mmol, 1.1 equiv) was added rapidly. The mixture was left stirring for 20 min, then all volatiles were removed *in vacuo*. Compound **1** was obtained as a yellow oil. Yield: 1,21 g (2.36 mmol, 88%).

^{1}H NMR (400.13 MHz, C_6D_6, 298 K): δ 5.85 (m, 1H, Si*H*).

^{13}C{^{1}H} NMR (100.61 MHz, C_6D_6, 298 K): δ 149.7 (d, $^{1}J_{C–F}$ = 248.8 Hz, *C*F_{Ar}), 145.4 (d, $^{1}J_{C–F}$ = 261.4 Hz, *C*F_{Ar}), 137.9 (d, $^{1}J_{C–F}$ = 257.1 Hz, *C*F_{Ar}), 119.0 (q, $^{1}J_{C–F}$ = 318.3 Hz, *C*F_3), 100.1 (m, C_{ipso}).

^{19}F{^{1}H} NMR (376.66 MHz, C_6D_6, 298 K): δ –76.6 (s, 3F, C*F*$_3$), –127.5 (m, 4F, C*F*$_{Ar}$), –142.6 (m, 2F, C*F*$_{para}$), –158.5 (m, 4F, C*F*$_{Ar}$).

^{29}Si{^{1}H} NMR (79.49 MHz, C_6D_6, 298 K): δ –24.9 (s, *Si*H).

CHN Analysis: Calcd for $C_{13}HF_{13}O_3SSi$: C, 30.48; H, 0.2. Found: C, 28.96; H, 0.62.

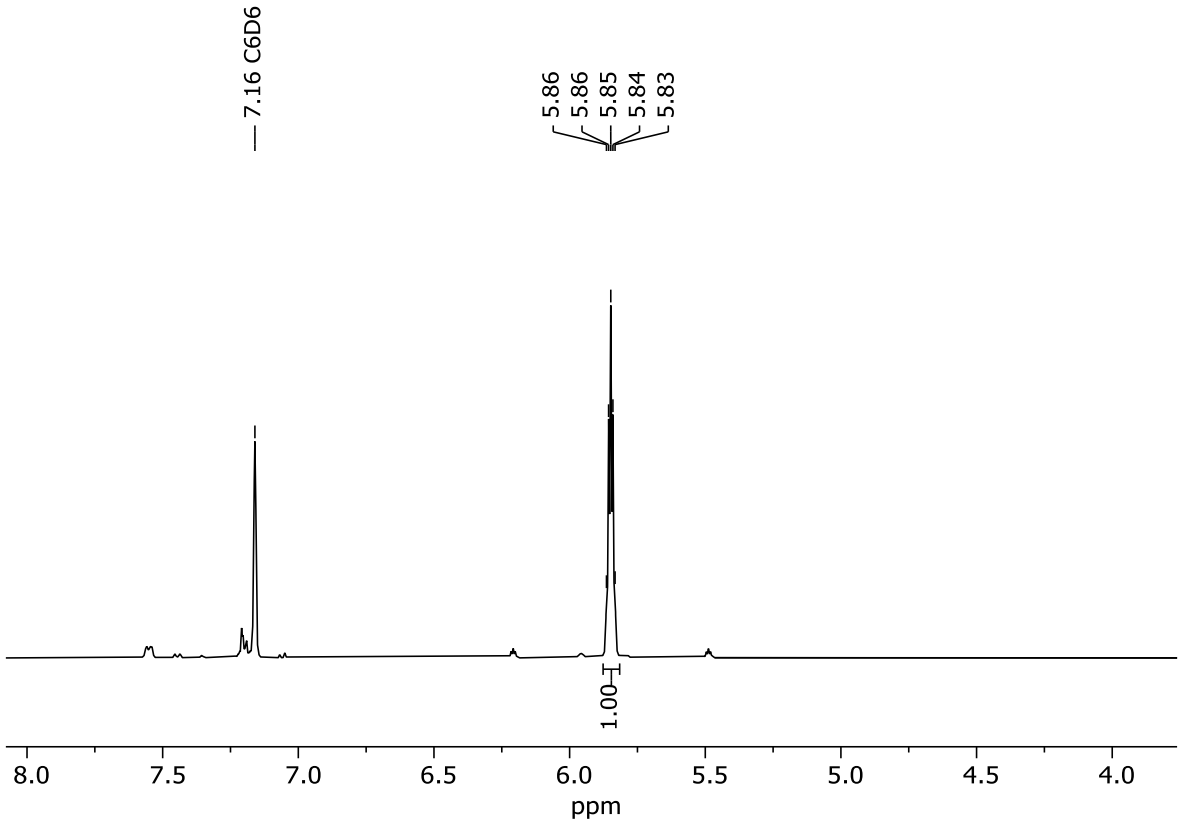

Figure S1: ^{1}H NMR (400.13 MHz, C_6D_6, 298 K) spectrum of compound **1**.

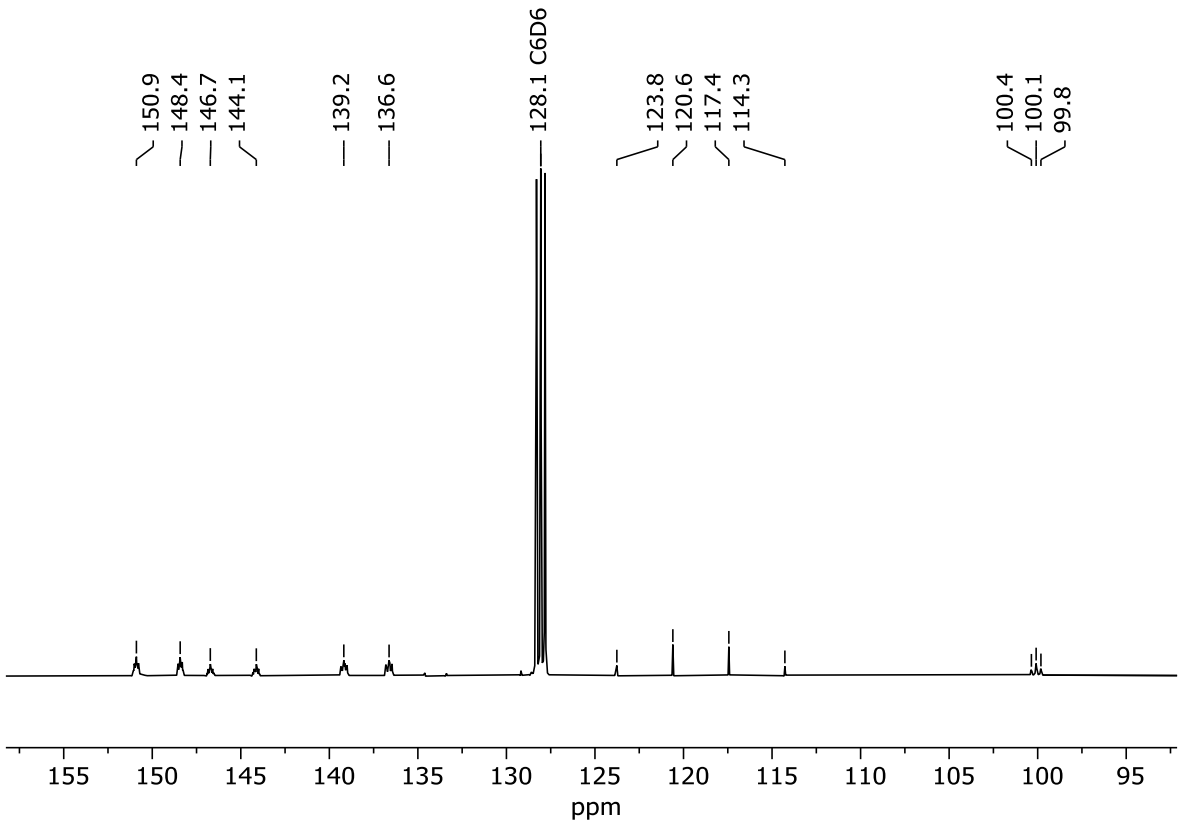

Figure S2: $^{13}C\{^{1}H\}$ NMR (100.61 MHz, C_6D_6, 298 K) spectrum of **1**.

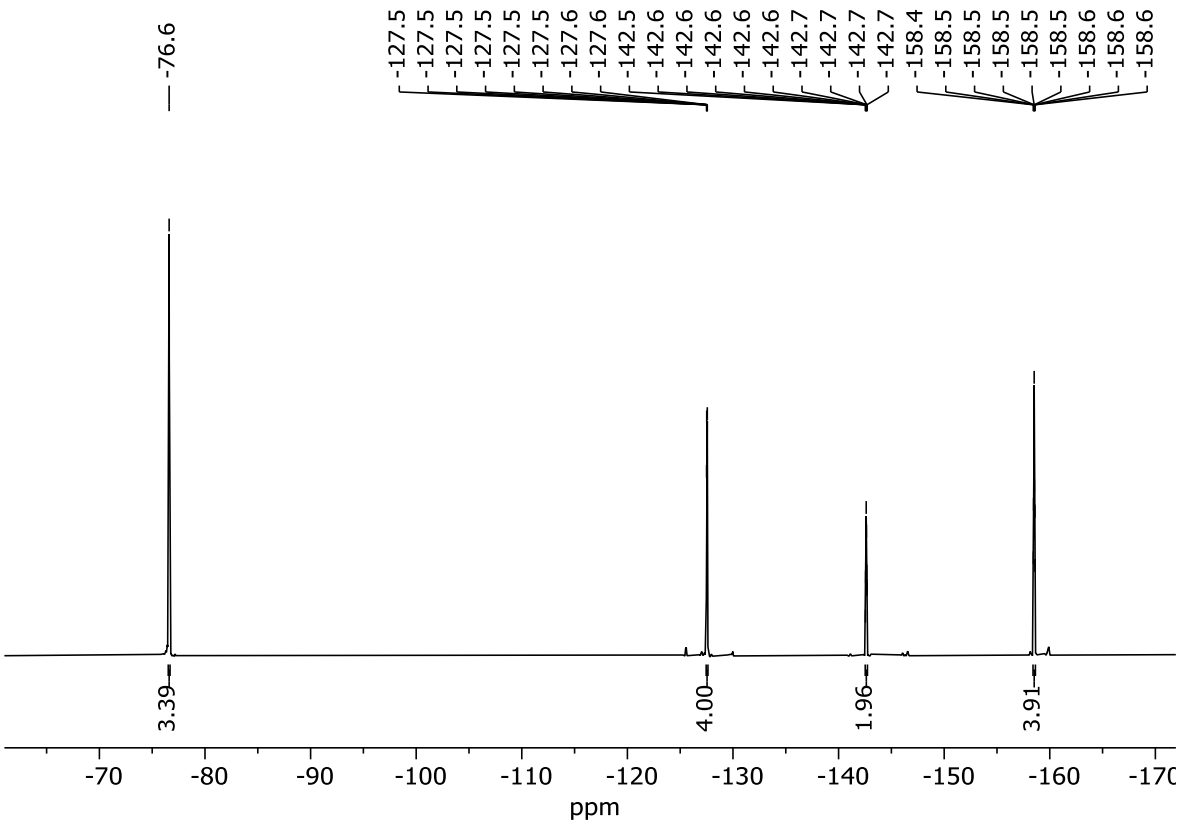

Figure S3: $^{19}F\{^{1}H\}$ NMR (376.66 MHz, C_6D_6, 298 K) of compound **1**.

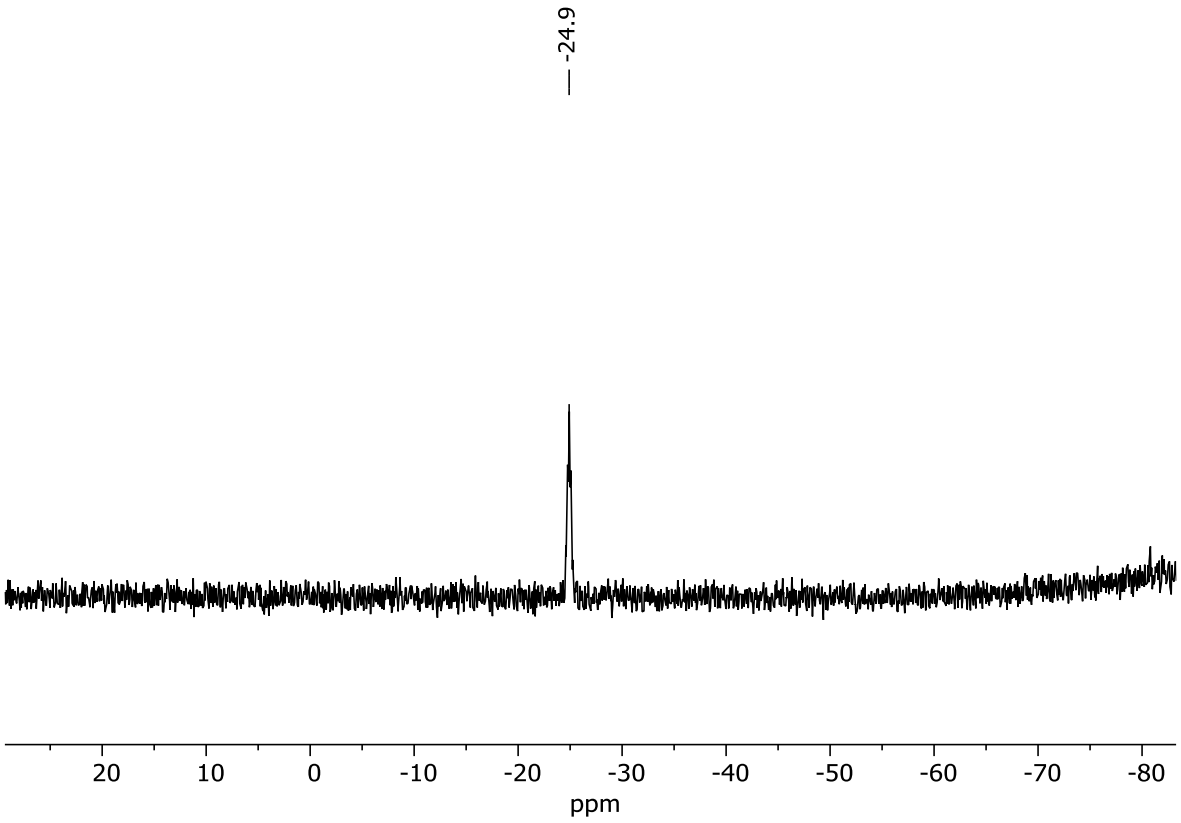

Figure S4: $^{29}Si\{^{1}H\}$ NMR (79.49 MHz, C_6D_6, 298 K) of compound **1**.

5.6.3 Synthesis of compound 2

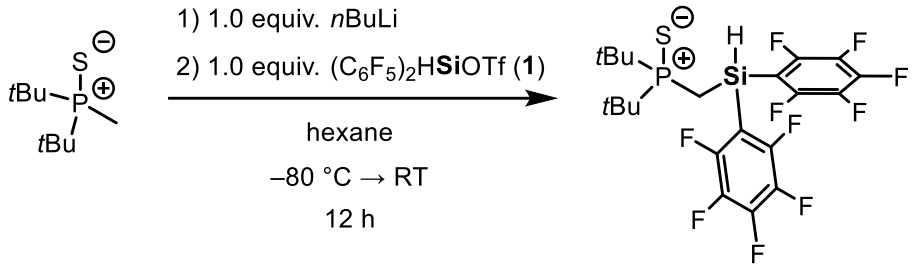

2

In a dry Schlenk di-*tert*-butyl(methyl)phosphine sulfide[1] (454 mg, 2.36 mmol, 1 equiv) was dissolved in 20 mL of hexane and cooled to 0°C. Then *n*-Butyllithium (0.944 mL of a 2.5 M solution in hexane, 2.36 mmol, 1 equiv) was added. This was stirred for 15 min at 0°C, then the suspension was cooled to –80°C. To this compound **1** (1.21 g, 2.36 mmol, 1 equiv) was added. The reaction mixture was subsequently stirred for 12 h at room temperature. Afterwards the brown suspension was filtered using a P3-Frit with added celite. The volume of the filtrate was reduced by half and placed at 8°C for crystallization. The crystals were isolated by filtration. Compound **2** was obtained as colorless crystals suitable for single-crystal X-ray diffraction analysis. Yield: 480 mg (0.865 mmol, 36%).

^{1}H NMR (400.13 MHz, C_6D_6, 298 K): δ 5.86 (m, 1H, Si*H*), 2.02 (dd, $^{2}J_{P–H}$ = 11.3 Hz, $^{3}J_{H–H}$ = 4.0 Hz, 2H, SiCH_2P), 1.07 {d, $^{3}J_{P–H}$ = 15.3 Hz, 18H, P[C(CH_3)$_3$]$_2$}.

^{13}C{^{1}H} NMR (100.61 MHz, C_6D_6, 298 K): δ 149.1 (d, $^{1}J_{C–F}$ = 243.6 Hz, *C*F$_{Ar}$), 143.3 (d, $^{1}J_{C–F}$ = 256.2 Hz, *C*F$_{Ar}$), 137.7 (d, $^{1}J_{C–F}$ = 242.8 Hz, *C*F$_{Ar}$), 106.4 (s, *C*$_{ipso}$), 38.6 {d, $^{1}J_{P–C}$ = 40.9 Hz, P[*C*(CH$_3$)$_3$]$_2$}, 26.9 {d, $^{2}J_{P–C}$ = 1.8 Hz, P[C(*C*H$_3$)$_3$]$_2$}, 7.7 (d, $^{1}J_{P–C}$ = 33.4 Hz, Si*C*H$_2$P).

^{31}P{^{1}H} NMR (162.04 MHz, C_6D_6, 298 K): δ 74.6 (s, *P*=S)

^{19}F{^{1}H} NMR (376.66 MHz, C_6D_6, 298 K): δ –126.9 (m, 4F, C*F*$_{Ar}$), –148.7 (m, 2F, C*F*$_{para}$), –160.4 (m, 4F, C*F*$_{Ar}$).

^{29}Si{^{1}H} NMR (79.49 MHz, C_6D_6, 298 K): δ –43.4 (s, *Si*H).

CHN Analysis: Calcd for $C_{21}H_{21}F_{10}PSSi$: C, 45.49; H, 3.82. Found: C, 45.48; H, 4.20.

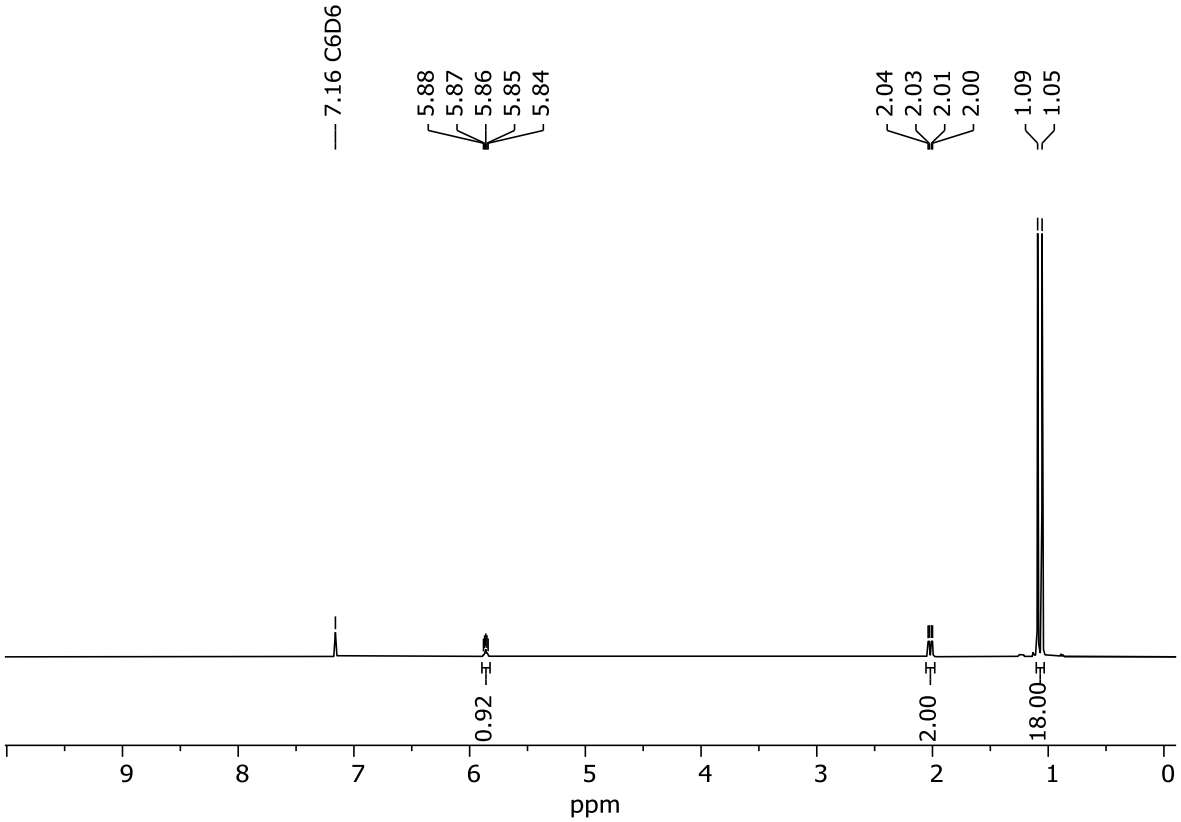

Figure S5: ^{1}H NMR (400.13 MHz, C_6D_6, 298 K) spectrum of compound **2**.

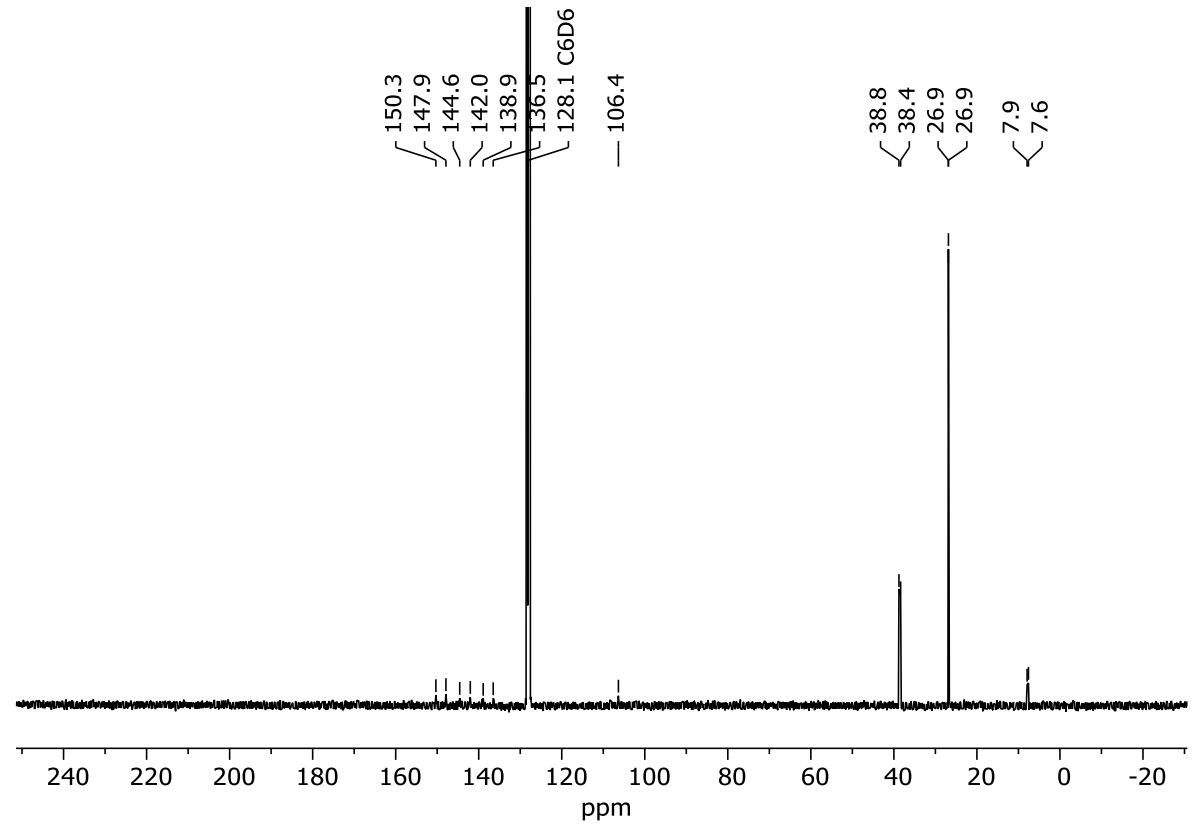

Figure S6: $^{13}C\{^{1}H\}$ NMR (100.61 MHz, C_6D_6, 298 K) spectrum of **2**.

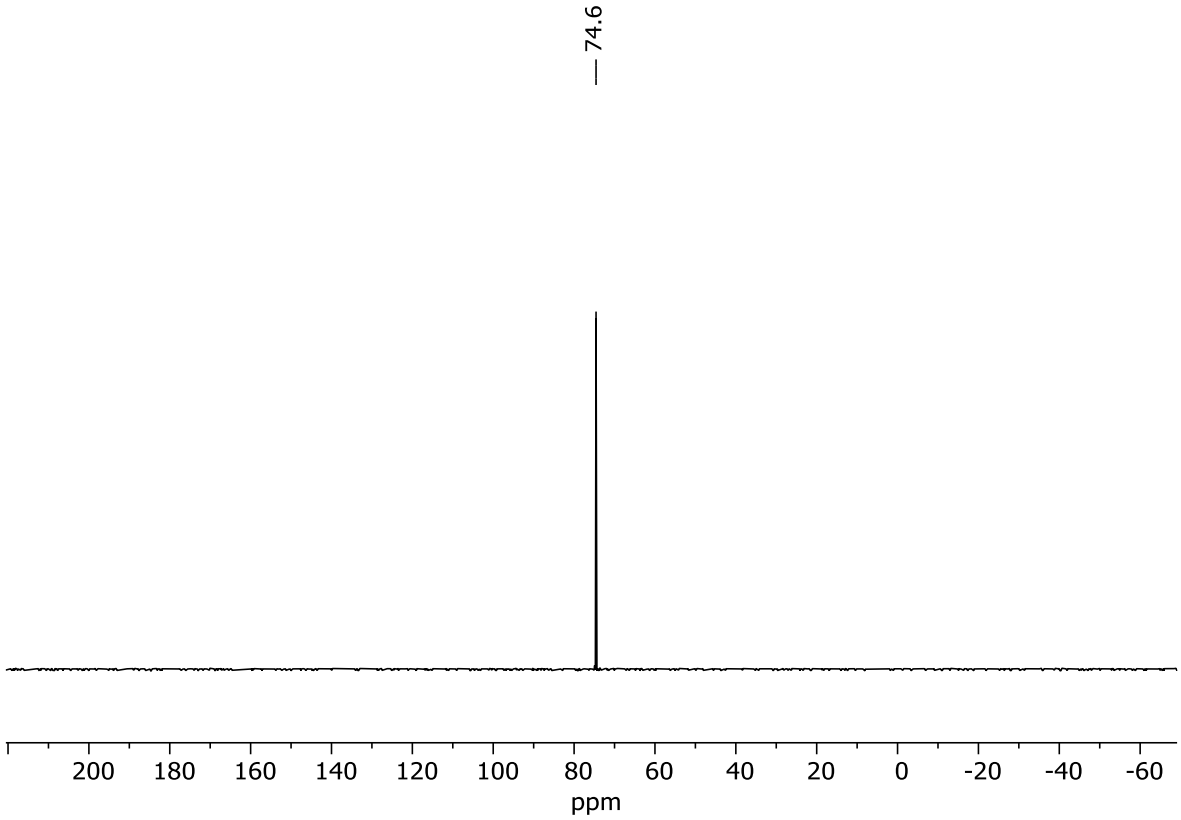

Figure S7: $^{31}P\{^{1}H\}$ NMR (162.04 MHz, C_6D_6, 298 K) of compound **2**.

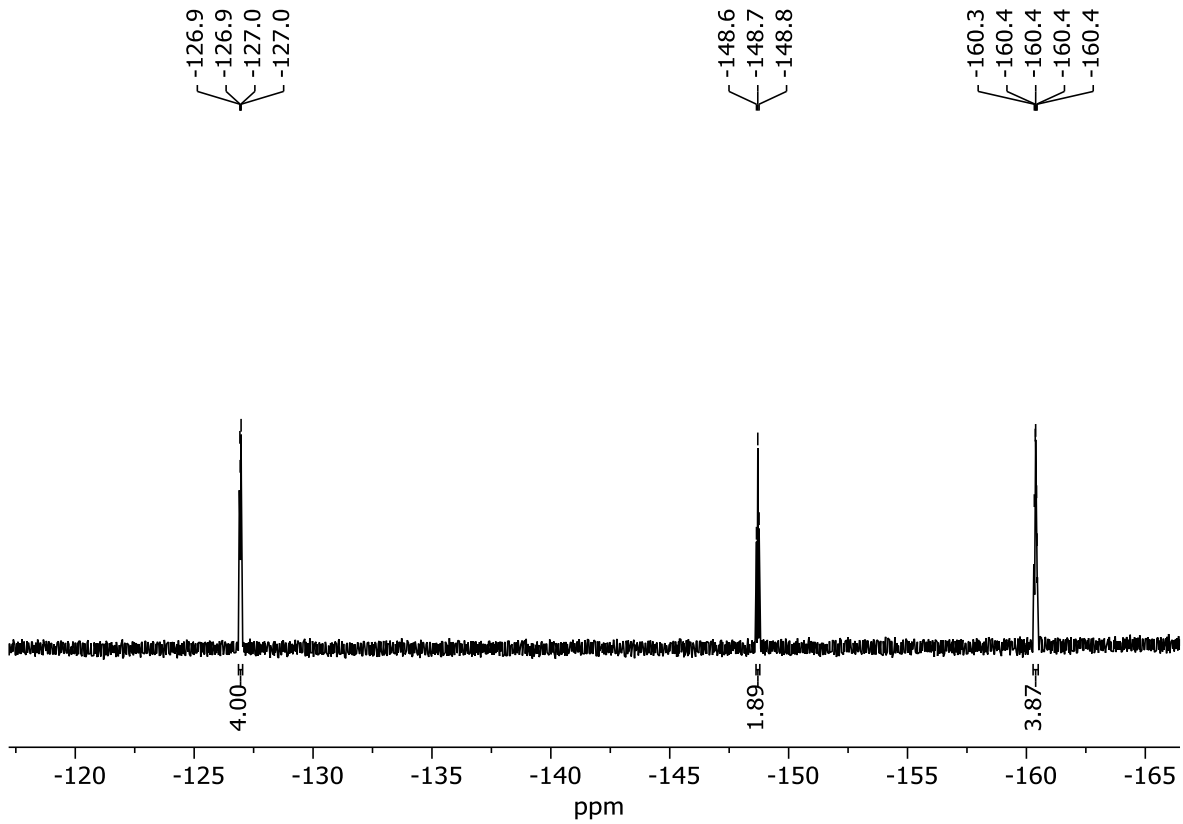

Figure S8: 19F{1H} NMR (376.66 MHz, C6D6, 298 K) of compound 2.

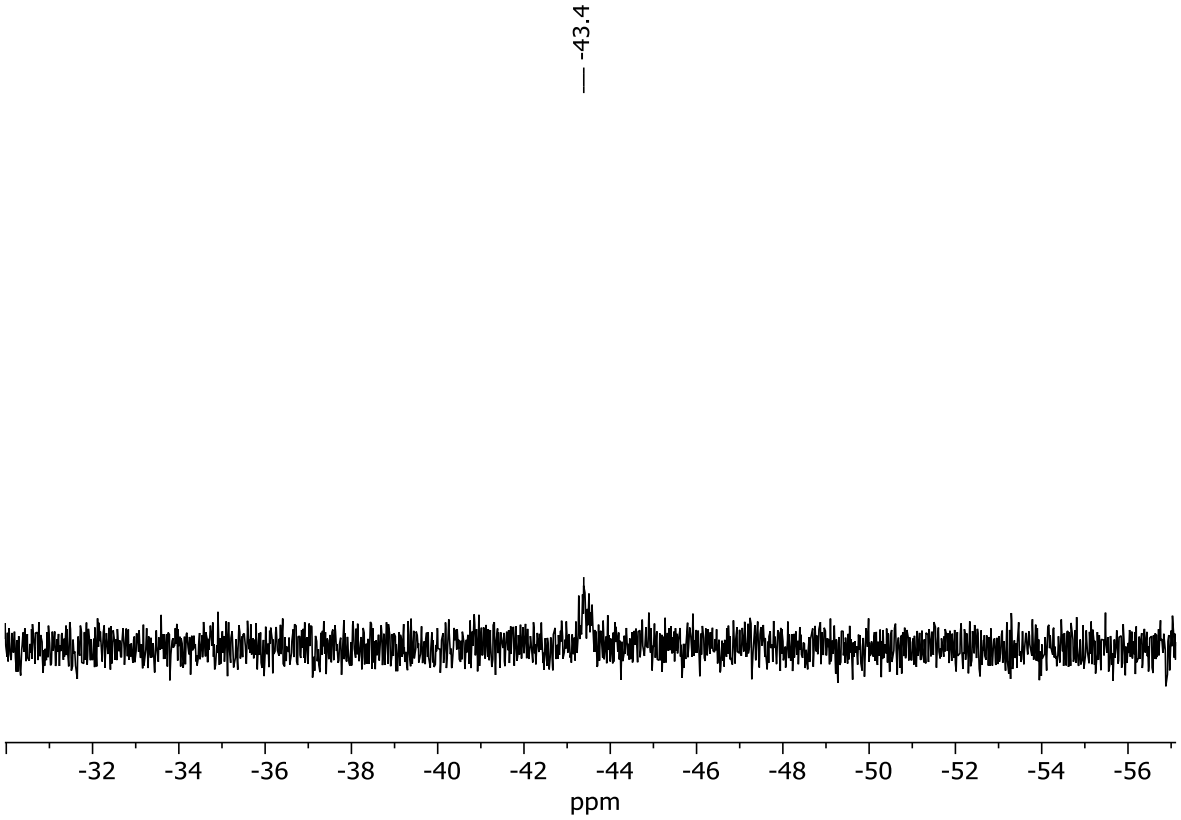

Figure S9: $^{29}Si\{^{1}H\}$ NMR (79.49 MHz, C_6D_6, 298 K) of compound **2**.

5.6.4 Synthesis of compound 3

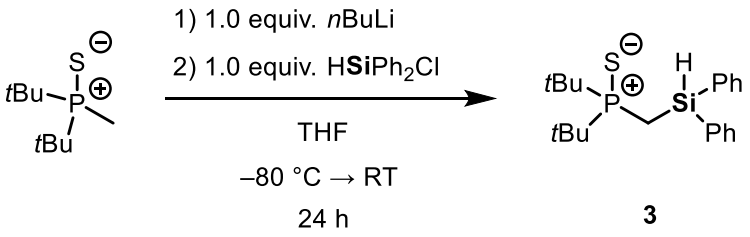

First di-*tert*-butyl(methyl)phosphine sulfide[1] (1.15 g, 5.98 mmol, 1 equiv) was dissolved in 30 mL of THF and cooled to –80°C. Next *n*-Butyllithium (2.39 mL of a 2.5 M solution in hexane, 5.98 mmol, 1 equiv) was added, and the mixture left to warm up to room temperature. The mixture was left to stir for 20 min at room temperature and then cooled to –80°C. Next dichloro(phenyl)silane (1.31 g, 5.98 mmol, 1 equiv) was added and the reaction mixture stirred for 12 h at room temperature. Then all volatiles were removed *in vacuo* and the remaining white solid was suspended with 20 mL of hot hexane and filtered using a P3-Frit with added celite. The filter cake was washed once with 10 mL of DCM. The combined filtrates were dried *in vacuo* and the resulting white powder dissolved in 5 mL Et_2O. After a few days at room temperature crystals formed from this solution. The product was isolated via filtration and dried *in vacuo*. Compound **3** was obtained as

colorless crystals suitable for single-crystal X-ray diffraction analysis. Yield: 1.13 g (3.02 mmol, 50 %).

^{1}H NMR (400.13 MHz, C_6D_6, 298 K): δ 7.75–7.73 (m, 4H, C*H*$_{Ph}$), 7.20–7.14 (m, 6H, C*H*$_{Ph}$), 5.77 (m, 1H, Si*H*), 1.66 (dd, $^{2}J_{P-H}$ = 12.5 Hz, $^{3}J_{H-H}$ = 2.8 Hz, 2H, SiC*H*$_2$P, 1.09 {d, $^{3}J_{P-H}$ = 14.8 Hz, 18H, P[C(C*H*$_3$)$_3$]$_2$}.

^{13}C{^{1}H} NMR (100.61 MHz, C_6D_6, 298 K): δ 136.0 (s, *C*H$_{Ph}$), 135.4 (d, $^{3}J_{P-C}$ = 3.2 Hz, *C*$_{Ph}$), 129.6 (s, *C*H$_{Ph}$), 128.4 (s, *C*H$_{Ph}$), 38.3 {d, $^{1}J_{P-C}$ = 42.1 Hz, P[*C*(CH$_3$)$_3$]$_2$}, 27.4 {d, $^{3}J_{P-C}$ = 1.9 Hz, P[C(*C*H$_3$)$_3$]$_2$}, 9.5 (d, $^{1}J_{P-C}$ = 32.7 Hz, Si*C*H$_2$P).

^{31}P{^{1}H} NMR (162.04 MHz, C_6D_6, 298 K): δ 76.0 [s, *P*(S)].

^{29}Si{^{1}H} NMR (79.49 MHz, C_6D_6, 298 K): δ –18.9 (d, $^{2}J_{P-Si}$ = 6.0 Hz, PCH$_2$*Si*).

CHN Analysis: Calcd for $C_{21}H_{31}PSSi$: C, 67.33; H, 8.34. Found: C, 67.22; H, 7.99.

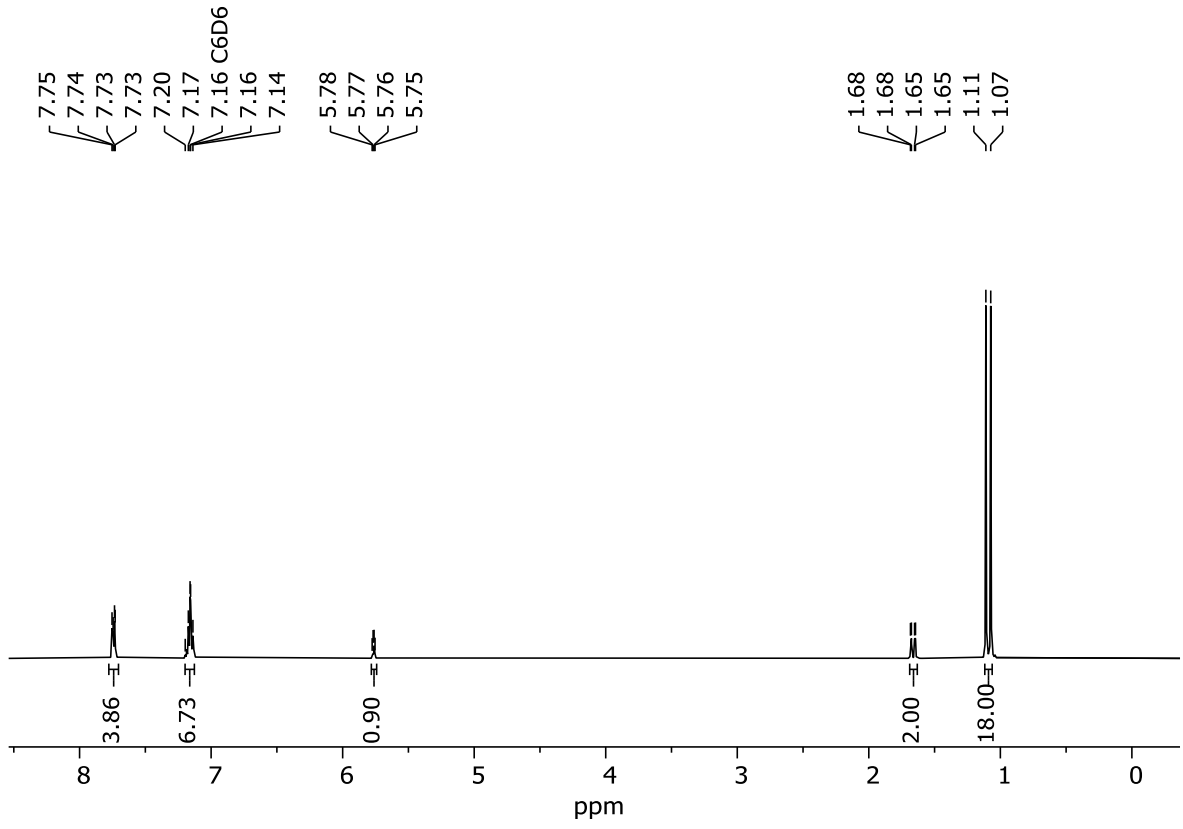

Figure S10: ^{1}H NMR (400.13 MHz, C_6D_6, 298 K) spectrum of compound **3**.

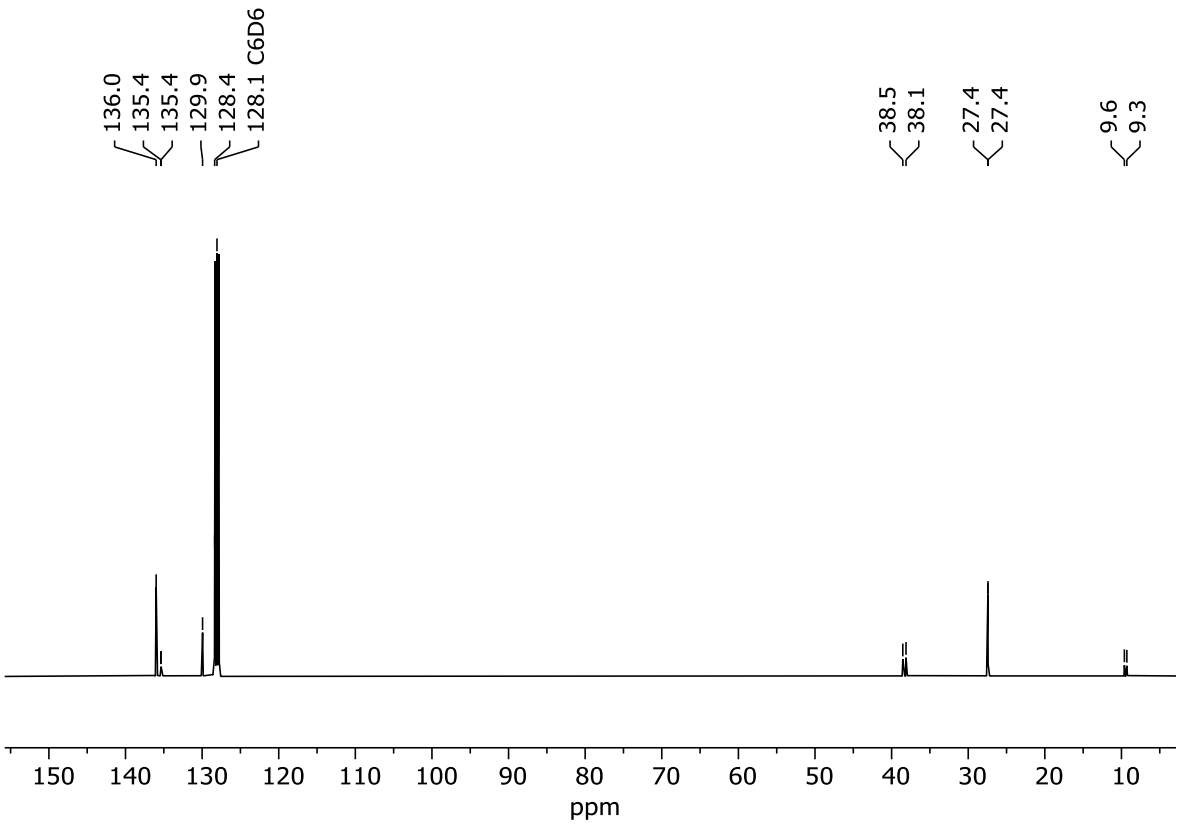

Figure S11: $^{13}C\{^{1}H\}$ NMR (100.61 MHz, C_6D_6, 298 K) spectrum of **3**.

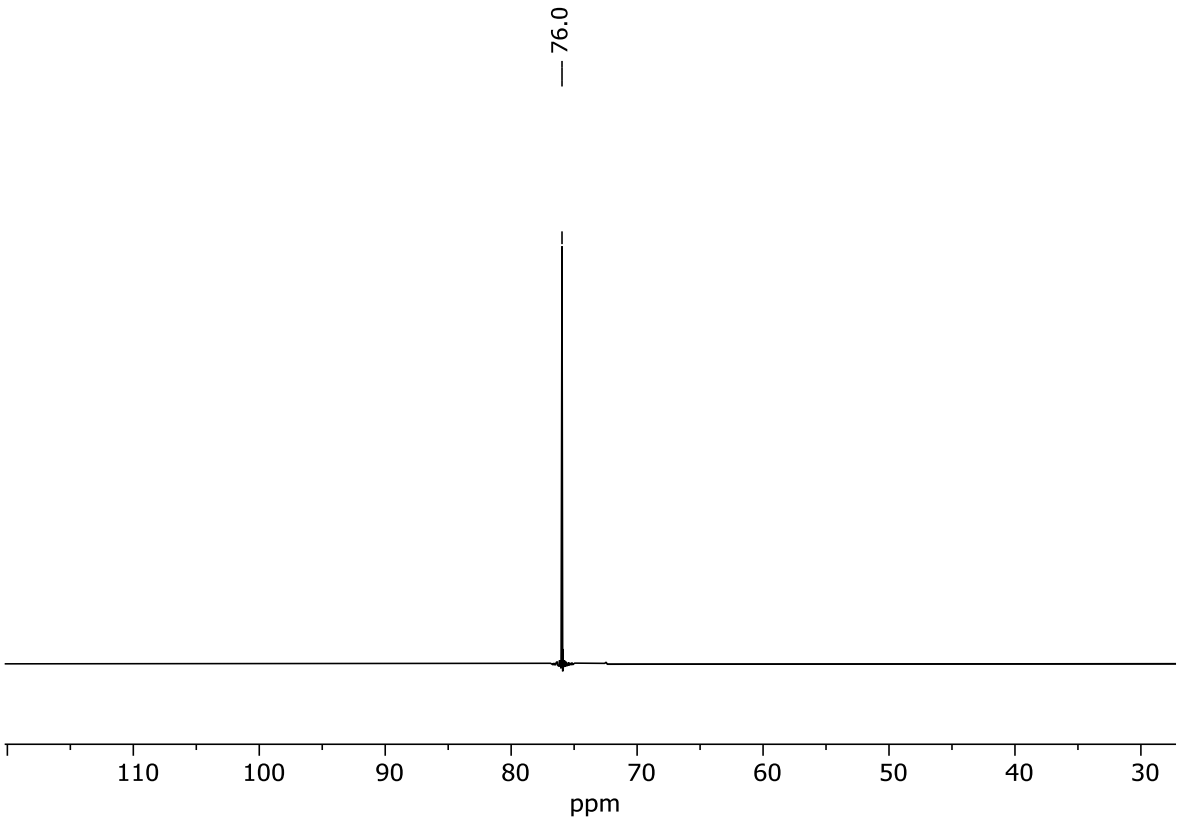

Figure S12: $^{31}P\{^{1}H\}$ NMR (162.04 MHz, C_6D_6, 298 K) of compound **3**.

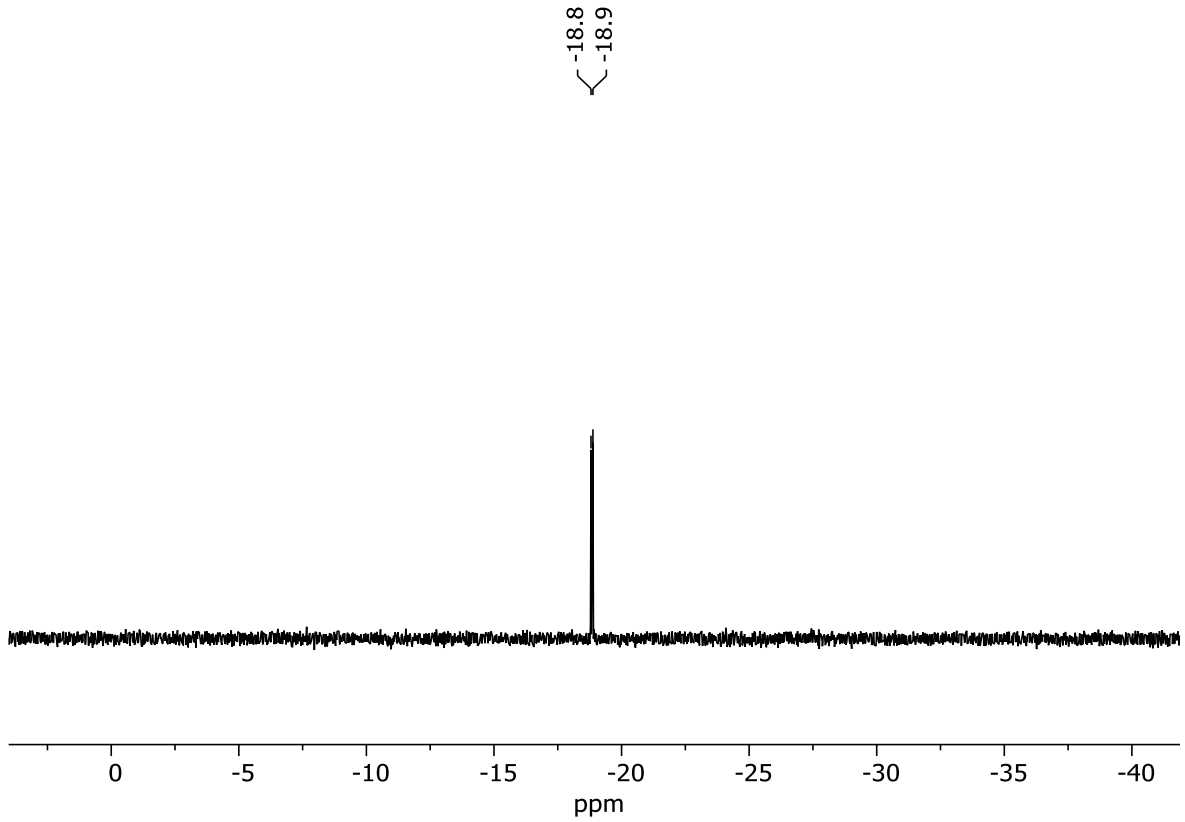

Figure S13: $^{29}Si\{^{1}H\}$ NMR (79.49 MHz, C_6D_6, 298 K) of compound **3**.

5.6.5 Synthesis of compound 4

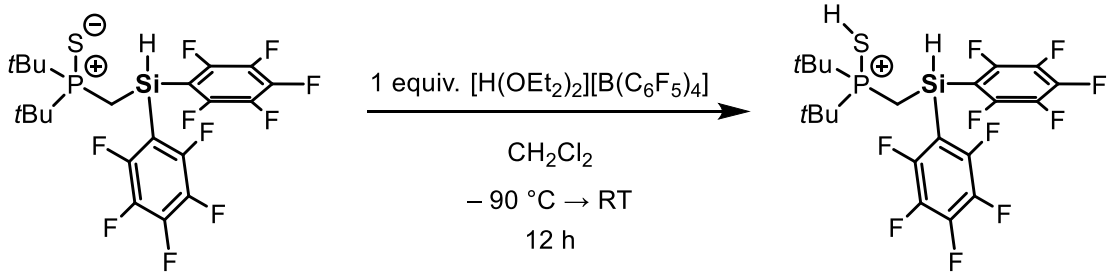

2 **4**

In a Glovebox a dry Schlenk flask was charged with compound **2** (400 mg, 0.721 mmol, 1 equiv) and $[H(OEt_2)_2][B(C_6F_5)_4]$[3] (597 mg, 0.721 mmol, 1 equiv). The solids were cooled to –90°C and then 6 mL of DCM were slowly added. The reaction mixture was left to warm up to room temperature and then stirred for 2 h. Next all volatiles were removed *in vacuo* and the resulting white solid suspended in 10 mL of DCM and stirred for 12 h at room temperature. The suspension was filtered using cannula filtration. Compound **4** was obtained as a white powder. Yield: 360 mg (0.291 mmol, 40%).

^{1}H NMR (400.13 MHz, CD_2Cl_2, 298 K): δ 5.65 (s, 1H, Si*H*), 2.54 (bs, 1H, P(S)*H*), 2.36 (dd, $^{2}J_{P–H}$ = 12.8 Hz, $^{3}J_{H–H}$ = 3.7 Hz, 2H, SiCH_2P), 1.52 {d, $^{3}J_{P–H}$ = 18.5 Hz, 18H, P[C(CH_3)$_3$]$_2$}.

^{13}C{^{1}H} NMR (100.61 MHz, CD_2Cl_2, 298 K): δ 149.5 (d, $^{1}J_{C–F}$ = 248.8 Hz, *C*F_{Ar}), 148.6 (d, $^{1}J_{C–F}$ = 242.3 Hz, *C*F_{borate}), 145.2 (d, $^{1}J_{C–F}$ = 263.1 Hz, *C*F_{Ar}), 138.7 (d, $^{1}J_{C–F}$ = 244.1 Hz, *C*F_{borate}), 136.7 (d, $^{1}J_{C–F}$ = 248.1 Hz, *C*F_{borate}), 124.7 (s, *C*$_{borate–ipso}$), 101.2 (s, *C*$_{ipso}$), 40.5 {d, $^{1}J_{P–C}$ = 27.0 Hz, P[*C*(CH$_3$)$_3$]$_2$}, 26.8 {s, P[C(*C*H$_3$)$_3$]$_2$}, 2.8 (d, $^{1}J_{P–C}$ = 30.3 Hz, Si*C*H$_2$P).

^{31}P{^{1}H} NMR (162.04 MHz, CD_2Cl_2, 298 K): δ 85.8 (s, *P*(S)H).

^{19}F{^{1}H} NMR (376.66 MHz, CD_2Cl_2, 298 K): δ –125.6 (m, 4F, C*F*$_{Ar}$), –133.0 (m, 8F, C*F*$_{borate}$), –143.6 (m, 2F, C*F*$_{Ar}$), –157.8 (m, 4F, C*F*$_{Ar}$), –163.7 (m, 4F, C*F*$_{borate}$), –167.5 (m, 8F, C*F*$_{borate}$).

CHN Analysis: Calcd for $C_{45}H_{22}BF_{30}PSSi$: C, 43.78; H, 1.80. Found: C, 43.89; H, 2.00.

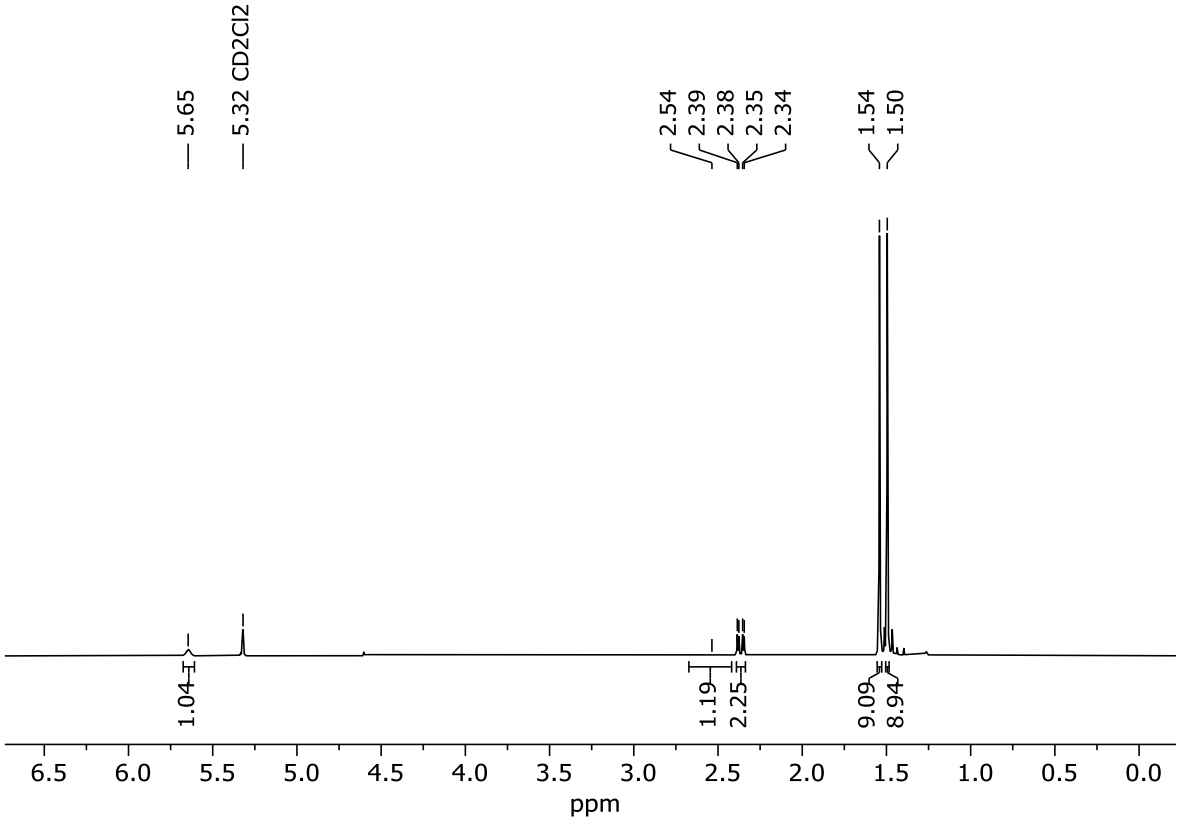

Figure S14: ^{1}H NMR (400.13 MHz, CD_2Cl_2, 298 K) spectrum of compound **4**.

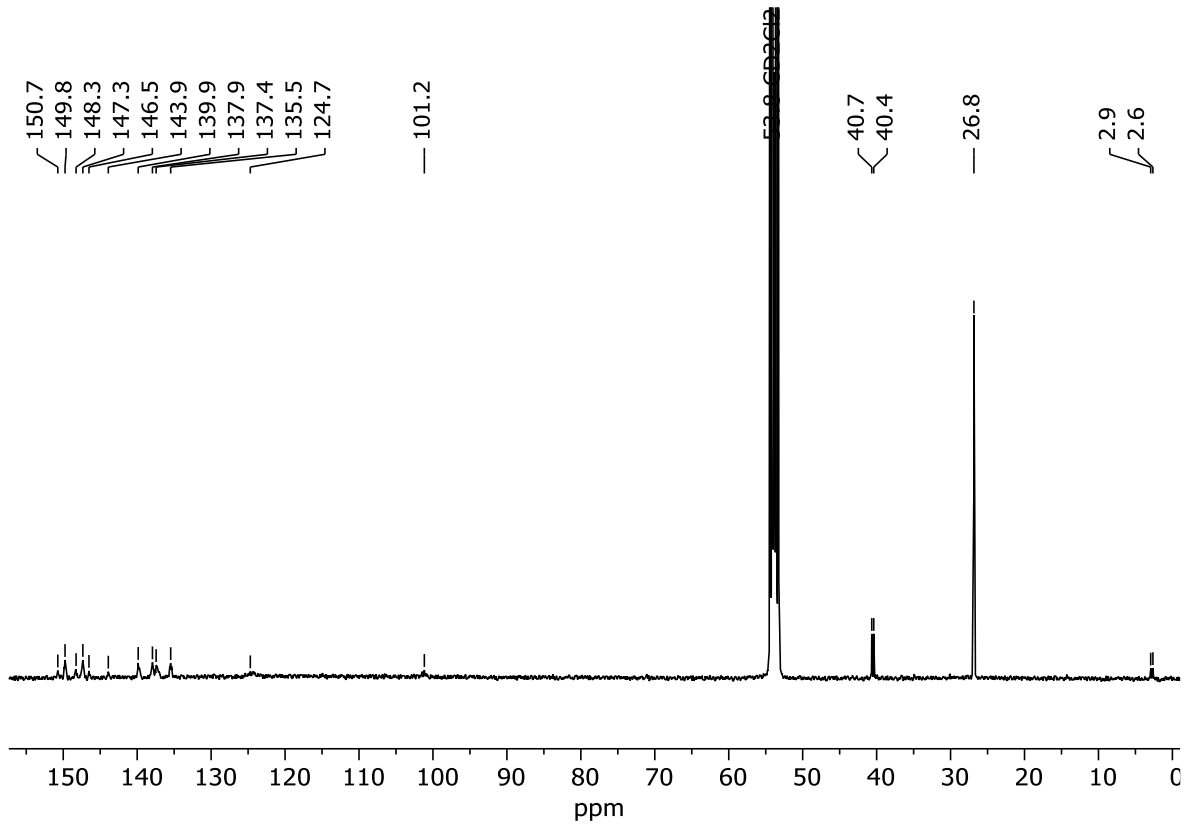

Figure S15: $^{13}C\{^{1}H\}$ NMR (100.61 MHz, CD_2Cl_2, 298 K) spectrum of **4**.

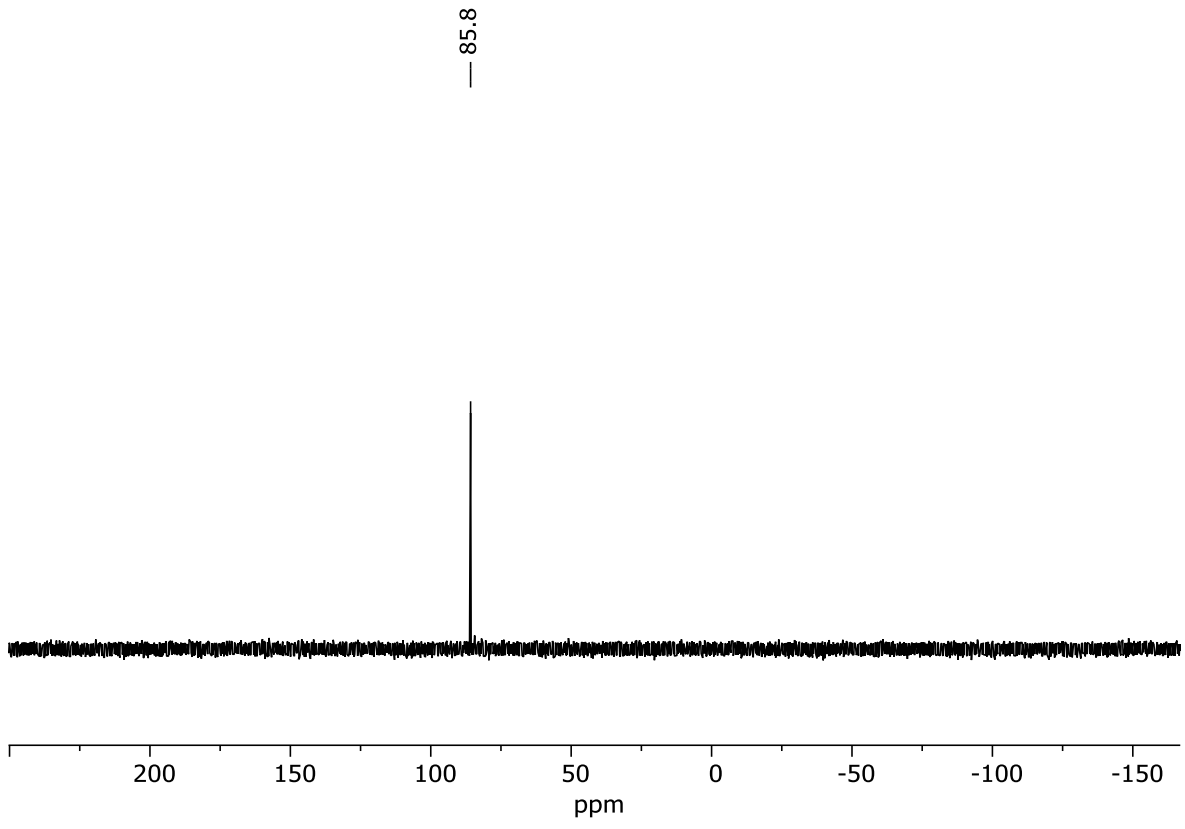

Figure S16: $^{31}P\{^{1}H\}$ NMR (162.04 MHz, CD_2Cl_2, 298 K) of compound **4**.

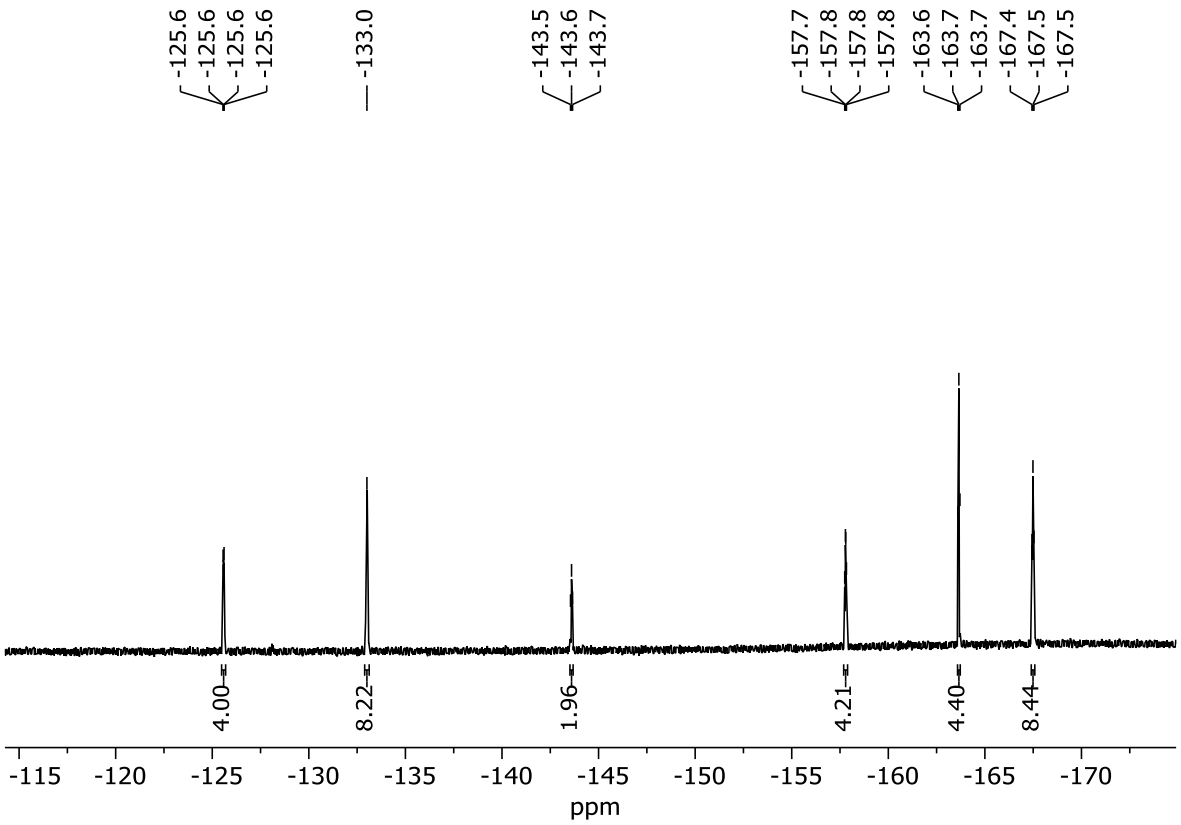

Figure S17: $^{19}F\{^{1}H\}$ NMR (376.66 MHz, CD_2Cl_2, 298 K) of compound **4**.

5.6.6 Synthesis of compound 5

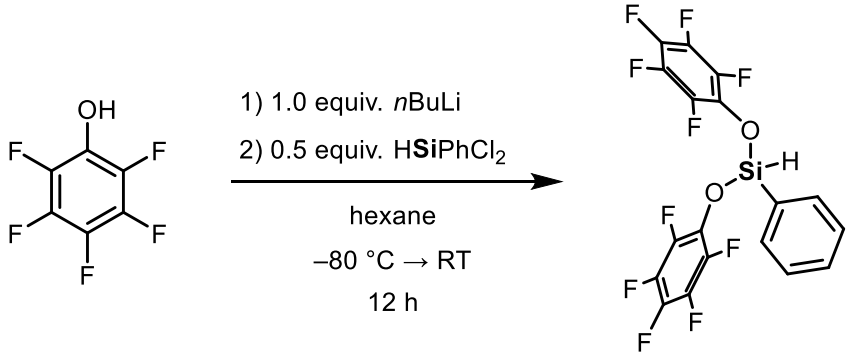

5

In a dry Schlenk flask pentafluorophenol (3.68 g, 20 mmol, 2 equiv) was dissolved in 20 mL of hexane and cooled to –80°C. Then *n*-Butyllithium (8.0 mL of a 2.5 M solution in hexane, 20 mmol, 2 equiv) was added. The mixture was left to slowly warm up to room temperature and then stirred for 30 min. To the resulting suspension dichloro(phenyl)silane (1.77 g, 10 mmol, 1 equiv) was added at room temperature. The reaction mixture was stirred for 12 h at room temperature and then filtered using cannula filtration. The filtrate was purified using Kugelrohr distillation (110°C oven temperature, 1 x 10^{-3} mbar). Compound **5** was obtained as a colorless oil. Yield: 3.55 g (7.52 mmol, 75%).

^{1}H NMR (400.13 MHz, C_6D_6, 298 K): δ 7.75–7.72 (m, 2H, C*H*$_{Ph}$), 7.23–7.14 (m, 3H, C*H*$_{Ph}$), 5.53 (m, 1H, Si*H*).

^{13}C{^{1}H} NMR (100.61 MHz, C_6D_6, 298 K): δ 141.9 (m, *C*F$_{Ar}$), 139.6 (m, *C*F$_{Ar}$), 139.5 (m, *C*F$_{Ar}$), 138.5 (m, *C*F$_{Ar}$), 137.0 (m, *C*F$_{Ar}$), 135.9 (m, *C*F$_{Ar}$), 134.2 (s, *C*H$_{Ph}$), 133.0 (s, *C*H$_{Ph}$), 128.9 (s, *C*H$_{Ph}$), 128.2 (s, *C*$_{Ph}$).

^{19}F{^{1}H} NMR (376.66 MHz, C_6D_6, 298 K): δ –158.7 (m, 4F, C*F*$_{Ar}$), –163.8 (m, 4F, C*F*$_{Ar}$), –164.6 (m, 2F, C*F*$_{Ar}$).

CHN Analysis: Calcd for $C_{18}H_6F_{10}O_2Si$: C, 45.77; H, 1.28. Found: C, 45.59; H, 1.75.

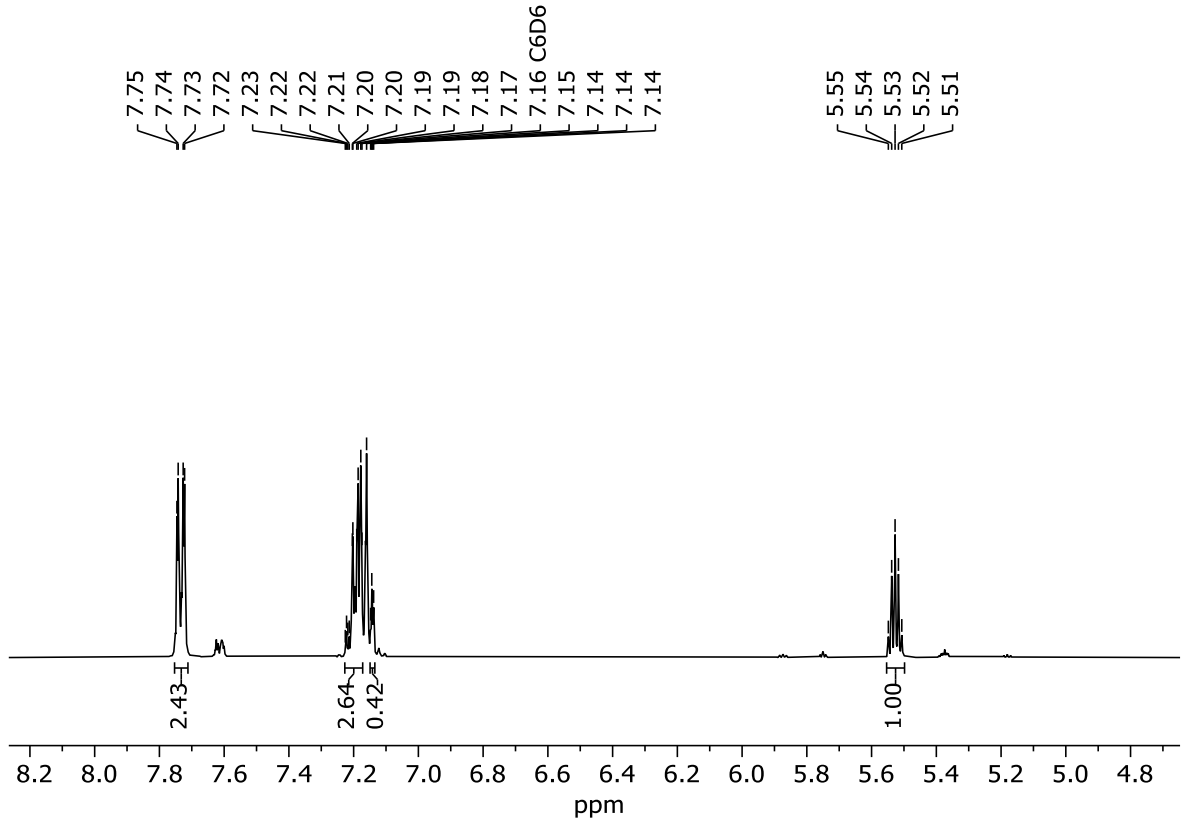

Figure S18: ^{1}H NMR (400.13 MHz, C_6D_6, 298 K) spectrum of compound **5**.

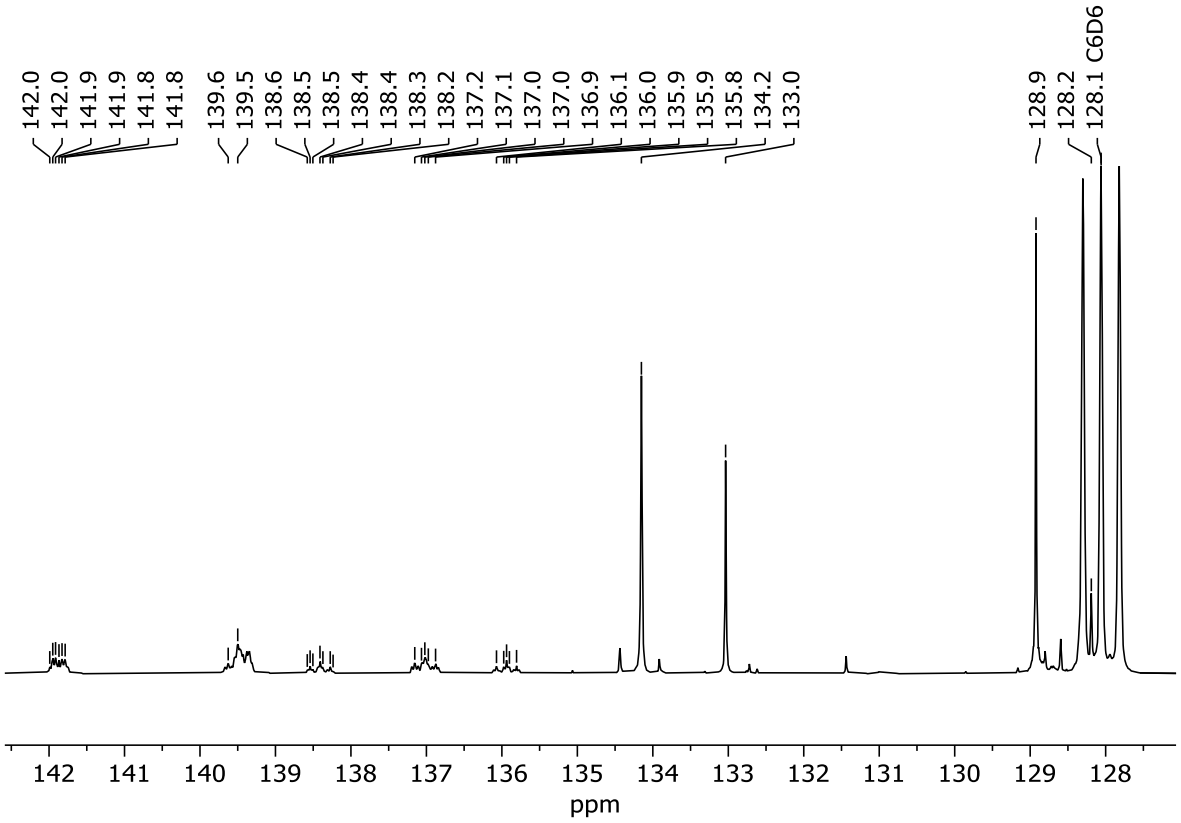

Figure S19: $^{13}C\{^{1}H\}$ NMR (100.61 MHz, C_6D_6, 298 K) spectrum of **5**.

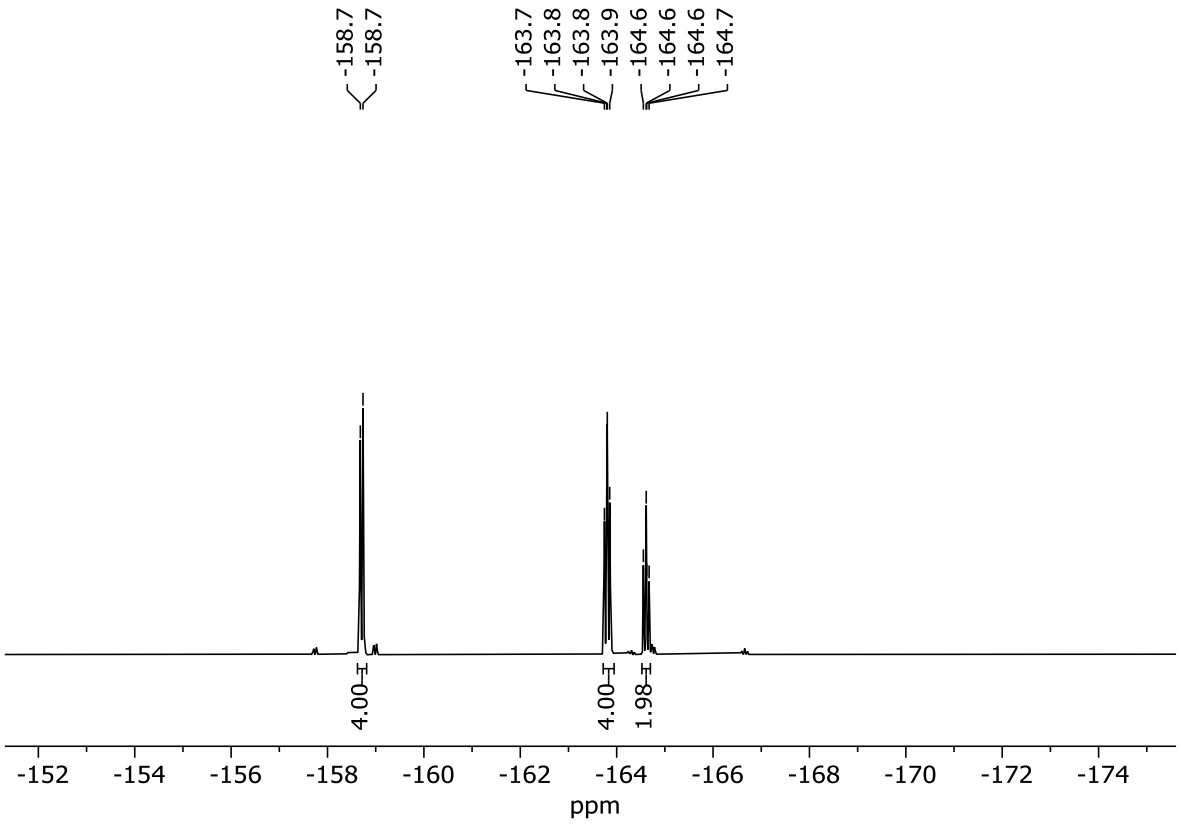

Figure S20: $^{19}F\{^{1}H\}$ NMR (376.66 MHz, C_6D_6, 298 K) of compound **5**.

5.6.7 Synthesis of di-pyrrolidine(chloro)silane

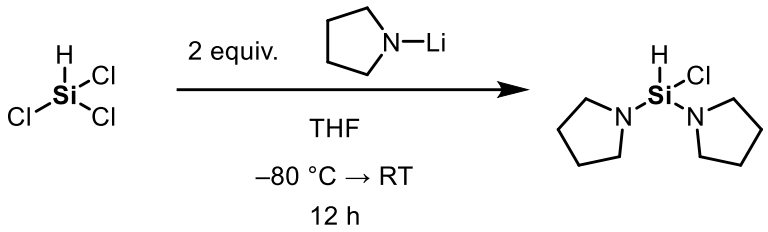

First dry freshly distilled pyrrolidine (5.69 g, 80 mmol, 2 equiv) was diluted in 150 mL of THF and then cooled to –80°C. Next *n*-Butyllithium (32 mL of a 2.5 M solution in hexane, 80 mmol, 2 equiv) was slowly added, and the reaction mixture was stirred for 30 min in the cooling bath. Subsequently trichlorosilane (5.42 mL, 40 mmol, 1 equiv) was added and the mixture stirred for 24 h at room temperature. Then all volatiles were *in vacuo* and the resulting white oily residue suspended in 50 mL of hexane. The suspension was filtered using a P3-Frit with added celite. The filtrate was purified using fractional Kugelrohr distillation (60°C oven temperature, 1 x 10^{-3} mbar). Di-pyrrolidine(chloro)silane was obtained as a colorless oil. Yield: 6.6g (32.23 mmol, 80%).

^{1}H NMR (400.13 MHz, C_6D_6, 298 K): δ 5.31 (m, 1H, Si*H*), 2.99–2.95 (m, 8H, CH_2), 1.53–1.49 (m, 8H, CH_2).

^{13}C{^{1}H} NMR (100.61 MHz, C_6D_6, 298 K): δ 46.3 (s, *C*H_2), 26.9 (s, *C*H_2).

CHN Analysis: Calcd for $C_8H_{17}ClN_2Si$: C, 46.92; H, 8.37; N, 13.68. Found: C, 45.46; H, 7.78; N, 12.93.

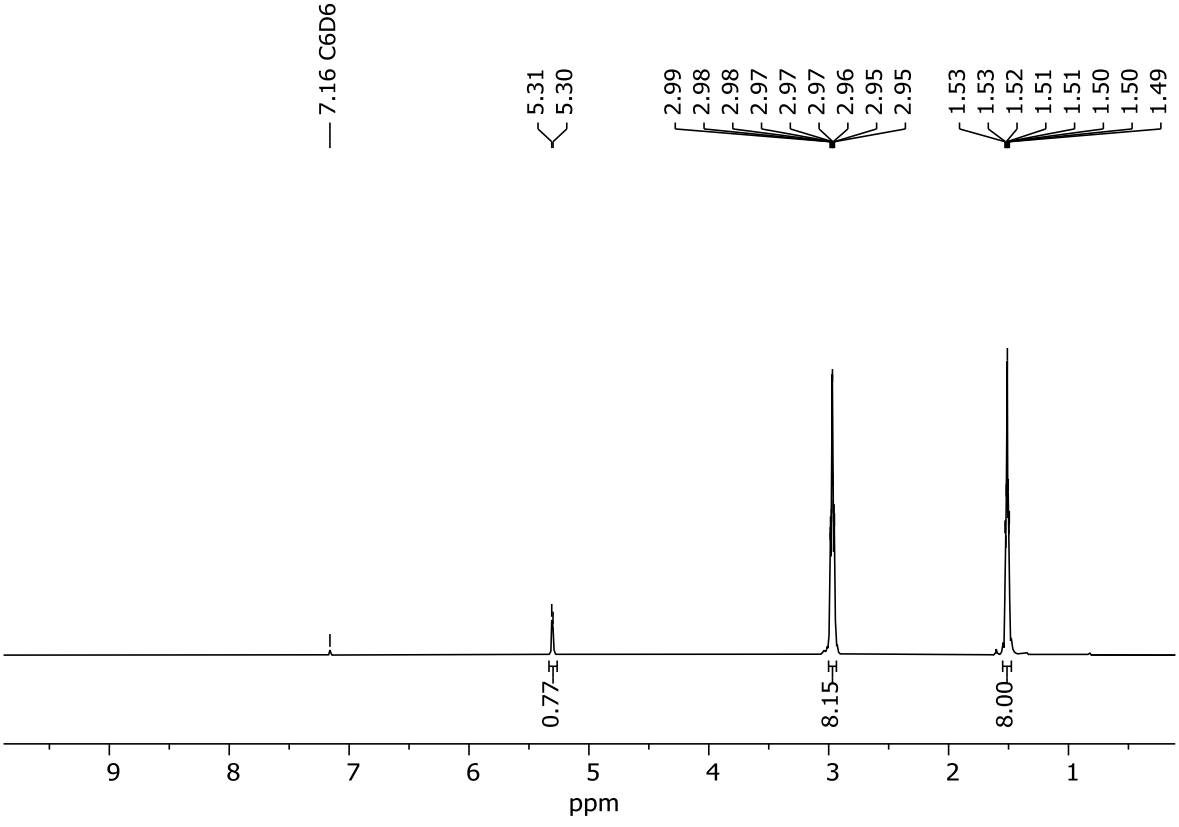

Figure S21: ^{1}H NMR (400.13 MHz, C_6D_6, 298 K) spectrum of di-pyrrolidine(chloro)silane.

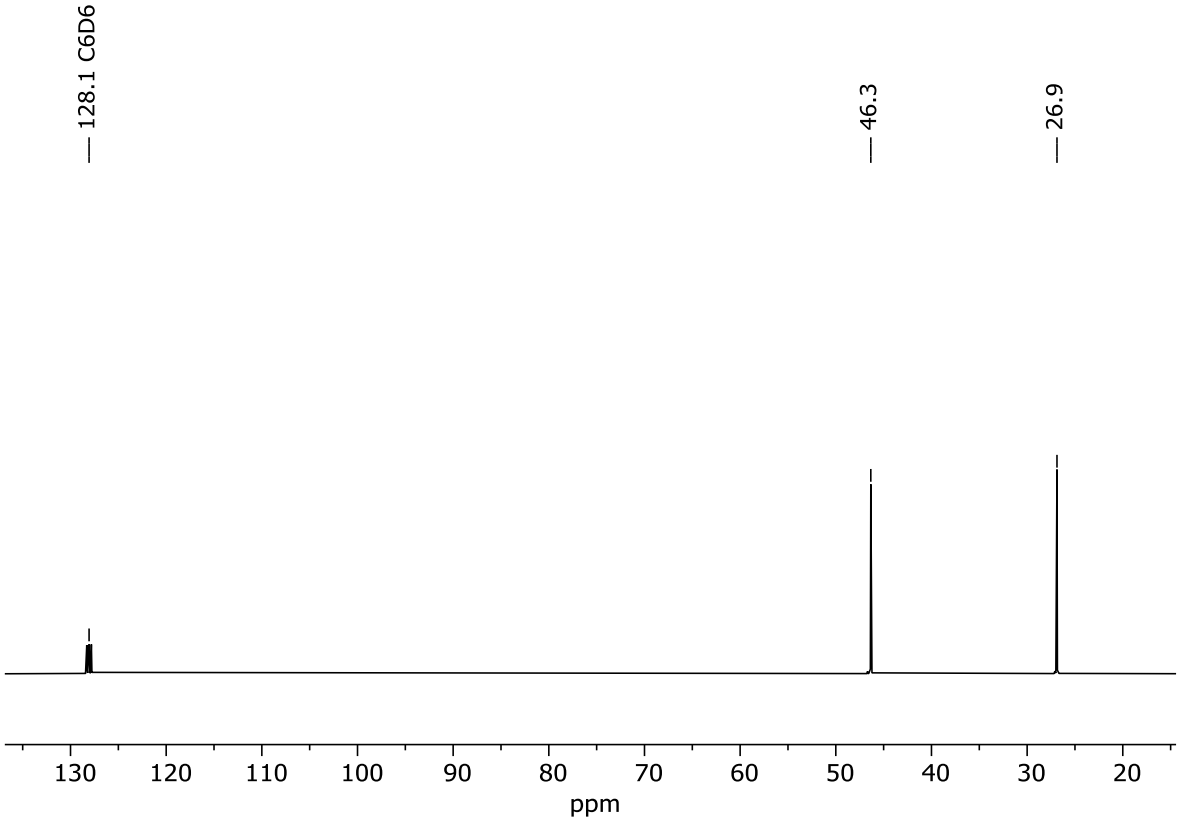

Figure S22: $^{13}C\{^{1}H\}$ NMR (100.61 MHz, C_6D_6, 298 K) spectrum of di-pyrrolidine(chloro)silane.

5.6.8 Synthesis of compound 6

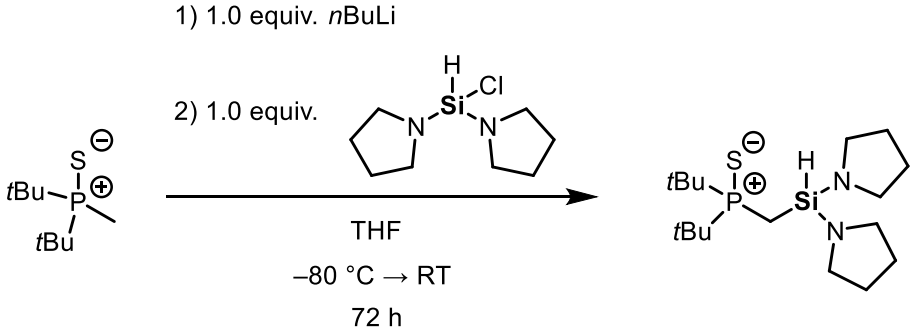

6

In a dry Schlenk flask di-*tert*-butyl(methyl)phosphine sulfide[1] (3.36g, 17.47 mmol, 1 equiv) was dissolved in 150 mL of THF and cooled to –80°C. Next *n*-Butyllithium (6.99 mL of a 2.5 M solution in hexane, 17.47 mmol, 1 equiv) was added. The mixture was stirred for 1 h in the cooling bath at –30°C. Then the reaction mixture was cooled to –80°C and di-pyrrolidine(chloro)silane (3.58 g, 17.47 mmol, 1 equiv) was slowly added. The reaction mixture was stirred for 3d at room temperature. Next all volatiles were removed *in vacuo* and the reaction mixture suspended with 20 mL of hot hexane. The resulting suspension was filtered using a P3-Frit with added celite and the filtrate crystallized at –80°C. The

product was isolated via filtration and dried *in vacuo*. Compound **6** was obtained as slightly yellow crystals suitable for single-crystal X-ray diffraction analysis. Yield: 5.49 g (15.22 mmol, 87%).

^{1}H NMR (400.13 MHz, C_6D_6, 298 K): δ 5.9 (m, 1H, Si*H*), 3.15–3.03 (m, 8H, CH_2), 1.64–1.61 (m, 8H, CH_2), 1.37 (dd, $^{2}J_{P-H}$ = 13.3 Hz, $^{3}J_{H-H}$ = 1.6 Hz, 2H, SiCH_2P), 1.23 {d, $^{3}J_{P-H}$ = 14.6 Hz, 18H, PC(CH_3)$_3$]$_2$}.

^{13}C{^{1}H} NMR (100.61 MHz, C_6D_6, 298 K): δ 47.5 (s, *C*H_2), 38.2 {d, $^{1}J_{P-C}$ = 42.5, P*C*(CH$_3$)$_3$]$_2$}, 27.6 {d,$^{3}J_{P-C}$ = 1.8 Hz, PC(*C*H$_3$)$_3$]$_2$}, 27.2 (s, *C*H_2), 8.8 (d, $^{1}J_{P-C}$ = 35.3 Hz, Si*C*H_2P).

^{31}P{^{1}H} NMR (162.04 MHz, C_6D_6, 298 K): δ 74.8 (s, *P*=S).

^{29}Si{^{1}H} NMR (79.49 MHz, C_6D_6, 298 K): δ –24.3 (s, PCH$_2$*Si*).

CHN Analysis: Calcd for $C_{17}H_{37}N_2PSSi$: C, 56.6; H, 10.3; N, 7.77. Found: C, 53.49; H, 9.80; N, 6.62.

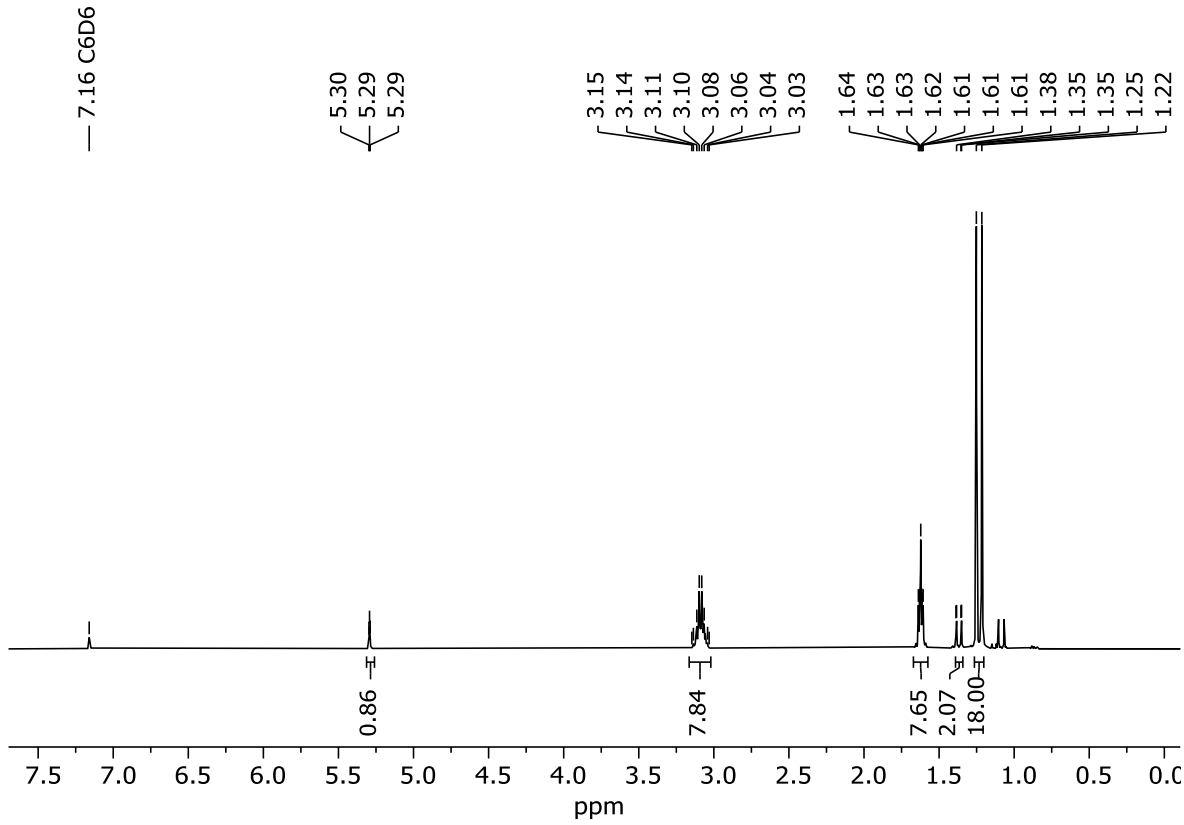

Figure S23: ^{1}H NMR (400.13 MHz, C_6D_6, 298 K) spectrum of compound **6**.

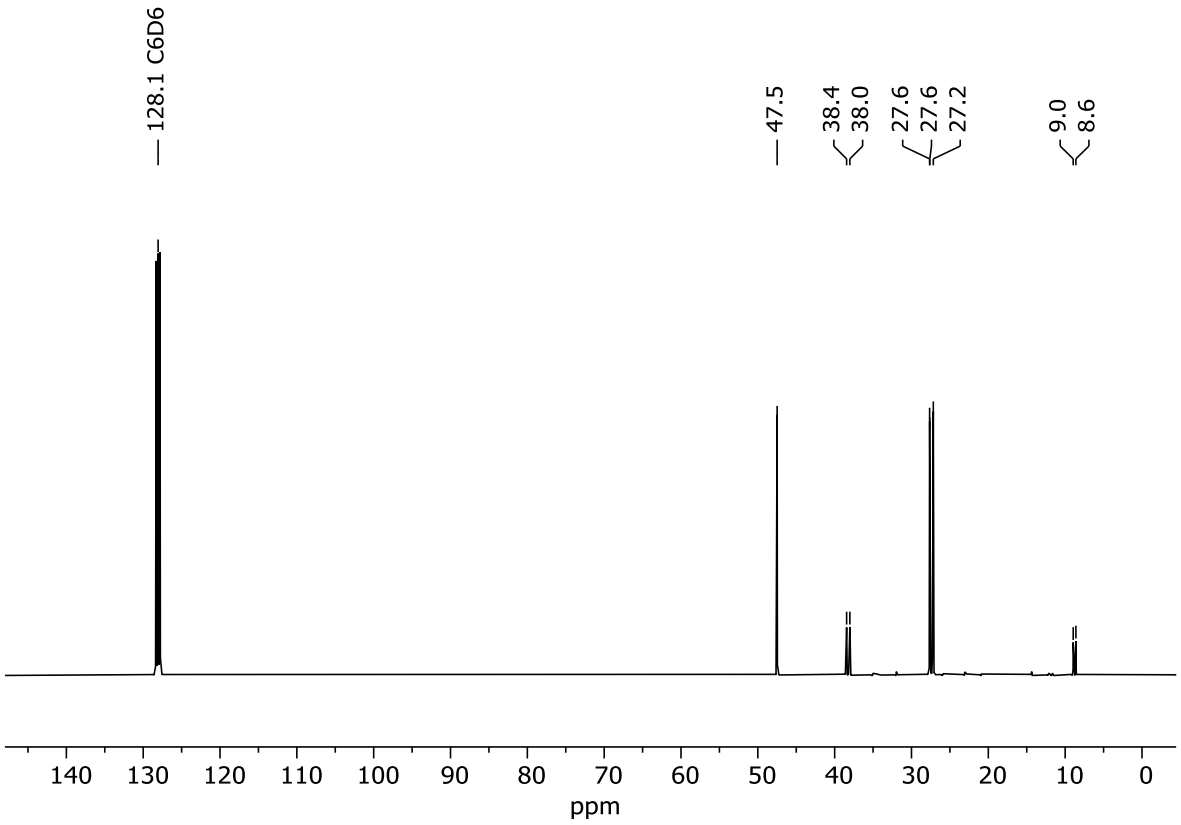

Figure S24: $^{13}C\{^{1}H\}$ NMR (100.61 MHz, C_6D_6, 298 K) spectrum of **6**.

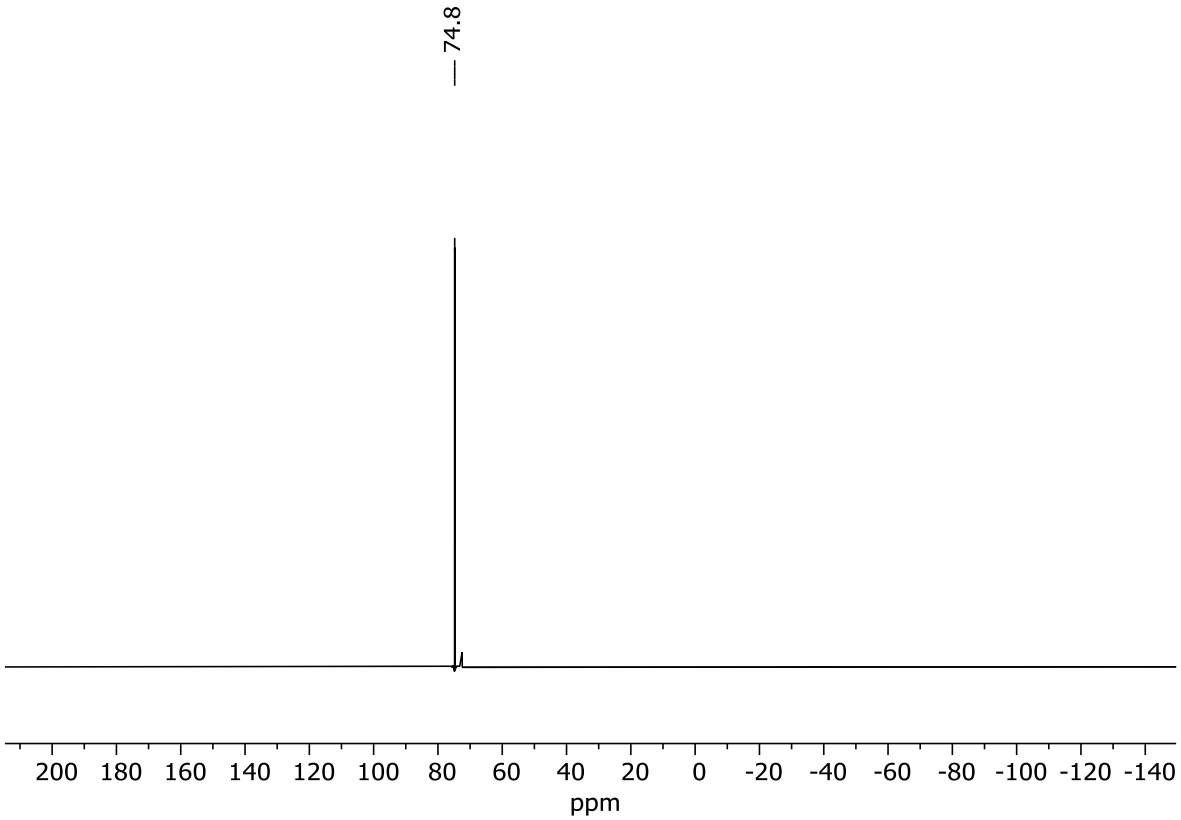

Figure S25: $^{31}P\{^{1}H\}$ NMR (162.04 MHz, C_6D_6, 298 K) of compound **6**.

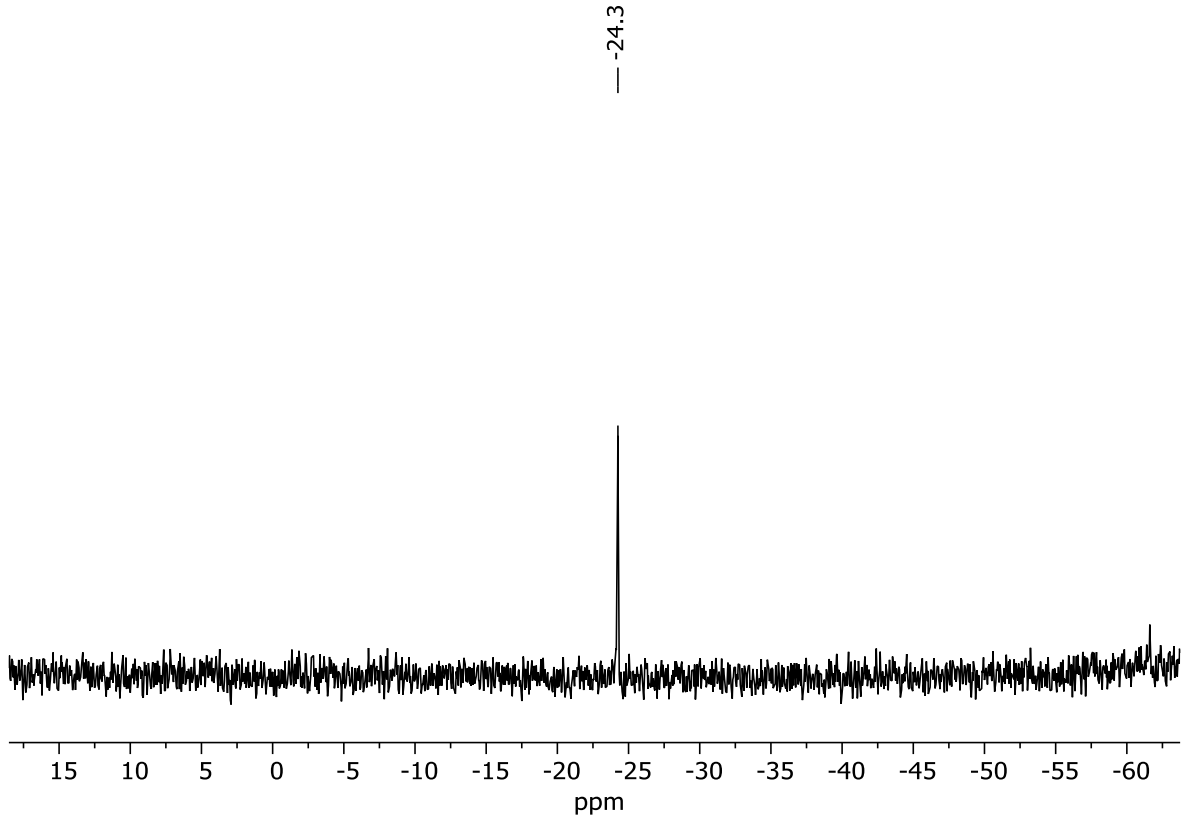

Figure S26: $^{29}Si\{^{1}H\}$ NMR (79.49 MHz, C_6D_6, 298 K) of compound **6**.

5.6.9 Synthesis of compound 7

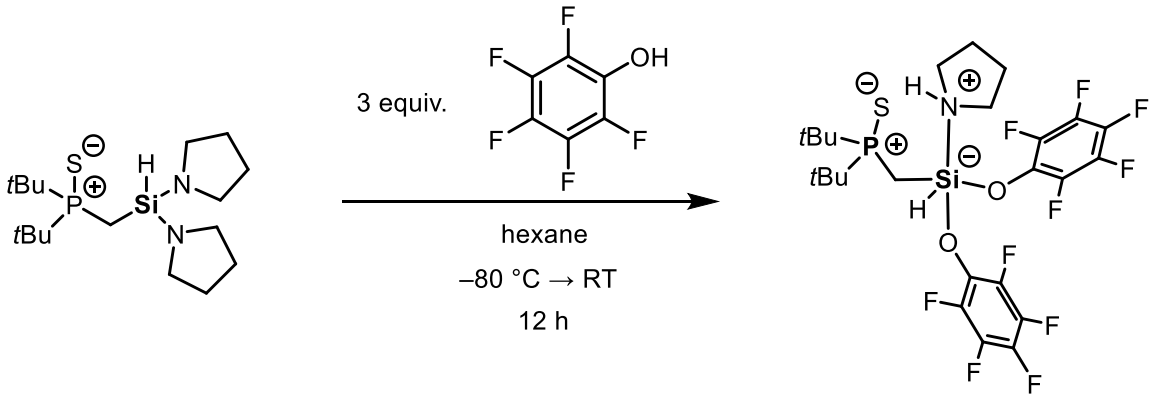

6 **7**

First compound **6** (800 mg, 2.22 mol, 1 equiv) was dissolved in 20 mL of hexane and cooled to –40 °C. Then pentafluorophenol (1.23 g, 6.66 mmol, 3 equiv) was dissolved in 10 mL of hexane and then slowly added to the cooled solution containing compound **6** via teflon cannula. The reaction mixture was left to stir for 24 h at room temperature.

Afterwards roughly half of the volume of the solution was removed *in vacuo* and the solution filtered. The filtrate was placed at –80 °C for crystallization. The next day the precipitated powder was filtered at –80 °C and washed once with 5 mL of cold CH_2Cl_2. The powder was then dissolved in 3 mL of toluene at –20 °C and again placed at –80 °C for crystallization. After 12 h compound **7** was obtained as single-crystals suitable for single crystal X-ray diffraction analysis. Due to the temperature sensitive nature of compound **7** no yield was determined.

^{1}H NMR (400.13 MHz, C_6D_6, 298 K): δ 7.39 (bs, 2H, N*H* + pyrrolidine N*H*), 5.49–5.46 (m, 1H, Si*H*), 3.19–3.00 (m, 4H, CH_2NCH_2), 1.64–1.54 (m, 2H, SiCH_2P), 1.52–1.49 (m, 4H, CH_2CH_2), 1.17 {d, $^3J_{P–H}$ = 15.1 Hz, 9H, PC(CH_3)$_3$]}, 1.08 {d, $^3J_{P–H}$ = 15.0 Hz, 9H, PC(CH_3)$_3$]}.

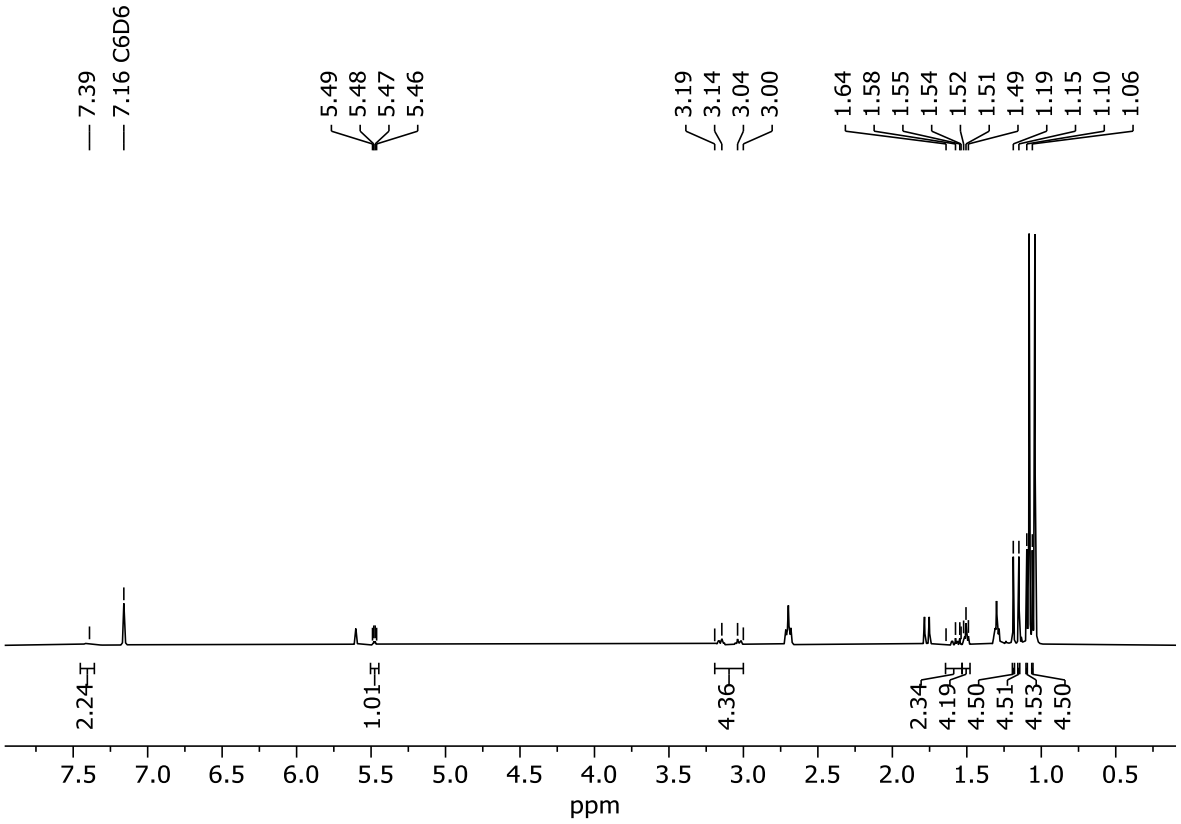

Figure S27: ^{1}H NMR (400.13 MHz, C_6D_6, 298 K) spectrum of compound **7**.

5.6.10 Synthesis of compound 9

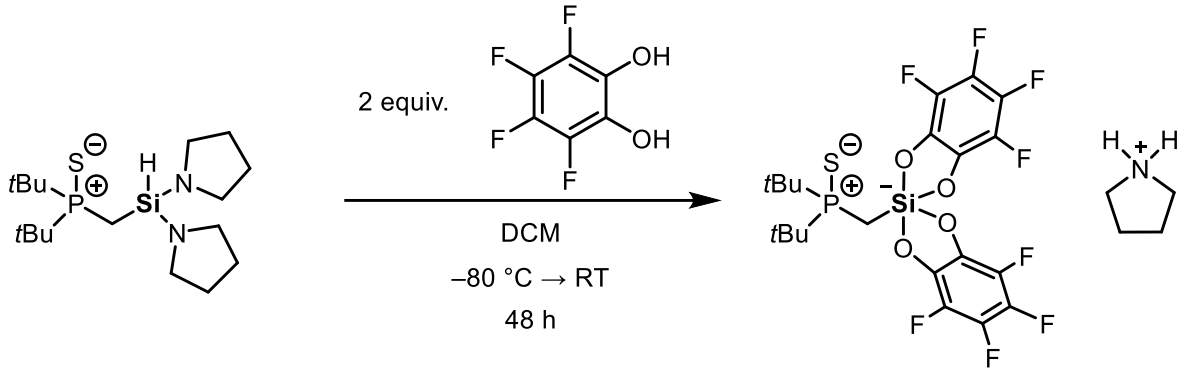

6 **9**

Compound **6** (800 mg, 2.22 mmol, 1 equiv) was dissolved in 2 mL of DCM. In a separate Schlenk flask 3,4,5,6-tetrafluorobenzene-1,2-diol (807.8 mg, 4.44 mmol, 2 equiv) was dissolved in 2 mL of DCM. Both solutions were cooled to –80°C. Then the solution containing 3,4,5,6-tetrafluorobenzene-1,2-diol was slowly added to the strongly stirred solution containing compound **6**, over the course of 30 min. Immediate strong gas evolution was observed. Afterwards the reaction mixture was stirred for 48 h at room temperature. Next all volatiles were removed *in vacuo* and the residue dissolved in 2 mL of Et_2O. The solution was crystallized at –30°C. The product was isolated via filtration and dried *in vacuo*. Compound **9** was obtained as colorless crystals suitable for single-crystal X-ray diffraction analysis. Yield: 1.2 g (1.84 mmol, 83%).

^{1}H NMR (400.13 MHz, CD_2Cl_2, 298 K): δ 8.28 (bs, 2H, NH_2), 3.57–3.53 (m, 4H, CH_2), 2.12–2.09 (m, 4H, CH_2), 1.51 (d, $^{2}J_{P–H}$ = 14.3 Hz, 2H, SiCH_2P), 1.19 {d, $^{3}J_{P–H}$ = 15.3 Hz, 18H, P[C(CH_3)$_3$]$_2$}.

^{13}C{^{1}H} NMR (100.61 MHz, CD_2Cl_2, 298 K): δ 136.6 (s, *C*F), 133.9 (s, *C*F), 46.3 (s, *C*H_2), 39.0 {d, $^{1}J_{P–C}$ = 42.9 Hz, P[*C*(CH_3)$_3$]$_2$}, 27.2 {d, $^{2}J_{P–C}$ = 1.7 Hz, P[C(*C*H_3)$_3$]$_2$}, 24.8 (s, *C*H_2), 12.6 (d, $^{1}J_{P–C}$ = 35.0 Hz, Si*C*H_2P).

^{31}P{^{1}H} NMR (162.04 MHz, CD_2Cl_2, 298 K): δ 76.8 [s, *P*(S)].

^{19}F{^{1}H} NMR (376.66 MHz, CD_2Cl_2, 298 K): δ –168.1 (m, 4H, CF_{Ar}), –174.5 (m, 4H, CF_{Ar}).

^{29}Si{^{1}H} NMR (79.49 MHz, CD_2Cl_2, 298 K): δ –75.2 (d, $^{2}J_{P–Si}$ = 6.5 Hz, PCH_2*Si*)

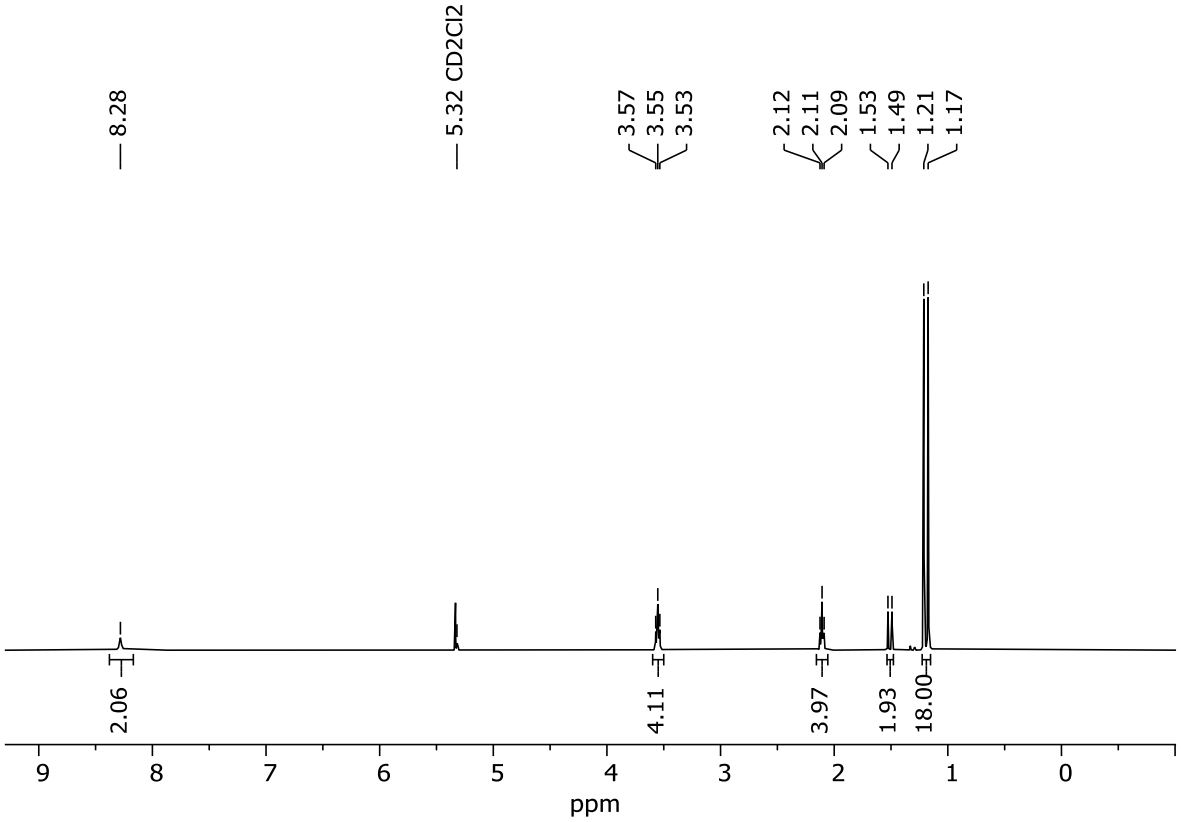

Figure S28: ^{1}H NMR (400.13 MHz, CD_2Cl_2, 298 K) spectrum of compound **9**.

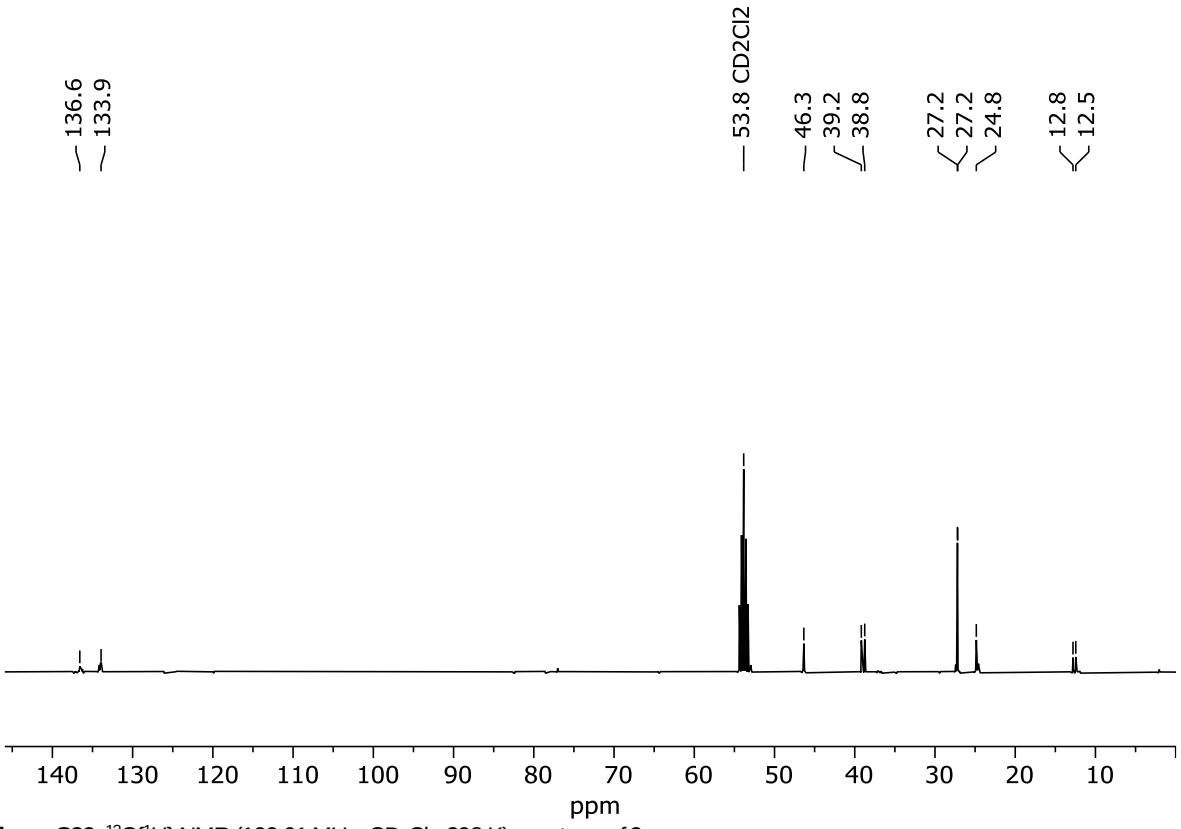

Figure S29: $^{13}C\{^{1}H\}$ NMR (100.61 MHz, CD_2Cl_2, 298 K) spectrum of **9**.

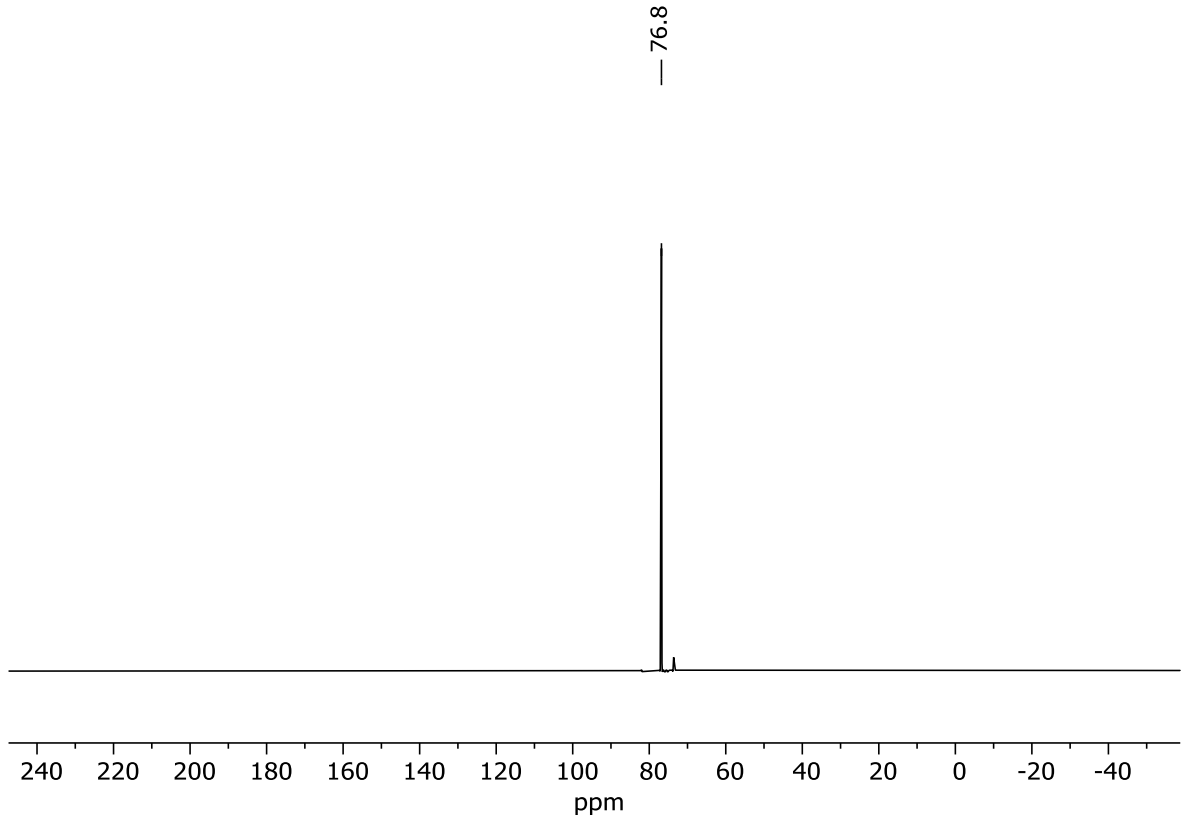

Figure S30: $^{31}P\{^{1}H\}$ NMR (162.04 MHz, CD_2Cl_2, 298 K) of compound **9**.

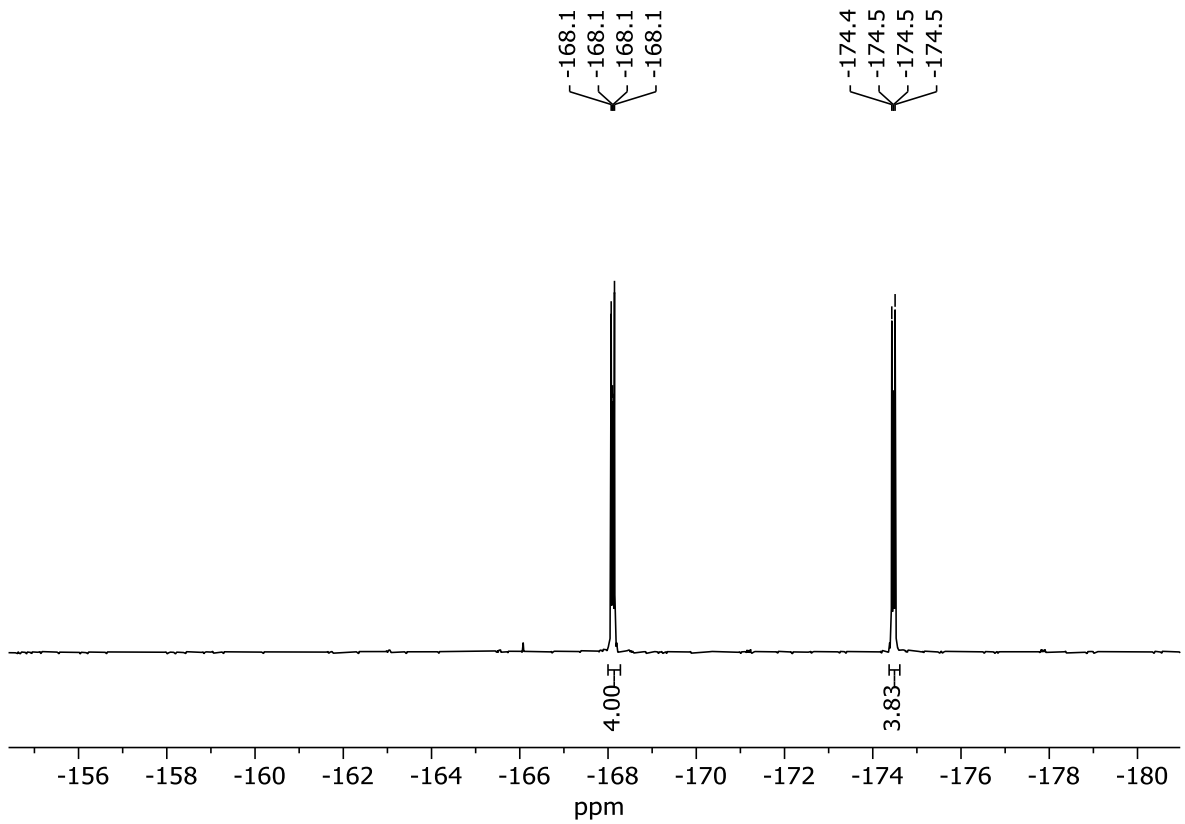

Figure S31: $^{19}F\{^{1}H\}$ NMR (376.66 MHz, CD_2Cl_2, 298 K) of compound **9**.

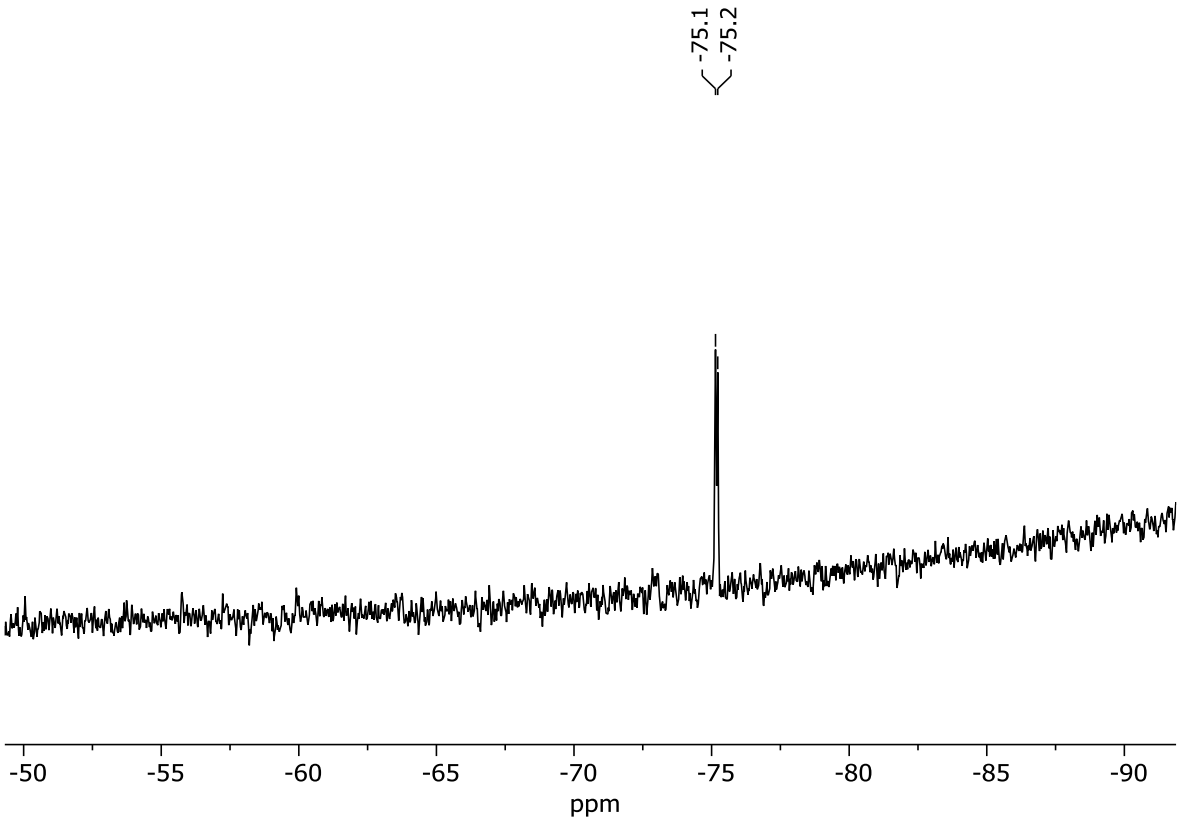

Figure S32: $^{29}Si\{^{1}H\}$ NMR (79.49 MHz, CD_2Cl_2, 298 K) of compound **9**.

5.6.11 X-ray crystallographic details

The crystals were selected and measured either on a SuperNova Dualflex diffractometer equipped with a TitanS2 detector (**2**, **6**) or a XtaLAB Synergy R, DW system, equipped with a HyPix-Arc 150 detector (**3**, **7**, **9**). Data collection and reduction were performed with CrysAlisPro {Version 1.171.43.36a for all compounds}.[5] A numerical absorption correction based on Gaussian integration over a multifaceted crystal model, and an empirical absorption correction using spherical harmonics, implemented in SCALE3 ABSPACK scaling algorithm was applied for all compounds. Using Olex2,[6] the structures were solved with ShelXT[7] and a least-square refinement on F^2 was carried out with ShelXL[7]. All non-hydrogen atoms were refined anisotropically. Hydrogen atoms at the carbon atoms were located in idealized positions and refined isotropically according to the riding model. Hydrogen atoms at the silicon and nitrogen atoms were located from the difference Fourier map and refined without restraints. The figures in the manuscript and Supporting Information were created with Olex2.[6]

Compound **2**: The asymmetric unit contains one molecule.

Compound **3**: The asymmetric unit contains one molecule.

Compound **6**: The asymmetric unit contains one molecule.

Compound **7**: The asymmetric unit contains one molecule.

Compound **9**: The asymmetric unit contains one molecule.

Table S1: Crystallographic information for compounds **2**,**3** and **6**.

Compound	**2**	**3**	**6**
Data Set (internal naming)	AF270	AF297	AF302
CCDC Number	-	-	-
Formula	$C_{21}H_{21}F_{10}PSSi$	$C_{21}H_{31}PSSi$	$C_{17}H_{37}N_2PSSi$
$\rho_{calc.}$ / g·cm^{-3}	1.541	1.188	1.167
μ/mm^{-1}	3.130	2.621	2.673
Formula Weight	554.50	374.58	360.60
Color	clear colorless	clear colorless	clear whiteish white
Shape	prism	needle	irregular
Size/mm^3	0.36 x 0.14 x 0.06	0.44 x 0.03 x 0.03	0.51 x 0.29 x 0.26
T/K	123.15	123.00(10)	123.00(10)
Crystal System	monoclinic	orthorhomic	monoclinic
Space Group	*Cc*	$P2_12_12_1$	*C*2/*c*
a/Å	16.2086(4)	6.1120(10)	20.010(2)
b/Å	11.8577(2)	13.7862(2)	6.71810(10)
c/Å	12.4651(2)	22.9828(4)	30.5927(4)
α/°	90	90	90
β/°	94.017(2)	90	93.1910(10)
γ/°	90	90	90
V/Å^3	2389.87(8)	2094.73	4106.32(9)
Z	4	4	8
Z'	1	1	1
Wavelength/Å	1.54184	1.54184	1.54184
Radiation Type	Cu K_α	Cu K_α	Cu K_α
$2\Theta_{min}$/°	9.248	7.478	8.852
$2\Theta_{max}$/°	133.67	145.884	133.588
Measured Refl.	11839	10127	14815
Independent Refl.	3123	3726	3610
R_{int}	0.0560	0.0235	0.0410
Parameters	317	227	209
Restraints	0	0	0
Largest Peak	0.38	0.24	0.34
Deepest Hole	-0.26	-0.21	-0.36
GooF	1.024	0.981	1.036
wR_2 (all data)	0.1106	0.0663	0.0923
wR_2	0.1096	0.0652	0.0917
R_1 (all data)	0.0445	0.0279	0.0345
R_1	0.0437	0.0258	0.0339

Table S2: Crystallographic information for compounds **7** and **9**.

Compound	**7**	**9**
Data Set (internal naming)	AF305b	AF306
CCDC Number	-	-
Formula	$C_{25}H_{30}F_{10}NO_2PSSi$	$C_{25}H_{30}F_8NO_4PSSi$
$\rho_{calc.}$ / g·cm^{-3}	1.511	1.511
μ/mm^{-1}	2.747	2.718
Formula Weight	657.62	651.62
Color	clear colorless	clear colorless
Shape	plate	needle
Size/mm^3	0.09 x 0.06 x 0.04	0.23 x 0.04 x 0.03
T/K	123.00(10)	123.00(10)
Crystal System	monoclinic	triclinic
Space Group	$P2_1/n$	$P\bar{1}$
a/Å	12.4717(4)	11.4317(8)
b/Å	13.9332(4)	12.1339(10)
c/Å	16.8142(7)	12.6030(9)
α/°	90	109.131(8)
β/°	98.438(4)	103.165(7)
γ/°	90	110.116(7)
V/Å^3	2890.19(18)	1432.1(2)
Z	4	2
Z'	1	1
Wavelength/Å	1.54184	1.54184
Radiation Type	Cu K_α	Cu K_α
$2\Theta_{min}$/°	8.274	8.042
$2\Theta_{max}$/°	151.956	156.736
Measured Refl.	27983	26777
Independent Refl.	5840	5758
R_{int}	0.0703	0.1329
Parameters	384	376
Restraints	0	0
Largest Peak	0.37	0.56
Deepest Hole	-0.55	-0.60
GooF	1.129	1.062
wR_2 (all data)	0.1594	0.3133
wR_2	0.1489	0.2713
R_1 (all data)	0.0758	0.1477
R_1	0.0545	0.0997

Compound **2**

Hydrogen atoms except Si–H are omitted for clarity.

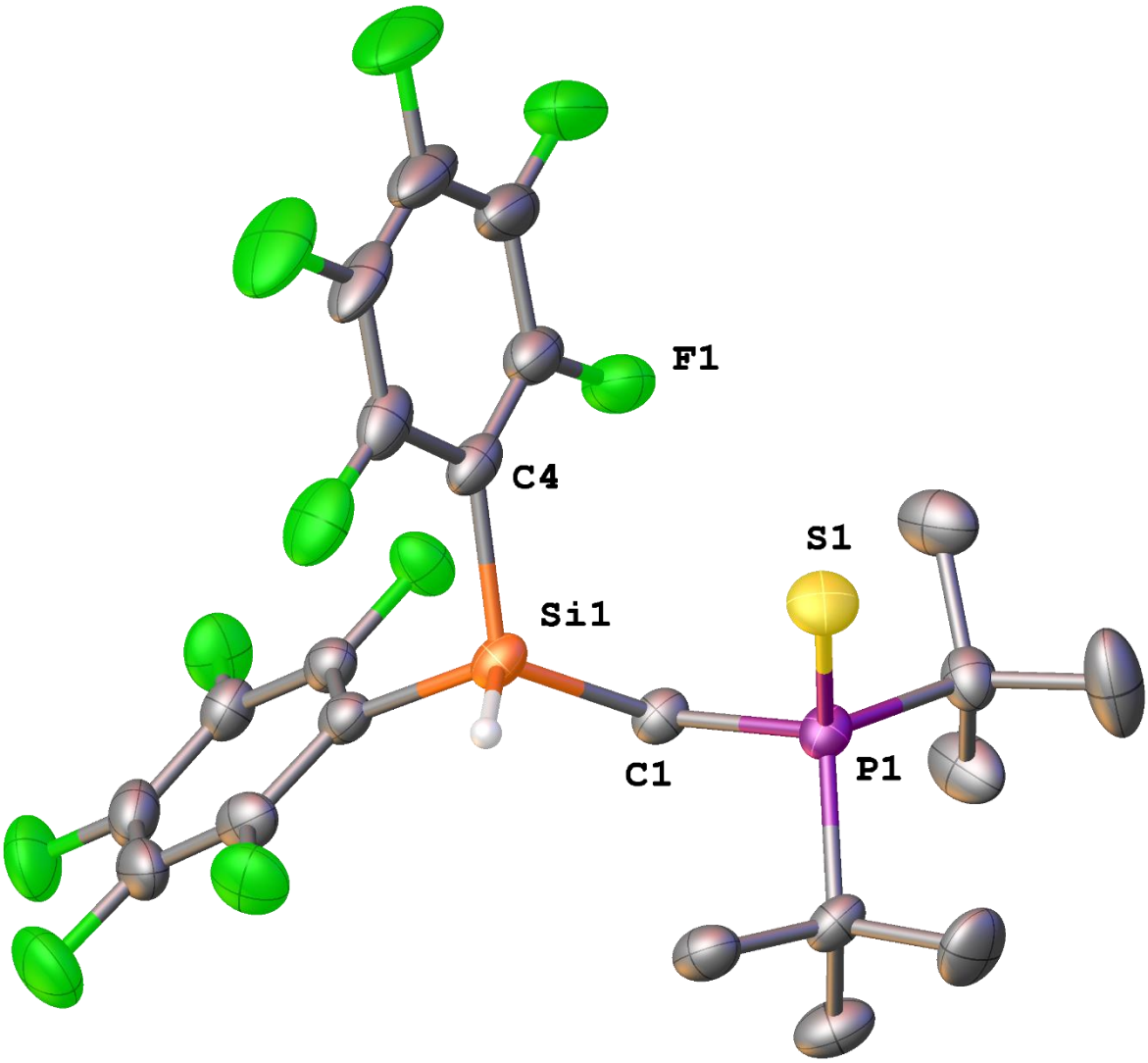

Selected Bond Lengths in Å		Selected Bond Angles in °	
P(1)–S(1)	1.9697(13)	**Si(1)–C(1)–P(1)**	116.8(2)
P(1)–C(1)	1.817(4)	**S(1)–P(1)–C(1)**	110.04(13)
Si(1)–C(4)	1.887(5)	**C(1)–Si(1)–C(4)**	116.79(19)

Compound **3**

Hydrogen atoms except Si–H are omitted for clarity.

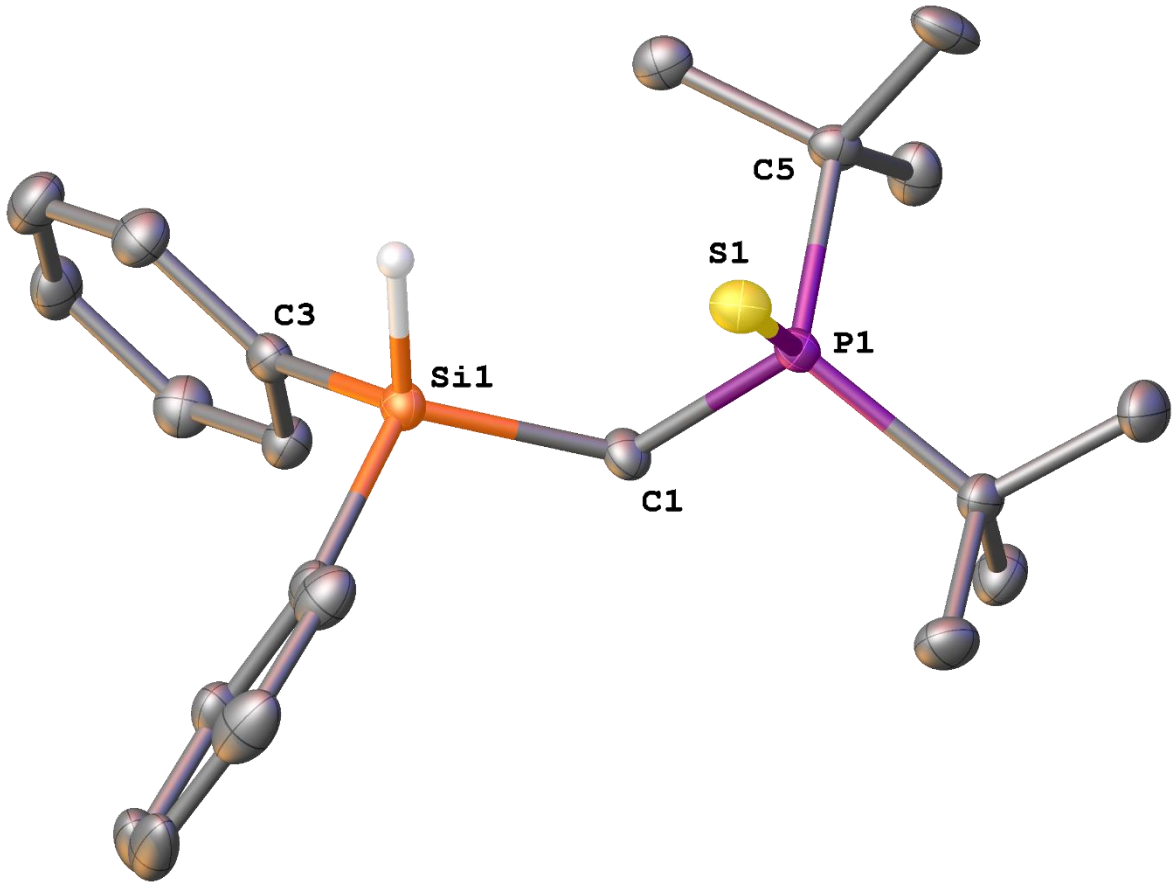

Selected Bond Lengths in Å		**Selected Bond Angles in °**	
P(1)–S(1)	1.9737(8)	**Si(1)–C(1)–P(1)**	117.64(11)
P(1)–C(1)	1.817(2)	**S(1)–P(1)–C(1)**	111.85(8)
Si(1)–C(1)	1.902(2)	**C(1)–Si(1)–C(3)**	109.55(10)

Compound **6**

Hydrogen atoms except Si–H are omitted for clarity.

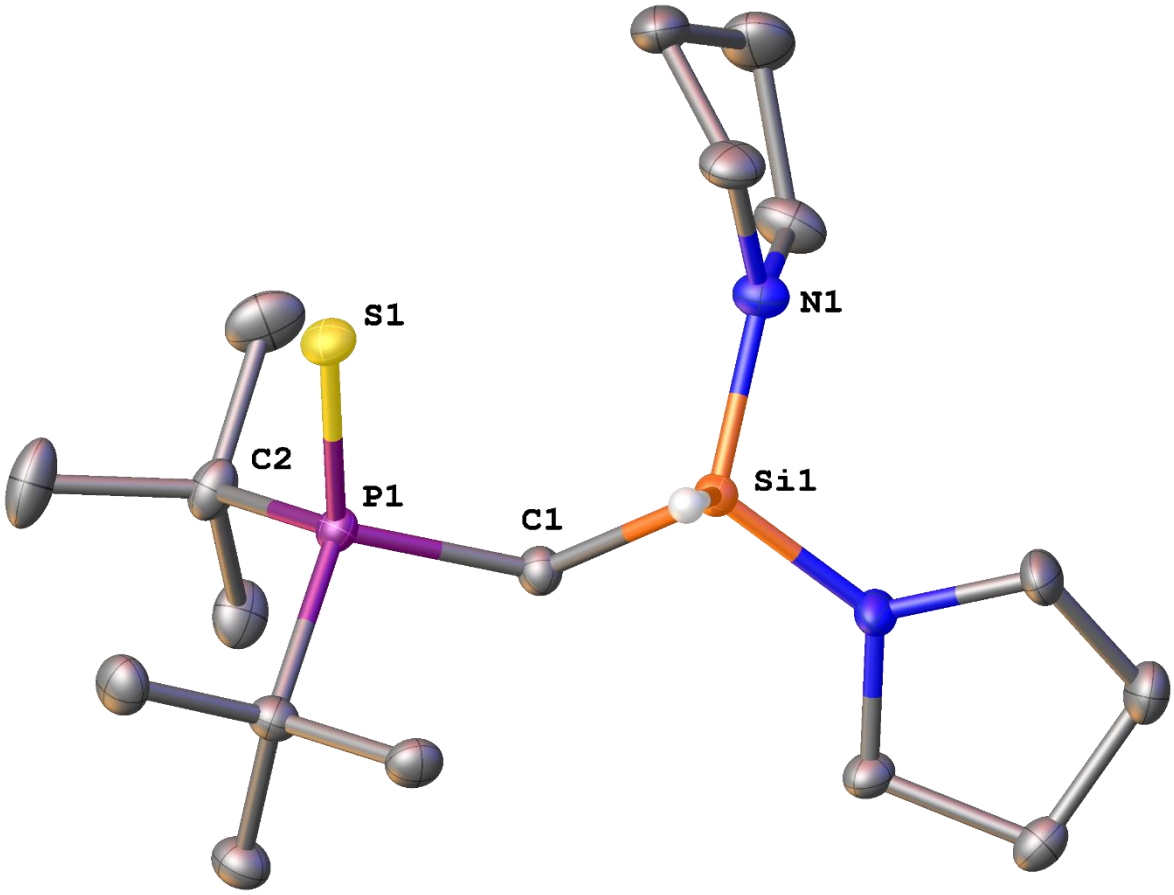

Selected Bond Lengths in Å		**Selected Bond Angles in °**	
P(1)–S(1)	1.9700(5)	**Si(1)–C(1)–P(1)**	117.15(9)
P(1)–C(1)	1.8144(16)	**S(1)–P(1)–C(1)**	113.06(5)
Si(1)–N(1)	1.7033(13)	**C(1)–Si(1)–N(1)**	113.65(7)

Compound **7**

Hydrogen atoms except Si–H and N–H are omitted for clarity.

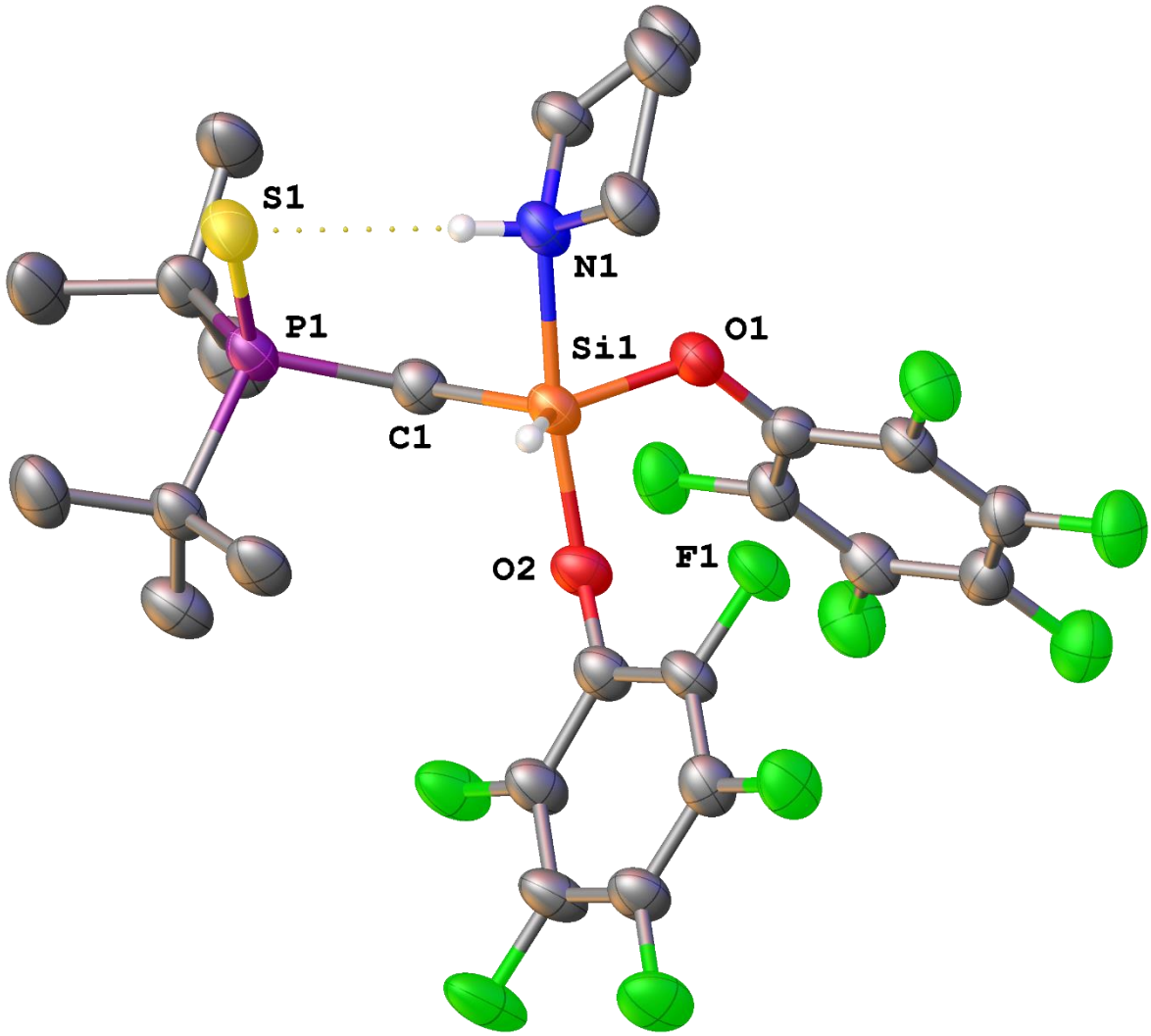

Selected Bond Lengths in Å		**Selected Bond Angles in °**	
P(1)–S(1)	1.9766(13)	**Si(1)–C(1)–P(1)**	125.25(18)
Si(1)–O(1)	1.702(2)	**N(1)–Si(1)–O(1)**	83.31(12)
Si(1)–N(1)	1.986(3)	**N(1)–Si(1)–O(2)**	173.18(11)

Compound **9**

Hydrogen atoms except N–H are omitted for clarity.

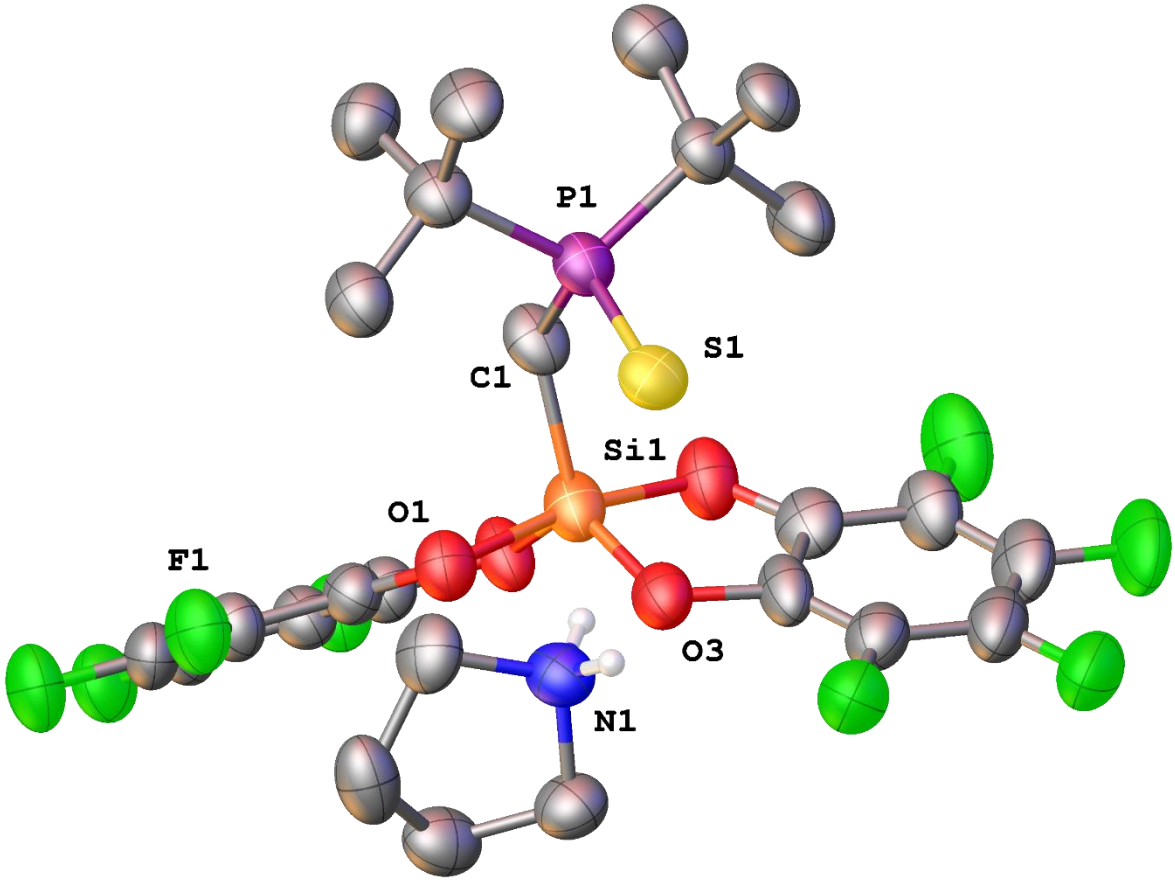

Selected Bond Lengths in Å		Selected Bond Angles in °	
P(1)–S(1)	1.988(2)	**Si(1)–C(1)–P(1)**	121.4(4)
Si(1)–O(1)	1.805(4)	**O(1)–Si(1)–O(3)**	84.7(2)
Si(1)–C(1)	1.891(7)	**C(1)–P(1)–S(1)**	114.4(2)

5.6.12 Supplementary references

(1) Hägele, G.; Tossing, G.; Kückelhaus, W.; Seega, J. Diastereomere Organophosphorverbindungen, I Darstellung und Eigenschaften von CH_3(*t*-C_4H_9)P(X)–Y–(Z)P(*t*-C_4H_9)CH_3. *Z. Naturforsch.* **1984**, *39b*, 1574–1580.

(2) Fearon, F. W. G.; Gilman, H. Polyhalo-organometallic and -organometalloidal compounds. VII. Preparation of some pentafluorophenyl substituted organosilicon compounds. *J. Organomet. Chem.* **1967**, *10*, 409–419.

(3) (a) Rach, S. F.; Herdtweck E.; Kühn, F. E. *J. Organomet. Chem.* **2011**, *696*, 1817. (b) Jutzi, P.; Müller, C.; Stammler, A.; Stammler, H.-G. Synthesis, Crystal Structure, and Application of the Oxonium Acid $[H(OEt_2)_2][B(C_6F_5)_4]$ -. *Organometallics* **2000**, *19*, 1442–1444.

(4) Levin, V. V.; Dilman, A. D.; Belyakov, P. A.; Korlyukov, A. A.; Struchkova, M. I.; Tartakovsky, V. A. Tris(pentafluorophenyl)silyl Triflate: Synthesis and Silylation of Carbonyl Compounds. *Eur. J. Org. Chem.* **2004**, *24*, 5141–5148.

(5) Rigaku Oxford Diffraction, CrysAlisPro Software System. 2020.

(6) Dolomanov, O. V.; Bourhis, L. J.; Gildea, R. J.; Howard, J. A. K.; Puschmann, H. *OLEX2*: a complete structure solution, refinement and analysis program. *J. Appl. Crystallogr.* **2009**, *42*, 339-341.

(7) Sheldrick, G. M. *SHELXT* – Integrated space-group and crystal-structure determination. *Acta Crystallogr*. **2015**, *A71*, 3-8.

(8) Sheldrick, G. M. Crystal structure refinement with *SHELXL*. *Acta Crystallogr.* **2015**, *C71*, 3-8.

6 Development of enantioselective silane thiol HAT catalysts

Preface

This chapter describes a detailed discussion about the synthesis and development of chiral silane thiol compounds. The complete study has already been published in:

Grotjahn, S.; Müller, L.; Pattanaik, A.; Falk, A.; Barison, G.; Bauer, J. O.; Rehbein, J.; Gschwind, R. M.; Burkhard, K. *Org. Chem. Front.* **2024**, 10.1039/D4QO01219D

Additionally compound **3** has already been published in:

Kümper, M.; Götz, T.; Espinosa-Jalapa, N. A.; Falk, A.; Rothfelder, R.; Bauer, J. O. *Z. Anorg. Allg. Chem.* **2023**, *649*.

Author contribution

All reported syntheses and characterizations in this chapter were performed by A. Falk. Catalysis screening of the synthesized catalysts and determination of the enantiomeric excess of the final substrate was performed by S. Grotjahn. The original script and supporting information were prepared by A. Falk and revised by Dr. J. O. Bauer.

Acknowledgements

This work was supported by the Deutsche Forschungsgemeinschaft (DFG, German Research Foundation) through the Research Training Group “Ion Pair Effects in Molecular Reactivity” (RTG 2620, project 426795949).

6.1 Abstract

This chapter presents the synthesis of various novel chiral silanethiols. In these compounds, the stereochemical information is either centered on the silicon atom or located in the backbone. The enantiomerically enriched silanethiols were then tested as catalysts in a photocatalyzed C–H activation reaction, where their potential in as asymmetric hydrogen-atom-transfer catalysts was studied.

6.2 Introduction

In the past decades, reports on silanethiols, the heavier analogs of silanols, have been relatively scarce. To the best of our knowledge, the first report on a silanethiol was published in 1951 by E. Larsson and R. Marin.[1] In this study, an alternative synthesis towards hexaalkyldisilathianes, first reported by C. Eaborn,[1b] was reported using trialkylamines and hydrogen sulfide gas. However, with the newly reported synthesis not only the hexaalkyldisilanthaines were obtained but also various trialkylsilanethiols.[1] The first report on the selective synthesis of a silanethiol, namely trimethylsilylsilanethiol, dates from 1952 and describes the reaction of LiSH with trimethylchlorosilane. Nevertheless, even in this synthesis, small amounts of hexamethyldisilathiane were produced as a byproduct.[2] A significant challenge in the general synthesis of silanethiols is the relatively low Si–S bond energy, when compared to the oxygen congeners (by 183 kJ/mol when substituent effects are neglected). This results in a higher tendency for condensation reactions, and especially their tendency to hydrolyze into the corresponding silanols when small quantities of water are present.[3] This implies that silanethiols must be either freshly prepared and subsequently stored in a cold environment or be kinetically stabilized by bulky ligands, as evidenced by numerous examples.[4] Consequently, the preparation of *Si*-stereogenic silanethiols represents a significant challenge and requires considerations of several factors to ensure the production of optically stable materials. It is therefore not surprising that the initial report on asymmetrically substituted Si–S compounds was published over a decade after their initial discovery by L. H. Sommer in 1966.[5] This publication describes the stereochemical aspects of a reaction sequence from the optically pure hydrosilane **1-I** to the silanethiol **6-I** (Scheme 1). In step 1 the initial hydrosilane **1-I** gets transformed with chlorine gas into the reactive chlorosilane **2-I**. Two equivalents of the chlorosilane **2-I** are reacted with dihydrogen sulfide gas in the presence of triethylamine to form the disilathiane **3-I**. Subsequent methanolysis of the reactive Si–S bond in **3-I** gives rise to the methoxysilane **4-I** in high optical purity as well as the ionic compound **5-I**. Since previous assignment of the reaction sequence from **1-I** to methoxysilane **4-I** proceeds with overall retention of configuration, and step 1 is known to proceed with retention of configuration, steps 2 and 3 have to proceed both with either retention or inversion of configuration.[5,6] The authors argue that predominantly inversion of configuration has been observed for reactions of chlorosilanes with various nucleophiles including alkoxide ions,[6b] and therefore steps 2 and 3 are more likely to proceed with inversion of configuration.[5] Furthermore the authors state, that compound **5-I** therefore forms with retention of configuration (Step 3.1) since the *Si* chiral center is not involved in the methanolysis of disilathiane **3-I**. Subsequently the ionic silathiolate **5-I** can be converted into the neutral silanethiol **6-I** by protonation with hydrochloric acid. Since step 4 also does not involve reaction the *Si*-chiral center, this step is also assumed to proceed with retention of configuration.

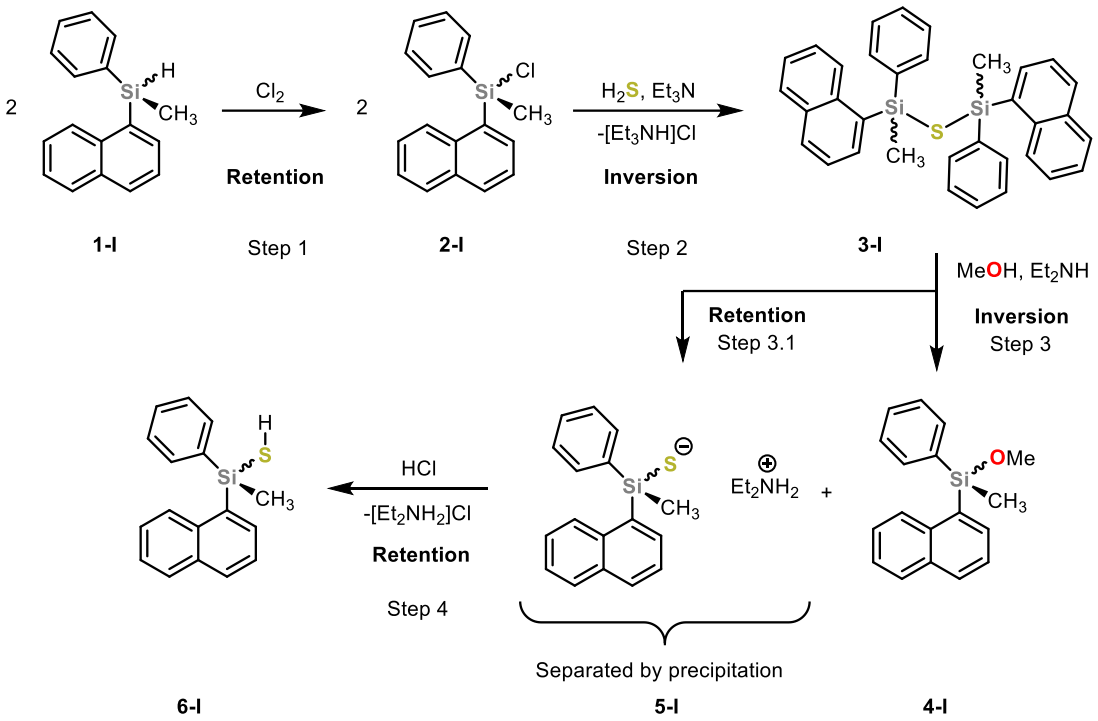

Scheme 1: First synthesis of optically active silanethiols as reported by L. H. Sommer in 1966.

However, no empirical proof of the absolute configuration nor for the optical purity was provided. To the best of our knowledge, this is the only publication to date that has addressed the topic of *Si*-stereogenic silanethiols and the stereochemical course of their synthesis. This finding is particularly notable considering that their smaller analogues, *Si*-stereogenic silanols, have been extensively investigated over the past decades.[7] One probable explanation is the complete absence of asymmetric catalytic methods for the formation of Si–SH moieties. This is in stark contrast to Si–OH moieties, where multiple approaches have been developed.[8] The reason for this is that hydrogen sulfide and other sulfides deactivate most catalytically active d-block metals, as evidenced by initial experiments on the dehydrogenative formation of silicon-sulfur bonds.[9] This together with the instability of the Si–S bond and the lack of applications for *Si*-chiral silanethiols made research on these compounds rather unattractive. However, times are changing and over the past two decades, silanethiols, particularly triisopropylsilanethiol and triphenylsilanethiol, have emerged as prominent polarity reversal catalysts.[10] The rates and selectivities of the hydrogen-atom abstractions in reactions involving electronically neutral free radicals are dependent upon polar effects operating within the transition states. This means electrophilic species, like silylthiyl radicals, are more likely to abstract hydrogen from an electron rich Si–H or C–H bond than from an electron deficient bond of similar strength. The idea of polarity-reversal catalysis (PRC) is to replace a single, because of mismatching polar effects slow, hydrogen atom abstraction reaction step with a polarity matching two-step process.[10] (Scheme 2).

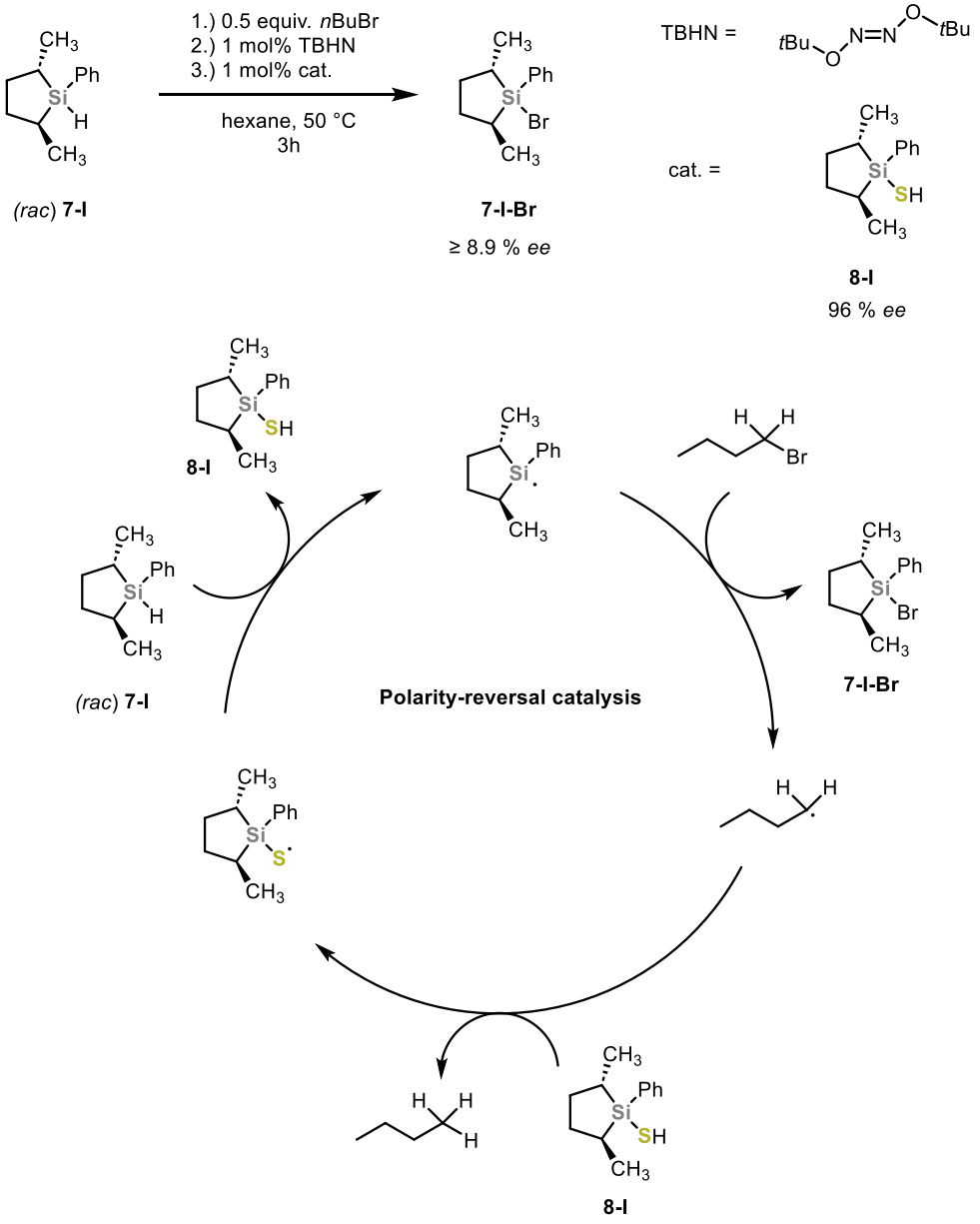

Scheme 2: Reported silanethiol catalyzed enantioselective PRC reported in 1995.

The silanethiol **8-I** has a dual role in the catalytic cycle depicted in Scheme 2. First and foremost, it serves as a polarity-reversal catalyst and therefore facilitates the otherwise slow reaction of the n-butyl radical with the hydrosilane (*rac*) **7-I**. However, in this case the silanethiol **8-I** is also chiral and therefore has a preferred enantiomer, from the racemic mixture of (*rac*) **7-I**, from which it abstracts the Si–H moiety. This leads to a slight enrichment of a single enantiomer (≥ 8.9 % *ee*) in the final brominated product **7-I-Br**. The potential of silanethiols in reactions involving radicals was soon recognized, and therefore silanethiols were also employed in photocatalyzed reactions as hydrogen atom transfer reagents.[11] One of the photocatalytic sequences employing silanethiols consist of a hydrogen-atom-transfer (HAT) facilitates by a silanethiol, a reductive radical-polar crossover (RRPCO) reducing the radicals to anions followed by a protonation step (HAT/RRPCO/protonation) (Scheme 3).[11]

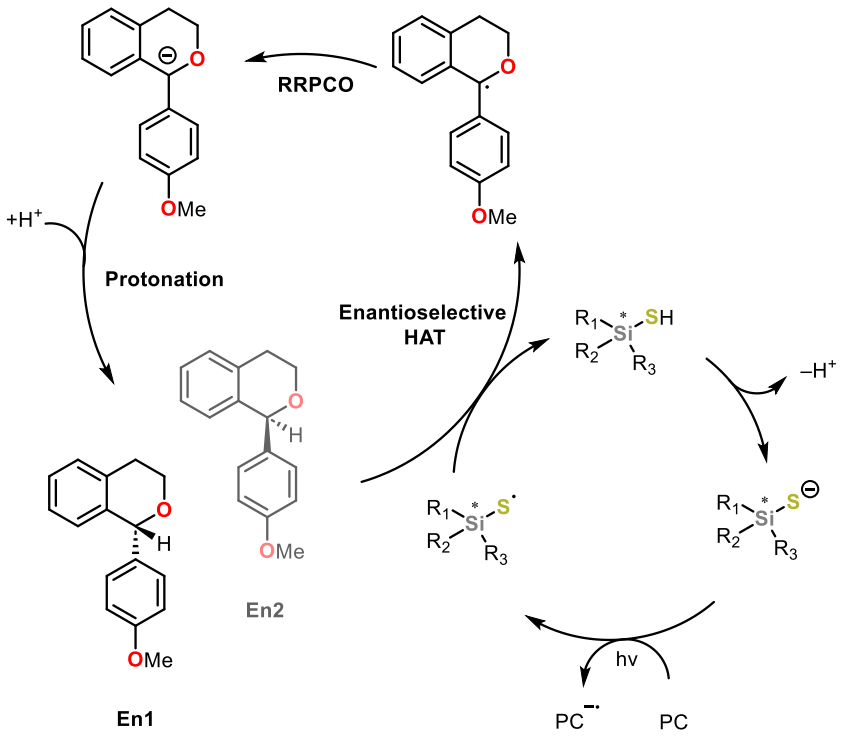

Scheme 3: Simplified photocatalytic HAT-RRPCO-Protonation sequence for the deracemization of benzylic C–H bonds (PC: Photocatalyst).

The mechanism of the enrichment of a single enantiomer relies on an enantioselective hydrogen-atom abstraction from a silylthiyl radical. However, the crucial difference between this approach and the one shown in Scheme 2 lies in the destruction of the chiral information during this step. Subsequent achiral transformation into a carbanion by RRPCO and protonation produces both enantiomers in a racemic mixture, but because the HAT step is enantioselective the more reactive enantiomer **En2** is also more likely to get racemized while the less reactive enantiomer **En1** is slowly enriched. The idea presented within this chapter was to design and synthesize silanethiols, which would both act as potent hydrogen-atom transfer catalysts and were able to deracemize substrates by enantioselective hydrogen-atom abstraction from the benzylic C–H bonds. In the following discussion several silanethiol design motives were synthesized and then tested for their catalytic activity and stereoselectivity within the presented HAT-RRPCO-Protonation sequence.

6.3 Results and Discussion

6.3.1 Preparation of silanethiols with backbone chirality

The investigation started with the synthesis of the (–)-menthol-substituted compound **1** (Scheme 4). The synthesis of (–)-menthol-substituted compound **1** (Scheme 3) commenced with the preparation of (–)-trimenthoxy(chloro)silane, which was obtained from a reaction between three equivalents of (–)-menthol and tetrachlorosilane in the presence of triethylamine. The subsequent introduction of the SH moiety was facilitated by the use of lithium hydrosulfide as a suitable reagent.[12]

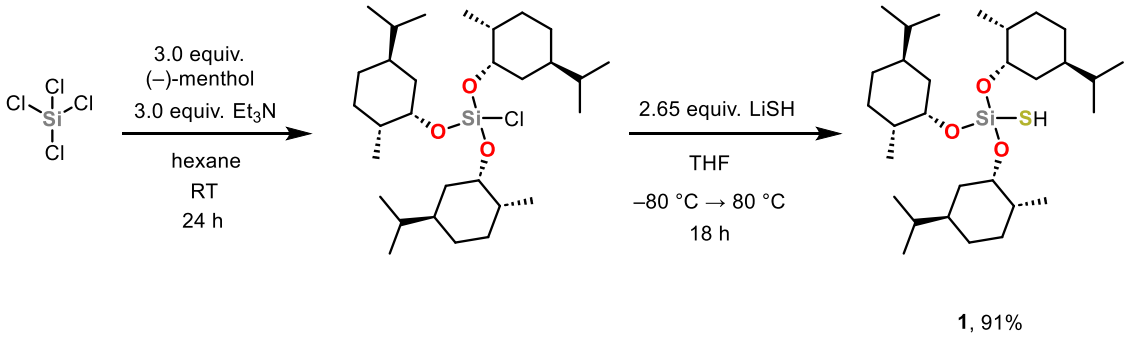

Scheme 4: Synthesis of compound **1** via nucleophilic substitution with lithium hydrosulfide.

Lithium hydrosulfide was freshly prepared from a 0.5 M H_2S solution in tetrahydrofuran (THF) and *n*-butyllithium. To ensure complete conversion, an excess of lithium hydrosulfide and heating to 80°C was employed. To our satisfaction, compound **1** was obtained in an excellent yield and exhibited no tendency for condensation, presumably due to hinderance by the bulky (–)-menthoxy groups. Compound **1** is a clear oil that became a waxy solid upon storage at room temperature over several months. Unfortunately, no single-crystals could be obtained. Nevertheless, the structure could be unambiguously identified as compound **1** by NMR spectroscopy and elemental analysis. The signal of the protic SH moiety was identified at 0.19 ppm in the ^{1}H-NMR spectrum, a value consistent with that observed in other tris(alkoxy)silanethiols.[13] When compound **1** was employed within the catalytic cycle depicted in Scheme 3 no enrichment of one enantiomer was found.[14] This lead us to focus on different systems.

6.3.2 Preparation of *Si*-chiral silanethiols

In order to maximize our chances of obtaining an enantioselective HAT catalyst based on silanethiols we expanded our synthesis efforts to *Si*-chiral thiosilanes. While this approach has the drawback of a more laborious synthesis it also brings the stereochemical information closer to the Si–S^- function which is active during the HAT step of the catalytic cycle (Scheme 3). This design might prove beneficial for the ability of the silylthiyl radical in the catalytic cycle to differentiate between both enantiomers. The structure of our choice should therefore be a silanethiol which is *Si*-chiral, easily accessible and possess bulky substituents to avoid condensation reactions. Luckily a method for easily obtaining bulky enantiomerically pure *Si*-chiral was already being developed by our group.[15] It involves the synthesis of compound **2** by reaction of di-methoxy(*tert*-butyl)phenylsilane with lithium (*S*)-

(1-phenylethyl)amide. Subsequently the pure diastereomer compound **2** was obtained from fractional crystallization from hexane at –30 °C (Scheme 5).[15] Our first attempt involved direct reaction of compound **2** with H_2S in THF (Scheme 5). However, no reaction with dihydrogen sulfide was observed. Instead, an alternative route was developed. The reaction of compound **2** with two equivalents of hydrogen chloride in diethyl ether resulted in the formation of the corresponding chlorosilane **2-Cl** in a smooth reaction. Subsequent reaction with freshly prepared lithium hydrosulfide yielded the final *Si*-chiral silanethiol **3** (Scheme 5). Compound **3** was obtained as a colorless oil, rendering the assignment of the absolute configuration difficult. The information in the literature does not allow for any clear statement on retention of inversion processes in the reaction sequence from **2** via **2-Cl** to **3**. While the majority of Si–N bond cleavages with hydrochloric acid in unpolar solvents proceeds with an inversion of configuration, indicating an S_N2-Si mechanism, some examples of retention of configuration are also known making a clear assignment of whether a retention or inversion process is present difficult.[16] As previously stated, only one publication to date has addressed the stereochemical course of the synthesis of silanethiols. However, the stereochemical course of substitution reactions of Si–Cl bonds with LiSH have not yet been studied.[5]

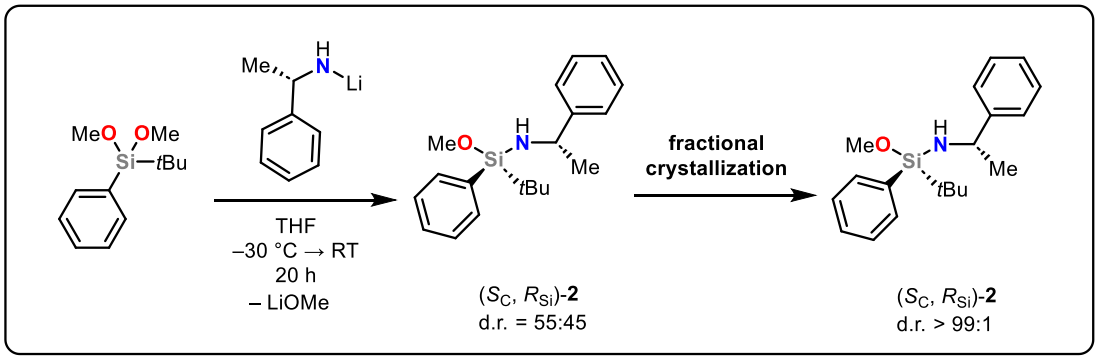

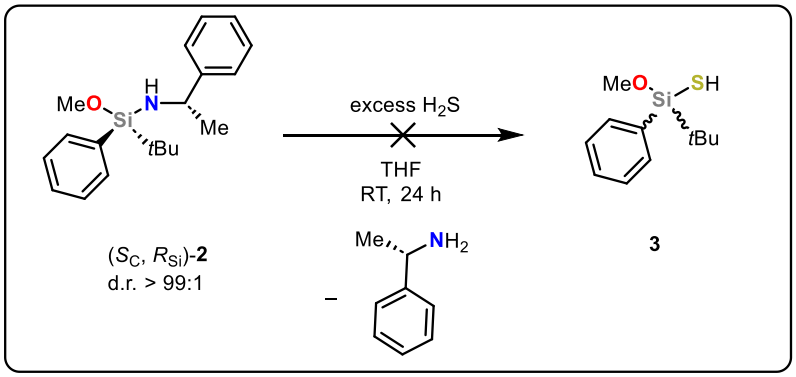

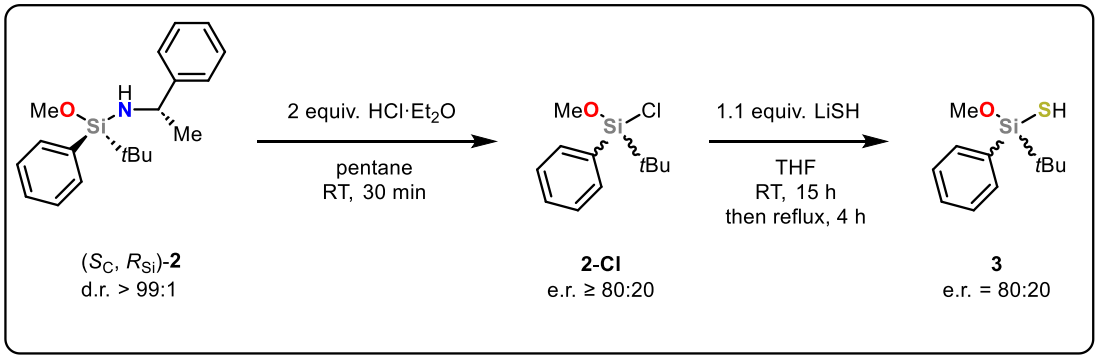

Scheme 5: Synthesis of compounds (S_C, R_{Si})-**2** and **3**, aswell as unsuccessful reaction of compound (S_C, R_{Si})-**2** with H_2S.

The enantiomeric ratio of **3** was determined by a reported ^{1}H-NMR spectroscopic method, developed by our group, using lithiated (*R*)-BINOL-dithiophosphoric acid [(*R*)-BINOL-PSSLi].[17] When compound **3** and (*R*)-BINOL-PSSLi are combined in CD_2Cl_2 and subjected to ^{1}H-NMR measurements at 223 K the enantiomeric ratio of **3** can be determined by integration of the S–H signals. Integration of the *Si*OMe signals in the ^{1}H-NMR at 298 K is also sufficient for the determination of enantiomeric ratio. Having our enriched silanethiol catalyst **3** at hand we tested it in the HAT-RRPCO-Protonation sequence (Scheme 3) found an 16 % *ee* in the final product.[14] This small success proved the viability of our approach and fueled our efforts to increase the stereoselectivity of the silanethiol catalysts. Subsequently, our next objective was to improve the stereoselectivity with a *Si*-chiral design which featured a rigid environment. Our initial approach involved the introduction of the chiral (*S*)-BINOL backbone (Scheme 6).

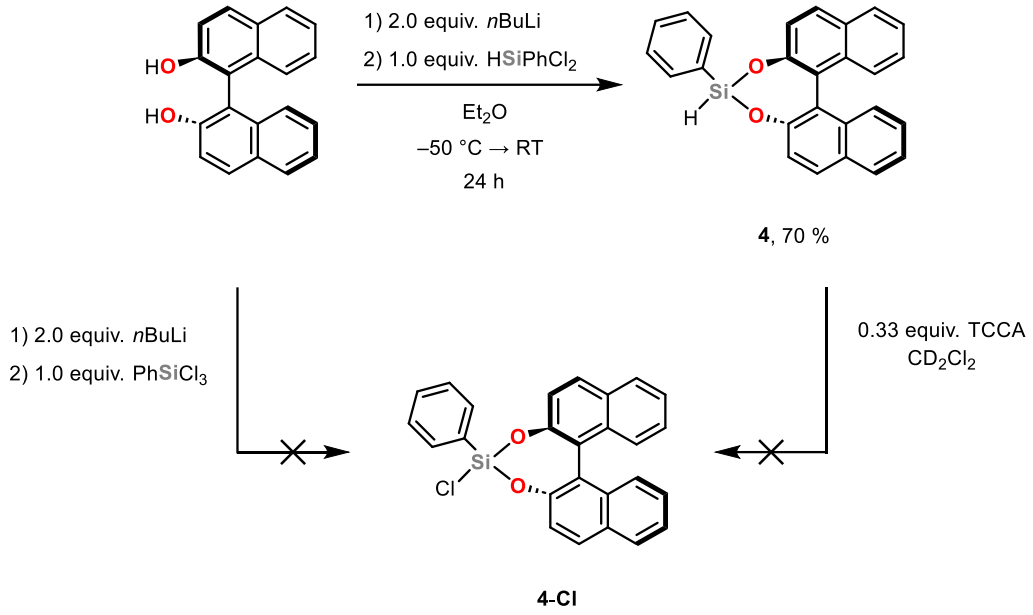

Scheme 6: Preparation of compound **4** and attempted routes towards target molecule **4-Cl**.

However, the synthesis towards the (*S*)-BINOL substituted chlorosilane **4-Cl** was troubled at the first step already. Direct synthesis from lithiated (*S*)-BINOL and $PhSiCl_3$ resulted in a complex mixture of unidentifiable products which were inseparable by Kugelrohrdistillation and flash column chromatography. Figuring that unselective substitutions might be taking place we modified the synthesis procedure towards **4-Cl**. To avoid unselective substitutions at the Si–Cl bonds we first synthesized the (*S*)-BINOL substituted hydrosilane **4**, which we obtained in good yield as a fine white powder. Subsequent chlorination of hydrosilane **4** with TCCA (trichloroisocyanuric acid) was initially successful, since no Si–H signal was observable within the ^{1}H-NMR spectrum. However, again a complex mixture of unidentifiable products was obtained. It is known that BINOL-substituted chlorosilanes can form transient Si(V)-species and this might interfere with the selective synthesis of **4-Cl**.[18] Therefore, we focused our attention other chiral *Si*-containing ring systems. In our search for alternative rigid *Si*-chiral systems we were drawn to *Si*-

chiral hydrosilanes encumbered within a rigid carbon-based ring system. Firstly, there are a multitude of reported methods for the stereospecific transformation of hydridosilanes into chlorosilanes[19]. Secondly, a large number of hydrosilanes can be introduced asymmetrically into carbon-based ring systems by dehydrogenative asymmetric Si–H/C–H coupling.[20] In particular, the ease of synthesis of ferrocene-based systems **5** and **6** (Scheme 7) led us to focus our attention on them. The synthesis of compounds **5** and **6** was carried out in accordance with the established procedure, employing an asymmetric rhodium-catalyzed Si–H/C–H coupling reaction.[20f] Both compounds feature one *Si*-chiral center in the *R*-configuration, and planar chirality with S_P configuration, as determined by single-crystal X-ray diffraction analysis.[20f] The subsequent step was the transformation of compounds **5** and **6** into silicon electrophiles, which could be reacted with LiSH. A variety of methods for transforming Si–H bonds were attempted, including reactions with bromine[6a,21], trichloroisocyanuric acid[19h], and carbon tetrachloride[19g]. However, all of these reactions were unsuccessful in our case, presumably due to a side reaction whereby ferrocene can be oxidized to its ferrocenium cation.

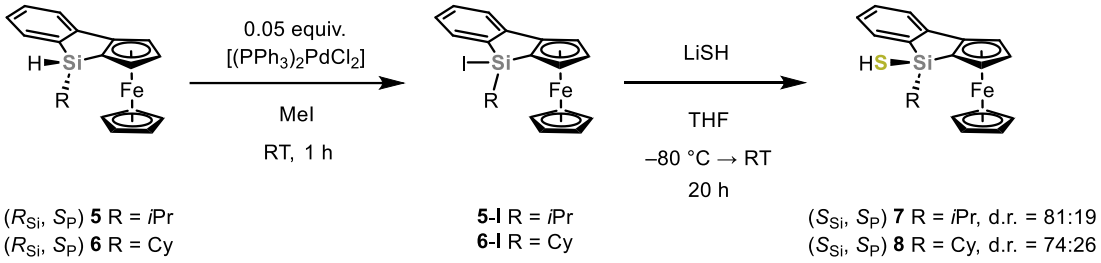

Scheme 7: Synthesis of chiral silane thiols **7** and **8** via an intermediate silyl iodide species.

Finally, we found a palladium dichloride-catalyzed iodination with methyl iodide as a suitable and mild method for the conversion of the hydrosilanes **5** and **6**.[19e] This gave the highly sensitive silyl iodide species **5-I** and **6-I**, which were directly reacted with LiSH in THF to form the desired chiral silane thiols **7** and **8**. Both species exhibit some degree of racemization, as evidenced by their determined diastereomeric ratios. However, the origin of this issue, whether it stems from the iodination step or the substitution step with LiSH, remains uncertain. This is because the diastereomeric ratios of the intermediates **5-I** and **6-I** could not be determined via chiral HPLC. The absolute configuration of compounds **7** and **8** was determined by single-crystal X-ray diffraction analysis (Figure 1).

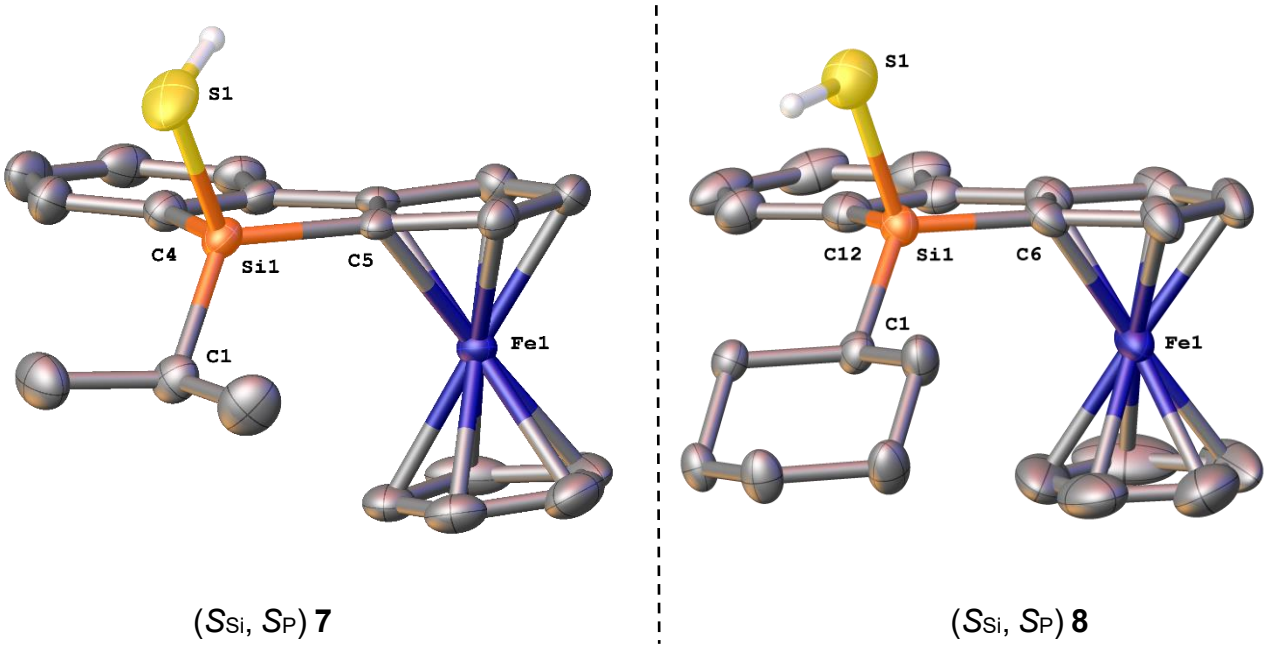

(S_{Si}, S_P) **7** (S_{Si}, S_P) **8**

Figure 1: Molecular structures of compounds **7** and **8** in the crystal (displacement ellipsoids set at the 50 % probability level). Selected bond lengths (Å) and angles (°) of **7**: Si(1)–S(1) 2.122(2), Si(1)–C(1) 1.868(6), Si(1)–C(5) 1.857(6), C(1)–Si(1)–S(1) 105.9(2), C(1)–Si(1)–C(5) 118.4(3), S(1)–Si(1)–C(5) 112.72(17). **8**: Si(1)–S(1) 2.132(3), Si(1)–C(1) 1.865(7), Si(1)–C(6) 1.846(7), C(1)–Si(1)–S(1) 109.2(2), C(1)–Si(1)–C(6) 117.2(3), S(1)–Si(1)–C(6) 111.4(2).

The planar chirality from compounds **5** and **6** are not affected during the subsequent iodination and substitution steps at silicon, therefore only partially racemizing the chiral *Si*-center giving diastereomers. However somewhat unclear is, whether the starting materials **5** and **6** are only diastereomerically pure or enantiomerically pure. The literature procedures from which these compounds were obtained states that compounds **5** and **6** were obtained in the ($Si_{R/S}$, R_P) configurations. However, only *ee* values were assigned to these compounds and neither the supplied chiral HPLC- nor the ^{1}H-NMR spectra show the presence of diastereomers.[20f] This led us to judge, that these compounds were indeed just obtained as a single enantiomerically pure diastereomer and during our modifications only the chiral *Si*-center was affected. Both compounds **7** and **8** crystallized in the orthorhombic crystal system with the space group $P2_12_12_1$ as large orange crystals. The Si–S bond distance is comparable in both compounds, with values of 2.122(2) Å in **7** and 2.132(3) Å in **8**. This is consistent with the expectation that the bond distance would be similar in compounds with just slightly differing alkyl substituents. At last compounds **7** and **8** were also subjected to the HAT-RRPCO-Protonation sequence, however immediately upon irradiation of the mixture decomposition of both catalysts was observed.[14] This may be caused by the ferrocene backbone of both compounds absorbing light in the same wavelength and engaging in undesired photooxidation processes.

6.4 Conclusions

In conclusion four novel silane thiols (**1**, **3**, **7**, and **8**) were synthesized and characterized. Of particular interest are the *Si*-chiral silane thiols **3**, **7**, and **8**, which represent three new examples in the field of *Si*-chiral thiosilanes. To the best of our knowledge, only two examples have been reported in the literature to date.[5,10d] Thus their synthesis and characterization adds valuable information to the scarce literature. Additionally, insights of

using these compounds as enantioselective HAT-catalysts in photochemical reactions were obtained. While compounds **7** and **8** were not stable under the reaction conditions employed, compounds **1** and **3** performed as excellent HAT catalysts. Although compound **1** was not stereoselective, compound **3** produced an *ee* of 16 % in the final product.[14] This lays the foundation for designs of future silanethiol HAT catalysts based on the general structure of compound **3**. In the future variation of reaction conditions will be employed to improve the obtained enantiomeric ratios, especially for compound **3** were only a moderately enriched sample produced an *ee* of 16 %.[14]

6.5 References

(1) (a) Larsson, E.; Marin, R. Notiz über die Reaktion zwischen Trialkyl-amino-silanen und Schwefelwasserstoff. *Acta Chem. Scand.* **1951**, *5*, 964–965. (b) Eaborn, C. A Conversion Series for Organosilicon Halides, Pseudohalides and Sulphides. *Nature* **1950**, *165*, 685–686.

(2) Champetier, G.; Etienne, Y.; Kullmann, R. Preparation of thiolsilanes and thiosilicones. *Compt. rend.* **1952**, *234*, 1985–1986.

(3) Luo, Y. R., *Comprehensive Handbook of Chemical Bond Energies*, CRC Press, Boca Ranton (FL), **2007**.

(4) (a) Baranowska, K.; Bulman, M.; Dołęga, A. (1*H*-Pyrazole-κ*N*)bis(tri-*tert*-butoxysilanethiolato-κ^2 *O*,*S*)cadmium. *Acta Crystallogr. Sect. E* **2012**, *68*, 1515. (b) I. J. S. Fairlamb (Ed.) *Specialist Periodical Reports*, Royal Society of Chemistry, Cambridge, **2010**. (c) Kays, D. L. in *Organometallic Chemistry*, pp. 56–76. (d) Khadka, C. B.; Macdonald, D. G.; Lan, Y.; Powell, A. K.; Fenske, D.; Corrigan, J. F. Trimethylsilylchalcogenolates of Co(II) and Mn(II): From mononuclear coordination complexes to clusters containing -ESiMe$_3$ moieties (E = S, Se). *Inorg. Chem.* **2010**, *49*, 7289–7297. (e) Komuro, T.; Kawaguchi, H.; Tatsumi, K. Synthesis and reactions of triphenylsilanethiolato complexes of manganese(II), iron(II), cobalt(II), and nickel(II). *Inorg. Chem.* **2002**, *41*, 5083–5090. (f) Pladzyk, A.; Kowalkowska-Zedler, D.; Ciborska, A.; Schnepf, A.; Dołęga, A. Complexes of silanethiolate ligands: Synthesis, structure, properties and application. *Coord. Chem. Rev.* **2021**, *437*, 213761. (g) Sydora, O. L.; Henry, T. P.; Wolczanski, P. T.; Lobkovsky, E. B.; Rumberger, E.; Hendrickson, D. N. Aggregation of (*t*Bu$_3$SiS)MX: Structures of {Br$_2$Fe(μ-SSi*t*Bu$_3$)$_2$)FeBr(THF)Na(THF)$_4$}$_\infty$, *cis*-(THF)FeI$_2$(μ-SSitBu$_3$)$_2$, (*t*Bu$_3$SiS)Fe$_2$(μ-SSi*t*Bu$_3$)$_2$, and comparative structure and magnetism studies of (*t*Bu$_3$SiS)MX$_n$ (M = Fe, Co, X = Cl, n = 12; M = Fe, Ni, X = Br, n = 12; M = Fe, X = I, n = 14). *Inorg. Chem.* **2006**, *45*, 609–626.

(5) Sommer, L. H.; McLick, J. Stereochemistry of asymmetric silicon. The silicon-sulfur bond. *J. Am. Chem. Soc.* **1966**, *88*, 5359–5361.

(6) (a) Sommer, L. H.; Frye, C. L.; Parker G. A. Stereochemistry of Asymmetric Silicon. I. Relative and Absolute Configurations of Optically Active α-Naphthylphenylmethylsilanes. *J. Am. Chem. Soc.* **1964**, *86*, 3276. (b) Sommer, L. H.; Frye, C. L.; Parker G. A.; Michael, K. W. Stereochemistry of Asymmetric Silicon. II. Alkoxy and Siloxy Leaving Groups. *J. Am. Chem. Soc.* **1964**, *86*, 3271.

(7) (a) Klare, H. F. T.; Oestreich, M. Chiral recognition with silicon-stereogenic silanes: remarkable selectivity factors in the kinetic resolution of donor-functionalized alcohols. *Angew. Chem. Int. Ed.* **2007**, *46*, 9335–9338. (b) Rendler, S.; Auer, G.; Oestreich, M. Kinetic resolution of chiral secondary alcohols by dehydrogenative coupling with recyclable silicon-stereogenic silanes. *Angew. Chem. Int. Ed.* **2005**, *44*, 7620–7624. (c) Rendler, S.; Oestreich, M. Kinetic resolution and desymmetrization by stereoselective silylation of alcohols. *Angew. Chem. Int. Ed.* **2008**, *47*, 248–250. (d) Mori, A.; Toriyama, F.; Kajiro, H.; Hirabayashi, K.; Nishihara, Y.; Hiyama, T. Synthesis and Optical Resolution of Novel Chiral Silanols. *Chem. Lett.* **1999**, *28*, 549–550. (e) Tomooka, K.; Nakazaki, A.; Nakai, T. A novel aryl migration from silicon to carbon: An efficient approach to asymmetric synthesis of a α-aryl β-hydroxy cyclic amines and silanols. *J. Am. Chem. Soc.* **2000**, *2*, 408–409. (f) Igawa, K.; Takada, J.; Shimono, T.; Tomooka, K. Enantioselecive Synthesis of Silanol. *J. Am. Chem. Soc.* **2008**, *48*, 16132–16133.

(8) (a) Huang, W.-S.; Xu, H.; Yang, H.; Xu, L.-W. Catalytic Synthesis of Silanols by Hydroxylation of Hydrosilanes: From Chemoselectivity to Enantioselectivity. *Chem. Eur. J.* **2024**, *30*, e202302458. (b) Wu, Y.; Wang, P. Silicon-Stereogenic Monohydrosilane: Synthesis and Applications. *Angew. Chem. Int. Ed.* **2022**, *134*. (c) Yang, W.; Liu, L.; Guo, J.; Wang, S.-G.; Zhang, J.-Y.; Fan, L.-W.; Tian, Y.; Wang, L.-L.; Luan, C.; Li, Z.-L. et al. Enantioselective Hydroxylation of Dihydrosilanes to *Si*-Chiral Silanols Catalyzed by In Situ Generated Copper(II) Species. *Angew. Chem. Int. Ed.* **2022**, *134*, e202205743. (d) Yuan, W.; Zhu, X.; Xu, Y.; He, C. Synthesis of *Si*-Stereogenic Silanols by

Catalytic Asymmetric Hydrolytic Oxidation. *Angew. Chem. Int. Ed.* **2022**, *61*, e202204912. (e) Zhu, J.; Chen, S.; He, C. Catalytic Enantioselective Dehydrogenative Si-O Coupling to Access Chiroptical Silicon-Stereogenic Siloxanes and Alkoxysilanes. *J. Am. Chem. Soc.* **2021**, *143*, 5301–5307.

(9) Sommer, L. H.; Citron, J. D. Group VIII metal-catalyzed reactions of organosilicon hydrides with amines, hydrogen halides, and hydrogen sulfide. *J. Org. Chem.* **1967**, *32*, 2470–2472.

(10) (a) Cai, Y.; Roberts, B. P. The mechanism of polarity-reversal catalysis as involved in the radical-chain reduction of alkyl halides using the silane–thiol couple. *J. Chem. Soc., Perkin Trans. 2* **2002**, 1858–1868. (b) Dang, H.-S.; Elsegood, M. R. J.; Kim, K.-M.; Roberts, B. P. Radical-chain reductive alkylation of electron-rich alkenes mediated by silanes in the presence of thiols as polarity-reversal catalysts. *J. Chem. Soc., Perkin Trans. 1* **1999**, 2061–2068. (c) Dang, H.-S.; Kim, K.-M.; Roberts, B. P. Radical-chain reductive carboxyalkylation of electron-rich alkenes: carbon–carbon bond formation mediated by silanes in the presence of thiols as polarity-reversal catalysts. *Chem. Commun.* **1998**, 1413–1414. (d) Dang, H.-S.; Roberts, B. P. Enantioselective Hydrogen-atom Abstraction by Homochiral Silanethiyl Radicals. *Tetrahedron Letters* **1995**, *36*, 3731–3734. (e) Dang, H.-S.; Roberts, B. P. Radical-chain addition of aldehydes to alkenes catalysed by thiols. *J. Chem. Soc., Perkin Trans. 1* **1998**, 67–76. (f) Dang, H.-S.; Roberts, B. P. Radical-chain cyclisation of unsaturated acetals and thioacetals in the presence of thiols as polarity-reversal catalysts. *Tetrahedron Letters* **1999**, *40*, 8929–8933. (g) Dang, H.-S.; Roberts, B. P. Selective radical-chain epimerisation at C-H centres *α* to oxygen under conditions of polarity-reversal catalysis. *Tetrahedron Letters* **1999**, *40*, 4271–4274. (h) Dang, H.-S.; Roberts, B. P.; Tocher, D. A. Selective radical-chain epimerisation at electron-rich chiral tertiary C–H centers using thiols as protic polarity-reversal catalysts. *J. Chem. Soc., Perkin Trans. 1* **2001**, 2452–2461. (i) Roberts, B. P. Polarity-reversal catalysis of hydrogen-atom abstraction reactions: Concepts and applications in organic chemistry. *Chem. Soc. Rev.* **1999**, *28*, 25–35.

(11) (a) Dong, J.-Y.; Xu, W.-T.; Yue, F.-Y.; Song, H.-J.; Liu, Y.-X.; Wang, Q.-M. Visible-light-mediated deuteration of aldehydes with D_2O via polarity-matched reversible hydrogen atom transfer. *Tetrahedron* **2021**, *82*, 131946. (b) Huang, Z.; Chen, Z.; Jiang, Y.; Li, N.; Yang, S.; Wang, G.; Pan, X. Metal-Free Hydrosilylation Polymerization by Merging Photoredox and Hydrogen Atom Transfer Catalysis. *J. Am. Chem. Soc.* **2021**, *143*, 19167–19177. (c) Schäfers, F.; Quach, L.; Schwarz, J. L.; Saladrigas, M.; Daniliuc, C. G.; Glorius, F. Direct Access to Monoprotected Homoallylic 1,2-Diols via Dual Chromium/Photoredox Catalysis. *ACS Catal.* **2020**, *10*, 11841–11847. (d) Vu, M. D.; Das, M.; Guo, A.; Ang, Z.-E.; Đokić, M.; Soo, H. S.; Liu, X.-W. Visible-Light Photoredox Enables Ketone Carbonyl Alkylation for Easy Access to Tertiary Alcohols. *ACS Catal.* **2019**, *9*, 9009–9014. (e) Zhang, M.; Yuan, X.-A.; Zhu, C.; Xie, J. Deoxygenative Deuteration of Carboxylic Acids with D_2O. *Angew. Chem. Int. Ed.* **2019**, *58*, 312–316. (f) Yan, C.; Li, L.; Liu, Y.; Wang, Q. Direct and Oxidant-Free Electron-Deficient Arylation of N-Acyl-Protected Tetrahydroisoquinolines. *Org. Lett.* **2016**, *18*, 4686–4689. (g) Meng, Q.-Y.; Schirmer, T. E.; Berger, A. L.; Donabauer, K.; König, B. Photocarboxylation of Benzylic C-H Bonds. *J. Am. Chem. Soc.* **2019**, *141*, 11393–11397.

(12) Beckmann, J.; Dakternieks, D.; Tiekink, E. R. T. Chiral trialkoxysilanols derived from terpene alcohols. Molecular structures of tris([1*S*)-*endo*]-(–)-bornoxy)silanol and tetrakis((–)-menthoxy)silane. *J. Organomet. Chem.* **2002**, *648*, 188–192.

(13) (a) Chojnacki, J.; Ciborska, A.; Wojnowski, W. A study of chirality in bis(1,2-dimethoxyethane-κ^2*O*,*O*')sodium bis(tri-*tert*-butoxysilanethiolato-κ^2*O*,*S*)sodate. *Acta Crystallogr. Sec. C* **2008**, *64*, m240-2. (b) Dołęga, A.; Marynowski, W.; Baranowska, K.; Smiechowski, M.; Stangret, J. Intramolecular interactions in crystals of tris(2,6-diisopropylphenoxy)silanethiol and its sodium salts. *Inorg. Chem.* **2012**, *51*, 836–843.

(14) Grotjahn, S.; Müller, L.; Pattanaik, A.; Falk, A.; Barison, G.; Bauer, J. O.; Rehbein, J.; Gschwind, R. M.; Burkhard, K. Regio-, diastereo- and enantioselectivity in the photocatalytic generation of

carbanions via hydrogen atom transfer and reductive radical-polar crossover. *Org. Chem. Front.* **2024**, 10.1039/D4QO01219D

(15) Kümper, M.; Götz, T.; Espinosa-Jalapa, N. A.; Falk, A.; Rothfelder, R.; Bauer, J. O. Stereochemically Pure Si -Chiral Aminochlorosilanes. *Z. Anorg. Allg. Chem.* **2023**, *649*.

(16) (a) Sommer, L. H.; Citron, J. D.; Frye, C. L. Stereochemistry of Asymmetric Silicon. The Silicon-Nitrogen Bond. *J. Am. Chem. Soc.* **1964**, *86*, 5684–5685. (b) Sommer, L. H.; Citron, J. D. Stereochemistry of asymmetric silicon. VII. Silicon-nitrogen bond. *J. Am. Chem. Soc.* **1967**, *89*, 5797–5801.

(17) Huber, T.; Espinosa-Jalapa, N. A.; Bauer, J. O. Access to Enantiomerically Pure P-Stereogenic Primary Aminophosphine Sulfides under Reductive Conditions. *Chem. Eur. J.* **2022**, *28*, e202202608.

(18) Wang, D.; Wang, Z. G.; Wang, M. W.; Chen, Y. J.; Liu, L.; Zhu, Y. Asymmetric allylation of aldehydes and glyoxylates through 'C-centered' chiral pentacoordinate allylsilicates or promoted by Lewis acid. *Tetrahedron: Asymmetry* **1999**, *10*, 327–338.

(19) (a) Chulsky, K.; Dobrovetsky, R. $B(C_6F_5)_3$ - Catalyzed Selective Chlorination of Hydrosilanes. *Angew. Chem. Int. Ed.* **2017**, *56*, 4744–4748. (b) Sommer; L. H.; Ulland, L. A. Chirality and Structure Organosilicon Radicals. *J. Org. Chem.* **1972**, *37*, 3878–3881. (c) Savela, R.; Zawartka, W.; Leino, R. Iron-Catalyzed Chlorination of Silanes. *Organometallics* **2012**, *31*, 3199–3206. (d) Sturm, A. G.; Schweizer, J. I.; Meyer, L.; Santowski, T.; Auner, N.; Holthausen, M. C. Lewis Base Catalyzed Selective Chlorination of Monosilanes. *Chem. Eur. J.* **2018**, *24*, 17796–17801. (e) Kunai, A.; Ohshita, J. Selective synthesis of halosilanes from hydrosilanes and utilization for organic synthesis. *J. Organomet. Chem.* **2003**, *686*, 3–15. (f) Nagai, Y.; Yamazaki, K.; Shiojima, I. Selectivity in the homolytic reduction of polyhaloalkanes with organosilicon hydrides. *J. Organomet. Chem.* **1967**, *9*, 25–26. (g) Sakurai, H.; Murakami, M.; Kumada, M. Stereochemical Course of the Rentention of an Opitcally Active Hydrosilane with Carbon Tetrachloride by a Free-Radical Mechanism. *J. Am. Chem. Soc.* **1969**, *91*, 519–520. (h) Varaprath, S.; Stutts, D. H. Utility of trichloroisocyanuric acid in the efficient chlorination of silicon hydrides. *J. Organomet. Chem.* **2007**, *692*, 1892–1897.

(20) (a) Su, B.; Zhou, T.-G.; Li, X.-W.; Shao, X.-R.; Xu, P.-L.; Wu, W.-L.; Hartwig, J. F.; Shi, Z.-J. A Chiral Nitrogen Ligand for Enantioselective, Iridium-Catalyzed Silylation of Aromatic C-H Bonds. *Angew. Chem. Int. Ed.* **2017**, *56*, 1092–1096. (b) Zhan, G.; Teng, H.-L.; Luo, Y.; Lou, S.-J.; Nishiura, M.; Hou, Z. Enantioselective Construction of Silicon-Stereogenic Silanes by Scandium-Catalyzed Intermolecular Alkene Hydrosilylation. *Angew. Chem. Int. Ed.* **2018**, *57*, 12342–12346. (c) Yang, B.; Yang, W.; Guo, Y.; You, L.; He, C. Enantioselective Silylation of Aliphatic C-H Bonds for the Synthesis of Silicon-Stereogenic Dihydrobenzosiloles. *Angew. Chem. Int. Ed.* **2020**, *59*, 22217–22222. (d) Huang, Y.-H.; Wu, Y.; Zhu, Z.; Zheng, S.; Ye, Z.; Peng, Q.; Wang, P. Enantioselective Synthesis of Silicon-Stereogenic Monohydrosilanes by Rhodium-Catalyzed Intramolecular Hydrosilylation. *Angew. Chem. Int. Ed.* **2022**, *61*, e202113052. (e) Zhang, Q.-W.; An, K.; Liu, L.-C.; Guo, S.; Jiang, C.; Guo, H.; He, W. Rhodium-Catalyzed Intramolecular C-H Silylation by Silacyclobutanes. *Angew. Chem. Int. Ed.* **2016**, *55*, 6319–6323. (f) Ma, W.; Liu, L.-C.; An, K.; He, T.; He, W. Rhodium-Catalyzed Synthesis of Chiral Monohydrosilanes by Intramolecular C-H Functionalization of Dihydrosilanes. *Angew. Chem. Int. Ed.* **2021**, *60*, 4245–4251.

(21) Sommer, L. H.; Frye, C. L.; Parker G. A.; Michael, K. W. Stereochemistry of Asymmetric Silicon. I. Relative and Absolute Configurations of Optically Active α-Naphthylphenylmethylsilanes. *J. Org. Biol. Chem.* **1964**, *86*, 3271-3276.

6.6 Synthesis and Characterizations

6.6.1 General remarks

All experiments were performed in an inert atmosphere of purified nitrogen by using standard Schlenk techniques or an MBraun Unilab 1200/780 glovebox. Glassware was heated at 600 °C prior to use. Dichloromethane (DCM), hexane, pentane, tetrahydrofuran (THF), and toluene were dried and degassed with an MBraun SP800 solvent purification system. *n*-Butyllithium (2.5 M solution in hexane, Merck KGaA), bis(triphenylphosphine)palladium(II) dichloride (98%, Merck KGaA), methyl iodide (99%, Merck KGaA), 1,3,5-trimethoxybenzene (≥99%, Merck KGaA) and hydrogen sulfide (0.8 M solution in THF, Merck KGaA). Trimenthoxy(chloro)silane[1], (*R*)-1-*tert*-butyl-1-methoxy-1-phenyl-*N*-((*S*)-1-phenylethyl)silanamine[2] (**2**), (^{R}*Si*, S_P) 8,8-isopropyl(hydrido)benzosilolo[2,3-a]ferrocene[3] and (^{R}*Si*, S_P) 8,8-cyclohexyl(hydrido)benzosilolo[2,3-a]ferrocene[3] were prepared according to literature procedures. A stock solution of hydrogen sulfide in THF was prepared by saturating THF with gaseous hydrogen sulfide and checking the concentration by NMR with 1,3,5-trimethoxybenzene as internal standard. C_6D_6 and CD_2Cl_2 used for NMR spectroscopy were dried over 3 Å molecular sieves and degassed by a standard freeze-pump-thaw procedure. NMR spectra were either recorded on a Bruker Avance 300 (300.13 MHz), a Bruker Avance 400 (400.13 MHz) or on a Bruker Avance III HD 400 (400.13 MHz) at 25 °C. Chemical shifts (δ) are reported in parts per million (ppm). ^{1}H and ^{13}C{^{1}H} NMR spectra are referenced to tetramethylsilane ($SiMe_4$, δ = 0.0 ppm) as external standard, with the deuterium signal of the solvent serving as internal lock and the residual solvent signal as an additional reference. ^{29}Si{^{1}H} NMR spectra are referenced to $SiMe_4$. For the assignment of the multiplicities, the following abbreviations are used: s = singlet, bs = broad singlet, d = doublet, t = triplet, bq = broad quartet, m = multiplet. Elemental analyses were performed on a Vario MICRO cube apparatus.

6.6.2 Synthesis of trimenthoxysilanethiol (1)

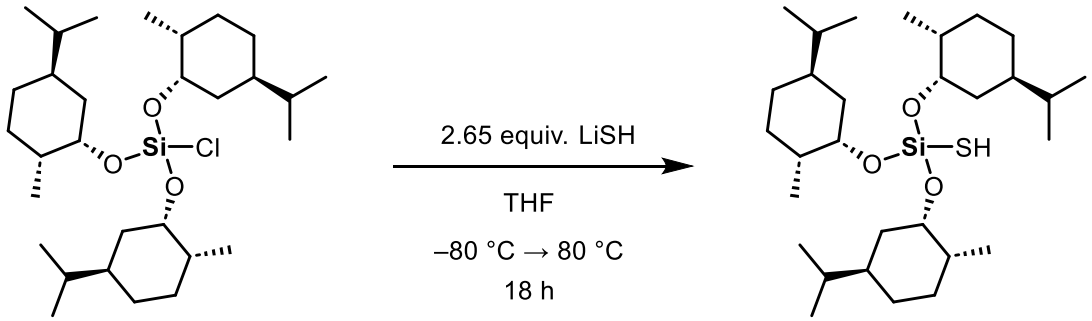

1

First H_2S (52.07 mL of a 1 M solution in THF, 52.07 mmol, 1.2 equiv) was diluted in 100 mL of THF and cooled to –78°C. Then *n*-Butyllithium (18.23 mL of a 2.5 M solution in hexane, 45.57 mmol, 1.05 equiv) was slowly added. The reaction mixture was stirred in the cooling bath until it reached a temperature of 0°C, then it was cooled to –78°C again. Next trimenthoxy(chloro)silane[1] (22.97 g, 43.40 mmol, 1 equiv) was added. The reaction was allowed to stir for 18 h at room temperature and then 18 h at 80°C. The reaction mixture was then checked by NMR analysis, and since no complete conversion was observed another portion of LiSH (26.4 mmol, 1.6 equiv) *in situ* prepared in the aforementioned manner was added. The reaction mixture was then stirred for 72 h at room temperature. Afterwards all volatiles were removed *in vacuo* and the oily suspension extracted with 50 mL of hot toluene. The cloudy suspension was filtered using a P3-Frit with added celite and silica. After removal of all volatiles *in vacuo* compound **1** was obtained as a slightly yellow oil. Yield: 20.8 g (39.47 mmol, 91%).

^{1}H NMR (400.13 MHz, C_6D_6, 298 K): δ 3.97–3.89 (m, 3H, C*H*), 2.54–2.44 (m, 3H, C*H*), 2.37–2.32 (m, 3H, CH_2), 1.57–1.48 (m, 6H, CH_2), 1.39–1.22 (m, 10H), 1.00–0.93 (m, 19H, CH_3), 0.89–0.87 (m, 9H, C*H*), 0.84–0.68 (m, 4H, CH_2), 0.19 (s, 1H, S*H*).

^{13}C{^{1}H} NMR (100.61 MHz, C_6D_6, 298 K): δ 74.4 (s, *C*H), 50.2 (s, *C*H), 45.3 (s, *C*H_2), 34.7 (s, *C*H_2), 31.9 (s, *C*H), 25.8 (s, *C*H), 23.1 (s, *C*H_2), 22.4 (s, *C*H_3), 21.5 (s, *C*H_3), 16.3 (s, *C*H_3).

^{29}Si{^{1}H} NMR (79.49 MHz, C_6D_6, 298 K): δ –59.2 (*Si*SH).

CHN Analysis: Calcd for $C_{30}H_{58}O_3SSi$: C, 68.38; H, 11.10. Found: C, 68.69; H, 10.72.

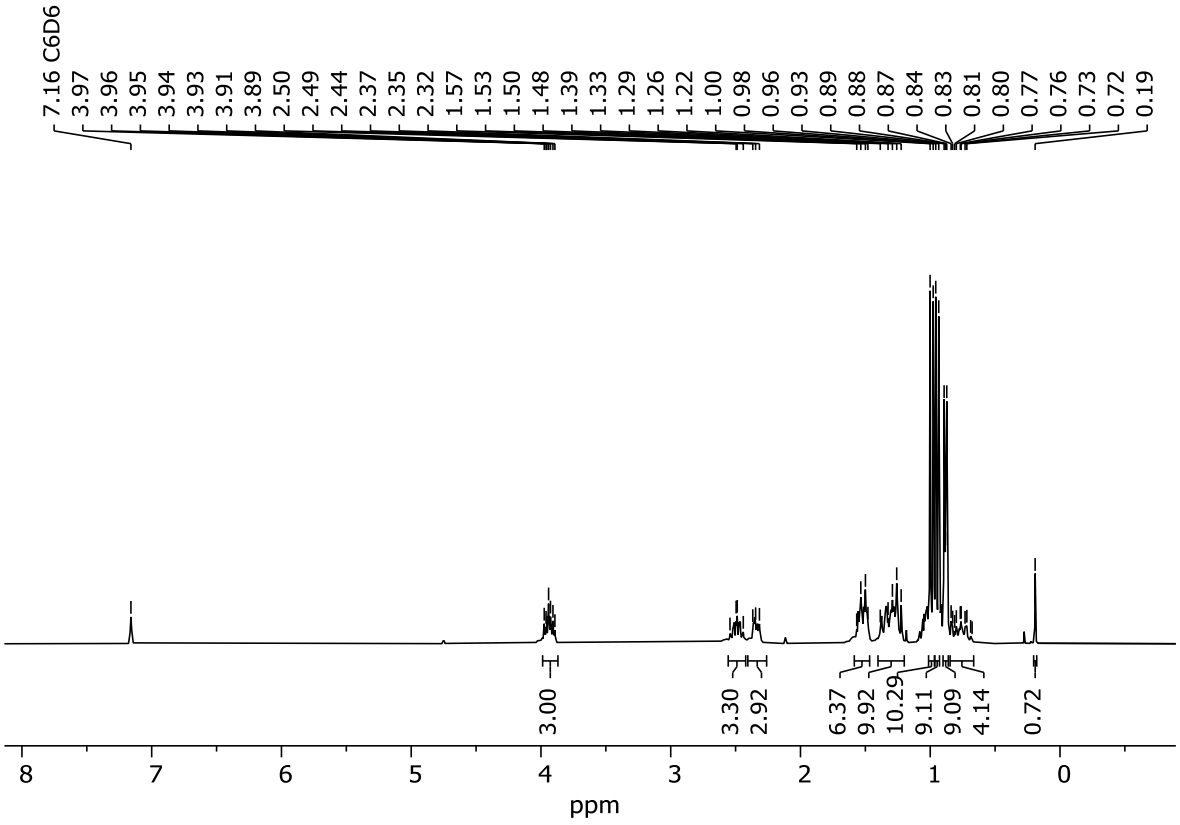

Figure S1: ^{1}H NMR (400.13 MHz, C_6D_6, 298 K) spectrum of compound **1**.

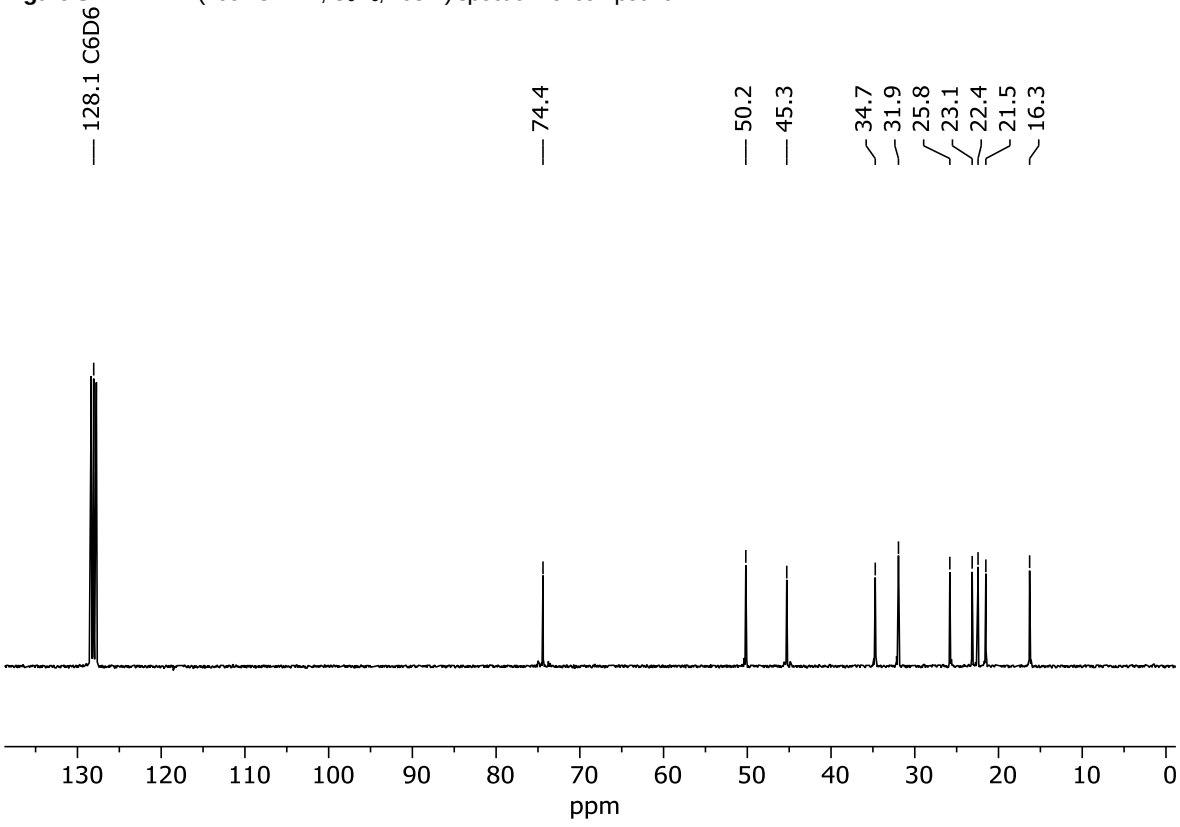

Figure S2: $^{13}C\{^{1}H\}$ NMR (100.61 MHz, C_6D_6, 298 K) spectrum of compound **1**.

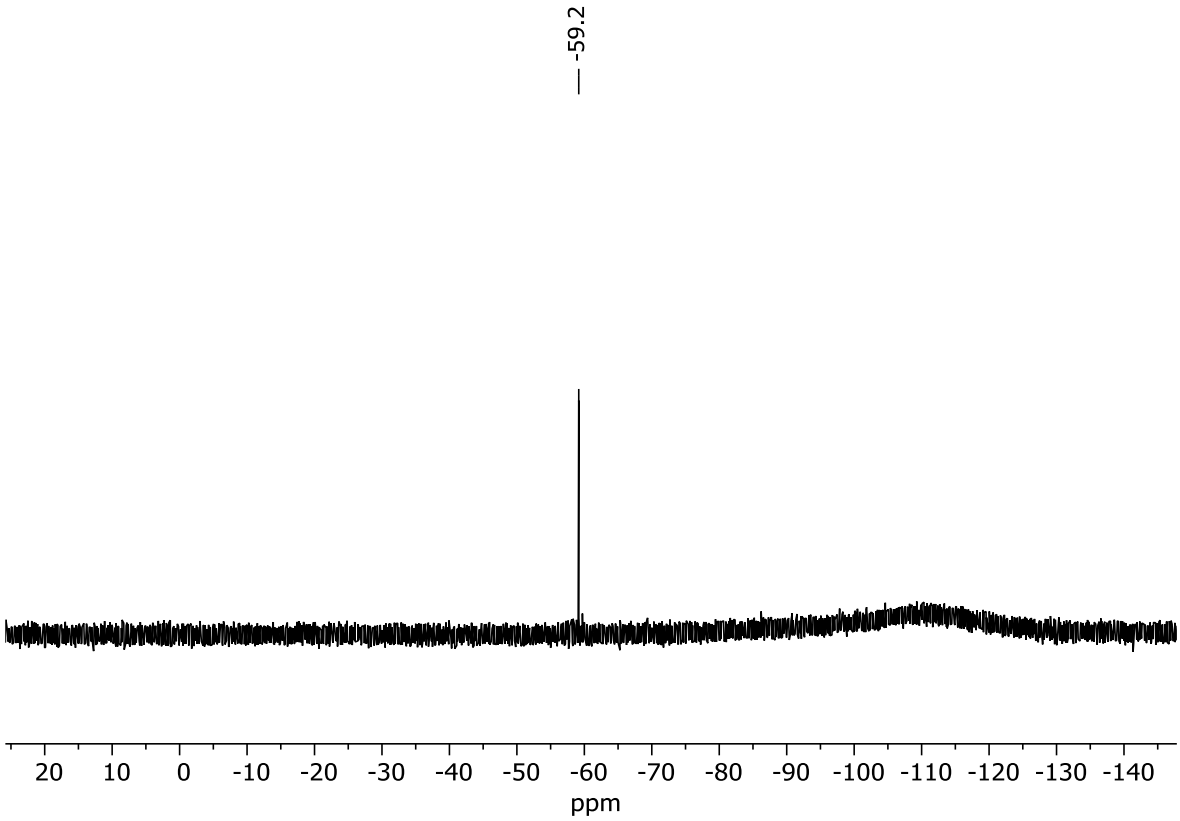

Figure S3: $^{29}Si\{^{1}H\}$ NMR (79.49 MHz, C_6D_6, 298 K) spectrum of compound **1**.

6.6.3 Synthesis of *tert*-Butylchloromethoxyphenylsilane (2-Cl)

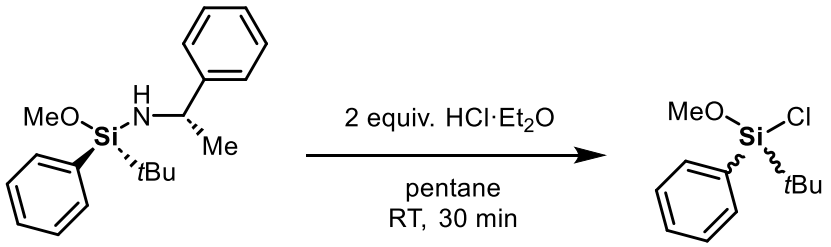

(S_C, R_{Si})-**2**
d.r. > 99:1

2-Cl
e.r. ≥ 80:20

This synthesis has already been reported in literature.[2]

Hydrogen chloride (6.9 mL of a 2.0 M solution in Et_2O, 13.10 mmol, 2.0 equiv.) was slowly added to a stirred solution of (S_C,R_{Si})-**2** (2.05 g, 6.55 mmol, 1.0 equiv., d.r. > 99:1) in pentane (100 mL) at −80 °C. A white solid precipitates immediately. The reaction mixture was allowed to slowly warm up to room temperature and kept stirring for 30 min. The mixture was then filtered through a fritted column layered with Celite® and the remaining solids washed with pentane (2 × 10 mL). The filtrates were collected and all volatiles removed in vacuo to yield **2-Cl** as a colorless oil (1.45 g, 6.55 mmol, 99%, e.r. ≥ 80:20).

^{1}H NMR (400.13 MHz, C_6D_6, 298 K): δ 1.04 [s, 9H, C(CH_3)$_3$], 3.35 (s, 3H, SiOCH_3), 7.17 (m, 3H, H_{Ph}), 7.67 (m, 2H, H_{Ph}).

^{13}C{^{1}H} NMR (100.62 MHz, C_6D_6, 298 K): δ 20.3 [s, C(CH_3)$_3$], 25.0 [s, C(CH_3)$_3$], 51.1 (s, SiOCH_3), 127.9 (s, C_{Ph}), 130.6 (s, C_{Ph}), 131.0 (s, C_{Ph}), 134.8 (s, C_{Ph}).

^{29}Si{^{1}H} NMR (79.49 MHz, C_6D_6, 298 K): δ 3.3 (s).

HRMS (EI+): Calcd *m*/*z* for $C_{11}H_{17}OClSi$ [M^+]: 228.07317. Found: 228.07354.

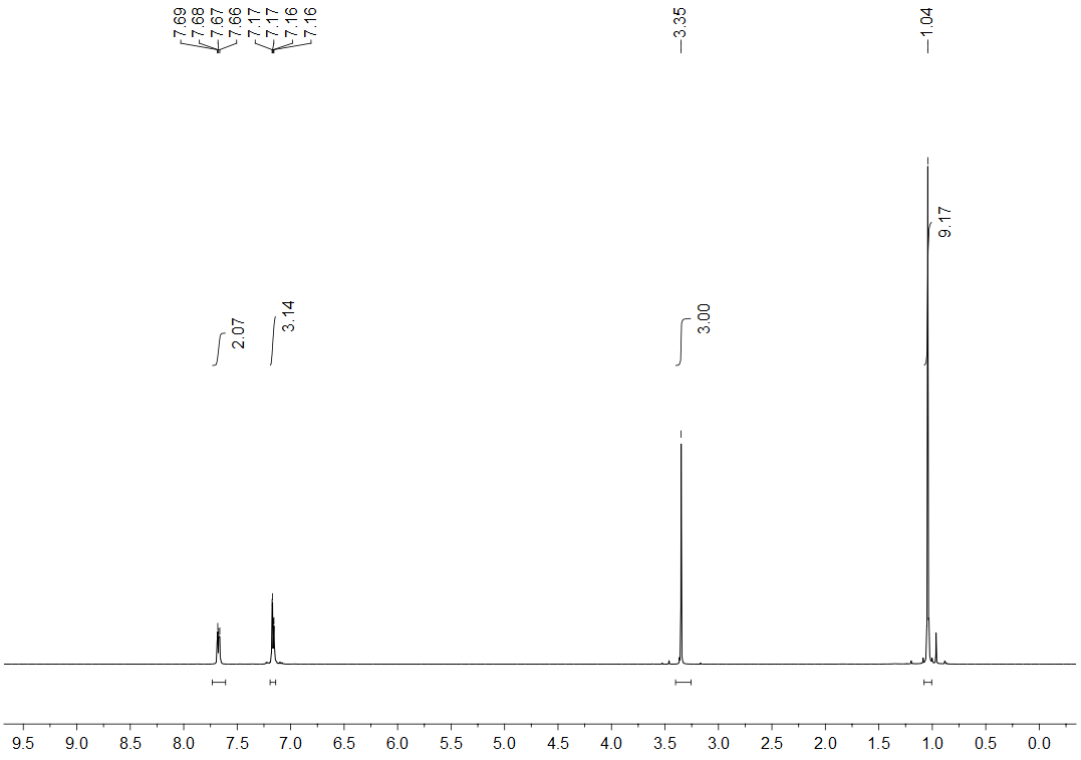

Figure S4: ^{1}H NMR (400.13 MHz, C_6D_6, 298 K) spectrum of compound **2-Cl**.

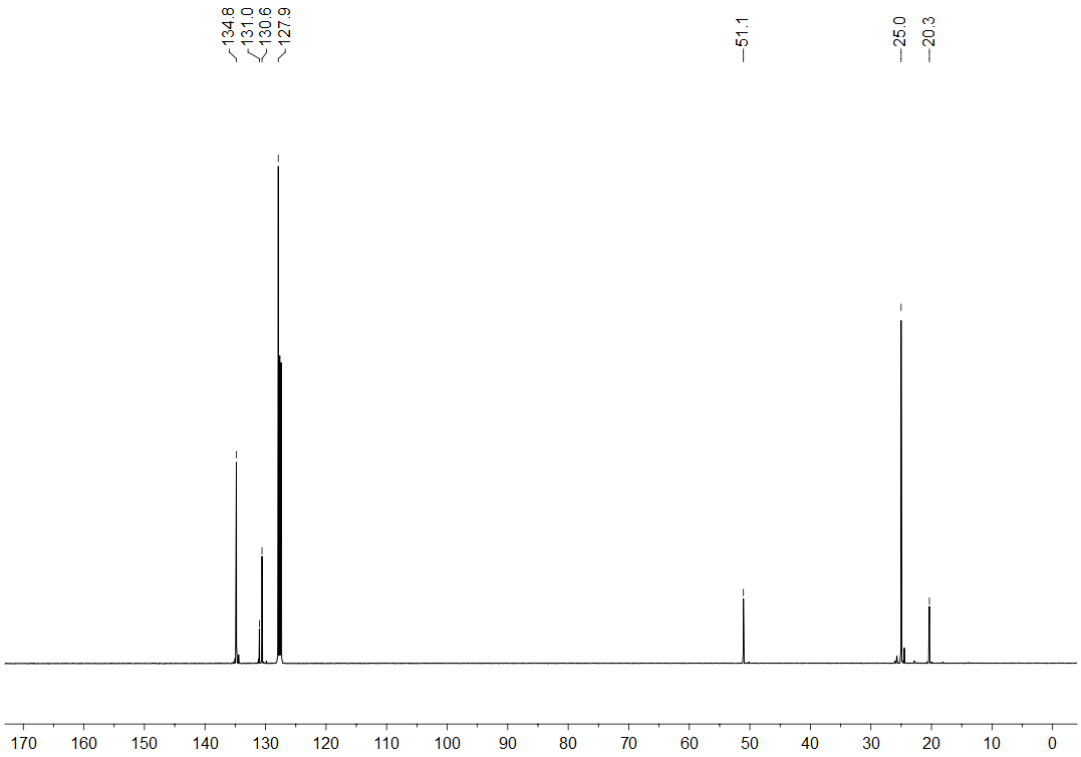

Figure S5: $^{13}C\{^{1}H\}$ NMR (100.61 MHz, C_6D_6, 298 K) spectrum of compound **2-Cl**.

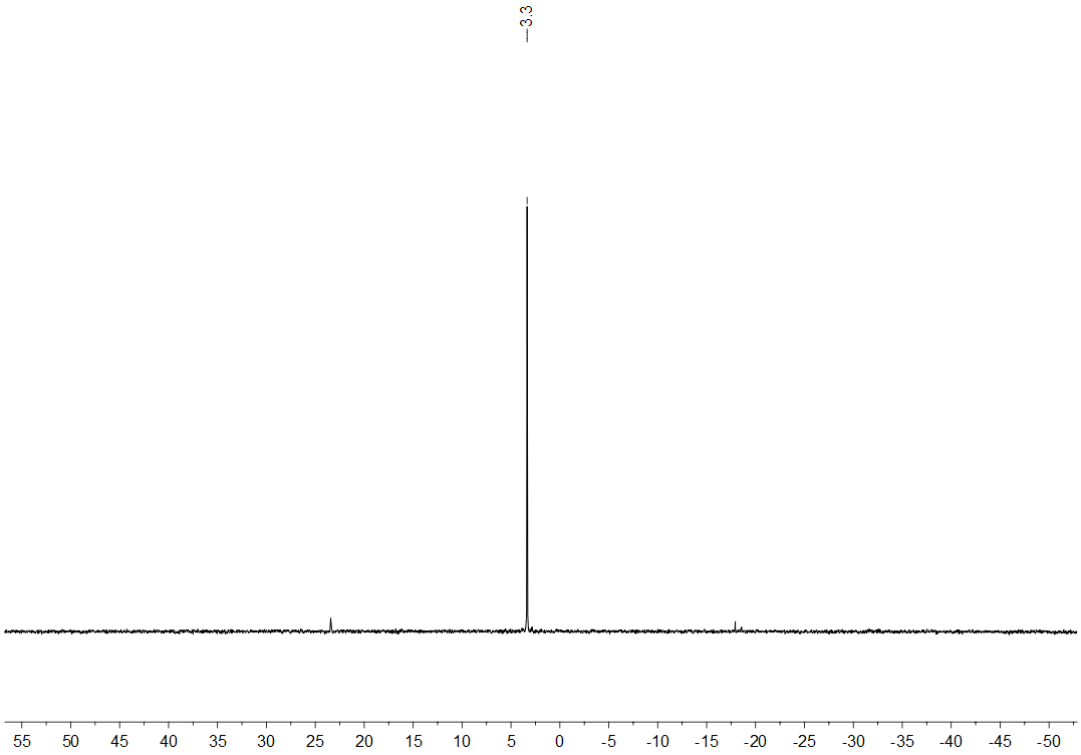

Figure S6: $^{29}Si\{^{1}H\}$ NMR (79.49 MHz, C_6D_6, 298 K) spectrum of compound **2-Cl**.

6.6.4 Synthesis of *tert*-Butylmethoxyphenylsilanethiol (3)

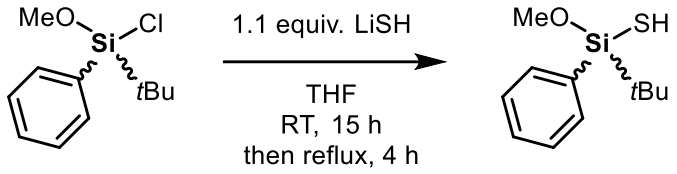

2-Cl
e.r. ≥ 80:20

3
e.r. = 80:20

This synthesis has already been reported in literature.[2]

n-Butyllithium (2.90 mL of a 2.5 M solution in hexane, 7.03 mmol, 1.1 equiv.) was slowly added to a solution of hydrogen sulfide (9.0 mL of a 0.8 M solution in tetrahydrofuran, 7.03 mmol, 1.1 equiv.) at 0 °C. The reaction mixture was then allowed to slowly warm up to room temperature and kept stirring for 20 min. The mixture was filtered and the solid washed with hexane (2 × 10 mL) Then, all volatiles were removed in vacuo to yield LiSH as a white powder. A solution of **2-Cl** (1.45 g, 6.55 mmol, 1.0 equiv., e.r. ≥ 83:17) in tetrahydrofuran (50 mL) was added to the freshly prepared LiSH at room temperature. The green-yellow suspension was kept stirring for 15 h and then heated at reflux for further 4 h. The mixture was cooled down to room temperature and all volatiles were removed in vacuo. The oily suspension was then diluted with hexane (50 mL) and filtered through a fritted column layered with Celite®. The remaining solids were washed with hexane (2 x 10 mL). Then, the filtrates were collected and all volatiles removed in vacuo. The crude oil was finally purified by silica gel flash column chromatography (EtOAc/Hex 2:8) (R_f = 0.4) to yield **3** as a pale yellow oil (0.49 g, 2.16 mmol, 33%, e.r. = 80:20).

^{1}H NMR (400.13 MHz, $CDCl_3$, 298 K): δ 0.01 (s, 1H, SiS*H*), 0.84 [s, 9H, C(CH_3)$_3$], 3.44 (s, 3H, SiOCH_3), 7.25 (m, 3H, H_{Ph}), 7.51 (m, 2H, H_{Ph}).

^{13}C{^{1}H} NMR (100.62 MHz, $CDCl_3$, 298 K): δ 20.5 [s, *C*(CH$_3$)$_3$], 25.9 [s, C(*C*H$_3$)$_3$], 51.6 (s, SiO*C*H$_3$), 128.0 (s, C_{Ph}), 130.4 (s, C_{Ph}), 133.2 (s, C_{Ph}), 134.9 (s, C_{Ph}).

^{29}Si{^{1}H} NMR (79.49 MHz, $CDCl_3$, 298 K): δ 9.4 (s).

CHN Analysis: Calcd for $C_{11}H_{18}OSSi$: C, 58.36; H, 8.01. Found: C, 59.08; H, 8.05.

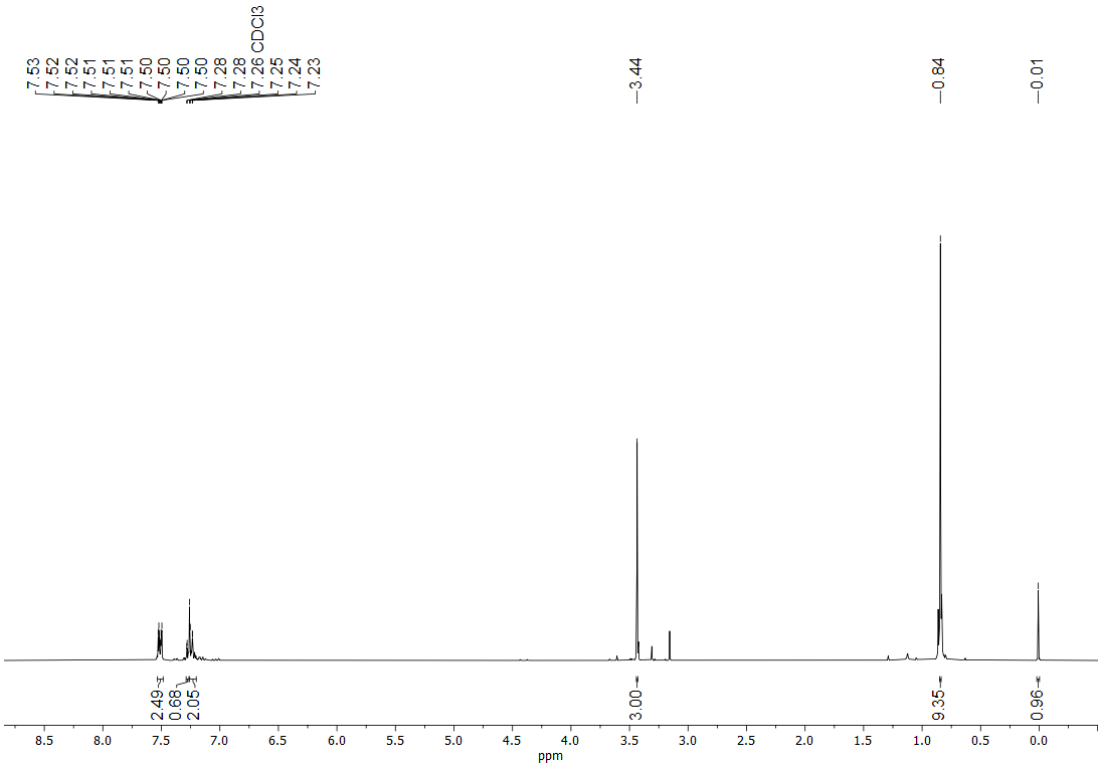

Figure S7: ^{1}H NMR spectrum (400.13 MHz, CDCl3, 298 K) of compound 3.

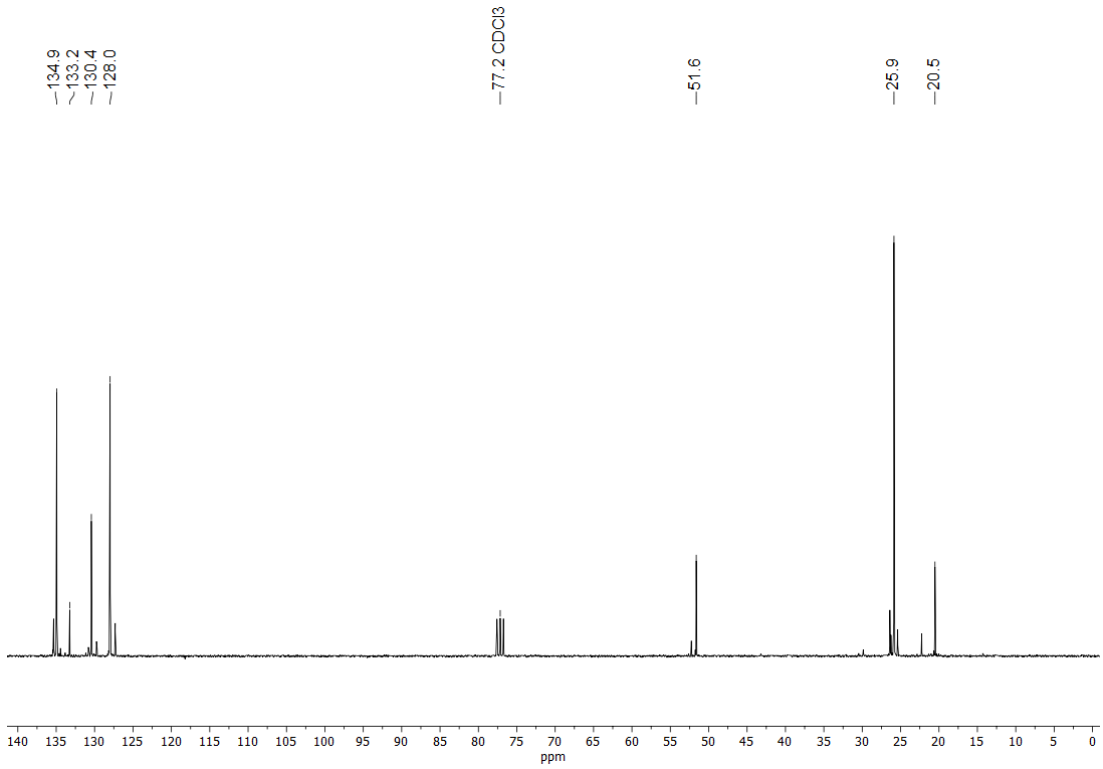

Figure S8: $^{13}C\{^{1}H\}$ NMR spectrum (100.61 MHz, CDCl3, 298 K) of compound **3**.

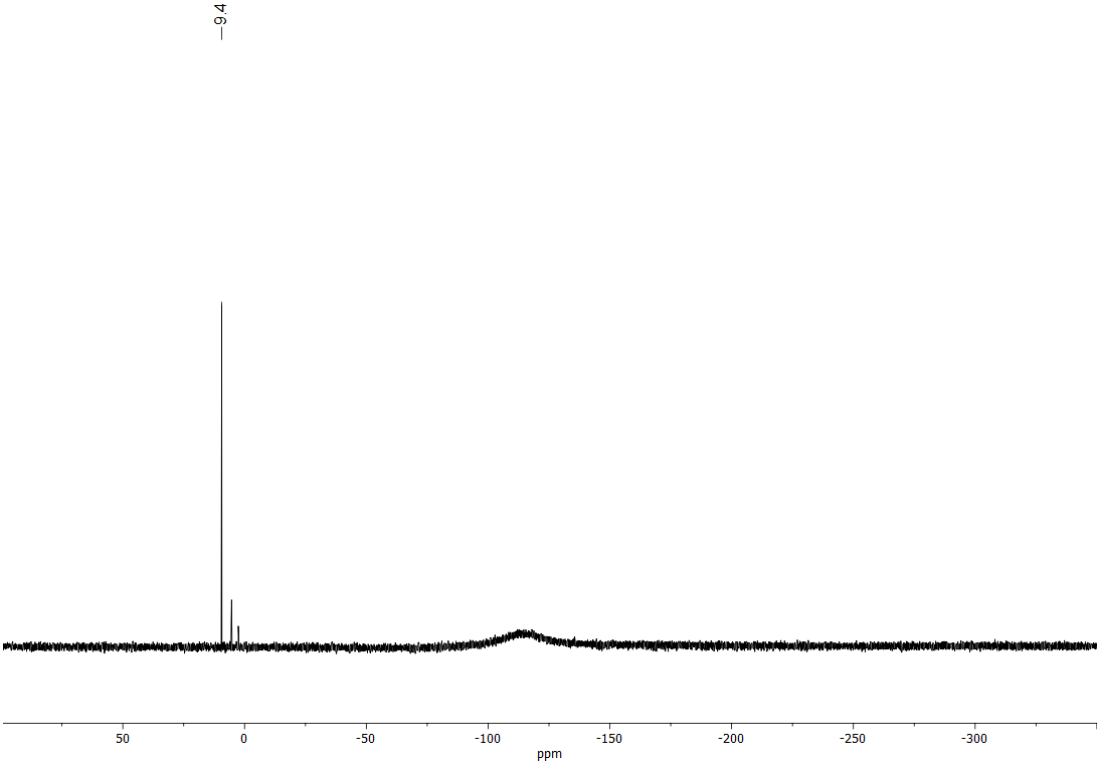

Figure S9: $^{29}Si\{^{1}H\}$ NMR spectrum (79.49 MHz, CDCl3, 298 K) of compound **3**.

6.6.5 Synthesis of compound 4

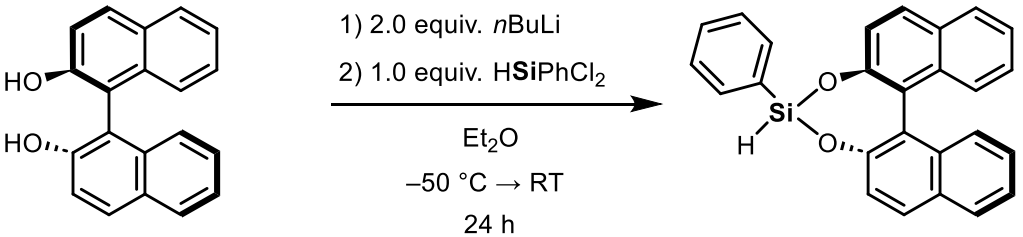

4

In a dry Schlenk flask (*S*)-(–)-[1,1'-binaphthalene]-2,2'-diol (4.85 g, 16.94 mmol, 1 equiv) was dissolved in 100 mL of Et_2O. The solution was cooled to –50°C and then *n*-Butyllithium (13.55 mL of a 2.5 M solution in hexane, 33.88 mmol, 2 equiv) was slowly added. The resulting suspension was allowed to warm up to room temperature and stirred for 30 min. The suspension was cooled to –20°C, then dichloro(phenyl)silane (3.00 g, 16.94 mmol, 1 equiv) was slowly added. The mixture was stirred for 24 h at room temperature. Then all volatiles were removed *in vacuo*. The remaining oily suspension was suspended in 30 mL hexane and filtered using a P3-Frit with added celite. The remaining filtrate was placed at –30°C to precipitate the product. The product was isolated by filtration and dried *in vacuo*. Compound **4** was obtained as an amorphous white powder. Yield: 4.6 g (11.85 mmol, 70%).

^{1}H NMR (400.13 MHz, C_6D_6, 298 K): δ 7.65–7.62 (m, 2H, CH_{Ar}), 7.57–7.55 (m, 1H, CH_{Ar}), 7.49–7.38 (m, 6H, CH_{Ar}), 7.14–7.06 (m, 4H, CH_{Ar}), 6.98–6.94 (m, 2H, CH_{Ar}), 6.92–6.87 (m, 2H, CH_{Ar}), 5.50 (s, 1H, Si*H*).

^{13}C{^{1}H} NMR (100.61 MHz, C_6D_6, 298 K): δ 150.8 (s, *C*H$_{Ar}$), 150.3 (s, *C*H$_{Ar}$), 134.4 (s, *C*H$_{Ar}$), 134.2 (s, *C*$_{Ar}$), 134.1 (s, *C*$_{Ar}$), 132.0 (s, *C*H$_{Ar}$), 131.3 (s, *C*$_{Ar}$), 131.1 (s, *C*$_{Ar}$), 131.0 (s, *C*H$_{Ar}$), 130.6 (s, *C*$_{Ar}$), 130.6 (s, *C*H$_{Ar}$), 128.6 (s, *C*H$_{Ar}$), 128.4 (s, *C*H$_{Ar}$), 127.6 (s, *C*H$_{Ar}$), 127.5 (s, *C*H$_{Ar}$), 126.7 (s, *C*H$_{Ar}$), 126.7 (s, *C*H$_{Ar}$), 124.8 (s, *C*H$_{Ar}$), 124.7 (s, *C*H$_{Ar}$), 122.2 (s, *C*H$_{Ar}$), 122.2 (s, *C*$_{Ar}$), 122.0 (s, *C*$_{Ar}$), 121.7 (s, *C*H$_{Ar}$).

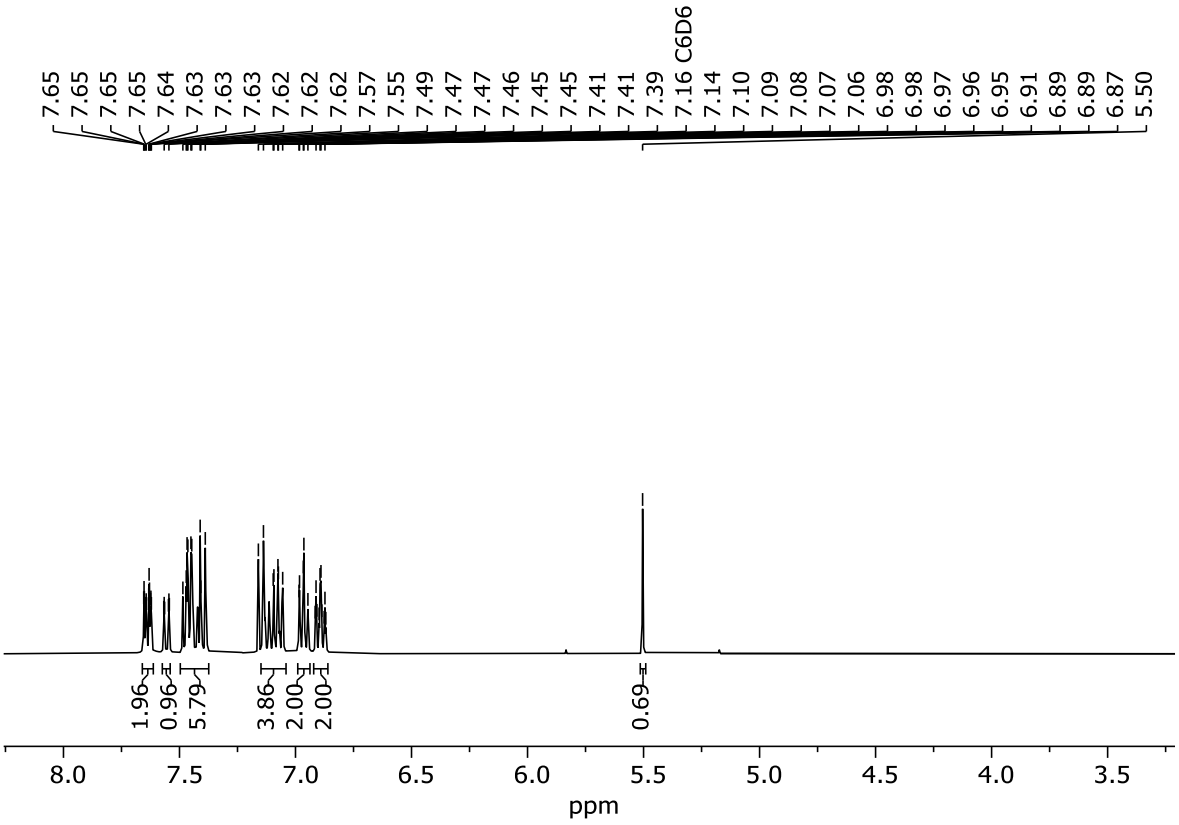

Figure S10: ^{1}H NMR (400.13 MHz, C_6D_6, 298 K) spectrum of compound **4**.

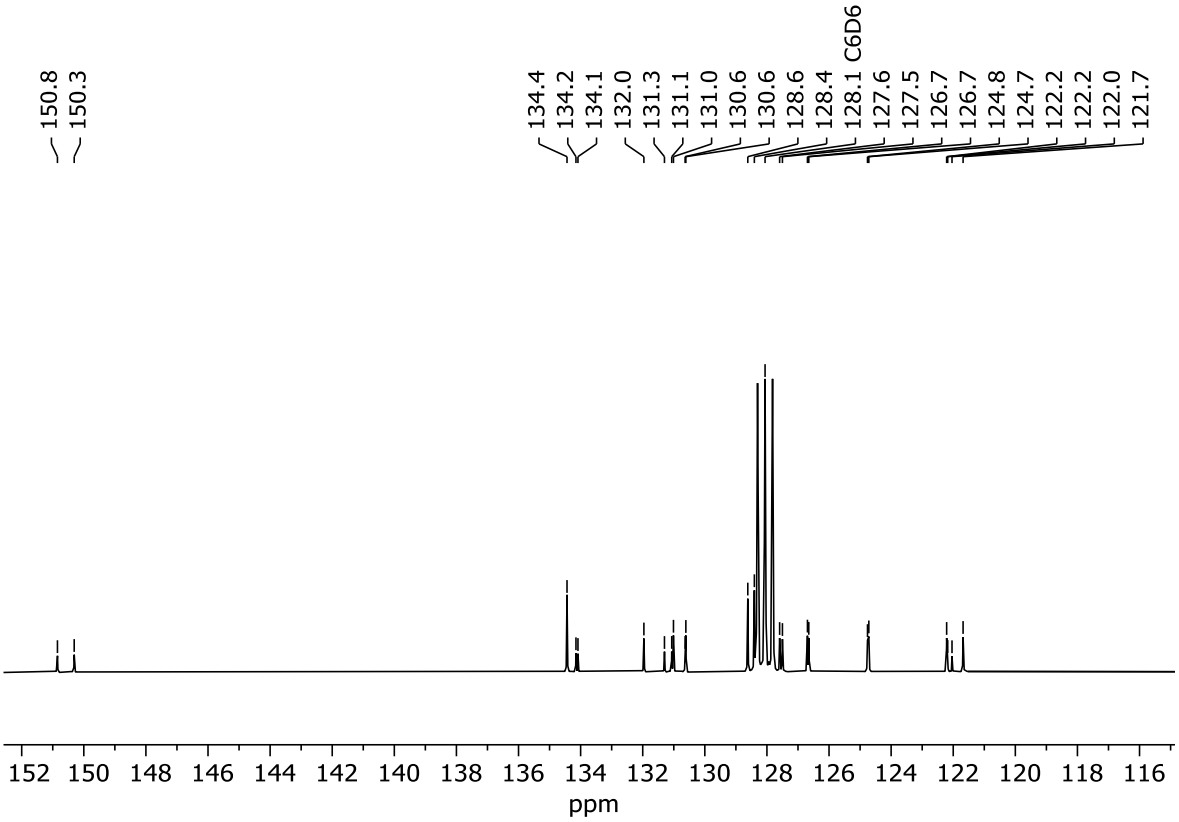

Figure S11: $^{13}C\{^{1}H\}$ NMR (100.61 MHz, C_6D_6, 298 K) spectrum of compound **4**.

6.6.6 General synthesis of iodosilanes 5-I and 6-I

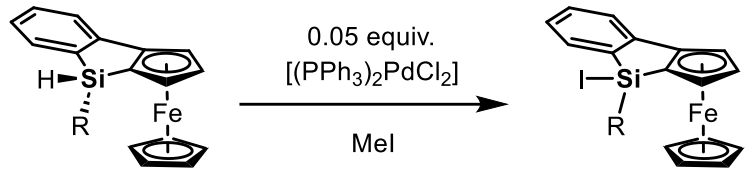

(R_{Si}, S_P) **5** R = *i*Pr
(R_{Si}, S_P) **6** R = Cy

5-I R = *i*Pr
6-I R = Cy

Prepared according to a modified literature procedure.[4]

First the respective hydridosilylferrocene[3] (150 mg, 0.45 mmol, 1 equiv) was combined with bis(triphenylphosphine)palladium(II) dichloride (15.84 mg, 0.022 mmol, 0.05 equiv) in a flame dried Schlenk flask. The mixture was then dissolved in methyl iodide (0.5 mL, 8.13 mmol, 18 equiv) and stirred for 1 h at room temperature. Afterwards all volatiles were removed *in vacuo*. The remaining red solids were immediately used in the next reaction step without further purification.

6.7.7 Synthesis of compound (S_{Si}, S_P) 7

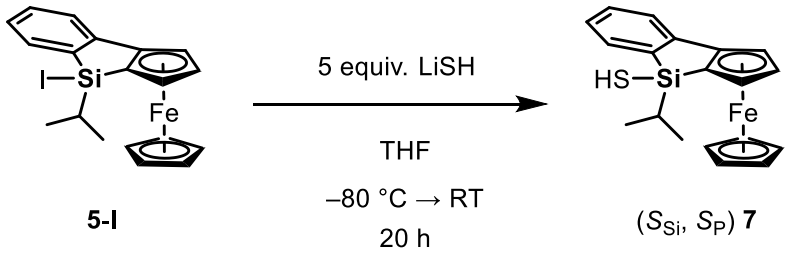

5-I (S_{Si}, S_P) **7**

First H_2S (8.99 mL of a 0.5 M solution in THF, 4.5 mmol, 10 equiv) was cooled to –80°C and then *n*-Butyllithium (0.9 mL of a 2.5 M solution in hexane, 2.25 mmol, 5 equiv) was added and the mixture stirred for 20 min. In a separate Schlenk flask 8,8-isopropyl(iodo)benzosilolo[2,3-a]ferrocene (**5-I**) (206 mg, 0.445 mmol, 1 equiv) was dissolved in 10 mL of THF and added to the cooled mixture. The reaction mixture was allowed to slowly warm up in the cooling bath, and then stirred for 20 h at room temperature. Next all volatiles were removed *in vacuo* and the black green residue suspended with 5 mL of hot hexane and filtered using a teflon cannula. The filtrate was concentrated *in vacuo* and purified by thin-layer chromatography (hexane, R_f = 0.4). Compound (S_{Si}, S_P) **7** was obtained as a red powder. Yield: 53 mg (0.145 mmol, 32%, 62% ee). Crystals suitable for single-crystal X-ray diffraction analysis were obtained from a concentrated pentane solution at –30°C.

^{1}H NMR (400.13 MHz, C_6D_6, 298 K): δ 7.52–7.50 (m, 1H, CH_{Ar}), 7.22–7.17 (m, 2H, CH_{Ar}), 7.05–7.01 (m, 1H, CH_{Ar}), 4.58–4.57 (m, 1H, CH_{Cp}), 4.36–4.34 (m, 1H, CH_{Cp}), 4.29–4.28 (m, CH_{Cp}), 3.83 (s, 5H, CH_{Cp}), 1.56–1.49 [m, 1H, SiCH(CH_3)$_2$], 1.37 [d, $^3J_{H–H}$ = 10.2 Hz, 3H, SiCH(CH_3)], 1.35 [d, $^3J_{H–H}$ = 10.4 Hz, 3H, SiCH(CH_3)], –0.19 (s, 1H, SiSH).

^{13}C{^{1}H} NMR (100.61 MHz, C_6D_6, 298 K): δ 147.8 (s, C_{Ar}), 140.0 (s, C_{Ar}), 133.7 (s, CH$_{Ar}$), 130.7 (s, CH$_{Ar}$), 126.3 (s, CH$_{Ar}$), 121.5 (s, CH$_{Ar}$), 96.3 (s, C_{Cp}), 74.4 (s, CH$_{Cp}$), 71.2 (s, CH$_{Cp}$), 71.0 (s, C_{Cp}), 70.4 (s, CH$_{Cp}$), 64.9 (s, CH$_{Cp}$), 17.8 [s, SiCH(CH$_3$)], 17.7 [s, SiCH(CH$_3$)], 16.3 [s, SiCH(CH_3)$_2$].

^{29}Si{^{1}H} NMR (79.49 MHz, C_6D_6, 298 K): δ 9.5 (s, *Si*SH).

CHN Analysis: Calcd for $C_{19}H_{20}FeSSi$: C, 62.6; H, 5.5. Found: C, 62.92; H, 5.80.

The enantiomeric excess was determined by HPLC on Chiralcel OD-H column (hexane, flowing rate = 1.0 mL/min, 35 °C, UV detection at λ = 241 nm) t_{R1} = 3.39 min (minor), t_{R2} = 3.77 min (major).

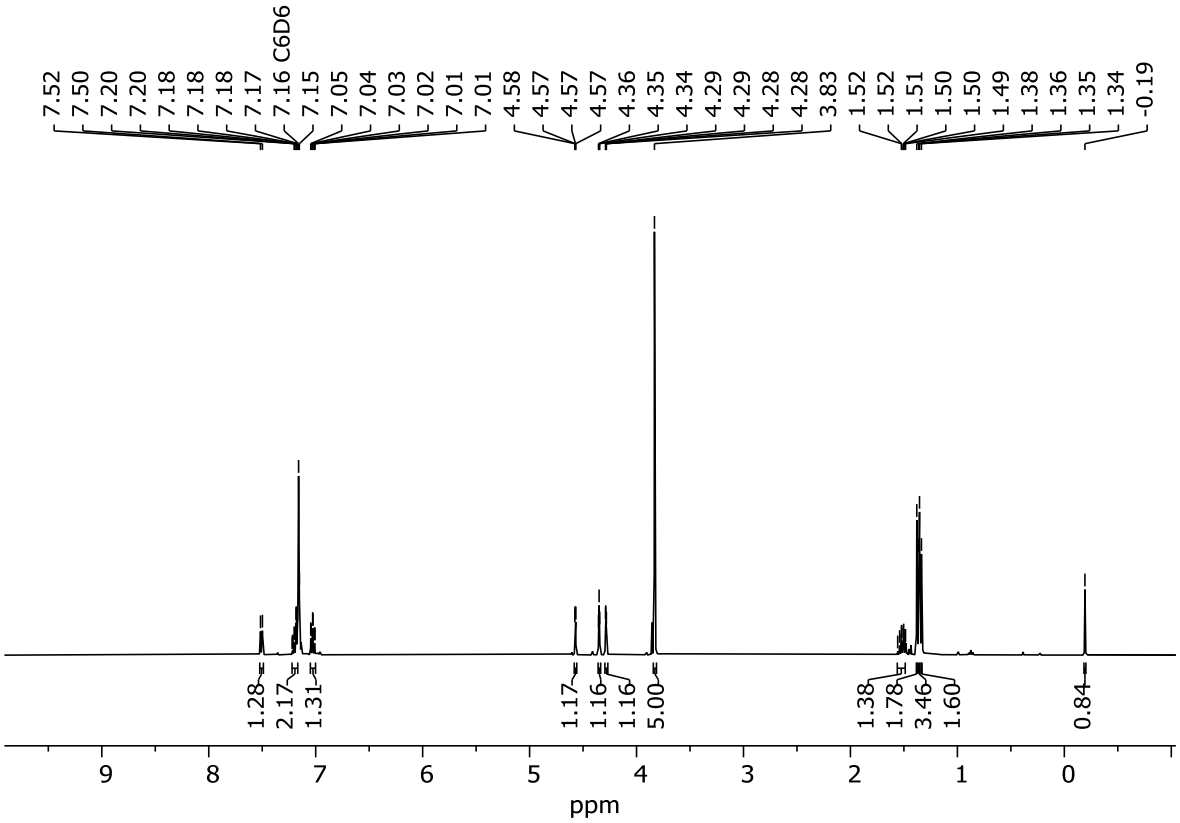

Figure S12: ^{1}H NMR (400.13 MHz, C_6D_6, 298 K) spectrum of compound (S_{Si}, S_P) **7**.

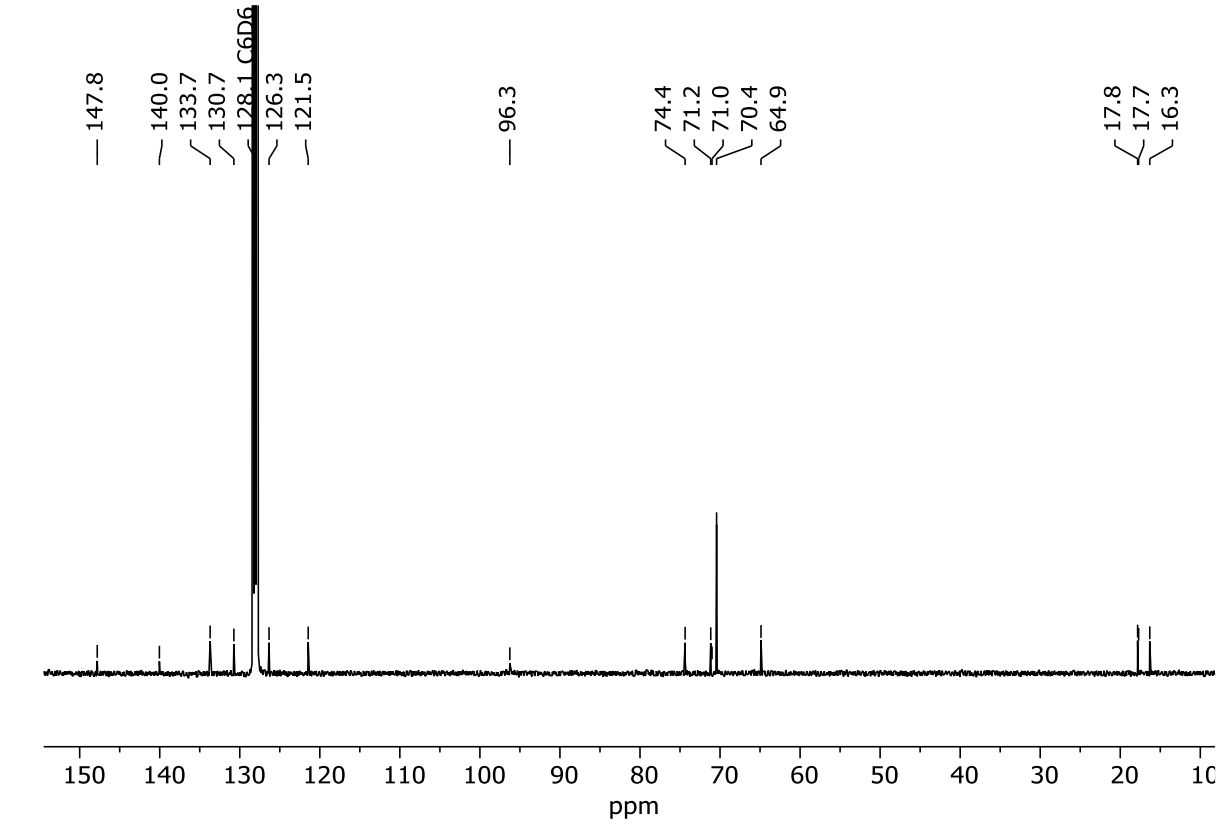

Figure S13: $^{13}C\{^{1}H\}$ NMR (100.61 MHz, C_6D_6, 298 K) spectrum of compound (S_{Si}, S_P) **7**.

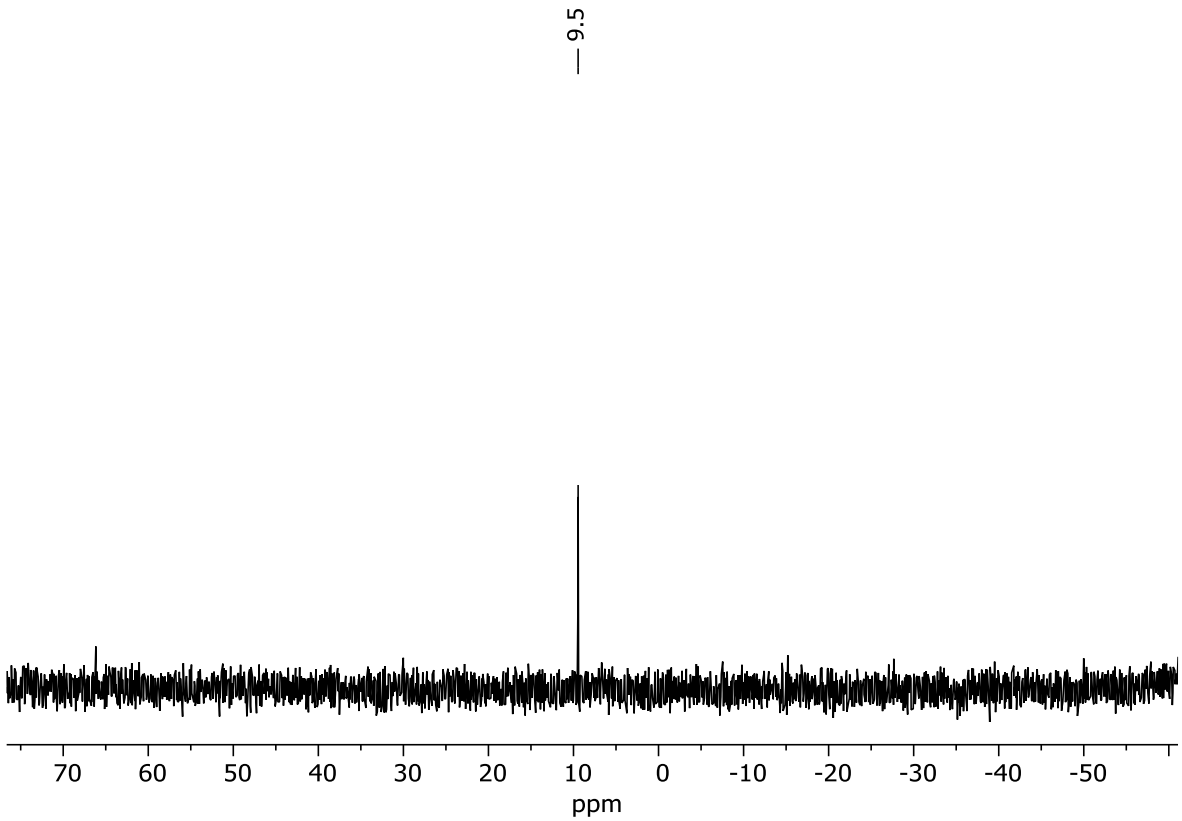

Figure S14: $^{29}Si\{^{1}H\}$ NMR spectrum (79.49 MHz, CDCl3, 298 K) of compound (S_{Si}, S_P) **7**.

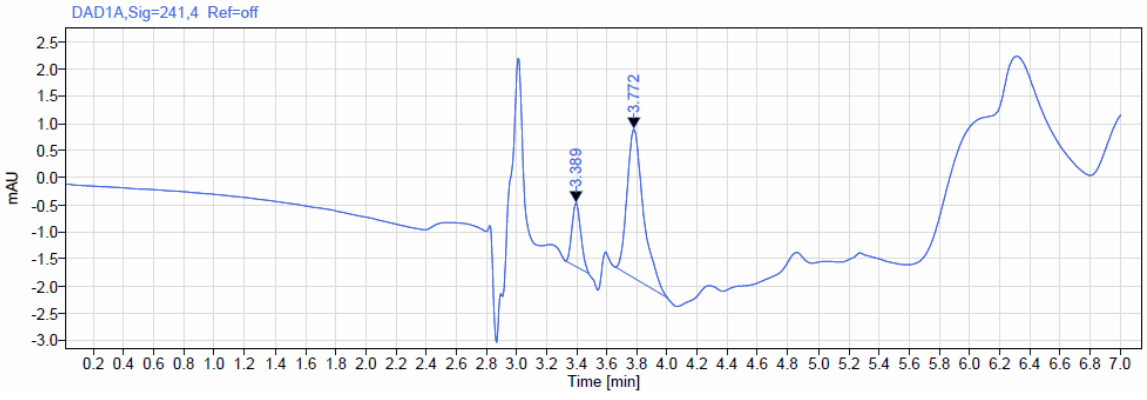

Signal: DAD1A,Sig=241,4 Ref=off

RT [min]	Type	Width [min]	Area	Height	Area%	Name
3.389	MM m	0.16	4.78	1.17	18.70	
3.772	MM m	0.34	20.78	2.74	81.30	
		Sum	**25.56**			

Figure S15: Chromatogram of compound (S_{Si}, S_P) **7** (other signals can be attributed to impurities in the eluent mixture).

6.6.8 Synthesis of compound (S_{Si}, S_P) 8

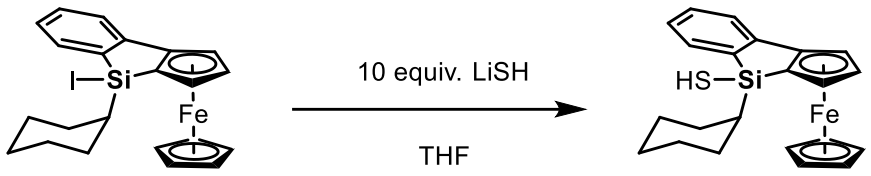

6-I (S_{Si}, S_P) **8**

First H_2S (11.24 mL of a 0.5 M solution in THF, 5.62 mmol, 20 equiv) was cooled to –80°C and then *n*-Butyllithium (1.12 mL of a 2.5 M solution in hexane, 2.81 mmol, 10 equiv) was added and the mixture stirred for 20 min. In a separate Schlenk flask 8,8-cyclohexyl(iodo)benzosilolo[2,3-a]ferrocene (**6-I**) (140 mg, 0.280 mmol, 1 equiv) was dissolved in 10 mL of THF and added to the cooled mixture. The reaction mixture was allowed to slowly warm up in the cooling bath, and then stirred for 12 h at room temperature. Next all volatiles were removed *in vacuo* and the residue suspended with 5 mL of hot hexane and filtered using a teflon cannula. Crystals suitable for single-crystal X-ray diffraction analysis were obtained from the filtrate at –30°C. The crystalline compound (S_{Si}, S_P) **8** was isolated via filtration and dried *in vacuo*. Compound (S_{Si}, S_P) **8** was obtained as orange red crystals. Yield: 83 mg (0.205 mmol, 73%, 47% ee).

^{1}H NMR (400.13 MHz, C_6D_6, 298 K): δ 7.52–7.50 (m, 1H, CH_{Ar}), 7.22–7.18 (m, 2H, CH_{Ar}), 7.06–7.02 (m, 1H, CH_{Ar}), 4.59 (m, 1H, CH_{Cp}), 4.37–4.36 (m, 1H, CH_{Cp}), 4.31–4.30 (m, 1H, CH_{Cp}), 3.87 (s, 5H, CH_{Cp}), 2.22–2.15 (m, 2H, CH_2), 1.81–1.76 (m, 2H, CH_2), 1.73–1.66 (m, 3H, CH_2), 1.50–1.42 (m, 1H, CH), 1.32–1.24 (m, 3H, CH_2), –0.13 (s, 1H, SiSH).

^{13}C{^{1}H} NMR (100.61 MHz, C_6D_6, 298 K): δ 147.8 (s, C_{Ar}), 140.1 (s, C_{Ar}), 133.9 (s, CH$_{Ar}$), 130.7 (s, CH$_{Ar}$), 126.3 (s, CH$_{Ar}$), 121.5 (s, CH$_{Ar}$), 96.4 (s, C_{Cp}), 74.3 (s, CH$_{Cp}$), 71.3 (s, CH$_{Cp}$, 71.2 (s, C_{Cp}), 70.4 (s, CH$_{Cp}$), 64.8 (s, CH$_{Cp}$), 28.1 (s, CH), 28.0 (s, CH$_2$), 28.0 (s, CH$_2$), 27.9 (s, CH$_2$), 26.9 (s, CH$_2$).

^{29}Si{^{1}H} NMR (79.49 MHz, C_6D_6, 298 K): δ 6.0 (s, *Si*SH).

CHN Analysis: Calcd for $C_{22}H_{24}FeSSi$: C, 65.34; H, 5.98. Found: C, 65.81; H, 6.35.

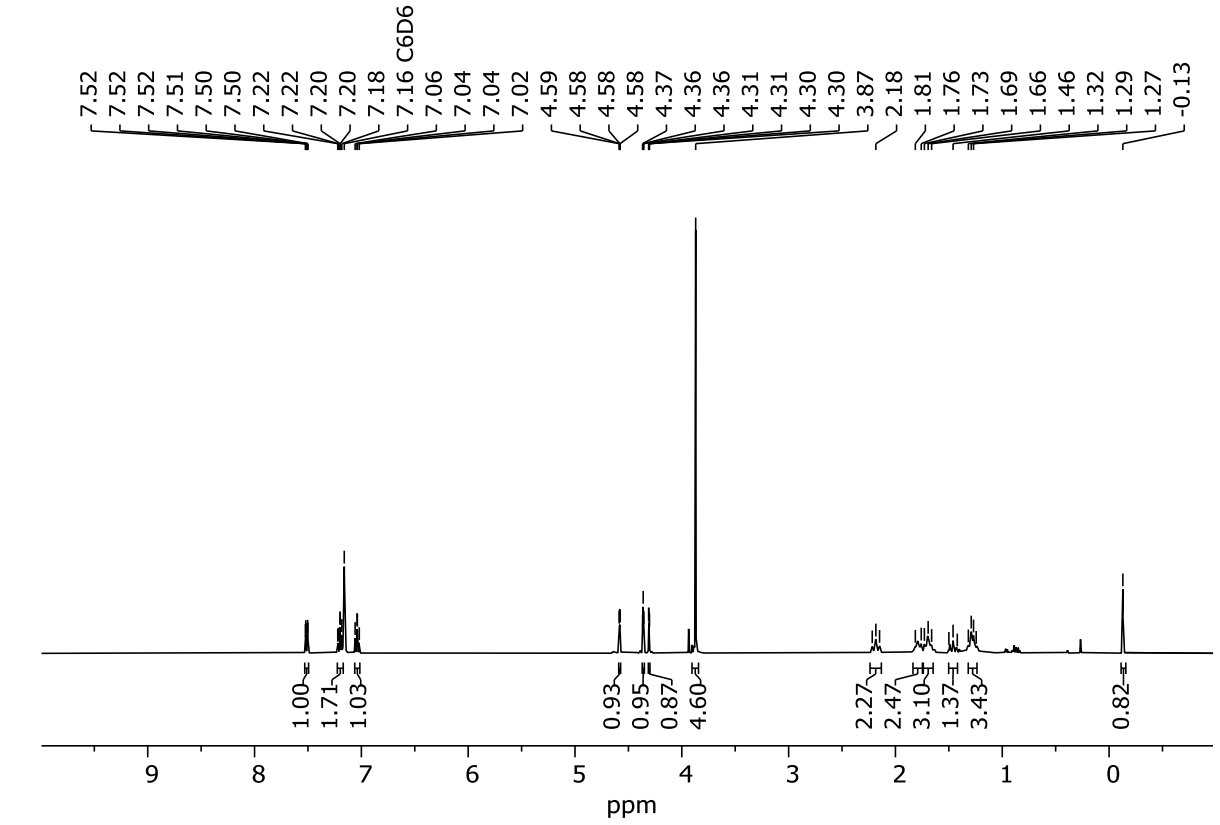

Figure S16: ^{1}H NMR (400.13 MHz, C_6D_6, 298 K) spectrum of compound (S_{Si}, S_P) **8**.

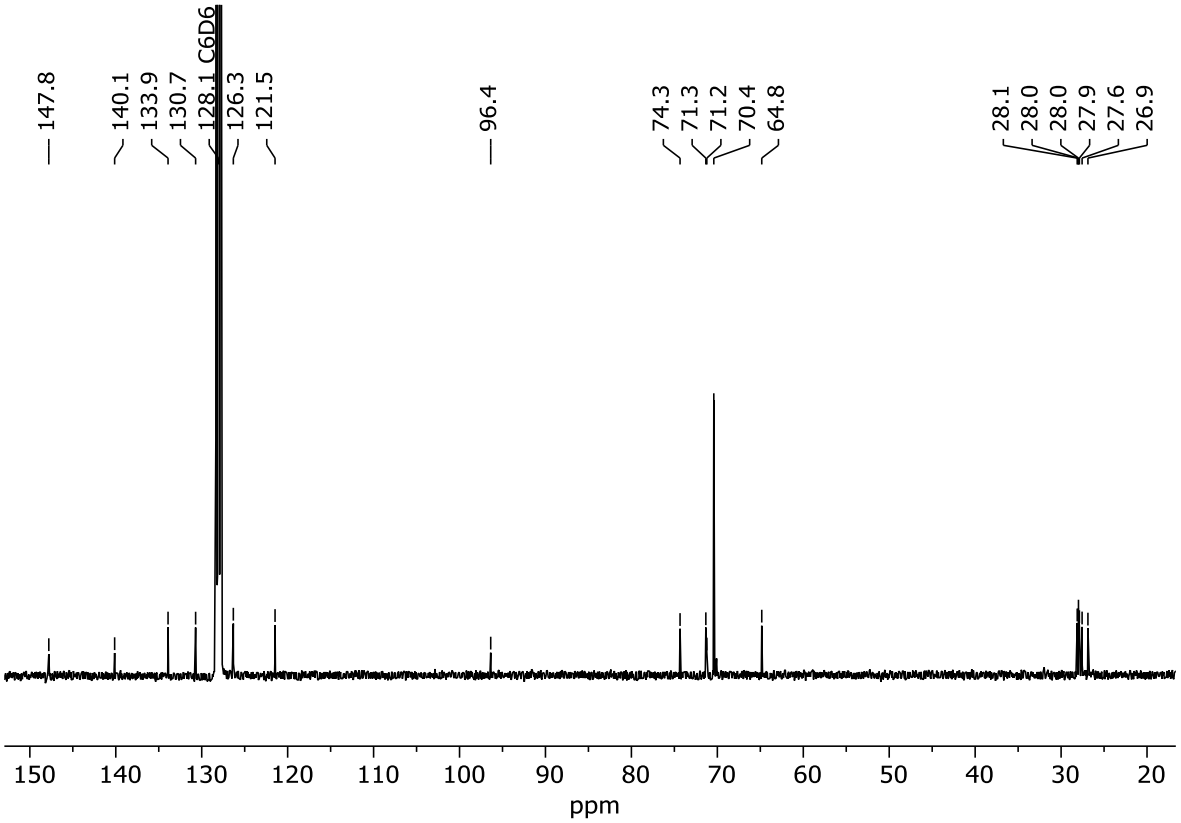

Figure S17: $^{13}C\{^{1}H\}$ NMR (100.61 MHz, C_6D_6, 298 K) spectrum of compound (S_{Si}, S_P) **8**.

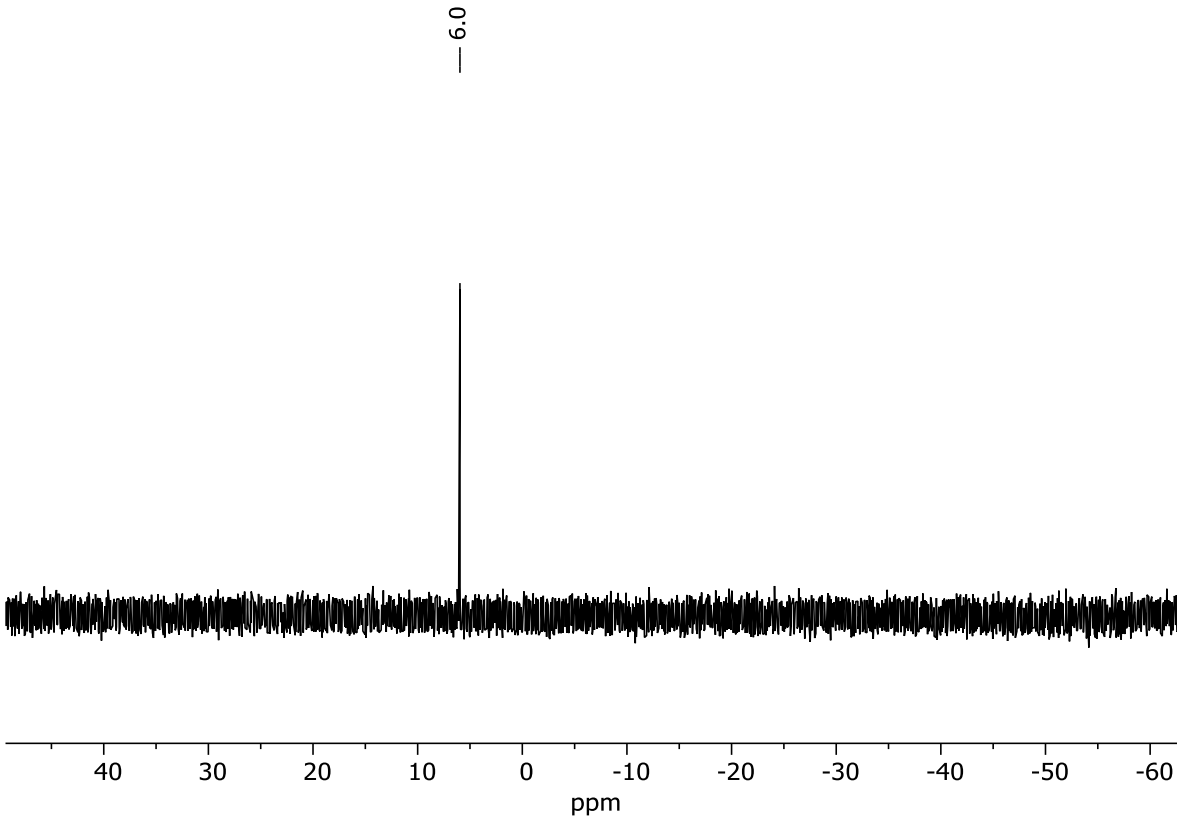

Figure S18: $^{29}Si\{^{1}H\}$ NMR spectrum (79.49 MHz, CDCl3, 298 K) of compound (S_{Si}, S_P) **8**.

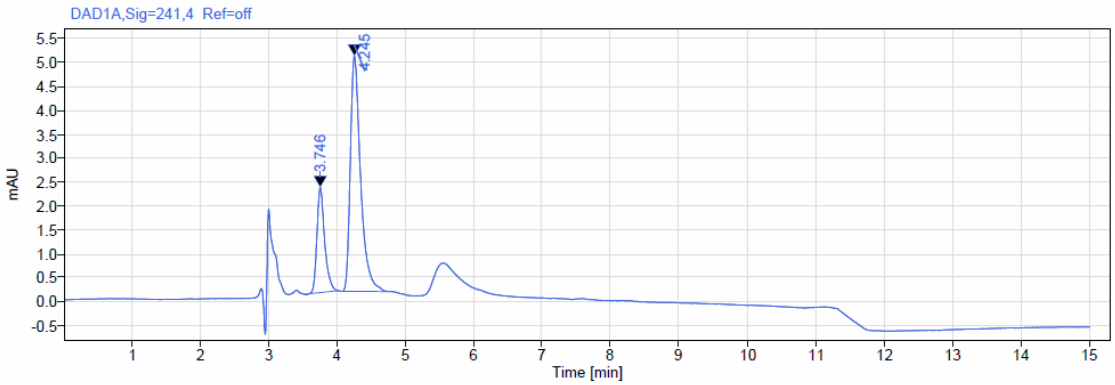

Signal: DAD1A,Sig=241,4 Ref=off

RT [min]	Type	Width [min]	Area	Height	Area%	Name
3.746	MM m	0.50	17.20	2.20	25.13	
4.245	MM m	0.74	51.24	4.92	74.87	
		Sum	**68.44**			

Figure S19: Chromatogram of compound (S_{Si}, S_P) **8** (other signals can be attributed to impurities in the eluent mixture).

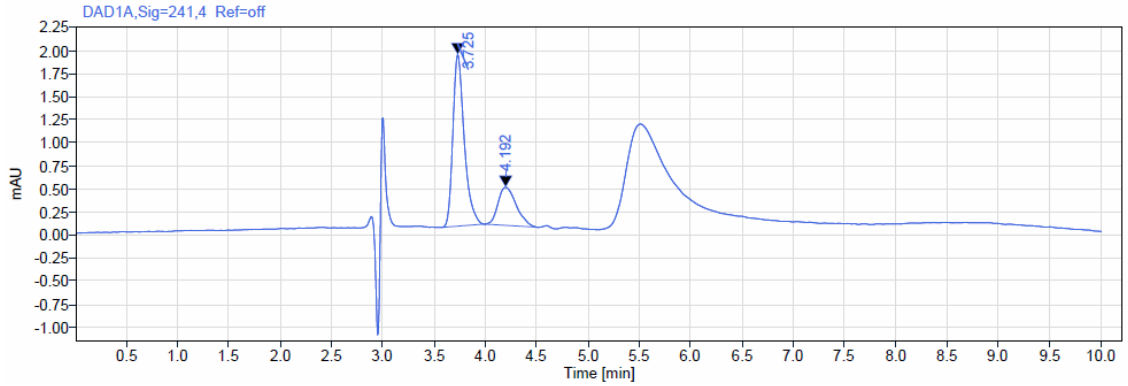

Signal: DAD1A,Sig=241,4 Ref=off

RT [min]	Type	Width [min]	Area	Height	Area%	Name
3.725	MM m	0.41	14.34	1.86	73.67	
4.192	MM m	0.54	5.12	0.41	26.33	
		Sum	**19.46**			

Figure S20: Chromatogram of compound (R_{Si}, R_P) **8** (other signals can be attributed to impurities in the eluent mixture).

6.6.9 X-ray crystallographic details

The crystals were selected and measured on a SuperNova Dualflex diffractometer equipped with a TitanS2 detector. Data collection and reduction were performed with CrysAlisPro {Version 1.171.43.36a}[5]. An analytical numeric absorption correction using a multifaceted crystal model, based on expressions derived by Clark and Reid[6]. A numerical absorption correction based on Gaussian integration over a multifaceted crystal model, and an empirical absorption correction using spherical harmonics, implemented in SCALE3 ABSPACK scaling algorithm was applied. Using Olex2,[7] the structures were solved with ShelXT[8] and a least-square refinement on F^2 was carried out with ShelXL[9]. All non-hydrogen atoms were refined anisotropically. Hydrogen atoms at the carbon atoms were located in idealized positions and refined isotropically according to the riding model. Hydrogen atoms on sulfur atoms were located from the difference Fourier map and refined without restraints. The figures in the Supporting Information were created with Olex2[7].

Compound (S_{Si}, S_P) **7**: The asymmetric unit contains one molecule.

Compound (S_{Si}, S_P) **8**: The asymmetric unit contains one molecule.

Compound	(S_{Si}, S_P) **7**	(S_{Si}, S_P) **8**
Data Set (internal naming)	AF 246(1)	AF250new_commented
CCDC Number	-	-
Formula	$C_{19}H_{20}FeSSi$	$C_{22}H_{24}FeSSi$
$\rho_{calc.}$ / g·cm^{-3}	1.403	1.413
μ/mm^{-1}	8.731	7.984
Formula Weight	364.35	404.41
Color	clear intense orange	clear intense orange
Shape	plate	irregular
Size/mm^3	0.38 x 0.22 x 0.1	0.3 x 0.2 x 0.17
T/K	12.98(10)	123.00(10)
Crystal System	orthorhombic	orthorhombic
Space Group	$P2_12_12_1$	$P2_12_12_1$
a/Å	7.5566(2)	8.3489(2)
b/Å	13.3052(3)	12.9052(2)
c/Å	17.1617(4)	17.6385(3)
α/°	90	90
β/°	90	90
γ/°	90	90
V/Å^3	1725.47(7)	1900.45(6)
Z	4	4
Z'	1	1
Wavelength/Å	1.54184	1.54184
Radiation Type	Cu K_α	Cu K_α
$2\Theta_{min}$/°	8.408	8.49
$2\Theta_{max}$/°	133.746	133.788
Measured Refl.	15492	17334
Independent Refl.	3049	3366
R_{int}	0.0866	0.0712
Parameters	205	226
Restraints	0	91
Largest Peak	0.50	0.79
Deepest Hole	-0.79	-0.93
GooF	1.031	1.032
wR_2 (all data)	0.1217	0.1584
wR_2	0.1175	0.1551
R_1 (all data)	0.0538	0.0603
R_1	0.0475	0.0572

Compound (S_{Si}, S_P) **7**

Hydrogen atoms except S–H are omitted for clarity.

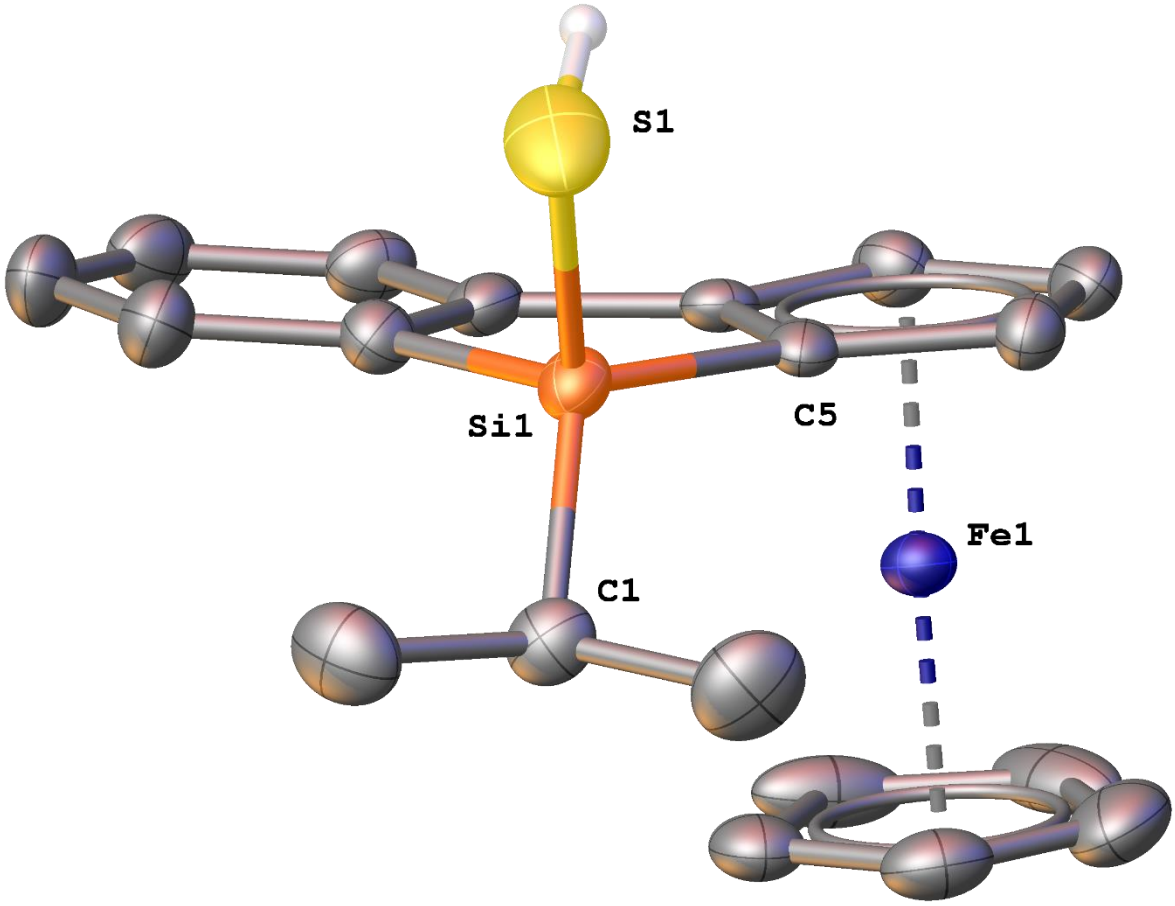

Selected Bond Lengths in Å		**Selected Bond Angles in °**	
Si(1)–S(1)	2.122(2)	**C(1)–Si(1)–S(1)**	105.9(2)
Si(1)–C(1)	1.868(6)	**C(1)–Si(1)–C(5)**	118.4(3)
Si(1)–C(5)	1.857(6)	**S(1)–Si(1)–C(5)**	112.72(17)

Compound (S_{Si}, S_P) **8**

Hydrogen atoms except S–H are omitted for clarity.

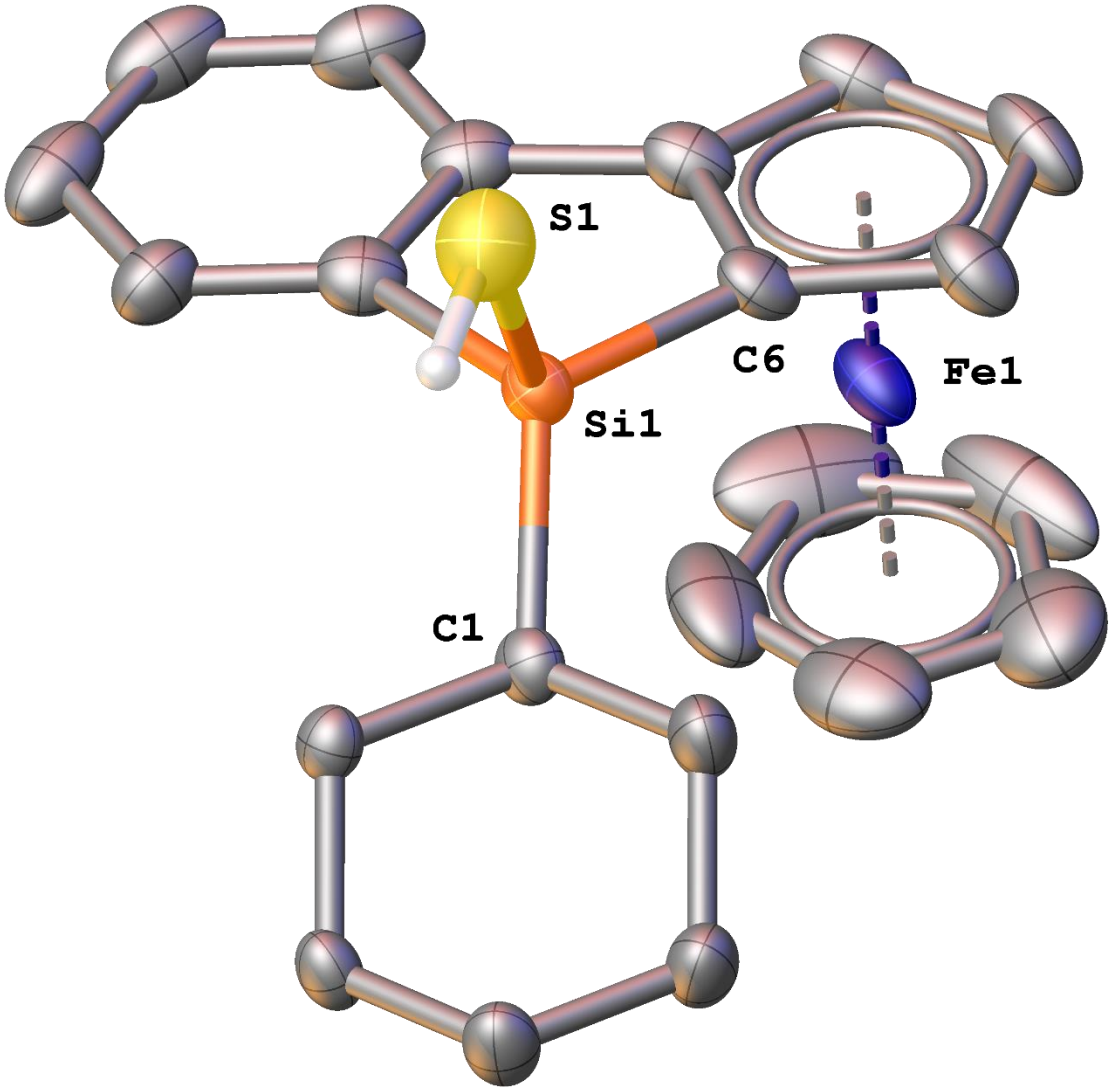

Selected Bond Lengths in Å		**Selected Bond Angles in °**	
Si(1)–S(1)	2.132(3)	**C(1)–Si(1)–S(1)**	109.2(2)
Si(1)–C(1)	1.865(7)	**C(1)–Si(1)–C(6)**	117.2(3)
Si(1)–C(6)	1.846(7)	**S(1)–Si(1)–C(6)**	111.4(2)

6.6.10 Supplementary references

(1) Beckmann, J.; Dakternieks, D.; Tiekink, E. R. T.; Chiral trialkoxysilanols derived from terpene alcohols.:Molecular structures of tris([(1*S*-*endo*]-(–)-bornoxy)silanol and tetrakis((–)-menthoxy)silane. *J. Organomet. Chem.* **2002**, *648*, 188-192.

(2) Kümper, M.; Götz, T.; Espinosa-Jalapa, N. A.; Falk, A.; Rothfelder, R.; Bauer, J. O. Stereochemically Pure *Si* -Chiral Aminochlorosilanes. *Z. anorg. allg. Chem.* **2023**, *649*.

(3) Ma, W.; Liu, Li-C.; An, K.; He, T.; He, W.; Rhodium-Catalyzed Synthesis of Chiral Monohydrosilanes by Intramolecular C–H Functionalization of Dihydrosilanes. *Angew. Chem. Int. Ed.* **2021**, *60*, 4245-4251.

(4) Kunai, A.; Ohshita, J.; Selective synthesis of halosilanes from hydrosilanes and utilization for organic chemistry. *J. Organomet. Chem.* **2003**, *686*, 3-15.

(5) Rigaku Oxford Diffraction, CrysAlisPro Software System. 2020.

(6) Clark, R. C.; Reid, J. S. The analytical calculation of absorption in multifaceted crystals. *Acta Crystallogr.* **1995**, *A51*, 887-897.

(7) Dolomanov, O. V.; Bourhis, L. J.; Gildea, R. J.; Howard, J. A. K.; Puschmann, H. *OLEX2*: a complete structure solution, refinement and analysis program. *J. Appl. Crystallogr.* **2009**, *42*, 339-341.

(8) Sheldrick, G. M. *SHELXT* – Integrated space-group and crystal-structure determination. *Acta Crystallogr.* **2015**, *A71*, 3-8.

(9) Sheldrick, G. M. Crystal structure refinement with *SHELXL*. *Acta Crystallogr.* **2015**, *C71*, 3-8.

7 Additional findings

Preface

The following chapter contains additional findings that were not discussed in the chapters before. It includes fully characterized compounds, but also some compounds where detailed characterization is missing. The collected procedures and data are available for further use by the group of PD Dr. J. O. Bauer.

Authors

A. Falk, J. O. Bauer

Author contribution

All the reported syntheses and characterizations were performed by A. Falk.

Acknowledgements

This work was supported by the Deutsche Forschungsgemeinschaft (DFG, German Research Foundation) through the Research Training Group “Ion Pair Effects in Molecular Reactivity” (RTG 2620, project 426795949).

7.1 Isolated intermediates in the synthesis of four-membered silyl phosphonium chalcogenides

7.1.1 Results and discussion

In the previous chapters, the synthesis of four-membered heterocycles was discussed. The preferred synthesis pathway proceeded *via* hydride abstraction with either tritylium tetrakis(pentafluorophenyl)borate or tris(pentafluorophenyl) borane. Both methods of silylium ion generation were well established within the literature.[1] However, other methods for the generation of silylium ions, which were previously successfully implemented,[1a] were also attempted. One of the aforementioned methods is the dehydrogenative generation of silylium ions *via* dehydrogenative protolysis with strong Brønsted acids, either Brookharts acid $[H(OEt_2)_2][B(3,5\text{-}(CF_3)_2C_6H_3)_4]$ or $[H(OEt_2)_2][B(C_6F_5)_4]$.[1a,2] However, for some protonated compounds, such as compounds **1** and **2**, no hydrogen evolution was observed (Scheme 1).

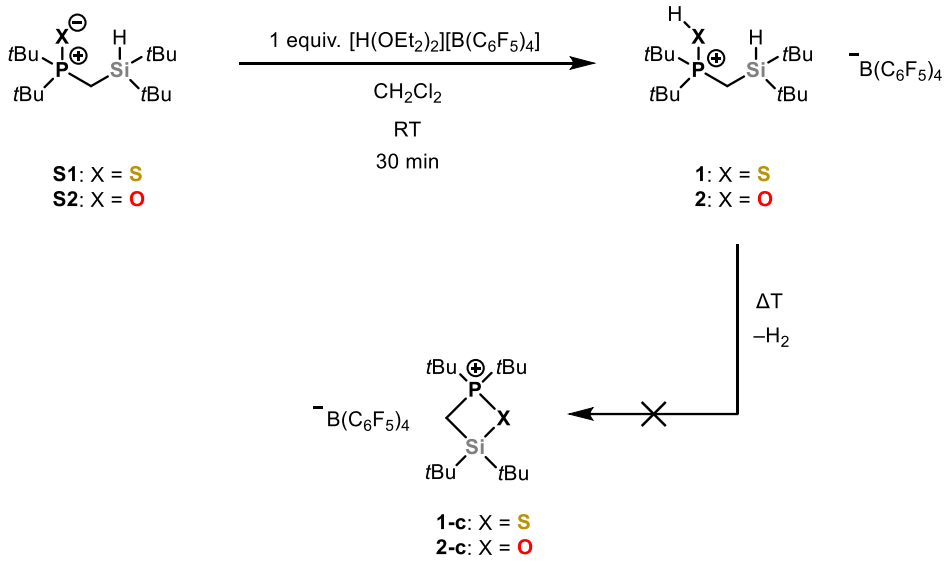

Scheme 1: Synthesis of protonated intermediates **1** and **2** and failed dehydrogenative ring closures.

Both compounds were readily obtained through protonation with $[H(OEt_2)_2][B(C_6F_5)_4]$ in CH_2Cl_2 from their respective silyl phosphine chalcogenides (**S1**, **S2**), whose respective syntheses are reported in the literature and within this work in chapter 3.[3] When compounds **1** and **2** were heated, no hydrogen evolution and ring closure was observed (Scheme 1). Instead, decomposition into several products occurred. One explanation for this observation is that the sterically demanding *tert*-butyl groups may hinder the ring closure through steric repulsion. This problem has been previously discussed in chapter 3. The higher polarization within the P^+–O^- bond in **2** compared to the P^+–S^- bond in **1** results in a shift of the ^{31}P-NMR signal of **2** to lower fields [**2**: 100.0 ppm] compared to **1** [**1**: 89.3 ppm]. Unfortunately, no crystal structure of compound **2** was obtained. However, a single-crystal X-ray diffraction analysis of compound **1** was successful (Figure 1). Compound **1** crystallized in the monoclinic crystal system with the space group $P2_1/n$. The molecular structure in the solid state exhibits a separate ion pair, which is consistent with the weakly coordinating $[B(C_6F_5)_4]^-$ anion. The structure shows that the hydridic Si–H bond

and the highly protic S–H bond are not engaged in any interactions. In contrast to the parent compound $[H(OEt_2)_2][B(C_6F_5)_4]$, where the two diethyl ether moieties are required for stabilization, no solvent molecules co-crystallized in this case. Due to the steric repulsion of the *tert*-butyl moieties, the Si(1)–C(1)–P(1) angle [124.98(8) °] is slightly enlarged to its ideal tetrahedral angle. This is accompanied by a twisting of the *tert*-butyl groups within the plane with a torsion angle of –30.5(1) °, which minimizes the steric interaction. Since an alternative synthesis of the four-membered CPSSi cycle **2-c** from compound **S1** was successful and described in chapter 3, no further effort was made to remove the hydride from compound **S1**. However, the alternative procedure employed for ring closure of compound **S1** and several other procedures (see chapter 3) were not successful for the preparation of oxygen containing cycle **2-c** (Scheme 1), and thus another attempt was made to remove the hydride using the strong silylium cation-based electrophile $[Et_3Si–H–SiEt_3]^+$ $[B(C_6F_5)_4]^–$. The silylium cation electrophile $[Et_3Si–H–SiEt_3]^+$ $[B(C_6F_5)_4]^–$ was prepared from $Ph_3C[B(C_6F_5)_4]$ in Et_3SiH according to the established procedure,[4] and then reacted with compound **S2** (Scheme 2). Unfortunately, the silylium cation does not abstract the hydride from the di-*tert*-butyl silyl hydride moiety in compound **S2**, but rather attaches itself onto the Lewis basic P–O moiety giving rise to compound **3** (Figure 1).

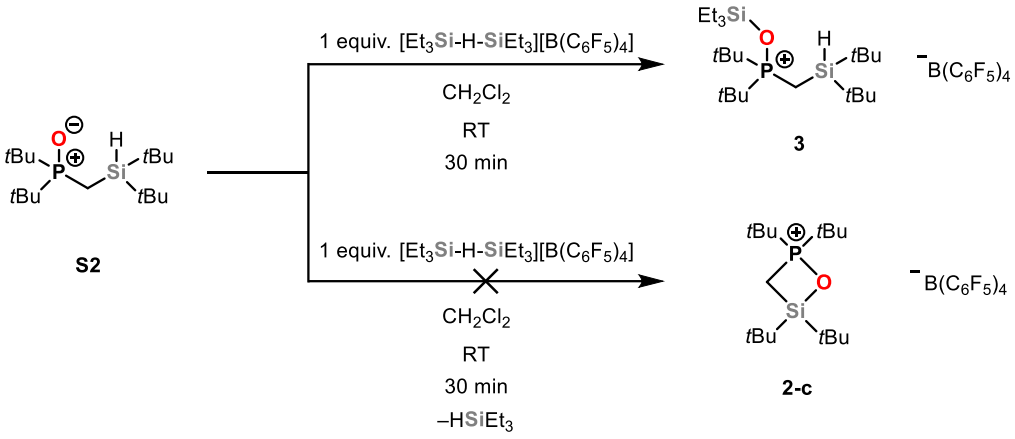

Scheme 2: Unsuccessful synthesis of compound **2-c** via hydride abstraction with $[Et_3Si–H–SiEt_3]^+$ $[B(C_6F_5)_4]^–$.

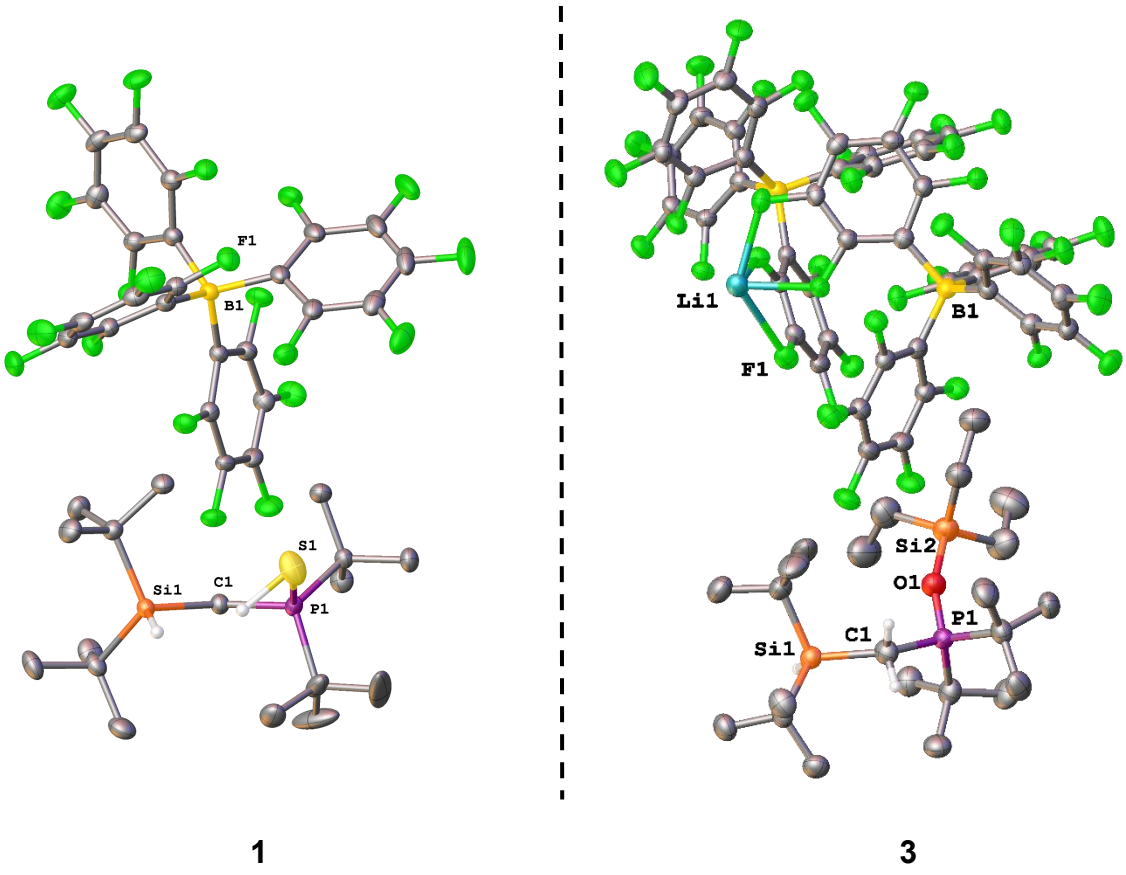

Figure 1: Molecular structures of compounds **1** and **3** in the crystal (displacement ellipsoids set at the 50 % probability level). Selected bond lengths (Å) and angles (°) of **1**: P(1)–S(1) 2.0647(6), P(1)–C(1) 1.8022(13), Si(1)–C(1) 1.9241(14), S(1)–P(1)–C(1) 110.22(5), P(1)–C(1)–Si(1) 124.98(8). **3**: P(1)–O(1) 1.557(3), O(1)–Si(2) 1.717(3), P(1)–C(1) 1.802(4), P(1)–O(1)–Si(2) 160.2(2), P(1)–C(1)–Si(1) 131.9(3), C(1)–P(1)–O(1) 109.14(18).

Compound **3** crystallized in the monoclinic crystal system with the spacegroup $P2_1/n$. The compound co-crystallized with one equivalent of $Li[B(C_6F_5)_4]$, which is an impurity from the synthesis of $Ph_3C[B(C_6F_5)_4]$ from which the $[Et_3Si–H–SiEt_3]^+$ $[B(C_6F_5)_4]^-$ was prepared. The lithium cation in **3** is coordinated by seven fluorine atoms from four $[B(C_6F_5)_4]^-$ moieties (Figure 2).

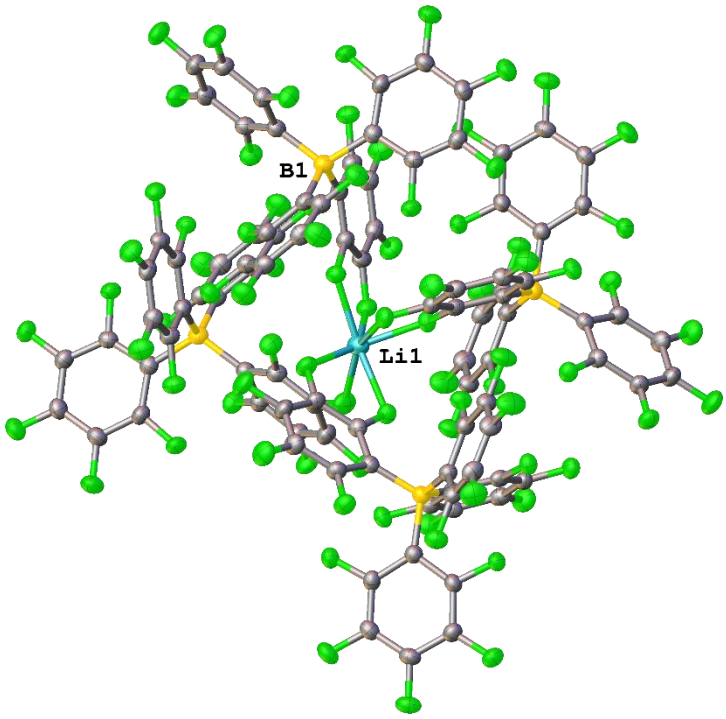

Figure 2: Part of the polymeric structure of compound **3** showing the Lithium cation being surrounded by four $[B(C_6F_5)_4]^-$ moieties.

The silylated phosphine oxide **3** does not exhibit any interaction with its counterion. The P(1)–O(1) bond length [1.557(3) Å] is slightly enlarged compared to the non-silylated compound **S2** [1.4958(8) Å] (see chapter 3).[3] Overall, all attempts at hydride abstraction from compound **S2** were unsuccessful. One major reason for this is definitely the previously discussed (chapter 3) short Si–O bond in the resulting cycle **2-c**, which forces the four *tert*-butyl groups in close proximity. Another reason might also be the higher basicity of the P^+–O^- group compared to the other phosphine chalcogenides (P^+–S^-, P^+–Se^-) (see calculations in chapter 3), which results in a higher competition for hydride abstraction (see introduction, Scheme 6).

7.2 Isolated intermediates in the synthesis of six-membered silyl phosphonium sulfides

7.2.1 Results and Discussion

Previous research conducted by our group has revealed the existence of a hitherto unidentified reactivity in six-membered silyl phosphine sulfides (Scheme 3).[5] Further research has highlighted the importance of steric factors in four-membered CPSSi cycles when looking at the ability of phosphine-sulfide donors to stabilize cationic silylium ion centers (chapter 3). Therefore the “hidden” FLP-type reactivity is also influenced by steric factors within these systems. Curious to see whether the same trends, observed during the study of the four-membered cycles, persist in the larger siloxane-based six-membered

cycles we set out to synthesize the di-*tert*-butylsilyl substituted compound **4** and compare its characteristics with the already known compound **S4**.

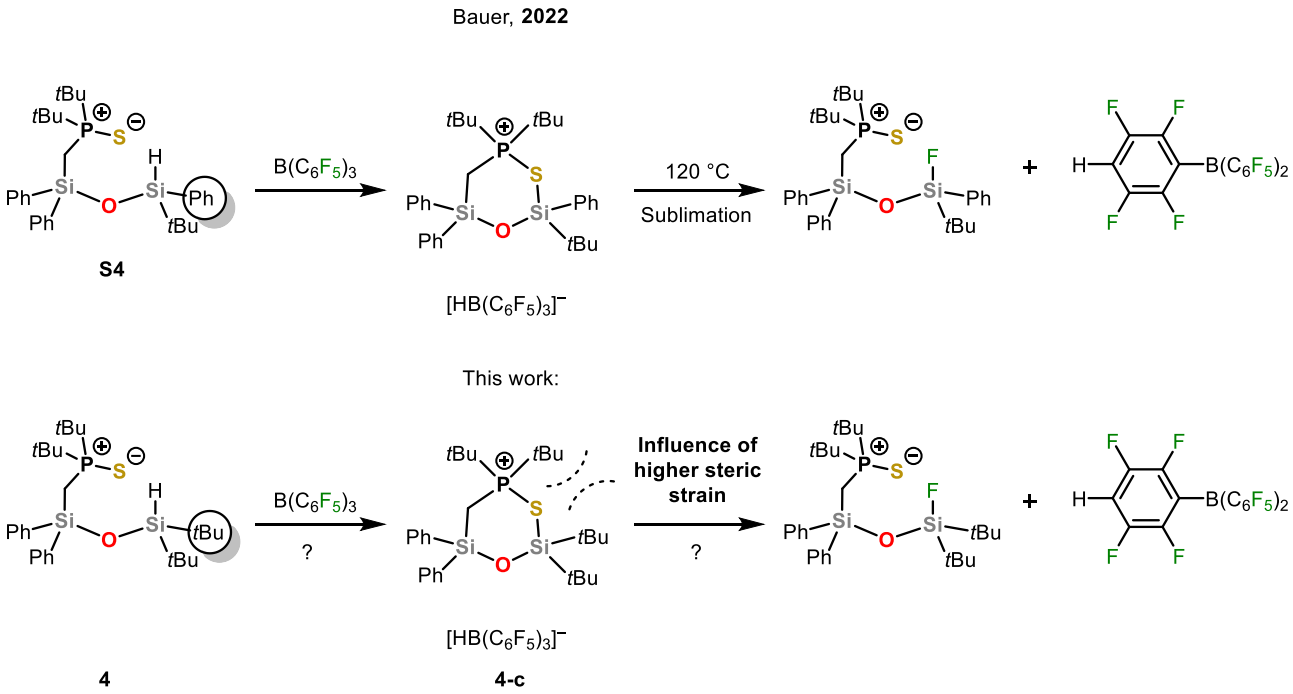

Scheme 3: Reported hidden silylium type reactivity and proposed comparison to the di-*tert*-butyl substituted compound **4**.

Compound **4** was obtained through the reaction of 3,3-di-*tert*-butyl-1-chloro-1,1-diphenyldisiloxane and ((di-*tert*-butylphosphorothioyl)methyl)lithium (Scheme 4).

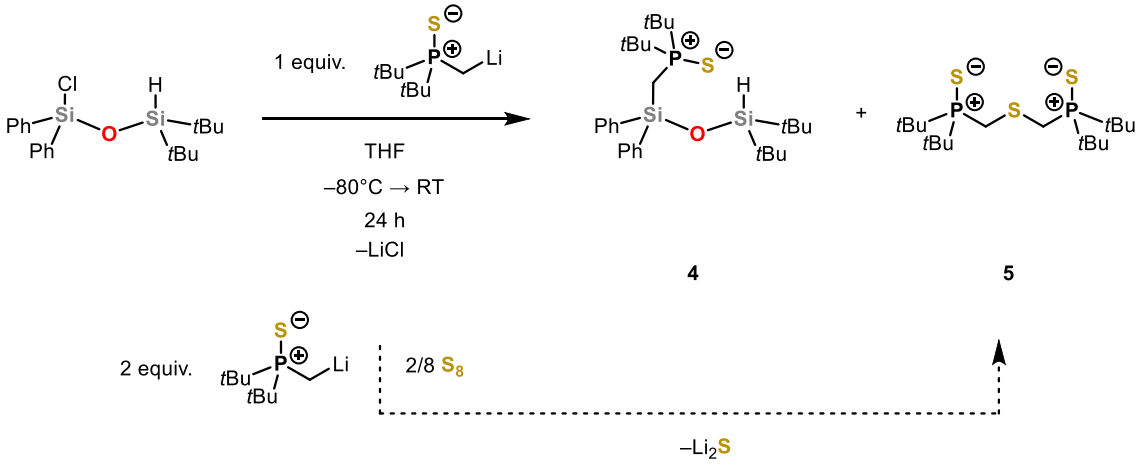

Scheme 4: Synthesis of compound **4** and possible formation of byproduct **5**.

Unfortunately, only a small quantity of crystals could be obtained from the reaction mixture, and was subjected to single-crystal X-ray diffraction analysis, which confirmed the

structure of the desired compound **4** (Figure 3). In addition to crystals of compound **4**, crystals of compound **5** could be obtained from the reaction mixture (Scheme 4) (Figure 3). This finding also serves as an indicator as to why only a small crop of **4** was obtained. It can be postulated that compound **5** resulted from a reaction between ((di-*tert*-butylphosphorothioyl)methyl)lithium and sulfur shown in Scheme 4. This ultimately points to the use of an apparently impure, excess sulfur containing, di-*tert*-butylmethylphosphine sulfide as a starting material for the synthesis of ((di-*tert*-butylphosphorothioyl)methyl)lithium. Further experiments utilising tris(pentafluorophenyl)borane as a hydride abstracting reagent demonstrated that compound **4** was unreactive. This suggests that the bulky di-*tert*-butyl moiety may be inhibiting the formation of the six-membered phosphonium sulfide ring **4-c** (Scheme 3). This is rather surprising, since the more strained four-membered all-*tert*-butyl substituted CPSSi ring-system can be obtained with this method (see chapter 3, Scheme 3). Compound **4** crystallized in the triclinic crystal system with the space group $P\bar{1}$, in conjunction with crystals from compound **5**, which crystallized in the monoclinic crystal system with the space group *C*2/*c*, from pentane at –30°C. Since we currently could not obtain the six-membered ring **4-c** with the previously proven methods we shifted our attention to other fields of research.[1,3,5] However, future research will focus on the synthesis of the di-*tert*-butyl substituted six-membered phosphonium sulfide cycle and its reactivity as a hidden frustrated Lewis pair.

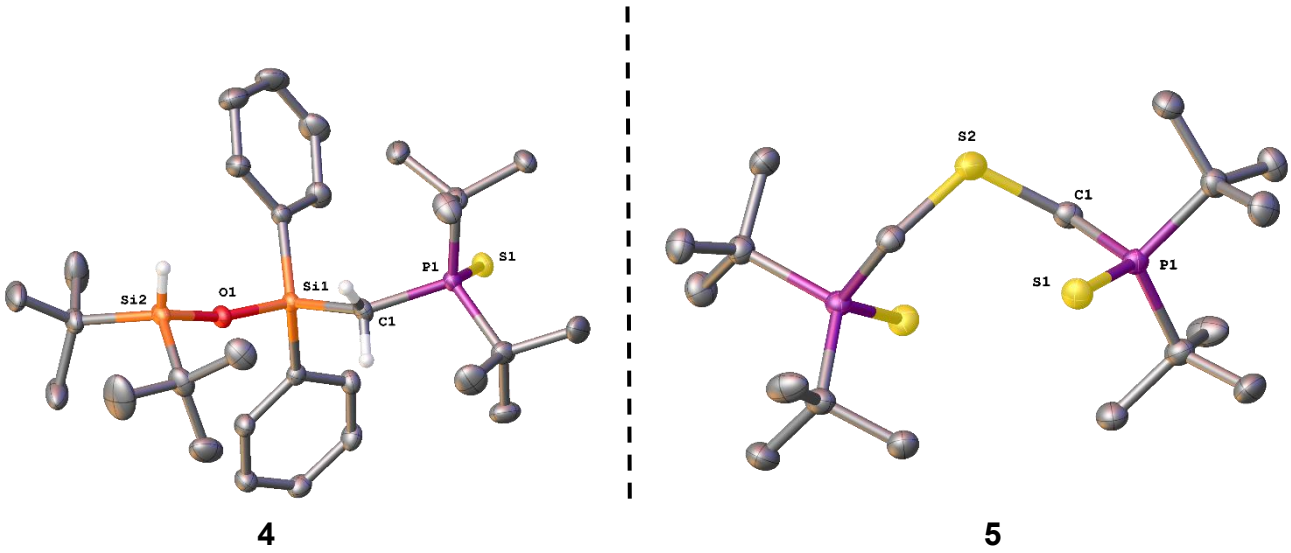

4 **5**

Figure 3: Molecular structures of compounds **4** and **5** in the crystal (displacement ellipsoids set at the 50 % probability level). Selected bond lengths (Å) and angles (°) of **4**: P(1)–S(1) 1.9701(5), Si(1)–O(1) 1.6289(10), Si(1)–C(1) 1.8860(15), Si(1)–O(1)–Si(2) 164.84(7), Si(1)–C(1)–P(1) 127.75(8), C(1)–P(1)–S(1) 115.07(5). **5**: P(1)–S(1) 1.9764(7), P(1)–C(1) 1.878(2), C(1)–S(2) 1.882(2), P(1)–C(1)–S(2) 119.41(12), C(1)–P(1)–S(1) 112.18(8), C(3)–P(1)–S(1) 111.79(7).

7.3 Di-*tert*-butyl(methyl)phosphaneyl-substituted compounds

The di-*tert*-butyl(methyl)phosphaneyl moiety has been employed extensively in the past as part of a ligand system for transition metals[6], as part of intramolecular donor-acceptor systems[7], and especially as the Lewis basic component of frustrated Lewis pairs.[8] The

high basicity of the phosphine and the simultaneous high steric shielding by the two *tert*-butyl groups, as well as the ease of incorporation into systems by lithiation with *tert*-butyllithium, render it an ideal candidate for intramolecular FLP systems.[9] The idea was to substitute the previously employed phosphine-chalcogenide (chapter 3) or phosphinimine (chapter 4) donors with the parent compound di-*tert*-butyl(methyl)phosphane (Figure 4).

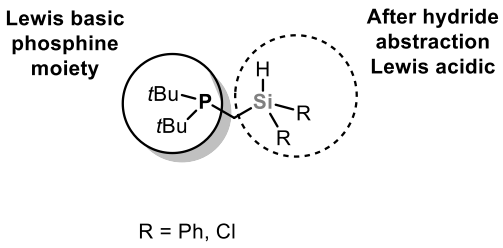

Figure 4: Proposed design of FLP systems containing the di-*tert*-butyl moiety.

The substitutions were chosen in order to study the effect of slightly (Ph) and strongly (Cl) electron withdrawing effects on the Lewis acidity of the silicon center (For further studies on electron withdrawing substituents see chapter 5). However, during the synthesis we were not able to obtain the desired compounds. Instead, compound **6** was obtained as the main product from the reaction of commercially available diphenyl(chloro)silane with freshly prepared di-*tert*-butylphosphaneyl lithium (Scheme 5).

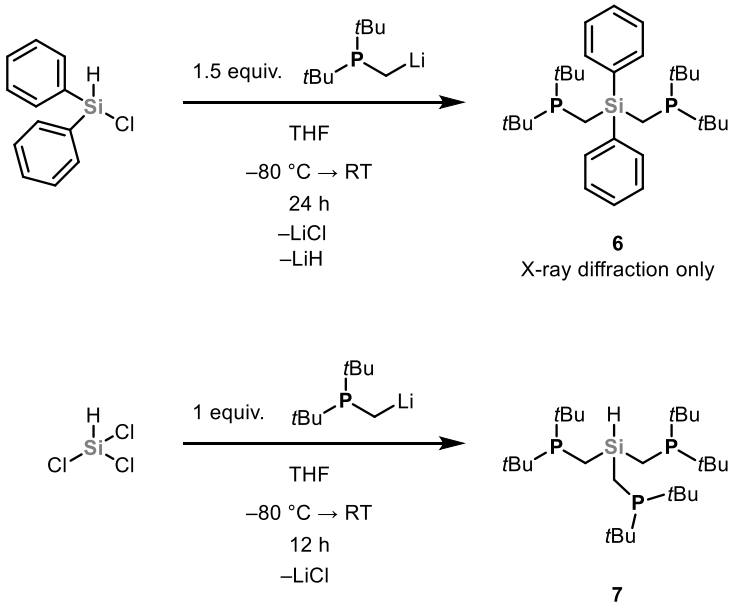

Scheme 5: Synthesis of compounds **6** and **7**.

To our surprise not the desired mono substituted product was obtained, but rather the disubstituted compound **6**. Apparently the high nucleophilicity of di-*tert*-butylphosphaneyl lithium also allows for the substitution of Si–H bonds. The highly nucleophilic nature of di-*tert*-butylphosphaneyl lithium was also observed when attempting to selectively substitute only one Si–Cl bond from trichlorosilane, however the substitution of all three Si–Cl bonds

was observed forming compound **7**. To obtain a sample clean enough for ^{1}H-NMR spectroscopic analysis the reaction was repeated with three equivalents di-*tert*-butylphosphaneyl lithium. From compound **6** single-crystal X-ray diffraction analysis was successful (Figure 5).

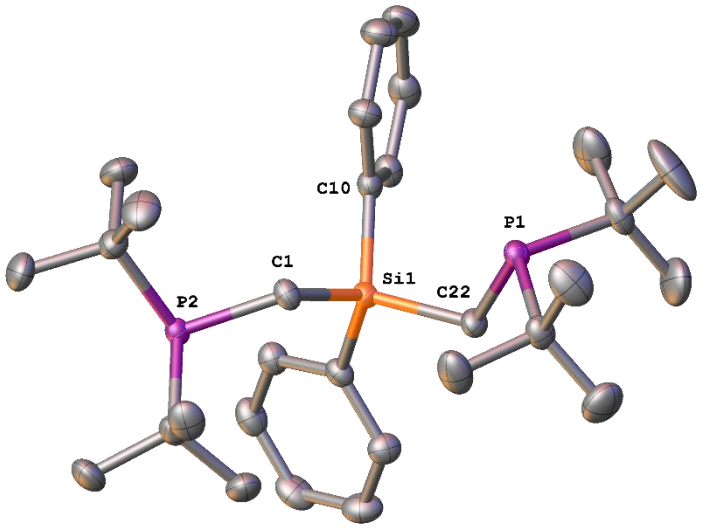

Figure 5: Molecular structure of compound **6** in the crystal (displacement ellipsoids set at the 50 % probability level). Selected bond lengths (Å) and angles (°) of **6**: Si(1)–C(1) 1.8810(16), C(1)–P(2) 1.8637(15), Si(1)–C(10) 1.8841(16), Si(1)–C(1)–P(2) 117.99(8), C(1)–Si(1)–C(10) 107.89(7), C(1)–Si(1)–C(22) 110.31(7).

Compound **6** crystallized in the monoclinic crystal system with the spacegroup $P2_1/c$. Both compounds **6** and **7** are currently investigated for possible lithium ion complexation in lithium siloxides, since they feature a bi-, tridentate chelating scaffold which is similar to picoline bearing systems reported previously in our group for lithium ion coordination.[10]

7.4 Transition metal modified substrates

7.4.1 Results and Discussion

Transition metals can act as both Lewis acids and bases in frustrated Lewis pairs.[11] A prominent example is the use of a ferrocene-stabilized silylium ion by the Oestreich group in 2009, which was used as catalyst for low-temperature Diels Alder reactions.[12]

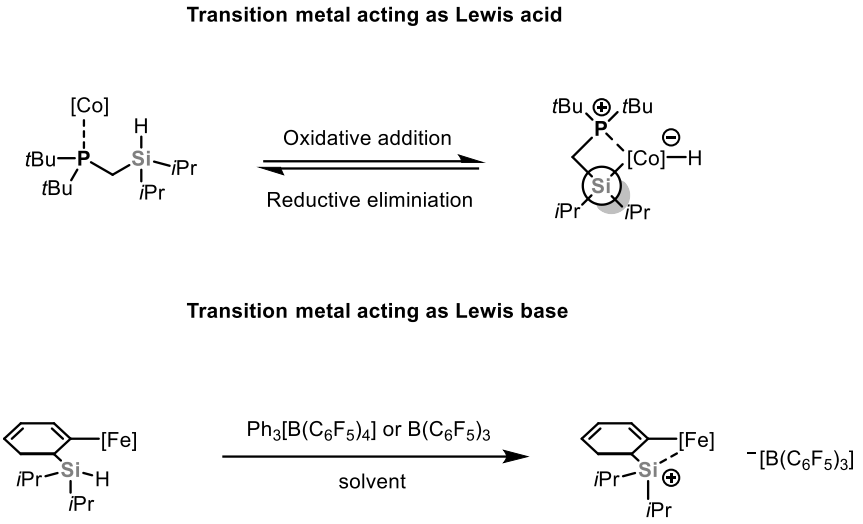

Scheme 6: Potential of using transition metals as stabilizing agents for silylium ions or activation of silicon hydrides.

Moreover, numerous transition metals are capable of performing an oxidative addition into Si–H bonds, thereby enhancing the electrophilicity of the silicon atom (Scheme 6).[13] Starting with the synthesis of compound **8** from di-*tert*-butyl((diisopropylsilyl)methyl)phosphane (see chapter 4 for the synthesis) and $Co_2(CO)_8$ (Scheme 7). Compound **8** was obtained as red prisms suitable for single-crystal X-ray diffraction analysis (Figure 6). It was observed that compound **8** undergoes a slow decomposition into unidentified products when stored in C_6D_6 at room temperature. Further modifications of **8**, including the removal of the hydride from the Si–H moieties with tritylium tetrakis(pentafluorophenyl)borate and tris(pentafluorophenyl)borane, were unsuccessful. Compound **9** was a byproduct obtained in a clean flash chromatography fraction from a literature synthesis (Synthesis of isopropyl(hydrido)benzosilolo[2,3-a]ferrocene, chapter 6).[14] Compound **9** was reacted with di-*iso*-propyl(chloro)silane to form compound **10**. Compound **10** was obtained as a red amorphous powder (Scheme 7). Subsequent attempts to perform hydride abstraction with both tritylium tetrakis(pentafluorophenyl)borate and tris(pentafluorophenyl) borane were unsuccessful.

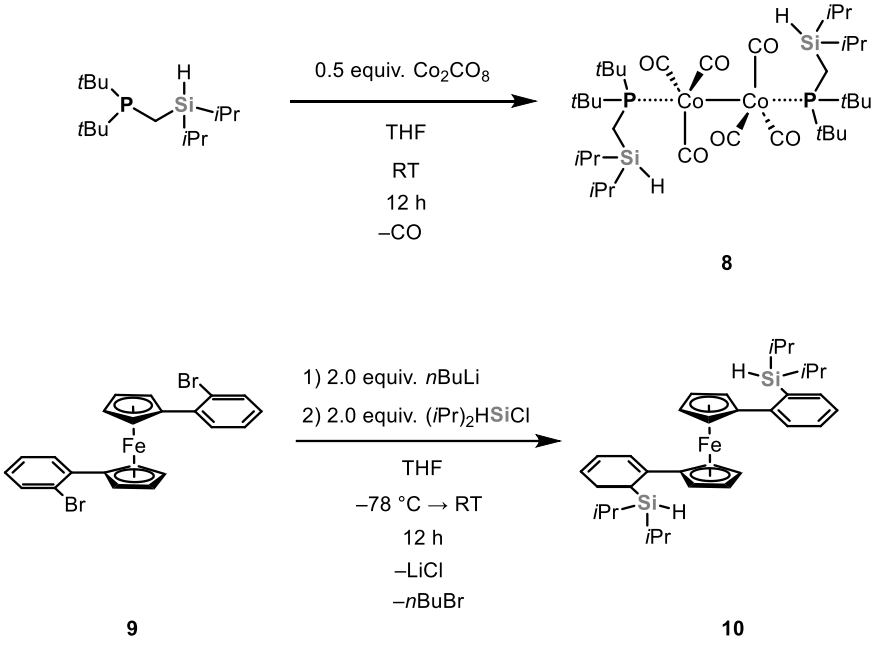

Scheme 7: Synthesis of transition metal functionalized compounds **8** and **10**.

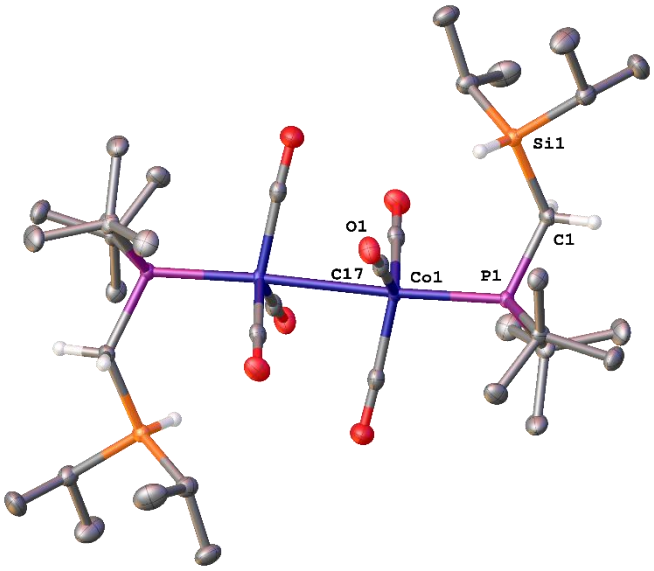

Figure 6: Molecular structure of compound **8** in the crystal (displacement ellipsoids set at the 50 % probability level). Selected bond lengths (Å) and angles (°) of **8**: Si(1)–C(1) 1.9103(17), P(1)–Co(1) 2.2382(5), C(17)–O(1) 1.147(2), Si(1)–C(1)–P(1) 122.76(9), C(1)–P(1)–Co(1) 112.73(6), P(1)–Co(1)–C(17) 97.20(6).

Compound **8** crystallized in the monoclinic crystal system with the spacegroup $P2_1/n$. Compound **8** features a symmetrical 18-VE cobalt complex with two di-*tert*-butyl((diisopropylsilyl)methyl)phosphane moieties acting as axial ligands. The Co(1)–P(1) bond length is 2.2382(5) Å, while the Co–Co bond length is 2.7066(5) Å. The cobalt atoms in compound **8** do not interact with the Si–H groups.

7.5 Compounds obtained as byproducts

7.5.1 Products obtained from the attempted synthesis of a *Si*-chiral thiosilane

In chapter 6 we discussed the synthesis of various chiral silanethiols and their application as an asymmetric HAT-catalyst in a HAT-RRPCO-Protonation sequence (HAT: hydrogen-atom transfer, RRPCO: reductive-radical-polar crossover).[15] Since no silanethiol achieved an enantiomeric excess in the product which was acceptable we envisioned a new silanethiol system in order to achieve a higher stereoselectivity (Figure 7). Our new design features an all alkyl/aryl substituted silane with no heteroatoms attached to silicon, as they are prone to react under the photocatalytic conditions. Importantly, we employed the 3,5-diphenylpheny-moiety to act as sort of a shield, selectively shielding one part of the catalyst and therefore enhancing the stereoselective properties of the HAT catalyst (Figure 7). Compounds (*rac*)-**11** and **12** were obtained from 3,5-diphenylphenyllithium and the corresponding dichlorosilanes (Scheme 8).

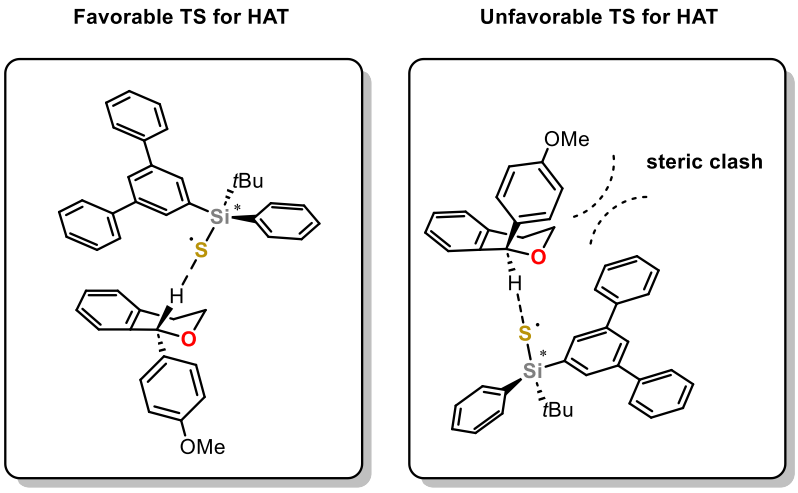

Figure 7: Design rational for the silanethiols with the 3,5-diphenylpheny-moiety attached.

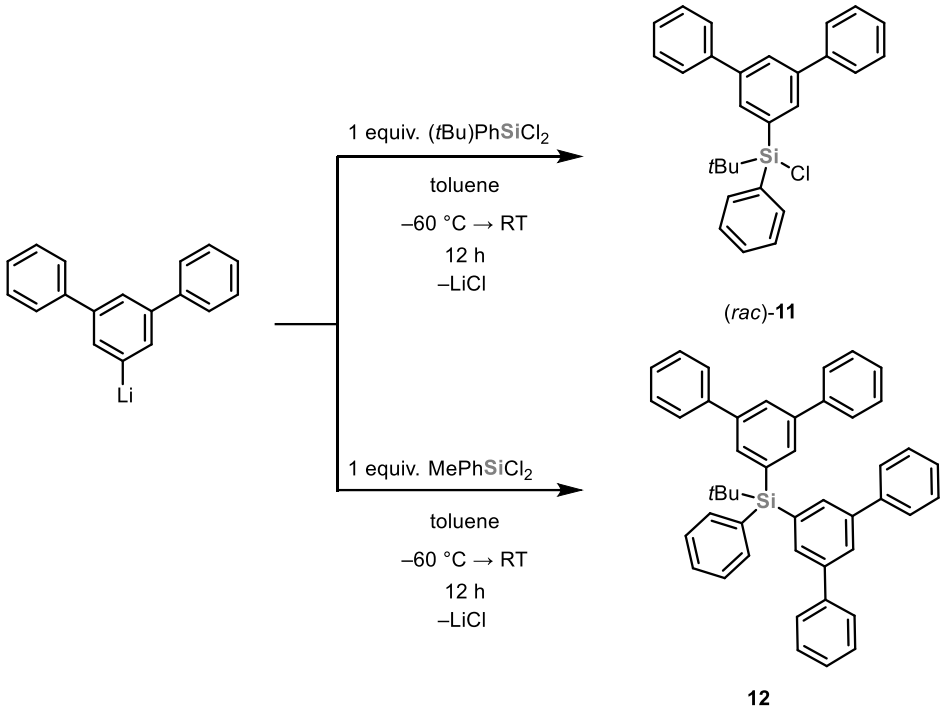

Scheme 8: Obtained compounds (*rac*)-**11** and **12** in the synthesis of a racemic chlorosilane.

(3,5-diphenyl)phenyllithium was freshly prepared from (3,5-diphenyl)bromobenzene and *n*-Butyllithium (2.5 M in hexanes) and then reacted with the one equivalent of the respective dichlorosilanes. In the case of (*rac*)-**11**, the expected monosubstituted product was obtained. However, when using the phenyl(methyl)dichlorosilane, only the disubstituted product **12** could be isolated. One reason for this discrepancy in reactivity is that the *tert*-butyl group, due to its steric hindrance, is less favored for multiple substitutions. A single-crystal X-ray structure was successfully obtained for compound **12** (see experimental results). Subsequently, compound (*rac*)-**11** was subjected to a reaction with H_2S and (*S*)-(1-phenylethyl)amine with the objective of forming separable diastereomers of silane thiolate salts. However, this reaction was unsuccessful (Scheme 9).

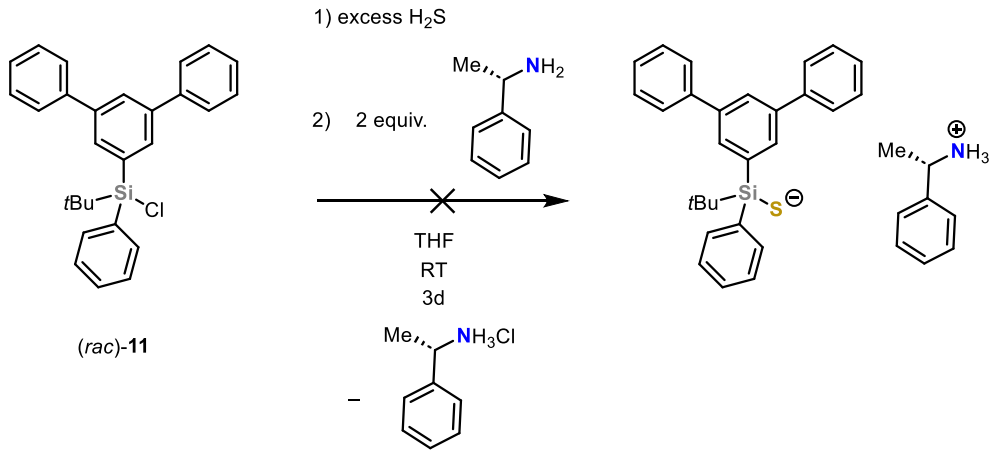

Scheme 9: Unsuccessful preparation of the diastereomeric silane thiolate salts by reaction of (*rac*)-**11** with H_2S and (*S*)-(1-phenylethyl)amine.

7.5.2 Intermediates in the stereodifferentation with the (*R*)-BINOL-PSSLi method

During our investigation of chiral silanethiols in chapter 6 we used lithiated (*R*)-BINOL-dithiophosphoric acid [(*R*)-BINOL-PSSLi] as a chiral shift reagent to determine the enantiomeric purity of our compounds.[16] This method is based on a previously published method for the enantiomeric determination of silyl pyridines, using the Brønsted acidic (*R*)-BINOL-dithiophosphoric acid [(*R*)-BINOL-PSSH] as a chiral shift reagent.[17] However this method does not discriminate between compounds with of low basicity as experiments with aminophosphine sulfides have shown (Scheme 10).[16] We adapted to this problem by lithiating the (*R*)-BINOL-PSSH and now a diastereomeric discrimination between both enantiomers was observed within the ^{1}H-NMR and ^{31}P-NMR spectra.

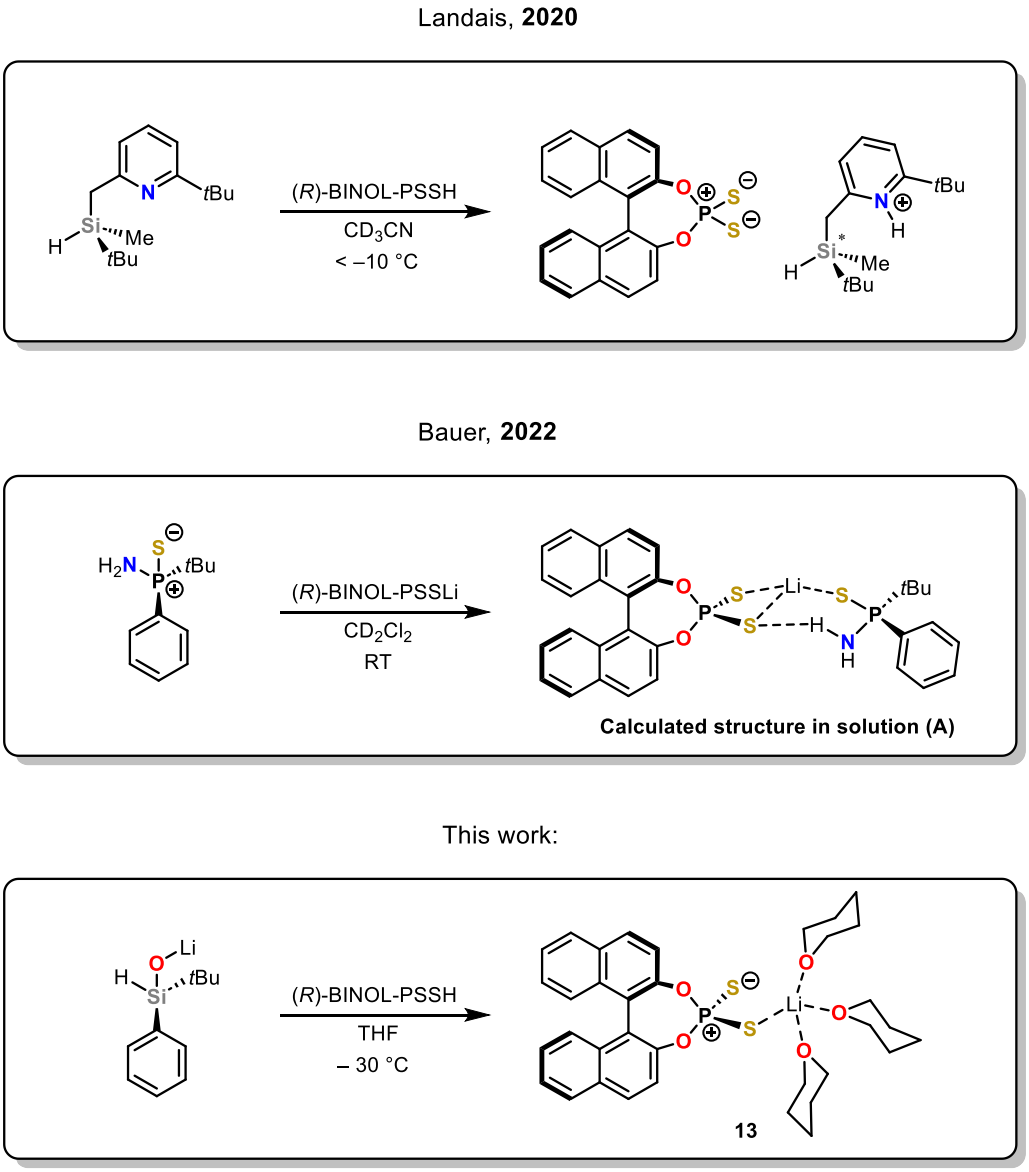

Scheme 10: Reactions with (*R*)-BINOL-PSSLi and (*R*)-BINOL-PSSH for stereo-differentiation of various molecules.

The lithium ion is therefore an important factor in the stabilization of the diastereomeric complex between (*R*)-BINOL-PSSLi and the aminophosphine sulfide substrate. Quantum chemical calculations show the structure in solution (**A**) where the lithium atom is coordinated in a trigonal planar fashion (Scheme 10).[16] The developed (*R*)-BINOL-PSSLi was also applied to *Si*-chiral silanols and silanethiols.[18] Due to the high Brønsted acidity of the employed (*R*)-BINOL-PSSH the substrate, for example a silanol, can be previously lithiated to form a lithium silanolate (Scheme 10) and then mixed with (*R*)-BINOL-PSSH to afford the same enantio-discrimination. In an effort to crystallize the stereo differentiating intermediate the racemic lithium phenyl(*tert*-butyl)hydridosilanolate was mixed with (*R*)-BINOL-PSSH in THF. We hoped that the THF would stabilize the intermediate enough to obtain a single-crystal solid state structure. However, it turned out that the THF solvent molecules stabilize the lithium cation too much and therefore only the THF stabilized (*R*)-BINOL-PSSLi was obtained (**13**) (Figure 7).

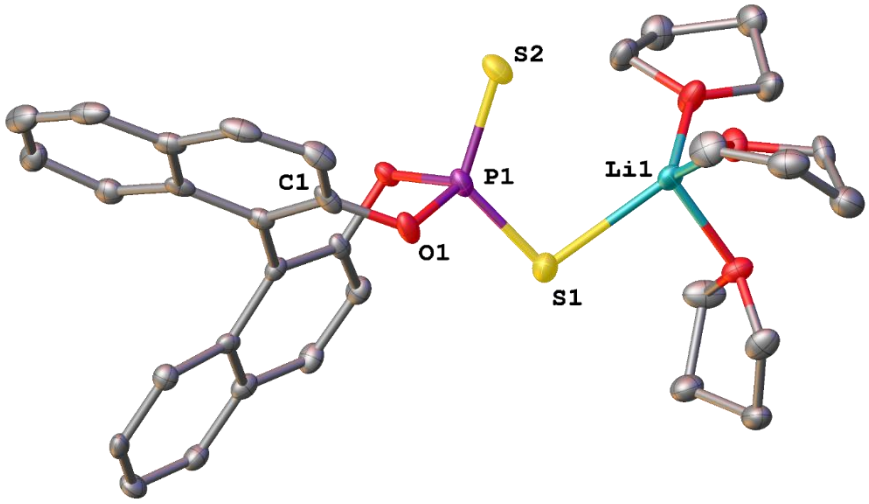

Figure 5: Molecular structure of compound **13** in the crystal (displacement ellipsoids set at the 50 % probability level). Selected bond lengths (Å) and angles (°) of **13**: P(1)–S(1) 1.9655(19), S(1)–Li(1) 2.481(8), P(1)–O(1) 1.637(3), P(1)–S(1)–Li(1) 100.7(2), S(2)–P(1)–O(1) 113.13(15), P(1)–O(1)–C(1) 120.1(3).

Compound **13** crystallized in the orthorhombic crystal system with the spacegroup $P2_12_12_1$, and a lithium cation which is coordinated by three THF solvent molecules. The coordination of the THF solvent is stronger than that of the chiral substrate, making the use of non-coordinating polar solvents like CD_2Cl_2 crucial for the discrimination of enantiomers with the (*R*)-BINOL-PSSLi method. Interestingly this is in strong contrast to the (*R*)-BINOL-PSSH method by Landais, where highly polar solvents like CD_3CN can be used.[17]

7.6 References

(1) (a) Fontana, N.; Espinosa-Jalapa, N. A.; Seidl, M.; Bauer, J. O. Easy Access to Enantiomerically Pure Heterocyclic Silicon-Chiral Phosphonium Cations and the Matched/Mismatched Case of Dihydrogen Release. *Chem. Eur. J.* **2021**, *27*, 2649–2653. (b) Y. Corey, J.; Gust, D.; Mislow, K. Generation of a ferrocenylsilicenium ion. *J. Organomet. Chem.* **1975**, *101*, C7-C8. (c) Corey, J. Y. Generation of a silicenium ion in solution. *J. Am. Chem. Soc.* **1975**, *97*, 3237–3238. (d) Corey, J. Y.; West, R. Hydrogen-Halogen Exchange between Silanes and Triphenylmethyl Halides. *J. Am. Chem. Soc.* **1963**, *85*, 2430–2433. (e) Bickart, P.; Llort, F. M.; Mislow, K. On the evidence for the generation of a ferrocenylsilicenium ion. *J. Organomet. Chem.* **1976**, *116*, C1-C2.

(2) (a) Jutzi, P.; Müller, C.; Stammler, A.; Stammler, H.-G. Synthesis, Crystal Structure, and Application of the Oxonium Acid $[H(OEt_2)_2][B(C_6F_5)_4]$ -. *Organometallics* **2000**, *19*, 1442–1444. (b) Chen, Q.-A.; Klare, H. F. T.; Oestreich, M. Brønsted Acid-Promoted Formation of Stabilized Silylium Ions for Catalytic Friedel-Crafts C–H Silylation. *J. Am. Chem. Soc.* **2016**, *138*, 7868–7871. (c) Wu, Q.; Irran, E.; Müller, R.; Kaupp, M.; Klare, H. F. T.; Oestreich, M. Characterization of hydrogen-substituted silylium ions in the condensed phase. *Science* **2019**, *365*, 168–172.

(3) Falk, A.; Bauer, J. O. Structural and Electronic Effects on Phosphine Chalcogenide Stabilized Silicon Centers in Four-Membered Heterocyclic Cations. *Inorg. Chem.* **2022**, *61*, 15576–15588.

(4) (a) Nava, M.; Reed, C. A. Triethylsilyl Perfluoro-Tetraphenylborate, $[Et_3Si^+][F_{20}\text{-}BPh_4^-]$, a widely used Non-Existent Compound. *Organometallics* **2011**, *30*, 4798–4800. (b) Connelly, S. J.; Kaminsky, W.; Heinekey, D. M. Structure and Solution Reactivity of (Triethylsilylium)triethylsilane Cations. *Organometallics* **2013**, *32*, 7478–7481.

(5) Fontana, N.; Espinosa-Jalapa, N. A.; Seidl, M.; Bauer, J. O. Hidden silylium-type reactivity of a siloxane-based phosphonium-hydroborate ion pair. *Chem. Commun.* **2022**, *58*, 2144–2147.

(6) (a) Kishino, M.; Takaoka, S.; Shibutani, Y.; Kusumoto, S.; Nozaki, K. Synthesis and reactivity of PC(sp^3)P-pincer iridium complexes bearing a diborylmethyl anion. *Dalton Trans.* **2022**, *51*, 5009–5015. (b) Szynkiewicz, N.; Chojnacki, J.; Grubba, R. Phosphinophosphoranes: Mixed-Valent Phosphorus Compounds with Ambiphilic Properties. *Inorg. Chem.* **2022**, *61*, 19925–19932.

(7) Pieper, M.; Auer, P.; Schwarzbich, S.; Kühn, F.; Neumann, B.; Stammler, H.-G.; Mitzel, N. W. Cationic, Methylene-Bridged, Intramolecular Donor-Acceptor Systems Based on Zirconium and Hafnium and Phosphino-methanides. *Z. Anorg. Allg. Chem.* **2017**, *643*, 909–915.

(8) (a) Samigullin, K.; Georg, I.; Bolte, M.; Lerner, H.-W.; Wagner, M. A Highly Reactive Geminal P/B Frustrated Lewis Pair: Expanding the Scope to C–X (X=Cl, Br) Bond Activation. *Chem. Eur. J.* **2016**, *22*, 3478–3484. (b) Kinder, T. A.; Pior, R.; Blomeyer, S.; Neumann, B.; Stammler, H.-G.; Mitzel, N. W. A Neutral Germanium/Phosphorus Frustrated Lewis Pair and Its Contrasting Reactivity Compared to Its Silicon Analogue. *Chem. Eur. J.* **2019**, *25*, 5899–5903. (c) Yang, Q.; Wang, L.; Li, Y.; Zhou, L.; Li, Z. A neutral germanium/phosphorus frustrated Lewis pair: Synthesis and reactivity. *J. Organomet. Chem.* **2021**, *954-955*, 122071. (d) Bertini, F.; Hoffmann, F.; Appelt, C.; Uhl, W.; Ehlers, A. W.; Slootweg, J. C.; Lammertsma, K. Reactivity of Dimeric P/Al-Based Lewis Pairs toward Carbon Dioxide and *tert* -Butyl Isocyanate. *Organometallics* **2013**, *32*, 6764–6769.

(9) Fink, L.; Samigullin, K.; Bodach, A.; Alig, E.; Wagner, M.; Lerner, H.-W. Donor-unsupported Phosphanylmethanides $Li[CH_2PR_2]$ (R = *t*Bu, Ph) – Crystal Structure of $Li[CH_2PtBu_2]$ Solved by XRPD and DFT-D Calculations. *Z. Anorg. Allg. Chem.* **2016**, *642*, 282–287.

(10) Espinosa-Jalapa, N. A.; Berg, N.; Seidl, M.; Shenderovich, I. G.; Gschwind, R. M.; Bauer, J. O. Complexation behavior of LiCl and $LiPF_6$ – Model studies in the solid-state and in solution using a bidentate picolyl-based ligand. *Chem. Commun.* **2020**, *56*, 13335–13338.

(11) Flynn, S. R.; Wass, D. F. Transition Metal Frustrated Lewis Pairs. *ACS Catal.* **2013**, *3*, 2574–2581.

(12) Klare, H. F. T.; Bergander, K.; Oestreich, M. Taming the silylium ion for low-temperature Diels-Alder reactions. *Angew. Chem. Int. Ed.* **2009**, *48*, 9077–9079.

(13) Denker, L.; Wullschläger, D.; Martínez, J. P.; Świerczewski, S.; Trzaskowski, B.; Tamm, M.; Frank, R. Cobalt(I)-Catalyzed Transformation of Si–H Bonds: H/D Exchange in Hydrosilanes and Hydrosilylation of Olefins. *ACS Catal.* **2023**, *13*, 2586–2600.

(14) Ma, W.; Liu, L.-C.; An, K.; He, T.; He, W. Rhodium-Catalyzed Synthesis of Chiral Monohydrosilanes by Intramolecular C-H Functionalization of Dihydrosilanes. *Angew. Chem. Int. Ed.* **2021**, *60*, 4245–4251.

(15) Grotjahn, S.; Müller, L.; Pattanaik, A.; Falk, A.; Barison, G.; Bauer, J. O.; Rehbein, J.; Gschwind, R. M.; Burkhard, K. Regio-, diastereo- and enantioselectivity in the photocatalytic generation of carbanions via hydrogen atom transfer and reductive radical-polar crossover. *Unpublished work* **2024**.

(16) Huber, T.; Espinosa-Jalapa, N. A.; Bauer, J. O. Access to Enantiomerically Pure *P*-Stereogenic Primary Aminophosphine Sulfides under Reductive Conditions. *Chem. Eur. J.* **2022**, *28*, e202202608.

(17) Fernandes A.; Laye, C.; Pramanik, S.; Palmeira, D.; Pekel, Ö. Ö.; Massip, S.; Schmidtmann, M.; Müller, T.; Robert, F.; Landais, Y. Chiral Memory in Silyl-Pyridinium and Quinolinium Cations. *J. Am. Chem. Soc.* **2020**, *1*, 564–572.

(18) Kümper, M.; Götz, T.; Espinosa-Jalapa, N. A.; Falk, A.; Rothfelder, R.; Bauer, J. O. Stereochemically Pure Si -Chiral Aminochlorosilanes. *Z. Anorg. Allg. Chem.* **2023**, *649*.

7.7 Synthesis and characterizations

7.7.1 General remarks

All experiments were performed in an inert atmosphere of purified nitrogen by using standard Schlenk techniques or an MBraun Unilab 1200/780 glovebox. Glassware was heated at 600 °C prior to use. Dichloromethane (DCM), hexane, pentane, tetrahydrofuran (THF), and toluene were dried and de-gassed with an MBraun SP800 solvent purification system. Diphenylchlorosilane (90%, Merck KGaA), trichlorosilane(99%, Merck KGaA), *n*-Butyllithium (2.5 M in hexane, Merck KGaA), methyl(phenyl)dichlorosilane (97%, Merck KGaA), di-*iso*-propyl(chloro)silane (97%, Merck KGaA), dicobaltoctacarbonyl (moistened with hexane (hexane 1-10%), ≥90% (Co), Merck KGaA), 3,5-diphenylbromobenzene (95%, Abcr GmbH) were used as received without further purification. Di-*tert*-butyl((di-*tert*-butylsilyl)methyl)phosphine sulfide[1], butylsilyl)methyl)phosphine oxide[1], di-*tert*-butyl(methyl)phosphine sulfide[2], di-*tert*-butyl(methyl)phosphaneyl lithium[3], (*tert*-butyl)phenyldichlorosilane[4] and $H(OEt_2)_2B(C_6F_5)_4$[5] were synthesized according to reported literature procedures. C_6D_6 and CD_2Cl_2 used for NMR spectroscopy were dried over 3 Å molecular sieves and degassed by a standard freeze-pump-thaw procedure. NMR spectra were either recorded on a Bruker Avance 300 (300.13 MHz), a Bruker Avance 400 (400.13 MHz) or on a Bruker Avance III HD 400 (400.13 MHz) at 25 °C. Chemical shifts (*δ*) are reported in parts per million (ppm). ^{1}H and $^{13}C\{^{1}H\}$ NMR spectra are referenced to tetramethylsilane ($SiMe_4$, δ = 0.0 ppm) as external standard, with the deuterium signal of the solvent serving as internal lock and the residual solvent signal as an additional reference. $^{19}F\{^{1}H\}$, $^{31}P\{^{1}H\}$, $^{11}B\{^{1}H\}$ and $^{29}Si\{^{1}H\}$ NMR spectra are referenced to $CFCl_3$, 85% H_3PO_4, $BF_3{\cdot}OEt_2$ and $SiMe_4$, respectively. For the assignment of the multiplicities, the following abbreviations are used: s = singlet, bs = broad singlet, d = doublet, t = triplet, bq = broad quartet, m = multiplet. For simplicity, multiplets of order higher than one are described by approximating them to the closest first order type. High resolution mass spectrometry was carried out on a Jeol AccuTOF GCX and an Agilent Q-TOF 6540 UHD spectrometer. Elemental analyses were performed on a Vario MICRO cube apparatus.

7.7.2 Synthesis of compound 1

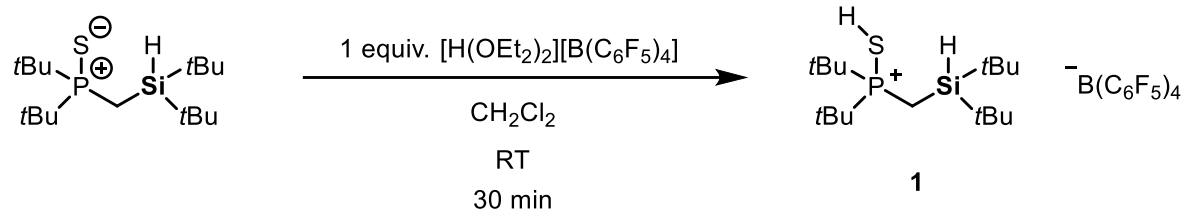

Di-*tert*-butyl((di-*tert*-butylsilyl)methyl)phosphine sulfide[1] (202 mg, 0.60 mmol, 1.0 equiv) and $[H(OEt_2)_2][B(C_6F_5)_4]$[5] (500 mg, 0.60 mmol, 1.0 equiv) were dissolved in dichloromethane (4 mL) and the resulting solution was stirred for 30 min at room temperature. All volatiles were removed *in vacuo* and the solid further dried. Then the white powder was washed twice with 2 mL of hexane. Subsequently the dry white powder was dissolved in 1 mL of DCM and layered with 3 mL of hexane. Compound **1** was obtained as fine colorless needles suitable for single crystal X-Ray crystallography. Yield: 585 mg (0.58 mmol, 95 %).

^{1}H NMR (400.13 MHz, CD_2Cl_2, 298 K): δ 3.90 (m, 1H, Si*H*), 2.42 (bs, 1H, S*H*), 1.55 (dd, $^{2}J_{P-H}$ = 14.4 Hz, $^{3}J_{H-H}$ = 2.0 Hz, 2H, PCH_2Si), 1.53 {d, $^{3}J_{P-H}$ = 17.8 Hz, 18H, P[C(CH_3)$_3$]$_2$}, 1.15 {s, 18H, Si[C(CH_3)$_3$]$_2$}.

^{13}C{^{1}H} NMR (100.61 MHz, CD_2Cl_2, 298 K): δ 148.6 (d, $^{1}J_{C-F}$ = 240.4 Hz, *C*F$_{Ar}$), 138.7 (d, $^{1}J_{C-F}$ = 245.1 Hz, *C*F$_{Ar}$), 136.7 (d, $^{1}J_{C-F}$ = 244.8 Hz, *C*F$_{Ar}$), 124.0 (bs, *C*$_{ipso}$), 40.7 [d, $^{1}J_{P-C}$ = 29.3 Hz, P*C*(CH$_3$)$_3$], 29.3 {s, Si[C(*C*H$_3$)$_3$]$_2$}, 27.4 {s, P[C(*C*H$_3$)$_3$]$_2$}, 20.0 {d, $^{3}J_{P-C}$ = 2.4 Hz, Si[*C*(CH$_3$)$_3$]$_2$}, –1.9 (d, $^{1}J_{P-C}$ = 27.1 Hz, P*C*H$_2$Si).

^{31}P{^{1}H} NMR (162.04 MHz, CD_2Cl_2, 298 K): δ 89.3 (P(S)H).

^{19}F{^{1}H} NMR (376.66 MHz, CD_2Cl_2, 298 K): δ –132.9 (m, 8F, C*F*$_{Ar}$), –163.5 (m, 4F, C*F*$_{Ar}$), –167.3 (m, 8F, C*F*$_{Ar}$).

^{11}B{^{1}H} NMR (128.43 MHz, CD_2Cl_2, 298 K): δ –16.9 (s, *B*$_{Ar^F}$).

^{29}Si{^{1}H} NMR (79.49 MHz, CD_2Cl_2, 298 K): δ 6.6 (d, $^{2}J_{P-Si}$ = 11.9 Hz, PCH$_2$*Si*).

CHN Analysis: Calcd for $C_{41}H_{40}BF_{20}PSSi$: C, 48.5; H, 3.97. Found: C, 48.45; H, 3.97.

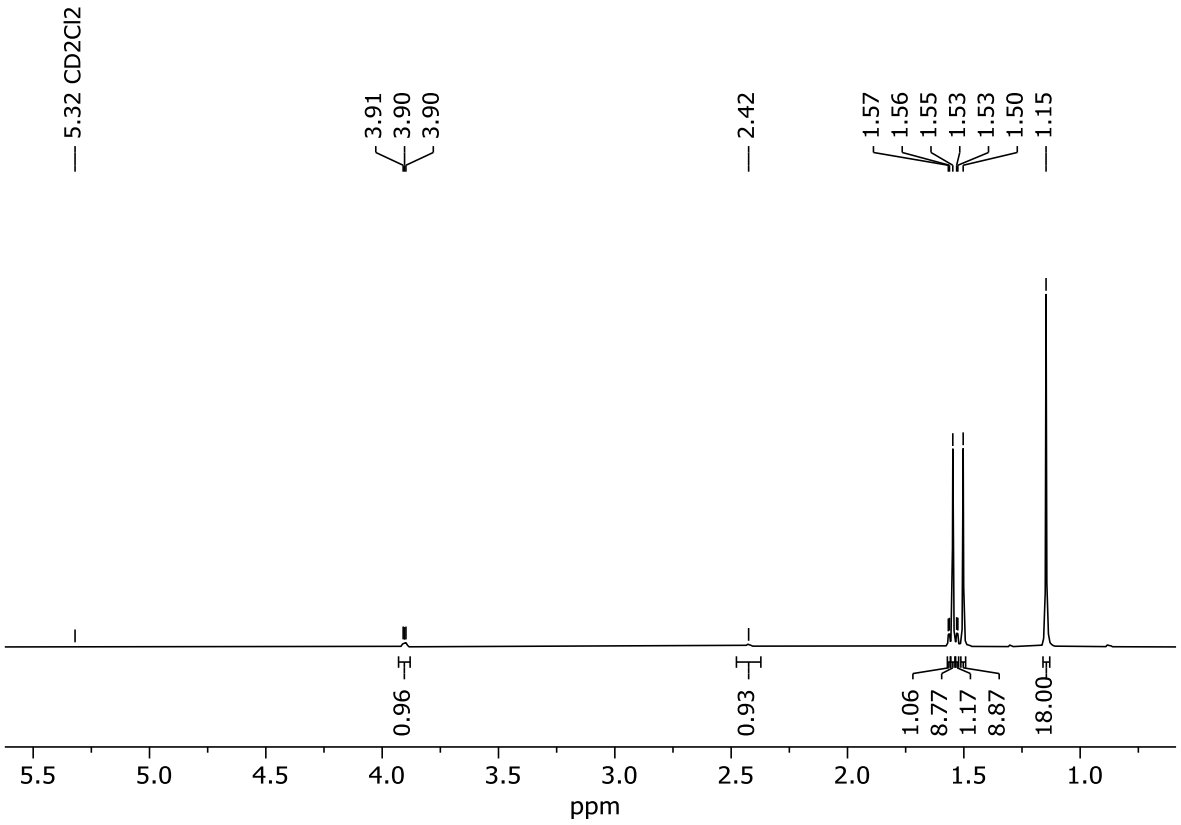

Scheme S1: ^{1}H NMR (400.13 MHz, CD_2Cl_2, 298 K) of compound **1**.

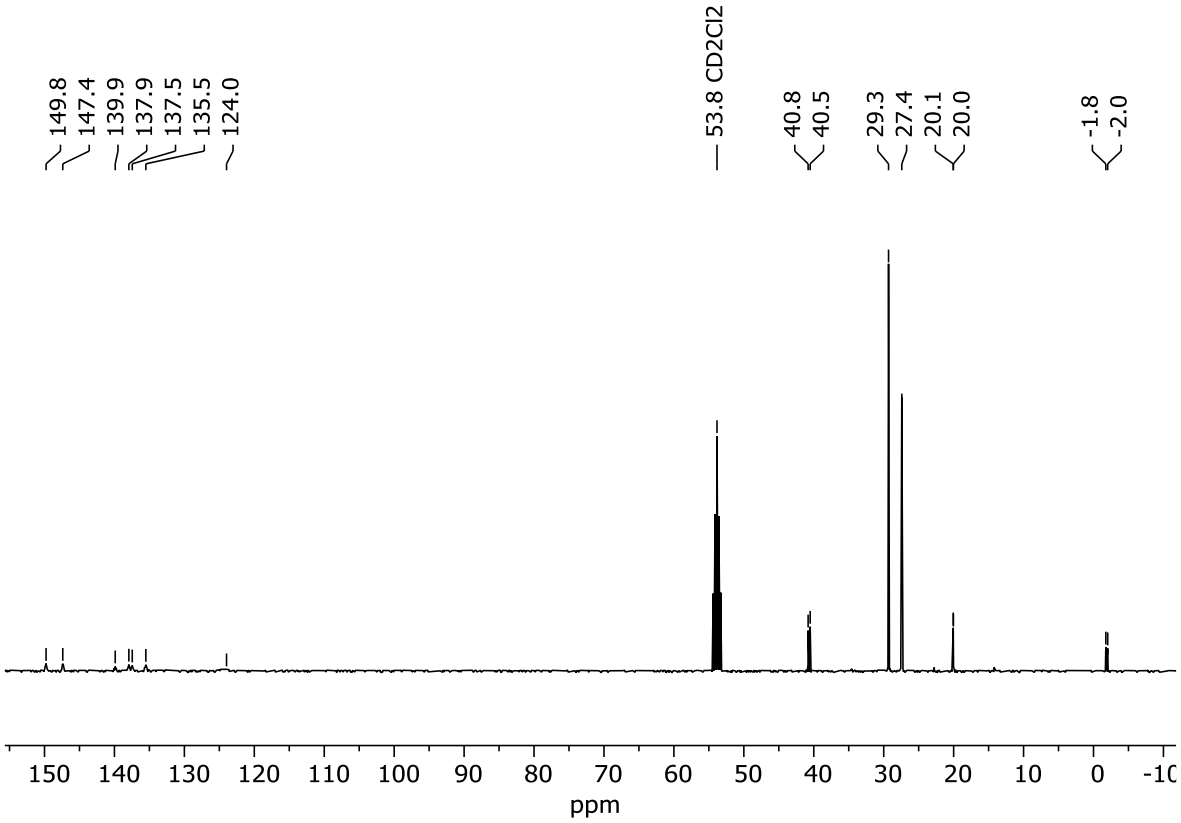

Scheme S2: $^{13}C\{^{1}H\}$ NMR (100.61 MHz, CD_2Cl_2, 298 K) of compound **1**.

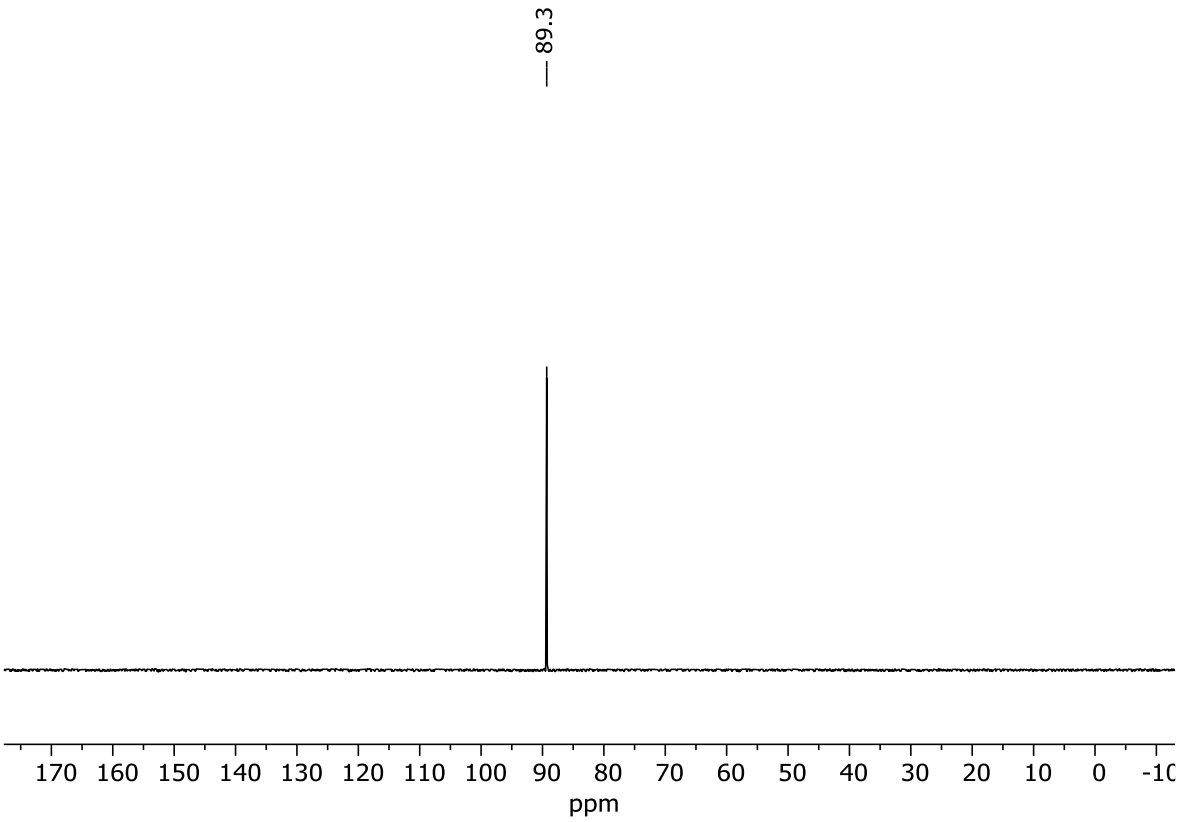

Scheme S3: $^{31}P\{^{1}H\}$ NMR (162.04 MHz, CD_2Cl_2, 298 K) of compound **1**.

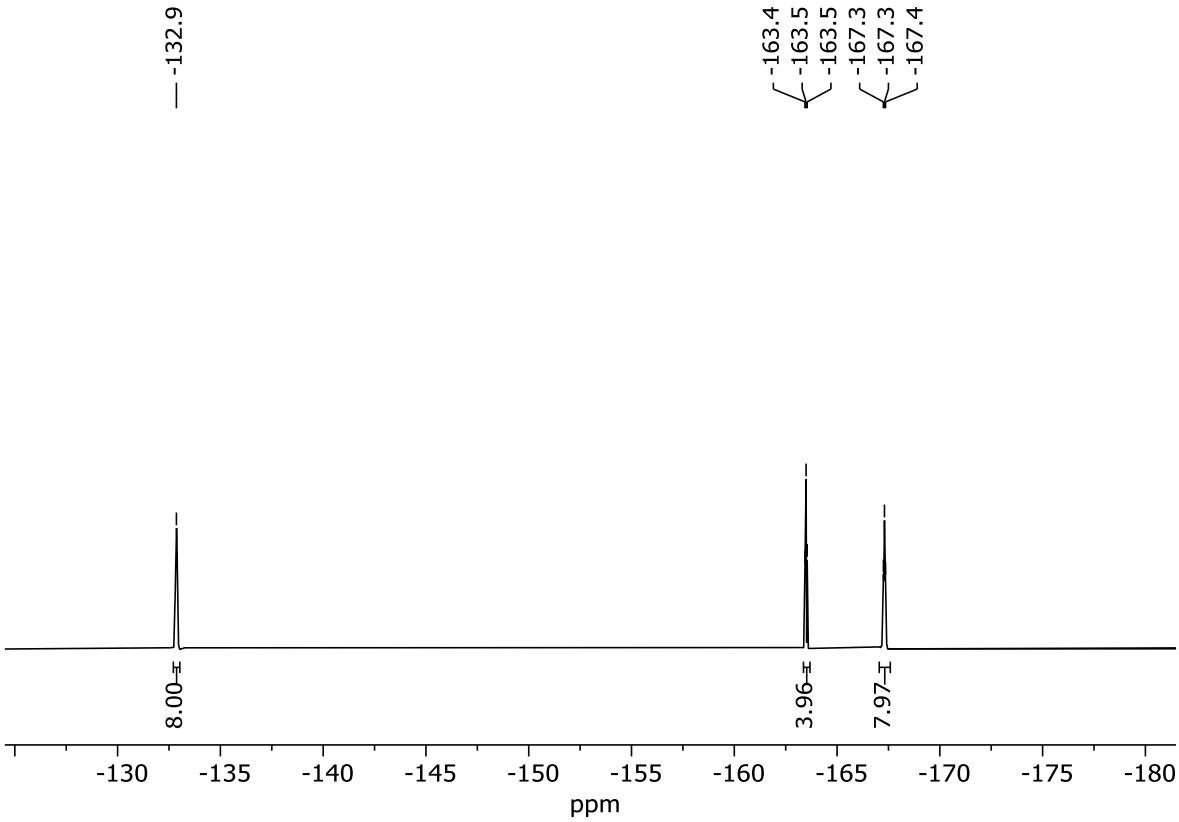

Scheme S4: $^{19}F\{^{1}H\}$ NMR (376.66 MHz, CD_2Cl_2, 298 K) of compound **1**.

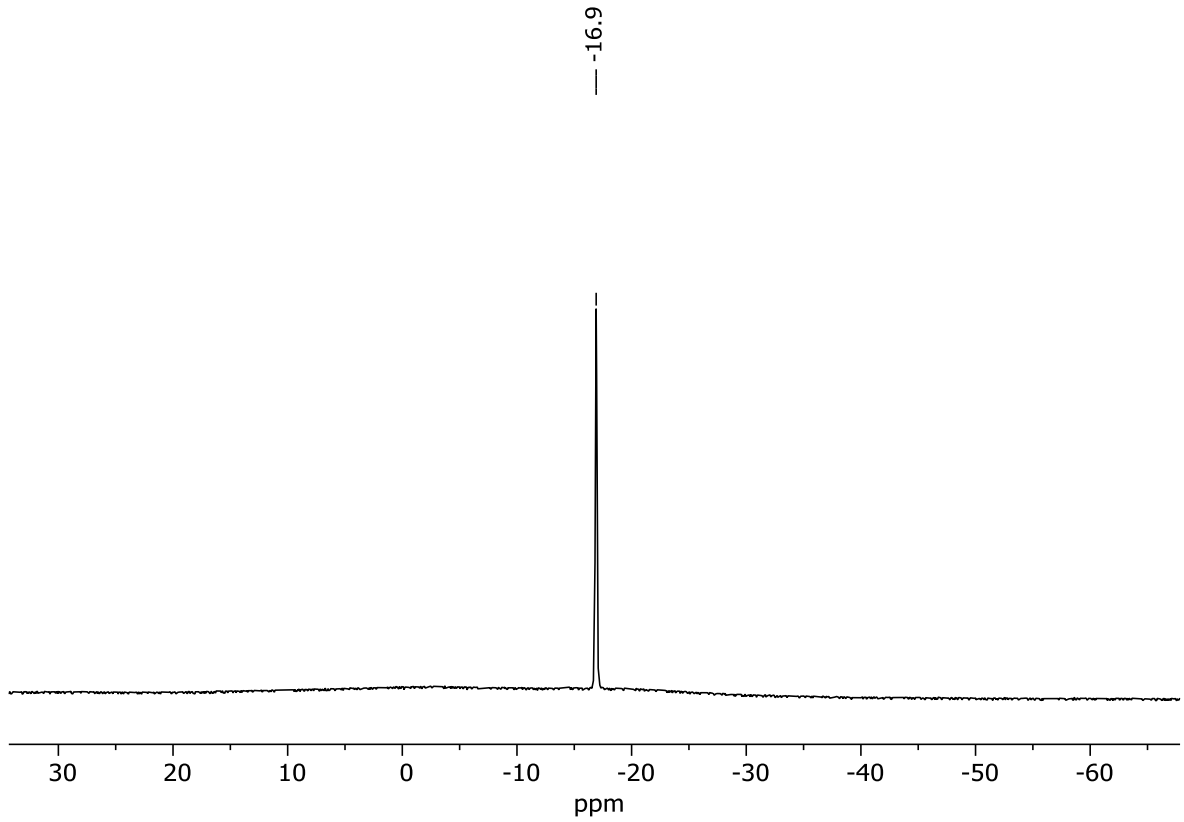

Scheme S5: $^{11}B\{^{1}H\}$ NMR (128.43 MHz, CD_2Cl_2, 298 K) of compound **1**.

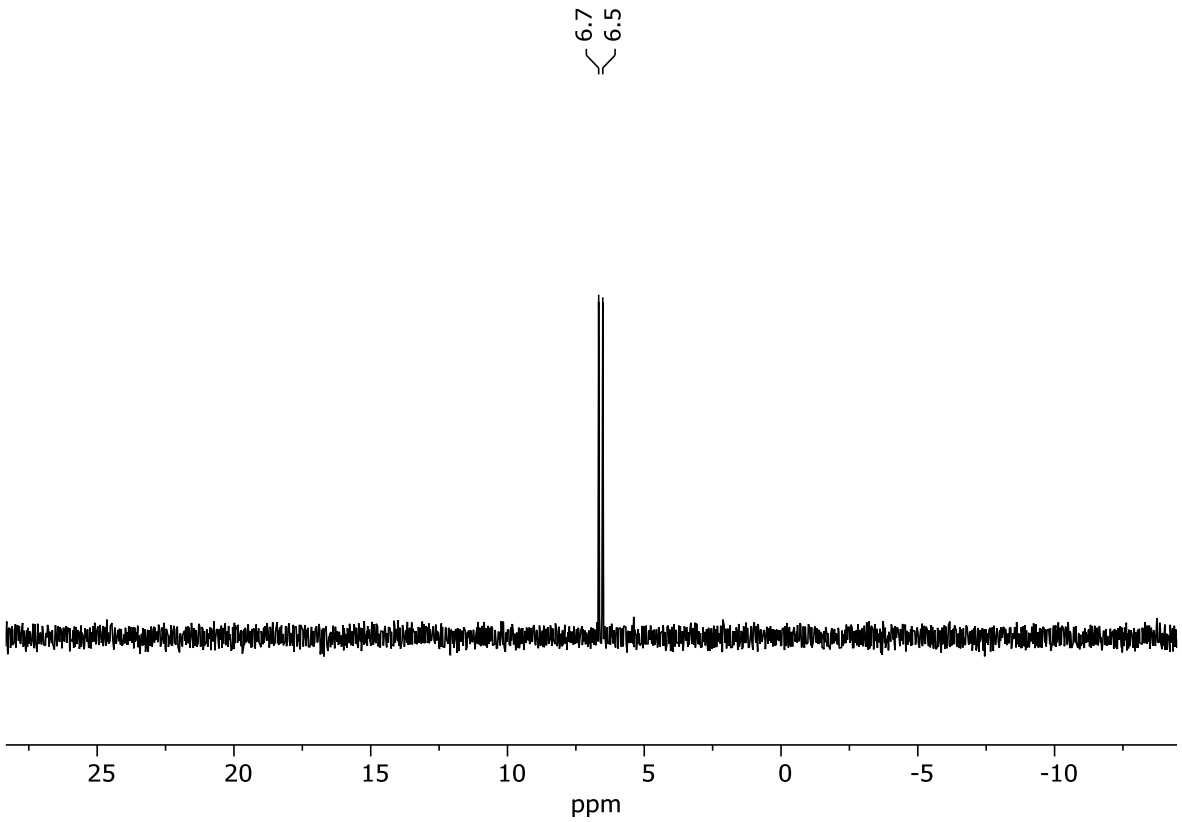

Scheme S6: $^{29}Si\{^{1}H\}$ NMR (79.49 MHz, CD_2Cl_2, 298 K) of compound **1**.

7.7.3 Synthesis of compound 2

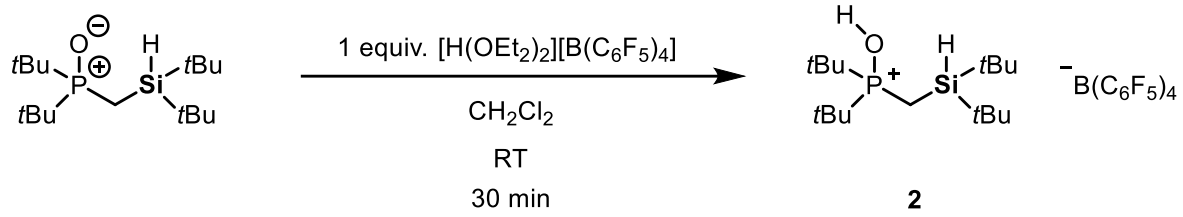

In a dry Schlenk flask di-*tert*-butyl((di-*tert*-butylsilyl)methyl)phosphine oxide[1] (100 mg, 0.313 mmol, 1 equiv) was combined with $[H(OEt_2)_2][B(C_6F_5)_4]$[5] (260 mg, 0.313 mmol, 1 equiv). Next 3 mL of DCM were added, and the mixture stirred for 30 min at room temperature. Afterwards all insoluble material was removed via cannula filtration. All volatiles of the filtrate were removed *in vacuo*. Compound **2** was obtained as a white powder. Yield: 214 mg (0.214 mmol, 68%).

^{1}H NMR (400.13 MHz, CD_2Cl_2, 298 K): δ 10.16 (bs, 1H, P(O)*H*), 3.87–3.85 (m, 1H, Si*H*), 1.43 [d, $^{3}J_{P-H}$ = 15.8 Hz, 20H, PC(C*H*$_3$)$_3$ + PC*H*$_2$Si], 1.11 [s, 18H, SiC(C*H*$_3$)$_3$].

^{13}C{^{1}H} NMR (100.61 MHz, CD_2Cl_2, 298 K): δ 148.6 (d, $^{1}J_{C-F}$ = 239.1 Hz, *C*F$_{borate}$), 138.7 (d, $^{1}J_{C-F}$ = 245.4 Hz, *C*F$_{borate}$), 136.7 (d, $^{1}J_{C-F}$ = 242.5 Hz, *C*F$_{borate}$), 37.5 [d, $^{1}J_{P-C}$ = 50.2 Hz, P*C*(CH$_3$)$_3$], 28.9 [s, PC(*C*H$_3$)$_3$], 26.7 [s, SiC(*C*H$_3$)$_3$], 19.7 [d, $^{3}J_{P-C}$ = 2.2 Hz, Si*C*(CH$_3$)$_3$], –0.6 (d, $^{1}J_{P-C}$ = 52.7 Hz, P*C*H$_2$Si).

^{31}P{^{1}H} NMR (162.04 MHz, CD_2Cl_2, 298 K): δ 100.0 (*P*(O)H).

^{19}F{^{1}H} NMR (376.66 MHz, CD_2Cl_2, 298 K): δ –132.9 (m, 8F, C*F*$_{Ar}$), –163.6 (m, 4F, C*F*$_{Ar}$), –167.4 (m, 8F, C*F*$_{Ar}$).

^{11}B{^{1}H} NMR (128.43 MHz, CD_2Cl_2, 298 K): δ –16.9 (s, *B*$_{Ar}^{F}$).

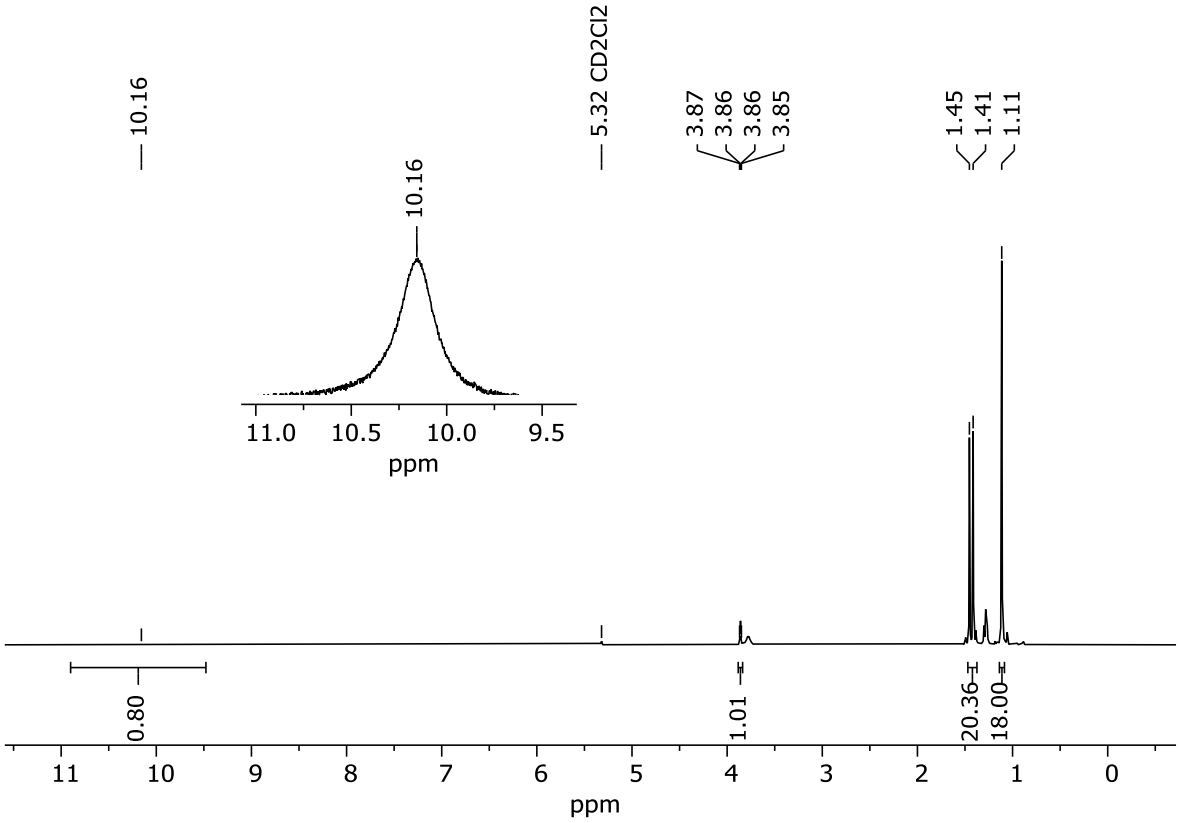

Scheme S7: ^{1}H NMR (400.13 MHz, CD_2Cl_2, 298 K) of compound **2**.

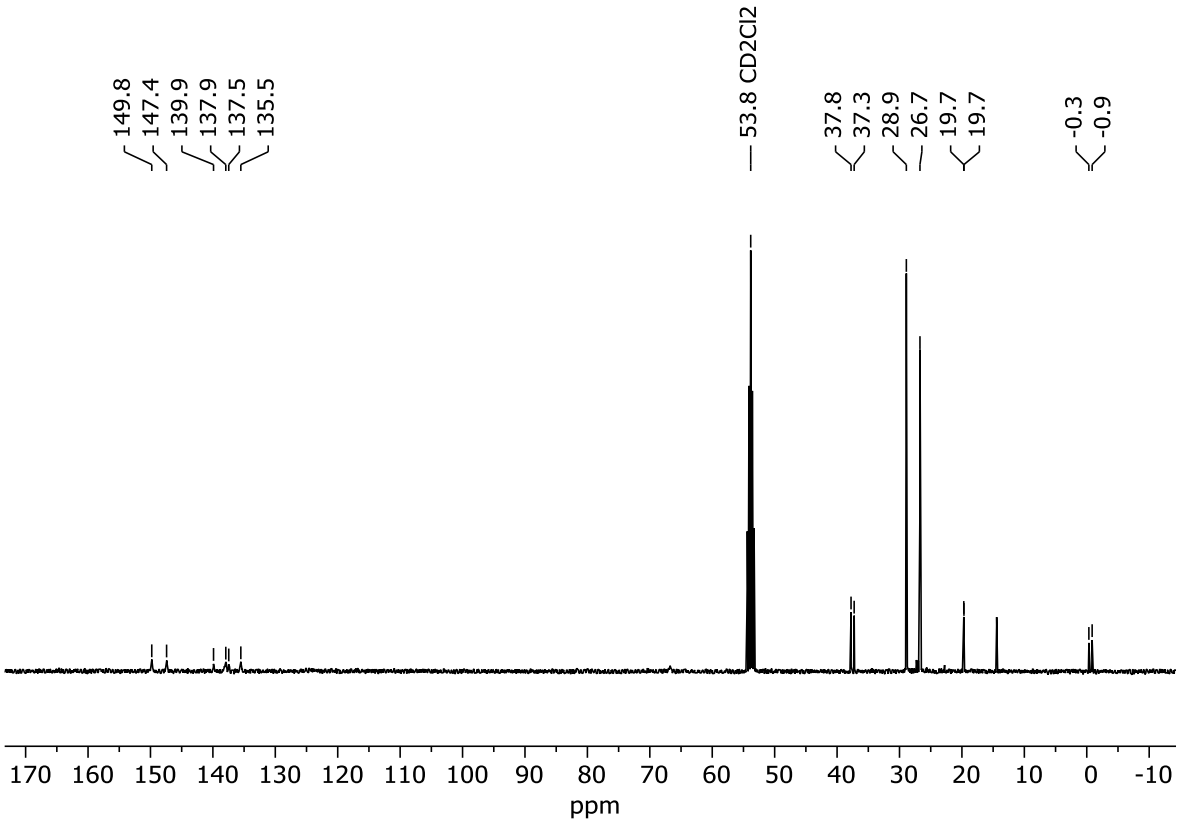

Scheme S8: $^{13}C\{^{1}H\}$ NMR (100.61 MHz, CD_2Cl_2, 298 K) of compound **2**.

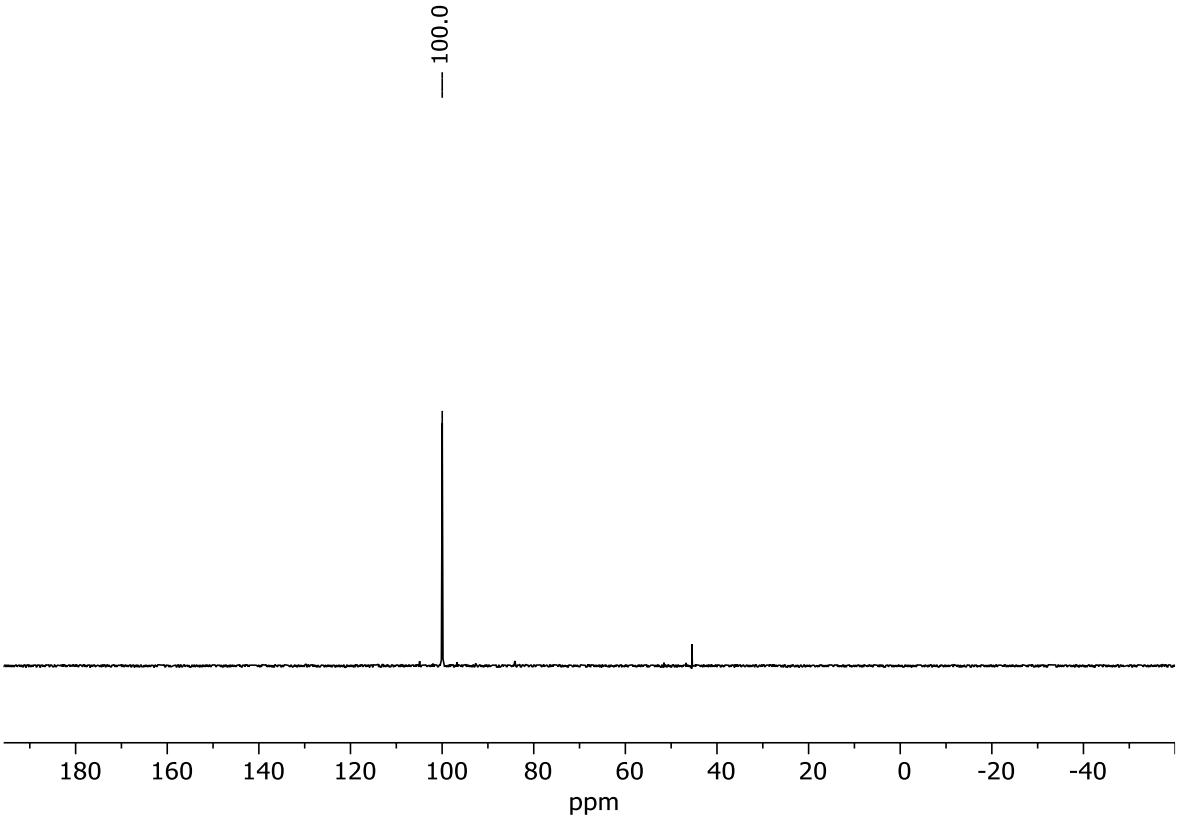

Scheme S9: $^{31}P\{^{1}H\}$ NMR (162.04 MHz, CD_2Cl_2, 298 K) of compound **2**.

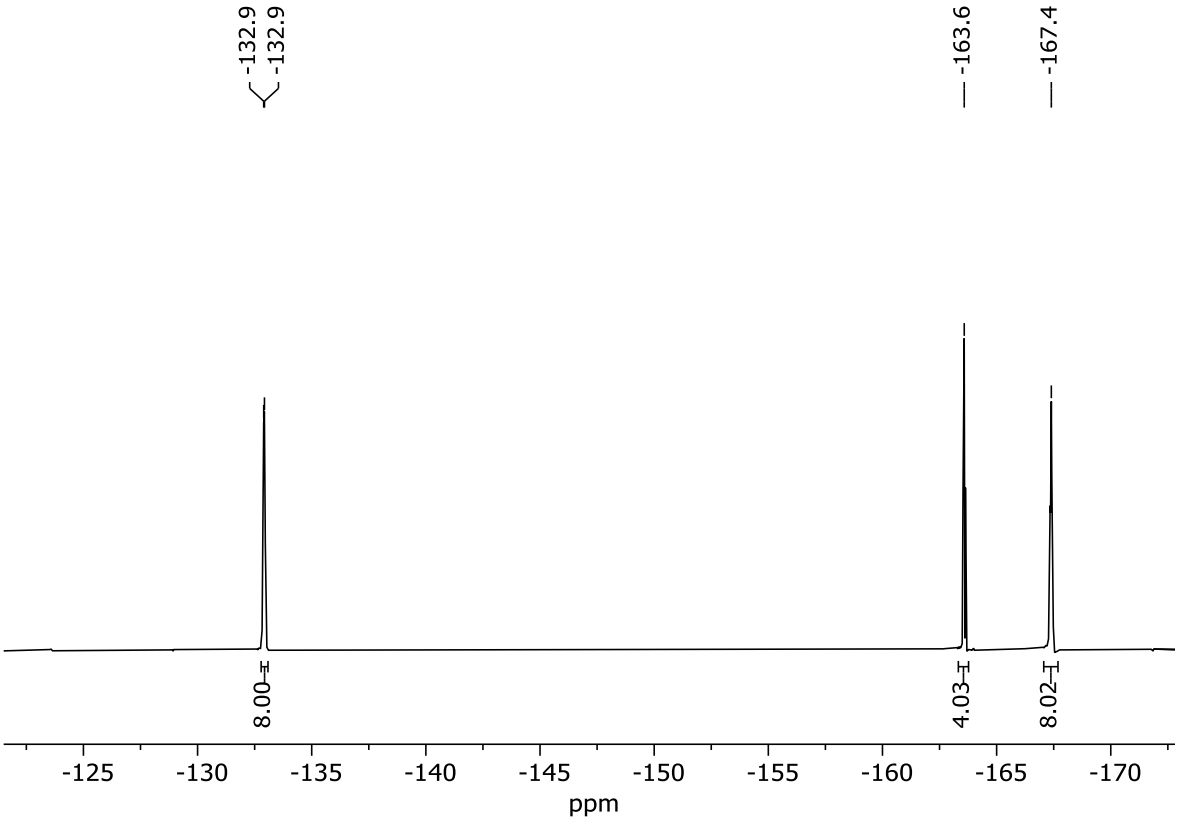

Scheme S10: $^{19}F\{^{1}H\}$ NMR (376.66 MHz, CD_2Cl_2, 298 K) of compound **2**.

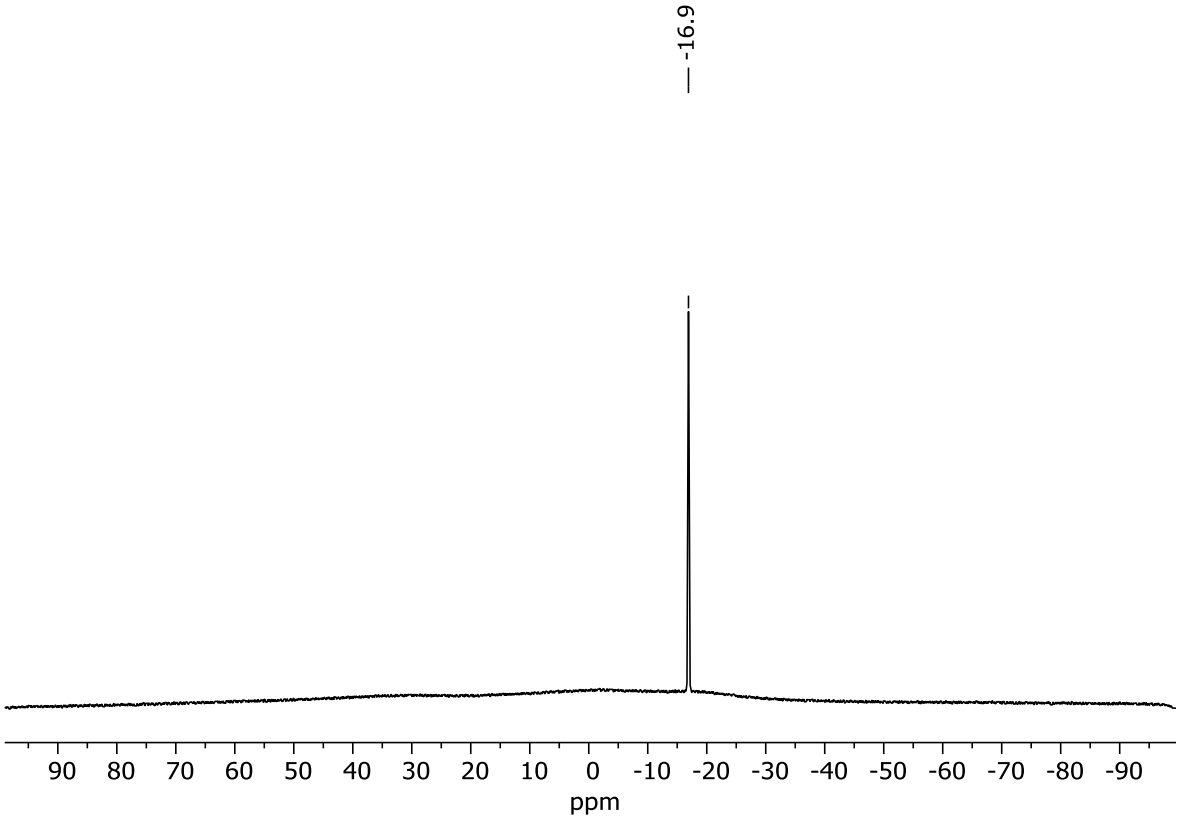

Scheme S11: $^{11}B\{^{1}H\}$ NMR (128.43 MHz, CD_2Cl_2, 298 K) of compound **2**.

7.7.4 Synthesis of compound 7

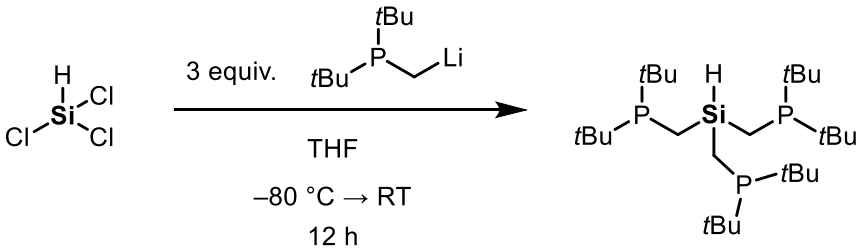

7

Trichlorosilane (0.877 mg, 6.48 mmol, 1 equiv) was diluted in 50 mL of THF and cooled to –80°C. In a separate Schlenk flash ((di-*tert*-butylphosphaneyl)methyl)lithium[3] (3.39 g, 20.41 mmol, 3.15 equiv) was dissolved in 20 mL of THF and added to the flask containing the trichlorosilane solution. The reaction mixture was left to warm up to room temperature and then stirred for 12 h. All volatiles were removed *in vacuo* and the white residue extracted with 10 mL of hot hexane. The solution was transferred to a Kugelrohr distillation apparatus and purified by fractional distillation (160°C oven temperature, 1.6 x 10^{-3} mbar). Compound **7** was obtained as a white polycrystalline solid. Yield: 1.53 g (3.02 mmol, 46%).

^{1}H NMR (400.13 MHz, C_6D_6, 298 K): δ 4.52–4.49 (m, 1H, Si*H*), 1.18 [d, $^{3}J_{P–H}$ = 10.8 Hz, 54H, PC(C*H*$_3$)$_3$], 0.96–0.94 (m, 6H, PC*H*$_2$Si).

^{31}P NMR (162.04 MHz, C_6D_6, 298 K): δ 19.4 (m, *P*CH_2Si).

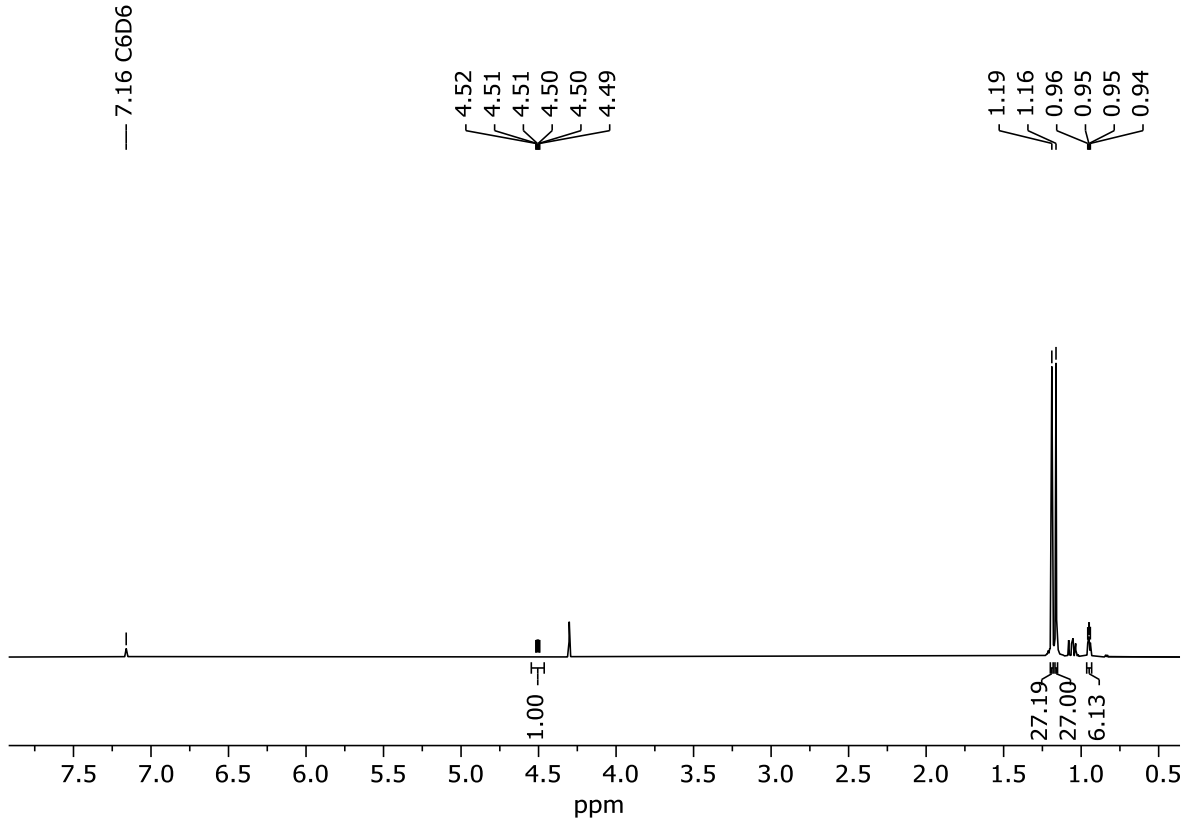

Scheme S12: ^{1}H NMR (400.13 MHz, C_6D_6, 298 K) of compound **7**.

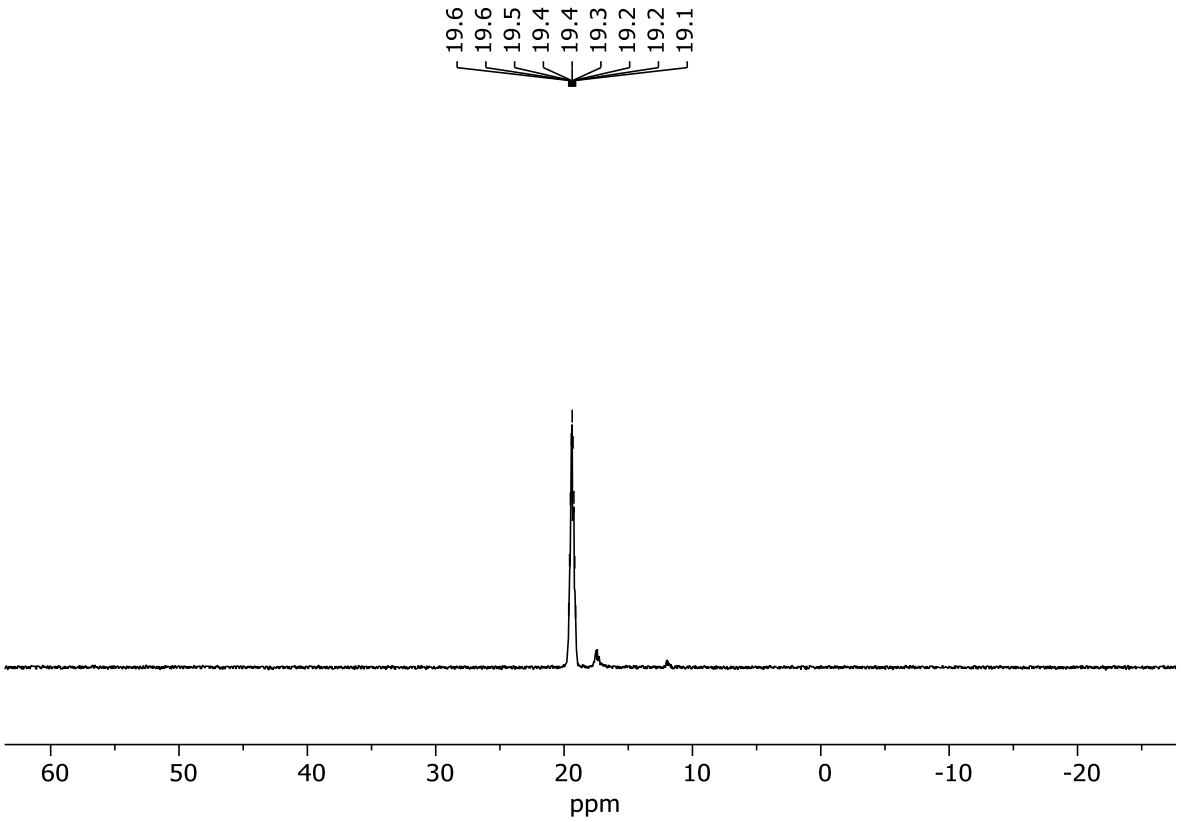

Scheme S13: ^{31}P NMR (162.04 MHz, C_6D_6, 298 K) of compound **7**.

7.7.5 Synthesis of compound 8

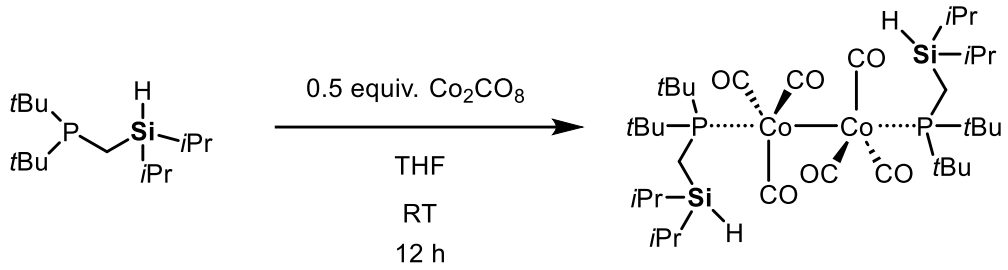

8

First octacarbonyldicobalt (629 mg, 1.84 mmol, 1 equiv) was dissolved in 10 mL of THF. Then di-*tert*-butyl((diisopropylsilyl)methyl)phosphane (1.01 g, 3.68 mmol, 2 equiv) was slowly added. Strong gas evolution was observed during addition. The reaction mixture was stirred for 12 h at room temperature, then all volatiles were removed *in vacuo*. The residue was suspended in 10 mL of hexane and filtered. The solid residue was resuspended in 10 mL hexane and filtered using a P3-Frit with added celite. This filtrate was left to crystallize at –30°C. The crystals were isolated by filtration and dried *in vacuo*. Compound **8** was obtained as red crystals suitable for single-crystal X-ray diffraction analysis. Yield: 650 mg (0.778 mmol, 42%).

^{1}H NMR (400.13 MHz, C_6D_6, 298 K): δ 4.39 (s, 2H, Si*H*), 1.50 [hept, $^{3}J_{H–H}$ = 7.6 Hz, 4H, SiC*H*$(CH_3)_2$], 1.25 [d, $^{3}J_{P–H}$ = 13.0 Hz, 36H, PC(C*H*$_3)_3$], 1.18–1.13 [m, 28H, SiCH(C*H*$_3)_2$ + PC*H*$_2$Si].

^{13}C{^{1}H} NMR (100.61 MHz, C_6D_6, 298 K): δ 206.0 (s, Co*C*O), 39.6 [d, $^{1}J_{P–C}$ = 14.6 Hz, P*C*$(CH_3)_3$], 30.1 [s, PC(*C*$H_3)_3$], 19.7 [s, SiCH(*C*$H_3)_2$], 18.9 [s, SiCH(*C*$H_3)_2$], 12.1 [s, Si*C*H$(CH_3)_2$], 5.9 (s, P*C*H_2Si).

^{31}P{^{1}H} NMR (162.04 MHz, C_6D_6, 298 K): δ 94.2 (Co*P*).

FD-MS: Calcd *m/z* for $C_{36}H_{70}Co_2O_6P_2Si_2$ $[M]^{+\bullet}$: 834.228447. Found: 834.28747 $[M]^{+\bullet}$.

CHN Analysis: Calcd for $C_{36}H_{70}Co_2O_6P_2Si_2$: C, 51.8; H, 8.46. Found: C, 52.14; H, 8.66.

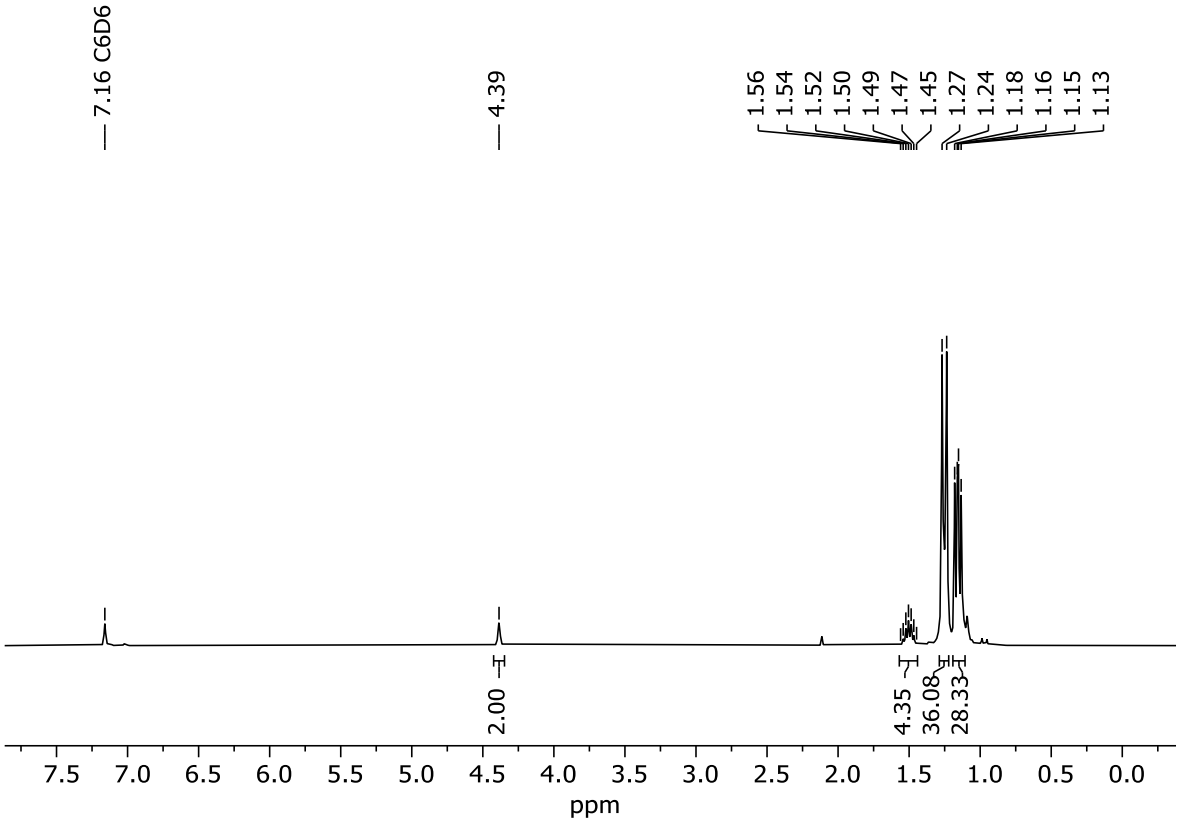

Scheme S14: ^{1}H NMR (400.13 MHz, C_6D_6, 298 K) of compound **8**.

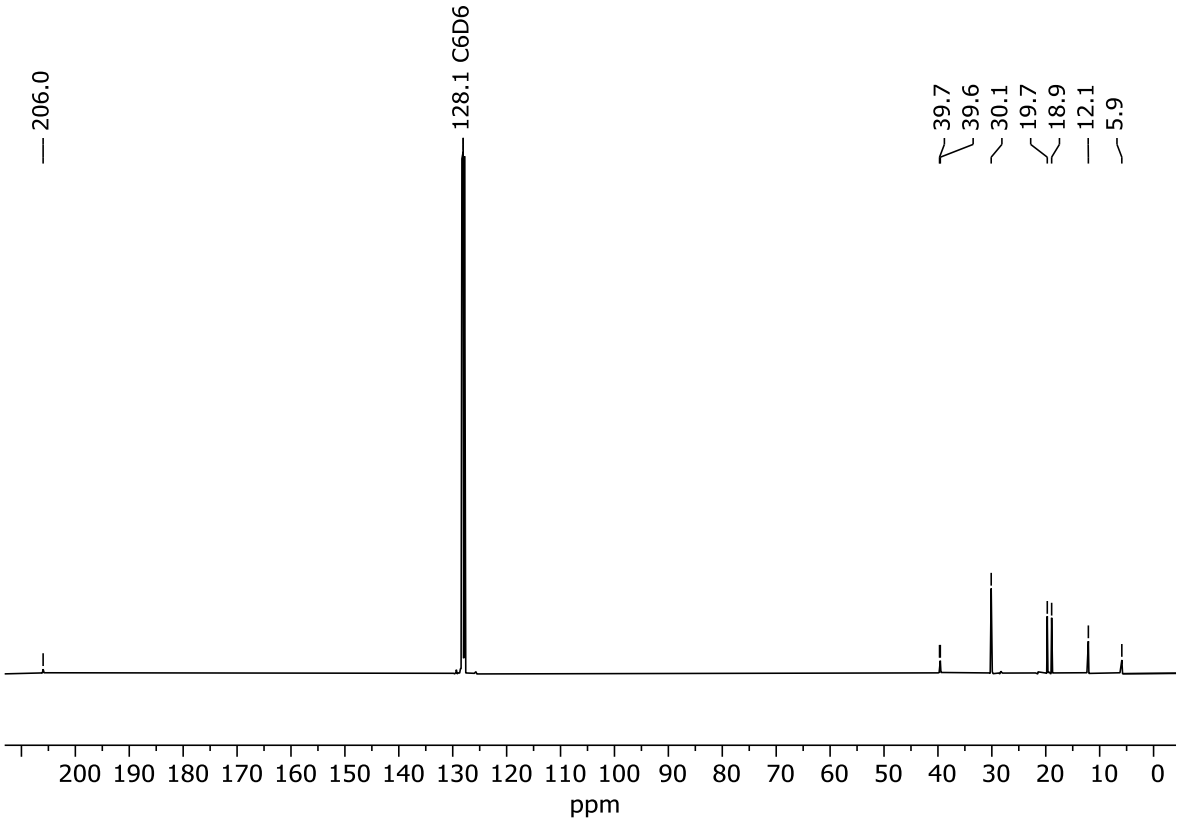

Scheme S15: $^{13}C\{^{1}H\}$ NMR (100.61 MHz, C_6D_6, 298 K) of compound **8**.

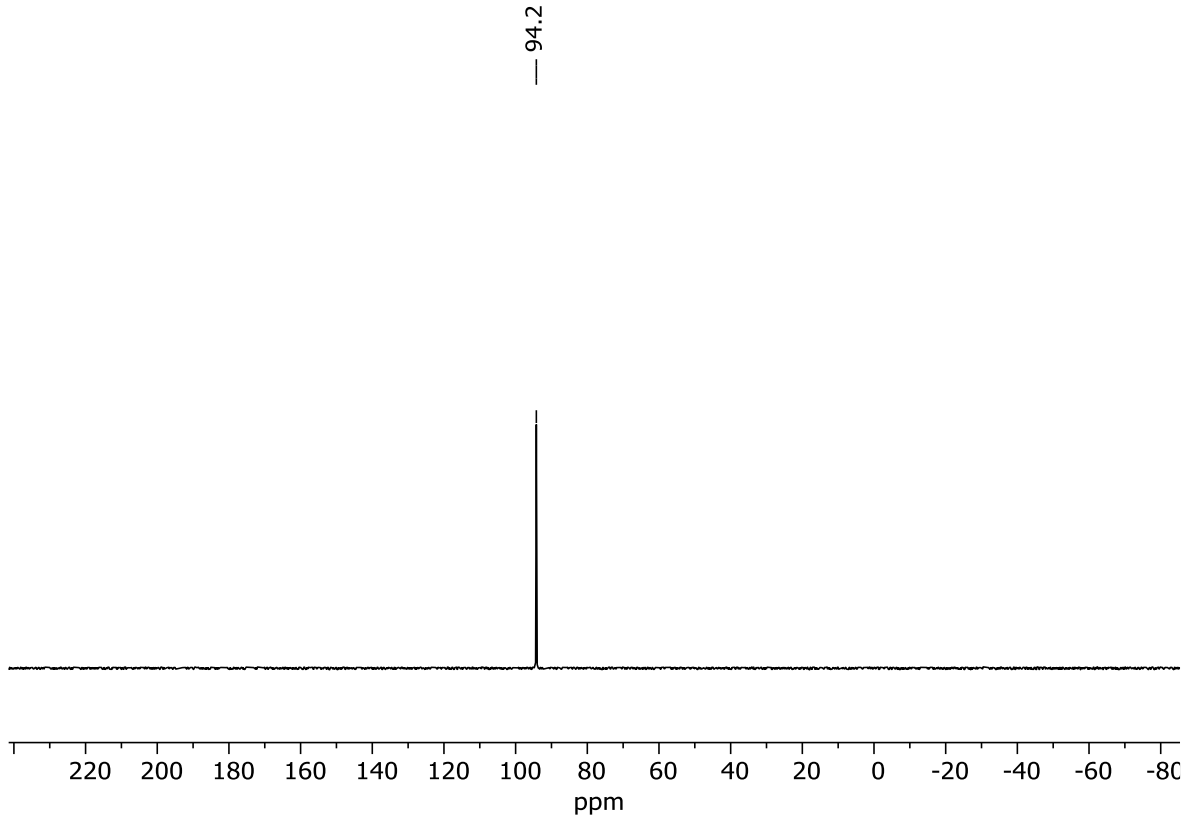

Scheme S16: $^{31}P\{^{1}H\}$ NMR (162.04 MHz, C_6D_6, 298 K) of compound **8**.

7.7.6 Compound 9

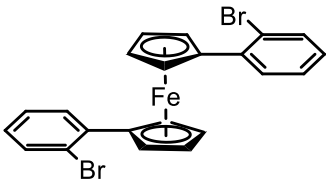

9

Compound **9** was obtained as a side-product within a literature synthesis.[6]

^{1}H NMR (400.13 MHz, C_6D_6, 298 K): δ 7.47–7.44 (m, 2H, C*H*$_{Ar}$), 7.39–7.36 (m, 2H, C*H*$_{Ar}$), 6.87–6.82 (m, 2H, C*H*$_{Ar}$), 6.66–6.60 (m, 2H, C*H*$_{Ar}$), 4.62–4.61 (m, 4H, C*H*$_{Cp}$), 4.04–4.03 (m, 4H, C*H*$_{Cp}$).

^{13}C{^{1}H} NMR (100.61 MHz, C_6D_6, 298 K): δ 138.7 (s, *C*Br$_{Ar}$), 134.0 (s, *C*H$_{Ar}$), 132.5 (s, *C*H$_{Ar}$), 127.6 (s, *C*H$_{Ar}$), 127.0 (s, *C*H$_{Ar}$), 122.9 (s, *C*$_{ipso}$), 87.2 (s, *C*$_{Cp}$), 72.1 (s, *C*H$_{Cp}$), 70.8 (s, *C*H$_{Cp}$).

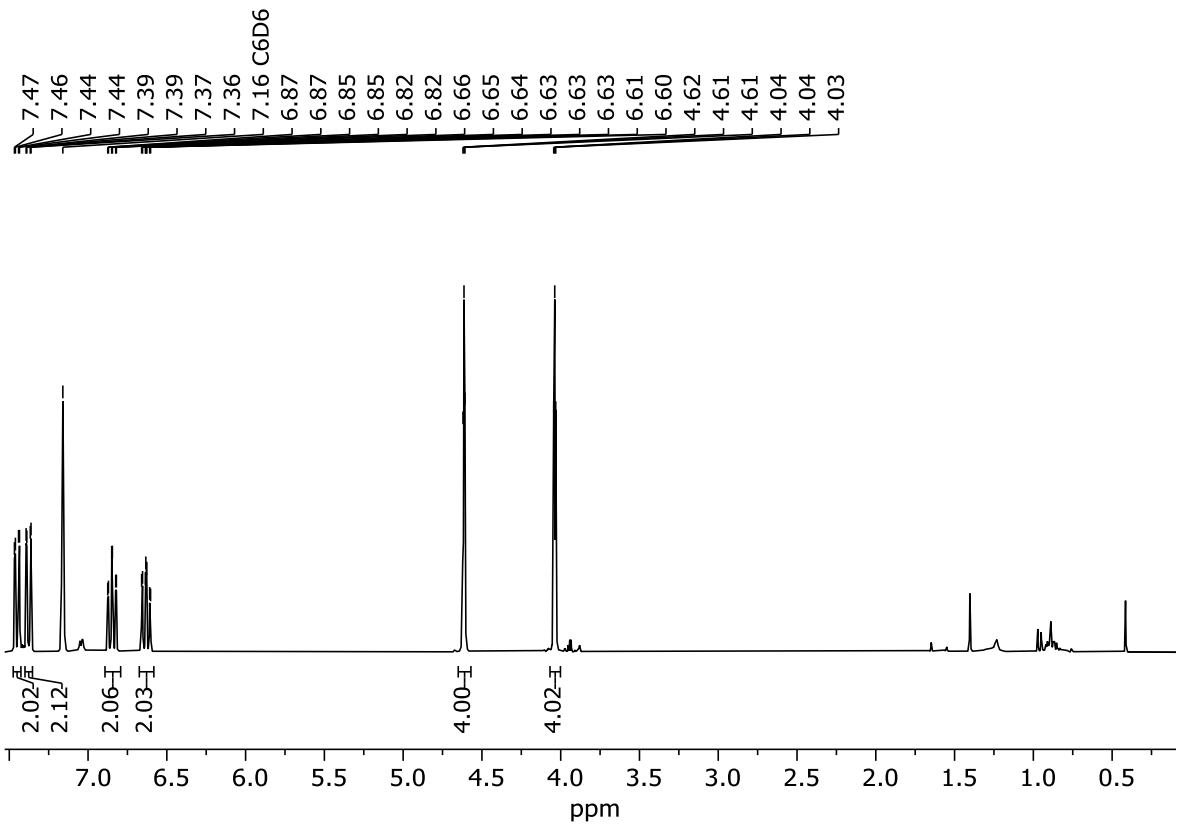

Scheme S17: ^{1}H NMR (400.13 MHz, C_6D_6, 298 K) of compound **9**.

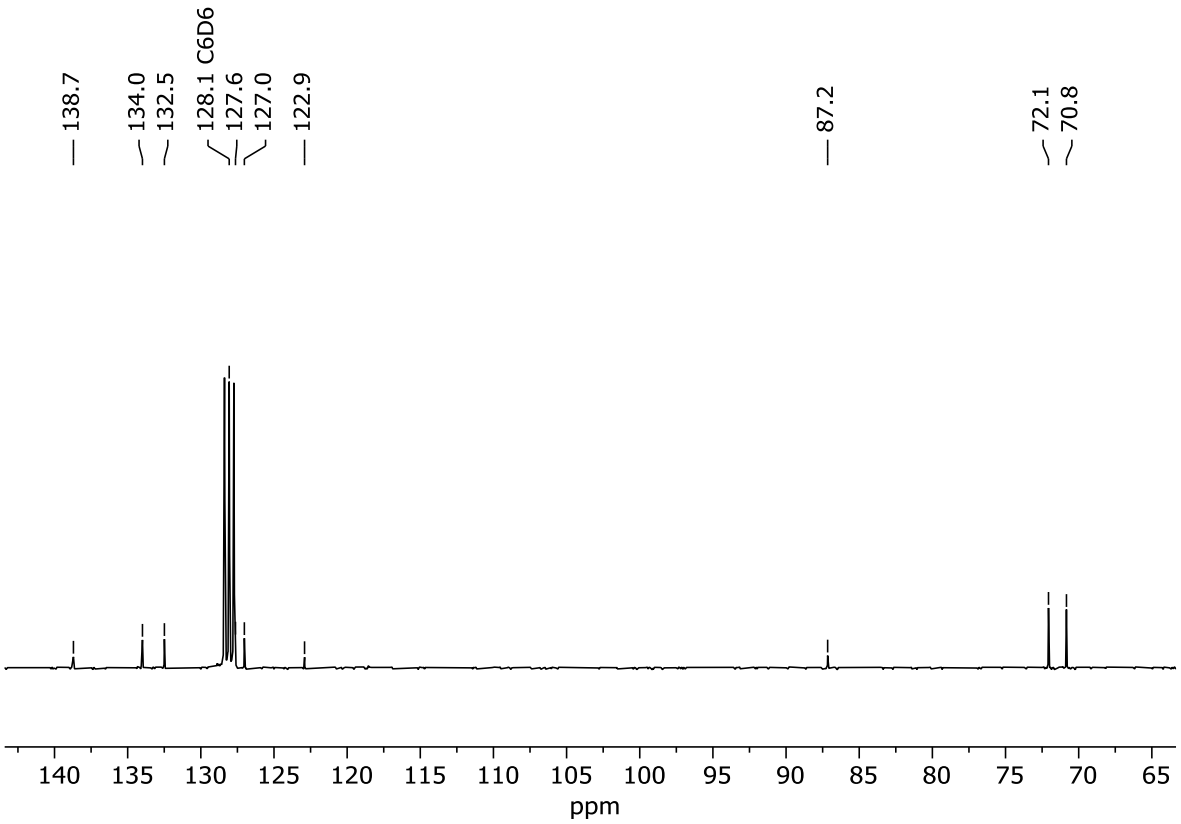

Scheme S18: $^{13}C\{^{1}H\}$ NMR (100.61 MHz, C_6D_6, 298 K) of compound **9**.

7.7.7 Synthesis of compound 10

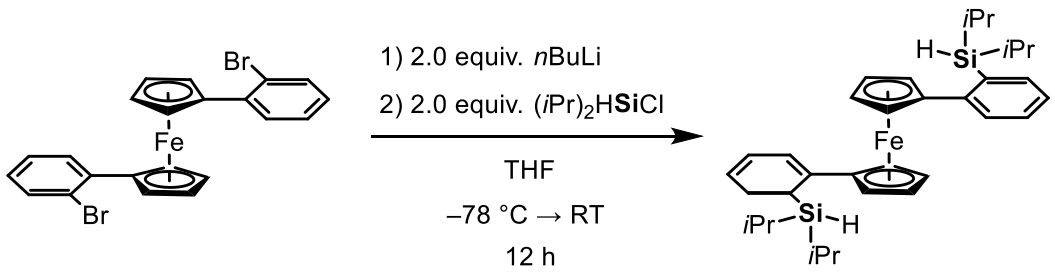

10

First compound **9** (1.07 g, 2.15 mmol, 1 equiv) was diluted in 10 mL of THF and cooled to –78°C. Next *n*-Butyllithium (1.72 mL of a 2.5 M solution in hexane, 4.30 mmol, 2 equiv) was added and the mixture stirred for 1 h in the cooling bath. Then di-*iso*-propyl(chloro)silane (648 mg, 4.30 mmol, 2 equiv) was added and the reaction mixture stirred for 12 h at room temperature. All volatiles were removed *in vacuo* and the residue suspended in pentane. The mixture was filtered using cannula filtration. The filtrate was crystallized at –80°C. Compound **10** was obtained as amorphous red crystals. Yield: 620 mg (1.09 mmol, 51%).

^{1}H NMR (400.13 MHz, C_6D_6, 298 K): δ 7.94–7.91 (m, 2H, C*H*$_{Ar}$), 7.47–7.44 (m, 2H, C*H*$_{Ar}$), 7.23–7.20 (m, 2H, C*H*$_{Ar}$), 7.13–7.07 (m, 2H, C*H*$_{Ar}$), 4.40–4.39 (m, 4H, C*H*$_{Cp}$), 4.26–4.23 (m, 2H, Si*H*), 4.10–4.09 (m, 4H, C*H*$_{Cp}$), 1.41–1.18 [m, 4H, SiC*H*$(CH_3)_2$], 1.04–1.02 [m, 12H, SiCH(C*H*$_3)_2$], 0.97–0.95 [m, 12H, SiCH(C*H*$_3)_2$].

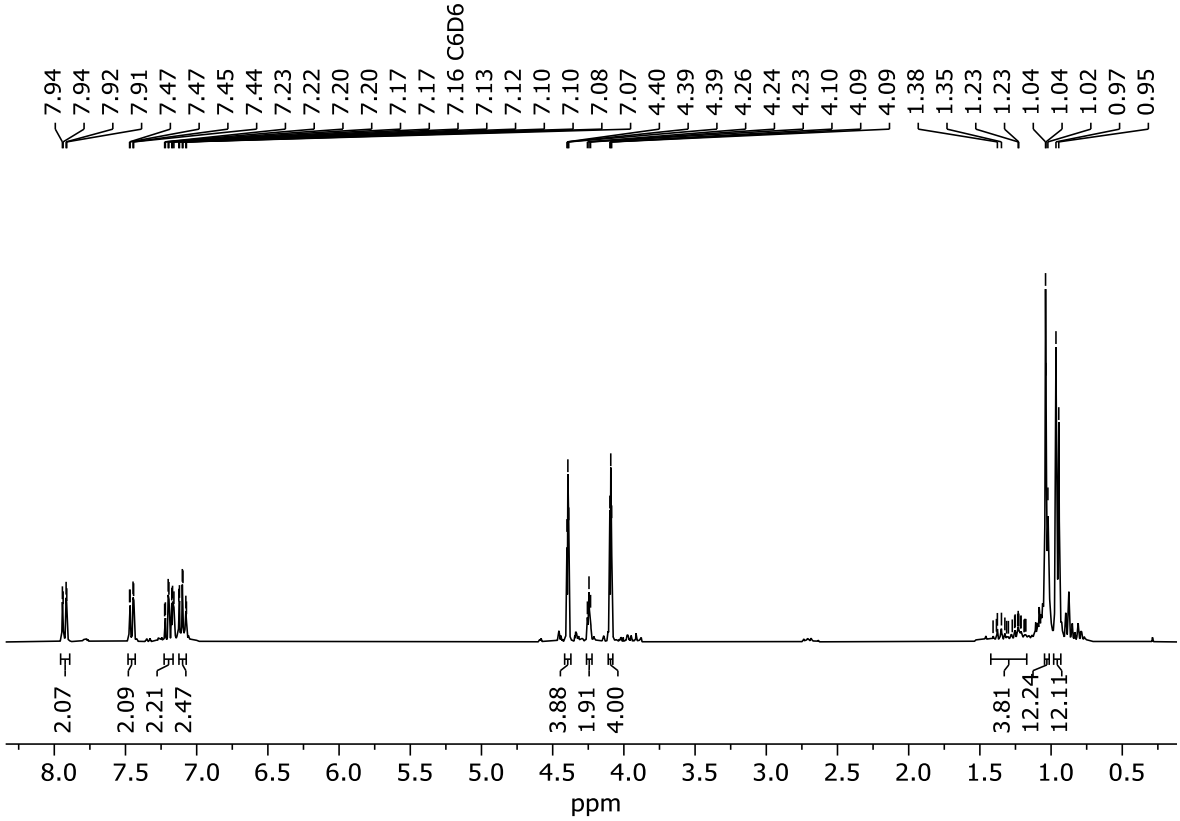

Scheme S19: ^{1}H NMR (400.13 MHz, C_6D_6, 298 K) of compound **10**.

7.7.8 Synthesis of compound 11

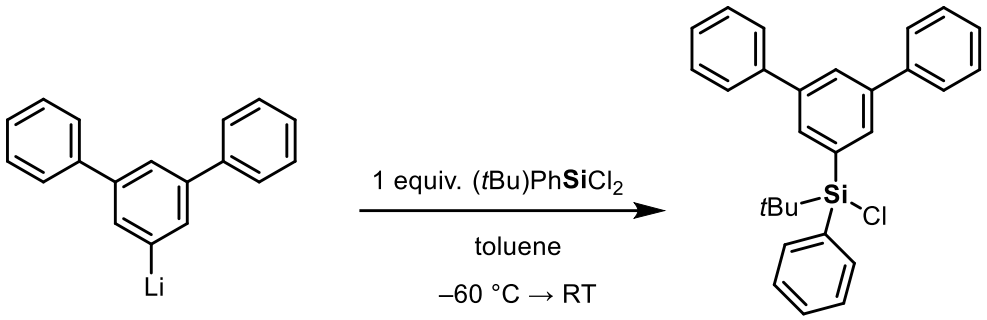

11

First freshly prepared (3,5-diphenyl)phenyllithium[7] (2.29 g, 9.70 mmol, 1 equiv) was suspended in 50 mL of toluene. The suspension was cooled to –60°C, and then *tert*-butyldichloro(phenyl)silane (2.26 g, 9.70 mmol, 1 equiv) was added. The reaction mixture was left to slowly warm up to room temperature and then stirred for 12 h. The crude suspension was purified using fractional Kugelrohr distillation (230°C oven temperature, 1 x 10^{-3} mbar). Compound **11** was obtained as a colorless oil. Yield: 1.33g (3.11 mmol, 32%).

^{1}H NMR (400.13 MHz, C_6D_6, 298 K): δ 8.28 (m, 2H, CH_{Ar}), 7.91–7.89 (m, 3H, CH_{Ar}), 7.56–7.54 (m, 4H, CH_{Ar}), 7.24–7.20 (m, 4H, CH_{Ar}), 7.17 (m, 1H, CH_{Ph}), 7.16–7.14 (m, 4H, CH_{Ph}), 1.21 [s, 9H, SiC(CH_3)$_3$].

^{13}C{^{1}H} NMR (100.61 MHz, C_6D_6, 298 K): δ 142.2 (s, C_{Ar}), 141.4 (s, C_{Ar}), 135.6 ((s, C_{Ar}), 134.4 (s, C_{Ar}), 133.3 (s, C_{Ar}), 132.7 (s, C_{Ar}), 130.7 (s, C_{Ar}), 129.2 (s, C_{Ar}), 128.9 (s, C_{Ar}), 128.4 (s, C_{Ar}), 127.9 (s, C_{Ar}), 127.7 (s, C_{Ar}), 26.8 [s, SiC(CH$_3$)$_3$], 21.0 [s, SiC(CH$_3$)$_3$].

^{29}Si{^{1}H} NMR (79.49 MHz, C_6D_6, 298 K): δ 13.9 [s, *Si*(Cl)C(CH$_3$)$_3$].

FD-MS: Calcd *m/z* for $C_{28}H_{27}ClSi$ [M]$^{+\bullet}$: 426.1565. Found: 426.1570 [M]$^{+\bullet}$.

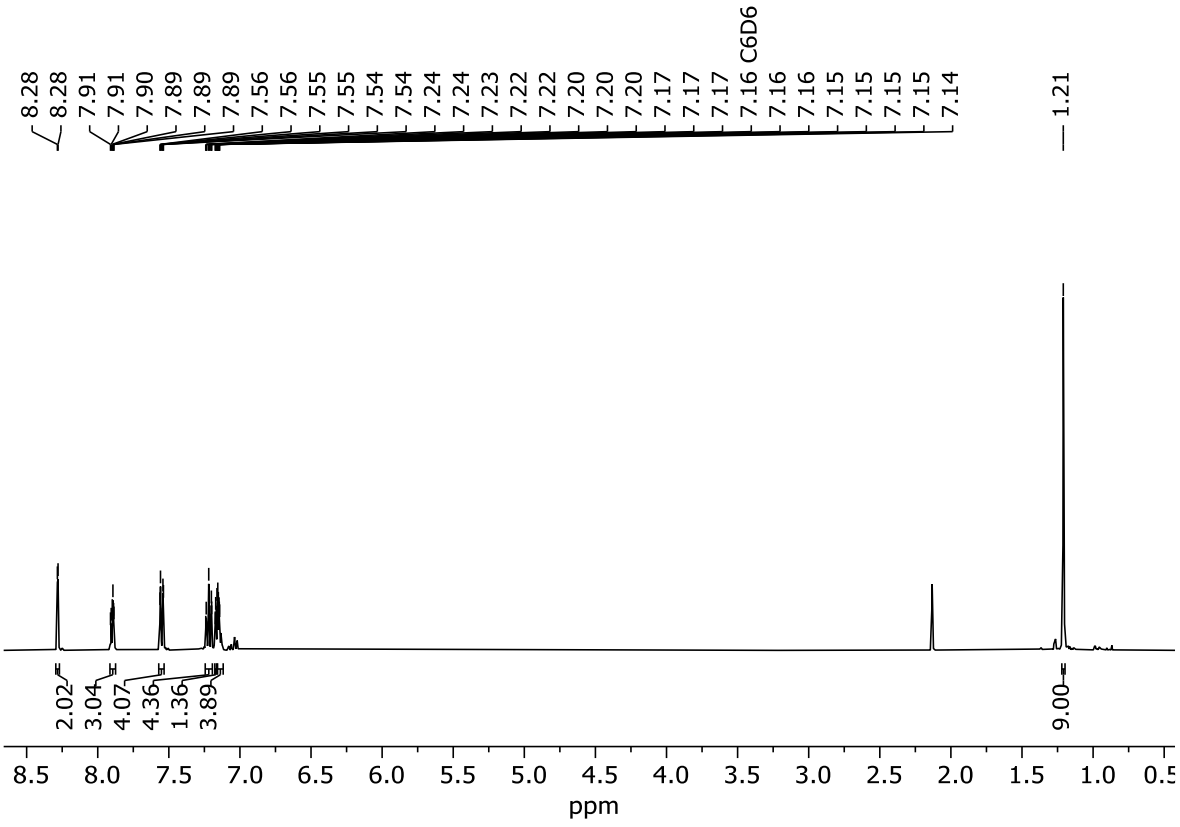

Scheme S20: ^{1}H NMR (400.13 MHz, C_6D_6, 298 K) of compound **11**.

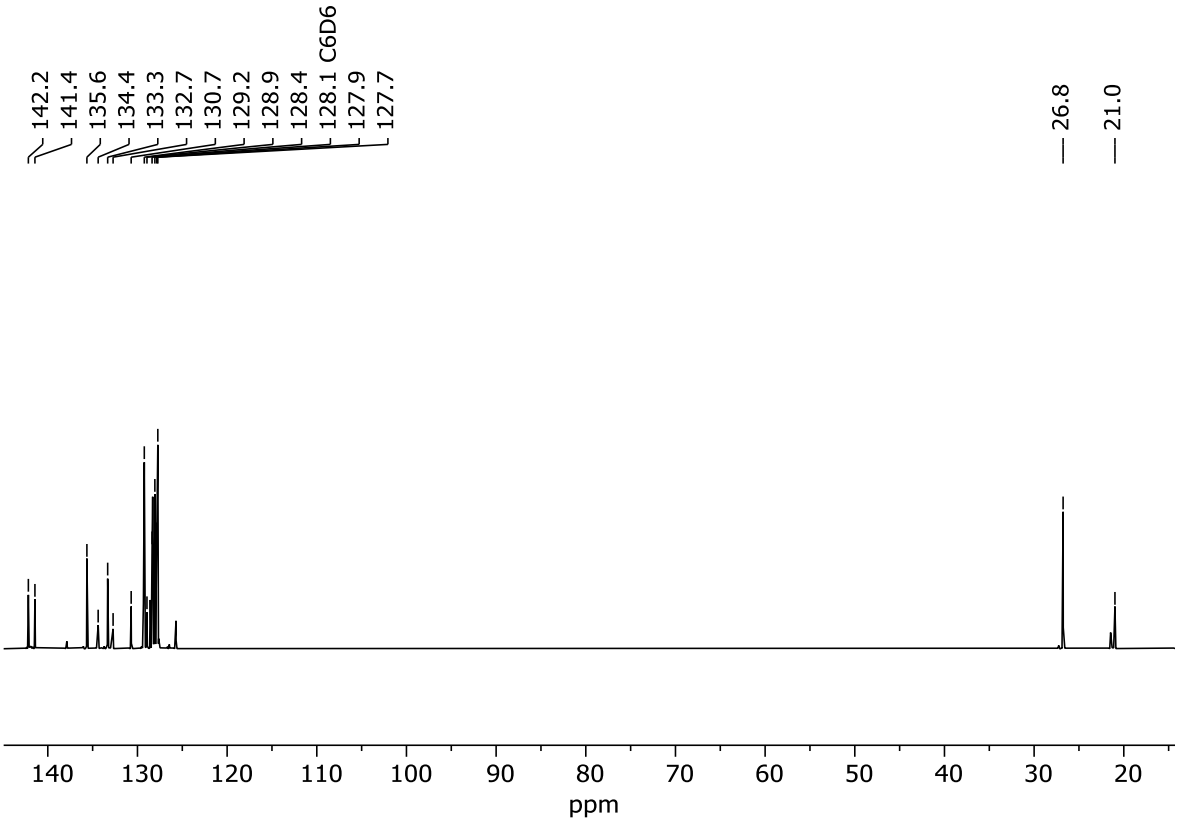

Scheme S21: $^{13}C\{^{1}H\}$ NMR (100.61 MHz, C_6D_6, 298 K) of compound **11**.

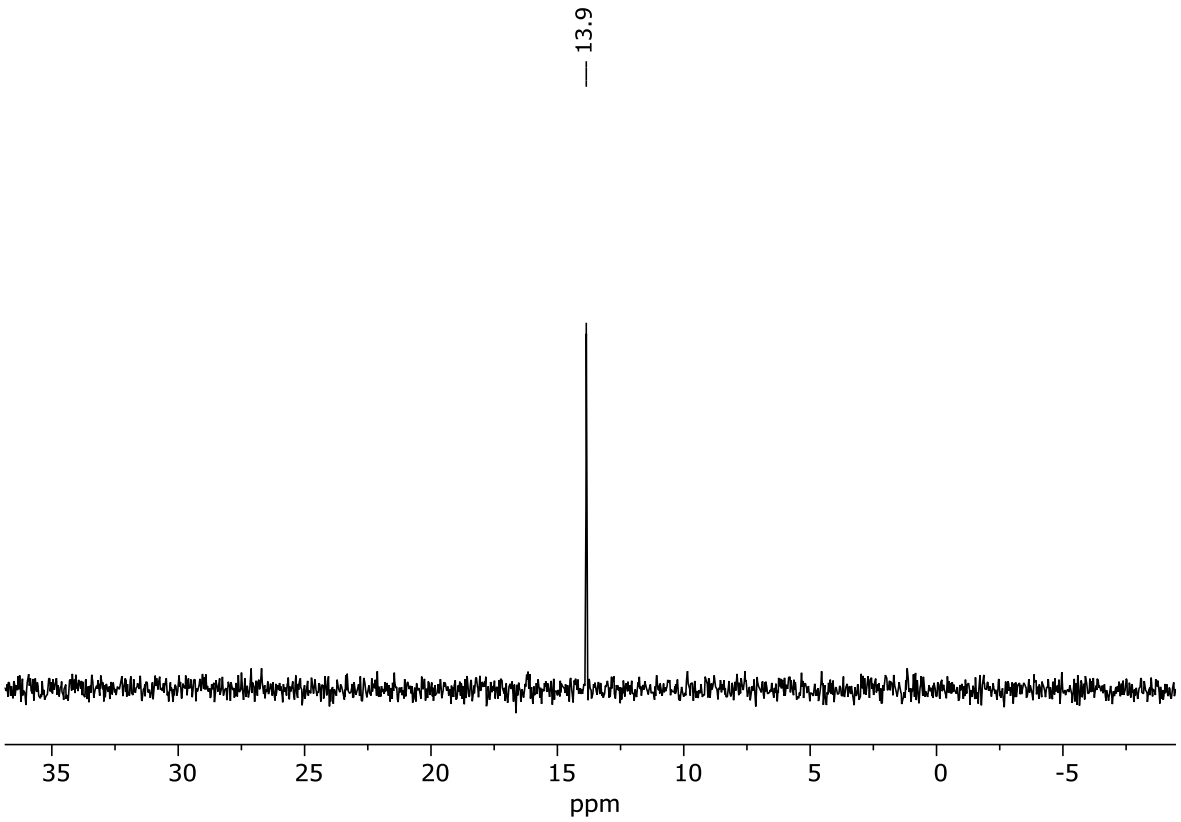

Scheme S22: $^{29}Si\{^{1}H\}$ NMR (79.49 MHz, C_6D_6, 298 K) of compound **11**.

7.7.9 X-ray crystallographic details

The crystals were selected and measured either on a SuperNova Dualflex diffractometer equipped with a TitanS2 detector (**5**, **8**, **12**, **13**), Xcalibur Gemini Ultra diffractometer equipped with a TitanS2 detector (**6**) or a XtaLAB Synergy R, DW system, equipped with a HyPix-Arc 150 detector (**1**, **3**, **4**). Data collection and reduction were performed with CrysAlisPro {Version 1.171.43.36a for all compounds}.[8] A numerical absorption correction based on Gaussian integration over a multifaceted crystal model, and an empirical absorption correction using spherical harmonics, implemented in SCALE3 ABSPACK scaling algorithm was applied for all compounds. Using Olex2,[9] the structures were solved with ShelXT[10] and a least-square refinement on F^2 was carried out with ShelXL[11]. All non-hydrogen atoms were refined anisotropically. Hydrogen atoms at the carbon atoms were located in idealized positions and refined isotropically according to the riding model. Hydrogen atoms at the silicon and nitrogen atoms were located from the difference Fourier map and refined without restraints. The figures in the manuscript and Supporting Information were created with Olex2[9].

Compound **1**: The asymmetric unit contains one molecule.

Compound **3**: The asymmetric unit contains one molecule.

Compound **4**: The asymmetric unit contains one molecule.

Compound **5**: The asymmetric unit contains one half of the molecule.

Compound **6**: The asymmetric unit contains one molecule.

Compound **8**: The asymmetric unit contains one half of the molecule.

Compound **12**: The asymmetric unit contains one molecule. A solvent mask was used for the structure refinement.

Compound **13**: The asymmetric unit contains one molecule.

Table S1: Crystallographic information for compounds **1**,**3** and **4**.

Compound	**1**	**3**	**4**
Data Set (internal naming)	AF119b	AF 216	AF 194
CCDC Number	-	-	-
Formula	$C_{41}H_{40}BF_{20}PSSi$	$C_{71}H_{54}B_2F_{40}LiOPSi_2$	$C_{29}H_{49}OPSSi_2$
$\rho_{calc.}$ / g·cm^{-3}	1.555	1.630	1.125
μ/mm^{-1}	2.357	1.994	2.254
Formula Weight	1014.66	1798.85	532.89
Color	clear colorless	clear colorless	clear colorless
Shape	cube	needle	irregular
Size/mm^3	0.16 x 0.15 x 0.07	0.82 x 0.08 x 0.07	0.11 x 0.1 x 0.07
T/K	123.00(10)	123.00(10)	100.0(10)
Crystal System	monoclinic	monoclinic	triclinic
Space Group	$P2_1/n$	$P2_1/n$	$P\bar{1}$
a/Å	13.96480(10)	15.4367(2)	9.72800(10)
b/Å	20.74560(10)	25.7214(3)	11.21580(10)
c/Å	15.03350(10)	19.3971(3)	14.73450(10)
α/°	90	90	88.6640(10)
β/°	95.6630(10)	107.837(2)	89.8790(10)
γ/°	90	90	78.2070(10)
V/Å^3	4334.07(5)	7331.48(19)	1573.27(2)
Z	4	4	2
Z'	1	1	1
Wavelength/Å	1.54184	1.54184	1.54184
Radiation Type	Cu K_α	Cu K_α	Cu K_α
$2\Theta_{min}$/°	7.286	5.892	6
$2\Theta_{max}$/°	150.602	146.876	150.832
Measured Refl.	46340	72841	75764
Independent Refl.	8842	14192	6397
R_{int}	0.0221	0.0683	0.0258
Parameters	606	1082	319
Restraints	0	0	0
Largest Peak	0.41	0.53	0.49
Deepest Hole	-0.47	-0.96	-0.51
GooF	1.109	1.096	1.072
wR_2 (all data)	0.1269	0.2049	0.0876
wR_2	0.1234	0.1850	0.0870
R_1 (all data)	0.0357	0.0966	0.0324
R_1	0.0326	0.0662	0.0312

Table S2: Crystallographic information for compounds **5**,**6** and **8**.

Compound	**5**	**6**	**8**
Data Set (internal naming)	AF266	AF 160	AF172
CCDC Number	-	-	-
Formula	$C_{18}H_{40}P_2S_3$	$C_{30}H_{50}P_2Si$	$C_{18}H_{35}CoOPSi$
$\rho_{calc.}$ / g·cm^{-3}	1.155	1.082	1.275
μ/mm^{-1}	4.077	1.752	5.736
Formula Weight	207.31	500.73	417.45
Color	clear light brown	clear colorless	clear intense red
Shape	plate	prism	prism
Size/mm^3	0.96 x 0.41 x 0.21	0.31 x 0.16 x 0.13	0.54 x 0.34 x 0.28
T/K	293(2)	122.99(10)	123.00(10)
Crystal System	monoclinic	monoclinic	monoclinic
Space Group	*C*2/*c*	*P*2$_1$/*c*	*P*2$_1$/*n*
a/Å	24.1383(4)	13.6629(5)	10.74150(10)
b/Å	8.4615(2)	14.2277(6)	16.9160(2)
c/Å	11.7514(2)	16.6887(7)	12.7900(2)
α/°	90	90	90
β/°	96.371(2)	108.696(4)	110.663(2)
γ/°	90	90	90
V/Å^3	2385.36	3073.0(2)	2174.49(5)
Z	8	4	4
Z'	1	1	1
Wavelength/Å	1.54184	1.54184	1.54184
Radiation Type	Cu K$_\alpha$	Cu K$_\alpha$	Cu K$_\alpha$
$2\Theta_{min}$/°	11.088	8.36	7.944
$2\Theta_{max}$/°	133.722	134.61	151.698
Measured Refl.	10736	27477	30153
Independent Refl.	2106	5465	6085
R_{int}	0.0495	0.0439	0.0974
Parameters	185	310	227
Restraints	0	0	0
Largest Peak	0.76	0.52	1.05
Deepest Hole	-0.75	-0.39	-1.15
GooF	1.050	1.046	1.035
wR_2 (all data)	0.1261	0.1083	0.1409
wR_2	0.1257	0.1054	0.1383
R_1 (all data)	0.0432	0.0425	0.0536
R_1	0.0429	0.0397	0.0520

Table S3: Crystallographic information for compound **12**.

Compound	**12**	**13**
Data Set (internal naming)	AF207_autored	AF 191b
CCDC Number	-	-
Formula	$C_{43}H_{34}Si$	$C_{32}H_{36}LiO_5PS_2$
$\rho_{calc.}$ / g·cm^{-3}	1.116	1.351
μ/mm^{-1}	0.796	2.464
Formula Weight	578.79	602.64
Color	clear colorless	clear colorless
Shape	prism	prism
Size/mm^3	0.27 x 0.21 x 0.16	0.12 x 0.09 x 0.08
T/K	123.00(10)	123.00(10)
Crystal System	monoclinic	orthorhombic
Space Group	*C*2/*c*	$P2_12_12_1$
a/Å	36.3442(11)	20.2114(3)
b/Å	10.13270(10)	14.5586(2)
c/Å	27.2225(8)	10.0663(2)
α/°	90	90
β/°	136.575(6)	90
γ/°	90	90
V/Å^3	6891.3(6)	2962.01(8)
Z	8	4
Z'	1	1
Wavelength/Å	1.54184	1.54184
Radiation Type	Cu K_α	Cu K_α
$2\Theta_{min}$/°	9.314	7.484
$2\Theta_{max}$/°	133.344	134.008
Measured Refl.	32028	21917
Independent Refl.	6051	5238
R_{int}	0.0703	0.0595
Parameters	398	370
Restraints	0	0
Largest Peak	0.22	0.24
Deepest Hole	-0.31	-0.27
GooF	1.040	1.197
wR_2 (all data)	0.1131	0.1057
wR_2	0.1062	0.1054
R_1 (all data)	0.0497	0.0446
R_1	0.0411	0.0441

Compound **1**

Hydrogen atoms except Si–H and S–H are omitted for clarity.

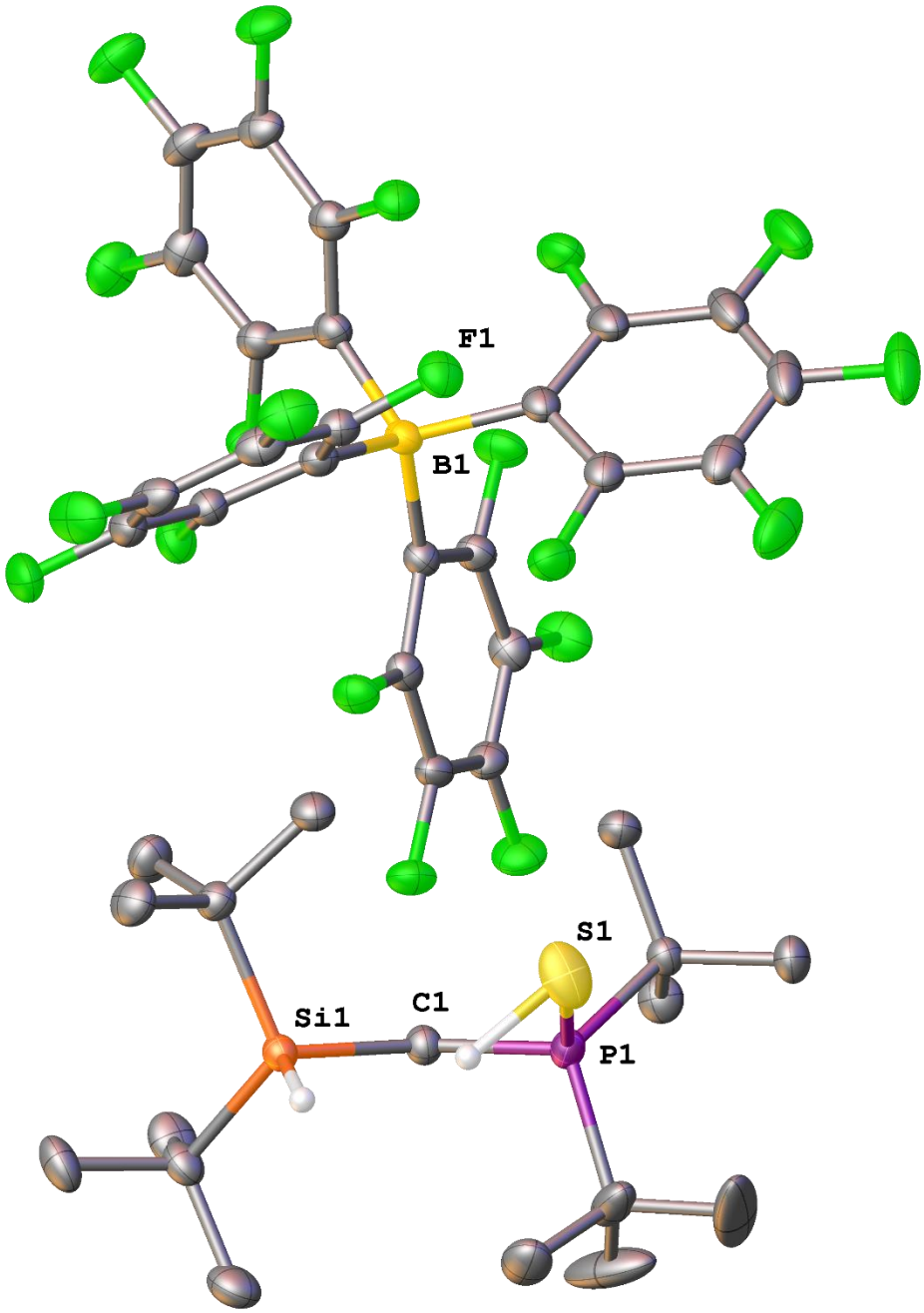

Selected Bond Lengths in Å		**Selected Bond and Torsion Angles in ˚**	
P(1)–S(1)	2.0647(6)	**S(1)–P(1)–C(1)**	110.22(5)
P(1)–C(1)	1.8022(13)	**P(1)–C(1)–Si(1)**	124.98(8)
Si(1)–C(1)	1.9241(14)	**Si(1)–C(1)–P(1)–Si(1)**	-30.53(10)

Compound **3**

Hydrogen atoms except Si–H are omitted for clarity.

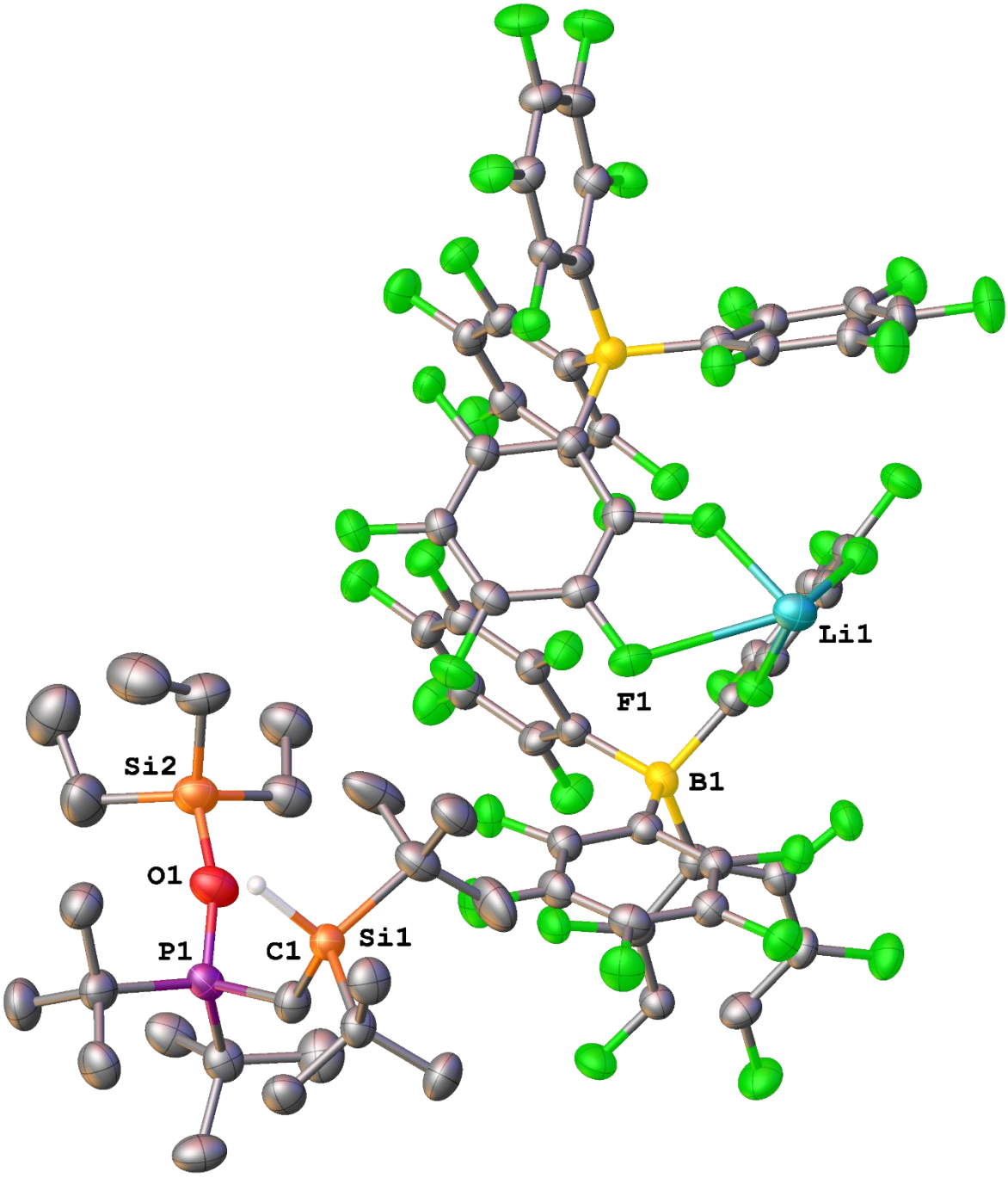

Selected Bond Lengths in Å		**Selected Bond Angles in °**	
P(1)–O(1)	1.557(3)	**P(1)–O(1)–Si(2)**	160.2(2)
O(1)–Si(2)	1.717(3)	**P(1)–C(1)–Si(1)**	131.9(3)
P(1)–C(1)	1.802(4)	**C(1)–P(1)–O(1)**	109.14(18)

Compound **4**

Hydrogen atoms except Si–H are omitted for clarity.

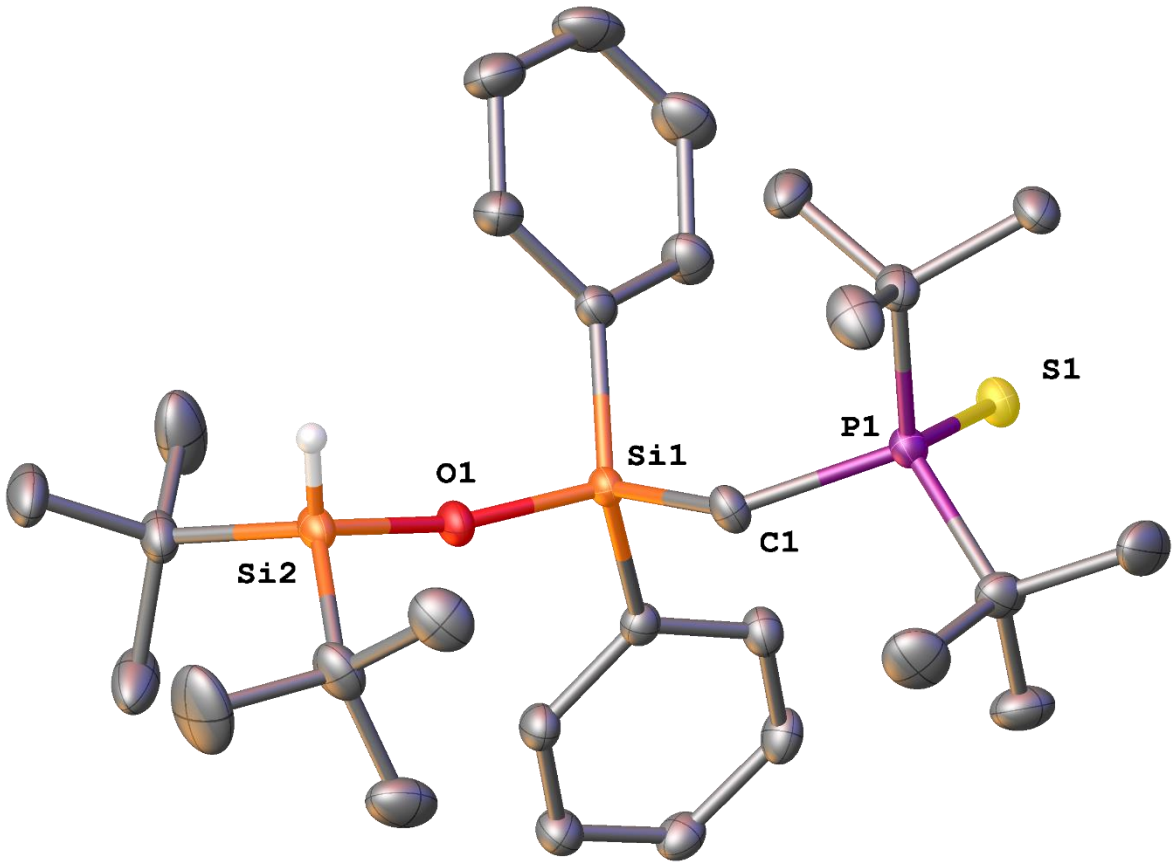

Selected Bond Lengths in Å		**Selected Bond Angles in °**	
P(1)–S(1)	1.9701(5)	**Si(1)–O(1)–Si(2)**	164.84(7)
Si(1)–O(1)	1.6289(10)	**Si(1)–C(1)–P(1)**	127.75(8)
Si(1)–C(1)	1.8860(15)	**C(1)–P(1)–S(1)**	115.07(5)

Compound **5**

Hydrogen atoms are omitted for clarity.

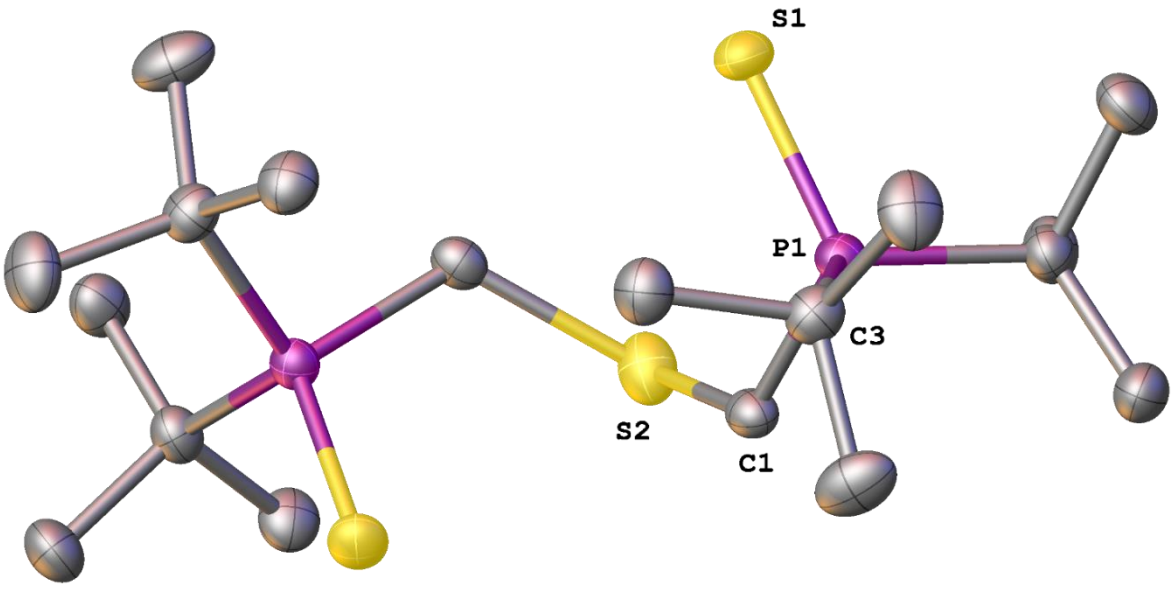

Selected Bond Lengths in Å		**Selected Bond Angles in °**	
P(1)–S(1)	1.9764(7)	**P(1)–C(1)–S(2)**	119.41(12)
P(1)–C(1)	1.878(2)	**C(1)–P(1)–S(1)**	112.18(8)
C(1)–S(2)	1.882(2)	**C(3)–P(1)–S(1)**	111.79(7)

Compound **6**

Hydrogen atoms are omitted for clarity.

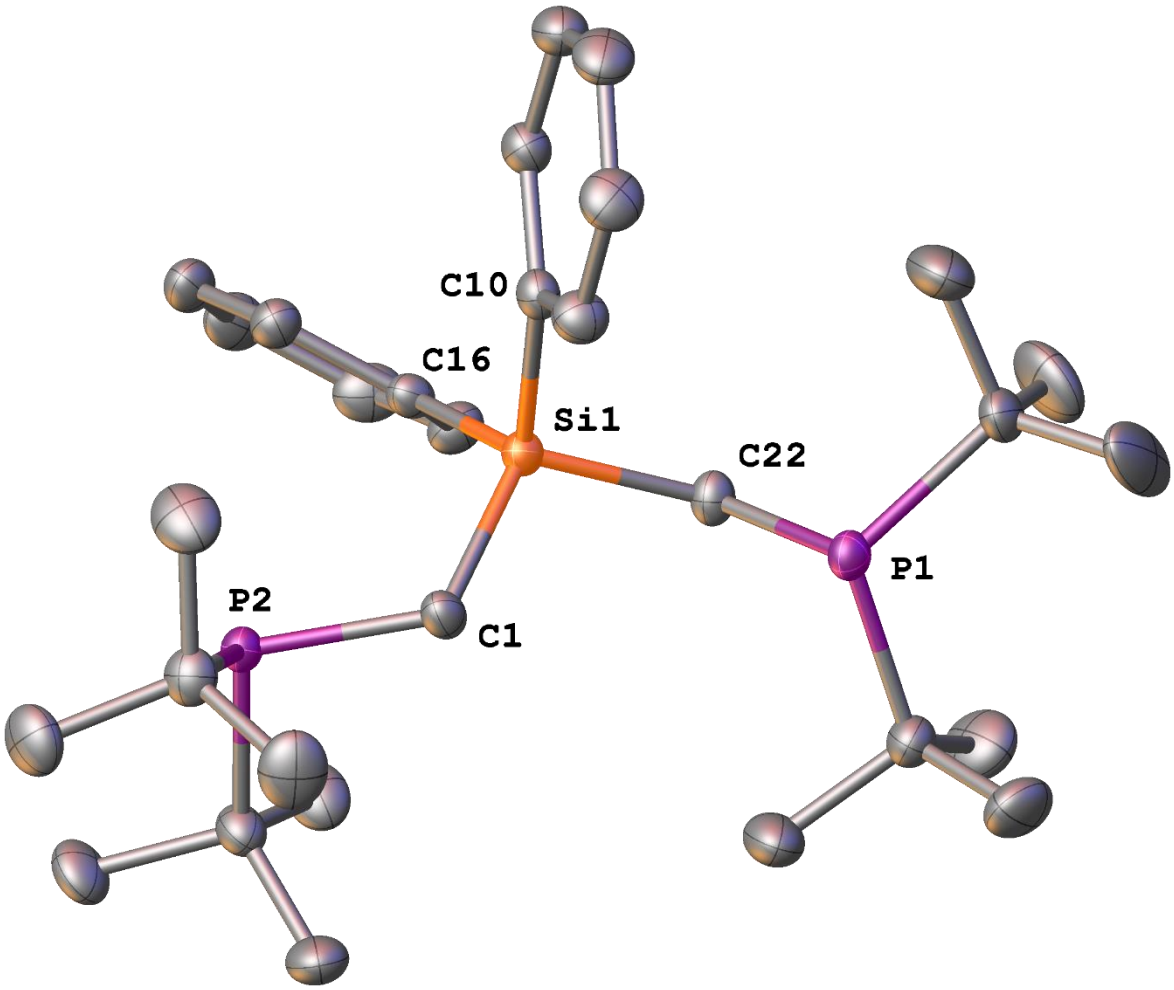

Selected Bond Lengths in Å		**Selected Bond Angles in °**	
Si(1)–C(1)	1.8810(16)	**Si(1)–C(1)–P(2)**	117.99(8)
C(1)–P(2)	1.8637(15)	**C(1)–Si(1)–C(10)**	107.89(7)
Si(1)–C(10)	1.8842(16)	**C(1)–Si(1)–C(22)**	110.31(7)

Compound **8**

Hydrogen atoms except Si–H are omitted for clarity and only one symmetrical half of the molecule is shown.

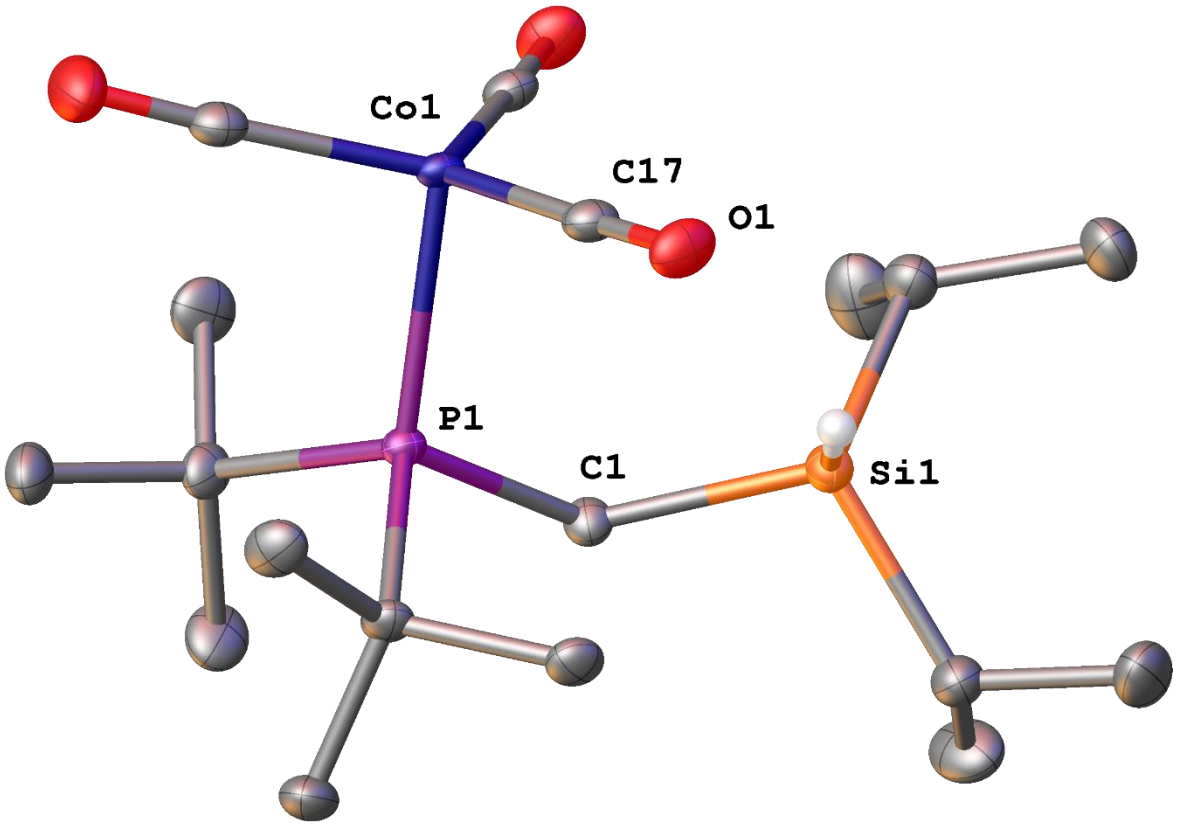

Selected Bond Lengths in Å		**Selected Bond Angles in °**	
Si(1)–C(1)	1.9103(17)	**Si(1)–C(1)–P(1)**	122.76(9)
P(1)–Co(1)	2.2382(5)	**C(1)–P(1)–Co(1)**	112.73(6)
C(17)–O(1)	1.147(2)	**P(1)–Co(1)–C(17)**	97.20(6)

Compound **12**

Hydrogen atoms are omitted for clarity.

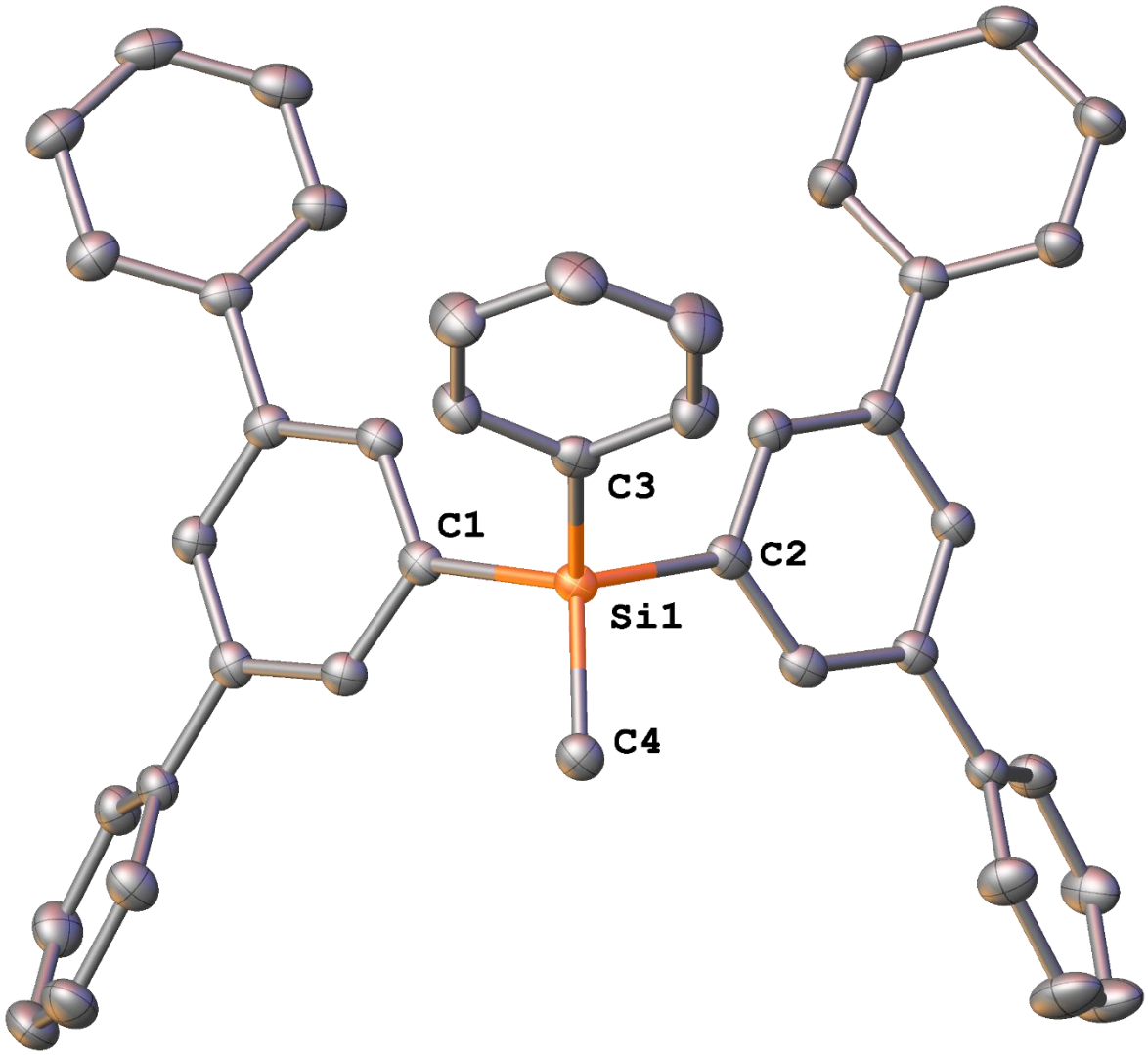

Selected Bond Lengths in Å		**Selected Bond Angles in ˚**	
Si(1)–C(1)	1.8825(16)	**C(1)–Si(1)–C(2)**	111.13(7)
Si(1)–C(4)	1.8577(16)	**C(3)–Si(1)–C(4)**	112.83(7)
Si(1)–C(3)	1.8762(17)	**C(1)–Si(1)–C(3)**	108.77(7)

Compound **13**

Hydrogen atoms are omitted for clarity.

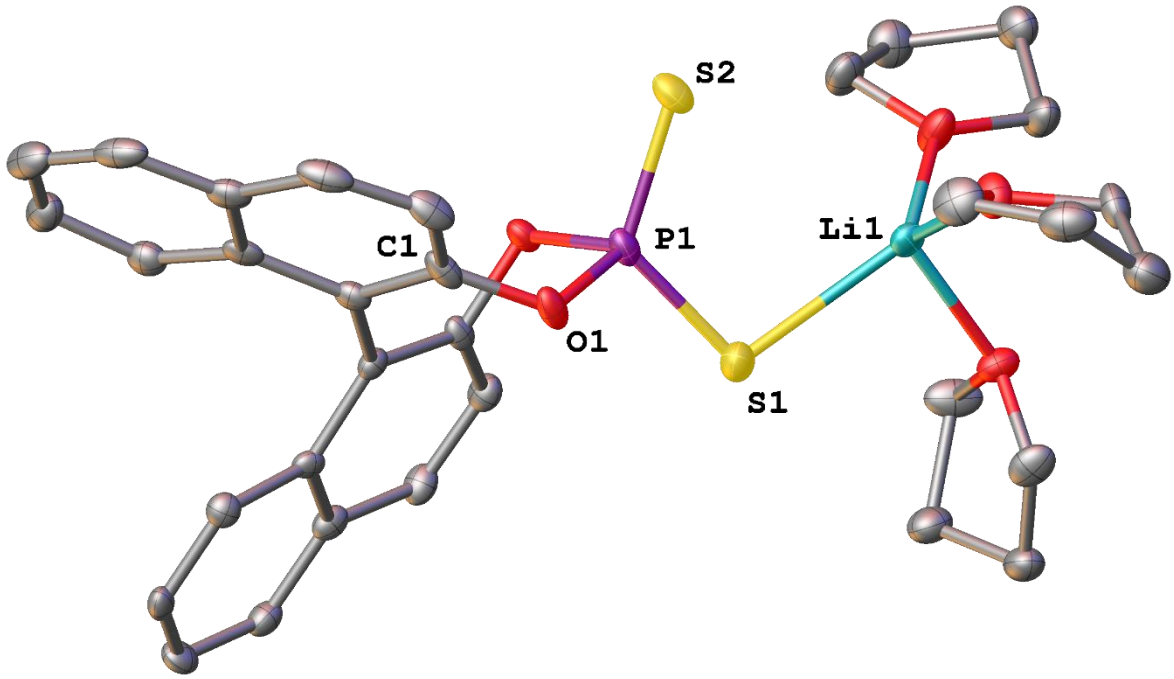

Selected Bond Lengths in Å		**Selected Bond Angles in °**	
P(1)–S(1)	1.9655(19)	**P(1)–S(1)–Li(1)**	100.7(2)
S(1)–Li(1)	2.481(8)	**S(2)–P(1)–O(1)**	113.13(15)
P(1)–O(1)	1.637(3)	**P(1)–O(1)–C(1)**	120.1(3)

7.7.10 Supplementary References

(1) Falk, A.; Bauer, J. O. Structural and Electronic Effects on Phosphine Chalcogenide Stabilized Silicon Centers in Four-Membered Heterocyclic Cations. *Inorg. Chem.* **2022**, *61*, 15576–15588.

(2) Hägele, G.; Tossing, G.; Kückelhaus, W.; Seega, J. Diastereomere Organophosphorverbindungen, I Darstellung und Eigenschaften von CH_3(*t*-C_4H_9)P(X)–Y–(Z)P(*t*-C_4H_9)CH_3. *Z. Naturforsch.* **1984**, *39b*, 1574–1580.

(3) (a) Fontana, N.; Espinosa-Jalapa, N. A.; Seidl, M.; Bauer, J. O. Hidden silylium-type reactivity of a siloxane-based phosphonium–hydroborate ion pair. *Chem. Commun.* **2022**, *58*, 2144-2147. (b) Fink, L.; Samigullin, K.; Bodach, A.; Alig, E.; Wagner, M.; Lerner, H.-W. Donor-unsupported Phosphanylmethanides Li[CH2P*R*$_2$] (*R* = *t*Bu, Ph) – Crystal Structure of Li[CH_2P*t*Bu_2] Solved by XRPD and DFT-D Calculations. *Z. Anorg. Allg. Chem.* **2016**, *642*, 282-287.

(4) Shainyan, B. A.; Suslova, E. N.; Phien, T. D.; Shlykov, S. A.; Oznobikhina, L. P. 1-*t*-Butyl-1-phenyl-1-silacyclohexane: Synthesis, conformational analysis in gas and solution by GED, FT-IR and theoretical calculations. *J. Organomet. Chem*. **2020**, *923*, 121433.

(5) (a) Rach, S. F.; Herdtweck E.; Kühn, F. E. *J. Organomet. Chem.* **2011**, *696*, 1817. (b) Jutzi, P.; Müller, C.; Stammler, A.; Stammler, H.-G. Synthesis, Crystal Structure, and Application of the Oxonium Acid [H(OEt_2)$_2$][B(C_6F_5)$_4$] -. *Organometallics* **2000**, *19*, 1442–1444.

(6) Ma, W.; Liu, L.-C.; An, K; He, T.; He, W. Rhodium-Catalyzed Synthesis of Chiral Monohydrosilanes by Intramolecular C–H Functionalization of Dihydrosilanes. *Angew. Chem. Int. Ed.* **2020**, *60*, 4245-4251.

(7) Yong, Q.; Zhanqi, L.; Duan, L. Pepraration of anthracene derivatives as fluorescent and phosphorescent materials. *Tsinghua University; Beijing Visionox Technology Co., Ltd.; Kunshan Visionox Display Technology Co., Ltd.* **2010**, CN102557856 A 2012-07-11.

(8) Rigaku Oxford Diffraction, CrysAlisPro Software System. 2020.

(9) Dolomanov, O. V.; Bourhis, L. J.; Gildea, R. J.; Howard, J. A. K.; Puschmann, H. *OLEX2*: a complete structure solution, refinement and analysis program. *J. Appl. Crystallogr.* **2009**, *42*, 339-341.

(10) Sheldrick, G. M. *SHELXT* – Integrated space-group and crystal-structure determination. *Acta Crystallogr*. **2015**, *A71*, 3-8.

(11) Sheldrick, G. M. Crystal structure refinement with *SHELXL*. *Acta Crystallogr.* **2015**, *C71*, 3-8.

8 Conclusions

Within this work, the modification of the substituents at silicon of heterocyclic four-membered silyl phosphonium ions was investigated. In chapter 1 a general overview of the current state of research, and the design principles, to which the structure of the four-membered phosphonium ions adhere, are presented. The focus of chapter 3 is the modification of previously known silyl phosphine chalcogenides with different substituents and Lewis basic chalcogenides. New synthesis routes towards these novel compounds were developed, the structures synthesized and thoroughly investigated by means of single-crystal X-ray diffraction analysis, NMR analysis and DFT calculations. Through this procedure a deep understanding of the governing principles of steric and electronic effects within these four-membered silyl phosphonium chalcogenides was obtained. When all substituents are replaced by sterically demanding *tert*-butyl substituents, the choice of chalcogen used as a Lewis base becomes crucial for successful ring formation (Scheme 8.1).

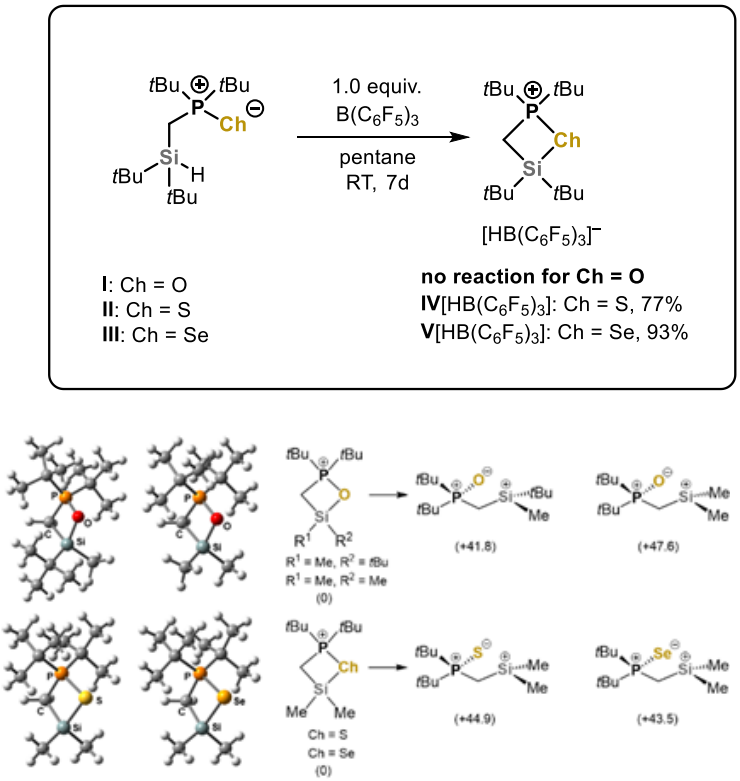

Scheme 8.1: Influence of chalcogen Lewis base type on the ability of all *tert*-butyl substituted silyl phosphine chalcogenides (**I**, **II**, **III**) to form the four-membered heterocycles.

The angular strain within the four-membered rings was found to be well balanced in all four-membered CPChSi rings investigated. Thermochemical investigations showed that the substituents on the silicon and phosphorus atoms play an important role for the strength of the intramolecular Ch–Si coordination. In the absence of large steric repulsions through bulky substituents (methyl groups on silicon, *tert*-butyl groups on phosphorus), a stability sequence depending on the chalcogen atom in the direction Se ≤ S < O can be

observed. However, the order is reversed (O < S < Se) in case of strong repulsions between sterically demanding substituents (*tert*-butyl groups on both silicon and phosphorus atoms). Due to the shorter Si–O bond length compared to the Si–S and Si–Se bond lengths, the substituents of the phosphorus and silicon atom are forced in closer proximity in the four-membered cations. In the case of all-*tert*-butyl substituted compound **I** this leads to a significant increase in steric repulsion in this cation, therefore hampering its synthesis. Building upon this knowledge, another second-row element, nitrogen, was investigated as a donor in chapter 4. The nitrogen atom was introduced as a phosphinimine moiety into the systems. In contrast to phosphine chalcogenides, phosphinimine donor moieties allow for further modification of donor strength by the influence of steric or electronic parameters. The introduction of either a trimethylsilyl or a bis(3,5-trifluoromethylphenyl)boryl moiety allows for additional ring strain in these systems. Furthermore, an electronic destabilization of the Si–N bond was expected to be achieved by either resonance stabilization by the bis(3,5-trifluoromethylphenyl)boryl moiety or by hyperconjugative n(N)→σ*(SiMe) interactions from the –$SiMe_3$ moiety. Taken together, these effects are expected to facilitate ring opening and enable small molecule activation or even catalytic transformations. The rational synthesis of these systems, the influence of steric and electronic factors, and the reactivity in terms of catalytic applications and FLP-like behavior were investigated. The silylated phosphinimines can be easily obtained in moderate to good yields (Figure 8.1).

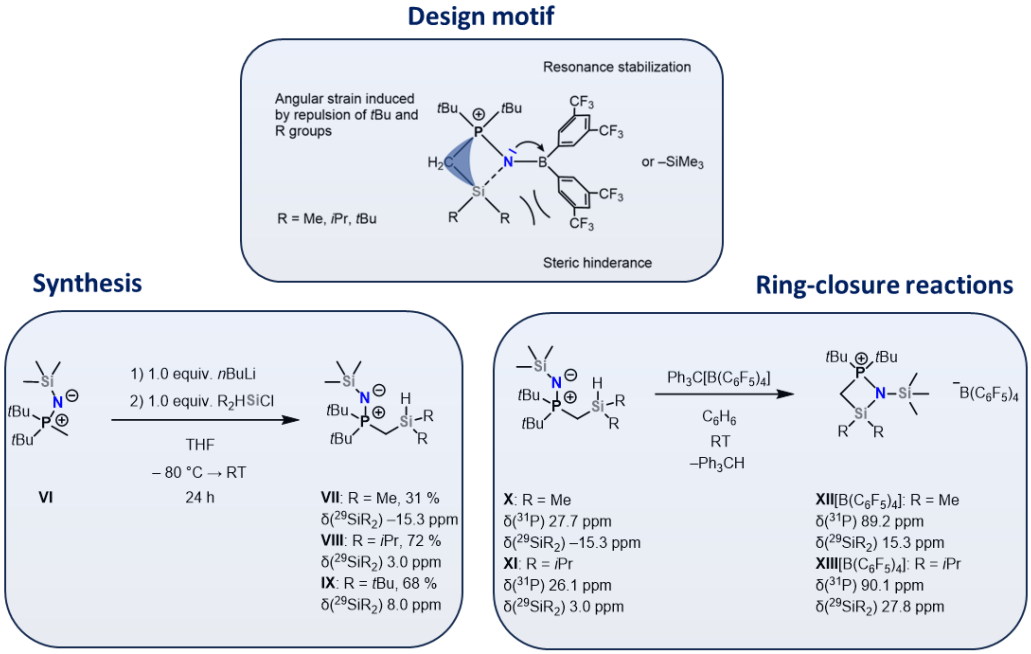

Figure 8.1: General design, synthesis and ring closure reactions with the silylated phosphinimines.

The ring-closure reactions of the methyl- and *iso*-propyl-substituted silanes (**X**, **XI**) proceeded smoothly, however the case of the all *tert*-butyl substituted silyl phosphinimine **IX** no ring closure was possible. Like the P–O bond length [1.4958(8) Å] in compound **I** the P–N bond length [1.538(2) Å] in compound **IX** is also very short, therefore the same effects hampering the ring formation in compound **I** were found to also affect the ring formation in compound **IX**. The Si–N bonds in the $SiMe_3$-substituted four-membered phosphonium ions **XII**[$B(C_6F_5)_4$] and **XIII**[$B(C_6F_5)_4$] were found to be covalent in nature, and did not possess

the ability to reversibly open as anticipated. Nevertheless, we were able to gain valuable insights from these results and therefore we set out to design a new system with a maximum of steric hinderance, while also preserving the desired ability to remove the hydride from the Si–H moiety. Therefore, an electrophilic boryl moiety was introduced to study the effect of electron-withdrawing groups on the reversible opening ability of these ring systems. With the zwitterionic compound **XIV** reversibility was finally achieved which was evidenced by the ability of compound **XIV** to catalyze the hydrosilylation of nitriles (Scheme 8.2).

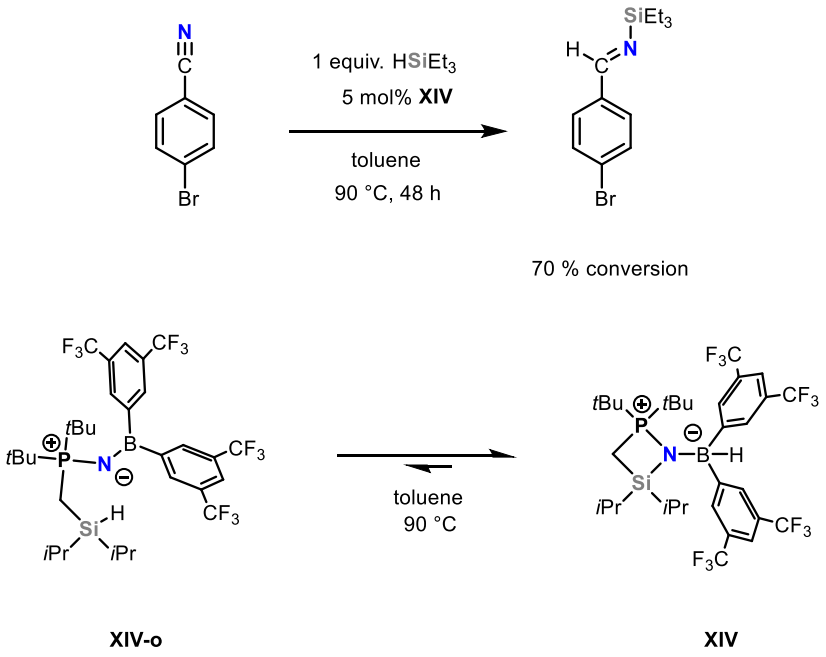

Scheme 8.2: Proposed reversibly opening compound **XIV** at elevated temperatures and its catalytic activity.

This validated our approach of combining steric and electronic factors to weaken the Si–N bond in compound **XIV**. Upon receiving preliminary confirmation through this experiment, that reversibility is in principle possible within these systems our attention shifted away from the strongly Lewis acidic silylium-based Lewis acids towards neutral silicon-based Lewis acids (Scheme 8.3).

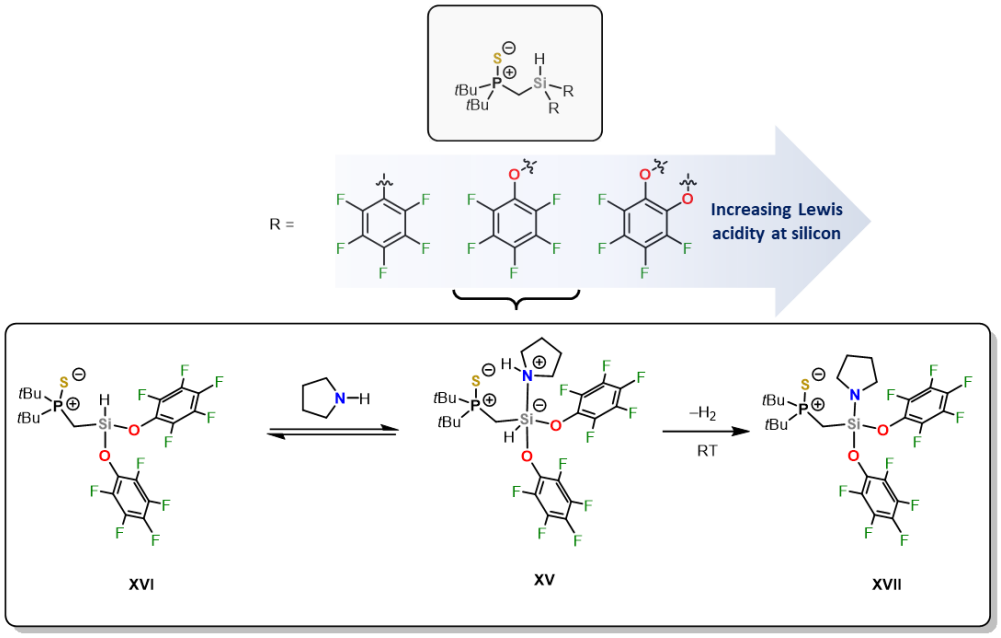

Scheme 8.3: Phosphine sulfide substituted neutral silanes with different electron-withdrawing substituents.

The rational was, that neutral silicon-based Lewis acids are of lower Lewis acidity compared to silylium ions, and therefore reversibility within these systems can be easier achieved. The question whether this really is the case was addressed in chapter 5. Several novel neutral Lewis acidic silanes were prepared and incorporated within the previously described CPSSi cycles (chapter 3). By varying the electron-withdrawing groups from pentafluorophenyl [-C_6F_5] over pentafluorophenoxy [-OC_6F_5] to tetrafluorocatecholato [-$O_2C_6F_4$] moieties, a discernible difference in Lewis acidity at the silicon center was observed (Scheme 8.3). While the pentafluorophenyl [-C_6F_5] substituted compound showed no Lewis acidity, the tetrafluorocatecholato [-$O_2C_6F_4$] substituted silane was strongly prone towards formation of the pentacoordinate state making the desired Si–H substituted tetravalent silane inaccessible. A good balance between Lewis acidity and stability of the tetravalent state was found with the pentafluorophenoxy [-OC_6F_5] substituted compound **XV**. Through in depth NMR spectroscopic experiments a equilibrium between compounds **XV** and **XVI** could be observed. Compound **XV** represents an intriguing structure as it combines a highly reducing anionic Si–H function, aswell as a protic cationic N–H function in close proximity to each other. To the best of our knowledge this is the only example were both motifs can be found within one molecule. Through additional time resolved NMR experiments it was also found that compound **XV** is not stable over a prolonged amount of time and slowly reacts with the loss of dihydrogen towards compound **XVII**. In conclusion the introduction of neutral Lewis acidic silanes indeed proved to ease the ability of the silicon Lewis acids to reversibly attach to Lewis bases.

In a second part of this doctoral project, chiral silanethiols were synthesized and investigated as enantioselective hydrogen-atom transfer (HAT) catalysts together with the group of Prof. König. The deracemization was achieved by a sequence of photocatalytic hydrogen-atom transfer, reductive radical-polar crossover (RRPCO), and protonation. Our goal was to design silanethiols which were able to act as potent and enantioselective HAT-

catalysts. To achieve this goal, different strategies were employed. The first attempt was made with a silanethiol which was equipped with chiral substituents (Figure 8.2). Therefore the (–)-menthol substituted silanethiol **XVIII** was prepared and tested, and while compound **XVIII** performed well as a HAT-catalysts no enantioselectivity was observed. Next, the *Si*-chiral silanethiol **XIX** was prepared and tested. The idea was to bring the chiral information closer to the reactive Si–S^- function, and therefore enhance enantioselectivity. This approach was successful and compound **XIX** performed well as a HAT catalyst and gave an enantiomeric excess of 16 % in the final product. While this finding served as proof that chiral silanethiols can indeed be used as enantioselective HAT-catalysts, the enantiomeric excess obtained was not good enough for practical use. In order to increase the enantioselectivity even further, the successful concept of using *Si*-chiral silanethiols was combined with a chiral backbone. A suitable motif, which combined both desired features was found in a class of silanthiols with a ferrocene backbone [(S_{Si},S_P)-**XX** and (S_{Si},S_P)-**XXI**] (Figure 8.2). While both compounds are *Si*-stereogenic, they also exhibit planar chirality in the ferrocenyl backbone. However, when employing compounds (S_{Si},S_P)-**XX** and (S_{Si},S_P)-**XXI** in the RRPCO-HAT-protonation sequence, decomposition was observed. No catalytic activity nor enantioselectivity was observed for both compounds, therefore concluding that the ferrocene backbone is not suitable for this application. In summary, this lays the foundation for the design of silanethiol HAT catalysts based on the general structure of compound **XIX**.

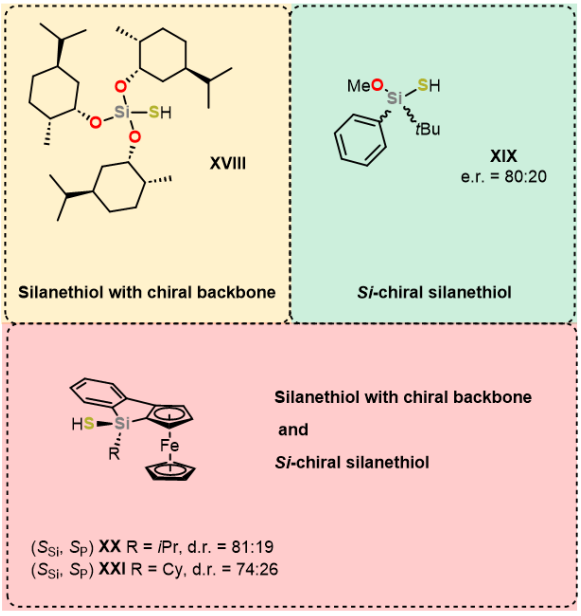

Figure 8.2: The synthesized and tested silanethiols.

9 Acknowledgements

Zum Schluss der Arbeit möchte ich noch allen Personen danken die mich während dieser lehrreichen und aufschlussreichen Zeit begleitet haben.

Als Erstes möchte ich Jonathan Bauer danken, der mich 2020 zuerst zum Abschluss meiner Masterarbeit in die Arbeitsgruppe aufgenommen hat und mir diese Promotion somit erst ermöglicht hat. Ich danke ihm vor allem für das stets mir entgegengebrachte Vertrauen sowie die zahlreichen interessanten wissenschaftlichen Diskussionen.

Prof. Dr. Manfred Scheer möchte ich für die Übernahme des Zweitgutachtens und die stetige Unterstützung unserer Arbeitsgruppe über die Jahre danken.

Prof. Dr. Frank-Michael Matysik und Prof. Dr. Hubert Motschmann möchte ich für die Übernahme des Drittprüfers bzw. Vorsitzenden meines Kolloquiums danken.

Meinen Kollegen im Arbeitskreis Bauer (Tanja, Tobi, Noel, Robin, Nikolo und Manuel) möchte ich für die stets angehnehme Arbeitsatmosphäre, die tollen Konferenzreisen sowie die äußerst wertvollen Tipps und Tricks zum praktischen Arbeiten danken. Durch eure kollegiale Art habe ich mich von Tag eins an wohl gefühlt.

Den Arbeitskreisen des dritten Stocks (AK Scheer, AK Wolf, AK Korber), den technischen Angestellten (Martina, Petra, Schotti, Lukas, Tuan, Birgit, Sabine) und Gabor möchte ich für das tägliche Miteinander sowie diverse technische Hilfe danken.

Ein weiter Dank geht an meine Freunde Sebastian und Dominik, die mich während meines Studiums und meiner Promotion begleitet haben.

Ein großer Dank geht auch an meine Eltern Dine und Hans sowie meinen Bruder Valentin und meine Freundin Saphia für die nie nachlassende Unterstützung in jedem Lebensabschnitt.